BASIN-SCALE PRODUCED-WATER MANAGEMENT TOOLS AND OPTIONS—GIS-BASED MODELS AND STATISTICAL ANALYSIS OF SHALE GAS/TIGHT SAND RESERVOIRS AND THEIR PRODUCED-WATER STREAMS, UINTA BASIN, UTAH
(Subcontract No. 11123-08)

FINAL REPORT

Submitted by

Utah Geological Survey
Salt Lake City, Utah 84114
November 2015

John Terneus, Contract Director,
National Energy Technology Laboratory (NETL), U.S. Department of Energy
and
Charlotte Schroeder, Manager, Unconventional Resources & Small Producer Program
Research Partnership to Secure Energy for America (RPSEA)

DISCLAIMER

Although this product represents the work of professional scientists, the Utah Department of Natural Resources, Utah Geological Survey, makes no warranty, expressed or implied, regarding its suitability for a particular use. The Utah Department of Natural Resources, Utah Geological Survey, shall not be liable under any circumstances for any direct, indirect, special, incidental, or consequential damages with respect to claims by users of this product.

BASIN-SCALE PRODUCED-WATER MANAGEMENT TOOLS AND OPTIONS—GIS-BASED MODELS AND STATISTICAL ANALYSIS OF SHALE GAS/TIGHT SAND RESERVOIRS AND THEIR PRODUCED-WATER STREAMS, UINTA BASIN, UTAH
(Subcontract No. 11123-08)

FINAL REPORT

Submitted by

Utah Geological Survey
Salt Lake City, Utah 84114
November 2015

Edited and Compiled by

Thomas C. Chidsey, Jr., Principal Investigator,
Utah Geological Survey
Salt Lake City, Utah

ABSTRACT

Oil and gas fields in the Uinta Basin of eastern Utah produced nearly 33 million barrels of oil and 363 billion cubic feet of gas in 2014 from the Tertiary Wasatch and Green River Formations and several formations in the Upper Cretaceous Mesaverde Group. Nearly 105 million barrels of water was also produced with these hydrocarbons. Extensive drilling for lenticular, tight gas sands in the Wasatch and Mesaverde occurred in the eastern part of the basin, whereas large drilling programs as part of expanding waterflood projects for oil in the Green River continued in the south-central basin; over 1300 wells were permitted in 2014 (before oil prices collapsed). The environmentally sound disposal of produced water affects the economics of the hydrocarbon resource development in the basin and has recently become a topic of much public debate because produced water is the largest-volume waste stream associated with these unconventional gas plays.

Managing produced water can be a significant cost fraction of the value of the gas extracted, so there is an economic incentive to minimize this waste stream, and/or generate revenue from treating and reusing produced water in hydrocarbon production or other applications. Balancing the water-use needs and produced-water disposal requirements associated with shale/tight-sand gas development creates significant material handling challenges to both industry and regulators. These challenges are complicated by an operating environment where many individual producers of varying sizes exist within a field, each with differing water needs and production, and a production timescale of decades for the basin as wells play out and new ones are completed. Specific Uinta Basin water issues include: water use/reuse for well drilling and completion (hydraulic fracturing), appropriate sites for disposal/reuse of water,

development of systems to manage the produced water streams, and differing challenges for gas versus oil producers.

Current produced water disposal practices in the Uinta Basin consist of (1) injection in deep wells below the base of a moderately saline aquifer in the Green River Formation, (2) storage and evaporation in lined disposal ponds, and (3) supplying water for flooding in enhanced-oil recovery programs. Potential uses for the produced water from Uinta Basin tight-sand gas reservoir include waterflooding for secondary recovery, drilling mud formulation, hydraulic fracturing fluid for well completion, and future possible oil shale production. Our study consisted of four major components: (1) compilation and analysis of past and new information on the thickness, structure, depth, lithology, porosity, permeability, water quality, and temperature of all aquifer/reservoir units in the basin from the Tertiary down through the Jurassic Glen Canyon Group; (2) statistical analysis of water production quantity and quality; (3) development of alluvial aquifer sensitivity/vulnerability models to potential contamination from fluids associated with tight-sand gas development; and (4) an evaluation of the existing infrastructure for produced water management/reuse and recommendations for best management practices and the energy generation potential of geothermal-produced waters.

Current best practices for produced water storage include: (a) disposal in deep injection wells below the base of the moderately saline aquifer, (b) storage and evaporation in lined disposal ponds, and (c) use for waterflooding enhanced-oil recovery. The “Birds Nest” aquifer in the upper Green River Formation is the most widespread and economically viable disposal unit in terms of depth, proximity to producing wells, and water quality. Statistical analysis of water production quantity and quality identified and forecasted volume trends. For example, the greatest need for water disposal results from drilling gas wells in the eastern part of the basin

whereas water is needed for enhanced-oil recovery projects in the south-central basin. These needs will continue, based on predicted drilling trends once prices return to the levels prior to the collapse and as producing wells mature leading to increased water production. Thus, we suggest that excess compatible produced water from gas wells be transported to oil fields undergoing enhanced oil recovery. Produced water could also be used for the water component in hydraulic fracturing, required for tight-gas sand reservoirs and potential shale-gas resouces in the basin. Finally, the heat content of produced waters could be used locally for space heating and engineering purposes.

CONTENTS

ABSTRACT i

EXECUTIVE SUMMARY xix

CHAPTER I – INTRODUCTION 1.1
LOCATION AND GENERAL GEOLOGIC SETTING 1.2
BASIC PETROLEUM GEOLOGY AND OIL AND GAS DEVELOPMENT HISTORY 1.3
PURPOSE AND SCOPE 1.6

CHAPTER II – STRATIGRAPHY AND DEPOSITIONAL HISTORY 2.1
UPPER TRIASSIC-JURASSIC ROCKS 2.2
Upper Triassic to Lower Jurassic Rocks 2.2
Wingate Sandstone 2.3
Kayenta Formation 2.4
Navajo Sandstone 2.4
Middle-Upper Jurassic Rocks 2.5
Carmel and Arapien Formations 2.5
Entrada 2.7
Curtis and Stump Formations 2.8
Summerville Formation 2.9
Morrison Formation 2.10
CRETACEOUS ROCKS 2.12
Lower to Lower-Upper Cretaceous Rocks 2.12
Cedar Mountain Formation 2.13
Dakota Sandstone 2.15
Upper Cretaceous Rocks 2.16
Mowry Shale 2.17
Frontier Formation 2.17
Mancos Shale 2.18
Mesaverde Group 2.20
Star Point Sandstone 2.21
Blackhawk Formation 2.21
Castlegate Sandstone 2.22
Sego Sandstone 2.23
Neslen Formation 2.24
Farrer Formation 2.25
Price River Formation 2.25
Tuscher Formation 2.26
Tertiary Rocks 2.27
North Horn Formation 2.28
Flagstaff Limestone 2.29
Colton Formation 2.30
Wasatch Formation 2.31
Green River Formation 2.32

Uinta Formation 2.36
Duchesne River Formation 2.37
Quaternary Deposits 2.38

CHAPTER III – STRUCTURAL SETTING 3.1
TECTONIC HISTORY 3.1
GENERAL BASIN STRUCTURE AND FOLDING 3.4
FAULTING 3.5
Uinta Basin-Mountain Boundary Fault 3.6
Duchesne Fault and Fracture Zone 3.7
JOINTING 3.8
FRACTURES 3.9
GILSONITE VEINS 3.11

CHAPTER IV – UINTA BASIN RESERVOIRS/AQUIFERS: TRIASSIC-JURASSIC GLEN CANYON GROUP THROUGH THE CRETACEOUS CEDAR MOUNTAIN AND DAKOTA FORMATIONS 4.1
METHODS 4.2
TRIASSIC-JURASSIC GLEN CANYON GROUP AND NUGGET SANDSTONE 4.4
Thickness 4.4
Depth 4.5
Lithology 4.5
Reservoir Properties 4.6
Water Quality 4.7
Water Production, Use, and Disposal 4.9
Hydrocarbon Production 4.10
JURASSIC ENTRADA SANDSTONE 4.11
Thickness 4.11
Depth 4.12
Lithology 4.12
Reservoir Properties 4.13
Water Quality 4.14
Water Production, Use, and Disposal 4.15
Hydrocarbon Production 4.15
CRETACEOUS CEDAR MOUNTAIN AND DAKOTA FORMATIONS 4.16
Thickness 4.16
Depth 4.17
Lithology 4.17
Reservoir Properties 4.18
Water Quality 4.19
Water Production, Use, and Disposal 4.20
Hydrocarbon Production 4.21
SUMMARY 4.22

CHAPTER V – UINTA BASIN RESERVOIRS/AQUIFERS: UPPER CRETACEOUS MANCOS SHALE 5.1

METHODS 5.2
UPPER CRETACEOUS MANCOS SHALE 5.2
Thickness 5.3
Depth 5.3
Lithology 5.5
Reservoir Properties 5.5
Water Quality 5.6
Water Production, Use, and Disposal 5.7
Hydrocarbon Production 5.8
SUMMARY 5.9

CHAPTER VI – UINTA BASIN RESERVOIRS/AQUIFERS: UPPER CRETACEOUS MESAVERDE GROUP AND UPPER PALEOCENE WASATCH/COLTON FORMATION 6.1
METHODS 6.2
UPPER CRETACEOUS MESAVERDE GROUP 6.14
Thickness 6.15
Depth 6.15
Lithology 6.16
Reservoir Properties 6.20
Water Quality 6.23
Water Production, Use, and Disposal 6.24
Hydrocarbon Production 6.25
UPPER PALEOCENE TO LOWER EOCENE WASATCH/COLTON FORMATION 6.26
Thickness 6.27
Depth 6.28
Lithology 6.28
Reservoir Properties 6.29
Water Quality 6.30
Water Production, Use, and Disposal 6.32
Hydrocarbon Production 6.34
SUMMARY 6.35

CHAPTER VII – UINTA BASIN RESERVOIRS/AQUIFERS: EOCENE GREEN RIVER FORMATION 7.1
METHODS 7.2
EOCENE GREEN RIVER FORMATION 7.4
Thickness 7.5
Depth 7.6
Lithology and Stratigraphy 7.6
Reservoir Properties 7.12
Water Quality 7.12
Water Production, Use, and Disposal 7.16
Hydrocarbon Production 7.17
SUMMARY 7.18

CHAPTER VIII – SUMMARY OF THE COMPILED FLUID GEOCHEMISTRY DATABASE FOR THE UINTA BASIN....8.1
BACKGROUND....8.1
DATA ANALYSIS....8.5
SUMMARY....8.10

CHAPTER IX – GROUNDWATER CHEMISTRY AND WATER QUALITY FOR SHALLOW ALLUVIAL WELLS AND SPRINGS IN THE UINTA BASIN....9.1
PREVIOUS WORK....9.1
Hydrogeology....9.2
Previous Water-Quality Data....9.5
WATER-QUALITY SAMPLING FOR SPRINGS AND ALLUVIAL WELLS....9.7
WATER-QUALITY RESULTS....9.8
Total-Dissolved-Solids Concentrations....9.9
Nitrate Concentrations....9.9
Arsenic....9.10
Boron....9.10
Other Constituents of Concern....9.11
Volatile Organic Compounds and Total Petroleum Hydrocarbons....9.11
Secondary Constituents....9.12
Oxygen and Deuterium Stable Isotopes....9.13
WHITE RIVER SPRING COMPLEX....9.15
DISCUSSION....9.18
SUMMARY....9.18

CHAPTER X – SENSITIVITY AND VULNERABILITY OF THE AQUIFERS AND SPRINGS IN THE UINTA BASIN, TO POTENTIAL CONTAMINATION ASSOCIATED WITH TIGHT-SAND GAS PRODUCTION AND POTENTIAL SHALE-GAS RESOURCE DEVELOPMENT....10.1
APPROACH AND BACKGROUND....10.2
Groundwater Quality Standards....10.4
Volatile Organic Compounds in the Uinta Basin....10.4
PREVIOUS WORK....10.5
METHODS....10.6
Methodologies for Groundwater Pollution....10.6
Combined Methodologies Applied to the Uinta Basin....10.8
SENSITIVITY ANALYSIS....10.10
Aquifer Permeability....10.10
Hydraulic Conductivity of Soils....10.11
VOC Retardation....10.12
VOC Attenuation....10.14
Depth to Groundwater (Permeability Layer)....10.16
GIS Analysis Methods....10.17
VULNERABILITY ANALYSIS....10.17
Groundwater Sensitivity....10.18
Proximity to Wells, Rivers, and Streams....10.19

Active/Producing Well Density 10.19
GIS Analysis Methods 10.20
RESULTS OF MAPPING 10.20
Groundwater Sensitivity 10.20
Groundwater Vulnerability 10.21
DISCUSSION 10.21
SUMMARY 10.22

CHAPTER XI – HANDLING AND MANAGEMENT OF WATER PRODUCED FROM OIL AND GAS RESERVOIRS IN THE UINTA BASIN 11.1
UTAH WATER QUALITY STANDARDS 11.2
Utah Groundwater Classification Scheme 11.3
Class I Groundwater 11.3
Class II Groundwater 11.6
Class III Groundwater 11.7
Class IV Groundwater 11.8
Utah Total Maximum Daily Loads 11.9
WATER FACILITIES 11.10
History of Utah Water Facility Development and Use 11.10
Produced Water Volume in the Uinta Basin 11.12
Water Disposal Wells 11.14
Waterflood Injection Projects 11.16
Water Evaporation Ponds 11.19
Water Used for Hydraulic Fracturing 11.23
UINTA BASIN PETROLEUM-RELATED WATER HANDLING PRACTICES 11.26
Introduction 11.26
Current Practices of Selected Companies 11.27
Anadarko Petroleum/Kerr-McKee (Natural Buttes Gas Field) 11.27
Drilling and completion practices 11.27
Produced water management practices 11.29
EOG Resources (Natural Buttes Gas Field) 11.32
Field development activities 11.33
Produced water management practices 11.33
XTO Energy (Natural Buttes Gas Field) 11.35
Field development activities 11.35
Produced water management practices 11.36
GASCO Energy (West Tavaputs Plateau Gas Development) 11.36
Field development activities 11.36
Produced water management practices 11.37
Enervest Operating, LLC (West Tavaputs Plateau Gas Development) 11.39
Field development activities 11.39
Produced water management practices 11.40
Newfield Exploration (Monument Butte Oil Field) 11.41
Field development activities 11.42
Produced water management practices 11.42
Opportunities for Water Reuse in Utah 11.46

Best Water Handling Practice Recommendations 11.48
SUMMARY 11.51

CHAPTER XII – GEOTHERMAL ASSESSMENT AND MODELING OF THE UINTA BASIN 12.1
BHT DATA 12.3
BHT Correction Methods 12.3
BHT Data Compilation 12.7
Heat Flow 12.8
Heat Flow Results 12.11
THERMAL MODELS 12.13
Background Data and Methods 12.13
Model Results and Discussion 12.14
GEOTHERMAL RESOURCE POTENTIAL 12.16
SUMMARY 12.20

CHAPTER XIII – CONCLUSIONS AND RECOMMENDATIONS 13.1
UINTA BASIN RESERVOIRS/AQUIFERS: TRIASSIC-JURASSIC GLEN CANYON GROUP THROUGH TERTIARY GREEN RIVER FORMATION 13.2
Triassic-Jurassic Nugget and Jurassic Navajo and Entrada Sandstones 13.2
Cretaceous Cedar Mountain and Dakota Formation 13.3
Upper Cretaceous Mancos Shale 13.4
Upper Cretaceous Mesaverde Group 13.5
Upper Paleocene to Lower Eocene Wasatch/Colton Formation 13.5
Eocene Green River Formation 13.6
SUMMARY OF THE COMPILED FLUID GEOCHEMISTRY DATABASE FOR THE UINTA BASIN 13.7
GROUNDWATER CHEMISTRY AND WATER QUALITY FOR SHALLOW ALLUVIAL WELLS AND SPRINGS IN THE UINTA BASIN 13.8
SENSITIVITY AND VULNERABILITY OF THE AQUIFERS AND SPRINGS IN THE UINTA BASIN, TO POTENTIAL CONTAMINATION ASSOCIATED WITH TIGHT-SAND GAS PRODUCTION AND POTENTIAL SHALE-GAS RESOURCE DEVELOPMENT 13.10
HANDLING AND MANAGEMENT OF WATER PRODUCED FROM OIL AND GAS RESERVOIRS IN THE UINTA BASIN 13.12
GEOTHERMAL ASSESSMENT AND MODELING OF THE UINTA BASIN 13.14

ACKNOWLEDGMENTS R.1

REFERENCES R.2

LIST OF ACRONYMS AND ABBREVIATIONS R.78

APPENDIX A: TECHNOLOGY TRANSFER A.1

APPENDIX B: POROSITY AND PERMEABILITY MEASUREMENTS FROM CORES FROM THE LOWER BLUE GATE SHALE MEMBER OF THE MANCOS SHALE..... attached

APPENDIX C: LIST OF WELLS USED IN CALCULATIONS AND STUDIES OF THE MESAVERDE GROUP AND WASATCH FORMATION ..... attached

APPENDIX D: CATIONS, ANIONS, TOTAL DISSOLVED SOLIDS, AND SALINITY VALUES FROM THE WASATCH FORMATION, MESAVERDE GROUP, AND MANCOS SHALE..... attached

APPENDIX E: WATER CHEMISTRY FOR THE WASATCH/COLTON FORMATION AND THE MESAVERDE GROUP..... attached

APPENDIX F: ZONE INFORMATION WASATCH/COLTON FORMATION AND THE MESAVERDE GROUP..... attached

APPENDIX G: COMPILED DATABASE OF FLUID CHEMISTRY ..... attached

APPENDIX H: SUMMARY STATISTICS FOR MAJOR ION CHEMISTRY FOR SELECT CHEMISTRY SAMPLES ..... attached

FIGURES

Figure 1.1. Oil and gas fields in the Uinta Basin of eastern Utah.....1.13
Figure 1.2. Production in the Uinta Basin in comparison to the rest of the state in 2014 .....1.14
Figure 1.3. Ancient Eocene lake basins of the Rocky Mountain west 1.15
Figure 1.4. Uinta Basin cross section from southwest flank to the north-central part of the basin showing producing reservoirs, general facies, and widely recognized stratigraphic markers.....1.16
Figure 1.5. Stratigraphic column from surface down through Triassic-Jurassic Nugget Sandstone in the Uinta Basin showing major producing reservoirs and aquifers evaluated 1.17
Figure 2.1. Generalized geologic map of the Uinta Basin with simplified north-south cross section 2.47
Figure 2.2. Representative outcrop of Upper Triassic-Lower Jurassic Wingate Sandstone.....2.49
Figure 2.3. Representative outcrop of Lower Jurassic Kayenta Formation.....2.50
Figure 2.4. Representative outcrop of the Lower Jurassic Navajo Sandstone.....2.51
Figure 2.5. Representative outcrop of Middle Jurassic Carmel Formation 2.52
Figure 2.6. Representative outcrop and facies of the Middle Jurassic Entrada Sandstone.....2.53
Figure 2.7. Representative outcrop of the Middle Jurassic Curtis Formation 2.54
Figure 2.8. Representative outcrop of the Middle Jurassic Summerville Formation 2.55
Figure 2.9. Representative outcrop of the Salt Wash and Brushy Basin Members of the Upper Jurassic Morrison Formation 2.55
Figure 2.10. Representative outcrops of the Lower to lower Upper Cretaceous Cedar Mountain Formation.....2.56

Figure 2.11. Typical exposures of Upper Cretaceous Dakota Sandstone....2.57
Figure 2.12. Chronostratigraphic chart for Late Cretaceous-Paleogene strata in the Book Cliffs-Wasatch Plateau region....2.57
Figure 2.13. Representative outcrop of Upper Cretaceous Mowry Shale....2.58
Figure 2.14. Representative outcrop of Upper Cretaceous Frontier Formation....2.59
Figure 2.15. Classic outcrop of the Tununk Shale Member of the Mancos Shale....2.59
Figure 2.16. Blackhawk Formation outcrops in the Book Cliffs....2.60
Figure 2.17. Castlegate Sandstone outcrops in the Book Cliffs....2.61
Figure 2.18. Paleogeography of the Uinta Basin during late Campanian through Maastrichtian....2.62
Figure 2.19. Outcrop lower Sego Sandstone and Buck Tongue of the Mancos Shale, eastern Book Cliffs....2.63
Figure 2.20. Stratigraphic section in Sego Canyon, eastern Book Cliffs....2.64
Figure 2.21. Representative outcrop of Upper Cretaceous Price River Formation....2.68
Figure 2.22. Representative outcrop of Tuscher Formation and underlying Farrer Formation, eastern Book Cliffs....2.66
Figure 2.23. Representative outcrop of late Upper Cretaceous-early Paleocene North Horn Formation, Book Cliffs....2.67
Figure 2.24. Representative outcrop of Paleocene Flagstaff Limestone, Book Cliffs....2.68
Figure 2.25. Paleogeography of the Uinta Basin during Paleocene through Eocene....2.69
Figure 2.26. Representative outcrop of Paleocene-Eocene Colton Formation, Roan Cliffs....2.70
Figure 2.27. Paleocene-Eocene Wasatch Formation, Hells Hole area, southeastern Uinta Basin....2.70
Figure 2.28. General stratigraphy and major marker beds of the Green River Formation in the Uinta Basin....2.71
Figure 2.29. Representative outcrops of the Eocene Green River Formation....2.72
Figure 2.30. Generalized depositional setting for Lake Uinta....2.74
Figure 2.31. Badland topography formed in the Eocene Uinta Formation....2.75
Figure 2.32. Representive outcrop of the Eocene Duchesne River Formation....2.76
Figure 3.1. Major structural features, surface faults, and fracture zones in and around the Uinta Basin....3.14
Figure 3.2. Structure contour map on the top of the Douglas Creek Member, Green River Formation, Red Wash field....3.15
Figure 3.3. North-south seismic profile showing Uinta Basin-Mountain boundary fault zone....3.16
Figure 3.4. North-south structural cross section from Red Wash field, Uinta Basin through the Uinta Basin-Mountain boundary fault zone....3.17
Figure 3.5. Duchesne fault and fracture zone....3.18
Figure 3.6. Fracturing in the Eocene Uinta Formation....3.19
Figure 3.7. Southeast-trending Cowboy gilsonite vein....3.20
Figure 4.1. Early Jurassic Wingate Sandstone paleogeography....4.37
Figure 4.2. Early Jurassic Kayenta Formation paleogeography....4.38
Figure 4.3. Early Jurassic Navajo and Nugget Sandstone paleogeography....4.39
Figure 4.4. Outcrop of the Glen Canyon Group....4.40
Figure 4.5. Navajo facies and bedform types....4.41
Figure 4.6. Heterogeneity within Navajo dune sets....4.42

Figure 4.7. Structure on top of Navajo–Nugget Sandstone, Uinta Basin 4.43
Figure 4.8. Thickness from top of Navajo–Nugget Sandstone to top of Chinle Formation 4.44
Figure 4.9. Frequency distribution of the gross thickness of Glen Canyon Group/Nugget Sandstone 4.45
Figure 4.10. Drill depth to top of Navajo-Nugget Sandstone 4.46
Figure 4.11. Frequency distribution of the drill depth to top of Glen Canyon Group/Nugget Sandstone 4.47
Figure 4.12. Outcrop of Navajo Sandstone with large dune sets 4.48
Figure 4.13. Feet of sandstone in Glen Canyon Group/Nugget reservoir with ≥ 6% porosity..4.49
Figure 4.14. Feet of sandstone in Glen Canyon Group/Nugget reservoir with ≥ 12% porosity 4.50
Figure 4.15. Frequency distribution graphs of feet of sandstone in Glen Canyon Group/Nugget Sandstone reservoir 4.51
Figure 4.16. Ratio of PhiE ≥ 6% and 12% to reservoir thickness versus drill depth, Glen Canyon Group/Nugget Sandstone 4.52
Figure 4.17. Porosity–permeability plot separated into facies, Nugget Sandstone, Anschutz Ranch East field 4.53
Figure 4.18. Drill depth from the base of the moderately saline water to the top of Navajo-Nugget Sandstone 4.54
Figure 4.19. Total dissolved solids with depth, Glen Canyon Group/Nugget Sandstone 4.55
Figure 4.20. Produced water chemistry, Glen Canyon Group/Nugget Sandstone.....4.56
Figure 4.21. Total water produced from Glen Canyon Group/Nugget reservoir.....4.57
Figure 4.22. Frequency diagram of total water per well produced from Glen Canyon Group/Nugget reservoir 4.58
Figure 4.23. Water produced from Glen Canyon Group/Nugget reservoir, December 2014....4.59
Figure 4.24. Frequency diagram of total gas produced per barrel of water per well from Glen Canyon Group/Nugget reservoir 4.60
Figure 4.25. Total gas produced per well from Glen Canyon Group/Nugget reservoir through December 2014 .....4.61
Figure 4.26. Gas produced from Glen Canyon Group/Nugget reservoir, December 2014 .....4.62
Figure 4.27. Frequency diagram of total gas produced per well from Glen Canyon Group/Nugget reservoir through December 2014 .....4.63
Figure 4.28. Frequency distribution diagram of gas produced per well from Glen Canyon Group/Nugget reservoir, December 2014 .....4.64
Figure 4.29. Paleogeographic interpretation of the Entrada Sandstone 4.65
Figure 4.30. Outcrop of Entrada Sandstone dune facies 4.66
Figure 4.31. Depositional model with eolian dunes encroaching on a tidal flat, Namibia Desert 4.67
Figure 4.32. Structure on top of the Entrada Sandstone, Uinta Basin 4.68
Figure 4.33. Gross thickness, Entrada Sandstone 4.69
Figure 4.34. Net sandstone, Entrada Sandstone 4.70
Figure 4.35. Frequency distribution of the gross thickness, Entrada Sandstone 4.71
Figure 4.36. Frequency distribution of the net sandstone, Entrada Sandstone 4.72
Figure 4.37. Drill depth to the top of Entrada Sandstone 4.73
Figure 4.38. Frequency distribution of the drill depth to top of Entrada Sandstone.....4.74
Figure 4.39. Feet of sandstone in Entrada Sandstone with 6% or more porosity 4.75

Figure 4.40. Feet of sandstone in Entrada Sandstone with 12% or more porosity 4.76
Figure 4.41. Frequency distribution graphs of the feet of sandstone, Entrada Sandstone 4.77
Figure 4.42. Ratio of PhiE ≥ 6% and 12%/net sandstone versus drill depth, Entrada Sandstone 4.78
Figure 4.43. Drill depth from base of moderately saline water to top of Entrada Sandstone....4.78
Figure 4.44. Total dissolved solids with depth, Entrada Sandstone 4.80
Figure 4.45. Produced water chemistry, Entrada Sandstone 4.81
Figure 4.46. Total barrels of water produced from Entrada Sandstone 4.82
Figure 4.47. Frequency diagram of total water per well produced from Entrada Sandstone 4.83
Figure 4.48. Frequency diagram of total gas produced per barrel of water from Entrada Sandstone 4.84
Figure 4.49. Gas produced from Entrada Sandstone, December 2014 .....4.85
Figure 4.50. Total gas produced per well from Entrada Sandstone through December 2014...4.86
Figure 4.51. Frequency diagram of total gas produced per well from Entrada Sandstone through December 2014 .....4.87
Figure 4.52. Frequency distribution diagram of gas produced per well from Entrada Sandstone, December 2014 .....4.88
Figure 4.53. Early Cretaceous paleogeography for Cedar Mountain and Dakota Formations..4.89
Figure 4.54. Structure on top of the Dakota Formation, Uinta Basin 4.90
Figure 4.55. Gross thickness of the Cedar Mountain and Dakota reservoir 4.91
Figure 4.56. Frequency distribution of the gross thickness of Cedar Mountain and Dakota reservoir 4.92
Figure 4.57. Net sandstone, Cedar Mountain and Dakota reservoir 4.93
Figure 4.58. Frequency distribution of the net sandstone, Cedar Mountain and Dakota reservoir 4.94
Figure 4.59. Drill depth to top of Dakota Formation 4.95
Figure 4.60. Frequency distribution of the drill depth to top of Dakota Formation 4.96
Figure 4.61. Feet of sandstone with porosity ≥ 6%, Cedar Mountain and Dakota reservoir.....4.97
Figure 4.62. Feet of sandstone with porosity ≥ 12%, Cedar Mountain and Dakota reservoir...4.98
Figure 4.63. Frequency distribution of feet of sandstone with ≥ 6% and ≥ 12% porosity, Cedar Mountain and Dakota reservoir 4.99
Figure 4.64. Ratio of feet of sandstone with ≥ 6% and ≥ 12% porosity/net sandstone versus depth.....4.100
Figure 4.65. Plot of percent porosity versus permeability, Cedar Mountain and Dakota reservoir 4.101
Figure 4.66. Drill depth from the base of the moderately saline water to top of Dakota Formation.....4.102
Figure 4.67. Total dissolved solids with depth, Cedar Mountain and Dakota.....4.103
Figure 4.68. Produced water chemistry, Cedar Mountain and Dakota reservoir.....4.104
Figure 4.69. Total water produced from the Cedar Mountain and Dakota reservoir through December 2015 .....4.105
Figure 4.70. Water produced from the Cedar Mountain and Dakota reservoir, December 2014 .....4.106
Figure 4.71. Frequency diagram of the total water produced from the Cedar Mountain and Dakota reservoir.....4.107

Figure 4.72. Frequency diagram of the gas per barrel of water produced per well, Cedar Mountain and Dakota....4.108
Figure 4.73. Total gas produced from the Cedar Mountain and Dakota reservoir through December 2014....4.109
Figure 4.74. Frequency diagram of total gas produced from the Cedar Mountain and Dakota reservoir through December 2014....4.110
Figure 4.75. Gas production from the Cedar Mountain and Dakota, December 2014....4.111
Figure 4.76. Frequency diagram of gas produced from the Cedar Mountain and Dakota reservoir, December 2014....4.112
Figure 5.1. Oil and gas fields in the Uinta Basin with known or potential reservoirs in the Mancos Shale....5.16
Figure 5.2. Stratigraphic relations of the Mancos Shale, its subunits and adjacent formations in the Uinta Basin....5.17
Figure 5.3. Isopach of the Mancos Shale in the Uinta Basin....5.18
Figure 5.4. Structural map of the base of the Mancos Shale in the Uinta Basin....5.19
Figure 5.5. Structural map of the top of the Mancos B Member in the Uinta Basin....5.20
Figure 5.6. Average porosities in cores, lower Blue Gate Shale Member, Mancos Shale....5.21
Figure 5.7. Average permeabilities in cores, lower Blue Gate Shale Member, Mancos Shale....5.22
Figure 5.8. Stiff diagrams of water samples from the Mancos Shale and adjacent units....5.23
Figure 6.1. Paleogeography during Late Cretaceous through early Eocene....6.53
Figure 6.2. Index map of geology and chemistry data sources from the Wasatch/Colton Formation and Mesaverde Group....6.54
Figure 6.3. Gamma-ray trend across the Uinta Basin based on normalizing GR curves....6.55
Figure 6.4. Isopach of the entire Mesaverde Group....6.56
Figure 6.5. Structure of the top of the Mesaverde Group....6.57
Figure 6.6. Mesaverde Group, Book Cliffs....6.58
Figure 6.7. Representative outcrops of Blackhawk, Castlegate, and Price River Formations....6.59
Figure 6.8. Isopach of the lower Castlegate Sandstone....6.60
Figure 6.9. Schematic block diagram of a braided stream environment....6.61
Figure 6.10. Castlegate Sandstone overlying the Desert Member of the Blackhawk Formation and the Mancos Shale....6.62
Figure 6.11. Isopach of the Bluecastle Sandstone Member of the Castlegate Sandstone....6.63
Figure 6.12. Typical outcrops of the Farrer and Tuscher Formations....6.64
Figure 6.13. Outcrops of the Mesaverde Group in Sego Canyon....6.65
Figure 6.14. Isopach of the Buck Tongue of the Mancos Shale....6.66
Figure 6.15. Combined isopach of the middle Castlegate, Sego, and Neslen Formations....6.67
Figure 6.16. Combined isopach of the Price River, Tuscher, and Farrer Formations....6.68
Figure 6.17. Outcrops of Buck Tongue of the Mancos Shale, Sego Sandstone, and coal-bearing Neslen Formation....6.69
Figure 6.18. Net to gross ratio of sands within the Mesaverde Group....6.70
Figure 6.19. Calculated TDS with depth in the Mesaverde Group....6.71
Figure 6.20. TDS map of the Mesaverde Group....6.72
Figure 6.21. Stiff diagrams from water samples sourced from the Mesaverde Group....6.73
Figure 6.22. Calcium/sodium ratio map for Mesaverde Group water....6.74

Figure 6.23. Cumulative water production from Mesaverde Group and/or the Wasatch/Colton Formation gas reservoirs 6.75
Figure 6.24. Locations and volumes for water disposal wells into the Mesaverde Group and Wasatch/Colton Formation 6.76
Figure 6.25. Cumulative natural gas production from Mesaverde Group and/or the Wasatch/Colton Formation reservoirs 6.77
Figure 6.26. Cumulative crude oil production from Mesaverde Group and/or the Wasatch/Colton Formation reservoirs 6.78
Figure 6.27. Isopach of the Colton/Wasatch Formation 6.79
Figure 6.28. Structure of the top of the Wasatch/Colton combined formations 6.80
Figure 6.29. Representative outcrops of the Wasatch/Colton Formation 6.81
Figure 6.30. Net to gross ratio of sands within the Wasatch/Colton Formation 6.82
Figure 6.31. Calculated TDS with depth in the Wasatch/Colton Formation 6.83
Figure 6.32. TDS map of the Wasatch/Colton Formation 6.84
Figure 6.33. Calcium/sodium ratio map for the Wasatch/Colton Formation water 6.85
Figure 6.34. Wells logs for NBU No. 921-21 L well, Natural Buttes field 6.86
Figure 7.1. Overview map showing location of study area, the outcrop of the top and base of the Green River Formation, and the outcrop of the Mahogany bed 7.26
Figure 7.2. Paleogeographic reconstruction of the Uinta Basin during the Eocene epoch 7.27
Figure 7.3. Isopach map of entire Green River Formation 7.28
Figure 7.4. Isopach map of lower Green River Formation, below the Mahogany bed 7.29
Figure 7.5. Isopach map of upper Green River Formation, above the Mahogany bed 7.30
Figure 7.6. Structure contour map of the top of the Green River Formation 7.31
Figure 7.7. General stratigraphic columns of the Green River Formation 7.32
Figure 7.8. Compilation of Green River Formation stratigraphic nomenclature 7.33
Figure 7.9. Extent of phase 1 saline interval, upper Green River Formation 7.34
Figure 7.10. Utah State No. 13X-2 core description and images of phase 2 saline zone 7.35
Figure 7.11. Extent of phase 2 saline interval (Birds Nest aquifer), upper Green River Formation 7.36
Figure 7.12. Isopach maps of "large-saline-nodule" facies (upper and lower Birds Nest aquifers), phase 2 saline zone 7.37
Figure 7.13. Shrine Hospital No. 1 core description and images of the phase 3 saline zone 7.38
Figure 7.14. Extent of phase 3 saline interval, upper Green River Formation 7.39
Figure 7.15. Map of total dissolved solids concentrations, lower Green River Formation 7.40
Figure 7.16. Map of total dissolved solids concentrations, upper Green River Formation 7.41
Figure 7.17. Map of total dissolved solids concentrations, Birds Nest aquifer (phase 2 saline zone) 7.42
Figure 7.18. Map of the depth from the base of the moderately saline water to the top of the Green River Formation 7.43
Figure 7.19. Bubble map showing cumulative produced water, Green River Formation 7.44
Figure 7.20. Histogram displaying total cumulative water production by well, Green River Formation 7.45
Figure 7.21. Location of injection wells currently disposing produced water into the Green River Formation 7.46
Figure 7.22. Bubble map showing the volume of water that has been injected into the Green River Formation from each injection well 7.47

Figure 7.23. Histograms displaying water) injected into the Green River Formation via disposal wells 7.48
Figure 7.24. Bubble map showing the volume of oil produced from the Green River Formation by field 7.49
Figure 7.25. Bubble map showing the volume of gas produced from the Green River Formation by field 7.50
Figure 7.26. Histograms displaying cumulative oil and gas by well from the Green River Formation 7.51
Figure 8.1. Pie graph of the number of samples for each geologic unit 8.17
Figure 8.2. Location of select fluid geochemical samples 8.18
Figure 8.3. Total dissolved solids versus depth for select samples 8.19
Figure 8.4. Summary of depths of samples by geologic unit 8.20
Figure 8.5. Summary of total dissolved solids by geologic unit 8.21
Figure 8.6. Summary of water types by geologic unit 8.22
Figure 8.7. Major ion chemistry versus total dissolved solids 8.23
Figure 8.8. Piper diagram of select samples 8.24
Figure 9.1. Map of study area showing sample wells/springs sites 9.27
Figure 9.2. Well, spring, and surface water sample site locations from a previous baseline water quality study for southeastern Uinta Basin 9.28
Figure 9.3. Piper plots of general solute chemistry for sampling sites in the Uinta Basin 9.29
Figure 9.4. Stiff diagrams for solute chemistry in the Uinta Basin 9.30
Figure 9.5. Total-dissolved-solids concentrations 9.31
Figure 9.6. White River spring 9.32
Figure 9.7. Monitoring well drilled to examine water quality in shallow alluvium, southeastern Uinta Basin 9.33
Figure 9.8. Plot of deuterium versus oxygen isotope for 22 samples in the Uinta Basin 9.34
Figure 9.9. White River spring complex along the White River recreational corridor 9.35
Figure 10.1. Location of sites sampled for water quality, public water supply wells, and drinking water source protection zones 10.31
Figure 10.2. Density of active oil/gas wells in the Uinta Basin 10.32
Figure 11.1. Graph of cumulative number of produced-water disposal wells in the Uinta Basin, from 1968 through 2014 ....11.64
Figure 11.2. Location of water disposal wells by field in the Uinta Basin 11.65
Figure 11.3. Location of enhanced-oil recovery, waterflooding projects and wells in the Uinta Basin 11.66
Figure 11.4. Water evaporation ponds in the Uinta Basin 11.67
Figure 11.5. Location of water evaporation ponds in the Uinta Basin 11.68
Figure 11.6. Graph showing the annual amount of water used in fracture stimulations by county for the Uinta Basin from 2011 through 2014 ....11.69
Figure 11.7. Example of Anadarko's Completion Technology System (ACTS) at Natural Buttes field 11.70
Figure 11.8. Exterior view of water and oil storage tanks at Newfield's Beluga water treatment facility 11.71
Figure 11.9. Schematic diagram of the Newfield Beluga plant's Veolia water-treatment process 11.72
Figure 12.1. Map of Uinta Basin showing geographic distribution of wells studied 12.24

Figure 12.2. Histogram showing the distribution of bottom-hole temperatures.....12.25
Figure 12.3. Simple Gradient and Thermal Resistance Methods plots.....12.26
Figure 12.4. Histogram showing the distribution of calculated heat-flow values 12.27
Figure 12.5. Thermal gradients of oil and gas wells, Uinta Basin.....12.28
Figure 12.6. Temperatures at depth 12.29
Figure 12.7. Thermal model framework including upper and lower boundary conditions 12.30
Figure 12.8. Residuals of model results to observed data for each model parameter set 12.31
Figure 12.9. Maps of the temperature field at planes of constant elevation below the average elevation of the Uinta Basin.....12.32
Figure 12.10. Surface heat flow from Uinta Basin thermal model and corrected well data....12.33
Figure 12.11. Map of depth to base moderately saline water, Uinta Basin 12.34
Figure 12.12. Histogram showing the distribution of calculated thermal output 12.35
Figure 12.13. Map of wells co-producing water at a sufficient volume to support greenhouse and wells meeting required temperature threshold binary power generation.....12.36

TABLES

Table 5.1. Water-chemistry data from wells that sampled the Mancos Shale 5.13
Table 5.2. Water, oil, and natural gas production from the Mancos Shale and adjacent units, 1984-2015 .....5.14
Table 5.3. Produced-water disposal wells that inject into the Mancos Shale 5.14
Table 5.4. Utah gas fields with reservoirs in the Mancos Shale 5.15
Table 6.1. Porosity values from sonic logs within the Mesaverde Group 6.48
Table 6.2. Porosity and permeability from the NBU No. 253 core, Natural Buttes field.....6.48
Table 6.3. Porosity and permeability from the NBU No. 921-21L core, Natural Buttes field 6.49
Table 6.4. Water classification based on TDS 6.50
Table 6.5. Cumulative production from the Wasatch Formation and the Mesaverde Group....6.50
Table 6.6. Total oil, gas, and produced water between January 2009 and March 2015 for producing zones in the Wasatch and Mesaverde Group 6.50
Table 6.7. Porosity values from sonic logs within the Wasatch/Colton Formation 6.50
Table 6.8. Calculated volume of water storage per radial foot in three Tuscher Formation channel sandstones, NBU No. 921-12L gas well, Natural Buttes field.....6.52
Table 6.9. Reservoir properties Wasatch/Colton Formation and Mesaverde Group.....6.52
Table 7.1. Examples of wells with varied water sample depths, dates, and total dissolved solid concentrations 7.25
Table 8.1. Summary of depth distribution of select water chemistry samples 8.14
Table 8.2. Summary of total dissolved solids distributions for select water chemistry samples.....8.15
Table 8.3. Water type distribution for select samples.....8.16
Table 9.1. Water quality data for shallow well and spring sample sites in the Uinta Basin.....9.23
Table 9.2. Isotope data for 22 sites in the Uinta Basin 9.26
Table 10.1. Chemical and physical properties of volatile organic compounds and maximum contaminant levels in drinking water.....10.26

Table 10.2. Summary of methods used, data sources used to calculate and derive parameters, and determination of ranges of values used to rank attributes from analysis of aquifer sensitivity and vulnerability in the Uinta Basin 10.26
Table 10.3. Permeability ranking of geologic units in the Uinta Basin 10.27
Table 10.4. Volatile organic compounds sensitivity and the attribute rankings used to assign sensitivity for the Uinta Basin 10.28
Table 10.5. Hydrologic soil groups, field capacity, bulk density, and fraction of organic carbon content generalized for Utah soils 10.29
Table 10.6. Volatile organic compounds vulnerability and the attribute rankings used to assign vulnerability for Uinta Basin 10.30
Table 11.1. Uinta Basin active wells and annual produced water volumes by county, 2008–2014.
Table 11.2. Uinta Basin annual produced water volumes per well by county, 2008–2014 ..... 11.58
Table 11.3. Uinta Basin disposal-well numbers with active disposal volumes by county, 2008–2014 ..... 11.58
Table 11.4. Uinta Basin disposal well injection volumes, 2008–2014 ..... 11.59
Table 11.5. 2014 Uinta Basin enhanced-oil recovery water injection and produced water volumes 11.59
Table 11.6. Uinta Basin enhanced-oil recovery water injection volumes, 2008–2014 ..... 11.60
Table 11.7. Produced water delivered to Uinta Basin evaporation ponds, 2010-2013 ..... 11.60
Table 11.8. Approved commercial disposal facilities as of June 9, 2015 ..... 11.61
Table 11.9. Annual number of wells with fracture stimulations in the Uinta Basin by county for the years 2011–2014 ..... 11.61
Table 11.10. Annual number of barrels of water used in fracture stimulations in the Uinta Basin by county for the years 2011–2014 ..... 11.62
Table 11.11. Annual number of barrels of water used per well in fracture stimulations in the Uinta Basin by county for the years 2011–2014 ..... 11.62
Table 11.12. Annual number of wells fracture stimulated, barrels of water used in stimulations, and the number of barrels used per well in Uintah County for the year 2013 ..... 11.62
Table 11.13. Veolia's reported processing performance data for waterflood applications 11.62
Table 11.14. Publicly operated waste water treatment plants in Duchesne and Uintah Counties, Utah and their average annual flow in barrels per year 11.63

PLATES

Plate 1: Preliminary Geologic Map of the Uinta Basin, Utah ..... attached

Plate 2: West to East Cross Section of the Wasatch/Colton Formation and the Mesaverde Group ..... attached

Plate 3: North to South Cross Section of the Wasatch/Colton Formation and the Mesaverde Group ..... attached

Plate 4: Groundwater Sensitivity to VOCs in the Uinta Basin ..... attached

Plate 5: Groundwater Vulnerability to VOCs in the Uinta Basin ..... attached

EXECUTIVE SUMMARY

The environmentally sound production and disposal of water from tight-sand reservoirs and potential shale-gas resources affects the economics of gas resource development and has recently become a topic of much recent public debate because produced water is the largest-volume waste stream associated with these unconventional gas plays. Managing produced water can be a significant cost fraction of the value of the gas extracted, so there is an economic incentive to minimize this waste stream, and/or generate revenue from treating and reusing produced water in hydrocarbon production or other applications. Several potential uses for this produced water exist, particularly in arid regions of the West, including waterflooding for secondary recovery, drilling mud formulation, hydraulic fracturing fluid for well completion, and future use in possible oil shale production or other industrial water uses. In addition, produced water from petroleum production has potential for geothermal energy production in some basins.

Oil and gas fields in the Uinta Basin of eastern Utah produced nearly 33 million barrels of oil and 363 billion cubic feet of gas in 2014 from the Tertiary Wasatch and Green River Formations and several formations in the Upper Cretaceous Mesaverde Group. Nearly 105 million barrels of water was also produced with these hydrocarbons. Extensive drilling for lenticular, tight gas sands in the Wasatch and Mesaverde occurred in the eastern part of the basin, whereas large drilling programs as part of expanding waterflood projects for oil in the Green River continued in the south-central basin; over 1300 wells were permitted in 2014 (before oil prices collapsed).

Balancing the water-use needs and produced-water disposal requirements associated with tight-sand and shale-gas development creates significant material handling challenges to both

industry and regulators in the Uinta Basin. Deciding how to manage large volumes of produced water, whether for disposal, reuse, or energy production presents a number of major decision options. These challenges include understanding the variable chemistry of the produced water; determining the various quality needs of the potential reuses; managing transport from widely distributed sources to use or disposal facilities; optimizing treatment facility siting to minimize transport distances and account for the varying volume and quality of water produced over time; and identification of available disposal options for unusable produced water. They are further complicated by an operating environment where many individual producers of varying sizes exist within a field or the Uinta Basin, each with differing water needs and production; and a production timescale of decades for a basin as wells play out and new ones are completed.

This three-year project investigated the integrated management of water production and disposal for shale/tight-sand gas in the Uinta Basin, across many producers, and with multiple reuse or disposal options. The study was comprised of four major components. (1) Compilation and analysis within a geographical information systems format of past and new information on: the thickness, structure, depth, porosity, permeability, and lithologic nature of all aquifer/reservoir units in the basin from the Tertiary through the Jurassic Glen Canyon Group; the regional variations in quality of water, flow direction, and temperature produced from the various shale/tight-sand gas reservoirs across the basin; the location, saturated volume, and quality of alluvial aquifers; the existing infrastructure for water management/reuse; the energy generation potential of geothermal-produced waters; and location and geochemical and hydrological characteristics of aquifers used/proposed for disposal of produced water or concentrated brines. (2) Compilation and statistical analysis of water production quantity and quality. This geostatistical characterization will help provide options for treatment,

transportation, disposal, geothermal energy production, and alternative use options. (3) Development of alluvial aquifer sensitivity/vulnerability models to potential contamination from fluids associated with shale/tight-sand gas development in the basin. (4) An evaluation of produced water management practices and recommendations for best management practices.

The following summarizes the significant findings of the study. The major recommendations for managing produced water from current tight-sand gas reservoirs and potential shale-gas resources in the Uinta Basin are also included.

- The Late Triassic-Early Jurassic Nugget and Early Jurassic Navajo Sandstone is an excellent potential aquifer for produced water disposal where less than 10,000 feet in depth; porosity decreases at greater depths. However, there are relatively few Navajo penetrations in the Uinta Basin and the economics for drilling new disposal wells at the required depths are difficult to justify. Old wells that encountered Navajo/Nugget could be re-entered and completed as water disposal wells.

- The Jurassic Entrada Sandstone is projected to have less than 20 feet of porous sandstone throughout much of the basin. The amount of sandstone with 6% usable porosity in begins to decrease rapidly below 5000 feet drill depth. There are few penetrations of the Entrada in the deeper portion of the basin but areas of high porosity and permeability could exist which could either be hydrocarbon bearing or store produced water depending on the depth and proximity to oil and gas production.

- The Cretaceous Cedar Mountain and Dakota Formations are fluvial channel and overbank deposits with some littoral marine deposits and coal in the upper Dakota. There is an overall northeast-southwest thickness trend in study area. Thickness ranges from less than 25 feet in southeast part of the Uinta Basin, to over 250 feet in the northeast part of the basin. A porous sand trend is parallel, but slightly southeast of net sandstone thickness trend. Thickness of porous sand with at least 6% porosity is generally less than half of the total sandstone thickness. However, porosity and permeability within the channel sandstones can be highly variable and difficult to predict. Channel deposits provide stratigraphic traps for hydrocarbons throughout the Uinta Basin. Production can be spotty and volumes highly variable due to the heterogeneity of the channel deposits. These sandstones have very limited potential for produced water disposal.

- The Mancos Shale is one of the thickest confining units in the Colorado Plateaus aquifer, separating the Dakota-Glen Canyon and Mesaverde aquifers. The sandstone content of the Mancos Shale, based on gamma-ray logs, show that sandstone constitutes less than 1% of the formation except where the Tununk and Blue Gate Shale Members interfinger with the Ferron and Emery Sandstone Members. The only produced-water disposal into the Mancos is local injection of water from coalbed methane operations in the Ferron on the southwestern margin of the Uinta Basin. With very low permeability, in the range of 0.05 to 160 nanodarcies, the Mancos is likely a poor candidate for produced-water disposal in most of the Uinta Basin. It continues to be a secondary drilling target for shale gas.

- The sandy formations in the upper part of the Mesaverde Group could make favorable produced water injection units, particularly around the margins of the Uinta Basin where their water saturation is lower. The Tuscher and Farrer Formations are good candidates for disposal wells on the eastern side of the basin. Both formations, especially the Tuscher, have thick-blocky sandstones with good porosity. The Farrer has significant candidate sandstone channels for water disposal that are generally finer-grained, thinner, and less massive than the Tuscher channels. We calculated that three sandstone channels in the upper Tuscher, or approximately 40 feet of sandstone, would store up to 4.2 million barrels of water in a 1000-foot radius around a well. Further subdivision of the Mesaverde Group into units or facies would provide a more accurate representation of high and low porosity zones within each formation, but this level of detail was beyond the scope of this project. Additional studies of the Mesaverde should be conducted to correlate total dissolved solids and sodium-chloride waters from laboratory analyses to formation water resistivity from well logs.

- The Colton/Wasatch Formation contains sandstones that are candidates for water disposal. However, the thickness and continuity of any sandstone channel will be localized and will require long perforated zones and targeted perforations for disposal. Generally higher net-to-gross sand ratios and average porosity in Colton/Wasatch suggest favorable conditions for water disposal. The Wasatch is an oil reservoir in the central parts of the basin and would lend itself to water flooding using produced water. There are two options recommended for disposing of produced water from the Colton/Wasatch (as well as the Mesaverde Group). One treatment option would desalinate produced water to decrease the volume of disposal, particularly where the water can be used in hydraulic fracturing operations, possibly for

irrigation water, or for other surface uses. The second option is injecting produced water into sandstone beds of the Colton/Wasatch (or Mesaverde) either for waterflooding to enhance hydrocarbon production or as waste disposal.

- The greatest potential for produced water storage is within the "Birds Nest" aquifer in the upper section of the Eocene Green River Formation in the easternmost part of the Uinta Basin. This shallow zone (which outcrops southeast of Natural Buttes field) represents the final stages of Lake Uinta when hypersaline conditions existed resulting the formation of evaporite minerals. Dissolution of these minerals has created both porosity (vuggy) and permeability, and groundwater water containing extremely high concentrations of total dissolved solids. The groundwater flow is towards the deeper, center of the basin where these characteristics could be very high. Thus, conditions are excellent for the aquifer to store produced water.

  The Birds Nest aquifer is divided into upper and lower zones. The upper zone covers an area of 359.0 square miles, has a mean thickness 82 feet, and a macro pore volume (at 2.5%) of 469,157 acre feet. The lower zone covers an area of 498.6 square miles, has a mean thickness of 85 feet, and a macro pore volume (at 2.5%) of 679,908 acre feet. The aquifer is located close to significant drilling activity but poses unique challenges and risks: (1) large areas with no mineral dissolution reduces potential, (2) cross-cutting gilsonite veins (and associated fractures) could transmit water vertically through the section, posing risks to "fresh" water aquifers, and (3) monitoring wells will be a key requirement, but an added expense.

- The compilation of fluid geochemistry for the Uinta Basin showed that the highest total dissolved solids (TDS) tends to correlate with sodium chloride or sodium bicarbonate water types that are typical of the upper and lower Green River, Wasatch-Colton, and Mesaverde units. These samples are predominately produced water and the high TDS and may be the result of oil and gas generation processes, long residence time, and or increased water rock interaction within these units. Lower TDS values and bicarbonate water types area typical of the Unconsolidated, Uinta-Duchesne River, Glen Canyon units. These chemistries likely result from a relatively active meteoric groundwater system within these units where they are near surface. The samples in this database represent a unique regional scale snapshot of fluid geochemistry across an active petroleum province including both the shallow meteoric groundwater system and the deeper basin fluid system. Further study and geochemical analysis of these data could yield insight into large scale fluid evolution in both active petroleum provinces and similar geographic setting elsewhere.

- Water samples collected from alluvial water wells and springs show variable water quality throughout the study area indicating there are multiple aquifers that are not connected. Total dissolved solids (TDS) concentrations for all samples range from 214 to 5532 milligram/liter (mg/L) and nitrate concentrations range from <0.1 to 5.32 mg/L for all samples. Dissolved-solids concentrations were lowest from a shallow well located in the northern part of the basin near recharge from the Uinta Mountains. Most sites have nitrate concentrations below 0.1 mg/L (the detection limit). Some samples had detectable volatile organic compounds (VOCs), but all were below the Environmental Protection Agency's (EPA's) maximum contaminant levels, except for some sites having elevated chloromethane. No samples had

detectable total petroleum hydrocarboons. To ensure good water quality is preserved, we recommend sampling most of the sites annually or every three years at the least.

- Using GIS analyses, we combined index-based, process-based, and overlay methods to determine aquifer sensitivity and vulnerability in the Uinta Basin. The resultant attribute and ranking assessment shows that the areas most sensitive to groundwater contamination by VOCs occur where near-surface permeable layers are near streams and lakes, especially in areas having relatively high hydraulic conductivities, high VOC retardation factors, and low VOC attenuation factors. High vulnerability areas are located near water bodies, water wells/springs, and in close proximity to high-density oil/gas wells.

- Current best practices for produced water storage in the four-county Uinta Basin study include: (1) disposal in deep injection wells (Environmental Protection Agency [EPA] Class II) below the base of the moderately saline aquifer, (2) storage and evaporation in lined disposal ponds, and (3) use for waterflooding enhanced-oil recovery in EPA Class II wells at oil fields. Produced water volumes from petroleum development in the basin study area have increased over the last seven years (2008-2014) from 86 to 116 million barrels per year. Current water management practices used by petroleum companies in the Uinta Basin for the disposition of the 116 million barrels of produced water in 2014 is estimated as follows: 68 million barrels (58.6%) to disposal wells, 24 million barrels (20.7%) used for enhanced-oil recovery, 13.7 million barrels (11.8%) sent to evaporation ponds, 1.5 million barrels (1.3%) reused in hydraulic fracturing, and 8.8 million barrels (7.6%) lost to evaporation.

The number of Uinta Basin disposal wells has increased with higher petroleum production. The disposal well count in the four-county Uinta Basin area has increased from 56 in 2008 to 92 in 2014. The greatest number of disposal wells are typically associated with natural gas production. On average there is about one disposal well for every 145 producing wells in the Uinta Basin.

There are 15 major waterflood projects in the Uinta Basin. The amount of water used in enhanced-oil recovery waterflood projects has increased from over 25 to over 44 million barrels per year from 2008 through 2014. Newfield Exploration reused up to 10 million barrels of produced water in 2014 for its 36 million-barrel waterflood needs at Monument Butte oil field. One approach that should be further investigated is transporting the excess produced water from the gas fields in the eastern part of the basin for use in waterflooding in the oil fields of the central part of the basin.

The amount of produced water delivered to commercial and private evaporation ponds has varied from 11.9 to 17.3 million barrels, and averaged about 13.7 million barrels per year. Commercial evaporation ponds take water for pay, generally from small producers with few wells that don't justify a water disposal system. Private ponds act as backup water storage for larger producers with integrated water disposal systems. However, ponds are losing favor with regulators and users alike.

Hydraulic fracturing fluid reuse of produced water is a technique where by flow-back fluids are captured and transferred between pads via temporary pipelines to reduce fresh-water usage. Anadarko Petroleum's best practices at Natural Buttes gas field in the eastern Uinta Basin involves recycling nearly 100% of the water recovered after the hydraulic fracturing process and reusing it in new well-completions, which conserves fresh water and

reduces truck traffic. On average this reuse is estimated involve about 1.5 million barrels of flow-back produced water. EOG Resources plans to minimize fresh water usage in the drilling and completion of new wells in the area by only using 12% from fresh water sources, and obtaining the remaining 88% from recycled water from the Bonanza power plant south of Vernal, Utah.

Regulatory agencies in Utah are encouraging petroleum development companies to reuse drilling wastes such as produced water to reduce fresh water consumption; however, many of the best management practices are practical only when the developments in an area reach a critical size where implementing centralized water collection, handling, treatment, and reuse or disposal achieves the economies of scale to become cost effective. Produced water management in Utah is a large and dynamic management challenge that requires a flexible, adaptive regulatory scheme to meet ever changing conditions and technologies in fields of variable size and with differing product and waste streams.

- Co-produced waters from sedimentary basins may represent a significant geothermal resource. This regional assessment of the geothermal potential for co-produced waters from oil and gas fields in the Uinta Basin used bottom-hole temperatures and co-produced water data from 776 oil and gas wells along with available lithological information. Calculations reveal an average geothermal gradient of about 27°C/km (1.48°F/100 ft), implying wells producing from depths greater than 2 kilometers (6562 ft) in the basin will likely have temperatures greater than 65°C (149°F). The average heat-flow value from wells with corrected BHTs is 67 milliwatts per square meter. These results are generally typical for gradient and heat-flow values in the Colorado Plateau. Co-produced water temperatures in

740 wells are above 50°C (122°F) and may be suitable for direct-use applications such as greenhouses, space heating, and aquaculture. Binary geothermal power plants generally require a minimum temperature of 140°C (284°F) to achieve acceptable efficiency and 36 wells (~5%) across the basin meet or exceed such temperatures. The thermal regime and existing infrastructure make the Uinta Basin a candidate for extensive direct-use geothermal applications and possibly binary geothermal power generation.

CHAPTER I

INTRODUCTION

Thomas C. Chidsey, Jr. and David E. Tabet

Utah ranked 11th in the United States in oil production and 10th in gas production in 2014 (Energy Information Administration, 2015). Oil and gas fields in the Uinta Basin (UB) of eastern Utah (figure 1.1) produced nearly 33 million barrels of oil (MMBO) and 363 billion cubic feet of gas (BCFG) in 2014 from the Tertiary Wasatch and Green River Formations and several formations in the Upper Cretaceous Mesaverde Group (Utah Division of Oil, Gas, and Mining, 2015a). Nearly 105 million barrels of water (MMBW) were also produced with these hydrocarbons. This production represents 81%, 80%, and 55% of the oil, gas, and water produced, respectively, in Utah (figure 1.2). Over the last 10 years, extensive drilling for lenticular, tight-gas sands in the Wasatch and Mesaverde occurred in the eastern part of the basin; shale beds within the Upper Cretaceous Mancos Shale were secondary targets for potential shale gas. Large drilling programs as part of expanding waterflood projects for oil in the Green River continued in the south-central basin in the Monument Butte-Brundage Canyon trend (figure 1.1). More recently operators targeted the Uteland Butte Limestone member of the Green River in the central basin successfully using long-reach horizontal wells. Over 1300 wells were permitted in 2014 in the UB (Utah Division of Oil, Gas, and Mining, 2015b). Even with the collapse of oil prices and continued depressed gas prices, resulting in significantly reduced drilling activity in the basin, existing wells will mature and produce increased amounts of water. As has been the

case throughout the history of the petroleum industry, prices will eventually rebound and exploration and development will undoubtedly return to pre-2015 levels in Utah's most prolific hydrocarbon-producing basin. Thus, the question this study sought to answer was: "What to do with the produced water in the UB?"

LOCATION AND GENERAL GEOLOGIC SETTING

The UB is located in the northern Colorado Plateau geologic province. It extends west from the Colorado state line to about Strawberry Reservoir in north-central Utah and from the east-west-trending Uinta Mountains south to the Book Cliffs. It is both a structural and topographic basin dissected and drained by the Green River and its tributaries as part of the Colorado River system. The average elevation of the UB is 5000 feet (Hamblin, 2004) and like most areas in eastern Utah it has a semi-arid climate with low humidity hot and dry summers and cold winters; the average annual precipitation is 9.2 inches. Water availability in this arid climate is, of course, a critical issue for agriculture, light industries, culinary use, and oil and gas development.

The Laramide orogeny, between latest Cretaceous and Eocene time, produced numerous basins and basement-cored uplifts in the Rocky Mountain states. The UB is a major depositional and structural basin that subsided during the early Cenozoic along the southern flank of the Uinta Mountains. More than 10,000 feet of alluvial and lake deposits filled the basin between the eroding Sevier highlands to the west and the rising Laramide-age Uinta Mountains, Uncompahgre uplift, and San Rafael Swell to the north, east, and south, respectively (Hintze and

Kowallis, 2009). The Eocene Lake Uinta formed within the UB and Colorado's Piceance Creek Basin (figure 1.3). At times of low water level, the Douglas Creek Arch separating the two basins was exposed, creating two distinct lakes.

The UB is asymmetrical to the north, paralleling the east-west trending Uinta Mountains. The north flank dips 10 to 35º into the basin and is bounded by a large north-dipping, basement-involved thrust fault. The southern flank gently dips between 4 to 6º north-northwest from the Book Cliffs. Regional uplift of the Colorado Plateau began during the Miocene (Hunt, 1956; Lucchitta, 1979) resulting in massive erosion removing of several thousand feet of sedimentary rocks and the relatively rapid incision of the Green River and its tributaries. The result is the spectacular exposure of rocks as old as Cretaceous along the southern flank of the basin, ideal for reservoir/aquifer analog studies (plate 1).

BASIC PETROLEUM GEOLOGY AND OIL AND GAS DEVELOPMENT HISTORY

The UB is the most productive petroleum province in Utah due to an ideal combination of depositional and structural events. During the Cretaceous, compressional forces of the Sevier orogeny produced highlands in western Utah and the Western Interior Seaway covered most of eastern Utah. Extensive coal-forming swamps and marshes near the coastline (Emery, Book Cliffs, and Sego coal fields) and fluvial and wave-dominated deltas migrated eastward across the state as the sea eventually retreated. During the Paleocene and Eocene, lakes Flagstaff and Uinta formed in the Uinta Basin where alluvial, marginal lacustrine, and open lacustrine sediments

accumulated in an intertonguing relationship. Trapping mechanisms (figure 1.4) for hydrocarbons in these deposits include (1) fractured-enhanced stratigraphic pinchouts of lenticular sandstone beds updip along the south flank of the basin or across minor flexures or subtle, plunging anticlines with no four-way closure, (2) basin-centered updip facies changes, a reduction of fluid pressure, and associated closing of fractures, (3) and unconventional "tight" shale and carbonate zones that require horizontal drilling. Cretaceous coals and shale and Eocene organic-rich lacustrine shale serve as hydrocarbon source rocks. Reservoirs consist mainly of (1) alluvial channel and bar, fluvial, deltaic, shoreface to shoreline, and eolian sandstone, (2) carbonate flat dolomitized ostracod and pellet grainstone and packstone, and (3) coalbeds produce methane (CBM) in the extreme southwest part of the UB. The major reservoirs are Eocene Uinta (gas) and Green River Formations (oil); and Paleocene/Eocene Colton/Wasatch Formations (oil and gas [tight-gas sands]); Cretaceous Mesaverde Group (gas [tight-gas sands]), Ferron Sandstone Member of the Mancos Shale (CBM), Dakota Sandstone, Cedar Mountain Formation (gas [tight-gas sands]); and Jurassic Morrison, Entrada, and Wingate Formations (gas) (figure 1.5).

Utah's drilling history has fluctuated greatly due to discoveries, oil and gas price trends, and changing exploration targets—the UB is no exception. The first commercial oil discovery in the UB was Roosevelt field (now part of Bluebell field, figure 1.1) in 1949; gas and oil were discovered at Ashley Valley field southeast of Vernal in 1925 and 1948, respectively, but the field is technically just outside of the basin. The Humble Oil Ute Tribal No. 1 well (section 21, T. 1 S., R. 1 E., Uinta Base Line & Meridian [UBL&M], Uintah County, American Petroleum Institute [API] No. 43-047-15550) had an initial flowing potential (IFP) 1633 barrels of oil per day (BOPD) out of the Green River Formation. The opening of Bluebell field was followed by a

number of major Green River oil discoveries: Red Wash (1951) (figure 1.1), Pleasant Valley (1952), Walker Hollow (1953), and Wonsits Valley (1962) among others (Hill and Bereskin, 1993). In 1952, gas was discovered in the Mesaverde Group with the completion of the Chapita Wells Unit No. 1 well (section 16, T. 9 S., R. 23 E., Salt Lake Base Line & Meridian [SLB&M], Uintah County, API No. 43-047-10095) for an of IFP 275 thousand cubic feet of gas per day (MCFGPD). In 1955, gas was discovered nearby in the Wasatch Formation with the completion of Chapita Wells Unit No. 2 well (section 28, T. 9 S., R. 23 E., SLB&M, Uintah County, API No. 43-047-15050) for an IFP of 4618 MCFGPD. Ultimately, these and others gas discoveries in the area were merged to create what is now Utah's largest gas field—Natural Buttes (figure 1.1) with over 3.3 trillion cubic feet of gas (TCFG) produced (Utah Division of Oil, Gas, and Mining, 2015c). Since then significant tight-gas sand discoveries have spread throughout the eastern UB. Along the southwest flank of the UB, multiple Tertiary and Cretaceous gas reservoirs were discovered with a trend that began with Peters Point field (figure 1.1) in 1953. In the center of the basin, deep, fractured, overpressured Wasatch oil and gas production was discovered by the Shell Oil Miles No. 1-35A4 well (section 35, T. 1 S., R. 4 W., USBL&M, Duchesne County, API No. 43-013-30029) that had an IPF of 1004 BOPD and 530 MCFGPD opening giant Altamont-Bluebell-Cedar Rim field in 1970 (figure 1.1) which has produced 338 MMBO and 607 BCFG (Utah Division of Oil, Gas, and Mining, 2015c). In 1981, Monument Butte field in the south-central UB (figure 1.1) was discovered with the completion of the Monument Butte Federal No. 1-35 (section 35, T. 8 S., R. 16 E., SLBL&M, Duchesne County, API No. 43-013-30561) for an IPF of 37 BOPD in the Green River. The Green River oil discoveries of Antelope Creek and Brundage Canyon followed in 1983. The Monument Butte-

Brundage Canyon trend has produced 111 MMBO and 366 BCFG (Utah Division of Oil, Gas, and Mining, 2015c).

At the end of 2014, there were about 60 active oil and gas fields in the UB (figure 1.1) and over active 10,800 wells. Average monthly production in 2014 was about 2.7 MMBO, 31 BCFG, and 8.7 MMBW (Utah Division of Oil, Gas, and Mining, 2015a). State-of-the-art horizontal drilling technology, improved hydraulic fracturing techniques, and waterflood projects have collectively resulted in a continued boost in production rates and ultimate recovery from known fields and new discoveries in the UB. Deeper exploration drilling in the eastern and southern Uinta Basin during the past five years has led to discoveries of substantial gas accumulations in Mesaverde, Entrada, and Wingate reservoirs (e.g., Hill Creek field, Uintah County, figure 1.1). There is also resurgence in interest in the UB's oil shale and tar sand resources. Just to the southwest of the UB proper, the development of CBM accumulations in the Ferron Sandstone, beginning with the discovery of Drunkards Wash field in 1992, has produced 1.3 TCFG. Significant potential exists for other coal fields around the Uinta Basin to yield CBM, and the extent of deeper conventional and tight gas plays remains to be explored.

PURPOSE AND SCOPE

The environmentally sound production and disposal of produced water from tight-sand reservoirs and potential shale-gas resources affects the economics of the hydrocarbon resource development in the UB and has recently become a topic of much public debate because produced water is the largest-volume waste stream associated with these unconventional gas plays.

Managing produced water can be a significant cost fraction of the value of the gas extracted, so there is an economic incentive to minimize this waste stream, and/or generate revenue from treating and reusing produced water in hydrocarbon production or other applications.

Balancing the water-use needs and produced-water disposal requirements associated with tight-sand and shale-gas development creates significant material handling challenges to both industry and regulators in the UB. Deciding how to manage large volumes of produced water, whether for disposal, reuse, or energy production presents a number of major decision options. These challenges include understanding the variable chemistry of the produced water; determining the various quality needs of the potential reuses; managing transport from widely distributed sources to use or disposal facilities; optimizing treatment facility siting to minimize transport distances and account for the varying volume and quality of water produced over time; and identification of available disposal options for unusable produced water. They are further complicated by an operating environment where many individual producers of varying sizes exist within a field or the UB, each with varying water needs and production, and a production timescale of decades for the basin as wells play out and new ones are completed. Specific UB water issues include: water use/reuse for well drilling and completion (hydraulic fracturing), appropriate sites for disposal/reuse of water, development of systems to manage the produced water streams, and differing challenges for gas versus oil producers.

Current produced water disposal practices in the UB consist of (1) injection in deep wells below the base of a moderately saline aquifer in the Green River Formation, (2) storage and evaporation in lined disposal ponds, and (3) supplying water for flooding in enhanced-oil recovery (EOR) programs. Potential uses for the produced water from these formations include

water flooding for secondary recovery, drilling mud formulation, hydraulic fracturing fluid for well completion, and future possible oil shale production.

This study had five main objectives: (1) create basin-wide, digital produced water management tools that integrate produced water character, water disposal/reuse, water transport, and groundwater sensitivity factors to allow for quicker and more efficient regulatory and management decisions related to unconventional gas developments in the UB; (2) seek to increase protection of critical UB alluvial aquifers; (3) promote maximized produced water reuse which will minimize use of freshwater in unconventional gas development and production; (4) compile UB produced water management practices and recommend best practices; and (5) investigate the option of beneficial use of produced water treatment for geothermal heat recovery or power generation in the UB. The study investigated the integrated management of water production and disposal for shale/tight-sand gas in the UB, across many producers, and with multiple reuse or disposal options. It was comprised of four major components.

1. Compilation and analysis within a geographical information systems format of past and new information on: the thickness, structure, depth, porosity, permeability, and lithologic nature of all aquifer/reservoir units in the basin from the Tertiary down through the Jurassic Glen Canyon Group (figure 1.5); the regional variations in quality of water, flow direction, and temperature produced from the various shale/tight-sand gas reservoirs across the basin; the location, saturated volume, and quality of alluvial aquifers; the existing infrastructure for water management/reuse; the energy generation potential of geothermal-produced waters; and location and geochemical and hydrological characteristics of aquifers used/proposed for disposal of produced water or concentrated brines.

2. Compilation and statistical analysis of water production quantity and quality to identify and forecast produced-water production volume trends for each discrete shale/tight-sand gas producing interval, and possibly include changes in water quality over the life of reservoir's production development if analyses over time were available. The geostatistical characterization of the basin's produced water streams helped analyze the quality and quantity of potential future produced-water streams and the options for treatment, transportation, disposal, geothermal energy production, and alternative use options.

3. Development of alluvial aquifer sensitivity/vulnerability models to potential contamination from fluids associated with shale/tight-sand gas development in the basin.

4. An evaluation of produced water management practices and recommendations for best management practices.

Science-based decision support models, such as outlined here, will help industry, particularly small producers, and regulators alike in making optimum management decisions, and provide sound scientific information to allay public concerns about the potential for drinking water contamination. The aquifer, produced-water quantity and quality geostatistical models, groundwater sensitivity evaluation, and best practice recommendations provide a framework to address the divergent water use and disposal interests of various stakeholders. The produced-water models for the various reservoirs in the basin allow stakeholders to evaluate the cause and effect of the timing and rate of unconventional gas development drilling decisions on both their

operations and those of other operators, allow the evaluation of water input and output impacts and consequences of various unconventional gas-development decisions, and ultimately allow an improved understanding of complex interactions typical of produced-water management systems. Decision support models built with components on estimates of water needs for drilling and fracture stimulation, options for treatment, distribution, disposal, and reuse of produced water will allow efficient management and improved reuse of produced water flows in an arid region on a basin-wide level (across the UB), and potentially for other unconventional gas production areas of the U.S. Finally, we hope that the research results, will foster extensive collaboration among producers, users, regulators, and local water management interests, providing insight and information necessary for effective protection of alluvial aquifers, sustainable produced-water management, as well as potential for beneficial use.

This report covers research and results of the Utah Geological Survey's (UGS) three-year study of the geology, chemistry, and best practices related to produced water in the Uinta Basin. The report includes: (1) statistical trends of UB water quality, (2) descriptions of UB reservoirs and aquifers, (3) groundwater chemistry for shallow alluvial wells and springs, (4) sensitivity and vulnerability of aquifers and springs to potential contamination associated with energy development, (5) produced water facilities and best handling practices, and (6) geothermal resource reuse potential. Appendices provide the complete data compilations, maps, etc., either collected or generated as part of the study.

The results of this study have been provided to industry and other researchers through a Technical Advisory Board (Consortium), an industry outreach program, digital project databases, and a project Web page. The Technical Advisory Board and collaborating government agencies were composed of industry representatives operating in the UB, groups with regulatory

responsibilities, and stakeholder having a financial interest within the study area. Project results were also disseminated via displays and technical presentations at national and regional professional conventions, papers or abstracts in various technical or trade journals, a non-technical UGS publication, and a field review. All project maps, studies, and results are, or will be, publicly available in digital (interactive, menu-driven products on compact disc) or hard-copy format. Refer to appendix A for a complete listing of technology transfer activities and project publications.

CHAPTER I FIGURE CAPTIONS

Figure 1.1. Oil and gas fields in the Uinta Basin of eastern Utah. Cross section A-A' shown on figure 1.4.

Figure 1.2. Production in the Uinta Basin in comparison to the rest of the state in 2014: A – oil, B – gas, and C – water (Utah Division of Oil, Gas, and Mining, 2015a).

Figure 1.3. Ancient Eocene lake basins of the Rocky Mountain west. Lake Gosiute occupied the Green River and Washakie Basins in Wyoming, while Lake Uinta filled the Uinta and Piceance Creek Basins in Utah and Colorado. Modified from Vanden Berg (2011).

Figure 1.4. Cross section extending from the southwest flank of the Uinta Basin to the north-central part of the basin showing producing reservoirs, general facies, and widely recognized

stratigraphic markers. Also shown are major fields, some projected into the line of section. Location of cross section A-A' shown on figure 1.1. Modified from Fouch (1975), Fouch and others (1992).

Figure 1.5. Stratigraphic column from the surface down through the Late Triassic-Early Jurassic Nugget section in the Uinta Basin showing major producing reservoirs and aquifers evaluated in this study. Modified from Hintze and Kowallis (2009).

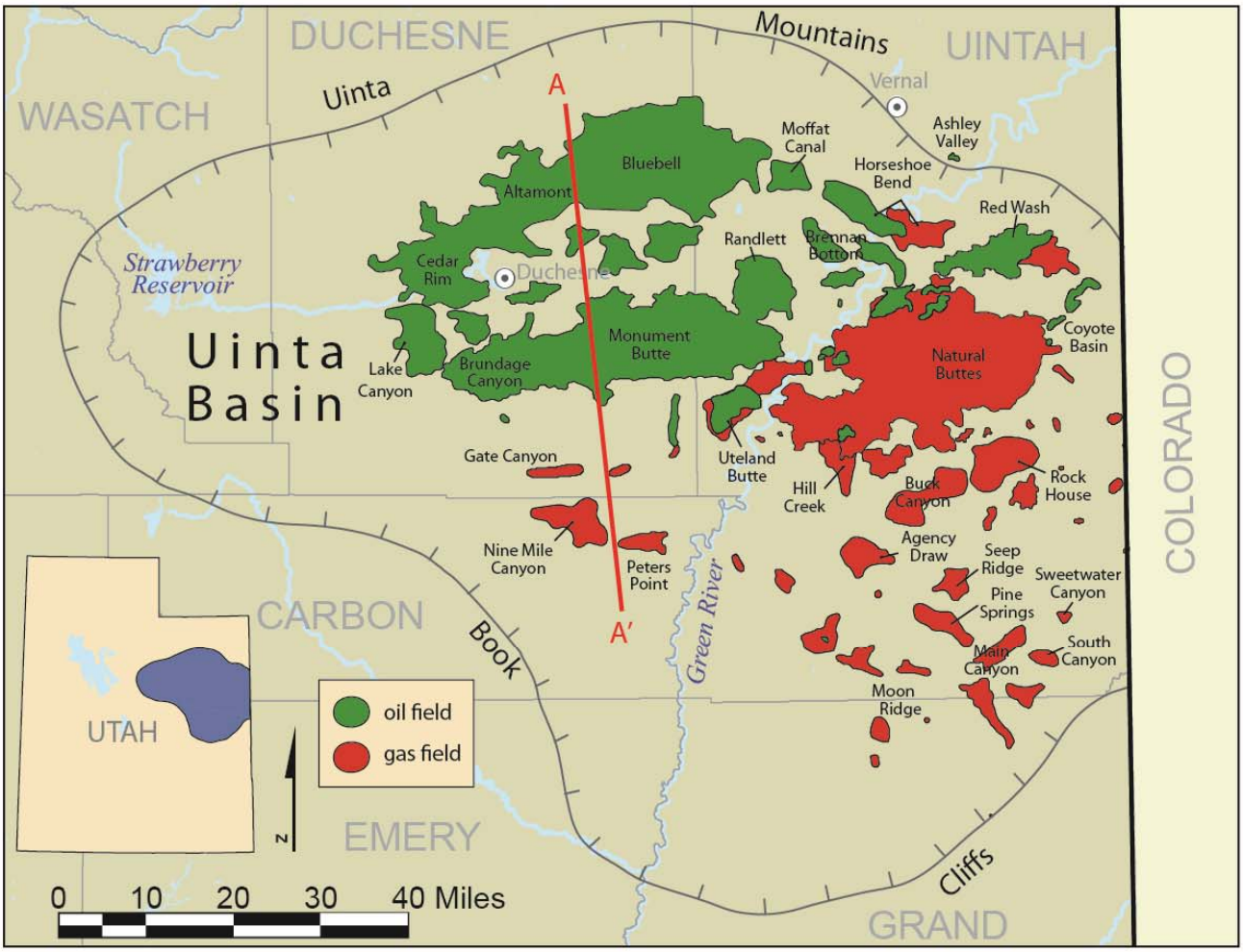

Figure 1.1. Oil and gas fields in the Uinta Basin of eastern Utah. Cross section A-A' shown on figure 1.4.

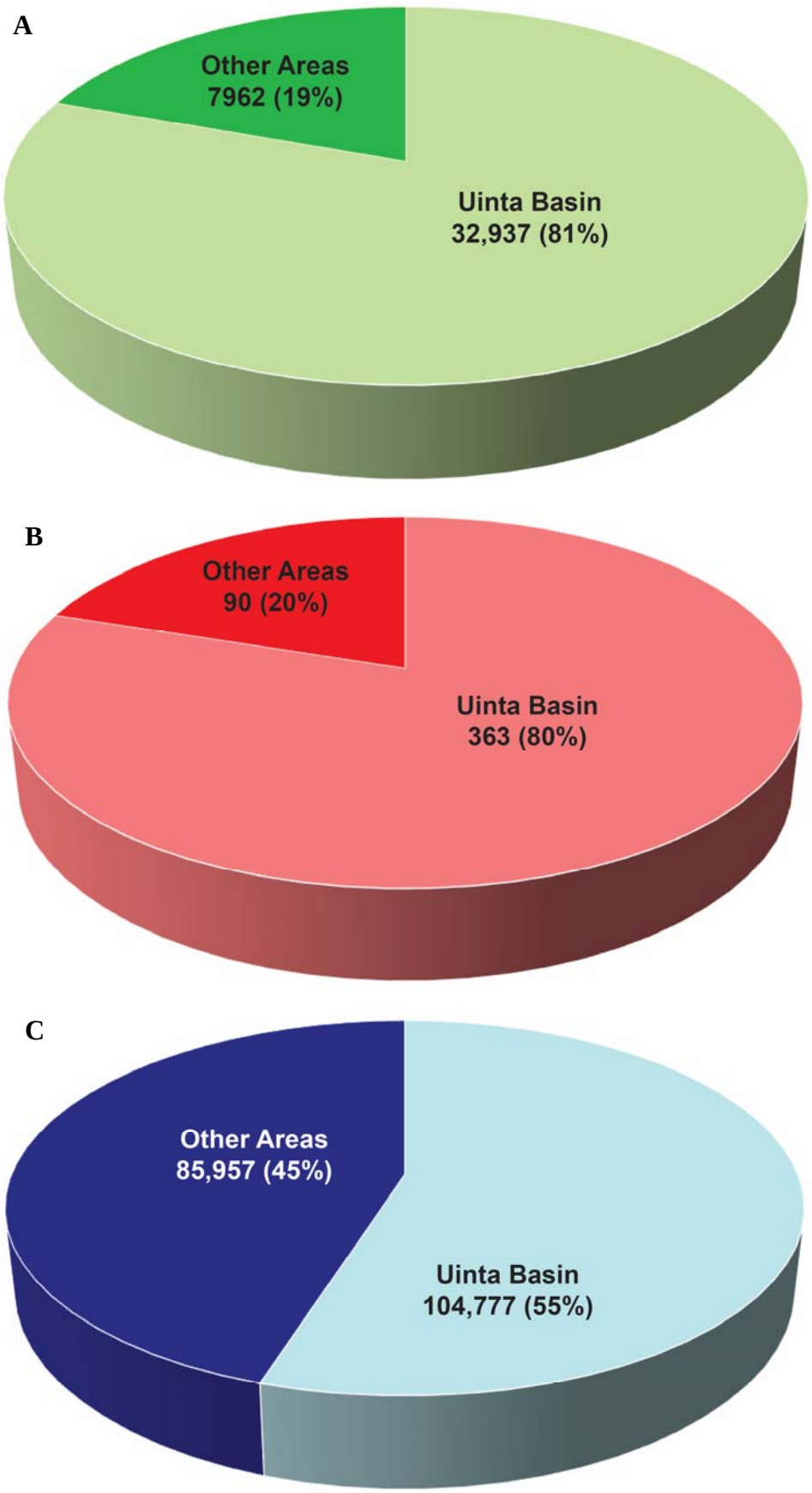

Figure 1.2. Production in the Uinta Basin in comparison to the rest of the state in 2014: A – oil, B – gas, and C – water (Utah Division of Oil, Gas, and Mining, 2015a).

Figure 1.3. Ancient Eocene lake basins of the Rocky Mountain west. Lake Gosiute occupied the Green River and Washakie Basins in Wyoming, while Lake Uinta filled the Uinta and Piceance Creek Basins in Utah and Colorado. Modified from Vanden Berg (2011).

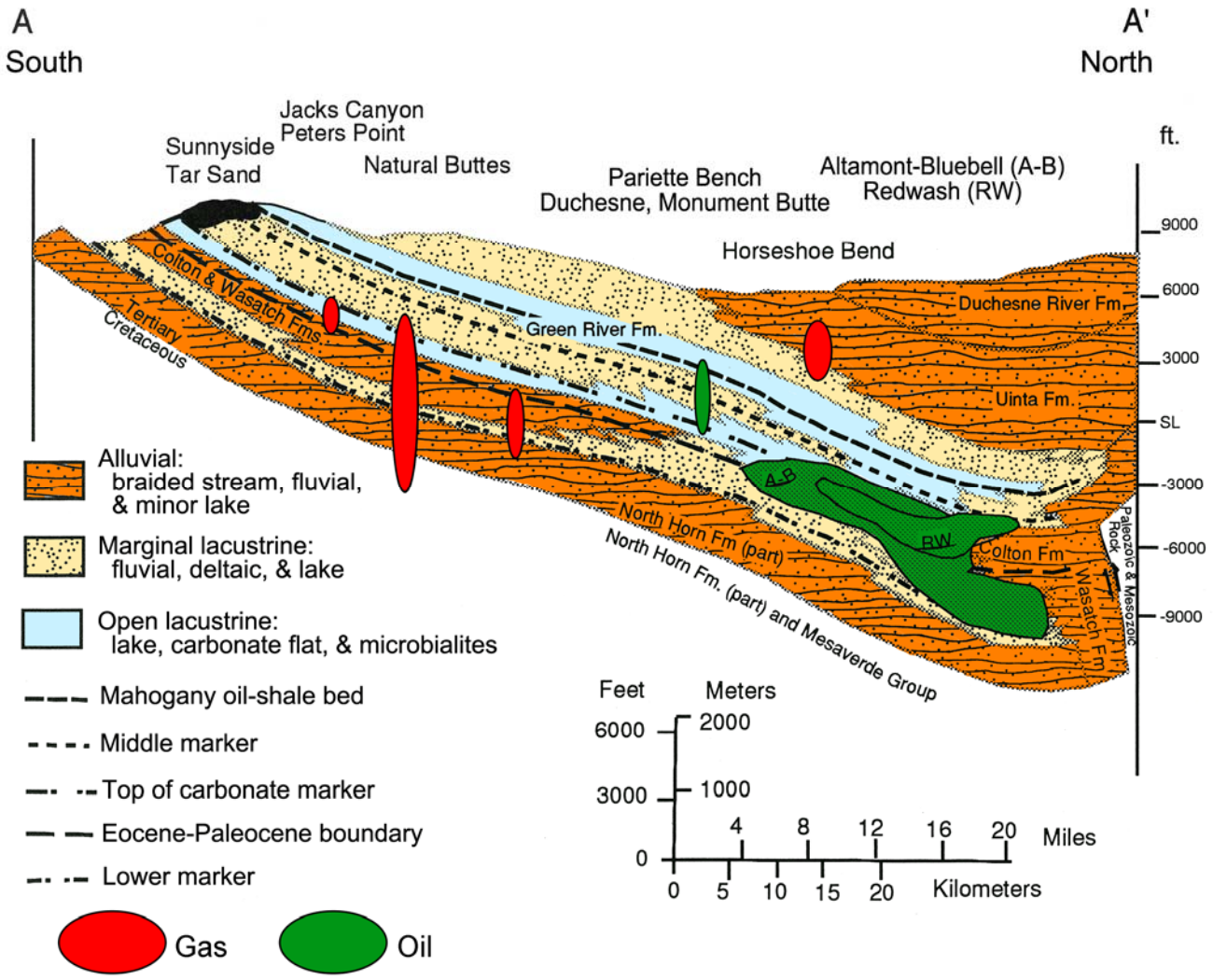

Figure 1.4. Cross section extending from the southwest flank of the Uinta Basin to the north-central part of the basin showing producing reservoirs, general facies, and widely recognized stratigraphic markers. Also shown are major fields, some projected into the line of section. Location of cross section A-A' shown on figure 1.1. Modified from Fouch (1975), Fouch and others (1992).

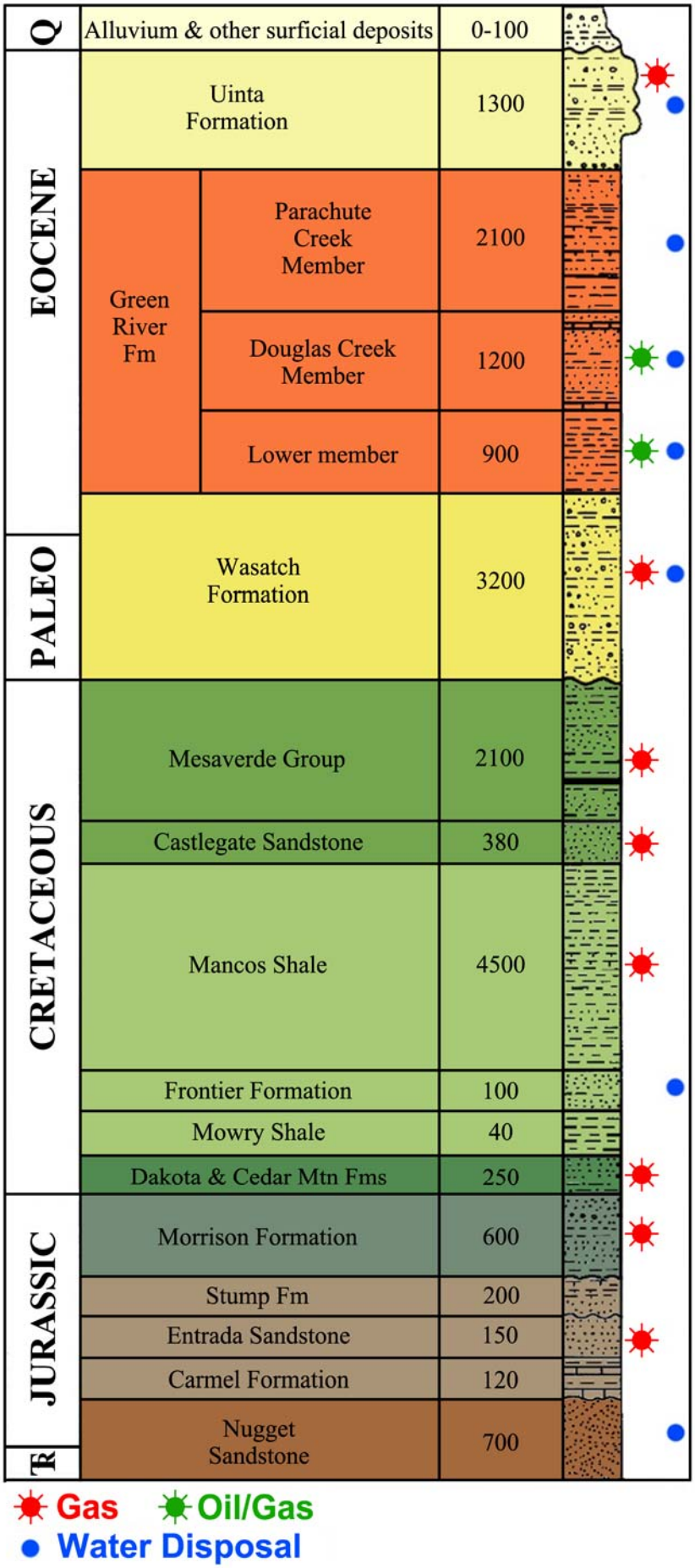

Figure 1.5. Stratigraphic column from the surface down through the Late Triassic-Early Jurassic Nugget section in the Uinta Basin showing major producing reservoirs and aquifers evaluated in this study. Modified from Hintze and Kowallis (2009).

CHAPTER II

STRATIGRAPHY AND DEPOSITIONAL HISTORY

Thomas C. Chidsey, Jr., Taylor Boden, and Stephanie M. Carney

Consolidated sedimentary rocks in the UB were deposited intermittently over the past 540 million years and have a cumulative average thickness of over nearly 22,000 feet (Hintze and Kowallis, 2009); however, rocks older than Cretaceous are not exposed in the basin. Exploratory drilling for hydrocarbons in the UB has penetrated the stratigraphic section to the Precambrian basement. Several major unconformities represent significant periods of erosion or non-deposition. The exposed strata in the UB, including the Book Cliffs along the southern boundary, and San Rafael Swell (SRS) to the southwest, which serve as outcrop reservoir and aquifer analogs, display changes in color, rock types, thicknesses, and weathering profiles representing various environments and geologic processes depending on their location within the region. In addition, unconsolidated gravel, sand, silt, and clay are found in a variety of settings—the products of weathering, running water, wind, and mass wasting as the UB is currently in a state of regional erosion. Figure 2.1 and plate 1 are generalized geologic maps showing the distribution of rock units across the UB and surrounding areas.

This study focuses on water produced from Late Triassic-Jurassic to Tertiary oil- and gas-bearing formations, aquifers within those formations, and Quaternary alluvial aquifers (figure 1.5). The stratigraphy and depositional history of Late Triassic through Quaternary deposits in the UB are discussed in general detail below.

UPPER TRIASSIC-JURASSIC ROCKS

Late Triassic and Jurassic rocks in the Uinta Basin are shallow marine, marginal marine, and terrestrial sedimentary formations deposited between 205 and 145 million years ago (Ma), coeval with the breakup of the supercontinent Pangea (Blakey and Ranney, 2008). Hintze and Kowallis (2009) grouped the strata into three packages: Late Triassic to Early Jurassic rocks which are primarily eolian and fluvial sandstones; Middle Jurassic marine and marginal marine rocks which reflect a change in conditions as an epicontinental seaway advanced and retreated from the north; and Late Jurassic rocks composed of continental interior fluvial and lacustrine deposits.

Upper Triassic to Lower Jurassic Rocks

There are three Upper Triassic to Lower Jurassic formations in the UB collectively called the Glen Canyon Group (figures 1.5 and 2.1, plate 1). In ascending order of deposition, these are the Triassic-Jurassic Wingate Sandstone, the Jurassic Kayenta Formation, and the Jurassic Navajo Sandstone (equivalent to the Upper Triassic-Lower Jurassic Nugget Sandstone in the eastern Uinta Mountains just outside the basin boundary). This sequence is spectacularly exposed on the SRS and consists of predominantly eolian and fluvial sandstone which generally thicken southwestward across the UB and Utah. The depositional limit of the Wingate and Kayenta Formations is near the central part of the UB, and they are not present in the north and

northeastern part of the basin based on deep wells. The thickness of the group ranges between 700 and 1000 feet, where all three formations are present in the basin (Hintze and Kowallis, 2009). In the central and southern part of the UB, the Upper Triassic-Lower Jurassic Wingate Sandstone comformably overlies the Triassic Chinle Formation, whereas in the north and northwest, the Nugget (Navajo) comformably overlies the Chinle. In outcrops and wells surrounding the Uinta Mountains, the Wingate and Kayenta Formations are not present and thus, the name Nugget Sandstone is applied to the predominately sandstone Upper Triassic to Lower Jurassic section (Sprinkel and others, 2011a).

Wingate Sandstone

The Wingate Sandstone is latest Triassic (Rhaetian) through the early part of Early Jurassic (early Sinemurian) in age, the basal formation of the Glen Canyon Group. The Wingate is composed of very fine to fine-grained, laminated to thin-bedded, flat- and cross-stratified sandstone, which contains very sparse shaly and silty partings (Gualtieri, 2004). It is light yellow-gray to orange-brown in color weathering dark brown and characteristically stained with dark-red-brown manganese oxide (desert varnish). The thick-bedded to massive Wingate forms sheer vertical to ledgey cliffs (figure 2.2), which are often jointed through the entire section.

The sandstone of the Wingate was deposited in a desert dune field (eolian erg) environment (Blakey and Ranney, 2008). The Wingate Sandstone contains only ichnofossils (mostly tracks from dinosaurs and other vertebrates) and no known ash beds; thus age dating has been difficult. Recent studies of dinosaur track sites elsewhere on the Colorado Plateau indicate that the lower Wingate is Triassic; other track sites showed that the upper Wingate was Early

Jurassic (Molina-Garza and others, 2003; Lockley and others, 2004; Lucas and others, 2005; Milner and Kirkland, 2006). Thus, the Triassic-Jurassic boundary lies within the Wingate (Sprinkel and others, 2011a).

Kayenta Formation

The Kayenta Formation (Sinemurian and Pliensbachian in age) is easy to distinguish from the underlying Wingate and overlying Navajo Sandstones. Whereas the formations above and below form large vertical cliffs, the Kayenta forms a series of ledges, small cliffs, and benches (figures 2.3). It is composed of gray, pinkish-gray, and red interbedded fine- to coarse-grained partly micaceous sandstone, siltstone and mudstone. The sandstone beds are thin- to medium-bedded, and flat- and cross-stratified (Gualtieri, 2004). The Kayenta forms gradational contacts with the underlying Wingate Sandstone and overlying Navajo Sandstone (Doelling, 2002).

The Kayenta Formation was deposited in a sandy, braided fluvial environment although the environment was arid. Perennial streams flowed west from the remaining Ancestral Rockies and the Appalachians far to the east (Lynds and Hajek, 2006; Blakey and Ranney, 2008). Subsidence in the Kayenta basin created accommodation space for deposition, and uplift in the adjacent Ancestral Rockies provided a source of sediment to the dominantly fluvial depositional system. Rise of the Ancestral Rockies may have also created wetter climatic conditions enhancing fluvial conditions in the Kayenta basin (Blakey and Ranney, 2008).

Navajo/Nugget Sandstone

The Navajo Sandstone (Pliensbachian and Toarcian in age) with its spectacular cross-stratification is perhaps the most well-known formation in Utah, where it forms the magnificent cliffs and canyons in Zion and other national parks, monuments, and recreational areas in the southern part of the state; it is equivalent to the upper (Lower Jurassic part) Nugget Sandstone north of the UB. The Navajo is light brown to light gray, thick-bedded to massive sandstone that is cross-stratified in large trough sets (figure 2.4). The sandstone beds are friable and composed of clean, fine- to medium-grained, frosted, subrounded to subangular, moderately to well-sorted quartz sand with minor amounts of feldspar and scattered heavy mineral grains. The Navajo forms steep cliffs and rounded knolls and locally contains thin, lenticular, light-gray limestone beds. The Navajo Sandstone is separated from the overlying Middle Jurassic Carmel Formation by the J-1 unconformity (Pipiringos and O'Sullivan, 1978).

The sandstone of the Navajo and age-equivalent rocks represents one of the largest eolian deposits in all of geologic time (Kocurek and Dott, 1983) and was deposited in a coastal to inland desert dune field (erg) environment, which extended from present-day Wyoming to Arizona (Blakey and Ranney, 2008). In Early Jurassic time, Utah had an arid climate and lay 15º north of the equator (Smith and others, 1981). The erg was comparable to the Sahara desert in North Africa or the Alashan area of the Gobi desert in northern China. The eolian deposits included dunes, interdunes, and sand sheets. Navajo dunes were large (widths up to 2200 feet) to small, straight-crested to sinuous, coalescing, transverse barchanoid ridges as suggested by the large-scale cross-stratification (Picard, 1975; Fryberger, 1990). Regional analyses of the mean dip of dune foreset beds indicate paleocurrent and paleowind directions were dominantly from the north and northwest (Kocurek and Dott, 1983; Peterson, 1988), as well displayed in the SRS.

A high paleo-water table produced oases; carbonate deposition occurred when springs and lakes existed for relatively long periods of time.

Middle-Upper Jurassic Rocks

Middle Jurassic rocks found in or exposed around the UB include the Carmel/Arapien Formation (Twin Creek Formation equivalent), Entrada Sandstone, Curtis/Stump, and Summerville Formations (Stump Formation equivalent) (figures 1.5 and 2.1, plate 1); these formations make up the San Rafael Group in the SRS. Middle Jurassic rocks in the basin range from 300 to 2000 feet thick (Hintze and Kowallis, 2009) and reflect a time of complex sedimentation resulting from the advance and retreat of a long, north-south oriented, narrow epicontinental seaway.

Carmel and Arapien Formations

The Carmel Formation (Bajocian through Callovian in age) is exposed in the SFS and north of the central and eastern part of the UB where it is divided into four members, which in ascending order are: Co-op Creek Limestone (or equivalent Judd Hollow), Crystal Creek, Paria River, and Winsor (figure 2.5). However, all four members are not always present with the SRS. Members of the Carmel and other Middle Jurassic formations in the region have been mapped, measured, and described by Sprinkel and others (in preparation). Along the western part of the south flank of the Uinta Mountains (near the town of Hanna), the stratigraphically equivalent Arapien Formation is exposed consisting of five members, which in ascending order

are: Sliderock, Rich, Boundary Ridge, Watton Canyon, and Twelvemile Canyon.

In general, the Carmel Formation consists of interbedded sandstone, siltstone, mudstone, and limestone with subordinate amounts of dolosiltite, doloarenite, calcarenite, and calcisiltite. The Paria and Windsor Members also gypsum beds. These lithotypes are generally thin to medium bedded, forming blocky ledges (weathering into slabs and plates) and steep slopes. The Arapien Formation consists mostly of thin- to medium-bedded, dense, micritic to grainstone-rich, and locally bioclastic limestone to dolomitic limestone; oolitic beds are common in the Sliderock and Watton Canyon Members (Sprinkel and others, 2011b). The Twelvemile Canyon Member is a mixed carbonate and clastic unit interbedded with gypsum (anhydrite) and salt.

The Carmel and Arapien Formations are the result of deposition during the transgression of the shallow marine Sundance Sea, which extended south from Canada into a narrow embayment or arm (called the Utah-Idaho trough) through northern, central, and southwestern Utah (Blakey and Ranney, 2008; Hintze and Kowallis, 2009). Shoreline fluctuations produced variations between restricted- and more open- to marginal-marine conditions, causing significant changes in deposition. This was especially the case along the eastern margin of the marine embayment, which is now exposed on the SRS and along the south flank of the Uinta Mountains.

Entrada Sandstone

Marine waters retreated northward out of Utah and the Entrada Sandstone was deposited on top of the Carmel Formation. The Entrada consists of orange-brown, red-brown, or light brown sandstone, siltstone, mudstone, and subordinate oolitic limestone (figure 2.6A). Red siltstone and silty sandstone dominant in the basal part (Gualtieri, 2004). Sandstone beds are

friable, porous, silty or very fine to fine grained with scattered coarse grains, poor to moderately sorted, and cemented with calcite or iron oxide. A variety of sedimentary structures are found in the Entrada: ripple marks, mudcracks, rip-up clasts, trough cross-stratification, micro-cross-lamination, and soft-sediment deformation. Bedding is thin to massive, forming earthy slopes and rounded ledges and cliffs. The Entrada Sandstone lies conformably above the Carmel Formation. It is separated from the overlying Curtis Formation by the regional J-3 unconformity of Pipiringos and O'Sullivan (1978).

The Entrada Sandstone was deposited primarily in broad, mud-dominated intertidal (low to high) and subtidal zones, supratidal sabkha mudflats and ponds, and related erg-margin coastal dunes (Hicks and others, 2010; Herbst and Morris, 2011; Thomas H. Morris, Brigham Young University, written communication, December 2012). Associated shoreface, ooid shoal and bar, foreshore, tidal channel, and storm deposits are also present (Marino and Morris, 1996; Hicks and others, 2010). Coastal dunes encroached on the region from the east, while the remaining part of the Sundance Sea lay to the west and northwest. These eolian deposits, found along the eastern flank of the SRS (figure 2.6B).

Curtis and Stump Formations

The final Jurassic marine incursion deposited the Curtis/Stump Formation (Oxfordian in age [Wilcox, 2007]); along the southern flank of the Uinta Mountains the Curtis is the lower member of the Stump (Hintze and Kowallis, 2009). The Curtis/Stump consists of light gray-green, light gray, to light brown sandstone (sublitharenite, lithicarenite, and subarkose), siltstone, and claystone/shale (figure 2.7) with subordinate conglomerate and limestone (Smith, 1976;

Witkind, 1988; Caputo and Pryor, 1991; Doelling, 2002, 2004). Sandstone is very fine to coarse-grained, poorly to moderately sorted, subrounded to subangular, and quartzose. The green color is attributed to the presence of glauconite in the matrix, although it may be iron-chlorite clay instead (written communication to Mario V. Caputo from Richard Pollastro, U.S. Geological Survey, October 1987). Bedding is finely laminated to medium, forming cliffs, ledgy benches, and slopes. The contact with the overlying Summerville Formation is gradational and conformable.

The Curtis/Stump Formation was deposited in a shallow-shelf and marginal-marine environment (Blakey and Ranney, 2008). The lithofacies display the effects of low-energy, marine (normal wave base) conditions, and tidal currents in intertidal and subtidal zones with tidal channels, shoals, storm deposits, tidal flats, etc. (Smith, 1976; Caputo and Pryor, 1991; Currie and Reeder, 2002; Currie and others, 2005).

Summerville Formation

The Summerville Formation (Oxfordian) commonly appears like chocolate-colored pages of a book displayed in prominent buttes and mesas (figure 2.8); it is only present in the southernmost part of the UB. The Summerville consists of red-brown, light to medium brown siltstone, mudstone, sandstone, and white gypsum with subordinate claystone/shale and gray limestone (Stanton, 1976; Witkind, 1988; Caputo and Pryor, 1991; Doelling, 2002, 2004). Siltstone is the most common lithotype, present both as mottled regular bedded units or small lenses, and is composed of silt with abundant clay. Sandstone is very fine to fine-grained, silty, and weathers into plates. Ripple marks are profuse throughout the Summerville. Bedding is

laminar to medium forming vertical cliffs and steep earthy slopes with a few smooth ledges. The Summerville Formation is separated from the overlying Morrison Formation by the regional J-5 unconformity of Pipiringos and O'Sullivan (1978).

The Summerville Formation was deposited in a broad, low-energy, muddy tidal flat/sabkha environment along an arid coastal plain during a supratidal stage of an upward-shallowing cycle (Stanton, 1976; Caputo and Pryor, 1991; Currie and others, 2005). These conditions were restricted, hypersaline, and evaporative; the narrow and receding sea was to the west and northwest of the SRS. In eastern Utah, eolian environments occurred on a coastal plain (Blakey and Ranney, 2008).

Morrison Formation

The Morrison Formation (Upper Jurassic – Kimmeridgian through Tithonian in age) is world famous for its dinosaur fossils and the outcrops in the SRS (figure 2.9) and the quarry in Dinosaur National Monument just east of Vernal. The Morrison is divided into three members within the region, which in ascending order are: Tidwell, Salt Wash, and Brushy Basin. The Tidwell Member consists of lavender, maroon, red, red-brown, or light gray interbedded siltstone, shale, limestone (marl), sandstone, and gypsum. The Salt Wash Member consists of red, gray, purple, or brown mudstone and siltstone with few sandy limestone beds and light yellow-gray, light gray to gray sandstone, conglomeritic sandstone, and conglomerate (Witkind, 1980, 1988; Doelling, 2002; Doelling and Kuehne, 2012). Sandstone beds are fine- to coarse-grained, subangular to well-rounded, arkosic or quartzose, and contain well-displayed trough cross-stratification. Conglomerate is composed of poorly sorted, subangular to well-rounded

chert and quartzite ranging in size from pebbles to cobbles in a matrix of coarse quartz sand. The Brushy Basin Member is produces the most colorful section of the Morrison consisting of purple, green, red, yellow, maroon, bluish gray, gray, and white colored bands of claystone (often bentonitic/smectitic), mudstone, siltstone interbedded with white, gray, and light brown sandstone with subordinate limestone and conglomerate (figure 2.9) (Witkind, 1980, 1988; Doelling, 2002; Gualtieri, 2004; Doelling and Kuehne, 2012). They form smooth, steep slopes composed of thin to thick bands that are devoid of vegetation. The Brushy Basin is separated from the overlying Lower Cretaceous Cedar Mountain Formation by the K-0 unconformity, representing a time gap of 25 million years (Pipiringos and O'Sullivan, 1978; Hintze and Kowallis, 2009).

The Morrison Formation represents entirely continental deposition when mountains were rising far to the west in Nevada and westernmost Utah, and the last Jurassic inland sea had retreated to the northeast. The regional structural setting was a back-bulge depozone of a foreland basin east of the thrust belt forebulge to the west (DeCelles and Coogan, 2006). The Tidwell Member was deposited in fluvial, lacustrine (numerous lakes and ponds), and coastal plain environments (Doelling and Kuehne, 2012). The Salt Wash Member was deposited in an anastomosing system of well-preserved braided or meandering rivers and streams on a broad floodplain (Doelling and others, 2010). These fluvial systems flowed in a general east-northeast direction from highlands in eastern Nevada and northern Arizona (Blakey and Ranney, 2008). The Brushy Basin Member was deposited by a northeast-flowing meandering river system (although individual channels flowed in different directions) on a floodplain that contained large lakes and ponds; the climate was hot and humid (Blakey and Ranney, 2008).

CRETACEOUS ROCKS

During the Cretaceous, North America was divided into two large landmasses by the north-south oriented Cretaceous Interior Seaway with part of the western shore located in present-day eastern Utah. Cretaceous deposition in the UB was controlled by the Sevier orogeny, which uplifted a north-south trending mountain belt in western Utah, and created a subsiding basin in eastern Utah that received some 15,000 feet of sedimentary outwash from the eroding mountain belt (Hintze and Kowallis, 2009). The mountain belt was composed of folded and thrust faulted Mesozoic, Paleozoic, and Precambrian rocks. Cretaceous deposits derived from these units largely consist of clastic rocks laid down along a coastal plain where coal-bearing non-marine sandstones and conglomerates interfinger with marine shale of the mid-continental Interior Seaway. They reflect a balance between changing sediment supply from the advancing Sevier orogenic belt in western Utah and changes in accommodation space resulting from transgressions and regressions of the Cretaceous Interior Seaway in eastern Utah (Armstrong, 1968; Hintze and Kowallis, 2009). In the UB and surrounding areas, the Cretaceous section consists of (in ascending order): the Cedar Mountain Formation, Dakota Sandstone, Mancos Shale, and Mesaverde Group (figures 1.5 and 2.1).

Lower and Lower-Upper Cretaceous Rocks

The Lower and lower-Upper Cretaceous Cedar Mountain and Dakota Formations are significant producers of gas from tight sandstone reservoirs in the UB. Productive units are

typically lenticular, discontinuous fluvial sandstone beds that can be observed in outcrop reservoir analogs around the basin.

Cedar Mountain Formation

The Cedar Mountain Formation (Early to early Late Cretaceous – Barremian to early Cenomanian in age [Doelling and Davis, 1989; Burton and others, 2006; Kirkland and others, 1998; Cifelli and others, 1997, 1999]) is divided into two members along the west flank of the SRS and to the east: the basal Buckhorn Conglomerate and the Ruby Ranch, (a third and uppermost member, the Mussentuchit, is best developed along the west flank of the SRS, figure 2.10). The Buckhorn, where present, is recognized in well logs in the UB whereas the others members are generally not discernable. The contact between the Cedar Mountain and the Morrison is also difficult to recognize when the Buckhorn Conglomerate Member is absent and thus the two formations are mapped together in the subsurface. In SRS outcrops, this situation places the Ruby Ranch Member of the Cedar Mountain over the Brushy Basin Member of the Morrison Formation—both create colorful, banded steep slopes and badland topography. However, the Cedar Mountain has (1) a more drab variegated color, (2) less smectite clay, (3) the presence of polished chert pebbles (gastroliths), (4) abundant carbonate nodules, and (5) a thick paleosol at the base (Kirkland and Madsen, 2007). The contact with the overlying Dakota Sandstone is an unconformity with about 2 feet of relief in some areas (Doelling and others, 2009).

The Buckhorn Conglomerate Member (Barremian to Aptian) is discontinuous within the SRS and UB ranging in thickness from nothing to 80 feet. It consists of gray to dark brown

conglomerate to conglomeratic sandstone with subordinate amounts of sandstone and mudstone (figure 2.10B). Pebbles and cobbles are composed of poorly to moderately sorted, subangular to well-rounded, clasts of white quartzite, and black, brown, light brown, and light gray chert (figure 2.10B inset). Conglomerate beds are either clast supported or supported by a matrix of clay or medium- to coarse-grained sandstone. Bedding is lenticular, thick to massive, trough cross-stratified, generally fines upward, and forms a single cliff or ledges. The Ruby Ranch Member (Aptian to Albian) ranges in thickness from 60 to 130 feet and consists of subtle bands of dark gray to dark purplish gray mudstone and tan to gray sandstone (figure 2.10A) (Doelling and others, 2009; Doelling and Kuehne, 2012). Mudstone is clayey and silty with local lenticular sandstone beds. Sandstone is fine-grained to pebbly, poorly sorted, trough cross-stratified, and discontinuous, and usually occurs in the upper half of the section. The Ruby Ranch is medium to thick bedded, with mudstone forming steep, rounded slopes, whereas sandstone produces ledges and cliffs.

The Cedar Mountain Formation represents the continuation of continental deposition that began during the Late Jurassic. By Early Cretaceous time, the Sevier orogenic belt was now emerging in western Utah (Armstrong, 1968). East-central Utah was the site of deposition in alluvial plains, fluvial channels, and floodplains (similar to the depositional environments of the Morrison Formation) in a back-bulge to foredeep setting; the climate was arid, becoming wetter near the top of the section (Currie, 1998; DeCelles and Coogan, 2006). The Buckhorn Conglomerate was deposited in gravel-filled channels of a northeast-flowing fluvial system originating from the rising highlands to the west (Yingling, 1987; Currie, 1998). The Ruby Ranch Member was deposited in fluvial channel and floodplain environments. Sandstone beds represent overbank, generally linear to low sinuosity channel-fill, and point-bar deposits.

Dakota Formation

The Dakota Formation is time-transgressive in the study area region and is considered to be Early Cretaceous (Albian) in the Uinta Basin (Sprinkel, 2007; Sprinkel, 2009) and Late Cretaceous (Cenomanian) farther south (Witkind, 1988; Gualtieri, 2004). The Dakota unlike other formations is not widespread SRS (figure 2.11) and within the UB (figure 2.12) it is often mapped together with the underlying Cedar Mountain Formation; the also production is commingled. It ranges in thickness from nothing to 100 feet, consisting of light yellow, tan, yellow-brown, orange-gray, light tan-gray, or light brown, sandstone, conglomeratic sandstone, conglomerate, shale, and coal, particularly east of the SRS (Witkind, 1979, 1980, 1988; Doelling, 2002; Doelling and others, 2009; Kirschbaum and Schenk, 2011; Doelling and Kuehne, 2012). Sandstones are friable, quartzitic, fine to coarse grained, and moderately to well sorted. Conglomerates contain rounded to subrounded pebbles of chert and quartzite. Sandstones and conglomerates are thin to thick bedded, cross-stratified (trough and planar); some ripple and convolute bedding are also present. The upper part is lenticular sandstone, 5 to 12 feet thick and encased in mudrock (Kirschbaum and Schenk, 2011). Shale beds are often the only rocks that represent the Dakota section. The Dakota weathers to form mound-like hills and discontinuous ridges or small cliffs (figure 2.11). The contacts with the conformable overlying Mancos or Mowry Shales in defined by the first appearance of deeper marine shale (Molenaar and Cobban, 1991; Doelling and others, 2009; Doelling and Kuehne, 2012).

In general, the Dakota Formation was deposited in swamps, beaches, bars, and marginal-marine environments associated with the approaching Cretaceous Interior Seaway from the

northeast (Blakey and Ranney, 2008). The section is interpreted as a fluvial/braided stream system whereas the upper section of mud-encased lenticular sandstone was deposited in low-energy, anastomosed channels on an alluvial and coastal floodplain setting (Kirschbaum and Schenk, 2011).

Upper Cretaceous Rocks

Upper Cretaceous deposits reflect transgressive-regressive cycles associated with the Cretaceous Interior Seaway, and contacts between formations are mostly gradational. The Mancos Shale epitomizes the various deposits resulting from the Cretaceous Interior Seaway on its western margin, and the influence of the Sevier orogenic belt in western Utah. The Upper Cretaceous Mesaverde Group overlies and interfingers with the Mancos Shale, and equivalent formations (e.g., Mowry Shale), and is composed of at least four to six main formations, depending on its location in the UB, that record several transgressive-regressive cycles (figure 2.13). The combined thickness of the Mancos and Mesaverde is nearly 8000 feet in the UB. Deposition took place from ~ 90 to 80 ma as the shoreline of the seaway transgressed to the south and west, and then gradually regressed back to the east.

The tight sandstone beds within the formations of the Mesaverde Group are the major gas producer (along with the Tertiary Wasatch Formation, to be discussed later) in the eastern UB. The coal beds in the Blackhawk and Neslen Formations in the Mesaverde are the source of much of the non-associated gas in the basin. The Mancos Shale is a secondary drilling target with shale-gas resource potential in the UB.

Mowry Shale

The Mowry Shale (Cenomanian) is found wells within the northeastern UB and in outcrop around the eastern Uinta Mountains (as well as in the subsurface of the Green River Basin of southwestern and other regions of Wyoming). The Mowry is a thin (less than 70 feet thick within the UB), dark gray, fissle, siliceous shale that weathers characteristically silver-gray (figure 2.12). It also contains bentonite beds (ash), with swelling clays, used to obtain radiometric dates. The Mowry forms slopes or strike valleys where often shale chips in the soil are the only evidence of its presence (Sprinkel, 2009; Gregson and others, 2010). In Wyoming, the Mowry is organic-rich and serves as a source rock for hydrocarbons in the thrust belt and elsewhere (Nixon, 1973). In the UB area, the contact with the overlying Frontier Formation is an unconformity represented by a time gap of about 5 million years (Sprinkel, 2009).

The Mowry Shale was deposited in a shallow, open-marine environment during the westernmost transgression of the Cretaceous Interior Seaway. The Mowry contains abundant fish scales, as well as ammonites, bivalves, and shark teeth (Hanson and others, 1983).

Frontier Formation

The Frontier Formation (Turonian), like the Mowry Shale, is found wells within the northeastern UB (figure 2.12) and in outcrop around the eastern Uinta Mountains (as well as in the subsurface of the Green River Basin of southwestern and other regions of Wyoming where it is a major hydrocarbon producer). In the Utah area of Dinosaur National Monument, the Frontier consists of upper and lower parts separated by a medial shale. The lower part consists

of soft, light to dark gray calcareous shale, silty shale, and siltstone with some minor limestone beds and coal; it forms slopes and saddles. The upper part is light brown to light greenish-gray, fine-grained sandstone that form prominent cliffs. It is thin bedded to massive containing cross-stratification, and ripple marks (Hansen and others, 1983; Sprinkel, 2009; Gregson and others, 2010).

The Frontier Formation was deposited in nearshore marine and coastal swamp environments as the sea temporarily retreated to the east (Gregson and others, 2010). As evidence, fossils include bivalves, ammonites, gastropods, and petrified wood (Hansen and others, 1983).

Mancos Shale

The Upper Cretaceous (Cenomanian to Campanian) Mancos Shale produces a drab, barren landscape (figure 2.14). The thickness of the Mancos exceeds 5000 feet in certain places within the UB (Hintze and Kowallis, 2009). The Mancos is divided into as many as five members along the west flank of the SRS, which in ascending order are: Tununk Shale, Ferron Sandstone, Lower Blue Gate Shale, Emery Sandstone, and Upper Blue Gate. The Ferron interfingers with the Juana Lopez Member to the east where much of the sandstone has pinched out; the Emery is equivalent to Prairie Canyon Member in the Book Cliffs and the Mancos B zone in the subsurface of the UB (Hintze and Kowallis, 2009). The Buck Tongue is the uppermost section of the Mancos and is a marine shale that thins and pinches out to the west interfingering with strata of the Mesaverde Group exposed in the eastern Book Cliffs and identified in the subsurface of the eastern UB.

The basal Tununk (Cenomanian-early Turonian), Lower Blue Gate and Upper Blue Gate Shale Members (Turonian-Coniacian), and Buck Tongue (Campanian) have very similar characteristics. They consist of light to dark gray, medium to dark brown or black shale, shaley siltstone, and mudstone. Shale is fissile breaking into platy, angular fragments. Some shale beds are bentonitic, providing regional correlation markers. Bedding is indistinct or even, thin, and laminated with a few siliceous zones that create small ledges. However, for the most part these members are soft and deeply weathered forming slopes and low, rounded hills devoid of vegetation (figures 2.14 and 2.15). They contain marine fossils including marine bivalves, cephalopods, fish scales, and a few shark teeth.

The Ferron Sandstone (Turonian) is spectacularly exposed along the west flank of the SRS (figure 2.15) where it consists of yellow-gray, light brown, to white sandstone and siltstone, gray sandy to black carbonaceous shale, and coal. Sandstone is very fine to medium grained, poor to moderately sorted, subrounded to angular. Sedimentary structures in sandstone that determine facies include ripples, channel scours, soft-sediment deformation to contorted bedding, cross-stratification (trough, swaley, and hummocky), and planar beds. Many beds contain rooted zones, a variety of burrows, or intense bioturbation. Bedding in sandstone is thin or lenticular to massive, forming vertical cliffs, whereas siltstone, shale, and coal create recesses and slopes. Coal beds are persistent but lenticular and often burned (due to spontaneous combustion or lightning strikes) leaving “clinker” zones with red oxidation staining. To the east Juana Lopez is light to dark gray, organic-rich, thin to medium bedded, heterolithic zone of shale and shaly siltstone.

The low cliff forming Emery Sandstone (Santonian) is divided into lower and upper sandstone units, which are separated by a middle shale unit. The lower and upper units consist

of light brown to yellowish-brown, thin- to medium-bedded, locally cross-stratified, very fine grained quartzose sandstone. The middle unit consists of light gray to gray, thin- and even-bedded shale and shaly siltstone. The Prairie Canyon Member (or Mancos B) (Santonian-Campanian) consists of thinly interbedded and interlaminated, very fine grained to fine-grained sandstone, siltstone, and claystone (Hettinger and Kirschbaum, 2002) and separates the Blue Gate into the upper and lower members in the central and eastern portion of the UB. The Mancos B is major gas producer in Colorado.

The shale members of the Mancos Shale were deposited in shallow, open-marine environments during major and rapid western transgressions of the Cretaceous Seaway. The Ferron Sandstone exposed along the west flank of the SRS was deposited in fluvial-dominated and wave-modified deltaic environments that prograded into the Cretaceous Interior Seaway. The alluvial to lower delta or coastal plain of the Ferron contained meander belts, swamps and peat bogs, levees, crevasse spays/overbanks, bays, distributary channels and mouth bars, shoreface, foreshore, prodelta facies. To the east, Juana Lopez and Prairie Canyon Members may represent offshore bars produced by longshore drift or sand plumes that accumulated on the shallow-marine shelf.

Mesaverde Group

The Late Cretaceous Mesaverde Group (Campanian-Maastrichtian) represent clastic deltaic packages that prograded east interfingering with the Mancos Shale (figure 2.13) (Cole and others, 2008). The Mesaverde Group ranges between 600 and about 4000 feet thick in and around the UB (Hintze and Kowallis, 2009) and is spectacularly exposed in the Book Cliffs

along the southern margin of the basin. In the western Books Cliffs, the Mesaverde includes, in ascending order, the Star Point, Blackhawk, Castlegate, and Price River Formations. In the eastern Book Cliffs near the state line, and the eastern UB including the Greater Natural Buttes area, the Mesaverde is composed of thinner Blackhawk and Castlegate (the Star Point has pinched out) and the Sego and Neslen Formations (equivalent to the middle and upper [Bluecastle Sandstone Member] Castlegate), and the Farrer and Tuscher Formations (equivalent to the lower Price River, the upper section also having pinched out) (figure 2.13).

Star Point Sandstone: The Star Point Sandstone (Campanian) consists of light brown to brown, fine- to medium-grained, platy, quartose sandstone, and some shale partings and interbeds of shale and shaly siltstone (Weiss and others, 1990). Depending on the facies, it displays graded bedding, laminated bedding, cross-stratification, burrowing, or flute casts and sole marks. The Star Point forms prominent cliffs in the western Book Cliffs and eastern Wasatch Plateau but thins and pinches out east and southwest of Price, Utah (Newman and Chan, 1991); it is not recognized in the subsurface of the central and eastern UB.

The Star Point Sandstone was deposited in deltaic to beach to nearshore marine environment (Weiss and others, 1990; Newman and Chan, 1991). Facies include prodelta, lower and upper delta front, and distributary mouth bar and channel.

Blackhawk Formation: The Blackhawk Formation (Campanian) is the major coal producer in Utah. The Blackhawk is dominantly light-brown, locally light-gray and brownish-gray, thin- to medium-bedded, fine- to medium-grained quartzose sandstone, with interbeds of shaly siltstone, shale, carbonaceous shale, and coal (figure 2.16A) (Weiss and others, 1990). Thin to medium

bedding contain a wide variety of sedimentary structures including burrowing or intense bioturbation, ripples, channel scours, soft-sediment deformation, cross-stratification and planar beds, hummocky beds, and rooted zones. The Blackhawk is composed of as many as six members, in ascending order: Spring Canyon, Aberdeen, Kenilworth, Sunnyside, Grassy, and Desert (Cole and others, 2008); only the non-coal bearing Desert Member is present in the eastern Books Cliffs (figure 2.16B). These members form steep slopes and cliffs (i.e., the Book Cliffs).

The Blackhawk Formation was deposited in marginal marine wave-dominated deltaic and beach environments along a coastal plain, with coal swampy areas behind barrier beach or deltaic sands. Facies include prodelta, shoreface, distributary mouth bar and channel, swamp and peat bogs, levees, crevasse spays/overbanks, bays, and coastal plain. The silt-rich lower shoreface and heavily bioturbated middle shoreface facies represent low energy deposition; hummocky bedding in sandstone indicates storm events. The "clean" cross-stratified upper shoreface and planar-bedded foreshore (beach) represent high energy; the tidal range was microtidal. The tops of foreshore sandstone beds are often a distinct white color and rooted with an overlying lower or middle shoreface sandstone representing a flooding event.

Castlegate Sandstone: The Castlegate Sandstone (Campanian) consists of light gray to dark gray, platy, very fine- to coarse-grained quartzose sandstone (figures 2.16B and 2.17), with some conglomerate beds (Weiss and others, 1990). In the eastern Book Cliffs, the Castlegate thins and along with the sandstone contains some siltstone, carbonaceous to non-carbonaceous shale, and lenses of sandy and silty marl (figure 2.16B) (Gualtieri, 1988). Bedding is laminated, thin, to medium and often lenticular, containing cross-stratification, cross-laminations, hummocky beds,

and ripple marks. In the central part of the Book Cliffs, the upper section of the Castlegate is called the Bluecastle Sandstone Member (figure 2.13). However, to the east, what remains of the lower Castlegate is overlain by the Buck Tongue of the Mancos Shale and the Bluecastle Sandstone Member is equivalent to the Neslen Formation (figure 2.13) or lower Farrer Formation (Fouch and others, 1983; Franczyk and others, 1990a; Cole and others, 2008; White and others, 2008). The Castlegate forms vertical cliffs and steep slopes. The contact with the underlying Desert Member of the Blackhawk Formation is a major flooding surface (transgressive surface of erosion) where Castlegate marine shoreface sandstone and shale overlie coal beds (Cole and others, 2005).

The Castlegate Sandstone in the western Book Cliffs represents a classic example of a sand-rich braided stream environment resulting from the continuing erosion of the Sevier orogenic belt to the west (figures 2.17 and 2.18A) (Blakey and Ranney, 2008). In the eastern Book Cliffs the Castlegate transitions into coastal plain/meanderbelt and deltaic/marginal marine environments (figures 2.16B and 2.18A) (Fouch and others, 1991; Cole and others, 2005). These include transitional shoreface, tidally influenced fluvial channels and estuarine facies (Cole and others, 2005).

Sego Sandstone: The Sego Sandstone (Campanian) consists of very light gray to light brown fine-grained sandstone with subordinate beds of sandy to silty shale that display a stacked series of coarsening and thickening upward intervals (figure 2.19) (Cole and others, 2008). Laminated to medium beds are horizontal, cross-laminated, trough and sigmoidal cross-stratification contain a variety of sedimentary structure including ripples, mud drapes, scours, and burrows (Cole and

others, 2008). The contact with the underlying Buck Tongue of the Mancos Shale is gradational (Gualtieri, 1988). The Sego forms cliffs and steep slopes (figures 2.19 and 2.20).

The Sego Sandstone was the last major marginal-marine complex in the Upper Cretaceous represented by a wide variety of depositional facies. These include deep marine, wave-dominated shelf, tidal bar and creek, estuarine distributary channel and fill, fluvial channel, and oyster bioherm (Wood and Dutton, 1999; Cole and others, 2008).

Neslen Formation: The Neslen Formation (Maastrichtian) consists of light brown and light gray, very fine to fine-grained sandstone and medium to dark gray, carbonaceous shale and silty shale, and coal in the lower half of the stratigraphic section (three coal zones were mined during the first half of the 20th century) (Gualtieri, 1988). Bedding is laminated to medium with planar and cross-stratification; the Thompson Canyon Sandstone unit forms a distinct tabular bed in outcrop near the middle of the Neslen. The Neslen generally coarsens upward with increasing channel-form sandstone toward the top of the formation (Cole and others, 2008). The Neslen forms ledges and steep slopes (figure 2.20). The contact with the underlying Sego Sandstone is sharp.

The Neslen Formation was deposited in a variety of depositional facies within a lower coastal plain environment (figure 2.18B). These facies include estuarine, swamp and marsh, meandering channels, and splays (Franczk and others, 1990; Cole and others, 2008; White and others, 2008). Sand bodies represent straight (anastomosed) to moderately or high-sinuosity rivers and distributary channels in wave-dominated deltas (White and others, 2008). The Thompson Canyon Sandstone represents a marginal-marine-strandline deposit.

Farrer Formation: The Farrer Formation (Maastrichtian) consists of gray to brown, fine to upper medium-grained sandstone and greenish-gray silty shale with subordinate amounts of carbonaceous shale in the lower section (Gualtieri, 1988). Bedding is thin to thick, and sandstone beds are commonly well sorted, cross-stratified, ripple laminated, or contorted (Cole and others, 2008). The Farrer Formation is sand-rich in comparison to the underlying Neslsen Formation (figure 2.20) and the contact is gradational. The Farrer forms small cliffs, ledges, and steep slopes.

The Farrer Formation was also deposited in an upper coastal plain to alluvial plain environment but farther west of the seaway (figure 2.18C) and thus the lacks the swamp and marsh facies observed in the underlying Neslen Formation. The Farrer facies include east- and northeast-flowing meandering, low- to moderate-sinuosity fluvial channels and braided streams represented by single and multistoried, sandstone bodies, and associated floodplain deposits with splay sands (Cole and others, 2008; White and others, 2008).

Price River Formation: The Price River Formation (Campanian) consists of a sequence of alternating beds composed of light gray to gray, and grayish-brown to dark gray poorly to fair sorted, fine- to medium-grained sandstone, siltstone, and mudstone, with some beds of conglomerate and conglomeratic sandstone farther west and carbonaceous shale beds to the east (Anderson, 1983; Weiss and others, 1990). The formation is thin bedded to massive, commonly thick bedded, and contains horizontal and cross-stratification, ripple marks, and disseminated carbonaceous material (Anderson, 1983). Sandstone beds in the lower section fine upward, are lenticular, and grade into one another (Anderson, 1983). The Price River forms steep, step-like slopes and ledges generally leading to an uppermost cliff (figure 2.21). Fouch and others (1983)

place an unconformity with in the Price River Formation (figure 2.13), however, it has been well established that a major unconformity separates it from the overlying Maastrichtian-Paleocene North Horn Formation (Hintze and Kowallis, 2009).

The Price River Formation represents northeast flowing sinuous to meandering fluvial deposition over a fluvial braidplain (Lawton, 1986; Hettinger and Kirschbaum, 2002) (figure 2.18C). Alluvial fans to the west as indicated by conglomerates were deposited in close proximity to the eroding Sevier orogenic belt.

Tuscher Formation: The Tuscher Formation (Maastrichtian) consists of brown and gray, well sorted, fine- to medium grained sandstone and greenish-gray silty shale with subordinate conglomerate in the upper most section (Gualtieri, 1988). The Tuscher has a significant higher sand content in comparison from the underlying Farrer Formation, however, in outcrop the contact between the two is often difficult to distinguish (Cole and others, 2008). The Tuscher section is characterized by a series of amalgamated, multi-storied sand bodies separated by thin mudrock beds that form vertical cliffs and small slopes (figure 2.22). These sandstone bodies are typically thick bedded containing low-angle inclined and cross-stratification, ripple laminations, contorted bedding, and scours and channel fills (Cole and others, 2008). The top of the Tuscher is marked by a major unconformity.

The Tuscher Formation was deposited on the upper coastal plain to alluvial braidplain (figure 2.18C). The Tuscher facies are similar to those of the underlying Farrer Formation but more sand-rich. The amalgamated sand bodies represents northeast to southeast flowing, high-energy to low sinuosity braided fluvial systems (Cole and others, 2008; White and others, 2008).

TERTIARY ROCKS

A major regional unconformity is found between the Mesaverde Group and the overlying Tertiary rocks (and the latest Late Cretaceous rocks where they are present [i.e., North Horn Formation]) in eastern Utah (figure 2.13). A transition from the Sevier orogeny to the Laramide orogeny occurred during the Late Cretaceous and early Tertiary, which resulted in the rise of the Uinta Mountains, the Uncompaghre uplift, and the San Rafael Swell, and the coeval subsidence of the UB in eastern Utah. In addition, during earliest Paleocene a depositional trough extended from the western UB to the southwest along the margin of the Sevier orogenic belt and was the site of clastic depositional. These deposits lie unconformably above Cretaceous strata tilted during the last phase of the Sevier orogeny (Hintze and Kowallis, 2009). During much of late Paleocene and Eocene time, the UB and much of central and southern Utah was dominated by freshwater lakes, and associated deltas, with periods of alluvial clastic deposition as the lakes eventually disappeared. The combined thickness of the alluvial and lacustrine Tertiary rocks in the UB ranges from 5000 feet to as great as 10,000 feet in the deepest part the asymmetric basin (Hintze and Kowallis, 2009).

The tight, lenticular sandstone beds within the Paleocene-Eocene Wasatch Formation are gas producers in the eastern UB, however, where naturally fractured and overpressured in the deep, center of the basin, they also produce oil. Fluvial-deltaic sandstone in the Eocene Green River Formation interfingering with carbonate and muddy lacustrine rocks are the major producers of oil in the basin. The organic-rich shale and marl within the Green River provide the source for these oil accumulations in the UB.

North Horn Formation

The North Horn Formation (includes late Maastrichtian but is mainly early Paleocene) consists of tan upward fine- to medium-grained, fining sandstone and reddish-brown and grayish-brown mudstone, with interbedded calcareous siltstone, limestone conglomerate, freshwater limestone (marlstone), and some carbonaceous shale and coal (Anderson, 1983; Weiss and others, 1990). Bedding is thin to medium bedded, and sandstone beds are lenticular, conglomeratic at the base, and laterally discontinuous; some units contain minor amounts of plant detritus or oncolites. The North Horn is divided into three intervals: lower and upper variegated intervals separated by a sandy coal-bearing middle section (Lawton, 1986; Lawton and others, 1993). These sections form steep slopes and ledges (figure 2.23) and thin rapidly east; the North Horn is not present in the eastern half of the UB. In the west part of the basin, the North Horn intertongues with the Flagstaff Limestone to such an extent that the two formations are often mapped as an undivided unit (Witkind, 1988; Weiss and others, 1990).

The Cretaceous-Tertiary boundary (K-T boundary) lies within the middle section of the North Horn Formation. Very late Cretaceous dinosaur bones are found in the lower North Horn and Paleocene mammals have been discovered in the upper section (Spieker, 1946; Anderson, 1983). However, there is no known iridium-rich clay layer to identify this boundary (Myung-Suk and Cross, 1997; Difley and Ekdale, 2002). A distinctive, white (bleached) kaolinite-rich sandstone can be traced throughout much of the formation; U.S. Geological Survey (USGS) geologists suggest this zone as the possible boundary (Weiss and others, 1990).

The North Horn Formation was deposited in a widespread terrestrial, high-energy environment. Facies are represented by fluvial, lacustrine, and floodplain deposits (Lawton, 1986; Lawton and others, 1993). Sediments accumulated in the depositional trough that extended from the western UB to the southwest along the margin of the Sevier orogenic belt (Hintze and Kowallis, 2009). The North Horn is the basal basin-filling deposit in the UB (Fouch, 1976).

Flagstaff Limestone

The Flagstaff Limestone (Paleocene) consists of dark gray to gray, dense limestone interbedded with tan to brown fine- to medium-grained sandstone, marlstone, and variegated mudstone (figure 2.24). Limestone units are thin bedded, and locally very fossiliferous containing freshwater gastropods, pelecypods, and ostracods (Anderson, 1983; Weiss and others, 1990). Some limestone beds, in places, are irregularly layered and contain many "bird's eye" algal nodules (Hintze and Kowallis, 2009). The Flagstaff is best expressed in outcrop as a prominent dip slope capping the Book Cliffs and dips towards the north into the UB. The formation is not presnt in the eastern UB. Its contact with the overlying Colton Formation is marked at the base of the Roan Cliffs.

The Flagstaff Limestone was deposited in a large freshwater lake (Lake Flagstaff) environment that extended from the central part of the UB through central and southwestern Utah. These lacustrine strata were deposited in the same elongated, northeast-southwest trending depositional trough as the North Horn Formation (Hintze and Kowallis, 2009) and included alluvial, marginal lacustrine, and open lacustrine facies. Lenticular sandstone bodies in the

Flagstaff represent fluvial deposits associated with the lake system as clastic material was into the along all of its margins. Clastic deposits gradually displaced Lake Flagstaff northward until all that remained was a crescent-shaped lake, partially within the UB (figure 2.25A) (Fouch, 1975).

Colton Formation

The Colton in the western UB and Wasatch Formations in the eastern part of the basin are equivalent (Paleocene-Eocene) (figure 2.13). The Colton consists of variegated mudstone and shaly siltstone interbedded with yellowish- to grayish-orange and grayish-brown, fine- to medium-grained quartzose sandstone with conglomerate at the base; there are some sparse limestone beds (figure 2.26) (Anderson, 1983; Weiss and others, 1990). Bedding is typically thin and lenticular in sandstone bodies that are cross-stratified and may be bioturbated by non-marine organisms (Anderson, 1983). Channel deposits are sometimes exhumed with outcrops topographically above the surrounding mudstone. The mudstone commonly contain root structures and mudcracks. The Colton forms the western part of the Roan Cliffs along the southern margin of the UB characterized by reddish steep, ledgey slopes and cliffs.

As the Uinta Mountains continued to rise during the late Paleocene and early Eocene, the alluvial Colton and Wasatch Formations began to fill the adjacent subsiding Uinta Basin. Thickness in the basin reaches up to 3200 feet (Hintze and Kowallis, 2009). The Colton is mainly of alluvial origin, but also contains fluvial, deltaic, and marginal lacustrine deposits. It is referred to as the Colton fan-delta which was associated with both freshwater Lake Flagstaff and the later Eocene-age Lake Uinta (figure 1.3) that occupied the UB (Weiss and others, 1990). It

was a large and arcuate delta that built into the lakes from the south-southwest intertonging with the lake sediments (figure 2.25B).

Wasatch Formation

The Colton and Wasatch Formations are often undivided in the UB, but in the central and east parts of the basin the Wasatch is more distinguishable where it consists of red, yellow, and light gray friable sandstone, siltstone, mudstone, conglomerate, and minor interfingering limestone of the Flagstaff Limestone (figure 2.27) (Sprinkel, 2009). Sandstone is moderately well sorted and fine to medium grained. Closely spaced, low permeability lenticular bedding in sandstone bodies represent the principle Tertiary-age, gas-producing reservoirs in the eastern UB, and range in thickness from 5 to 50 feet. They contain ripple lamination, small- to-medium cross-stratification, and horizontal beds (Cole and others, 2008). Conglomerate beds are thin and contain chert and quartzite pebbles (Sprinkel, 2007). A few thin ostradodal limestone (grainstone) beds are also found within the Wasatch. In the eastern UB, the major hiatus between the Wasatch and the underlying Upper Cretaceous Tuscher Formation (described above) is marked at the base of a conglomeratic section or lowest red or gray shale interval (Gualtieri, 1988). The Wasatch forms steep slopes, ledges, and small cliffs. It thin east where in onlaps the Douglas Creek arch along the Utah-Colorado border.

The Wasatch Formation was deposited predominantly in a non-lacustrine alluvial plain environment significantly beyond the margins of Lakes Flagstaff and Uinta (figure 2.25B) (Fouch, 1975; Ryder and others, 1976). This alluvial plain included fluvial channels, overbanks, and small lakes and ponds. Channel were eventually sand-filled channels and often encased by

thin clay creating small traps for hydrocarbons suppled later when regional fracturing provided migration pathways from Cretaceous source rocks below.

Green River Formation

The lacustrine Eocene Green River Formation is the primary oil producer in the UB (figure 1.1). It contains the oil source beds, seals, and a variety of reservoir facies and stratigraphic traps for major accumulations of oil (figure 1.4). Deep oil traps are overpressured and naturally fractured whereas shallower traps are normal pressure and require major hydraulic fracturing techniques, waterflooding programs, and/or horizintal drilling. The oils produced are high in paraffin (black or yellow wax) and require special wellsite and transportation infrastructure.

The Green River Formation consists of as much as 6000 feet of sedimentary strata (Hintze and Kowallis, 2009; Sprinkel, 2009). The stratigraphy is complex and there are many different unit names and marker beds that are in the literature or used by industry for decades (see Fouch, 1975, 1976; Ryder and others, 1976; Fouch and others, 1992; Morgan and others, 2003, and the references pertaining to Green River nomenclature therein); describing and explaining these are beyond the scope of this discussion but we provide a general summation in figure 2.28. The signature of each marker bed on wireline well logs is used to identify and correlate units in the subsurface throughout much of the basin. Briefly, the Wasatch Formation grades into and intertongues with the Green River Formation in the UB forming the Green River-Wasatch Formation Transition unit (Sprinkel, 2009). In general, the lower member, that is not always present, consists of the basal Uteland Butte limestone and overlying carbonate marker

unit (sometimes referred to as the black shale facies) (figure 2.28). The lower and middle members are separated by the Carbonate Marker bed and interfinger in the subsurface. The middle member is called the Douglas Creek Member in most maps and publications and contains the what is referred to as the "Delta Facies" and Green Shale Facies" (figure 2.28). The middle and upper members of the Green River are separated by the C Marker bed. The upper member, named the Parachute Creek Member, contains the famous Mahogany oil shale bed (zone) above the "Transitional Facies" (figure 2.28). The Parachute Creek intertongues with the overlying Uinta Formation, having an irregular contact where bedding is contorted due to soft-sediment deformation.

In the lower member, the basal Uteland Butte limestone ranges in thickness from less than 60 feet to more than 200 feet and consists of limestone, dolomite, organic-rich calcareous mudstone, siltstone, and rare sandstone (figures 2.29A). Recent tight-oil horizontal drilling and exploration activities in the UB are targeting relatively thin porous carbonate beds of the Uteland Butte, particularly in an area referred to as the "Central Basin region" between Altamont-Bluebell field to the north and Monument Butte field to the south (figure 1.1). The Uteland Butte has historically been a secondary oil objective of wells tapping shallower overlying Green River reservoirs and deeper fluvial-lacustrine Colton Formation sandstone units in the western UB. The dolomite, the horizontal drilling target, often has more than 20% porosity, but is so finely crystalline that the permeability is very low. The Uteland Butte is separated from the upper section by a tongue of the Colton Formation. The upper section of the lower Green River consists of light brown to light gray, fissle shale and limestone or marl. Limestone beds are lensoid and contain ostracods and algal laminae (Weiss and others, 1990). The lower member forms steep slopes, ledges, and small cliffs.

The Douglas Creek Member (or middle member) consists of light- to medium-gray, light- to medium-brown, yellow, and light-gray siltstone, sandstone, shale, chert, and limestone (Weiss and others, 1990; Gualtieri, 1988; Sprinkel, 2009). Thick sections of sandstone dominate in the south-central part of the UB as seen in Ninemile Canyon (figure 2.29B) are represent the main producing reservoirs in the Monument Butte field area in the subsurface to the north (figure 1.1). The Douglas Creek is dominated by shallowing-upward sequences of mudstones, siltstones, and sandstones often gradually transitioning to well-developed microbial carbonate intervals, topped by erosional flooding surfaces. Sandstone is generally fine-grained, moderately to well-sorted, thin to thick bedded, discontinuous, lenticular and channel form, and contain cross-stratification to planar beds, ripple marks, and scours. Limestone is consists of boundstone, rudstone, grainstone, packstone, wackestone, and mudstone carbonate fabrics. Constiuent carbonate grains includes ooids, pisoids, peloids, oncoids, coated grains, skeletal material especially ostracods and/or storm-generated carbonate rip-up clasts. Microbial carbonates include both stromatolites and thrombolites (clotted) that developed on a grainstone substrate (figure 2.29C) (Chidsey and others, 2015). The member also contains some thin bluish-gray to dark brown oil shale. The Douglas Creek forms large vertical cliffs, ledges, and steep slopes.

The Parachute Creek Member (or upper member) consists of moderately resistant, light- to medium-gray, light- to medium-brown, yellow, shale, marlstone and limestone, siltstone, and sandstone (Weiss and others, 1990; Gualtieri, 1988; Sprinkel, 2009). The lower Parachute Creek records fully carbonate-dominated shallowing-upward sequences, with carbonate mudstones transitioning to dolomitic microbial carbonates, again topped by an erosional flooding surface (Chidsey and others, 2015). Carbonates are similar to those in the underlying Douglas Creek Member dominated by oolites and microbialites. Both marlstone and shale can be dark brown,

organic-rich that include several oil shale beds, the most significant being the Mahogany oil-shale zone (figure 2.29D). Sandstone is very fine to medium-grained, thin- to thick-bedded containing cross-laminations and ripple marks (Gualtieri, 1988). The Parachute Creek also contains tuff beds that have been dated and pods of the evaporite mineral nachcolite that, in some places, have been leached leaving dissolution cavities (Sprinkel, 2009); i.e, the "Birds Nest" aquifer (figure 2.29E) discussed in later chapters. The Parachute Creek forms steep slopes, cliffs, and ledges.

The Green River Formation was deposited in marginal lacustrine and lacustrine environments, associated with an areally extensive, shallow, saline to freshwater lake (Lake Uinta) in the subsiding UB (figures 1.3 and 2.30). The Green River contains three major depositional facies associated with Lake Uinta sedimentation: alluvial, marginal lacustrine, and open lacustrine (figure 2.25C) (Fouch, 1975). The Uteland Butte records the first major transgression of Eocene Lake Uinta after the deposition of the alluvial Colton Formation, and thus it is relatively widespread in the basin. The marginal lacustrine facies, where most of the hydrocarbon production is found, consists of fluvial-deltaic, interdeltaic, and carbonate flat deposits (figures 2.29B and 2.30), including microbialites. These deposits changed as the lake shoreline shifted rapidly in response to sediment input and lake-level fluctuations (figure 2.30). The Uinta Mountains were the source for the sediments in the northern portion of Lake Uinta while sediments in the southern portion of the lake were sourced from the much larger Four Corners area. The open-lacustrine facies is represented by nearshore and deeper water offshore muds, including the Mahogany oil shale zone, which represents Lake Uinta's highest water level. Lake Uinta existed for about 13 million years and at at its maximum extended into northwest Colorado (Weiss and others, 1990). As climate changed during the late middle to early late

Eocene, Lake Uinta began to shink in size creating hypersaline conditions, similar to the modern Great Salt Lake in northern Utah, and now expressed by the evaporite minerals found in the upper Parachute Creek Member (figure 2.29E).

Uinta Formation

The Eocene Uinta Formation is exposed extensively throughout the UB (figure 2.1, plate 1). The Uinta, in places, is divided into lower, middle, and upper members (Members A, B, and C of Sprinkel (2007, 2009). Member A consists of yellowish-gray and yellowish-brown, very fine to fine-grained sandstone and siltstone, with minor conglomerate, shale, marlstone, and tuffaceous interbeds. It forms resistant ledges and cliffs. The member B consists of light gray, light greenish-gray, light-brown, and light-purple, mudstone and claystone, with interbeds of greenish-gray, yellow, and brown fine-grained sandstone, and minor conglomerate and tuffaceous beds. It forms slopes and thin ledges. Member B contains gilsonite beds which are mined in the eastern UB (Boden and Tripp, 2012). Member C consists of soft, light gray, greenish-gray, white, grayish-purple, red, and pale-yellow, shale, mudstone, claystone, and minor sandstone with local tuffaceous interbeds. It forms classic badland topography (figure 2.31).

The Uinta Formation represents sediments from the east and northeast that filled the UB as Lake Uinta waned and withdrew to the west (Weiss and others, 1990). The Uinta was deposited primarily in fluvial environments, but it also contains some marginal lacustrine deposits near the base.

Duchesne River Formation

The Duchesne River Formation, like the Uinta Formation, is widely exposed throughout the UB (figure 2.1, plate 1) and characterized by its dominant red color (figure 2.32). The basal part of the Duchesne River intertongues with the underlying Uinta. However, it lies unconformably on beds of the Green River Formation in certain areas. The Duchesne River has four members, inscending order: Brennan Basin, Dry Gulch Creek, Lapoint, and Starr Flat. Lower members of the Duchesne River are Eocene age and the upper members are Eocene to Oligocene age (Sprinkel, 2007). The basal Eocene Brennan Basin Member consists of light- to medium-red, light reddish-brown, and yellowish-gray, fine- to medium-grained lithic sandstone and siltstone, with minor amounts of mudstone and conglomerate; it also contains well-developed paleosols. The overlying Eocene Dry Gulch Creek consists of medium reddish-brown and purplish-gray, fine-grained sandstone, siltstone, mudstone, and conglomerate. The Eocene-Oligocene Lapoint consists of light reddish-brown and yellowish-gray, fine-grained sandstone, siltstone, and mudstone, with abundant light-greenish-gray bentonite beds. The Oligocene aged Starr Flat consists of reddish-brown, reddish-purple, yellowish-gray, and greenish-gray, fine- to coarse-grained sandstone, siltstone, mudstone, and conglomerate. It is dominated by thick-bedded sandstone that coarsen upward. The Starr Flat is correlative to, and may be part of, the Bishop Conglomerate due to its similar stratigraphic relation and age (Sprinkel, 2007). Overall the Duchesne River is very thin to medium bedded containing lenticular, channel form sand bodies. The Duchesne River forms ledges, small cliffs, and slopes that produce badland topography in some areas.

The Duchesne River Formation was deposited mainly in a fluvial environment as the UB continues to fill with sediment during the late Eocene and Oligocene. It contains a diverse assemblage of late Eocene age vertebrate fossils in the lower members.

QUATERNARY DEPOSITS

Quaternary deposits are widespread in the UB (figure 2.1, plate 1) and make of the shallow groundwater aquifers. The beginning of the Quaternary in the Colorado Plateau is characterized by the development of stream and river drainage patterns across the lower elevations of the landscape and glaciers forming at higher elevations. The deposits are mostly unconsolidated and vary in thickness depending on depositional environment. The most common Quaternary materials are alluvial-fluvial deposits, but colluvial, glacial, eolian, landslide, and debris-flow deposits occur as well and are mixed with alluvial-fluvial deposits in places.

Glaciation was extensive in the Uinta Mountains during the Pleistocene, and the mountains were covered by Utah's most extensive ice cap. Large amounts of glacial till and outwash from melting glaciers were deposited on the southern flanks of the Uinta Mountains and the northern boundary of the UB (figure 2.1, plate 1). Till deposits generally consist of unconsolidated, poorly sorted, angular to rounded boulders, cobbles, and pebbles of mostly red sandstone and quartzite sourced from the Precambrian Uinta Mountain Group. Outwash deposits generally consist of unconsolidated, well-rounded, boulders to pebbles and sand composed of

mostly red sandstone and quartzite also sourced from the Uinta Mountain Group (Sprinkel, 2006).

Pleistocene and Holocene alluvial fan deposits occur adjacent to uplands where there is periodic heavy rainfall, and they generally consist of unconsolidated, poorly sorted boulder, gravel, sand, and silt material. Pleistocene alluvial-fluvial and Holocene fluvial terrace deposits occur along major drainages and generally consist of unconsolidated to locally cemented silt, sand, gravel, cobbles, and boulders. Holocene fluvial stream channel and floodplain sediments consist of unconsolidated, moderately sorted, silt, sand, gravel, and cobbles deposited along both major and minor drainages. Extensive surficial sand dunes produced by wind action are present in wide, flat valley areas. Landslide and slump deposits occur in formations prone to slope failure. Debris-flow deposits occur in major drainages and consist of unconsolidated and poorly sorted heterogeneous mixture of boulders, cobbles, gravel, sand, silt, and mud. Rocks in these Quaternary deposits are mainly composed of sandstones, quartzites, and limestones derived from local bedrock or the Uinta Mountains.

CHAPTER II FIGURES

Figure 2.1. Generalized geologic map of the Uinta Basin and surrounding areas with simplified north-south cross section (modified from Hintze, 1975). Seismic line shown on figure 3.2; cross section B-B' shown on figure 3.3.

Figure 2.2. Eolian, cross-stratified Upper Triassic-Lower Jurassic Wingate Sandstone, Glen Canyon Group; northern San Rafael Swell. Photograph by Michael Chidsey, Sqwak Productions Inc.

Figure 2.3. Lenticular sandstone beds representing the sandy braided steam environment of the Lower Jurassic Kayenta Formation, Glen Canyon Group; northern San Rafael Swell. Photograph by Michael Chidsey, Sqwak Productions Inc.

Figure 2.4. Outcrop of the Lower Jurassic Navajo Sandstone displaying spectacular eolian trough cross-stratification representing multiple dune sets; dune foreset beds indicate paleowind directions were dominantly from the north and northwest; northern San Rafael Swell. Photograph by Michael Chidsey, Sqwak Productions Inc.

Figure 2.5. Excellent exposure of Middle Jurassic Carmel Formation, San Rafael Group, west flank of the San Rafael Swell, Devils Canyon south of Interstate 70 (I-70), view to the east. The Co-op Creek, Crystal Creek, Paria River, and part of the Winsor Members are shown. The Carmel is in direct contact with the underlying Navajo Sandstone represented by the J-1 unconformity. Photograph by Michael Chidsey, Sqwak Productions Inc.

Figure 2.6. Two representative facies in the Middle Jurassic Entrada Sandstone, San Rafael Group. A – Orange-brown, red-brown, or light brown sandstone, siltstone, and mudstone, deposited in broad, mud-dominated intertidal and subtidal zones, supratidal sabkha mudflats and ponds; view to the northwest on west flank of the San Rafael Swell south of I-70. B – Mudstone

and medium-grained, cross-stratified sandstone representing tidal flats and coastal dunes; view to the southeast on the east flank of the San Rafael Swell north of I-70. Photographs by Michael Chidsey, Sqwak Productions Inc.

Figure 2.7. Typical greenish colored, thin- to thick-bedded, shallow marine sandstone of the Middle Jurassic Curtis Formation, San Rafael Group; west flank of the San Rafael Swell along I-70, view west. Note this person is standing on a thin sandstone bed containing trough cross-stratification representing a possible migrating sand bar. Photograph by Michael Chidsey, Sqwak Productions Inc.

Figure 2.8. Tidal flat and sabkha siltstone, mudstone, and sandstone of the Middle Jurassic Summerville Formation, San Rafael Group; west flank of the San Rafael Swell along I-70, view north. The contact with the underlying Curtis Formation is conformable and gradational. Photograph by Michael Chidsey, Sqwak Productions Inc.

Figure 2.9. Fluvial channel sandstone of the Salt Wash Member and pastel-colored floodplain mudstone and shale of the Brushy Basin Member, Upper Jurassic Morrison Formation; west flank of the San Rafael Swell along I-70, view northeast. Photograph by Michael Chidsey, Sqwak Productions Inc.

Figure 2.10. Representative outcrops of the Lower to lower Upper Cretaceous Cedar Mountain Formation; west flank of the San Rafael Swell along I-70, view north. A – Floodplain and fluvial channel deposits of the Ruby Ranch and Mussentuchit Members (separated by an

unconformity) capped by the Upper Cretaceous Dakota Formation. B – Basal, and often discontinuous, Buckhorn Conglomerate Member overlying the Brushy Basin Member of the Upper Jurassic Morrison. The contact is marked by the K-0 unconformity. Inset is a close up of typical Buckhorn conglomerate consisting of pebbles and cobbles composed of poorly to moderately sorted, subangular to well-rounded clasts of white quartzite, and black, brown, light brown, and light gray chert. Photographs by Michael Chidsey, Sqwak Productions Inc.

Figure 2.11. Typical exposures of Upper Cretaceous Dakota Formation; west flank of the San Rafael Swell along I-70, view north. Photograph by Michael Chidsey, Sqwak Productions Inc.

Figure 2.12. Typical exposures of the brownish Upper Cretaceous Dakota, silver gray Mowry Shale, and overlying brownish slope and cliff of the Frontier Sandstone along U.S. 191 east of Steinaker Reservoir near Vernal, Utah. The Dakota consists of basal and upper sandstone units separated by a middle carbonaceous mudstone. The Frontier consist of a slope-forming zone of calcareous shale, silty shale, and whereas the upper part is composed of fine-grained sandstone that forms the prominent cliff (from Sprinkel and others, 2012).

Figure 2.13. Chronostratigraphic chart for Late Cretaceous-Paleogene strata in the Book Cliffs-Wasatch Plateau region (modified from Fouch and others, 1983; Franczyk and others, 1990a; White and others, 2008).

Figure 2.14. Classic outcrop of the Tununk Shale Member of the Mancos Shale composed of soft and deeply weathered slopes and low, rounded hills devoid of vegetation, and small vertical

cliffs; west flank of the San Rafael Swell near I-70, view to the northwest. Photograph by Michael Chidsey, Sqwak Productions Inc.

Figure 2.15. The Tununk Shale and Ferron Sandstone Members of the Upper Cretaceous Mancos Shale along the west flank of the San Rafael Swell near I-70, view to the east. Photograph by Michael Chidsey, Sqwak Productions Inc.

Figure 2.16. Blackhawk Formation outcrops in the Book Cliffs. A – Typical section of the Blackhawk Formation showing shoreface sandstone beds and coal. B – The Desert Member of the Blackhawk Formation overlying the Mancos Shale and underlying the Castlegate Sandstone in the eastern Book Cliffs. Note all other members of the formation are missing as well as any coal beds. The Castlegate consists of shoreface, fluvial, and estuarine facies.

Figure 2.17. Castlegate Sandstone outcrop showing classic sand-rich braided stream facies, western Book Cliffs.

Figure 2.18. Paleogeography of the Uinta Basin during the late Campanian through Maastrichtian time (modified from Fouch, 1975; Fouch and others, 1992). A – Deposition of the coastal plain/meanderbelt and deltaic/marginal marine environments of the Castlegate Sandstone. B – Deposition of the Neslen Formation in a coastal plain environment. C – Deposition of the Farrer and Tuscher Formations in an alluvial plain environment.

Figure 2.19. Outcrop of coarsening upward lower Sego Sandstone in gradational contact with the Buck Tongue of the Mancos Shale, eastern Book Cliffs (Sego Canyon).

Figure 2.20. Stratigraphic section in Sego Canyon, eastern Book Cliffs, showing, in ascending order, Sego Sandstone, Neslen Formation, and Farrer Formation; view west.

Figure 2.21. Representative outcrop of fluvial siltstone and sandstone in the Upper Cretaceous Price River Formation along the Green River, Desolation Canyon; view east. From Morgan, 2003a; photo by Logan MacMillan.

Figure 2.22. Representative outcrop of stacked amalgamated sandstone bodies of the Tuscher Formation, eastern Book Cliffs (Sego Canyon); view northwest.

Figure 2.23. Representative outcrop of fluvial siltstone and sandstone in the late Upper Cretaceous-early Paleocene North Horn Formation, Soldier Canyon, Book Cliffs; view east. From Morgan, 2003a.

Figure 2.24. Representative outcrop of the Paleocene Flagstaff Limestone, Price River Canyon, Book Cliffs; view south.

Figure 2.25. Paleogeography of the Uinta Basin during the Paleocene through Eocene time (modified from Fouch, 1975; Fouch and others, 1992). A – Deposition in lacustrine and marginal lacustrine environments during the waning stages of Lake Flagstaff, i.e., the Flagstaff

Limestone. B – Deposition of the alluvial Colton (Colton fan-delta) laterally equivalent Wasatch Formation during the late Paleocene and early Eocene. C – Deposition of the Green River Formation in open lake and marginal lacustrine environments during deposition of the Douglas Creek Member (middle member).

Figure 2.26. Paleocene-Eocene Colton Formation forming the western part of the Roan Cliffs.

Figure 2.27. Paleocene-Eocene Wasatch Formation, Hells Hole area, southeastern Uinta Basin. From Cole and others, 2008; photo by Rex Cole.

Figure 2.28. General stratigraphy and major marker beds of the Green River Formation in the Uinta Basin (not to scale).

Figure 2.29. Representative outcrops of the Eocene Green River Formation. A – Fresh road cut exposure of Uteland Butte limestone consisting of interbedded dolomite and mudstone/limestone, Nine Mile Canyon, southern Uinta Basin; view north. B – Depositional sequence of carbonate, green shale, and fluvial-deltaic sandstone sandstone cycles, Douglas Creek Member, Nine Mile Canyon; view north. C – A typical microbialite interval and associated facies, Hells Hole area, eastern Uinta Basin. The light tan interval near the base is composed of pisoids and oncoids (as a grainstone/rudstone). The tan beds beneath the hammer are stomatolitic, whereas a thrombolite dominates the area to the right of the hammer. D – Mahogany oil shale zone, Parachute Creek Member, Evacuation Creek area, eastern Uinta Basin; view west. E –The “Birds Nest” aquifer zone with nahcolite cavities in the upper Parachute

Creek Member, representing the hypersaline conditions during the waning stage of Lake Uinta, Evacuation Creek, eastern Uinta Basin; view north.

Figure 2.30. Generalized depositional setting for Lake Uinta: (A) high-lake levels, and (B) low-lake levels. From Morgan and others (2003).

Figure 2.31. Badland topography formed in the C member of the Eocene Uinta Formation about 30 miles southeast of Vernal, Utah. Photo by Doug Sprinkel, UGS.

Figure 2.32. Representive outcrop of the Eocene Duchesne River Formation along a meander of the Green River near Horseshoe Bend about 12 miles south of Vernal, Utah. The Duchesne River Formation was deposited by a fluvial system, possibly similar to the modern Green River providing an example of ancient and modern fluvial environments. Photo by Doug Sprinkel, UGS.

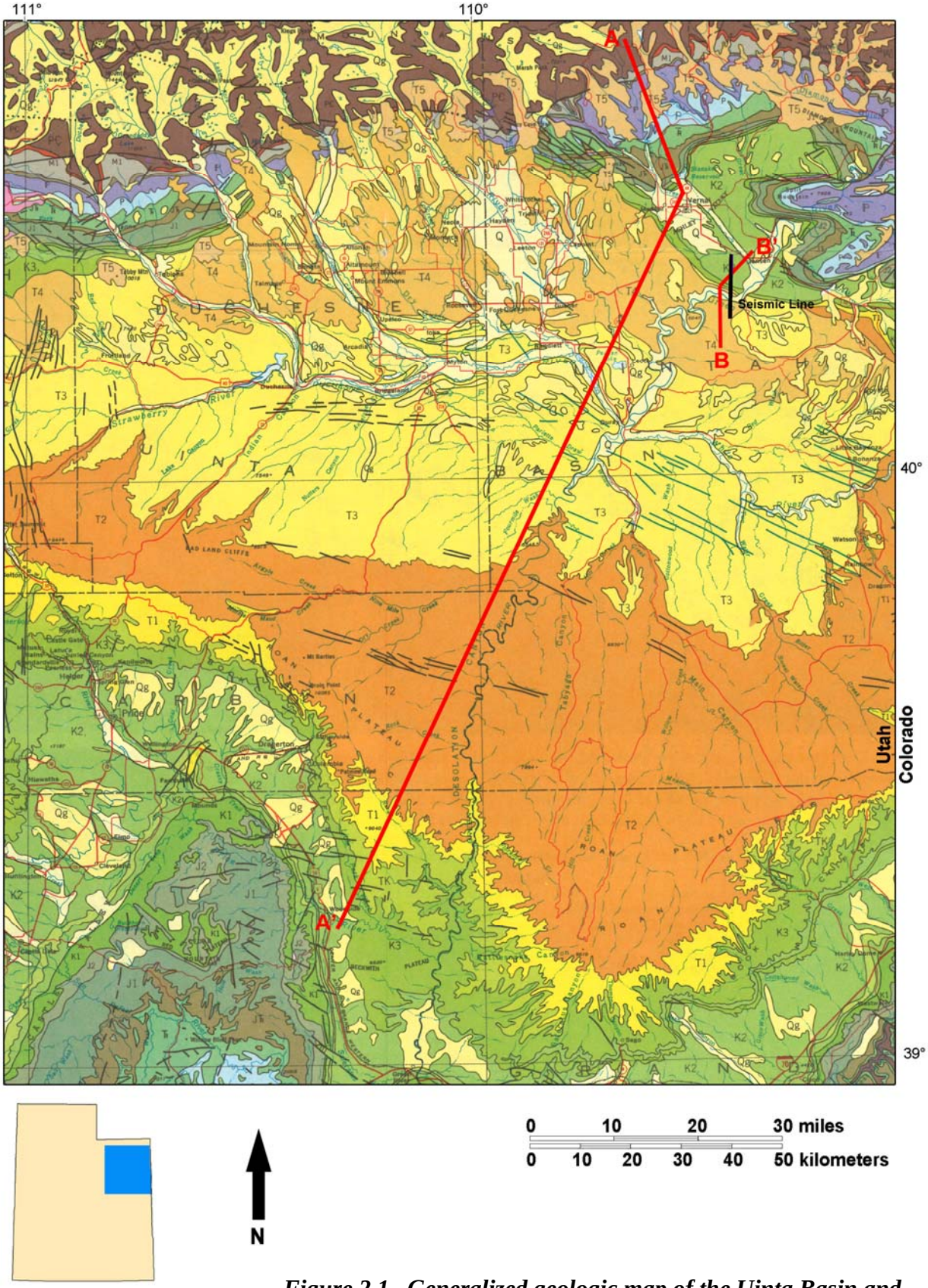

Figure 2.1. Generalized geologic map of the Uinta Basin and surrounding areas with simplified north-south cross section (modified from Hintze, 1975). Seismic line shown on figure 3.2; cross section B-B' shown on figure 3.3.

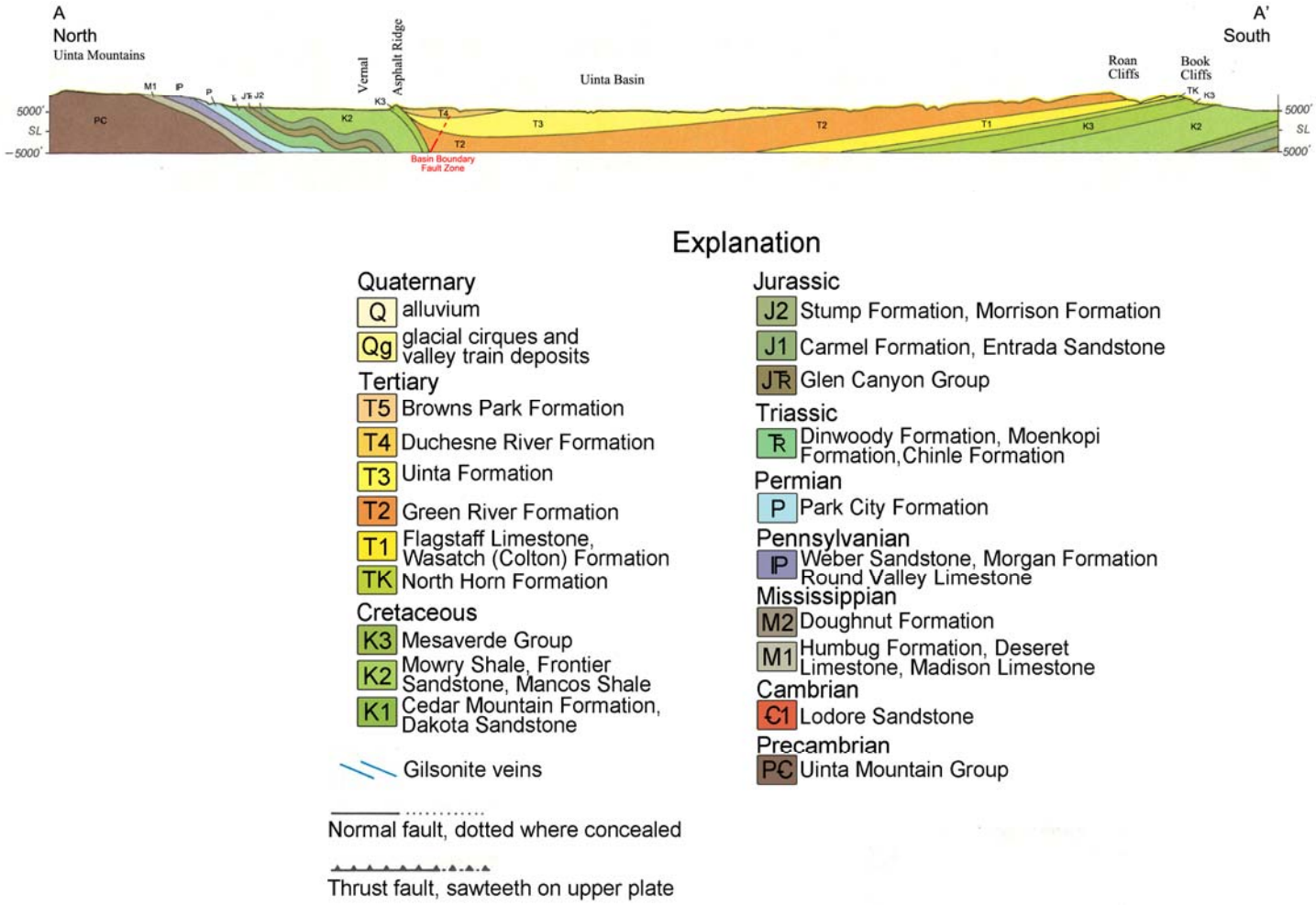

Figure 2.1 continued. Generalized geologic map of the Uinta Basin and surrounding areas with simplified north-south cross section. Modified from Hintze, 1975.

Figure 2.2. Eolian, cross-stratified Upper Triassic-Lower Jurassic Wingate Sandstone, Glen Canyon Group; northern San Rafael Swell. Photograph by Michael Chidsey, Sqwak Productions Inc.

Figure 2.3. Lenticular sandstone beds representing the sandy braided steam environment of the Lower Jurassic Kayenta Formation, Glen Canyon Group; northern San Rafael Swell. Photograph by Michael Chidsey, Sqwak Productions Inc.

Figure 2.4. Outcrop of the Lower Jurassic Navajo Sandstone displaying spectacular eolian trough cross-stratification representing multiple dune sets; dune foreset beds indicate paleowind directions were dominantly from the north and northwest; northern San Rafael Swell. Photograph by Michael Chidsey, Sqwak Productions Inc.

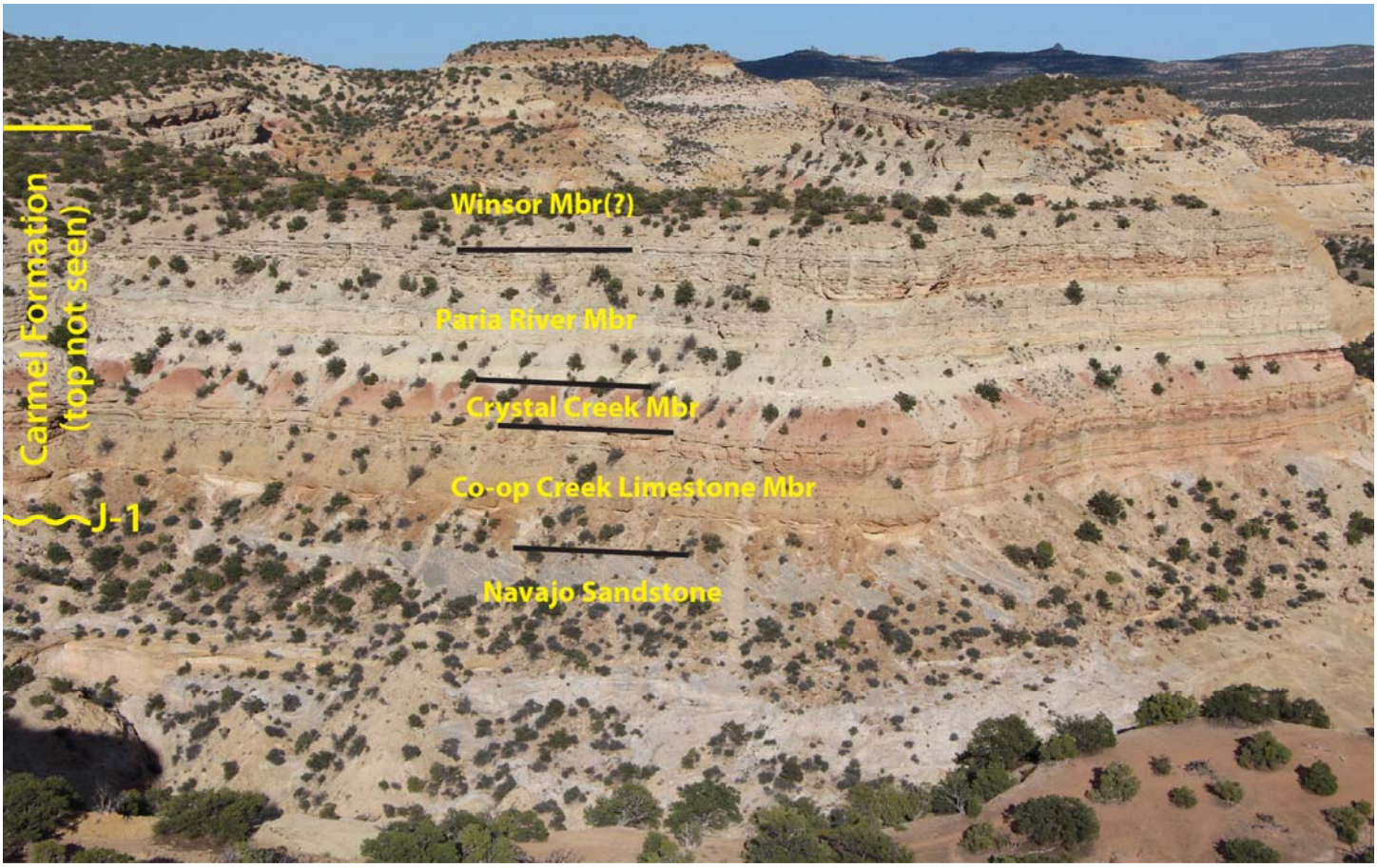

Figure 2.5. Excellent exposure of Middle Jurassic Carmel Formation, San Rafael Group, west flank of the San Rafael Swell, Devils Canyon south of Interstate 70 (I-70), view to the east. The Co-op Creek, Crystal Creek, Paria River, and part of the Winsor Members are shown. The Carmel is in direct contact with the underlying Navajo Sandstone represented by the J-1 unconformity. Photograph by Michael Chidsey, Sqwak Productions Inc.

Figure 2.6. Two representative facies in the Middle Jurassic Entrada Sandstone, San Rafael Group. A – Orange-brown, red-brown, or light brown sandstone, siltstone, and mudstone, deposited in broad, mud-dominated intertidal and subtidal zones, supratidal sabkha mudflats and ponds; view to the northwest on west flank of the San Rafael Swell south of I-70. B – Mudstone and medium-grained, cross-stratified sandstone representing tidal flats and coastal dunes; view to the southeast on the east flank of the San Rafael Swell north of I-70. Photographs by Michael Chidsey, Sqwak Productions Inc.

Figure 2.7. Typical greenish colored, thin- to thick-bedded, shallow marine sandstone of the Middle Jurassic Curtis Formation, San Rafael Group; west flank of the San Rafael Swell along I-70, view west. Note this person is standing on a thin sandstone bed containing trough cross-stratification representing a possible migrating sand bar. Photograph by Michael Chidsey, Sqwak Productions Inc.

Figure 2.8. Tidal flat and sabkha siltstone, mudstone, and sandstone of the Middle Jurassic Summerville Formation, San Rafael Group; west flank of the San Rafael Swell along I-70, view north. The contact with the underlying Curtis Formation is conformable and gradational. Photograph by Michael Chidsey, Sqwak Productions Inc.

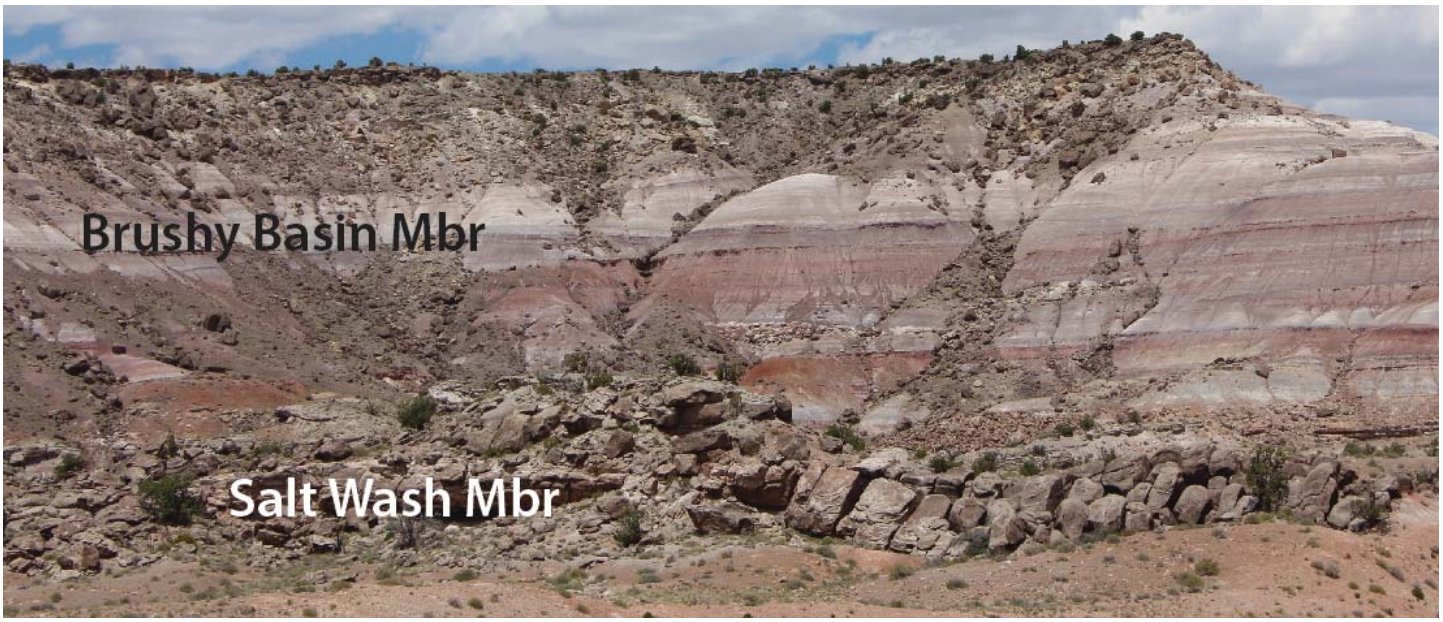

Figure 2.9. Fluvial channel sandstone of the Salt Wash Member and pastel-colored floodplain mudstone and shale of the Brushy Basin Member, Upper Jurassic Morrison Formation; west flank of the San Rafael Swell along I-70, view northeast. Photograph by Michael Chidsey, Sqwak Productions Inc.

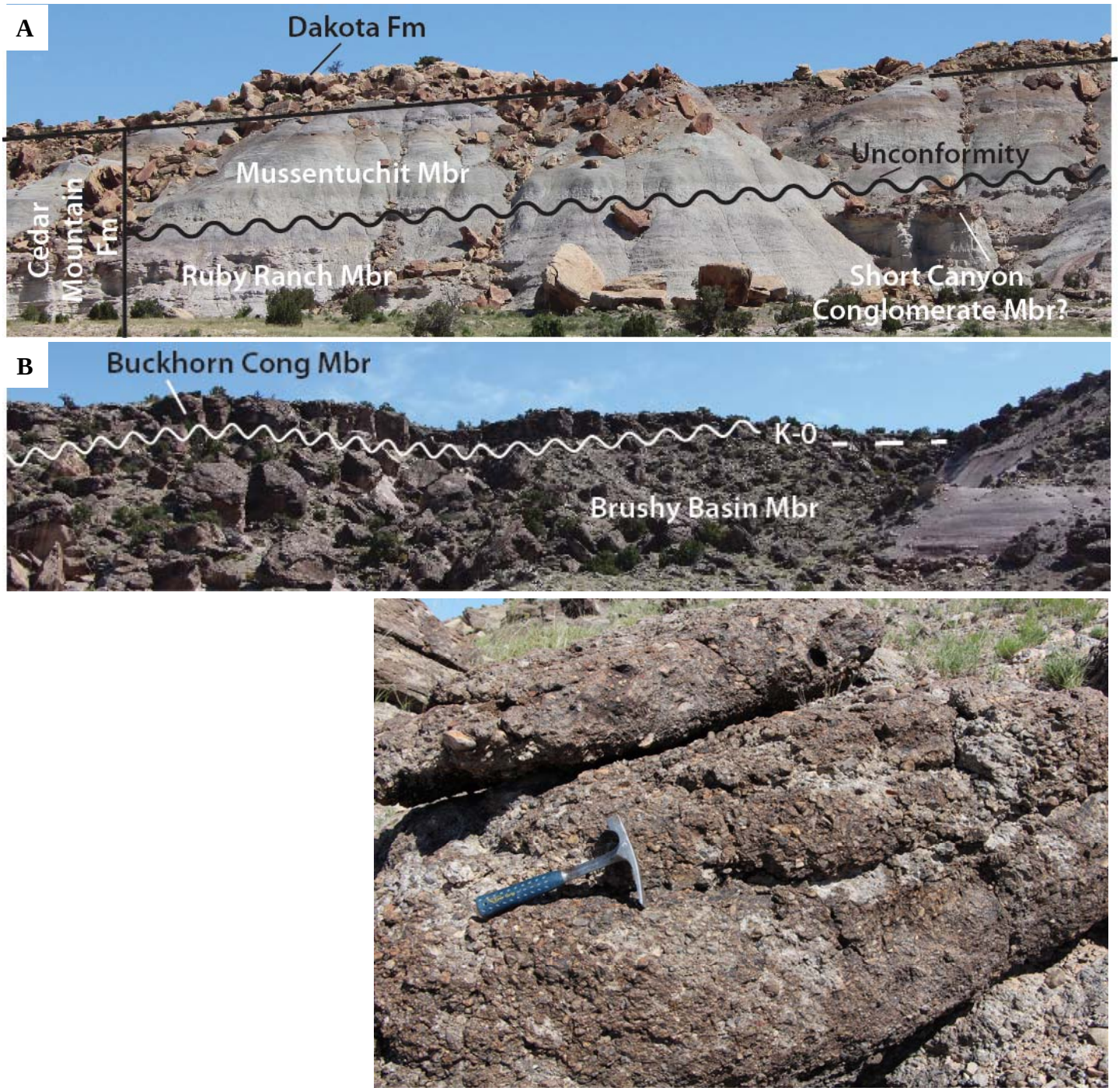

Figure 2.10. Representative outcrops of the Lower to lower Upper Cretaceous Cedar Mountain Formation; west flank of the San Rafael Swell along I-70, view north. A – Floodplain and fluvial channel deposits of the Ruby Ranch and Mussentuchit Members (separated by an unconformity) capped by the Upper Cretaceous Dakota Formation. B – Basal, and often discontinuous, Buckhorn Conglomerate Member overlying the Brushy Basin Member of the Upper Jurassic Morrison. The contact is marked by the K-0 unconformity. Inset is a close up of typical Buckhorn conglomerate consisting of pebbles and cobbles composed of poorly to moderately sorted, subangular to well-rounded clasts of white quartzite, and black, brown, light brown, and light gray chert. Photographs by Michael Chidsey, Sqwak Productions Inc.

Figure 2.11. Typical exposures of Upper Cretaceous Dakota Formation; west flank of the San Rafael Swell along I-70, view north. Photograph by Michael Chidsey, Sqwak Productions Inc.

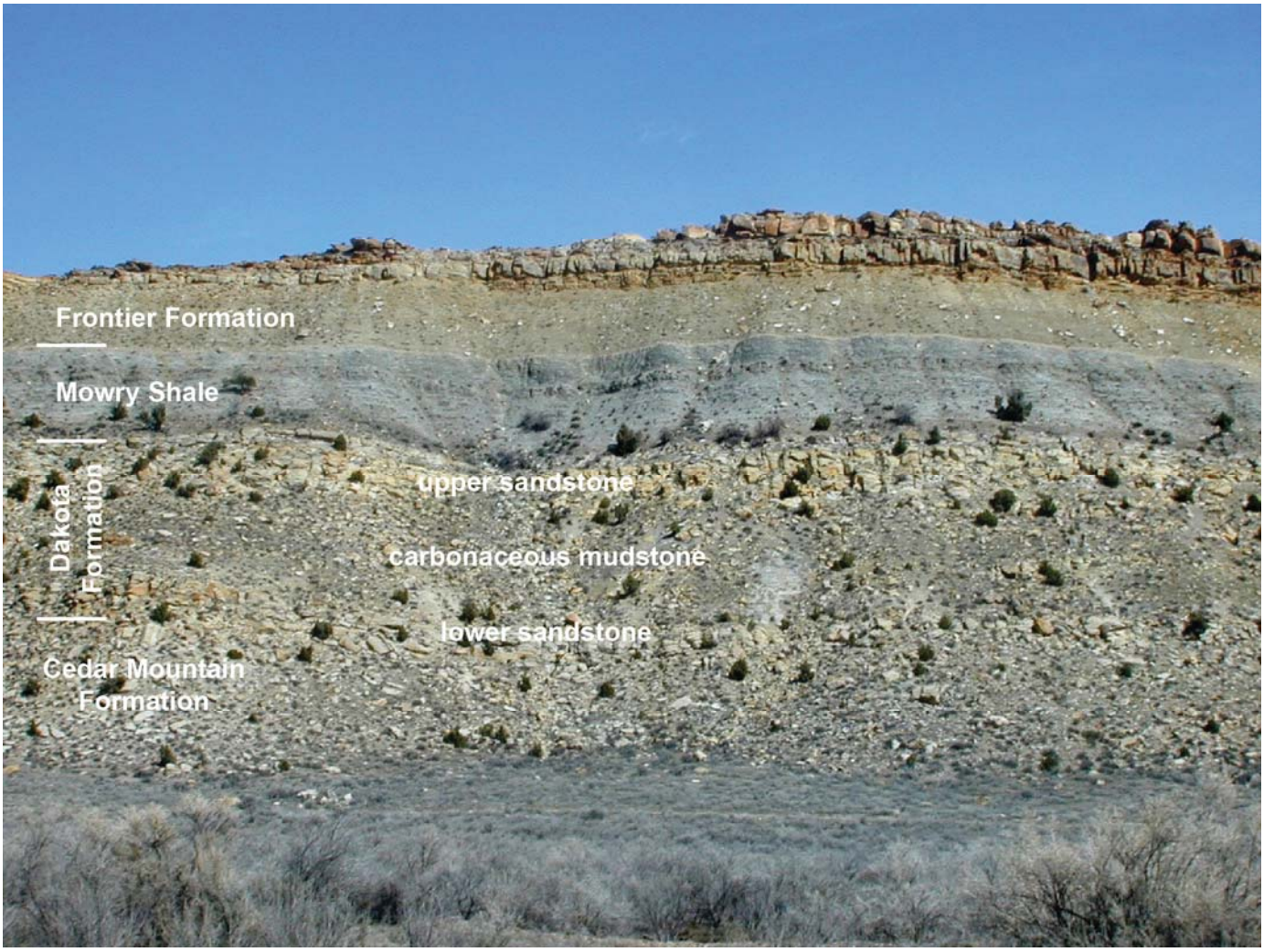

Figure 2.12. Typical exposures of the brownish Upper Cretaceous Dakota, silver gray Mowry Shale, and overlying brownish slope and cliff of the Frontier Sandstone along U.S. 191 east of Steinaker Reservoir near Vernal, Utah. The Dakota consists of basal and upper sandstone units separated by a middle carbonaceous mudstone. The Frontier consist of a slope-forming zone of calcareous shale, silty shale, and whereas the upper part is composed of fine-grained sandstone that forms the prominent cliff (from Sprinkel and others, 2012).

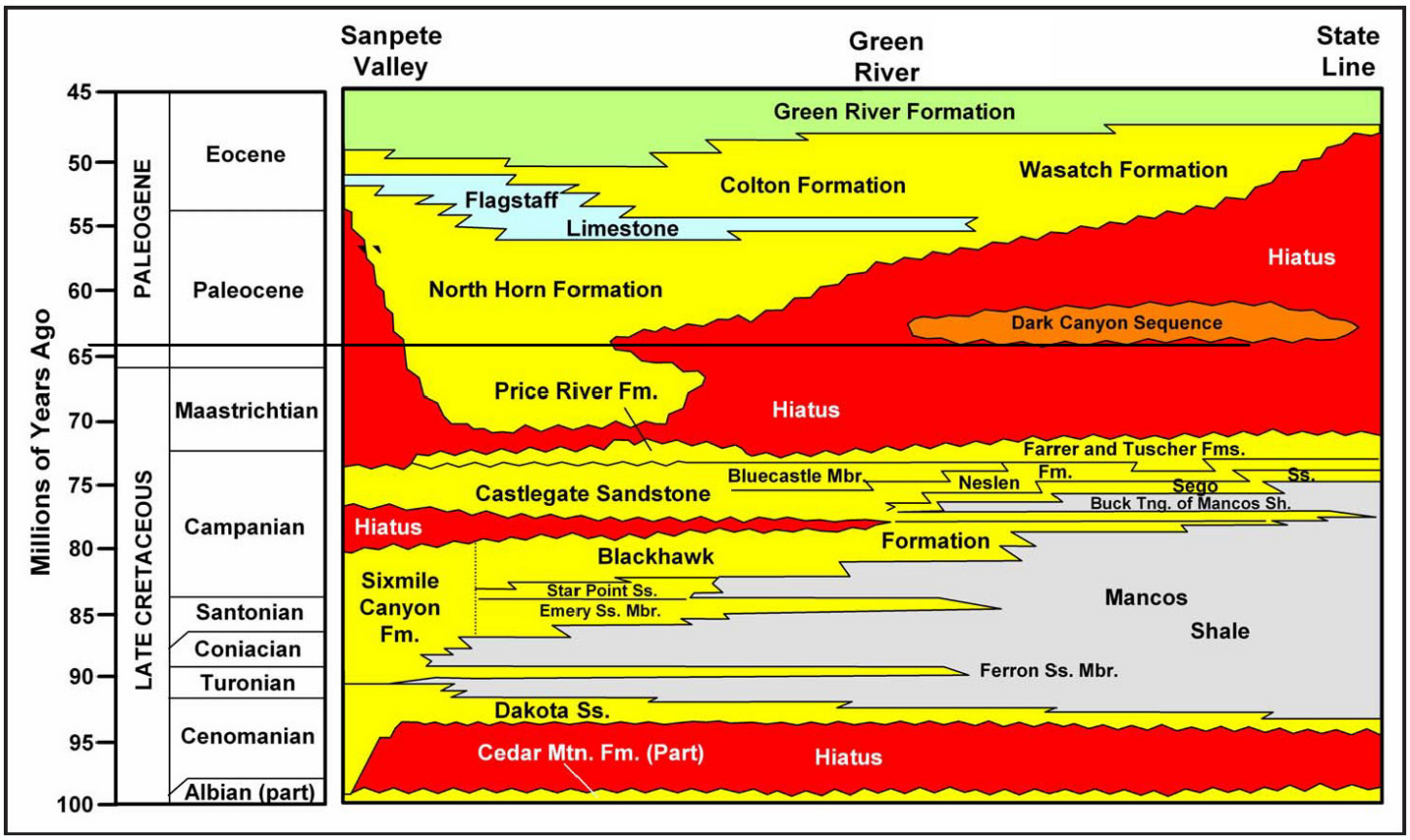

Figure 2.13. Chronostratigraphic chart for Late Cretaceous-Paleogene strata in the Book Cliffs-Wasatch Plateau region (modified from Fouch and others, 1983; Franczyk and others, 1990a; White and others, 2008).

Figure 2.14. Classic outcrop of the Tununk Shale Member of the Mancos Shale composed of soft and deeply weathered slopes and low, rounded hills devoid of vegetation, and small vertical cliffs; west flank of the San Rafael Swell near I-70, view to the northwest. Photograph by Michael Chidsey, Sqwak Productions Inc.

Figure 2.15. The Tununk Shale and Ferron Sandstone Members of the Upper Cretaceous Mancos Shale along the west flank of the San Rafael Swell near I-70, view to the east. Photograph by Michael Chidsey, Sqwak Productions Inc.

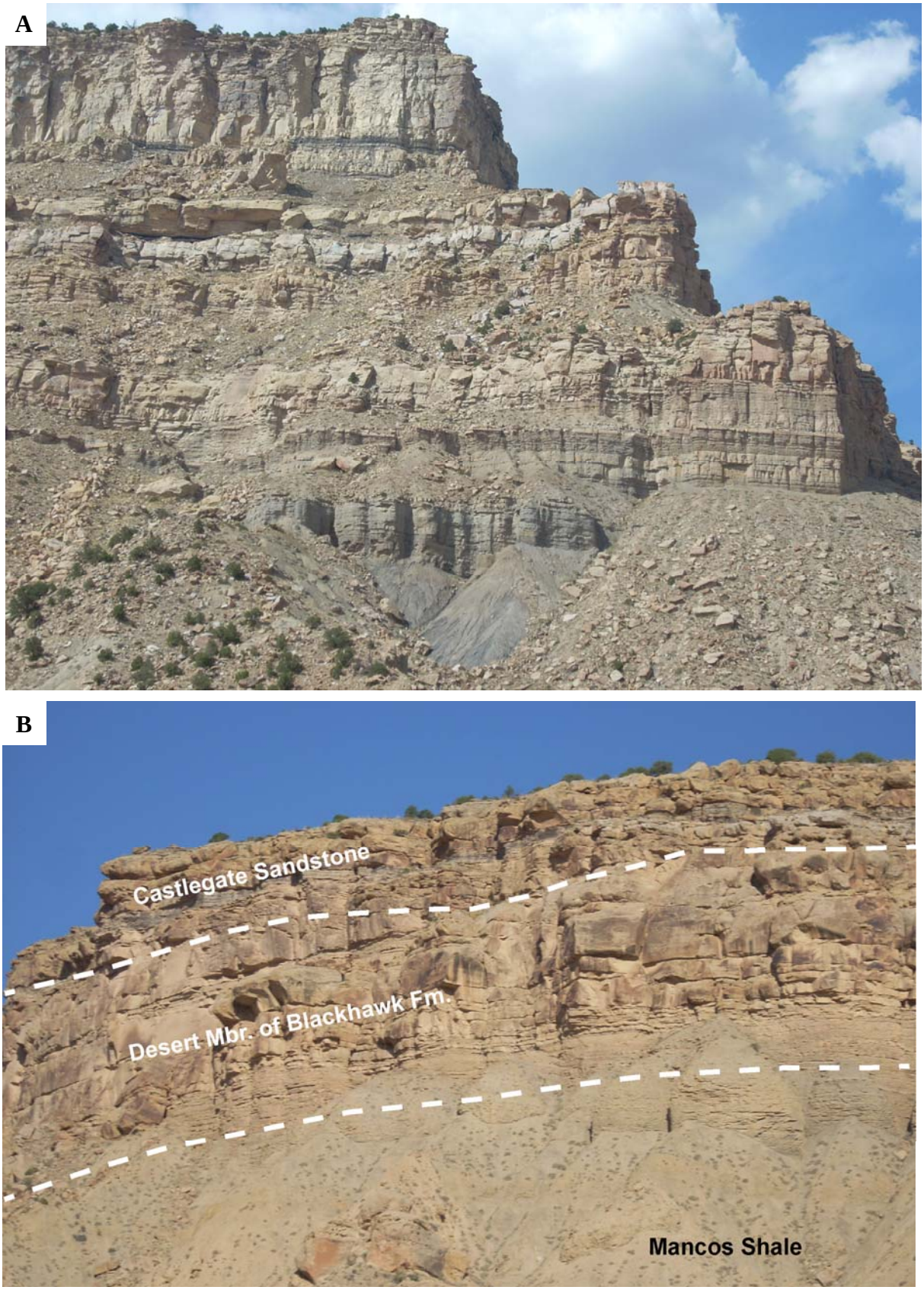

Figure 2.16. Blackhawk Formation outcrops in the Book Cliffs. A – Typical section of the Blackhawk Formation showing shoreface sandstone beds and coal. B – The Desert Member of the Blackhawk Formation overlying the Mancos Shale and underlying the Castlegate Sandstone in the eastern Book Cliffs. Note all other members of the formation are missing as well as any coal beds. The Castlegate consists of shoreface, fluvial, and estuarine facies.

Figure 2.17. Castlegate Sandstone outcrop showing classic sand-rich braided stream facies, western Book Cliffs.

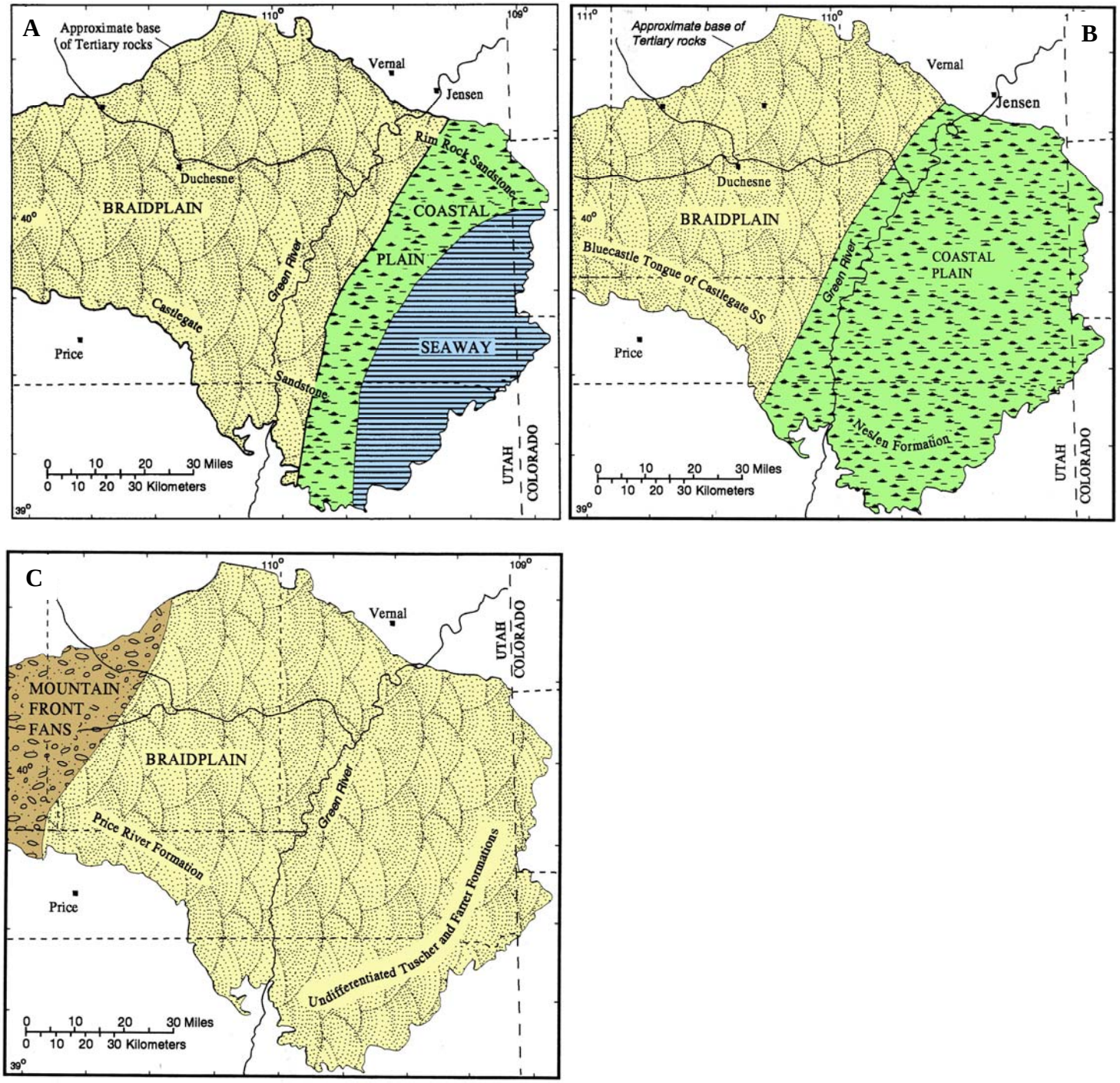

Figure 2.18. Paleogeography of the Uinta Basin during the late Campanian through Maastrichtian time (modified from Fouch, 1975; Fouch and others, 1992). A – Deposition of the coastal plain/meanderbelt and deltaic/marginal marine environments of the Castlegate Sandstone. B – Deposition of the Neslen Formation in a coastal plain environment. C – Deposition of the Farrer and Tuscher Formations in an alluvial plain environment.

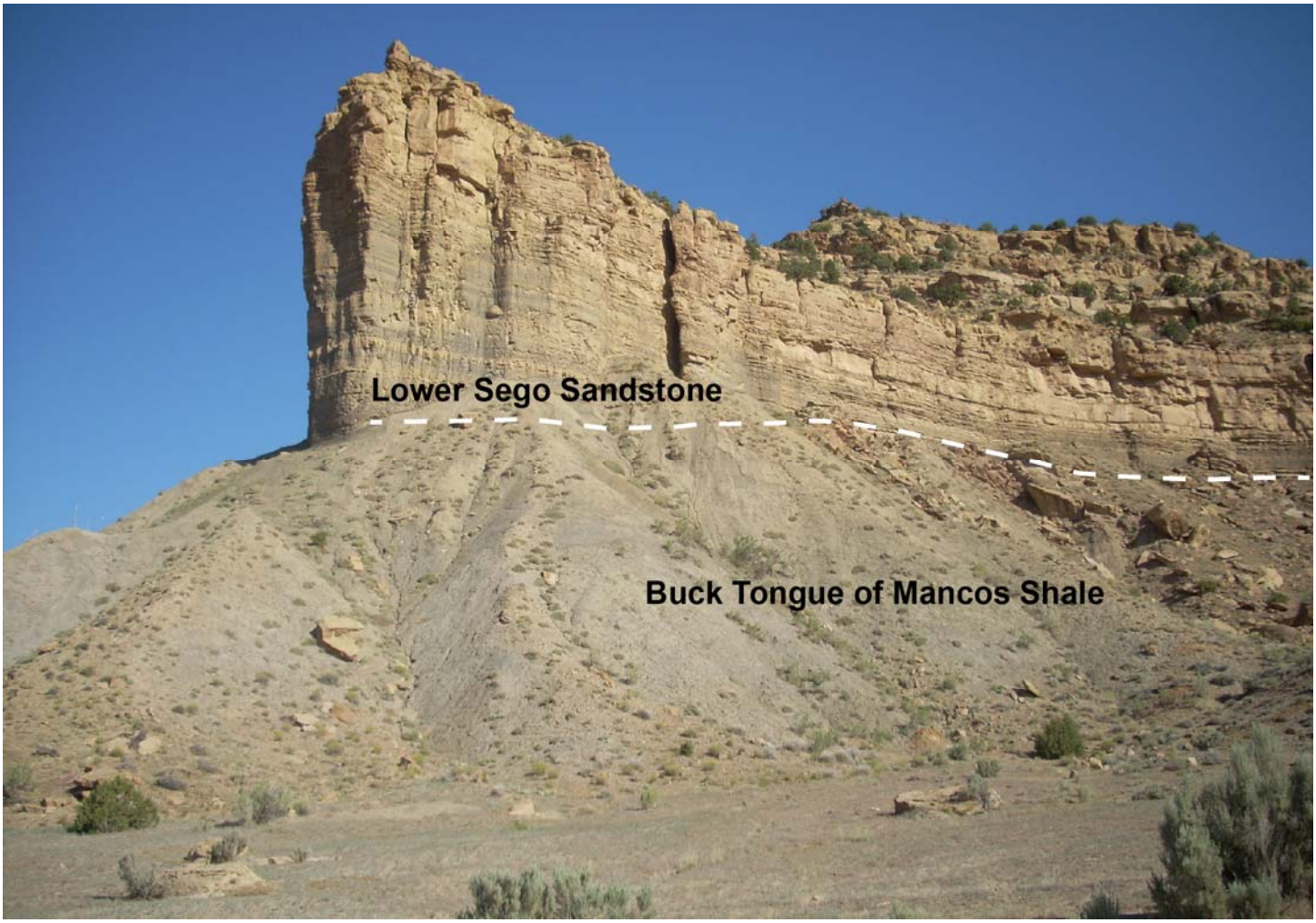

Figure 2.19. Outcrop of coarsening upward lower Sego Sandstone in gradational contact with the Buck Tongue of the Mancos Shale, eastern Book Cliffs (Sego Canyon).

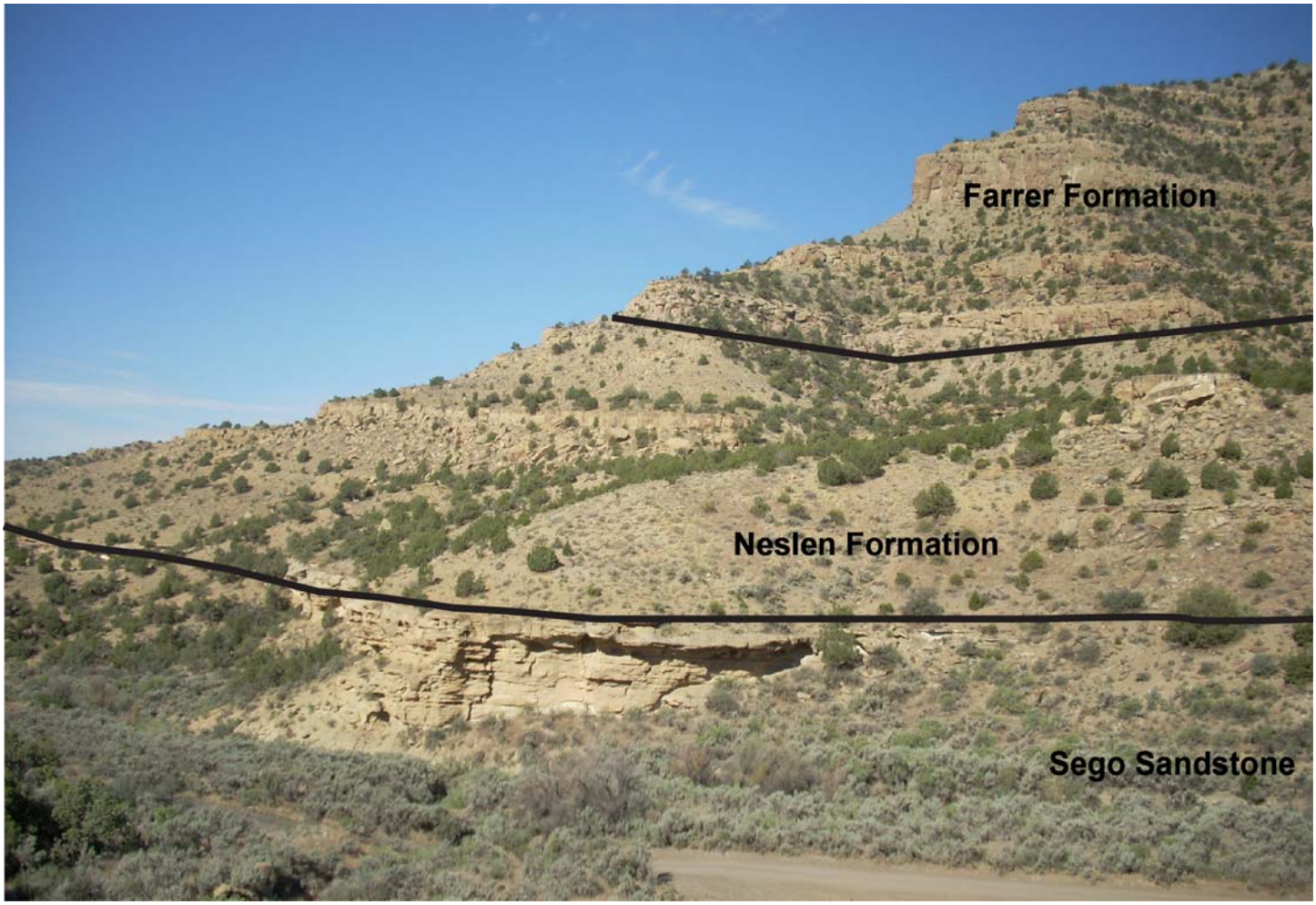

Figure 2.20. Stratigraphic section in Sego Canyon, eastern Book Cliffs, showing, in ascending order, Sego Sandstone, Neslen Formation, and Farrer Formation; view west.

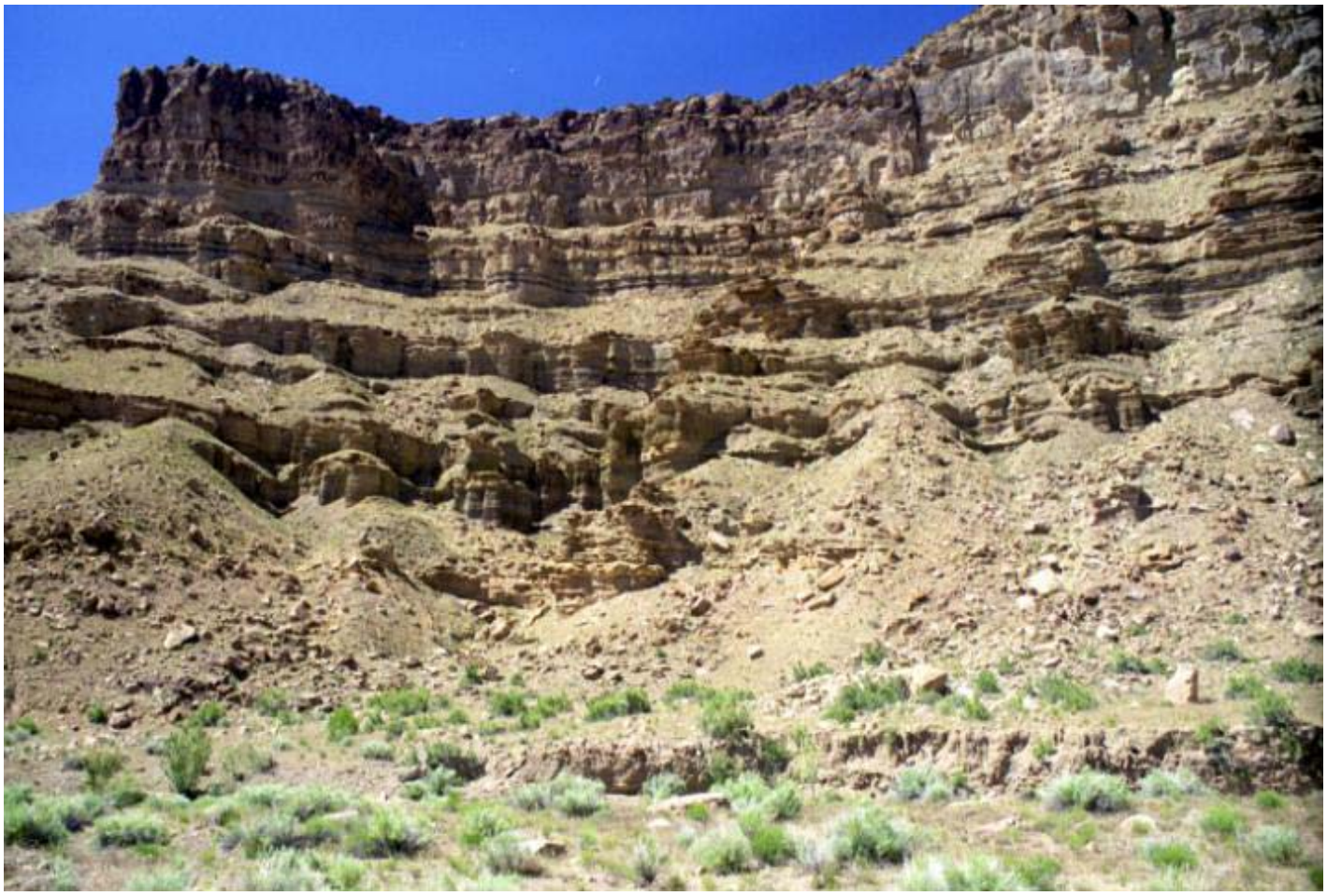

Figure 2.21. Representative outcrop of fluvial siltstone and sandstone in the Upper Cretaceous Price River Formation along the Green River, Desolation Canyon; view east. From Morgan, 2003a; photo by Logan MacMillan.

Figure 2.22. Representative outcrop of stacked amalgamated sandstone bodies of the Tuscher Formation, eastern Book Cliffs (Sego Canyon); view northwest.

Figure 2.23. Representative outcrop of fluvial siltstone and sandstone in the late Upper Cretaceous-early Paleocene North Horn Formation, Soldier Canyon, Book Cliffs; view east. From Morgan, 2003a.

Figure 2.24. Representative outcrop of the Paleocene Flagstaff Limestone, Price River Canyon, Book Cliffs; view south.

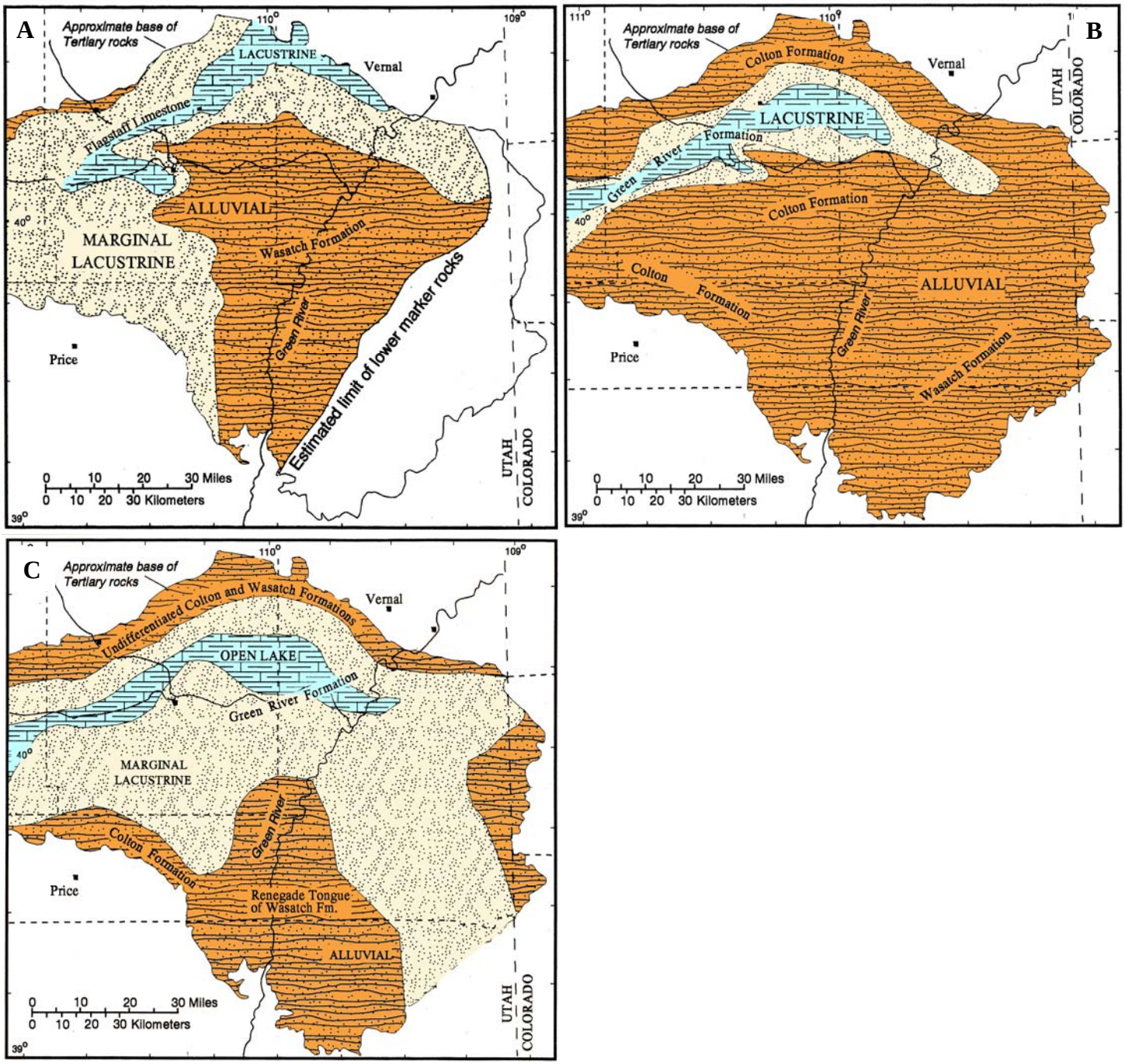

Figure 2.25. Paleogeography of the Uinta Basin during the Paleocene through Eocene time (modified from Fouch, 1975; Fouch and others, 1992). A – Deposition in lacustrine and marginal lacustrine environments during the waning stages of Lake Flagstaff, i.e., the Flagstaff Limestone. B – Deposition of the alluvial Colton (Colton fan-delta) laterally equivalent Wasatch Formation during the late Paleocene and early Eocene. C – Deposition of the Green River Formation in open lake and marginal lacustrine environments during deposition of the Douglas Creek Member (middle member).

Figure 2.26. Paleocene-Eocene Colton Formation forming the western part of the Roan Cliffs.

Figure 2.27. Paleocene-Eocene Wasatch Formation, Hells Hole area, southeastern Uinta Basin. From Cole and others, 2008; photo by Rex Cole.

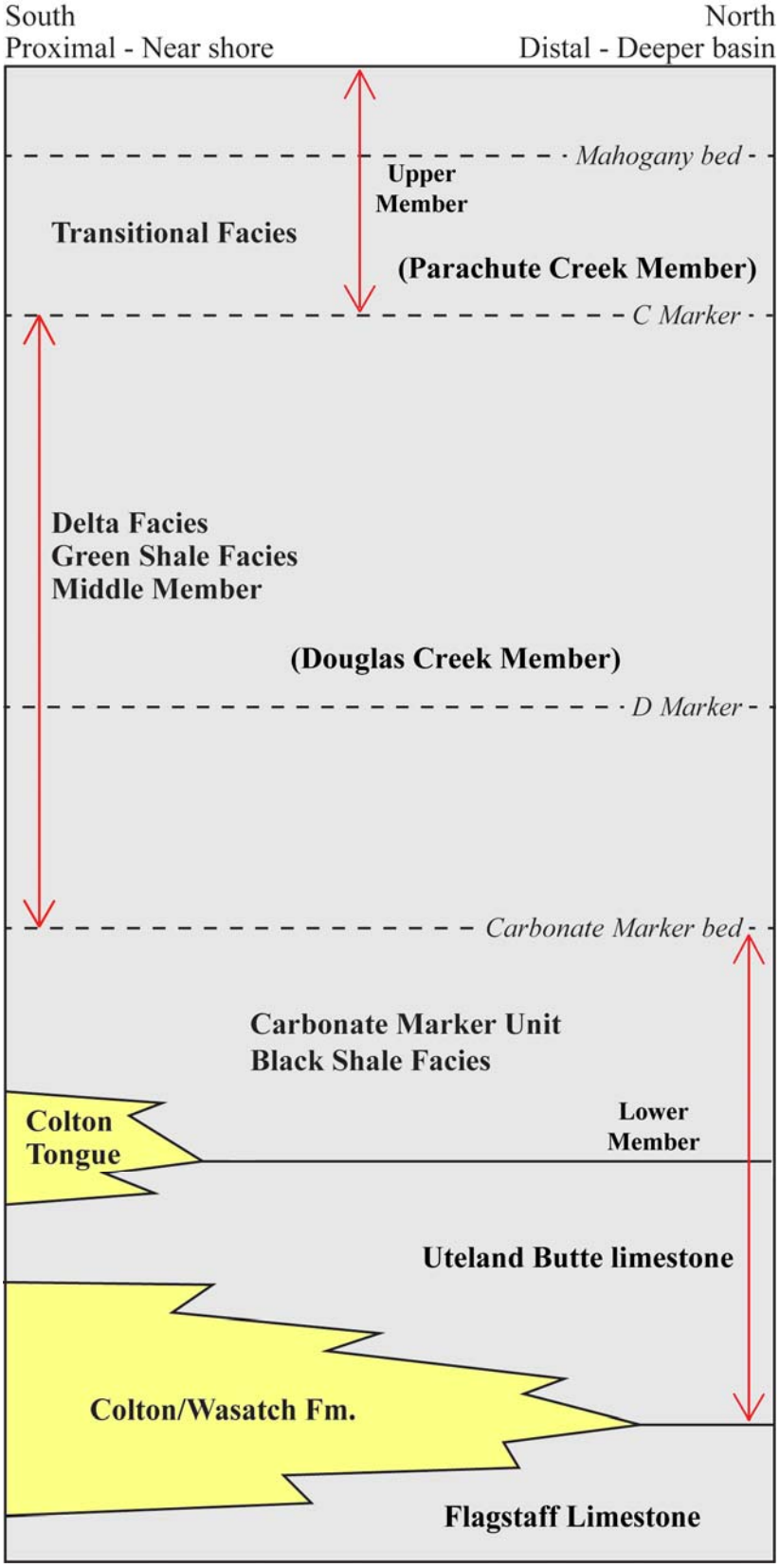

Figure 2.28. General stratigraphy and major marker beds of the Green River Formation in the Uinta Basin (not to scale).

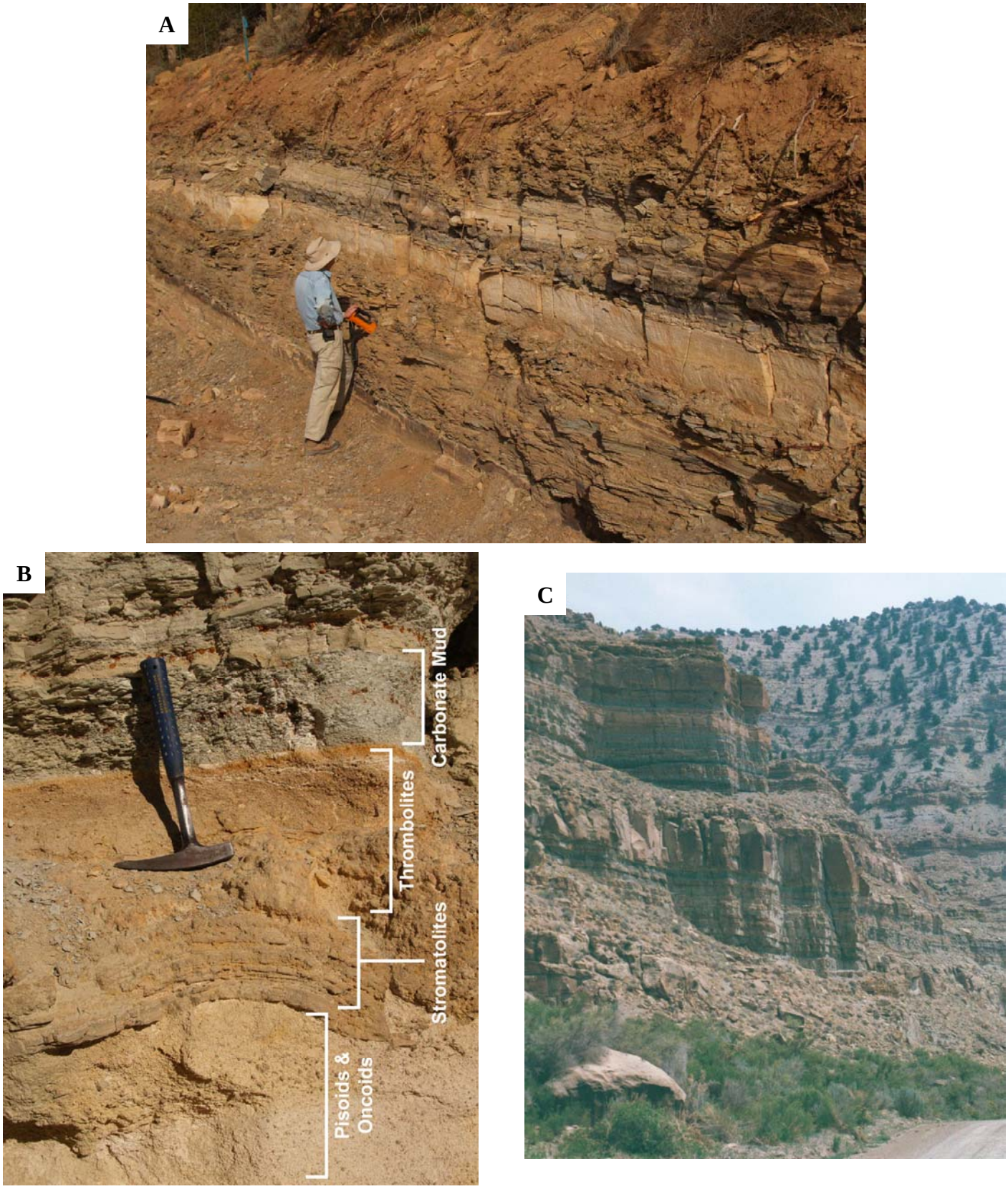

Figure 2.29. Representative outcrops of the Eocene Green River Formation. A – Fresh road cut exposure of Uteland Butte limestone consisting of interbedded dolomite and mudstone/limestone, Nine Mile Canyon, southern Uinta Basin; view north. B – Depositional sequence of carbonate, green shale, and fluvial-deltaic sandstone sandstone cycles, Douglas Creek Member, Nine Mile Canyon; view north. C – A typical microbialite interval and associated facies, Hells Hole area, eastern Uinta Basin. The light tan interval near the base is composed of pisoids and oncoids (as a grainstone/rudstone). The tan beds beneath the hammer are stomatolitic, whereas a thrombolite dominates the area to the right of the hammer.

Figure 2.29 continued. Representative outcrops of the Eocene Green River Formation. D – Mahogany oil shale zone, Parachute Creek Member, Evacuation Creek area, eastern Uinta Basin; view west. E –The "Birds Nest" aquifer zone with nahcolite cavities in the upper Parachute Creek Member, representing the hypersaline conditions during the waning stage of Lake Uinta, Evacuation Creek, eastern Uinta Basin; view north.

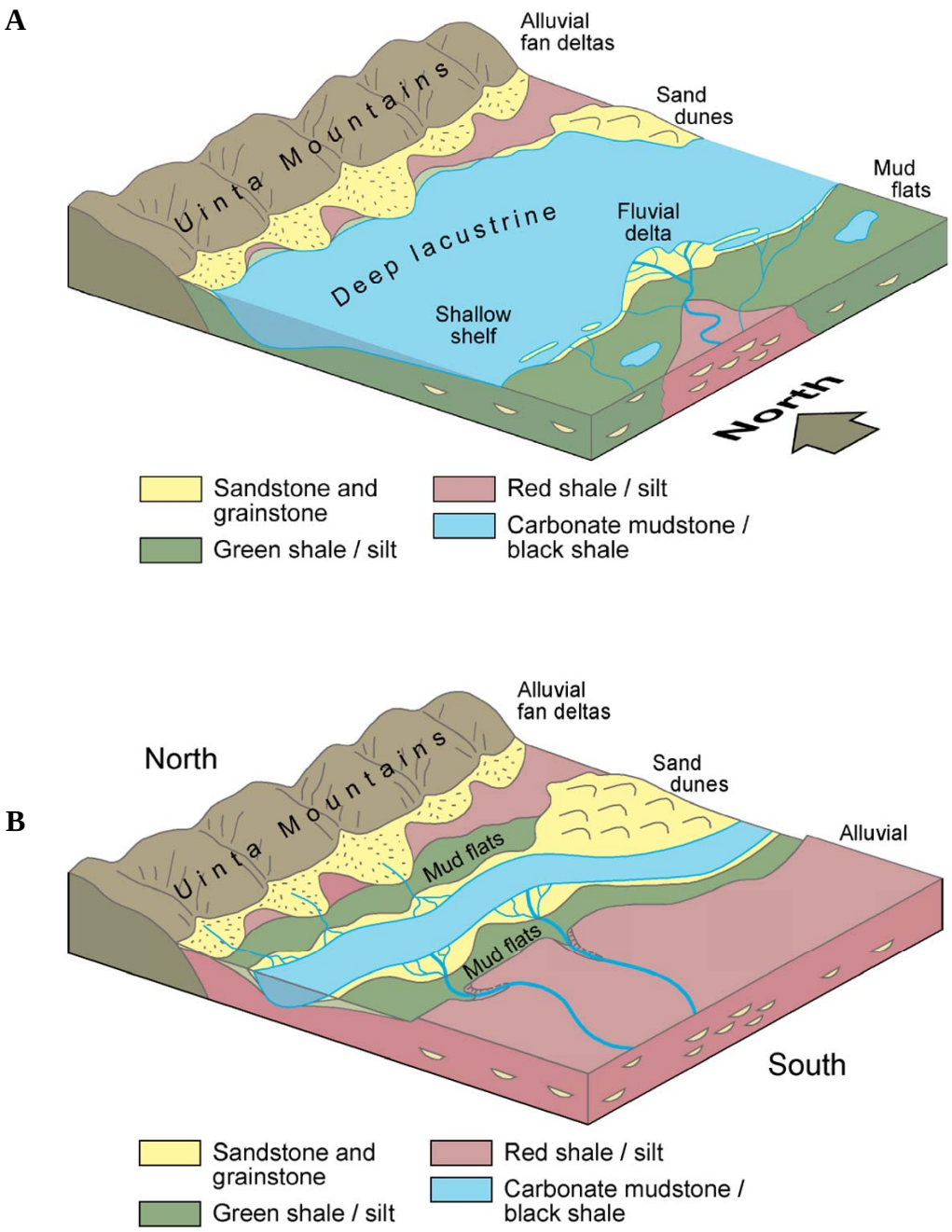

Figure 2.30. Generalized depositional setting for Lake Uinta: (A) high-lake levels, and (B) low-lake levels. From Morgan and others (2003).

Figure 2.31. Badland topography formed in the C member of the Eocene Uinta Formation about 30 miles southeast of Vernal, Utah. Photo by Doug Sprinkel, UGS.

Figure 2.32. Representive outcrop of the Eocene Duchesne River Formation along a meander of the Green River near Horseshoe Bend about 12 miles south of Vernal, Utah. The Duchesne River Formation was deposited by a fluvial system, possibly similar to the modern Green River providing an example of ancient and modern fluvial environments. Photo by Doug Sprinkel, UGS.

CHAPTER III

STRUCTURAL SETTING

Thomas C. Chidsey, Jr., Stephanie M. Carney, and Taylor Boden

The rocks in the UB have been faulted, fractured, jointed, folded, and uplifted. The resultant structural features have had a significant impact on the generation and trapping of hydrocarbons in the basin as well as potential for produced water disposal. Two major structural events helped shape the UB and create the structures within it: the Late Cretaceous to early Tertiary Laramide Orogeny and Tertiary-Quaternary uplift of the Colorado Plateau. Some structures in the UB also reflect overprinting regional Miocene extension.

Oil and gas migration along faults and fractures in Cretaceous and Tertiary strata in the eastern UB has been proposed by Rice and others (1992). Migration along fracture networks within the Green River Formation in the central part of the basin has been noted by several workers, including Chidsey and Laine (1992) and Groeger and Bruhn (2001). These faults and fractures could also influence vertical movement of groundwater throughout the basin and within the Mesaverde, Wasatch, and Green River reservoirs.

TECTONIC HISTORY

The Colorado Plateau is relatively undeformed in comparison to the central Utah thrust

belt to the west. Precambrian-age, basement-involved normal faults lie deep in the subsurface, several of which are exposed in the Grand Canyon. Late Cretaceous thrust faulting of the Sevier orogenic belt, specifically the Charleston-Nebo thrust, extended into the westernmost edge of the east-central Utah (Hintze, 1980). Synorogenic nonmarine deposition near the UB suggests a transition from "thin skinned" Sevier-thrust deformation to Laramide basement-cored uplift occurred during late Campanian (Lawton, 1985, 1986).

Structural basins, e.g., the Uinta and Kaiparowits in Utah, and broad, large-scale, elongate anticlinal uplifts like the SRS, are developed throughout the Colorado Plateau. These basins and uplifts formed in response to Laramide orogenic compressional forces between latest Cretaceous time (about 70 million years ago [Ma]) and the Eocene (about 40 Ma) (Hintze and Kowallis, 2009). Stratigraphic evidence (Molenaar and Cobban, 1991) suggests that uplift began possibly in Turonian (94-89 Ma) and ended by the close of the early Eocene (48.6 Ma).

Regional extension beginning during the Miocene (about 17 Ma) (Hintze and Kowallis, 2009) produced major north-south-trending, high-angle normal faults. These faults often bound plateaus and valleys, and have lengths over 100 miles in Utah and northern Arizona. Smaller faults also dissect high plateaus, such as the Wasatch Plateau to the southwest of the UB and extend into the western part of the basin (figure 3.1, plate 1) and earlier Laramide features in the western part of the Colorado Plateau.

The compression associated with the Laramide Orogeny also caused the Colorado Plateau and most of the western U.S. to rise. Some workers believe that as the hot, young, Farallon oceanic plate slid beneath the continental plate (underplating), the crust was forced to rise in compensation (Burchfiel and others, 1992; Anderson and others, 2010; Grant C. Willis, UGS, written communication, 2011). Most of the uplift occurred in the early Tertiary, but some

uplift continued throughout the remainder of the Cenozoic to the present (Hunt, 1956; Lucchitta, 1979; Graf and others, 1987; Young and Spamer, 2001). By middle Tertiary time, parts of the Colorado Plateau stood as a broad high plain (Anderson and others, 2010; Grant C. Willis, UGS, written communication, 2011). Of particular note in northeastern Utah was a period of crustal stability that occurred during the Oligocene about 30 Ma which replaced UB subsidence and Uinta Mountain uplift (Hansen, 1986). The result was the development of an extensive pediment around the flanks of the Uinta Mountains. This pediment is called the Gilbert Peak erosion surface; it is capped by the Oligocene-age Bishop Conglomerate where present (Hintze and Kowallis, 2009; Sprinkel, 2010).

The uplifting of the Colorado Plateau turned the region from one of deposition to one of massive erosion by running water, mass wasting, and wind. Burial history models for the area south of the UB near Green River, Utah, estimate the removal of 8000 feet, equating to a long-term average vertical erosion rate of 0.2 feet per thousand years (Nuccio and Condon, 1996; Nuccio and Roberts, 2003). Other estimates of the stream incision rates on the Colorado Plateau range from 0.6 feet per thousand years over the last one million years (Willis and Biek, 2001; Pederson and others, 2002), up to 1.3 to 1.6 feet per thousand years over the last several hundred thousand years (Davis and others, 2001; Hanks and others, 2001; Marchetti and Cerling, 2001).

Most of the eroded material from the Colorado Plateau has been carried to the sea by the Colorado River system. During the early Tertiary, the regional drainages in the Colorado Plateau flowed north from central Arizona toward the UB and other lacustrine basins (Dickinson and others, 1989; Potochnik and Faulds, 1998; Young and Spamer, 2001). About 5.5 Ma, southwest-flowing drainages in the southern Nevada, which had been lowered by structural collapse of the Basin and Range Province between 10 and 15 Ma, succeeded in cutting headward into the higher

Colorado Plateau to the east (Grant C. Willis, UGS, written communication, 2011). Eventually, headward erosion managed to capture and integrate the drainages of the Colorado Plateau (including those within the UB), reversing flow directions. As a result, the modern Colorado River system was formed. Due to the great topographic relief between the southern Nevada area and the higher Colorado Plateau, the Colorado River, Green River, and their tributaries had tremendous erosional energy and rapidly cut the Grand Canyon over a few million years (Lucchitta, 1989; Grant C. Willis, UGS, written communication, 2011). The new drainage system quickly eroded the soft Mesozoic strata of the Colorado Plateau creating wide valleys, narrow canyons, and entrenched meanders—many of which are found in the UB.

GENERAL BASIN STRUCTURE AND FOLDING

The UB is a classic example of a large Laramide basin on the Colorado Plateau. The basin is asymmetrical to the north, paralleling the east-west-trending Uinta Mountains (figures 2.1 and 3.1). The north flank dips 10 to 35 degrees into the basin and is bounded by a large, north-dipping, basement-involved reverse fault—the Uinta Basin-Mountain boundary fault (UBMBF) (Campbell, 1975; Stone, 1993; Bryant, 2010). The southern flank gently dips between 4 to 6 degrees north. The syncline axis of the UB is located near the north margin of the basin. It is related to and closely parallels UBMBF zone and Uinta Mountains (Rowley and others, 1985; Bryant, 2010). The UBMBF controlled the development and down warping of the basin in the north, while the southern part of the basin was influenced by the uplift of adjacent Laramide structures and remained elevated (Bryant, 2010).

Subtle structural noses are common in Tertiary rocks throughout the UB and are typically the sites of oil and gas accumulations such as Bluebell (Lucas and Drexler, 1975) and Redwash (figure 3.2) (Schuh, 1993) fields. They possibly developed as adjustments of basement faulting. Large structural features only occur along the flanks of the basin. The Jacks Canyon anticline is located along the southwestern margin (figure 3.1) and includes Nine Mile Canyon, Peters Point, and Stone Canyon fields (figure 1.1) which developed on subsidiary structures to the fold.

FAULTING

High-angle normal faults are common in south-central and westernmost UB (figures 2.1 and 3.1) (Weiss and others, 1990; Sprinkel, 2009, 2014). These faults are linear to slightly sinuous, ranging in length from several hundreds of feet to miles, have displacements less than 100 feet, and are often paired to form grabens. The orientation of the south-central set is northwest-southeast reflecting the northernmost extension of the ancestral Uncompahgre uplift to the south. They likely developed during the Paleozoic along the north and northeast flanks of the Uncompahgre uplift (Stone, 1977) and were reactivated during the Laramide Orogeny in the Late Cretaceous/early Tertiary (Fouch and others, 1992a, 1992b). The western fault set generally strikes north-south likely represents the eastern continuation of Miocene regional extension.

Two structural components are unique to the UB in comparison to many other Laramide-age Rocky Mountain basins: the Uinta Basin-Mountain boundary fault and the Duchesne fault and fracture zone (DFZ) (figure 3.1, plate 1). These are described in detail in the following sections.

Uinta Basin-Mountain Boundary Fault

The UBMBF, as previously discussed, is a major basement-involved reverse fault along the northern border of the UB. Movement along the UBMBF zone began during Laramide time and is partly responsible for uplift of the Uinta Mountains as well as contributing to the development of the UB (Bryant, 2010; Sprinkel, 2014). Several fault segments offsetting members of the Eocene/Oligocene Duchesne River Formation are exposed along its length of the UBMBF (Sprinkel, 2007, 2014). A series of normal fault scarps cut gravels (glacial outwash) of pre-Blacks Fork age (middle to early[?] Pleistocene) along the northwest margin of the UB, and generally align with exposed faults that may be surface traces of the UBMBF where extension and relaxation has occurred. Displacement of Pleistocene deposits along the UBMBF system shows that segments of the fault have been active in the Quaternary and may continue to the present (Sprinkel, 2014). To the east, Mesozoic and middle Eocene rocks are juxtaposed across the UBMBF zone (Sprinkel, 2006, 2007).

Although the UBMBF generally does not reach the surface along much of its length, it is identifiable on seismic profiles or from well data. Figure 3.3 is a north-south seismic profile from the northern UB to through Ashley Valley field (figure 1.1). This high-quality, time-migrated profile was acquired in 1985 using an airgun source (Stone, 1993). It has a horizontal exaggeration of 1.3 to 1 at 2.0 seconds two-way time (TWT), and a record length of 5 seconds TWT (Stone, 1993). The UBMBF is prominently displayed dipping north and appears to become relatively low-angle at depth. Strong reflectors on the profile delineate the Tertiary, Paleozoic-Mesozoic, and Precambrian Uinta Mountain Group and Red Creek Quartzite sections.

Figure 3.4 is a cross section parallel to the southern portion of the seismic profile from Red Wash field in the UB through Ashley Valley field, constructed using surface geologic maps, subsurface data from oil and gas exploratory wells, and the seismic interpretation shown on figure 3.3 supplemented with other geophysical information (Stone, 1993). The UBMBF dies out and is covered by the Green River and younger formations along most of its length. At depth, the UBMBF places the Precambrian through Jurassic section in contact with source rocks within the Upper Cretaceous Mancos Shale. The oil produced from the Pennsylvanian Weber Sandstone at Ashley Valley field is a mixture from source rocks in the Mancos Shale and Permian Phosphoria Formation based on analysis of saturated biomarkers, carbon isotopes, gas chromatography, and other geochemical techniques (Stone, 1986; Sprinkel and others, 1997; Lillis and others, 2003).

Duchesne Fault and Fracture Zone

The DFZ is a prominant east-west-trending, series of normal faults and associated intense fracturing (figures 3.1 and 3.5) that creates a discontinuous graben cutting beds of the Uinta Formation at the surface in the north-central part of the UB parallel to the Monument Butte-Brundage Canyon field trend just to the south (figure 3.1, plate 1) (Sprinkel, 2014). The faults may be related deep-seated fractures in basement. The DFZ is thought to have formed during the Larmide Orogeny prior to 30 to 35 Ma (Groeger and Bruhn, 2001). A subtle anticline follows the length of the DRZ; other minor folds are also present (Groeger and Bruhn, 2001; Smith, 2004). The faults in the DRZ can be mapped east to west for over 40 miles along a belt about 3 miles wide (Ray and others, 1956). The stratigraphic displacement on these relatively high angle faults

range from a few inches to 100 feet with no observable horizontal component (figure 3.5) (Bereskin and others, 1993; Smith, 2004). In the western DFZ, a shallow basal detachment on a south-dipping fault produces a half-graben (Groeger and Bruhn, 2001). The northwest-trending belt of gilsonite veins (discussed later) intersects the eastern end of the DFZ. The DFZ likely predates the formation of the gilsonite veins based on spatial relationships (Lemmon and others, 1998).

Fracturing in the DFZ was induced by high fluid pressures applied to low-permeable rocks on local subtle folding (Smith, 2004). The deep part of the UB to the north of the DFZ (Altamont-Bluebell field trend, figure 1.1) is characterized by overpressusing in the Green River and Wasatch/Colton reservoirs. The intense fracturing within the DFZ is postulated to have resulted from repeated cycles of (1) fluid pressure buildup, (2) fracturing, (3) fluid flow through the DFZ, (4) calcite precipitation by calcite-saturated fluids, and (5) sealing of fracture permeability (Smith, 2004). Fluid pressures were not as high to the south of the DFZ and thus, the intensity of the fractures was significantly less.

JOINTING

Sandstone beds in the UB are quartz rich and brittle, and when folded or bent produce joints and fractures. Joints are also a prominent feature in the strata of the UB. Large sets of joints are observed chiefly in sandstone of the Green River, Uinta, and Duchesne River Formations. These joints developed in response to the subtle folding in the UB, regional uplift of the Colorado Plateau, and the removal of several thousand feet of overlying rock by erosion.

Joints are closely spaced in many areas of the UB, but spacing varies with bedding thickness, lithology, and structural setting, i.e., folding, regional dip, proximity to faults, etc. Three types of joints are common: (1) near-vertical, (2) inclined, and (3) surficial. These joints are best displayed close to cliff faces where slope retreat is actively taking place. They are spaced from five to hundreds of feet apart, and are as much as several miles in length. Surficial joints are near-parallel to cliff faces and form from the expansion of the sandstone after rapid unloading of overlying strata. In cross section, surficial joints are closely spaced near the cliff face, from inches to a few feet apart, but disappear at depth.

There are five major regional joint sets in the eastern UB identified by Verbeek and Grout (1992) where tight-sand gas reservoirs produce at Natural Buttes and other fields (figure 1.1) listed as follows, including their strike range, starting with the oldest: F1 – N 15-30º W, F2 – N 55-85º W, F3 – N 60-80º E, F4 – N 15-40º E, and F5 – N 65-85º W. Joint sets F2 and F4 are very abundant, F3 is moderate, and F1 and F5 are sparse (Verbeek and Grout, 1992). Joint sets F1 through F3 formed 43 to 10 Ma whereas sets F4 and F5 are dated beginning 10 Ma during regional uplift (Verbeek and Grout, 1992).

FRACTURES

Fractures are closely associated with jointing and fault zones (not just the DFZ). Fracturing in the UB plays a major role in creating effective porosity and permeability that results in reservoir quality capble of hydrocarbon production. Understanding the characteristics and orientation of these naturally occurring fractures is also crtical for planning horizontal wells

and hydraulic fracturing of tight-sand and potential shale-gas reservoirs in the basin.

Regional fracture systems (tens of mile long) in the UB are near-parallel and are possibly genetically related to major structural features bordering the basin (Stearns and Friedmen, 1972). These features include the Uinta Mountains, Douglas Creek arch, San Rafael uplift, Wasatch Plateau, the buried Uncompahgre uplift, and the Charleston-Nebo thrust (figure 3.1, plate 1).

Fractures in the UB began to develop during burial of the Wasatch and Green River Formations (Narr and Currie, 1982). Hydrocarbon generation, with resultant overpressuring, may have caused fractures to form in the deeper parts of the basin (Sweeny and others, 1987). Fractures also developed as the result of tectonic stress in the region. Subsequent uplift of the Tertiary section expanded these existing fracture networks and possibly created additional fracture systems. Narr and Currie (1982) studied the origin of fracturing in Altamont field (figure 1.1) and suggest fractures in the basin are commonly open as a result of unloading by erosion of the overburden.

The distribution and abundance of natural fractures in the subsurface are strongly controlled by lithology and bedding characteristics (figure 3.6). They are found in most brittle units such as sandstone and carbonate beds. However, fractures also are present in shale or mudstone beds that contain significant amounts quartz silt and sand. Lucas and Drexler (1975) concluded that dense carbonate mudstone is fractured the most followed by sandstone and then shale.

Locally, the abundance and most importantly the orientation of fractures is controlled by folds. In Bluebell, Peters Point, and Natural Buttes fields (figure 1.1), fractures are concentrated along subtle surface or subsurface anticlines and structural noses (Clem, 1985) and are generally parallel to the axis of these structures. Lucas and Drexler (1975) showed by determining the

direction of reservoir drainage and pressure changes between wells, that the direction of connected fractures trend east-west in the shallow part of Bluebell field (parallel to the structural nose).

GILSONITE VEINS

Gilsonite veins are an unsual but significant component of the structural geology in the eastern UB (figures 2.1 and 3.1). Gilsonite is a naturally occurring, solid, black, lightweight asphaltite (solid hydrocarbon) sourced from the Mahogany oil shale zone of the Green River Formaion (Tripp, 2004; Boden and Tripp, 2012). Gilsonite is used in wide a variety of products: printers ink, pavement sealant, adhesives, and drilling mud to name a few. It has been mined in the UB since 1868 as open cuts (figure 3.7) and later underground (Tripp, 2004).

Deep burial and overpressuring of Mahogany oil shale zone generated hydrocarbons and expelled large quantities thermal water that hydrofractured the overlying rocks. Later viscous petroleum was expelled and intruded into the existing fractures, enlarging and forcing them open, subsequently solidified into gilsonite (Tripp, 2004; Boden and Tripp, 2012).

Gilsonite veins in the eastern UB are commonly several miles long (the longest vein system extends 24 miles) and hosted in the Wasatch, Green River, Uinta, and Duchesne Formation (Boden and Tripp, 2012). Nearly 60 veins and vein systems totaling over 120 miles in length in outcrop have been mapped by Boden and Tripp (2012). These veins vary in width from fractions of an inch to almost 18 feet averaging 3 to 6 feet (Tripp, 2004). They are vertical and continue into the subsurface for hundreds to as much as 2000 feet or more with only small

variations in vein width (Tripp, 2004). The 60-mile by 30-mile belt of gilsonite veins trends west-northwest suggesting a genetical structural relationship to the basement-involved Uncompahgre uplift (Narr and Currie, 1992).

CHAPTER III FIGURE CAPTIONS

Figure 3.1. Major structural features, surface faults, and fracture zones in and around the Uinta Basin. Uinta Basin-Mountain boundary fault after Osmond (1986); other faults and gilsonite veins taken from (Hintze; 1975; Hintze and others, 2000).

Figure 3.2. Structure contour map on the top of the Douglas Creek Member of the Green River Formation, Red Wash field. Contour interval is 100 feet; datum = mean sea level. From Schuh (1993).

Figure 3.3. North-south interpreted seismic profile showing prominently the Uinta Basin-Mountain boundary fault zone and the Ashley Valley field structure. Strong reflectors identify the Tertiary and Paleozoic-Mesozoic sections, and the Uinta Mountain Group and Red Creek Quartzite (the latter two of Precambrian age). Line of profile shown on figure 2.1. Seismic profile courtesy of Halliburton Geophysical Services, Inc. Modified from Stone (1993).

Figure 3.4. North-south structural cross section from Red Wash field in the Uinta Basin through the Uinta Basin-Mountain boundary fault zone and the Ashley Valley field area showing the

features identified on the seismic profile (figure 3.3). Line of section shown on figure 2.1. Modified from Stone (1993).

Figure 3.5. Duchesne fault and fracture zone in the Eocene Uinta Formation, Duchense field area (see figure 1.1). A – High angle normal fault with over 50 feet of displacement. B – Minor displacement on a fault dipping 78º north. C – Multiple faults creating south dip in the bedding. D – Small fault and associated closely spaced vertical fractures.

Figure 3.6. Fracturing in the Eocene Uinta Formation. A – Closely spaced, vertical fracturing in fine-grained sandstone along the Duchesne fault and fracture zone, Duchesne field area. Fracture sets generally strike N 62 E., N 84 E, and N 72 E (from Chidsey and Laine, 1992). B – Orthagonal fracture sets in fine-grained sandstone, Sowers Canyon field area. See figure 1.1 for field locations.

Figure 3.7. Abandoned mine workings along the southeast-trending Cowboy gilsonite vein, Uinta Formation, Uintah County. Mining occurred during the first half of the 20th century.

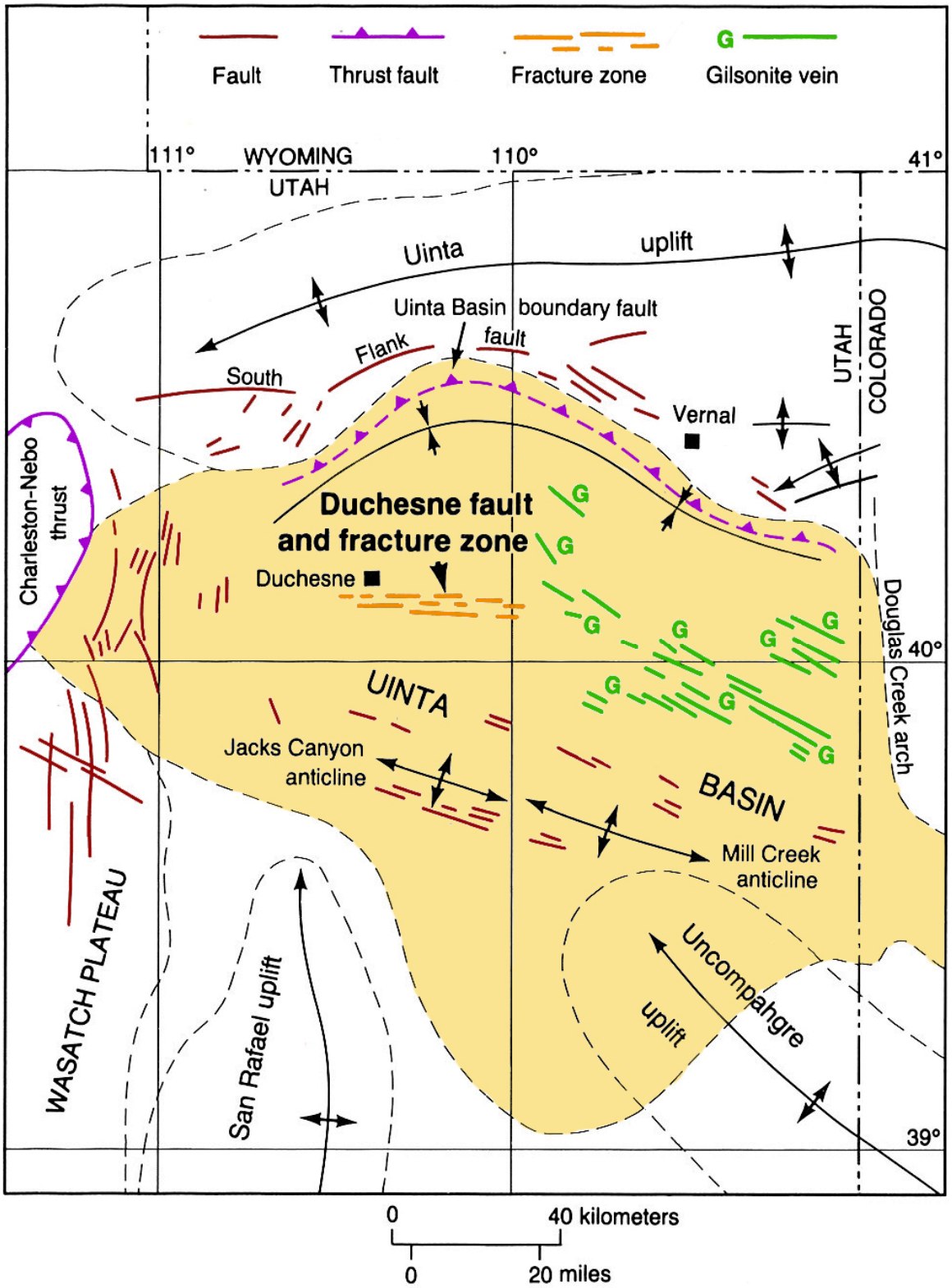

Figure 3.1. Major structural features, surface faults, and fracture zones in and around the Uinta Basin. Uinta Basin Mountain boundary fault after Osmond (1986); other faults and gilsonite veins taken from Hintze (1975).

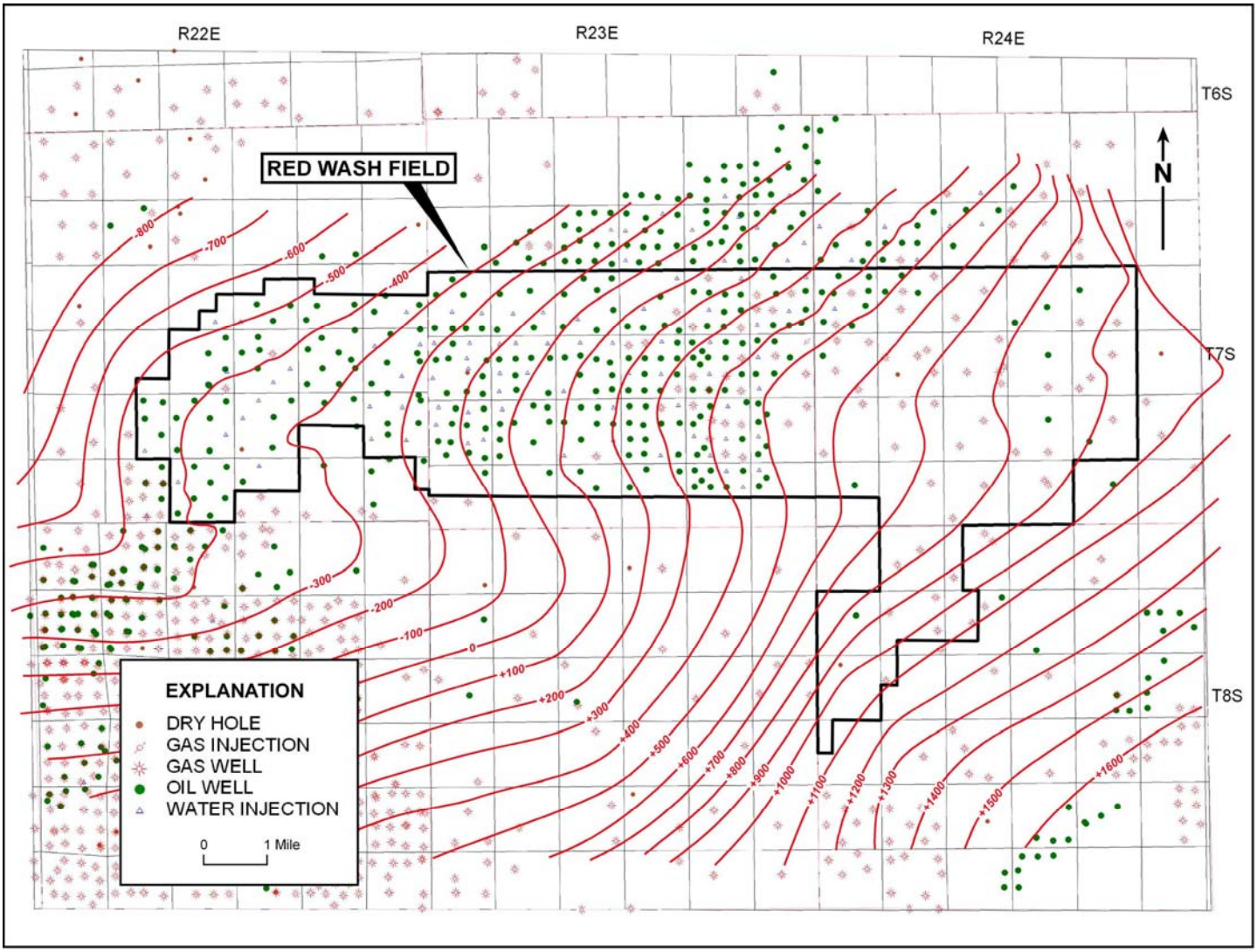

Figure 3.2. Structure contour map on the top of the Douglas Creek Member of the Green River Formation, Red Wash field. Contour interval is 100 feet; datum = mean sea level. From Schuh (1993).

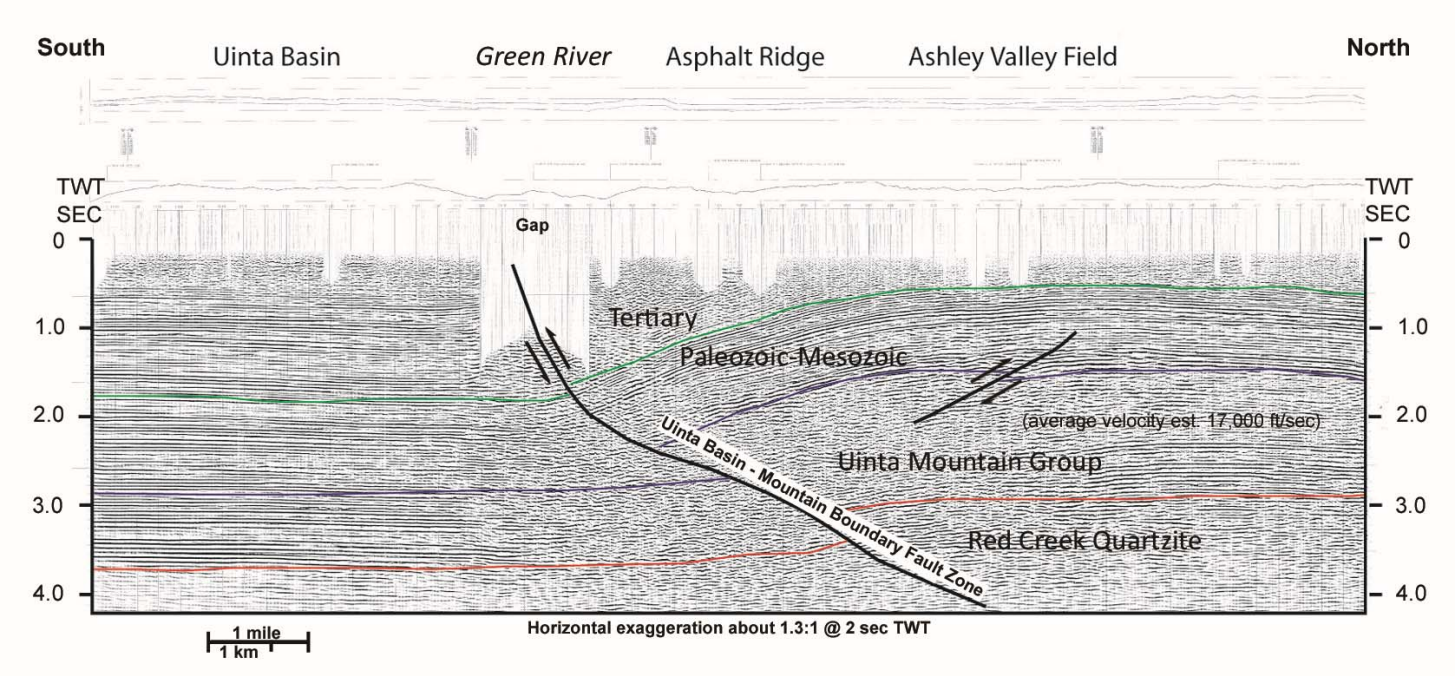

Figure 3.3. North-south interpreted seismic profile showing prominently the Uinta Basin-Mountain boundary fault zone and the Ashley Valley field structure. Strong reflectors identify the Tertiary and Paleozoic-Mesozoic sections, and the Uinta Mountain Group and Red Creek Quartzite (the latter two of Precambrian age). Line of profile shown on figure 2.1 Seismic profile courtesy of Halliburton Geophysical Services, Inc. Modified from Stone (1993).

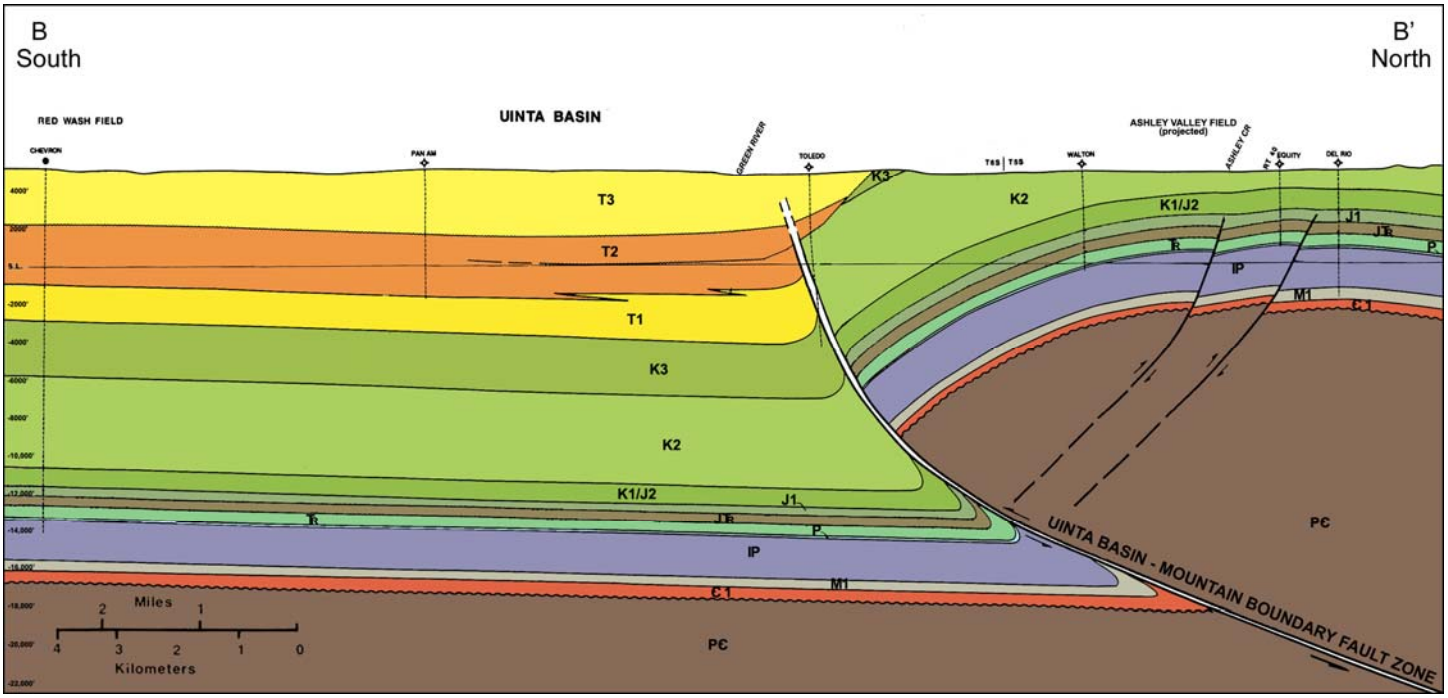

Figure 3.4. North-south structural cross section from Red Wash field in the Uinta Basin through the Uinta Basin-Mountain boundary fault zone and the Ashley Valley field area showing the features identified on the seismic profile (figure 3.3). Line of section shown on figure 2.1. Modified from Stone (1993).

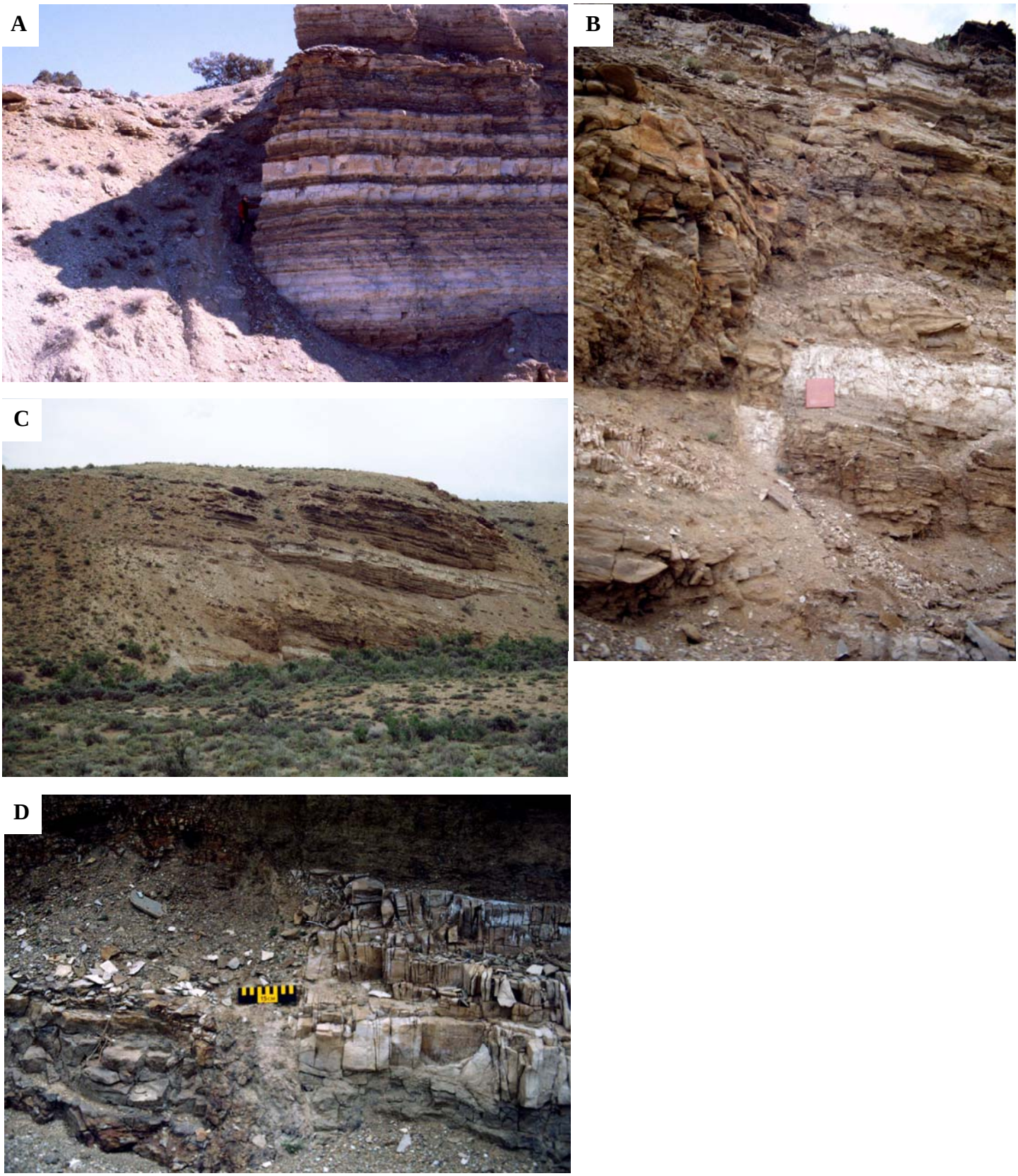

Figure 3.5. Duchesne fault and fracture zone in the Eocene Uinta Formation, Duchesne field area (see figure 1.1). A – High angle normal fault with over 50 feet of displacement. B – Minor displacement on a fault dipping 78º north. C – Multiple faults creating south dip in the bedding. D – Small fault and associated closely spaced vertical fractures.

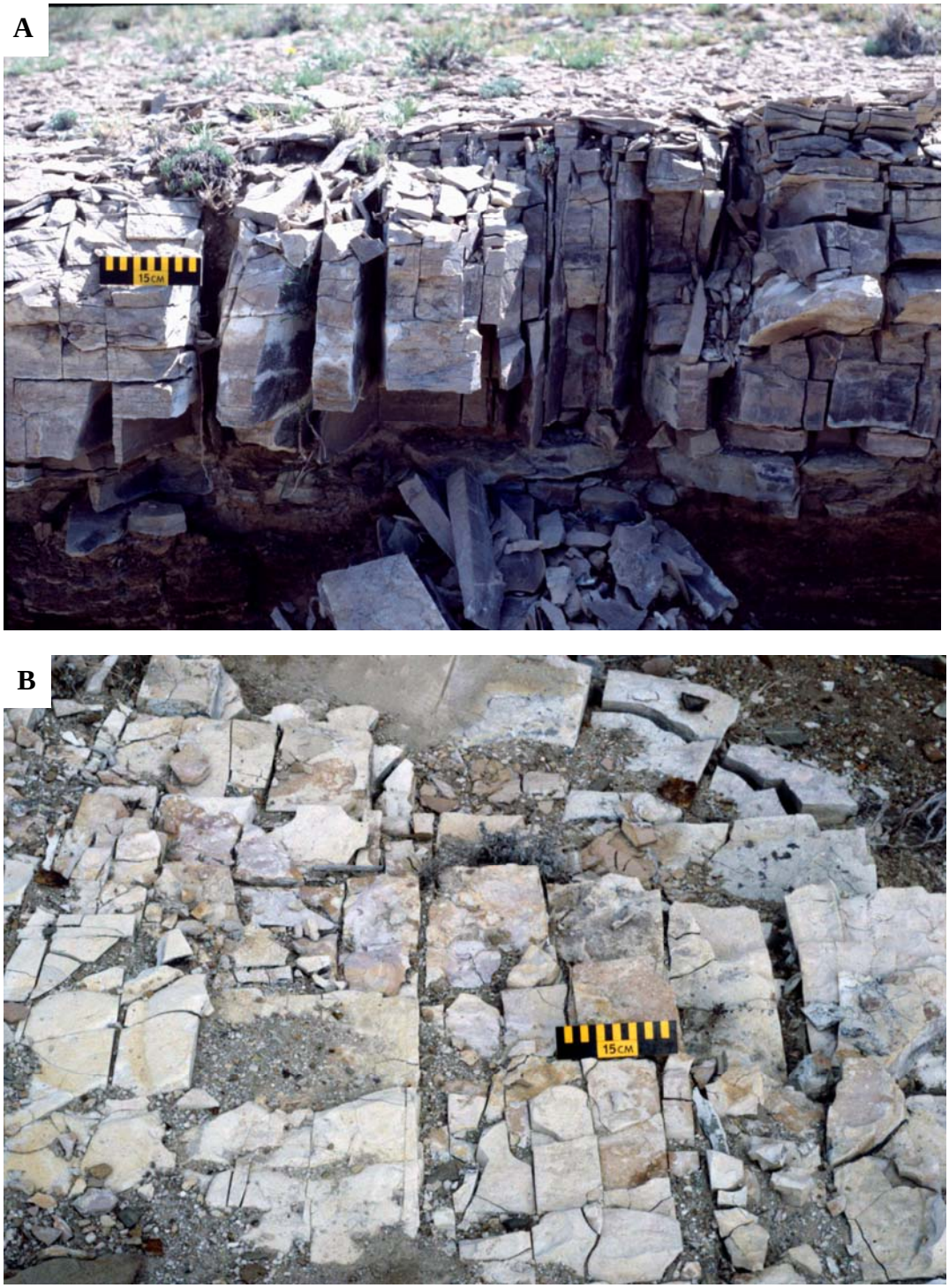

Figure 3.6. Fracturing in the Eocene Uinta Formation. A – Closely spaced, vertical fracturing in fine-grained sandstone along the Duchesne fault and fracture zone, Duchesne field area. Fracture sets generally strike N 62 E., N 84 E, and N 72 E (from Chidsey and Laine, 1992). B – Orthagonal fracture sets in fine-grained sandstone, Sowers Canyon field area. See figure 1.1 for field locations.

Figure 3.7. Abandoned mine workings along the southeast-trending Cowboy gilsonite vein, Uinta Formation, Uintah County. Mining occurred during the first half of the 20th century.

CHAPTER IV

UINTA BASIN RESERVOIRS/AQUIFERS: TRIASSIC-JURASSIC GLEN CANYON GROUP THROUGH THE CRETACEOUS CEDAR MOUNTAIN AND DAKOTA FORMATIONS

Craig D. Morgan

The Upper Triassic-Jurassic Glen Canyon Group, Jurassic Entrada Sandstone, and Cretaceous Cedar Mountain and Dakota Formations represent both aquifers for produced water storage and hydrocarbon production in the UB (figure 1.5). These rocks were deposited in a wide variety of environments including eolian, alluvial floodplain, fluvial, marine, etc., each with varying lithologies and petrophysical (porosity and permeability) properties. In the asymmetrical UB, the Upper Triassic and Lower Cretaceous sections reach depths of more than 26,000 feet (7900 m).

The following sections describe the (1) thickness, (2) depth, (3) lithology, (4) porosity and permeability, (5) general water quality, (6) water production, use, and disposal, and (7) hydrocarbon production of these important, but deep formations in the UB. These characteristics and companion maps provide the basic information required to assess or model those formations that may best serve as produced water storage aquifers.

METHODS

Well databases, along with structure and thickness maps, were developed for each reservoir (Glen Canyon Group/Nugget, Entrada, and Dakota/Cedar Mountain Formations, figure 1.5) as part of a previous study for the Rocky Mountain Carbon Capture and Storage (RMCCS) project (RMCCS reference). All data was gridded at 1 square kilometer (km^2) and then up scaled to 10 km^2 for the NATCARB database. For the RMCCS study, the Glen Canyon/Nugget and Entrada were mapped as a single reservoir. For this project, the Glen Canyon/Nugget and Entrada data were separated and mapped as separate reservoirs. This project expanded on the RMCCS research by correlating additional wells and calculating the thickness (feet of porosity) for each reservoir. The drill depth and thickness of each reservoir were gathered from numerous well databases such as Utah Division of Oil, Gas, and Mining (DOGM), published geologic reports, internal UGS databases, and well correlations. Many of the well logs were digitized into LAS format for easier correlation; others were viewed in tiff image format downloaded from the DOGM website (http://oilgas.ogm.utah.gov). Formation boundaries in the databases were quality checked by correlating logs and making corrections as needed.

The Dakota structure by Roberts (2003) was constructed by using Dakota well tops and projecting to Dakota from the hundreds of shallower wells in the deeper part of the basin. This resulted in a very accurate structure contour map for the UB. The UGS took the digital structural contour data from Roberts (2003) and converted the lines to points every 2000 meter (6505 ft). This point data was added to the UGS Dakota well database. The well database was used to grid (1 km^2) the Dakota structure in the UB. The structural elevations from the Entrada and

Navajo/Nugget well top databases were plotted on base maps. Structure contour maps of the top of Entrada and top of Glen Canyon Group/Nugget were hand contoured using the well data and following similar strike and dip of the Dakota structure map. The hand contoured maps were digitized and the contours were converted to point data which were added to the respective well databases. The expanded well databases were used to grid the structure of the top of the Entrada and Navajo/Nugget.

Thickness maps of the Glen Canyon Group/Nugget, Entrada, and Dakota reservoirs were hand contoured using values from the respective well databases. The contour lines were digitized, converted to point data and added to the respective well databases. The well databases were used to generate structure and thickness maps for each of the reservoirs in ArcMap®. The datasets were gridded using 1 km^2 grid cells. A digital elevation model (DEM) was gridded using the same grid pattern for each reservoir. The structural elevation grids from each reservoir were subtracted from the respective DEM grids to produce overburden, or drill depth, grids.

Previously for the RMCCS project, a single average porosity value was assigned to each reservoir evaluated based on a review of geophysical well logs and published reports for the respective reservoir. This average porosity does not capture geographic and depth variations. For this project, porosity logs (density or sonic) for each reservoir were reviewed, recording depth to the top of the reservoir, feet of porosity at 6% or more and 12% or more for each reservoir. Graphs were generated for feet of porosity versus depth for 6% or more and 12% or more porosity for each reservoir. This data was used to develop predictive equations for feet of porosity at varying depths for each of the reservoirs. The equations were used to calculate the grid data of feet of porosity for each reservoir for each 1 km^2 cell.

Hydrocarbon and produced water data were obtained from the DOGM website (Utah Division of Oil, Gas, and Mining, 2015d). Cumulative and monthly production bubble maps were constructed for each reservoir.

TRIASSIC–JURASSIC GLEN CANYON GROUP AND NUGGET SANDSTONE

The Glen Canyon Group (Wingate Sandstone, Kayenta Formation, and Navajo Sandstone) and equivalent Nugget Sandstone (GCN/N) were deposited as large erg systems throughout parts of Utah, Arizona, Wyoming, and Colorado (figures 4.1 through 4.3) during Late Triassic and Early Jurassic. The Navajo is the thickest and highest quality reservoir in the Glen Canyon Group. The Nugget may be time equivalent to the Glen Canyon Group or just the Navajo, or just the Wingate. Figures 4.5 shows an outcrop of the Glen Canyon Group (figure 2.4 show just the Navajo Sandstone in outcrop) and figure 4.5 shows facies and bedforms found within an eolian dune reservoir. The bed forms result in complex heterogeneity within the reservoir (figure 4.6). Structure on top of the GCG/N reservoir shows an asymmetrical UB with the reservoir more than 20,000 feet (6100 m) below mean sea level in the northern portion of the basin (figure 4.7).

Thickness

The GCG/N reservoir appears to be more than 1700 feet (500 m) thick in the northern portion of the mapped area. This may not be the true thickness due to steep dips and/or reverse faulting along the southern flank of the Uinta Mountains. Most wells to the west and southwest have a maximum thickness of 800 to 1200 feet (250-350 m), thinning to less than 400 feet (120 m) to the east (figure 4.8). Most of the GCG/N is sandstone, therefore a net sandstone map was not prepared.

The gross thickness of the GCG/N reservoir in 375 wells studied ranges from 178 to 1725 feet (54-526 m) with an average of 882 feet (269 m) and a median of 869 feet (265 m) (figure 4.9). The Glen Canyon Group is more than 800 feet (250 m) thick throughout much of the study area, the Navajo accounts for a significant portion of that thickness. The Navajo is thin to completely absent over portions of the Uncompahgre uplift; however, this is not fully represented in the thickness map (figure 4.8).

Depth

Drill depth to the GCG/N in the deepest part of the basin, where no well has penetrated the reservoir, is projected to be more than 28,000 feet (8500 m) (figure 4.10). Drill depths in the wells studied range from 30 to 16,960 feet (9-5169 m) with an average depth of 3198 feet (975 m) and median of 2397 feet (731 m) (figure 4.11).

Lithology

The Navajo and Nugget Sandstone represent a coastal to inland dune field (Hintze and Kowallis, 2009). The dunes may have been the largest recorded in Earth's history (Kocurek and Dott, 1983) (figure 4.12). Dune deposits of the Navajo and Nugget are generally composed of well sorted fine- to medium-grained sandstone. The Wingate Sandstone is typically composed of smaller dunes and dune sets than in the Navajo and Nugget. Numerous interdune deposits of reworked sand during relative rises in the water table resulted in a higher concentration of clay minerals in the Wingate. The Kayenta Formation is a series of channels deposited in a sand-rich braided stream or wadi environment separating the Wingate Sandstone from the Navajo Sandstones.

Reservoir Properties

The extensive winnowing of fines by wind resulted in clean sandstone with high porosity and permeability in the eolian facies of the Navajo and Nugget Sandstones. In the deeper portions of the basin, compaction and secondary diagenesis has greatly reduced the reservoir quality (figures 4.13 and 4.14). Although the Navajo and Nugget appear to be a thick, homogenous reservoir, the dune surfaces, dune set boundaries, and low permeability interdunal deposits, can affect fluid flow (figure 4.6). The Kayenta Formation is dominantly channel deposits with higher clay content than the overlying and underlying eolian deposits. Some individual channel deposits have moderate porosity and permeability but they are laterally discontinuous. The Wingate Sandstone is considered a tight sandstone reservoir with much lower porosity and permeability than the Navajo and Nugget. The Wingate has smaller dune sets and numerous interdune sandstone deposits with high concentration of clay minerals.

Based on porosity determined from density or sonic well logs, feet of sandstone with 6% or more effective porosity (PhiE) ≥ 6%) range from 14 to 1280 feet (4-390 m) with an average of 675 feet (206 m) and median of 761 feet (232 m). PhiE ≥ 12% range from 0 to 1138 feet (0-347 m) with an average of 417 feet (127 m) and median of 350 feet (107 m) (figure 4.15). The ratio of PhiE ≥ 6% and PhiE ≥ 12% to gross reservoir thickness was plotted against drill depth (figure 4.16). Down to a depth of 5000 feet (1500 m) values range from 0.0 to 1.0 but many are in the 0.8 to 1.0 range. Below 5000 feet (1500 m) the ratio begins to decrease rapidly. The feet of sandstone with 6% (PhiE ≥ 6%) and 12% porosity (PhiE ≥ 12%) in the GCG/N reservoir decreases rapidly with depth of burial (figures 4.16). However, since there are few penetrations of the GCG/N reservoir in the deeper portions of the basin, some areas of high porosity and permeability could exist at depth.

Very few GCG/N cores have been taken in the UB. As a result, little is known about the spatial distribution or the porosity to permeability relationship of the reservoir. Numerous Nugget Sandstone cores were taken in the Utah thrust belt northwest of the UB. Keele and Evans (2008) studied the Nugget Sandstone cores from Anschutz Ranch East field in Summit County, Utah, and developed a porosity-to-permeability plot based on facies (figure 4.17). The Nugget in the Utah thrust belt has undergone a much different structural and fluid-flow history than in the UB. Therefore, the thrust belt data was used as a proxy until more porosity and permeability data is gathered from the GCG/N reservoir in the UB.

Water Quality

The northern portion of the Freethey and Stolp (2010) Glen Canyon aquifer study area in east-central Utah overlaps part of our study area. They describe groundwater flow and solute transport between the San Rafael Swell and San Rafael Desert recharge areas and the San Rafael and Green River discharge areas. The area north of Price (in the UB) has little or negligible groundwater flow. Additional recharge areas exist along the southern boundary of the study area and along the northern mountain front boundary. There are no significant discharge areas within the basin.

Anderson and others (2012) mapped the base of the moderately saline water (BMSW) (defined as 10,000 total dissolved solids [TDS]) in the UB. The structure on top of the Navajo-Nugget Sandstone was subtracted from the structure on the BMSW to generate a map of the difference between the BMSW and GCG/N reservoir (figure 4.18). Throughout most of the basin, the GCG/N reservoir is thousands of feet below the BMSW except in Ashley Valley field (figure 1.1) where the water in the GCG/N is less than 10,000 TDS (GCG/N above the BMSW). Freethey and Stolp (2010) found that "dissolved-solids concentrations in the Glen Canyon aquifer in the area south of Price, Utah, increases from about 3000 milligrams/liter (mg/L) to greater than 10,000 mg/L in a horizontal distance of less than 5 miles (8 km) as depth of burial increases by about 1500 feet (460 m)." Anderson and others (2012) mapping did not extend far enough south to capture the 10,000 TDS line in the GCG/N but the 2000-foot (610-m) drill depth is used as an approximation (figure 4.18).

Freethey and Cordy (1991) reported that Mesozoic aquifers in the upper Colorado River basin generally have sodium chloride water in the deep basins in excess of 35,000 mg/L and calcium bicarbonate water in shallow water with less than 2000 mg/L. Both waters have

concentrations of iron and manganese. The hydrologic conductivity of the GCG/N aquifer is 0.1 to 10.0 feet per day (Freethey and Cordy, 1991).

Water quality data for GCG/N from oil and gas wells in the UB is very sparse; we only found 16 samples we believe are reliable. The data shows increasing TDS with depth (figure 4.19). The trend line indicates water is below 10,000 TDS to a depth greater than 6000 feet (2000 m), much deeper than expected from the work of Anderson and others (2012) and Freethey and Stolp (2010). The trend line is not considered reliable due to the few data points and the commingling of production water from other formations. The water types are sodium chloride from one deep well and a mix of all water types, except potassium chloride, from shallow depths (figure 4.20).

Water Production, Use, and Disposal

Hydrocarbon and associated water production from the GCG/N reservoir come from fields on the Uncompahgre uplift and Tavaputs Plateau (in the south-central UB) with some water production from west of the town of Green River. Through December 2014, 15 wells produced a total of 292,418 barrels of water (BW) but nearly half of that volume came from one well (figure 4.21). The average total production per well is 19,495 BW with a median of 4615 BW (figure 4.22). During December 2014, 5 wells produced 276 BW with more than half coming from one well. Four of the wells currently producing water are on the Tavaputs Plateau, the other well is southeast along the Uncompahgre uplift (figure 4.23). Water production per well during the month of December 2014 ranged from 0 to 140 BW.

The ratio of produced gas per barrel of water (GWR) produced per well range from 1 to 276 thousand cubic feet of gas (MCFG)/BW/well (figure 4.24). The average is 127 MCFG/BW with a median of 71 MCFG/BW.

The Navajo reservoir is used for produced water disposal in the coal-bed methane fields in central Utah but is currently not used for disposal in the UB. Freethey and Stolp (2010) developed a numerical simulation model to study the results of injecting into the Navajo. The model involved injecting 25,000 acre-feet over a 36-year period. Simulated water levels in the injection areas increased by 50 feet (15 m) and dissolved-solids concentrations increased by 100 mg/L or more. The increases are accrued into the aquifer storage. Similar results can be expected if the GCG/N reservoir is used for water disposal in the UB. Produced water from the Navajo is probably disposed of in one or more of the four water disposal wells in the Tavaputs Plateau area.

Hydrocarbon Production

Methane production from the GCG/N reservoir occurs along the Uncompahgre uplift and Tavaputs Plateau with minor oil and associated gas production west of the Greater Cisco area (figure 4.25). Most of the methane production is from the Navajo Sandstone with minor amounts from the Wingate Sandstone. Carbon dioxide (CO_2) is produced from the Navajo at Farnham Dome field near Wellington, Utah (figure 4.25). Total methane produced through December 2014 from 15 wells is more than 27 billion cubic feet (BCF) coming mostly from the Tavaputs Plateau (figure 4.26). Methane production from the GCG/N reservoir during December 2015 was primarily from the Tavaputs Plateau with lesser amounts from the

Uncompahgre uplift and Green River Town areas. Total production ranges from 0 (oil with no associated gas) to 8,012,292 MCFG/well with an average of 1,819,612 MCFG/well and a median of 556,422 MCFG/well (figure 4.27). Methane produced during December 2014 from 8 wells was 105,024 MCFG with an average of 13,128 MCFG/well and median of 7768 MCFG/well (figure 4.28).

JURASSIC ENTRADA SANDSTONE

The Jurassic Entrada Sandstone is a coastal eolian and tidal flat-alluvial plain deposit (figure 4.29) underlain by the marine Jurassic Carmel Formation and overlain by the J-3 unconformity, which defines the base of the marginal-marine Curtis Formation (Pipiringos and O'Sullivan, 1978). The Entrada consists of two primary facies: (1) eolian dune deposits in eastern Utah and (2) mudstone-rich, red-bed facies in central Utah. Figure 4.30 is an example of the dune facies near Moab and mudstone-rich facies in the San Rafael Swell. Figure 4.31 is a modern day example in the Namibia Desert of the depositional interpretation of the Entrada. Structure on top of the Entrada shows an asymmetrical UB with the Entrada more than 20,000 feet (6100 m) below mean sea level in the northern portion of the basin (figure 4.32).

Thickness

The Entrada Sandstone is more than 500 feet (150 m) thick in the west, but net sandstone (gamma ray ≤ 60 API) dramatically thins from east to west (figures 4.33 and 4.34). The Entrada

is composed of stacked dune deposits in eastern Utah that typically are well-sorted sandstones with good porosity and permeability. The Entrada in central and western Utah has been described as sand flats or mud-rich red-bed facies. Deposits in the red-bed facies have been interpreted as marine tidal flat, sabkha, and supratidal (Smith, 1976; Marino, 1992; Marino and Morris, 1996; and Hicks and others, 2010). Jennings (2014) describes the Entrada in the west-central portion of the state as dominantly alluvial flood-plain channels sourced from the Elko Fold Belt to the west. The red-bed facies has some thin, (10-foot [3-m]) laterally limited eolian sandstone beds with good reservoir properties.

The gross thickness of the Entrada Sandstone in 329 wells studied ranges from 26 to 1210 feet (8-369 m) with an average of 340 feet (103 m) and median of 273 feet (83 m) (figure 4.35). The net sandstone shows rapid thinning from east (eolian facies) to west (red-bed facies) (figure 4.34). The net sandstone thickness ranges from 6 to 670 feet (2-204 m) with an average of 210 feet (64 m) and median of 194 feet (59 m) (figure 4.36).

Depth

Drill depth to the Entrada Sandstone in the deepest part of the UB, where no well has penetrated the reservoir, is projected to be more than 28,000 feet (8500 m) (figure 4.37). Drill depths in the wells studied range from 19 to 16,550 feet (6-5044 m) with an average of 3974 feet (1211 m) and median of 2684 feet (818 m) (figure 4.38).

Lithology

The eolian facies of the Entrada Sandstone consists of fine-grained feldspathic arenite with alternating clay-rich and less clay-rich laminae (Morris and others, 2005). The eolian facies consists of high angle, trough cross-stratified sandstones with horizontal bedded, occasionally algal-laminated interdunal sandstone, siltstone, and shale. The red-bed facies typically consist of red silty shale and interbedded red channel sandstone beds and thin overbank deposits. In most areas the red-bed facies contains abundant clay.

Reservoir Properties

Porosity and permeability are well developed in the eolian facies of the Entrada Sandstone. Density and sonic logs were used to determine the feet of sandstone with 6% or more porosity (PhiE ≥ 6%) and 12% or more porosity (PhiE ≥ 12%) in 120 wells. Maps of PhiE ≥ 6% and PhiE ≥ 12% follow the paleogeographic trend of the eolian facies but with porosity decreasing in the deeper basin (figures 4.39 and 4.40). Porosity in the red-bed facies is generally developed in thin isolated sandstone beds. PhiE ≥ 6% has a range of 0 to 640 feet (0-195 m) with an average of 114 feet (35 m) and median of 72 feet (22 m) (figure 4.41). PhiE ≥ 12% has a range of 0 to 558 feet (0-170 m) with an average of 66 feet (20 m) and median of 17 feet (5 m) (figure 4.41). The ratio of PhiE ≥ 6% and PhiE ≥ 12% to net sandstone thickness was plotted against drill depth (figure 4.42). Down to a depth of 5000 feet (1500 m), values range from 0.0 to 1.0, with many in the 0.8 to 1.0 range. Below 5000 feet (1500 m) the ratio begins to decrease rapidly. Throughout much of the basin, the Entrada is projected to have less than 20 feet (6 m) of porous sandstone (figures 4.39 and 4.40). There are few penetrations of the Entrada in the

deeper portion of the basin, and undrilled areas of high porosity and permeability could exist at depth.

Very few Entrada Sandstone cores have been taken in the UB. As a result, little is known about the spatial distribution or the porosity-to-permeability relationship of the Entrada. Dyer and Donoho (2008) indicate that in Flat Rock field along the Uncomphagre uplift that overlaps the southeastern UB, the Entrada reservoir has an average porosity of 13%, a maximum of 36%, an average permeability of 5 millidarcies (mD) and maximum of 36 mD, at an average depth of 11,500 feet (3500 m).

Water Quality

The northern portion of the Freethey and Stolp's (2010) east-central Utah Glen Canyon aquifer study area overlaps part of our study area as described in the GCG/N section previously, and is also applicable to the Entrada Sandstone. As was done with the GCG/N, the structure on top of the Entrada was subtracted from the base of the BMSW of Anderson and others (2012) to generate a map of the difference between the BMSW and Entrada reservoir (figure 4.43). Throughout most of the basin, like the GCG/N, the Entrada reservoir is also thousands of feet below the BMSW except in Ashley Valley field (figure 1.1) where the water in the Entrada is less than 10,000 TDS (Entrada above the BMSW). Anderson and others (2012) mapping did not extend far enough south to capture the 10,000 TDS line in the Entrada but the 2000-foot (610-m) drill depth is used as an approximation (figure 4.43).

Water quality data for the Entrada from oil and gas wells in the UB is very sparse; we only found 10 samples we believe are reliable. The data shows increasing TDS with depth

(figure 4.44). The trend line indicates water is below 10,000 TDS to nearly 7000 feet (2000 m), much deeper than expected from the work of Anderson and others (2012) and Freethey and Stolp (2010). The trend line is not considered reliable due to the few data points and the commingling of production water from other formations. The water types are dominantly sodium chloride in deep wells and a mixture of calcium bicarbonate, magnesium bicarbonate, and magnesium sulfate from shallow depths (figure 4.45) generally agreeing with Freethey and Cordy (1991). The hydrologic conductivity of the Entrada aquifer is 0.1 to 10.0 feet per day (Freethey and Cordy, 1991).

Water Production, Use, and Disposal

Nearly all of the hydrocarbon and associated water production from Entrada reservoirs has come fields along the Uncompahgre uplift (figure 4.46). During December 2014, 23 wells produced 2670 BW from the Entrada, water volumes per well for the month ranged from 0 to 399 BW/well. Total water produced from the Entrada through December 2014 is 448,348 BW. Total volume per well from 37 wells range from 0 to 62,286 BW/well with an average of 12,118 BW/well and median of 9249 BW/well (figure 4.47). The GWR has a range from 7 to 134,536 MCFG)/BW (figure 4.48) excluding three wells that produced more than 9 BCFG and no water. The average GWR per well is 5670 MCFG/BW with a median of 200 MCFG/BW.

Hydrocarbon Production

Gas production from the Entrada reservoirs occurs along the Uncompahgre uplift (figure 4.49 and 4.50) in structural and fault traps. Total gas produced through December 2014 from 36 wells completed in the Entrada is 126 BCF. Total gas volumes per well, range from 14,878 to 12,276,656 MCF with an average of 3,509,967 MCFG and a median of 1,931,987 MCFG (figure 4.51). During the month of December 2014, 23 wells produced 406,387 MCF from the Entrada (figure 4.52).

CRETACEOUS CEDAR MOUNTAIN AND DAKOTA FORMATIONS

The Cretaceous Cedar Mountain and Dakota (CMKD) Formations (figure 1.5) were mapped as one reservoir unit. Almost all production is commingled and the boundary between the two formations can be very difficult to identify in many geophysical well logs. The Jurassic Morrison Formation was originally included in the group, but the gas and water production is not regionally significant. Also, most wells drilled to test the Cretaceous through Morrison interval only partially penetrate the Morrison. The CMKD consists of southwest to northeast trending fluvial channel, associated overbank deposits, and marginal marine deposits in the upper Dakota (figure 5.53). Structure on top of the Dakota shows an asymmetrical UB with the Dakota more than 20,000 feet (6000 m) below mean sea level in the northern portion of the basin (figure 5.54). Significant recent studies of the CMKD Formations funded by the UGS are: McPherson and, others, 2006; Currie and others, 2007, 2011.

Thickness

The CMKD reservoir generally thins regionally from the southwest to northeast (figure 4.55) reflecting the general channel flow direction illustrated in figure 4.53. Gross thickness of the CMKD reservoir ranges from 15 to 1048 feet (5-319 m) with an average of 220 feet (67 m) and a median of 203 feet (62 m) (figure 4.56). The net sandstone (gamma ray ≤ 60 API or less) shows a southwest to northeast trend with some northwest to southeast trends in the northeast portion of the UB possibly reflecting the influence of littoral marine sandstone deposits of the advancing Cretaceous sea (Currie and others, 2011) (figure 4.57). Net sandstone thickness of the CMKD reservoir ranges from 0 to 218 feet (0-66 m) with an average of 61 feet (19 m) and a median of 56 feet (17 m) (figure 4.58).

Depth

Drill depth to the CMKD reservoir in the deepest part of the basin, where no well has penetrated the Dakota, is projected to be more than 26,000 feet (7900 m) (figure 4.59). Drill depths in the wells studied range from 21 to 18,902 feet (6-5761 m) with an average depth of 4036 feet (1230 m) and median of 2683 feet (818 m) (figure 4.60).

Lithology

The CMKD Formations are fluvial channel and overbank deposits, some littoral marine deposits, with carbonaceous shale and coal in the upper Dakota Sandstone. The primary reservoir lithologies are conglomerate and coarse- to fine-grain sandstone. Most of the

conglomerate and coarse-grain sandstone is in the Cedar Mountain and lower Dakota. Young (1973) describes the Cedar Mountain as generally conglomerate to coarse-grain sandstone with carbonate cement. Cedar Mountain sandstones are commonly cemented with calcite and rarely silica. The Dakota typically has conglomerate sandstone at the base, a middle unit consisting of carbonaceous shale, coal, sandstone, and siltstone, and an upper unit of massive medium-grain sandstone (Young, 1973). The Dakota sandstones are commonly cemented by silica, kaolinite, smectite, hematite, and rarely calcite (McPherson and others, 2006; Currie and others, 2007, 2011).

Reservoir Properties

Porosity and permeability within the channel sandstones can be highly variable and difficult to predict. Density and sonic logs were used to determine the feet of sandstone with 6% or more porosity (PhiE ≥ 6%) and 12% or more porosity (PhiE ≥ 12%) in 428 wells. A map of the PhiE ≥ 6% (figure 4.61) shows similar trends as the net sandstone thickness map (figure 4.57), indicating porosity distribution is dominated by the sandstone thickness. A porous sand trend is parallel, but slightly southeast of net sandstone thickness trend and the thickness of porous sand with at least 6% porosity is generally less than half of the total sandstone thickness. The map of the PhiE ≥ 12% (figure 4.62) has a similar pattern, but greatly reduced thickness with most of the basin being less than 20 feet (6 m). PhiE ≥ 6% ranges from 0 to 152 feet (0-46 m) with an average of 50 feet (15 m) and a median of 46 feet (14 m). PhiE ≥ 12% ranges from 0 to 144 feet (0-44 m) with an average of 30 feet (14 m) and a median of 26 feet (8 m) (figure 4.63). The ratio of PhiE ≥ 6% and PhiE ≥ 12% to net sandstone thickness was plotted against

drill depth (figure 4.64). Many wells have a PhiE ≥ 6%/net sandstone ratio of 0.8 to 1.0 down to a depth of 10,000 feet (3050 m). Below 10,000 feet (3050 m) the ratio of PhiE ≥ 6%/net sandstone decreases but has a random distribution. Many of the wells have a PhiE ≥ 12%/net sandstone ratio of 0.7 to 1.0 down to a depth of 9000 feet but with a range of 0.0 to 1.0. Below 9000 (2750 m) feet the ratio of PhiE ≥ 12%/ net sandstone decreases rapidly. Both ratios (6% and 12%/net sandstone) show a significant drop in porous reservoir with increasing depth.

Permeability is highly variable in the heterolithic channel deposits of the CMKD reservoir. Variability occurs spatially in the basin, with depth, and within individual channel deposits. Currie and others (2011) used core data to plot porosity versus permeability based on grain size (figure 4.65). Permeability varied from 0.01 mD (lower limit of the core measurement) to 100 mD. A best fit logarithmic relationship is shown, but the permeability varies by several orders of magnitude at almost every value of porosity.

Water Quality

The CMKD outcrops along the southern and northern margins of the UB. The southern margin receives 6 to 10 inches (15-25 cm) of annual rainfall (Freethey and Cordy, 1991). The structural configuration creates geometry similar to a bowl with no groundwater discharge. Deep burial suggests little or no recharge into the basin resulting in a bowl filled with dense brine (Freethey and Stolp, 2010). As with the GCG/N and the Entrada Sandstone, the structure on top of the Dakota Formation was subtracted from the base of the BMSW of Anderson and others (2012) to generate a map of the difference between the BMSW and CMKD reservoir (figure 4.66). Again, throughout most of the basin, the CMKD reservoir is thousands of feet below the

BMSW except in Ashley Valley field where the water in the CMKD reservoir is less than 10,000 TDS (CMKD above the BMSW). As with the GCG/N and Entrada, Anderson and others (2012) mapping did not extend far enough south to capture the 10,000 TDS line in the CMKD but the 2000-foot (610-m) drill depth is used as an approximation (figure 4.66).

Water quality data for CMKD from oil and gas wells in the UB is also very sparse; only eight reliable samples were found. As expected, the data shows increasing TDS with depth (figure 4.67). As in the deeper section, the trend line indicates water is below 10,000 TDS to a depth greater than 10,000 feet (3000 m), again much deeper than expected from the work of Anderson and others (2012) and Freethey and Stolp (2010). Therefore, as was the case in the GCG/N and Entrada, the trend line is not considered reliable due to the few data points and the commingling of production water from other formations. The water types are dominantly sodium chloride in deep wells and sodium bicarbonate (one sample) from shallow depth (figure 4.68) in general agreement with Freethey and Cordy (1991). The hydrologic conductivity of the Dakota aquifer is 0.001 to 1.0 feet per day (Freethey and Cordy, 1991).

Water Production, Use, and Disposal

Historically, most of the production from the CMKD reservoir came from fields in the southern portion of the basin along the Uncompahgre uplift and Greater Cisco field (figure 1.1). Recently, several wells have been drilled to the CMKD in the greater Natural Buttes field area. The GNB wells are typically completed with commingled production from the CMKD, Mancos, Mesaverde, and occasionally Wasatch reservoirs (figure 1.5). Production from individual reservoirs is not reported in these wells, so the volume of water and hydrocarbons produced from

the CMKD alone cannot be determined. The production shown in this report as CMKD is often commingled production. The largest volume of CMKD produced water comes from the GNB area (figure 4.69), but much of this water is probably coming from the Mancos and Mesaverde. Water production for the month of December 2014 shows a similar pattern (figure 4.70). The frequency distribution of cumulative produced water (figure 4.71) ranges from 0 to 4,784,213 BW/well with an average of 121,730 BW/well and a median of 2908 BW/well. The frequency distribution of produced gas per barrel of water produced (GWR) (figure 4.72) has a range of 0.2 to 710.662.0 MCFG/BW with an average of 4692.2 MCFG/BW and a median of 79.2 MCFG/BW from 351 wells. Eighty-one CMKD gas wells have no associated water production.

Hydrocarbon Production

Channel and some marginal-marine deposits in the CMKD provide stratigraphic traps for hydrocarbons in the UB. Methane is produced throughout the basin from the CMKD reservoir. Production can be spotty and volumes highly variable due to the heterogeneity of the channel deposits. Large volumes of gas have been produced from both the northern greater Natural Buttes field and Uncompahgre areas (figure 4.73). Production from the Natural Buttes field is generally from newer wells that may eventually exceed production from wells in the rest of the basin. However, production from the field is commingled and the CMKD contribution is unknown. The total gas production from the CMKD (including commingled production) ranges from 143 to 12,123,393 MCFG/well averaging 737,753 MCFG/well and a median of 422,803 MCFG/well (figure 4.74). Gas production for the month of December 2014 shows larger volumes of gas per well are being produced from the greater Natural Buttes field area (figure

4.75). December production ranges from 0 to 59,485 MCFG/well averaging 3383 MCFG/well with a median of 957 MCFG/well (figure 4.76) from 432 wells, of which 77 wells had no production during the month of December.

SUMMARY

The Triassic-Jurassic GCG/N is more than 800 feet (250 m) thick throughout much of the UB; the Lower Jurassic eolian Navajo Sandstone is the thickest and highest quality reservoir/aquifer. Drill depth to the GCG/N in the deepest part of the basin is projected to be more than 28,000 feet (8500 m). The lithology of dune deposits of the Navajo (and equivalent section of the Nugget Sandstone) are generally composed of well sorted fine- to medium-grained sandstone. Feet of sandstone with 6% or more porosity range from 14 to 1280 feet (4-390 m) with an average of 675 feet. Throughout most of the basin, the GCG/N reservoir is thousands of feet below the BMSW. TDS with increases with depth and the water types are sodium chloride from one deep well and a mix of all water types, except potassium chloride, from shallow depths. Hydrocarbon and associated water production from the mainly from the Navajo Sandstone come from fields on the Uncompahgre uplift and Tavaputs Plateau; CO_2 is produced from the Navajo at Farnham Dome field. The Navajo reservoir is used for produced water disposal in the coal-bed methane fields in central Utah but is currently not used for disposal in the UB.

The Jurassic Entrada Sandstone ranges in thickness from 26 to 1210 feet (8-369 m) and thins from east to west. Drill depths to the Entrada in the wells studied reach up to 16,550 feet (5044 m). The lithology of coastal eolian facies consists of fine-grained feldspathic sandstone,

whereas the tidal flat-alluvial plain red-bed facies is composed of red silty shale and interbedded red channel sandstone. The Jurassic Entrada Sandstone is projected to have less than 20 feet of porous sandstone throughout much of the basin with the best porosity and permeability in the eolian facies; however, the usable porosity begins to decrease rapidly below 5000 feet drill depth. The Entrada reservoir is also thousands of feet below the BMSW and as expected the TDS increase with depth. The water types are dominantly sodium chloride in deep wells and a mixture of calcium bicarbonate, magnesium bicarbonate, and magnesium sulfate from shallow depths. Hydrocarbon and associated water production from Entrada reservoirs comes fields along the Uncompahgre uplift. The Entrada is not used for produced water disposal in the UB.

The Cretaceous CMKD are mainly fluvial deposits that thin regionally from less than 25 feet in the southwest to over 250 feet in the northeast part of the UB. Drill depths to the CMKD reservoirs in the wells studied range from 21 to 18,902 feet (6-5761 m). The primary reservoir lithologies are conglomerate and coarse- to fine-grain sandstone. Porosity and permeability within the channel sandstones are highly variable, however, a porous sand trend is parallel, but slightly southeast of net sandstone thickness trend. The thickness of porous sand with at least 6% porosity is generally less than half of the total sandstone thickness. Again, throughout most of the basin, the CMKD reservoir is thousands of feet below the BMSW and the water types are dominantly sodium chloride in deep wells and sodium bicarbonate from shallow depths. Hydrocarbon and associated water production from the CMKD reservoir comes stratigraphic traps created by small, lenticular channel deposits. CMKD fields are located in the southern portion of the basin along the Uncompahgre uplift and the greater Natural Buttes field area where production is commingled with that of the Mancos, Mesaverde, and Wasatch reservoirs.

CHAPTER IV FIGURE CAPTIONS

Figure 4.1. Early Jurassic paleogeography was dominated by dune deposits of the Wingate Sandstone. Red arrows indicate prevailing wind directions. Modified from Blakey and Ranney, 2008.

Figure 4.2. Early Jurassic Kayenta Formation paleogeography. Sand-rich braided streams flowed west across a broad floodplain from the Ancestral Rockies to the east. Red arrow indicate prevailing wind direction. Modified from Blakey and Ranney, 2008.

Figure 4.3. Early Jurassic Navajo and Nugget Sandstone paleogeography. Most of the Colorado Plateau and all of the Uinta Basin were covered by extensive dune deposits. Red arrows indicate prevailing wind directions. Modified from Blakey and Ranney, 2008.

Figure 4.4. Outcrop of the Glen Canyon Group, in ascending order: Wingate, Kayenta, and Navajo Formations along the Buckhorn Wash road, northern San Rafael Swell. The contact between the Kayenta and overlying Navajo Sandstone is gradational.

Figure 4.5. Navajo facies and bedform types showing some of the depositional details that can affect fluid flow in an eolian dune reservoir. From Allen and others, 2011.

Figure 4.6. Heterogeneity within dune sets. Three-dimensional model of a portion of the Navajo Sandstone along the west flank of the San Rafael Swell. From Allen and others, 2011.

Figure 4.7. Structure on top of the Navajo–Nugget Sandstone, Uinta Basin.

Figure 4.8. Thickness from the top of the Navajo–Nugget Sandstone to the top of the Chinle Formation for areas greater than 2000 feet deep.

Figure 4.9. Frequency distribution of the gross thickness of the GCG/N reservoir in the geophysical well logs studied. The thickness ranges from 178 to 1725 feet (54-526 m), with an average of 882 feet (269 m) and median of 869 feet (265).

Figure 4.10. Drill depth greater than 2000 feet (600 m) to the top of the Navajo-Nugget Sandstone.

Figure 4.11. Frequency distribution of the drill depth to the top of the GCG/N reservoir in the geophysical well logs studied. The drill depth ranges from 30 to 16,960 feet (9-5169 m) with an average of 3198 feet (975 m) and median of 2397 feet (731 m).

Figure 4.12. Outcrop of a portion of the Navajo Sandstone with large dune sets. Harris Wash in the Grand Staircase-Escalante National Monument, southeast of the town of Escalante in south-central Utah.

Figure 4.13. Feet of sandstone in the GCG/N reservoir with ≥ 6% porosity. Porosity determined from density and sonic well logs for areas primarily with greater than 2000 feet of depth.

Figure 4.14. Feet of sandstone in the GCG/N reservoir with ≥ 12% porosity for areas at more than 2000 feet deep. Porosity determined from density and sonic well logs.

Figure 4.15. Frequency distribution graphs of the feet of sandstone with (A) PhiE ≥ 6% and (B) ≥ (PhiE ≥ 12% in the GCG/N reservoir. PhiE ≥ 6% ranges from 14 to 1280 feet (4-390 m) with an average of 675 feet (206 m) and a median of 761 feet (232 m). PhiE ≥ 12% ranges from 0 to 1138 feet (0-347 m), with an average of 417 feet (127 m) and median of 350 feet (350 m).

Figure 4.16. (A) Ratio of PhiE ≥ 6% to reservoir thickness versus drill depth, and (B) ratio of PhiE ≥ 12% to reservoir thickness versus drill depth in the GCG/N reservoir. Porosity calculated from density or sonic logs.

Figure 4.17. Porosity–permeability plot separated into facies. The dune facies has the highest reservoir potential. Core data from the Nugget Sandstone, Anschutz Ranch East field, Summit County, Utah. From Keele and Evans, 2008.

Figure 4.18. Drill depth (feet) from the base of the moderately saline water (BMSW) to the top of the Navajo-Nugget Sandstone. The Nugget is above the BMSW in Ashley Valley (see figure 1.1 for field location). The map was created using ArcScene® by subtracting the drill depth map (figure 4.10) from the BMSA map of Anderson and others (2012).

Figure 4.19. Total dissolved solids (milligrams/liter [mg/L]) with depth (feet). The exponential trend line (Expon.) indicates less than 10,000 TDS to a depth of 10,000 feet (3000 m). The limited number of samples from deep wells (one) is insufficient to be statistically significant for such a large area.

Figure 4.20. Water produced from the GCG/N is sodium chloride (Na-Cl) from one deep well (> 5000 feet [150]) and a mix of all the water types except potassium chloride, at shallower depths. The number of samples from deep wells (one) is not statistically significant for such a large area.

Figure 4.21. Total water produced from the GCG/N reservoir.

Figure 4.22. Frequency diagram of total water per well produced from the GCG/N reservoir. Total water produced through December 2014 is 292,418 BW, nearly half coming from one well. Water volumes range from 0 to 140,079 BW/well, the average is 19,495 BW with a median of 4615 BW.

Figure 4.23. Water produced from the GCG/N reservoir during the month of December 2014.

Figure 4.24. Frequency diagram of total gas produced per barrel of water per well from the GCG/N reservoir. Gas volumes are in thousand cubic feet (MCF). The range is from 1 to 276 MCFG/BW, with an average of 127 MCFG/BW and a median of 71 MCFG/BW. Five wells not included in this data set, produce gas and no water.

Figure 4.25. Total gas produced per well from the GCG/N reservoir through December 2014.

Figure 4.26. Gas produced from the GCG/N reservoir during the month of December 2014.

Figure 4.27. Frequency diagram of total gas produced per well from the GCG/N reservoir through December 2014. Gas volumes range from 0 to 8,012,292 MCFG/well with an average of 1,819,612 MCFG/well and a median of 556,422 MCFG/well.

Figure 4.28. Frequency distribution diagram of gas produced per well from the GCG/N reservoir during December 2014. Production ranges from 1 to 48,628 MCFG/well with an average of 13,128 MCFG/well and median of 7768 MCFG/well.

Figure 4.29. Paleogeographic interpretation of the Entrada Sandstone. Riggs and Blakey (1993) and Peterson (1994) refer to the Entrada deposits in central Utah as sand flats, also commonly referred to as red-bed or mud-rich facies. Jennings (2014) describes the Entrada in central Utah as dominantly alluvial plain deposits sourced from the Elko Fold Belt to the west. Red arrows indicate wind direction during the Early and Middle Jurassic. Modified from Blakey and Ranney, 2008.

Figure 4.30. Entrada Sandstone dune facies (A) in Arches National Park near Moab and mud-rich facies (B) in the San Rafael Swell. Photograph B from Morris and Hicks, 2011.

Figure 4.31. Working depositional model (Morris and others, 2005) with eolian dunes encroaching on a tidal flat, Namibia Desert.

Figure 4.32. Structure on top of the Entrada Sandstone, Uinta Basin.

Figure 4.33. Gross thickness of the Entrada Sandstone for areas greater than 2000 feet (610 m) deep.

Figure 4.34. Net sandstone (gamma ray ≤ 60 API) in the Entrada Sandstone for areas greater than 2000 feet (610 m) deep.

Figure 4.35. Frequency distribution of the gross thickness of the Entrada Sandstone in the geophysical well logs studied. The thickness ranges from 26 to 1210 feet (8-369 m), with an average of 340 feet (104 m) and a median of 273 feet (83 m).

Figure 4.36. Frequency distribution of the net sandstone (≤ 60 API gamma ray) in the Entrada Sandstone in the geophysical well logs studied. The thickness ranges from 6 to 670 feet (2-204 m) with an average of 210 feet (64 m) and a median of 194 feet (59 m).

Figure 4.37. Drill depth to the top of the Entrada Sandstone for areas greater than 2000 feet (60 m) deep.

Figure 4.38. Frequency distribution of the drill depth in feet to the top of the Entrada Sandstone in the geophysical well logs studied. The drill depth ranges from 19 to 16,550 feet (6-5044 m) with an average of 3974 feet (1211 m) and median of 2684 feet (818 m).

Figure 4.39. Feet of sandstone in the Entrada Sandstone with 6% or more porosity for areas greater than 2000 feet (210 m) deep. Porosity determined from density or sonic well logs.

Figure 4.40. Feet of sandstone in the Entrada Sandstone with 12% or more porosity for areas greater than 2000 feet (210 m) deep. Porosity determined from density or sonic well logs.

Figure 4.41. Frequency distribution graphs of the feet of sandstone with (A) ≥ 6% porosity (PhiE ≥ 6%) and (B) ≥ 12% porosity (PhiE ≥ 12%) in the Entrada Sandstone. PhiE ≥ 6% ranges from 0 to 640 feet (195 m) with an average of 114 feet (35 m) and a median of 72 feet (22 m). PhiE ≥ 12% ranges from 0 to 558 feet (0-170 m) with an average of 66 feet (20 m) and median of 17 feet (5 m).

Figure 4.42. (A) Ratio of PhiE ≥ 6%/net sandstone versus drill depth, and (B) ratio of PhiE ≥ 12%/net sandstone versus drill depth in the Entrada Sandstone. Porosity calculated from density or sonic logs.

Figure 4.43. Drill depth (feet) from the base of the moderately saline water (BMSW) to the top of the Entrada Sandstone. The Entrada is above the BMSW in Ashley Valley (see figure 1.1 for

field location). The map was created using ArcScene® by subtracting the drill depth map (figure 4.37) from the BMSA map of Anderson and others (2012).

Figure 4.44. Total dissolved solids (mg/L) with depth (feet). The exponential trend line (Expon.) indicates less than 10,000 TDS to a depth of 7000 feet. The limited number of samples (10) is insufficient to be statistically significant for such a large area.

Figure 4.45. Water produced from the Entrada is mostly sodium chloride (Na-Cl) at depths greater than 7000 feet, and a mix of calcium bicarbonate (Ca-HCO_3), magnesium bicarbonate (Mg-HCO_3), and magnesium sulfate (Mg-SO_4), at shallower depths. The number of samples (10) is not statistically significant for such a large area.

Figure 4.46. Total barrels of water produced from the Entrada Sandstone.

Figure 4.47. Frequency diagram of total water per well produced from the Entrada Sandstone. Water volumes range from 0 to 62,286 BW/well, the average is 12,118 BW with a median 9249 BW.

Figure 4.48. Frequency diagram of total gas produced per barrel of water (BW). Gas volumes are in thousand cubic feet (MCF). The range is from 7 to 134,536 MCFG/BW with an average of 5670 MCFG/BW and median of 200 MCFG/BW. Three wells not included in this data produced more than 9 BCF of gas and no water.

Figure 4.49. Gas produced from the Entrada Sandstone during the month of December 2014.

Figure 4.50. Total gas produced per well from the Entrada Sandstone through December 2014.

Figure 4.51. Frequency diagram of total gas produced per well from the Entrada Sandstone through December 2014. Gas volumes range from 14,878 to 12,276,656 MCFG/well with an average of 3,509,967 MCFG/well and median of 1,931,987 MCFG/well.

Figure 4.52. Frequency distribution diagram of gas produced per well from the Entrada Sandstone during December 2014. Production ranges from 118 to 181,310 MCFG/well with an average of 17,669 MCFG/well and a median of 6954 MCFG/well.

Figure 4.53. Early Cretaceous paleogeography. A – Cedar Mountain Formation, Early Cretaceous (125 Ma). B – Dakota Formation, Early Cretaceous (105 Ma). From Blakey and Ranney, 2008.

Figure 4.54. Structure on top of the Dakota Formation, Uinta Basin.

Figure 4.55. Gross thickness of the CMKD reservoir for areas greater than 2000 feet (610 m) deep.

Figure 4.56. Frequency distribution of the gross thickness of CMKD reservoir in the geophysical well logs studied. The thickness ranges from 15 to 1048 feet (5-319 m), with an average of 220 feet (67 m) and a median 203 feet (62 m).

Figure 4.57. Net sandstone (gamma ray ≤ 60 API) thickness of the CMKD reservoir for areas greater than 2000 feet (210 m) deep.

Figure 4.58. Frequency distribution of the net sandstone (≤60 API gamma ray) in the CMKD reservoir in the geophysical well logs studied. The thickness ranges from 0 to 218 feet (0-66 m), with an average of 61 feet (19 m) and a median of 56 feet (17 m).

Figure 4.59. Drill depth to the top of the Dakota Formation for areas greater than 2000 feet (610 m) deep.

Figure 4.60. Frequency distribution of the drill depth to the top of the Dakota Formation. The drill depth ranges from 21 to 18,902 feet (6-5761 m) with an average depth of 4038 feet (1230 m) and a median of 2685 feet (818 m).

Figure 4.61. Feet of sandstone with porosity ≥ 6% in the CMKD reservoir for areas greater than 2000 feet (610 m) deep. Porosity derived from density or sonic geophysical well logs.

Figure 4.62. Feet of sandstone with porosity ≥ 12% in the CMKD reservoir for areas greater than 2000 feet (610 m) deep. Porosity derived from density or sonic geophysical well logs.

Figure 4.63. Frequency distribution graphs of the feet of sandstone with ≥ 6% porosity (A) and ≥ 12% porosity (B) in the CMKD reservoir. The feet of sandstone with ≥ 6% porosity ranges from 0 to 152 feet (0-46 m), with an average of 50 feet (15 m) and a median of 46 feet (14 m). The feet of sandstone with ≥ 12% porosity ranges from 0 to 144 feet (0-44 m) with an average of 30 feet (9 m) and a median of 26 feet (8 m).

Figure 4.64. (A) Ratio of feet of sandstone with ≥ 6% porosity/net sandstone versus depth, and (B) ratio of ≥ 12% porosity/net sandstone, in the CMKD reservoir. Porosity calculated from density or sonic logs.

Figure 4.65. Plot of percent porosity versus permeability for 364 core data points. Values are color coded by grain size. From Currie and others, 2011.

Figure 4.66. Drill depth (feet) from the base of the moderately saline water (BMSW) to the top of the Dakota Formation. The Dakota is above the BMSW in Ashley Valley field (see figure 1.1 for field location). The map was created using ArcScene® by subtracting the drill depth map (figure 4.59) from the BMSA map of Anderson and others (2012).

Figure 4.67. Total dissolved solids (mg/L) with depth (feet). The exponential trend line (Expon.) indicates less than 10,000 TDS to a depth of 10,000 feet (3000 m). The limited number of samples (eight) is insufficient to be statistically significant for such a large area.

Figure 4.68. Water produced from the KDCM is mostly sodium chloride (Na-Cl) at depths greater than 5000 feet (1500 m) and sodium bicarbonate (Na-HCO_3) at shallower depth (one sample). The number of samples (eight) is not statistically significant for such a large area.

Figure 4.69. Total water produced from the CMKD reservoir through December 2015. Many wells are completed in more than just the CMKD. As a result, much of the water may be coming from other reservoirs.

Figure 4.70. Water produced from the CMKD reservoir during December 2014. Many wells are commingled with other reservoirs and the majority of the produced water may not be from the CMKD.

Figure 4.71. Frequency diagram of the total water produced from the CMKD reservoir. Water volumes range from 0 to 4,784,213 BW, the average is 121,730 BW with a median of 2908 BW. Many of the wells producing from the CMKD reservoir are commingled with shallower reservoirs such as Mancos, Mesaverde, and Wasatch. Production volumes cannot be separated from the numerous commingled reservoirs.

Figure 4.72. Frequency diagram of the gas per barrel of water produced per well (GWR). Gas volumes are in thousand cubic feet (MCFG). The range is from 0 to710,622 MCFG/BW with an average of 469 MCFG/BW and a median of 79 MCFG/BW.

Figure 4.73. Total gas (MCFG) produced from the CMKD through the month of December 2014. Many of the wells producing from the CMKD reservoir are commingled with shallower reservoirs such as Mancos, Mesaverde, and Wasatch. Wells in the north are generally younger and commingled with Mancos and Mesaverde.

Figure 4.74. Frequency diagram of total gas (MCFG) produced from the CMKD reservoir through December 2014. Production ranges from 143 to 12,123,393 MCFG/month with an average of 737,753 MCFG and median of 422,803 MCFG. Many of the wells producing from the CMKD reservoir are commingled with shallower reservoirs such as Mancos, Mesaverde, and Wasatch.

Figure 4.75. Gas production (MCFG) from the CMKD during the month of December 2014. Many of the wells producing from the CMKD reservoir are commingled with shallower reservoirs such as Mancos, Mesaverde, and Wasatch. Wells in the north are generally younger and commingled with Mancos and Mesaverde.

Figure 4.76. Frequency diagram of gas produced (MCFG) from the CMKD reservoir during December 2014. Production ranges from 0 to 59,485 MCFG/month with an average of 3383 MCFG and median of 958 MCFG. Many of the wells producing from the CMKD reservoir are commingled with shallower reservoirs such as Mancos, Mesaverde, and Wasatch.

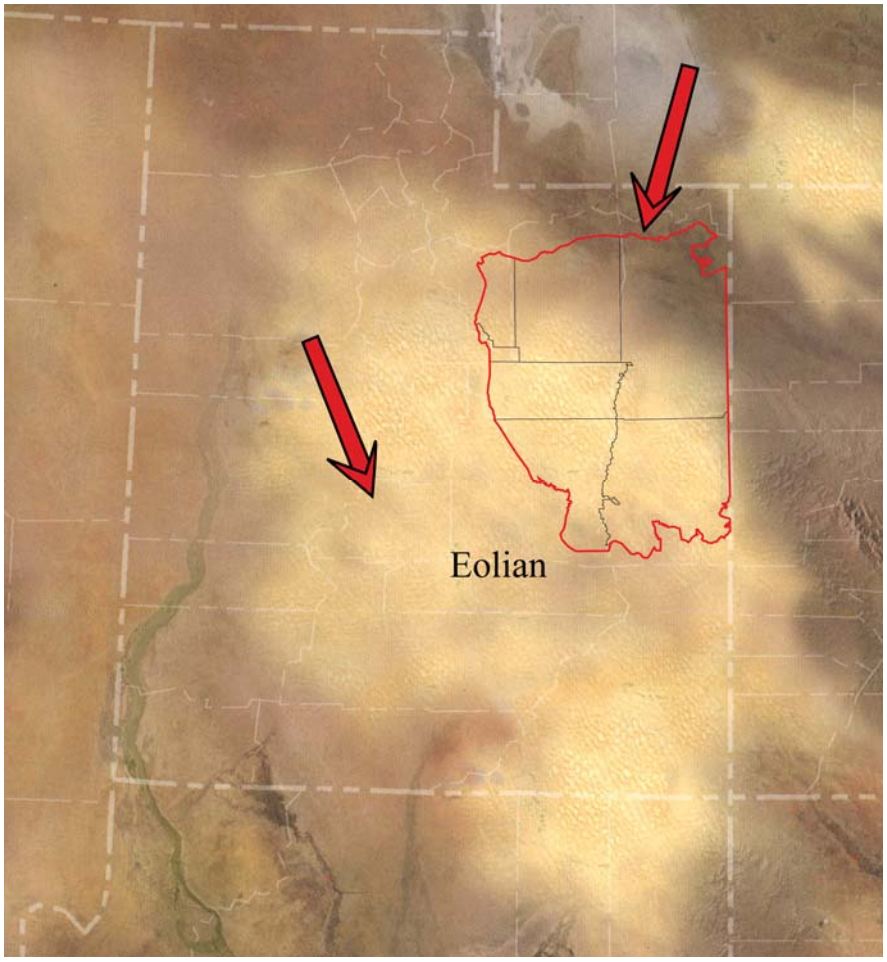

Figure 4.1. Early Jurassic paleogeography was dominated by dune deposits of the Wingate Sandstone. Red arrows indicate prevailing wind directions. Modified from Blakey and Ranney, 2008.

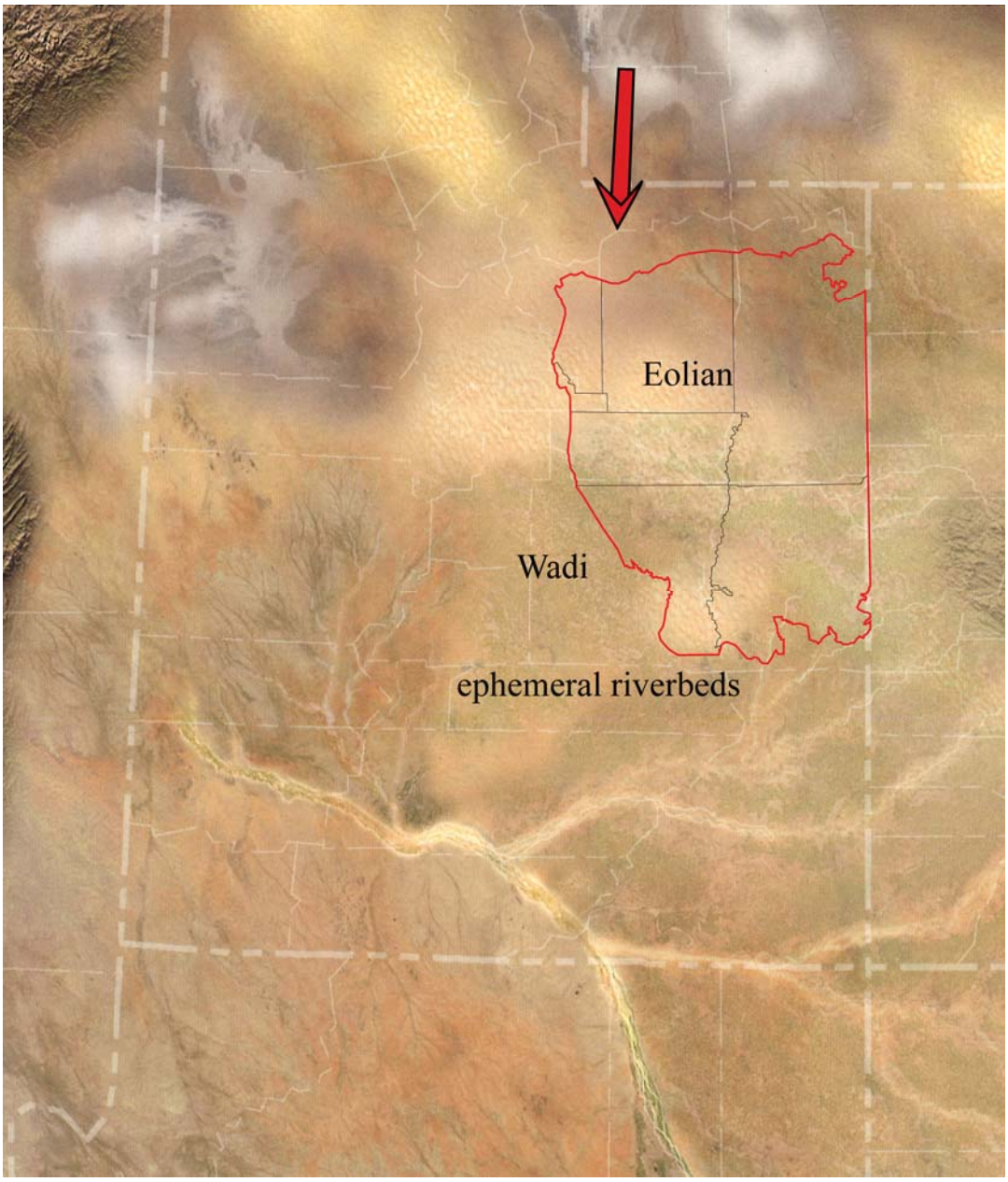

Figure 4.2. Early Jurassic Kayenta Formation paleogeography. Sand-rich braided streams flowed west across a broad floodplain from the Ancestral Rockies to the east. Red arrow indicate prevailing wind direction. Modified from Blakey and Ranney, 2008.

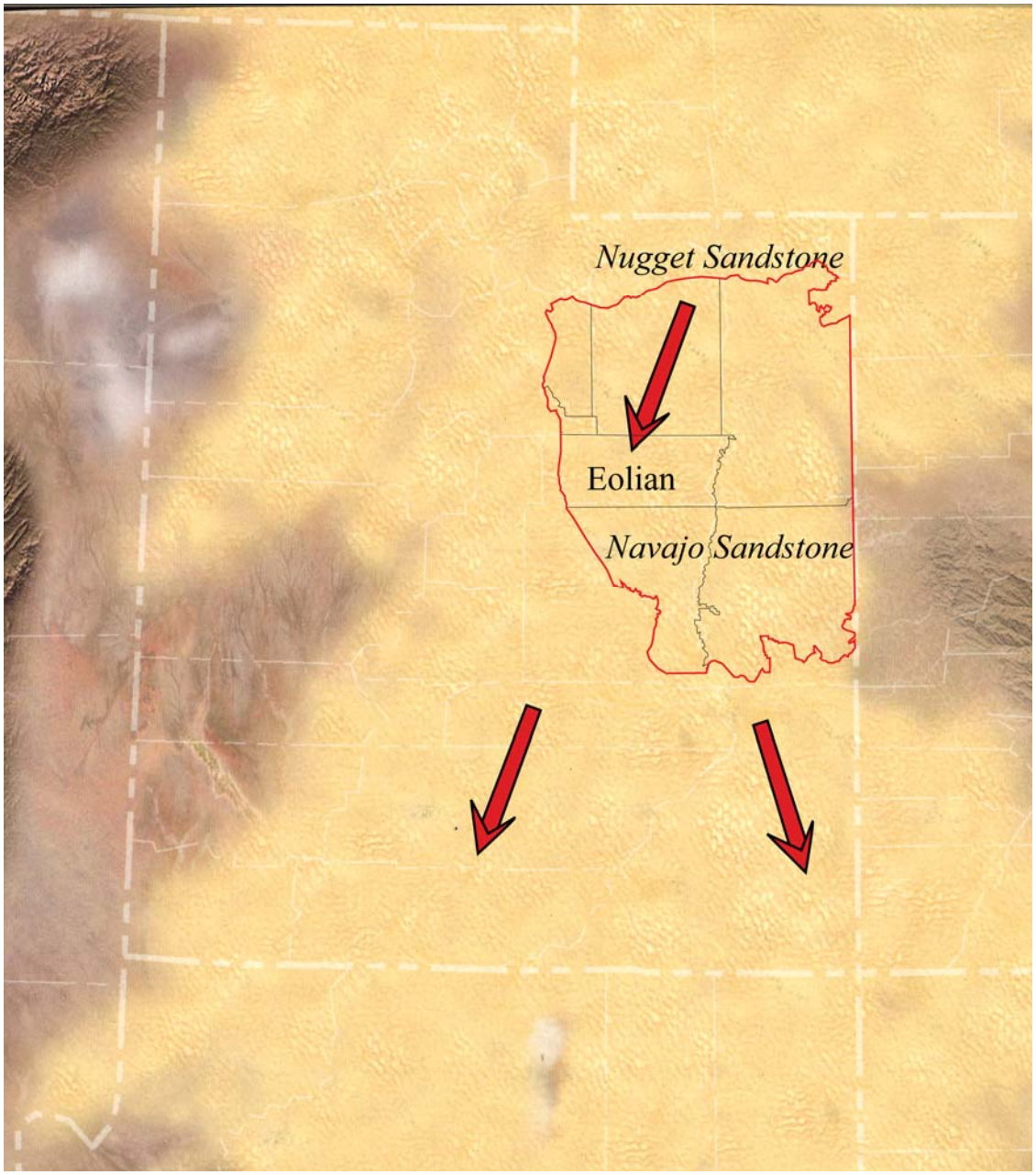

Figure 4.3. Early Jurassic Navajo and Nugget Sandstone paleogeography. Most of the Colorado Plateau and all of the Uinta Basin were covered by extensive dune deposits. Red arrows indicate prevailing wind directions. Modified from Blakey and Ranney, 2008.

Figure 4.4. Outcrop of the Glen Canyon Group, in ascending order: Wingate, Kayenta, and Navajo Formations along the Buckhorn Wash road, northern San Rafael Swell. The contact between the Kayenta and overlying Navajo Sandstone is gradational.

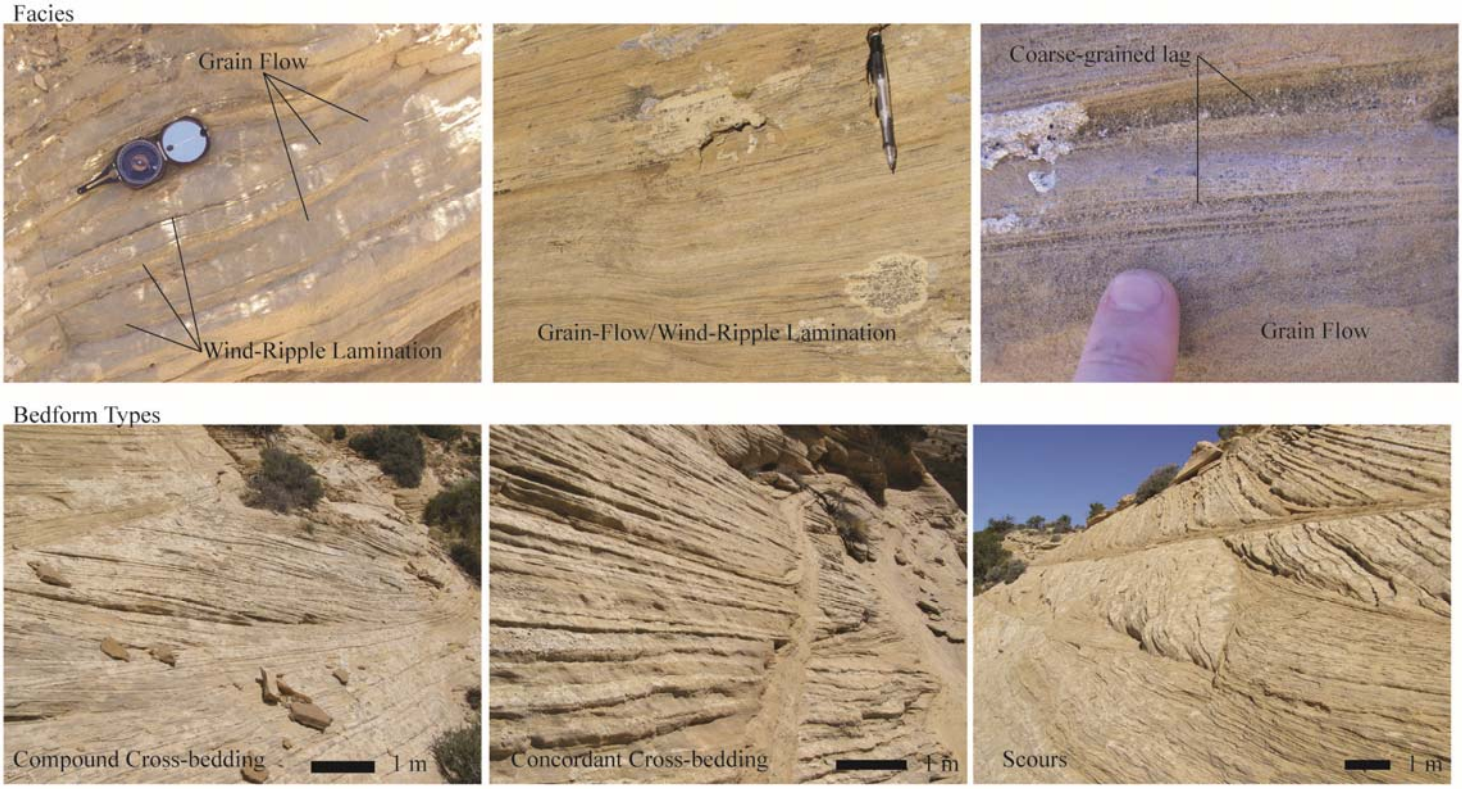

Figure 4.5. Navajo facies and bedform types showing some of the depositional details that can affect fluid flow in an eolian dune reservoir. From Allen and others, 2011.

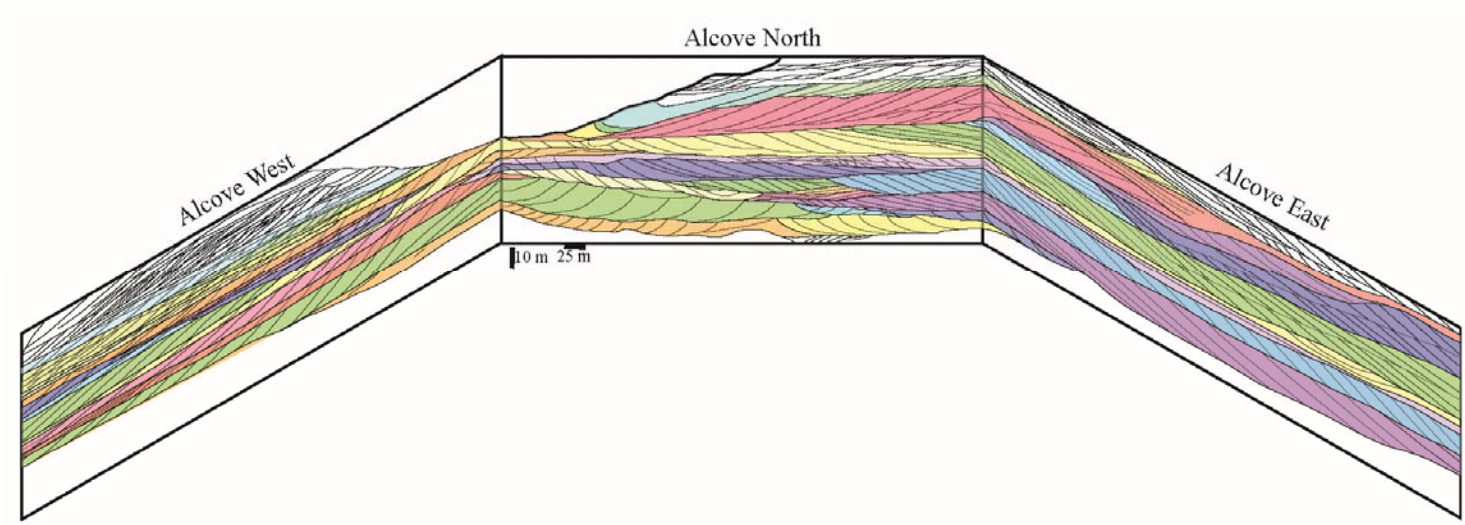

Figure 4.6. Heterogeneity within dune sets. Three-dimensional model of a portion of the Navajo Sandstone along the west flank of the San Rafael Swell. From Allen and others, 2011.

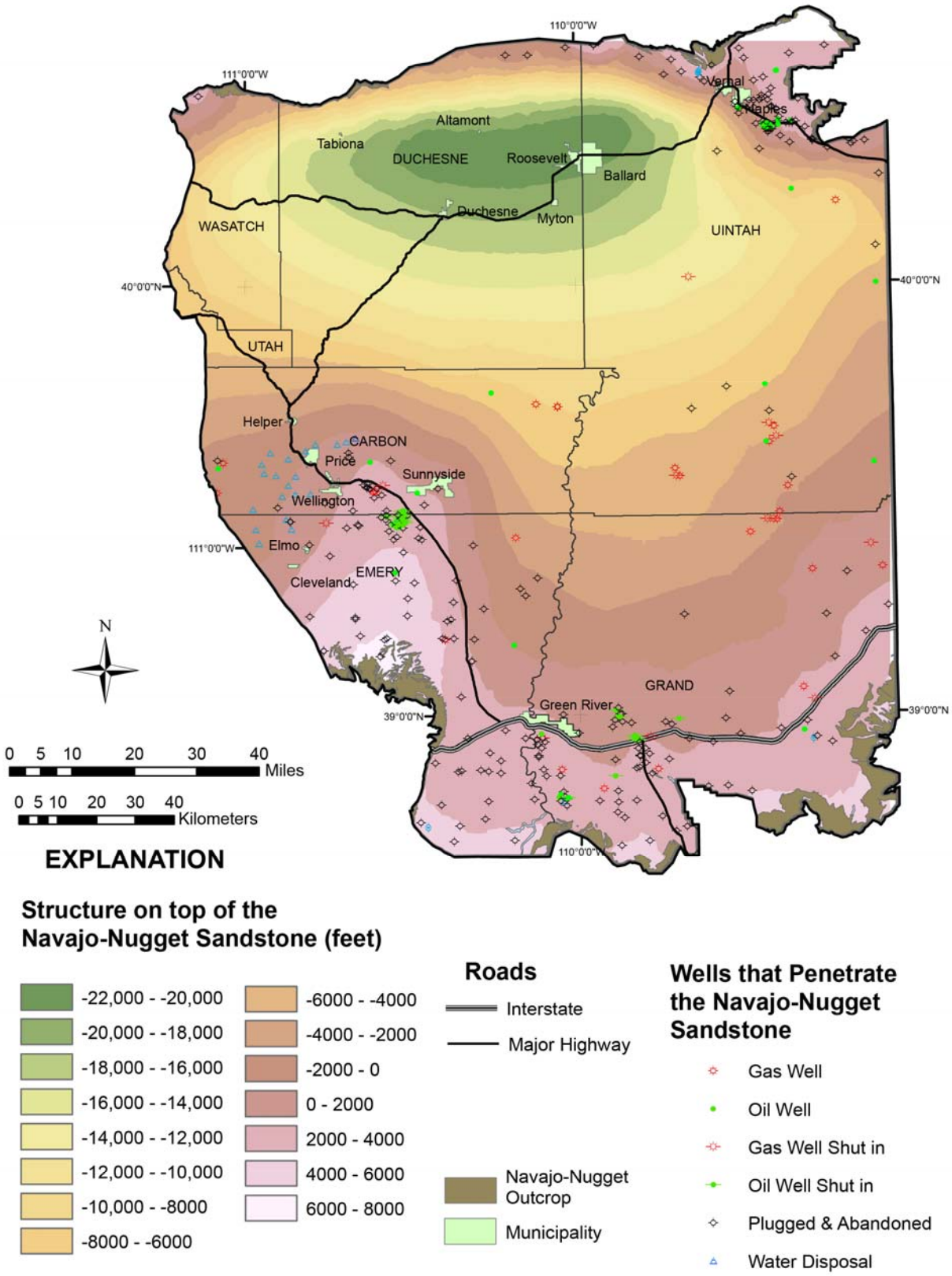

Figure 4.7. Structure on top of the Navajo–Nugget Sandstone, Uinta Basin.

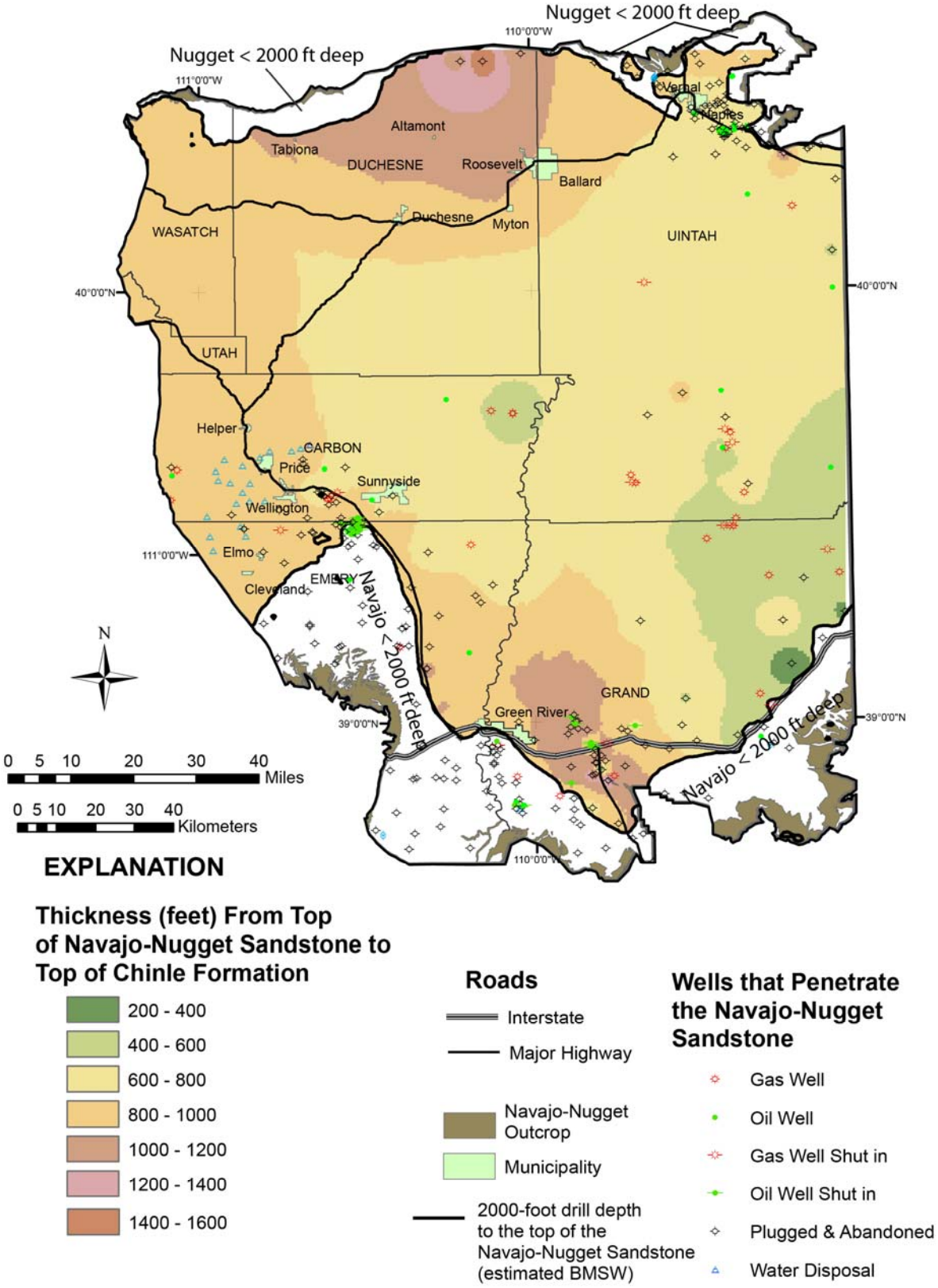

Figure 4.8. Thickness from the top of the Navajo–Nugget Sandstone to the top of the Chinle Formation for areas greater than 2000 feet deep.

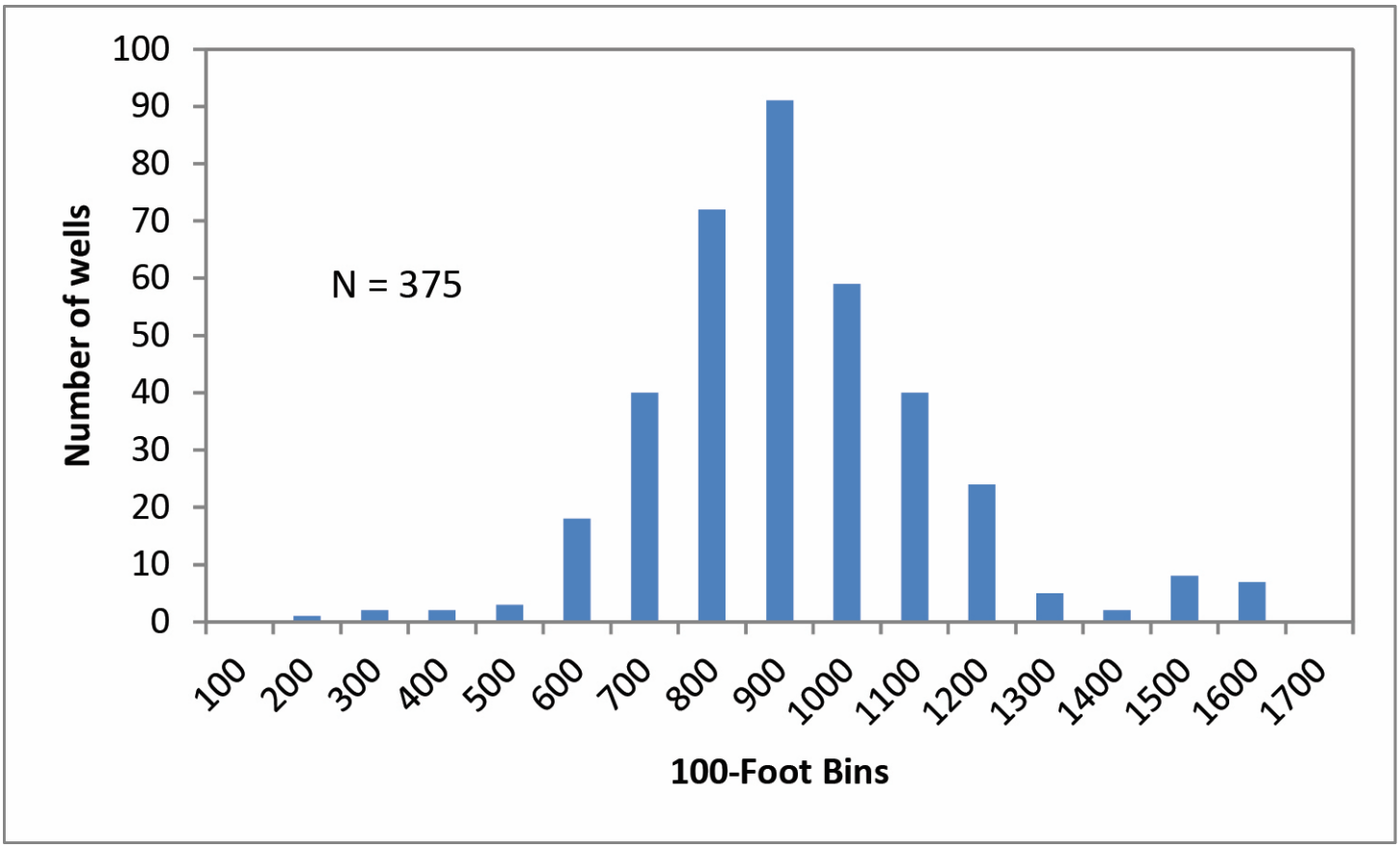

Figure 4.9. Frequency distribution of the gross thickness of the GCG/N reservoir in the geophysical well logs studied. The thickness ranges from 178 to 1725 feet (54-526 m), with an average of 882 feet (269 m) and median of 869 feet (265).

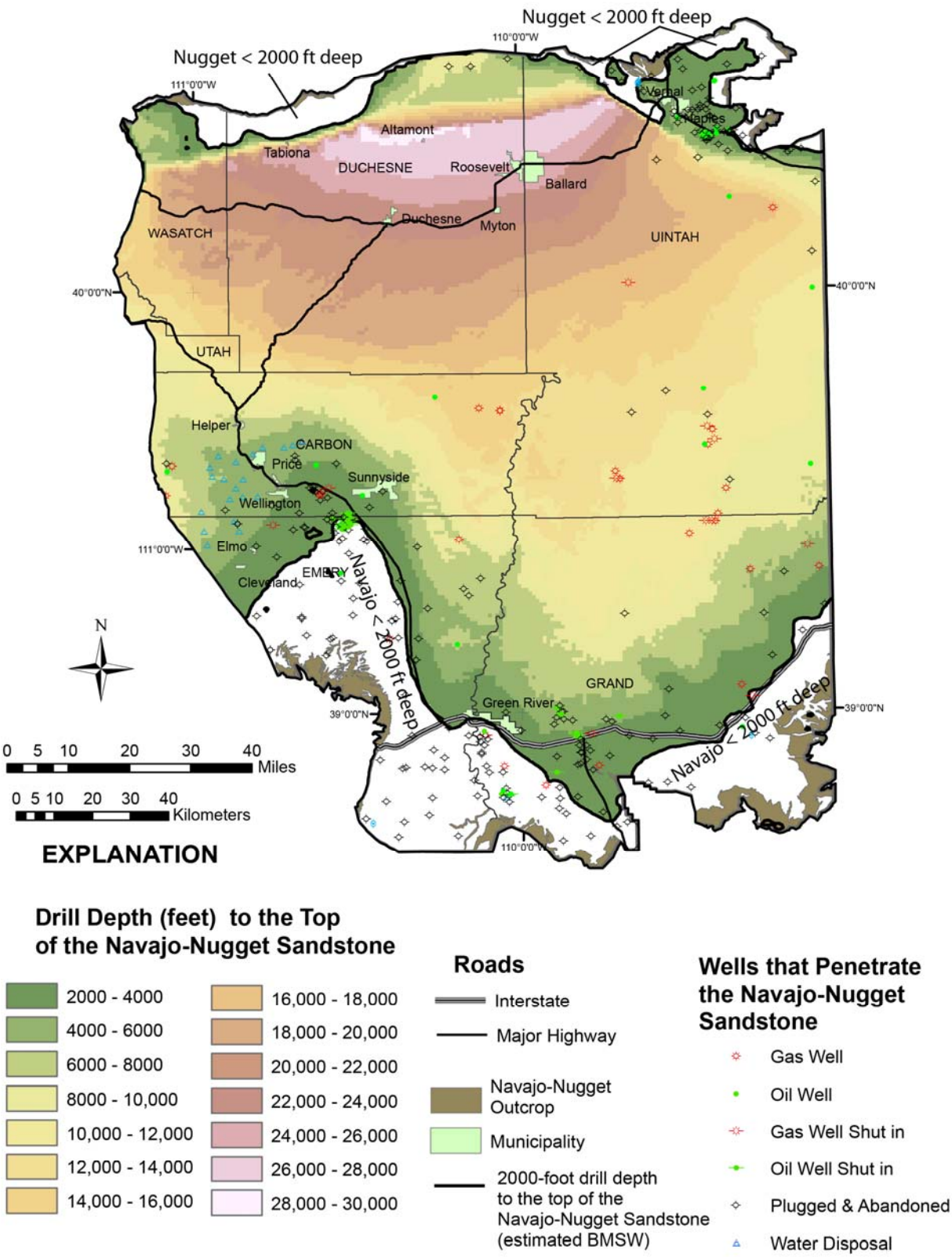

Figure 4.10. Drill depth greater than 2000 feet (600 m) to the top of the Navajo-Nugget Sandstone.

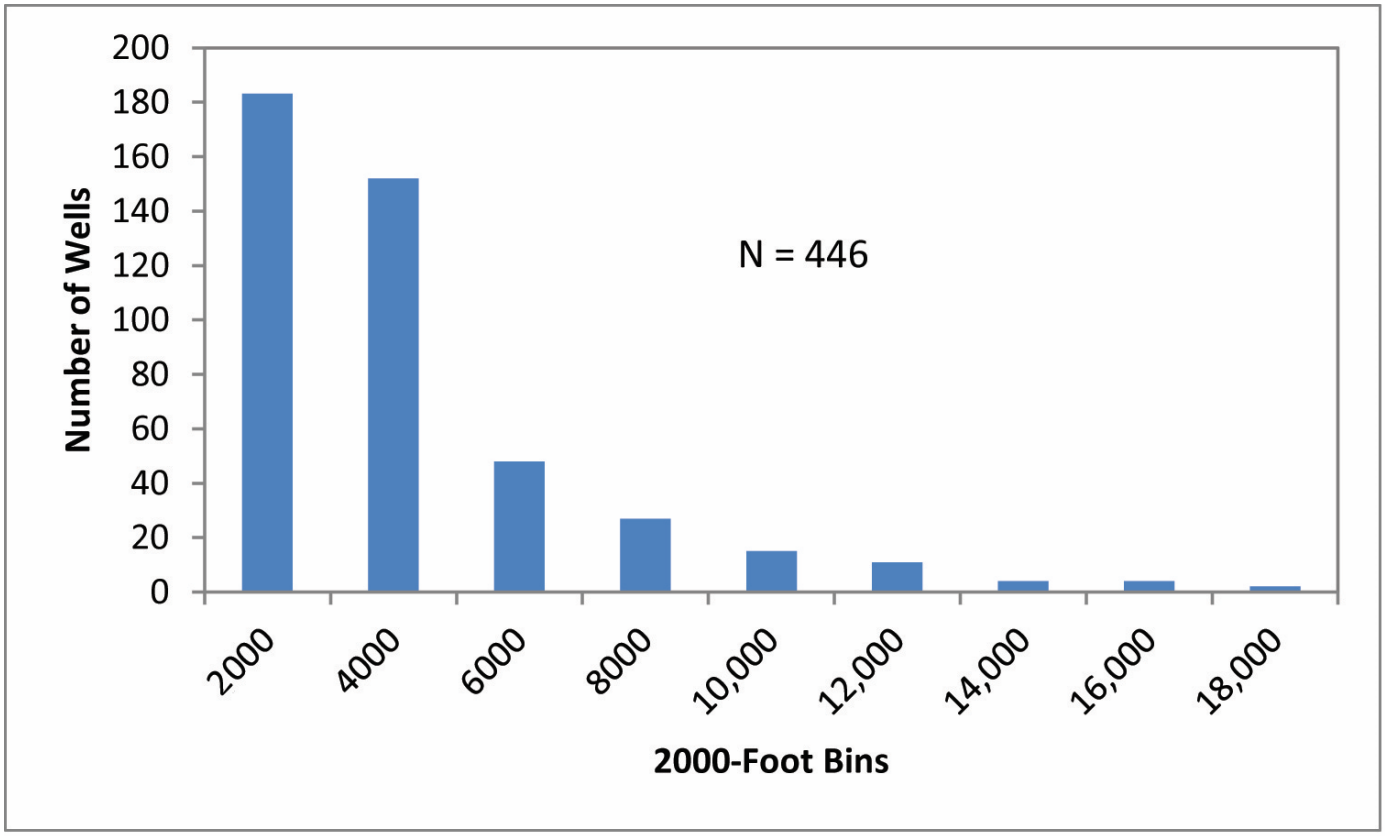

Figure 4.11. Frequency distribution of the drill depth to the top of the GCG/N reservoir in the geophysical well logs studied. The drill depth ranges from 30 to 16,960 feet (9-5169 m) with an average of 3198 feet (975 m) and median of 2397 feet (731 m).

Figure 4.12. Outcrop of a portion of the Navajo Sandstone with large dune sets. Harris Wash in the Grand Staircase-Escalante National Monument, southeast of the town of Escalante in south-central Utah.

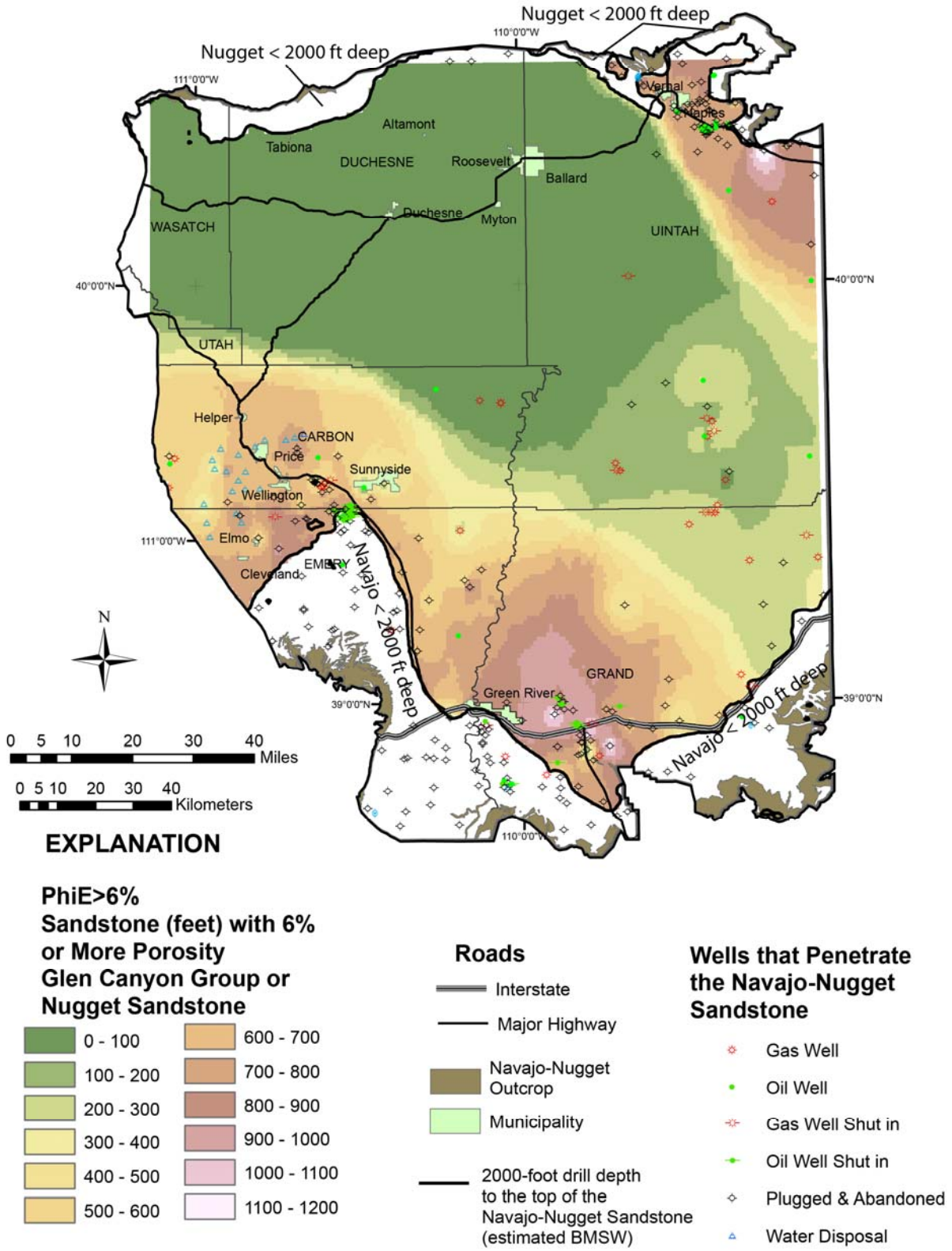

Figure 4.13. Feet of sandstone in the GCG/N reservoir with ≥ 6% porosity. Porosity determined from density and sonic well logs for areas primarily with greater than 2000 feet of depth.

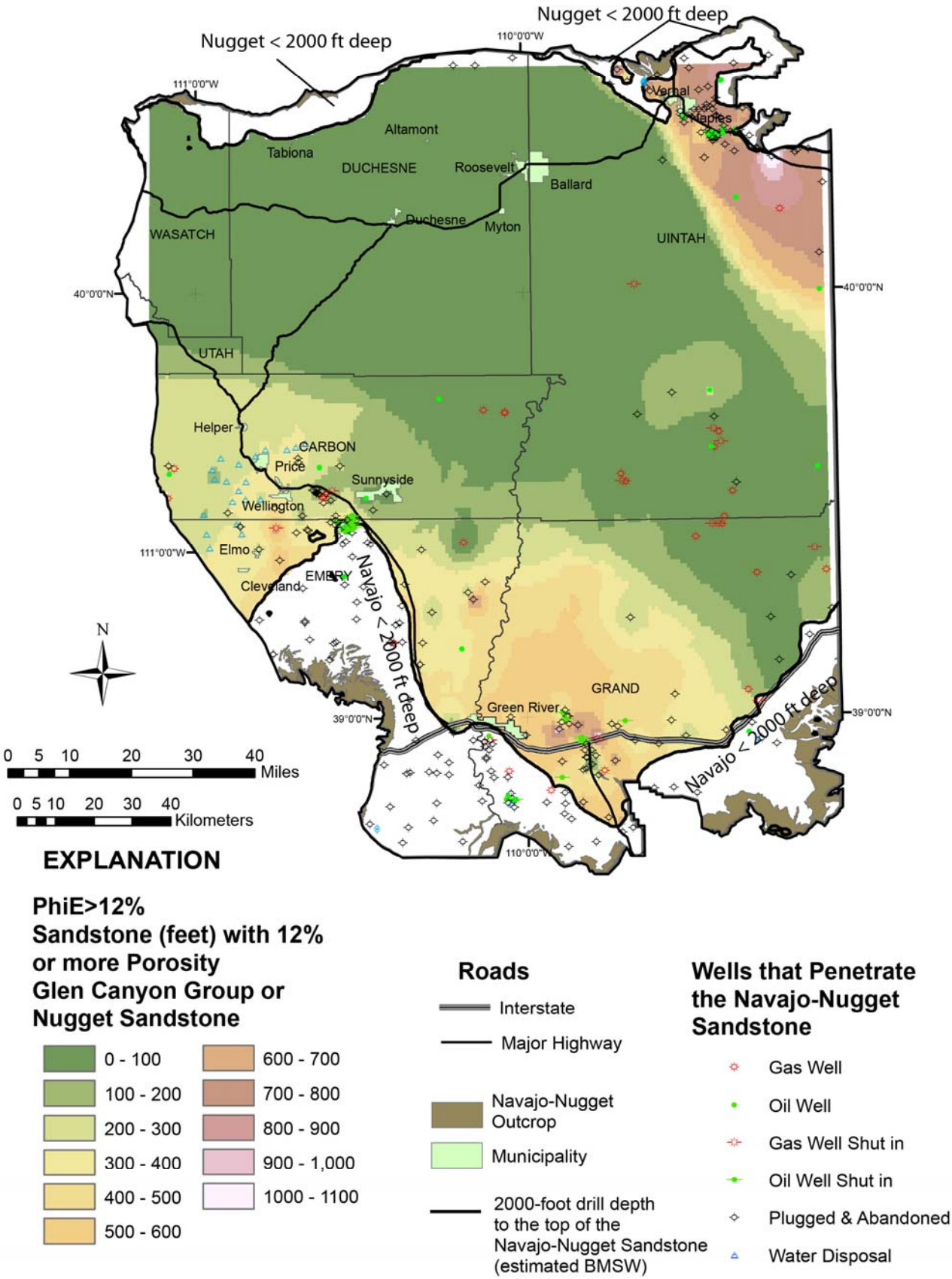

Figure 4.14. Feet of sandstone in the GCG/N reservoir with ≥ 12% porosity for areas at more than 2000 feet deep. Porosity determined from density and sonic well logs.

A

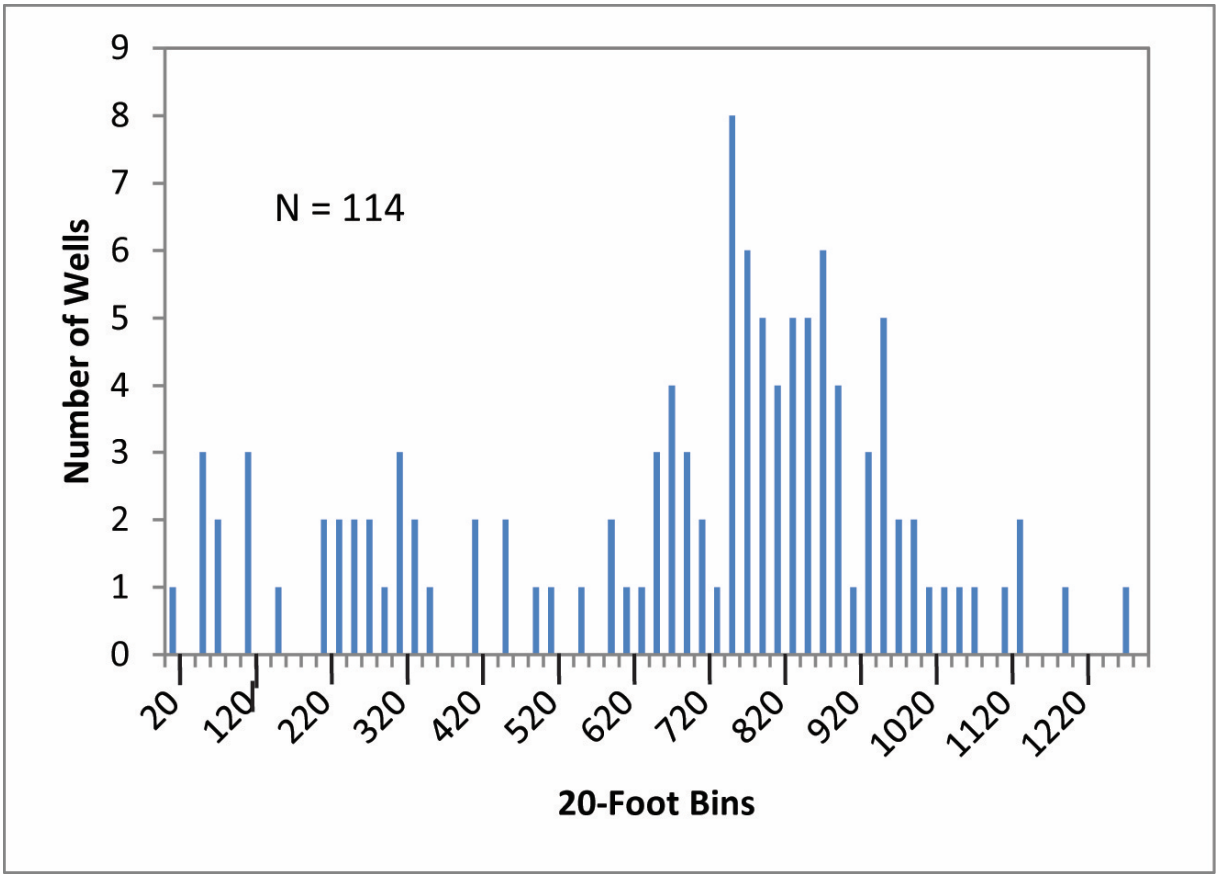

B

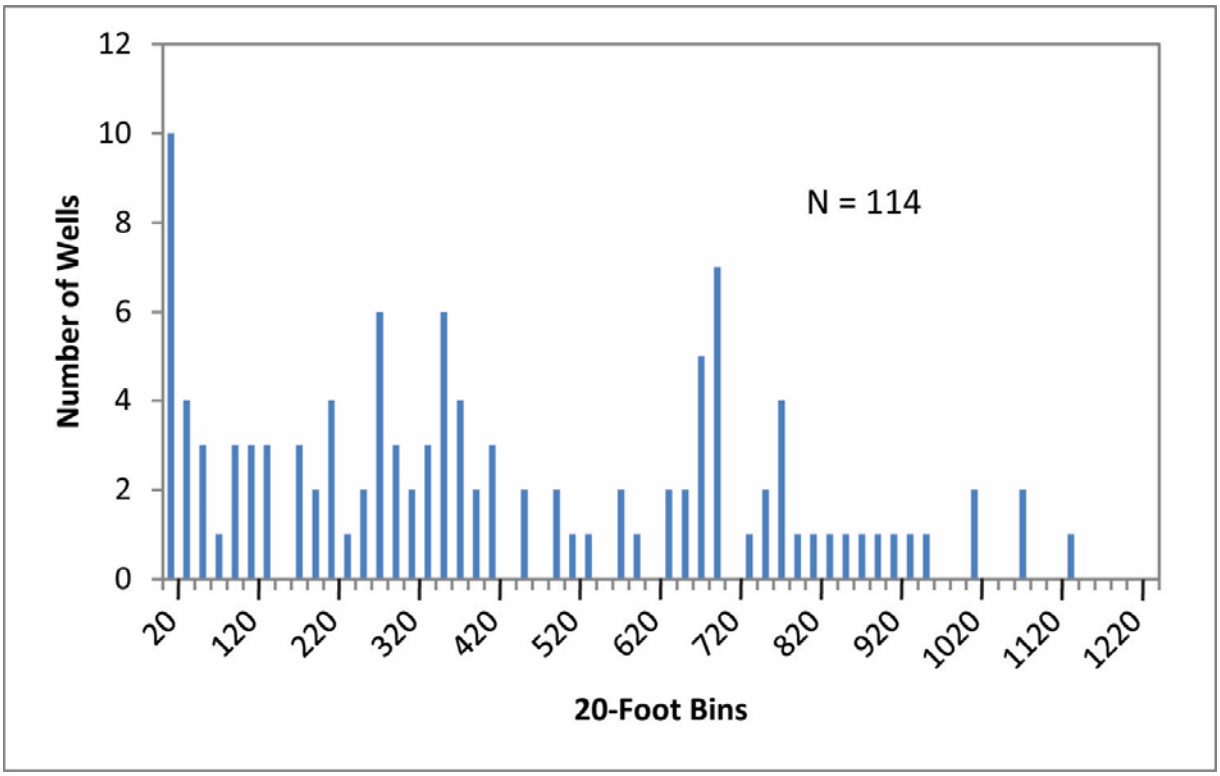

Figure 4.15. Frequency distribution graphs of the feet of sandstone with (A) PhiE ≥ 6% and (B) ≥ (PhiE ≥ 12% in the GCG/N reservoir. PhiE ≥ 6% ranges from 14 to 1280 feet (4-390 m) with an average of 675 feet (206 m) and a median of 761 feet (232 m). PhiE ≥ 12% ranges from 0 to 1138 feet (0-347 m), with an average of 417 feet (127 m) and median of 350 feet (350 m).

A

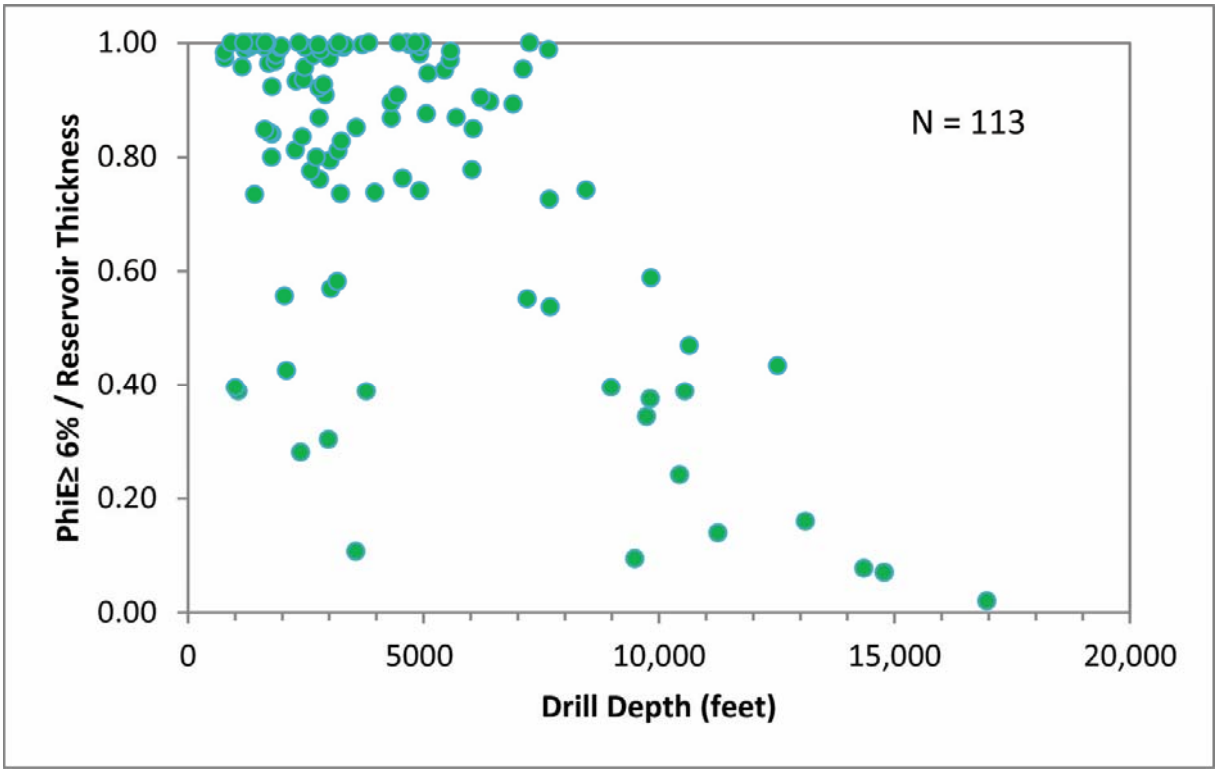

B

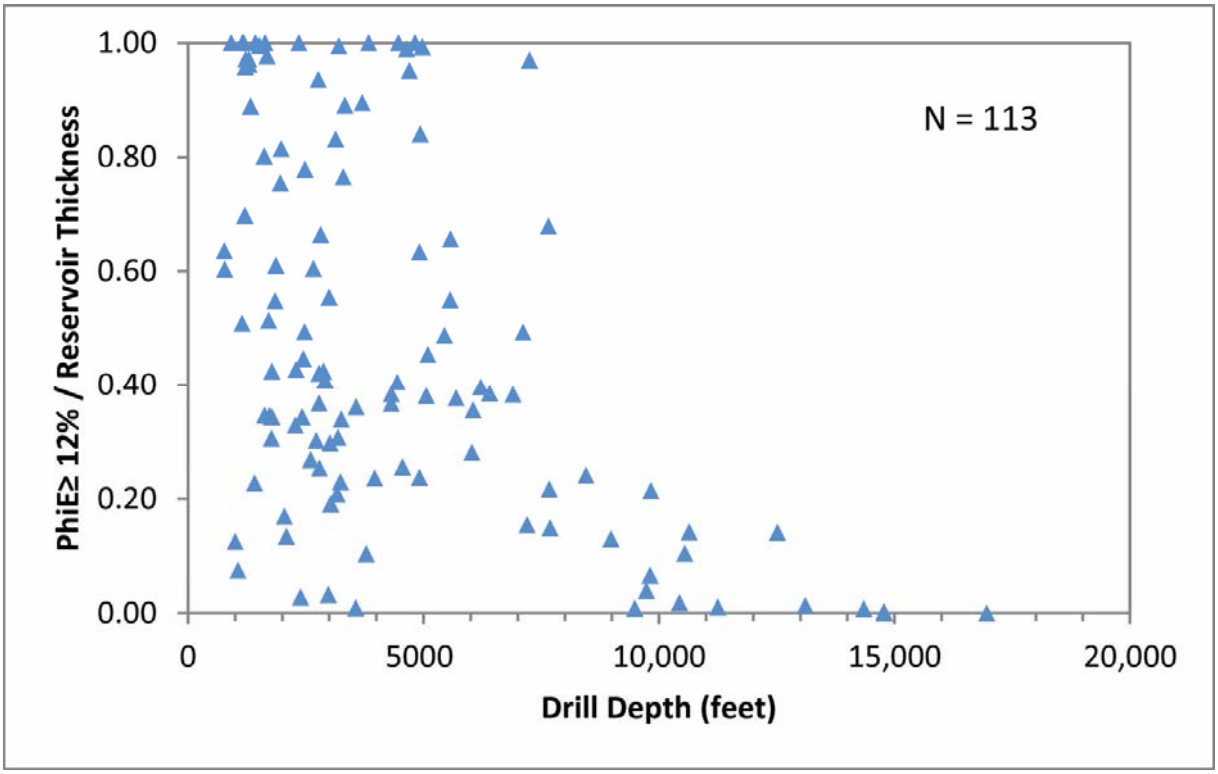

Figure 4.16. (A) Ratio of PhiE ≥ 6% to reservoir thickness versus drill depth, and (B) ratio of PhiE ≥ 12% to reservoir thickness versus drill depth in the GCG/N reservoir. Porosity calculated from density or sonic logs.

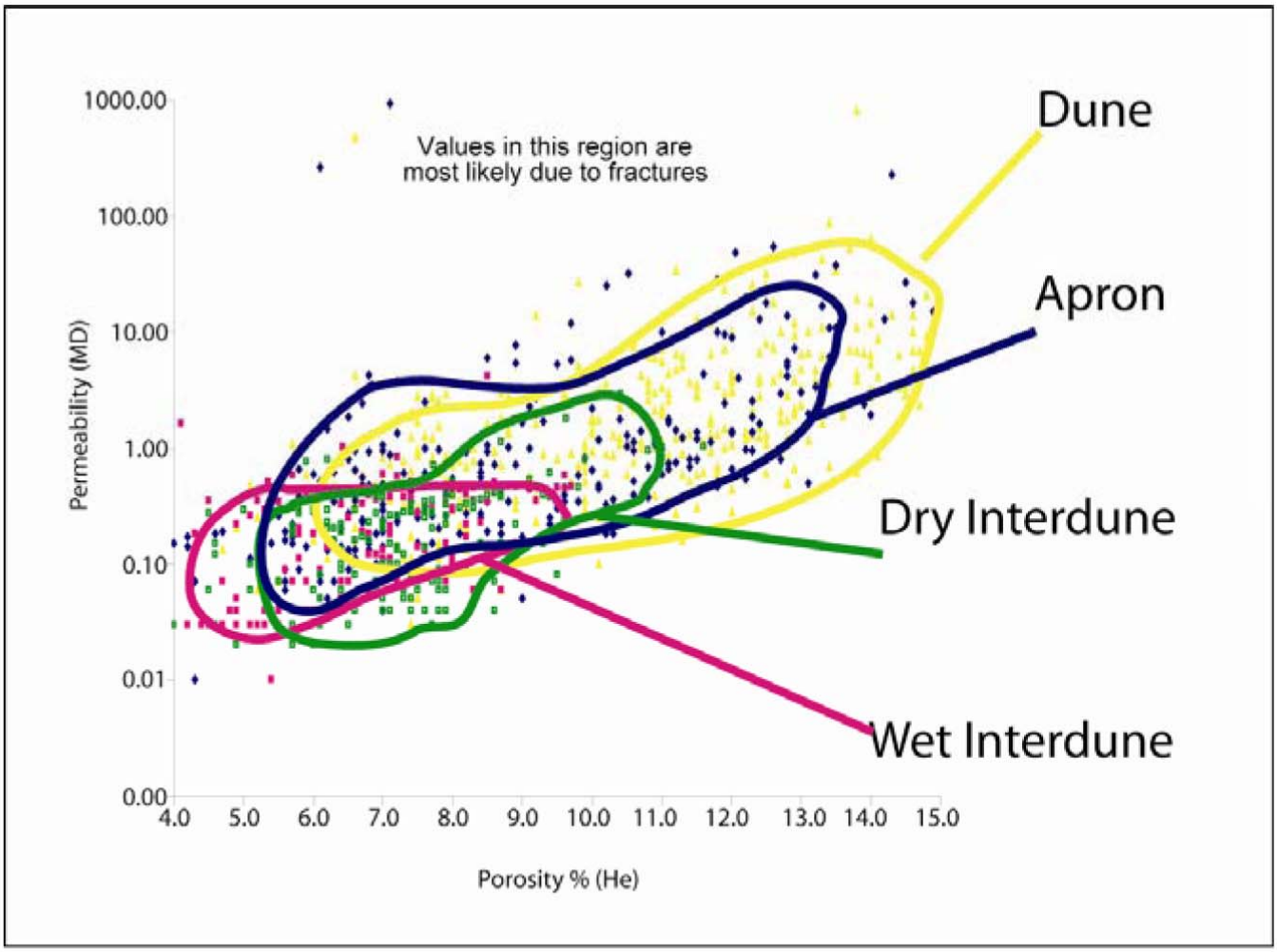

Figure 4.17. Porosity–permeability plot separated into facies. The dune facies has the highest reservoir potential. Core data from the Nugget Sandstone, Anschutz Ranch East field, Summit County, Utah. From Keele and Evans, 2008.

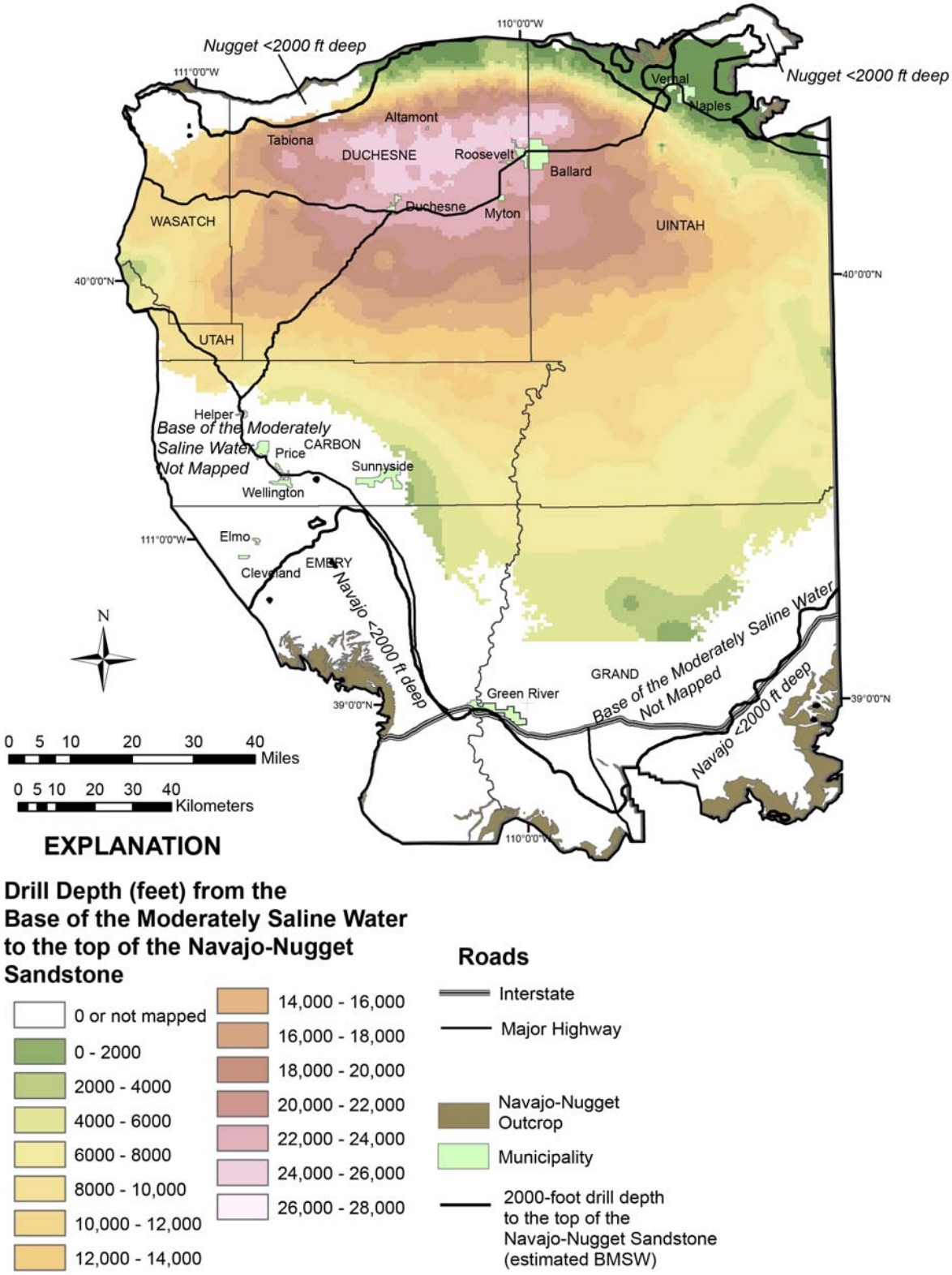

Figure 4.18. Drill depth (feet) from the base of the moderately saline water (BMSW) to the top of the Navajo-Nugget Sandstone. The Nugget is above the BMSW in Ashley Valley (see figure 1.1 for field location). The map was created using ArcScene® by subtracting the drill depth map (figure 4.10) from the BMSA map of Anderson and others (2012).

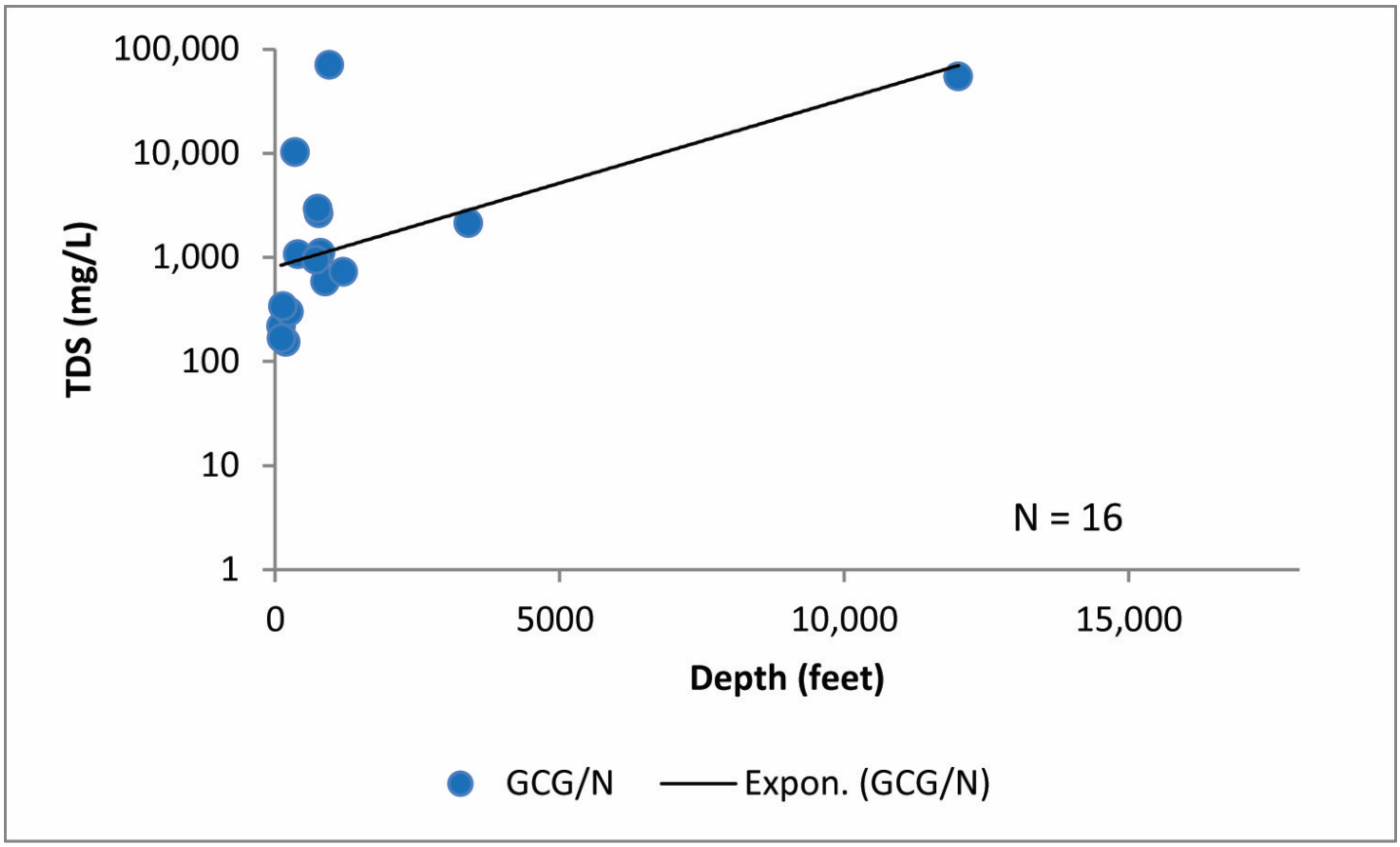

Figure 4.19. Total dissolved solids (milligrams/liter [mg/L]) with depth (feet). The exponential trend line (Expon.) indicates less than 10,000 TDS to a depth of 10,000 feet (3000 m). The limited number of samples from deep wells (one) is insufficient to be statistically significant for such a large area.

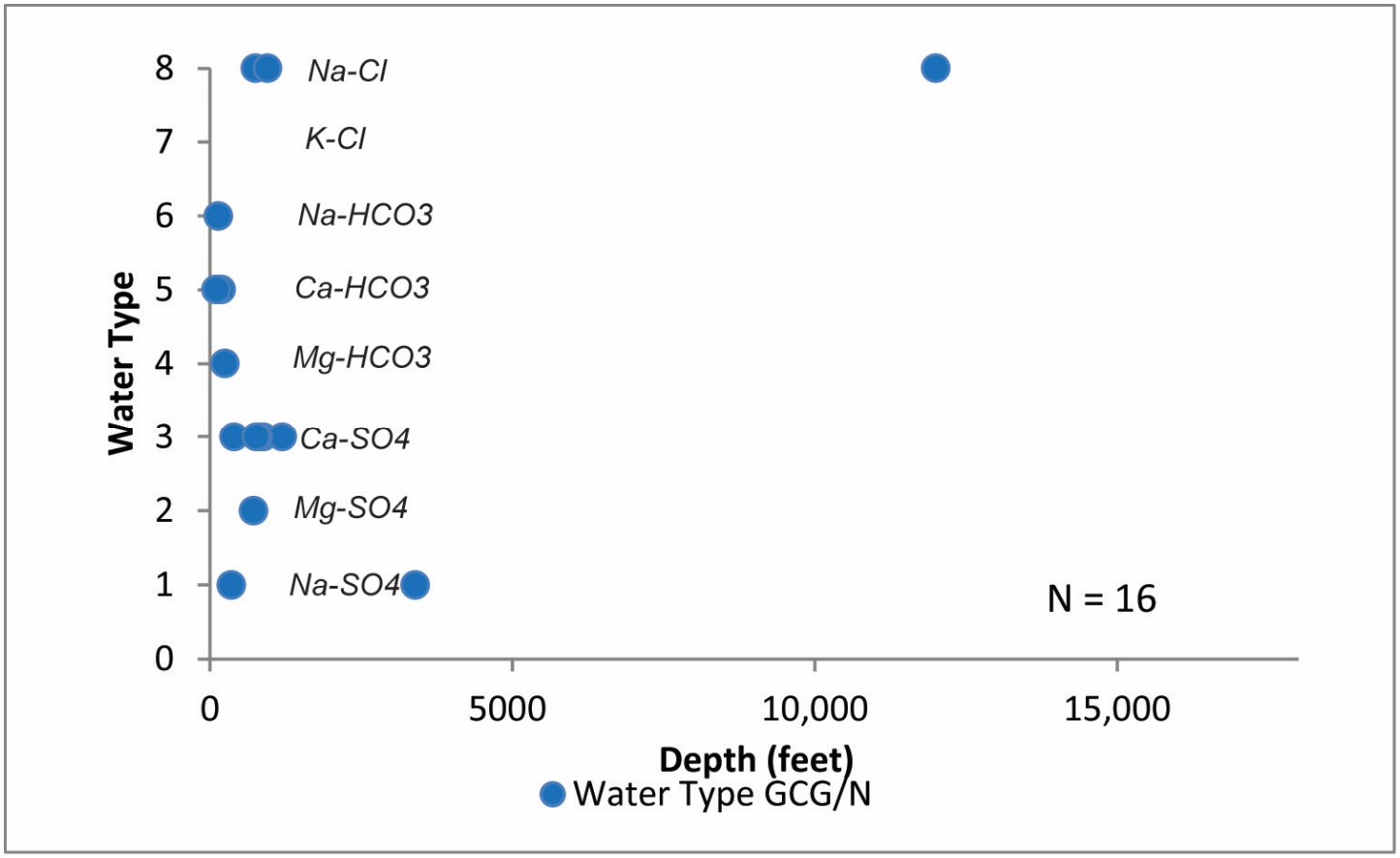

Figure 4.20. Water produced from the GCG/N is sodium chloride (Na-Cl) from one deep well (> 5000 feet [150]) and a mix of all the water types except potassium chloride, at shallower depths. The number of samples from deep wells (one) is not statistically significant for such a large area.

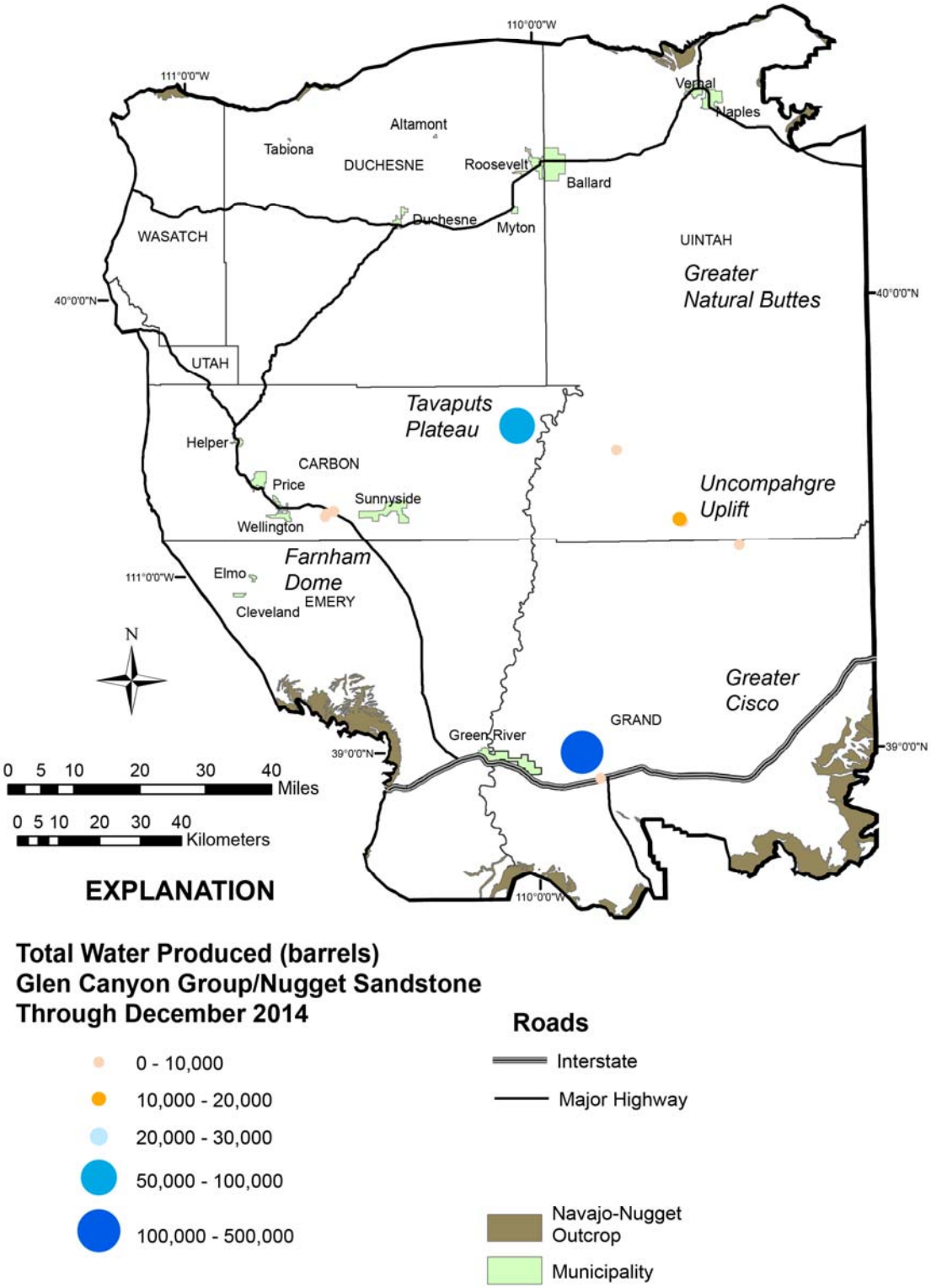

Figure 4.21. Total water produced from the GCG/N reservoir.

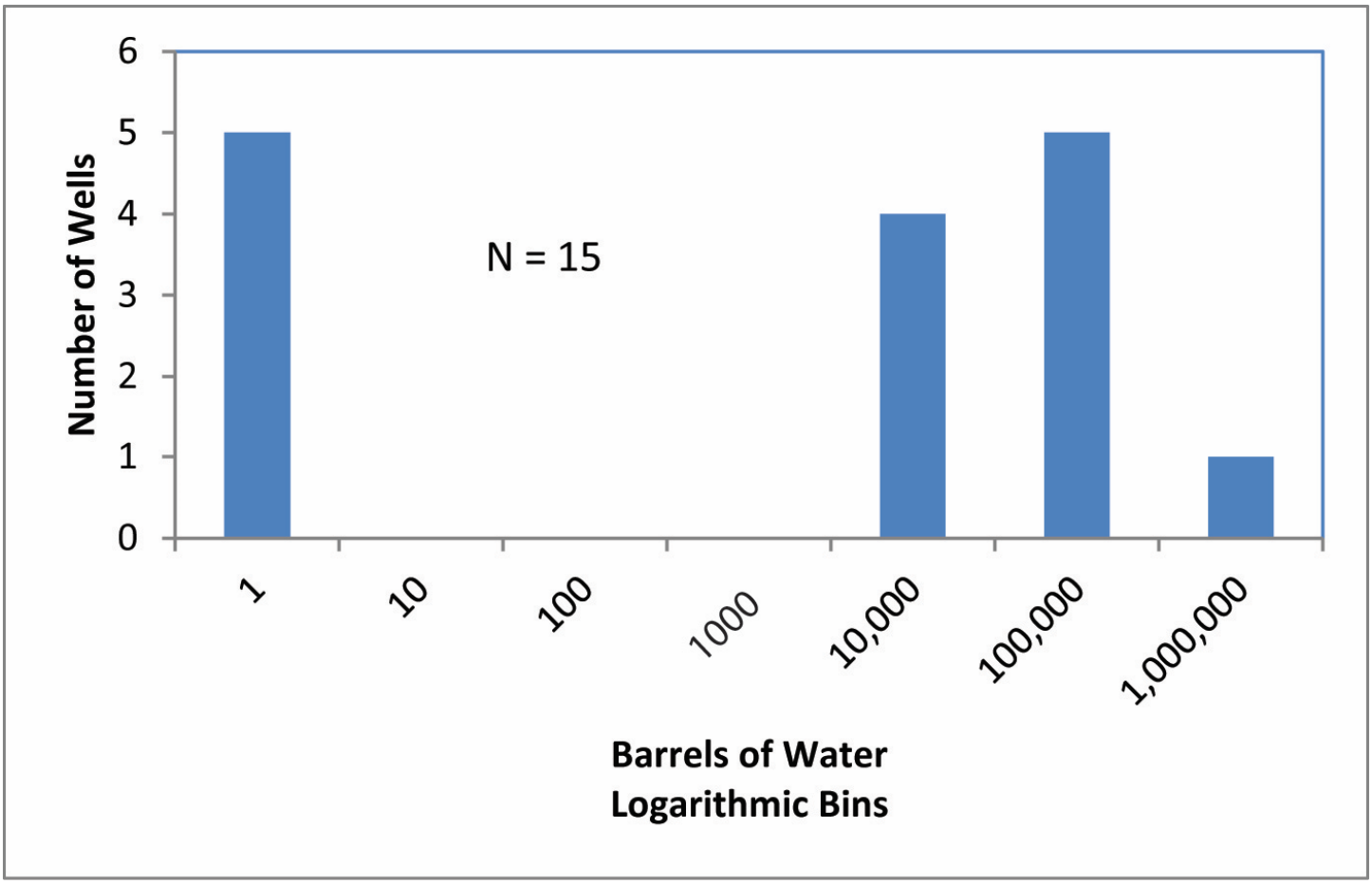

Figure 4.22. Frequency diagram of total water per well produced from the GCG/N reservoir. Total water produced through December 2014 is 292,418 BW, nearly half coming from one well. Water volumes range from 0 to 140,079 BW/well, the average is 19,495 BW with a median of 4615 BW.

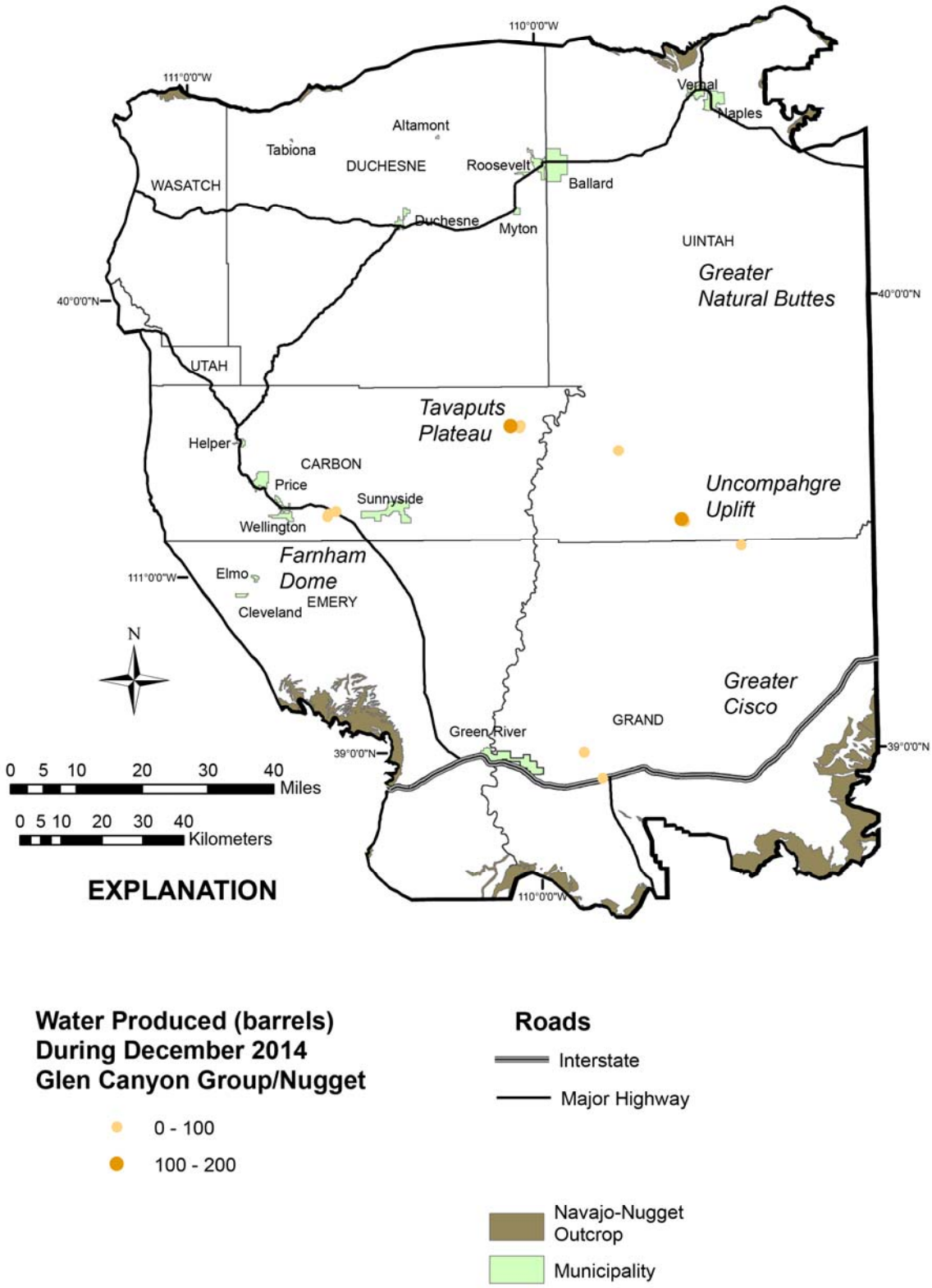

Figure 4.23. Water produced from the GCG/N reservoir during the month of December 2014.

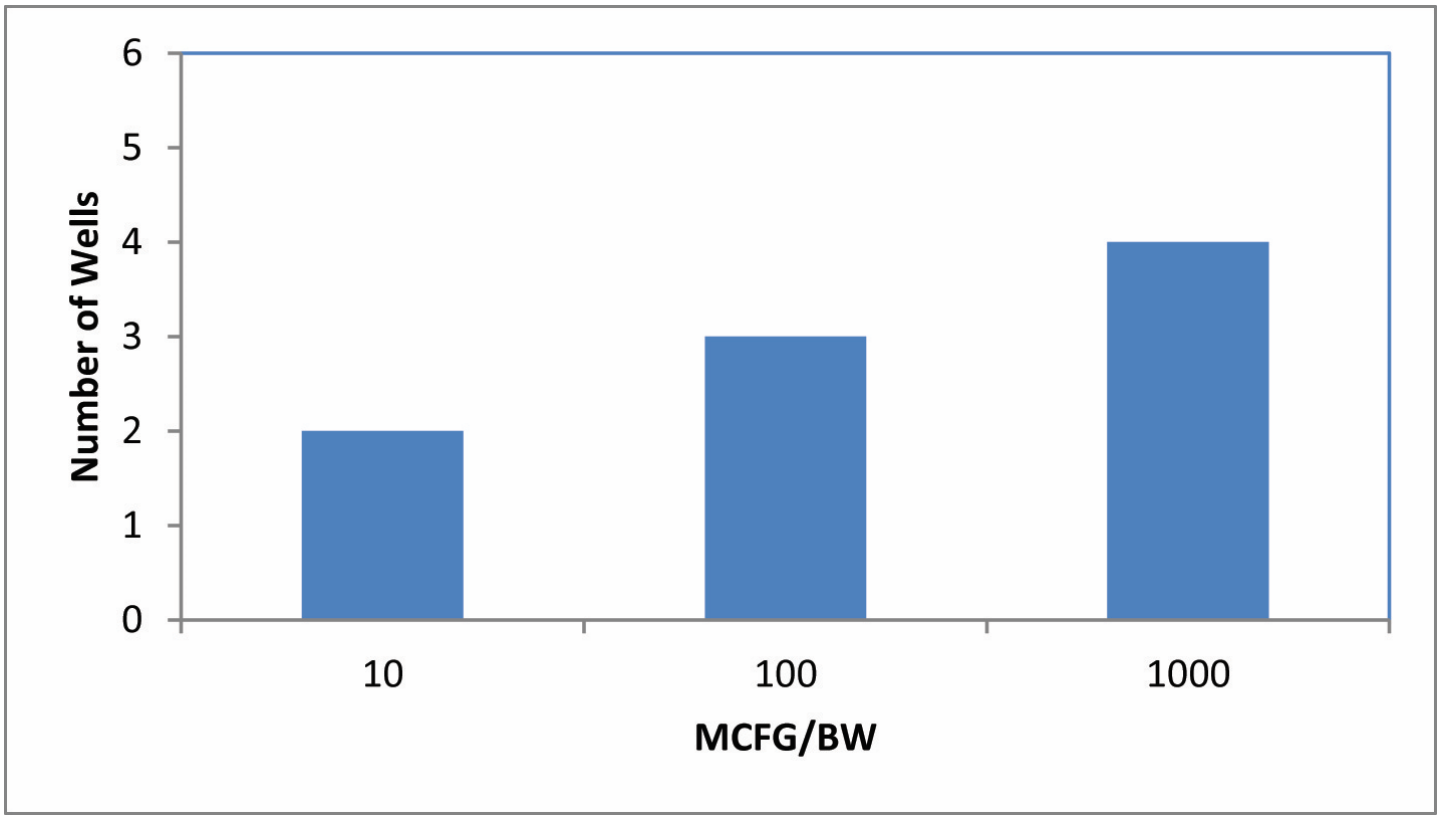

Figure 4.24. Frequency diagram of total gas produced per barrel of water per well from the GCG/N reservoir. Gas volumes are in thousand cubic feet (MCF). The range is from 1 to 276 MCFG/BW, with an average of 127 MCFG/BW and a median of 71 MCFG/BW. Five wells not included in this data set, produce gas and no water.

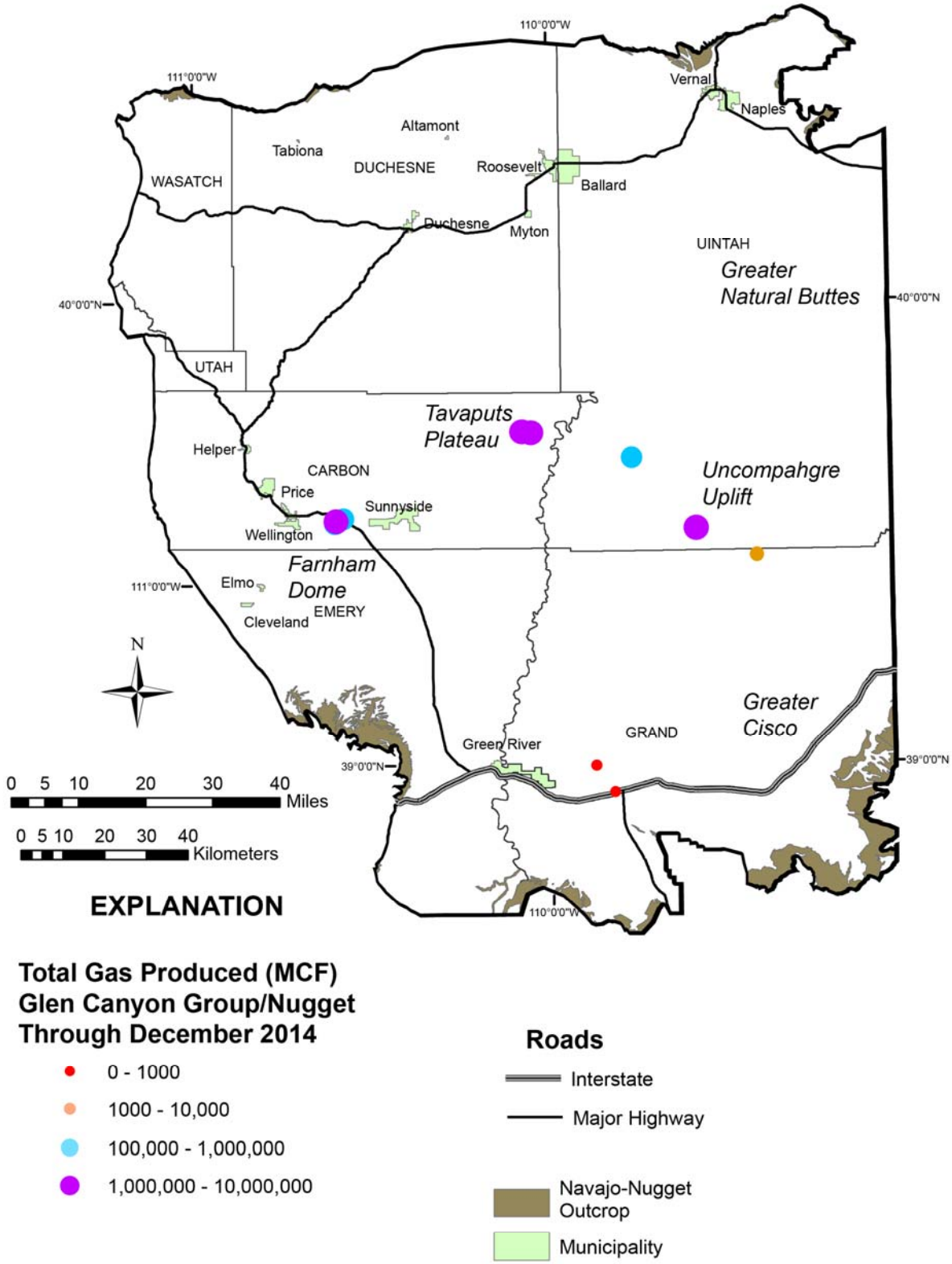

Figure 4.25. Total gas produced per well from the GCG/N reservoir through December 2014.

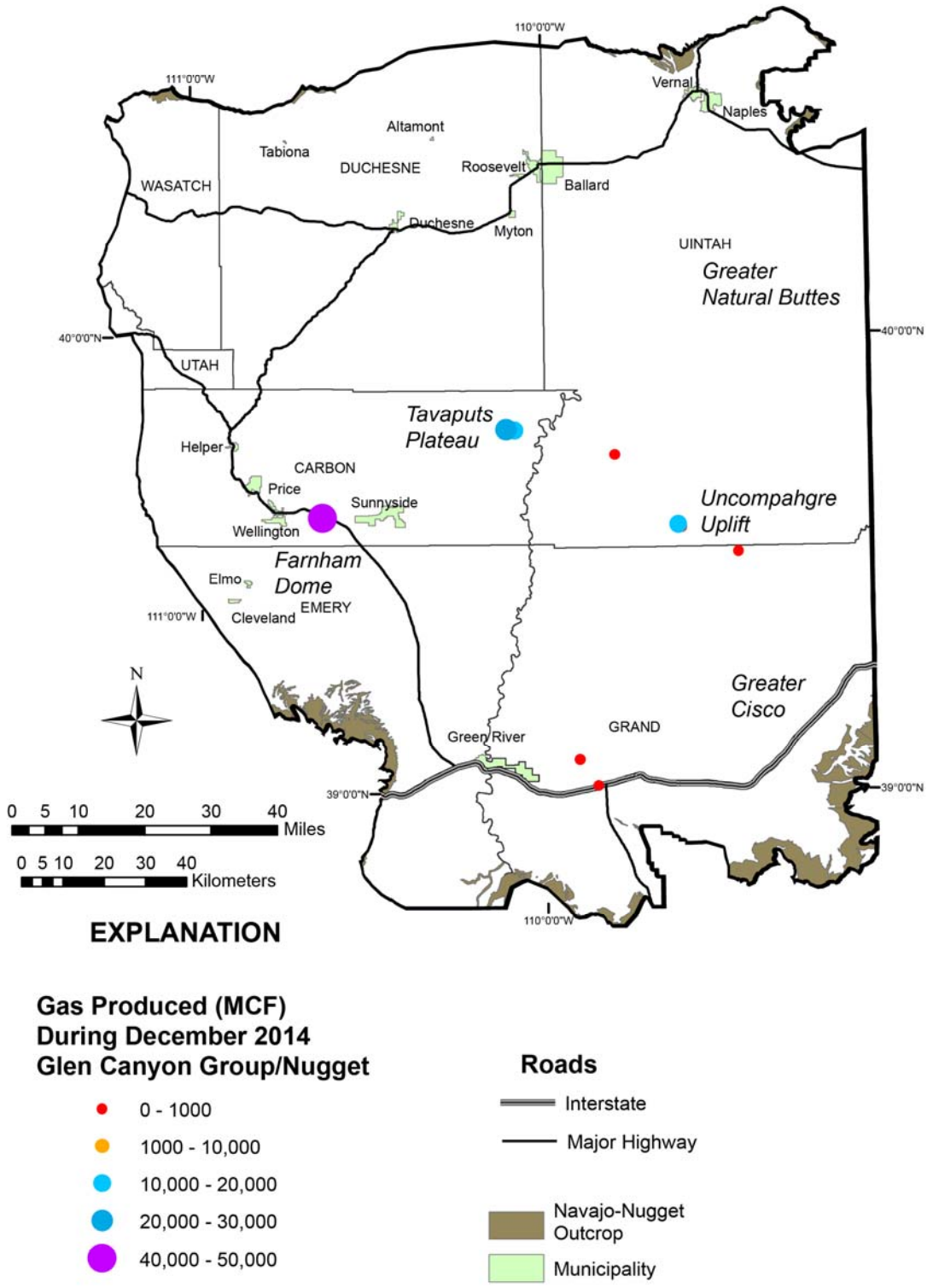

Figure 4.26. Gas produced from the GCG/N reservoir during the month of December 2014.

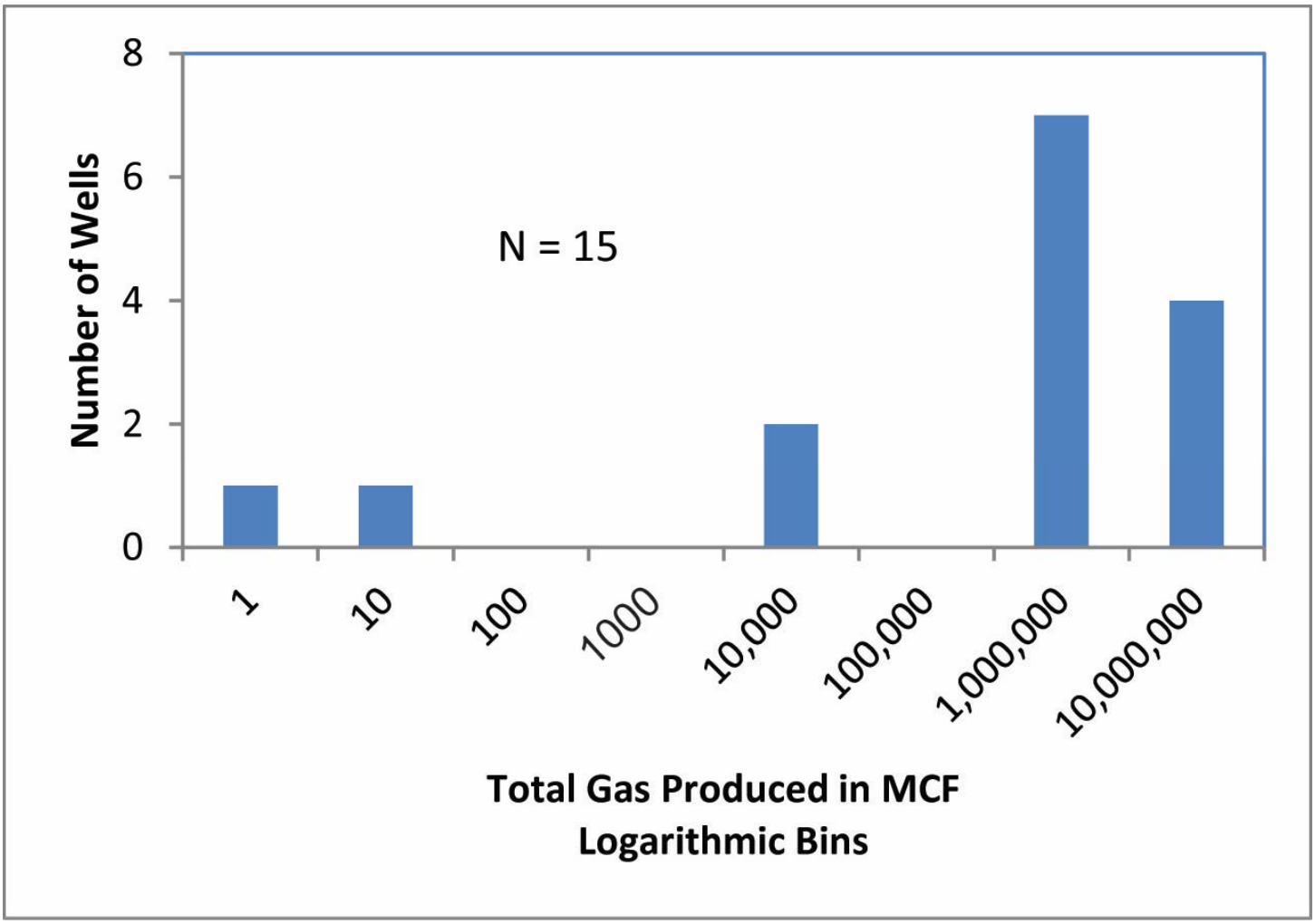

Figure 4.27. Frequency diagram of total gas produced per well from the GCG/N reservoir through December 2014. Gas volumes range from 0 to 8,012,292 MCFG/well with an average of 1,819,612 MCFG/well and a median of 556,422 MCFG/well.

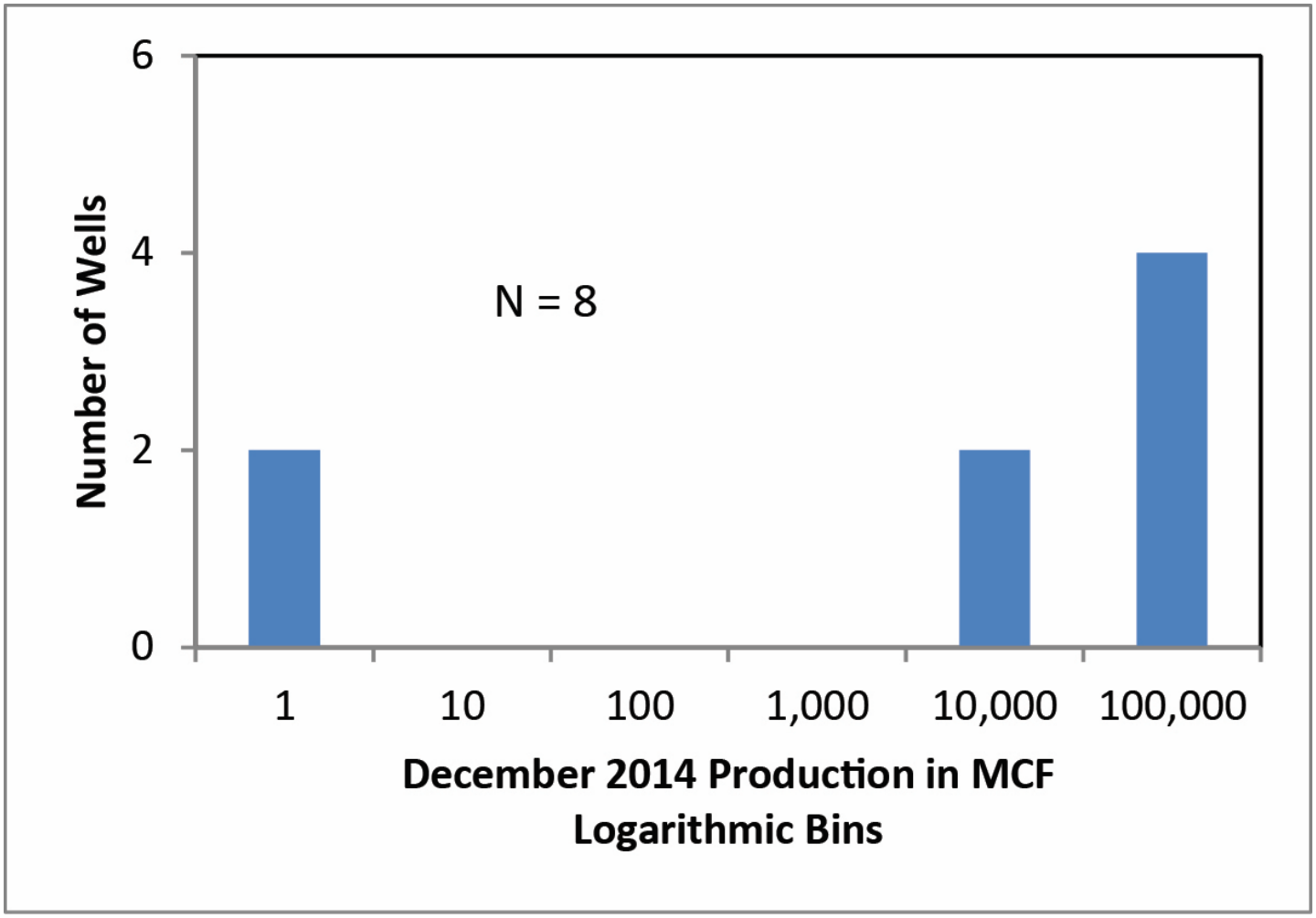

Figure 4.28. Frequency distribution diagram of gas produced per well from the GCG/N reservoir during December 2014. Production ranges from 1 to 48,628 MCFG/well with an average of 13,128 MCFG/well and median of 7768 MCFG/well.

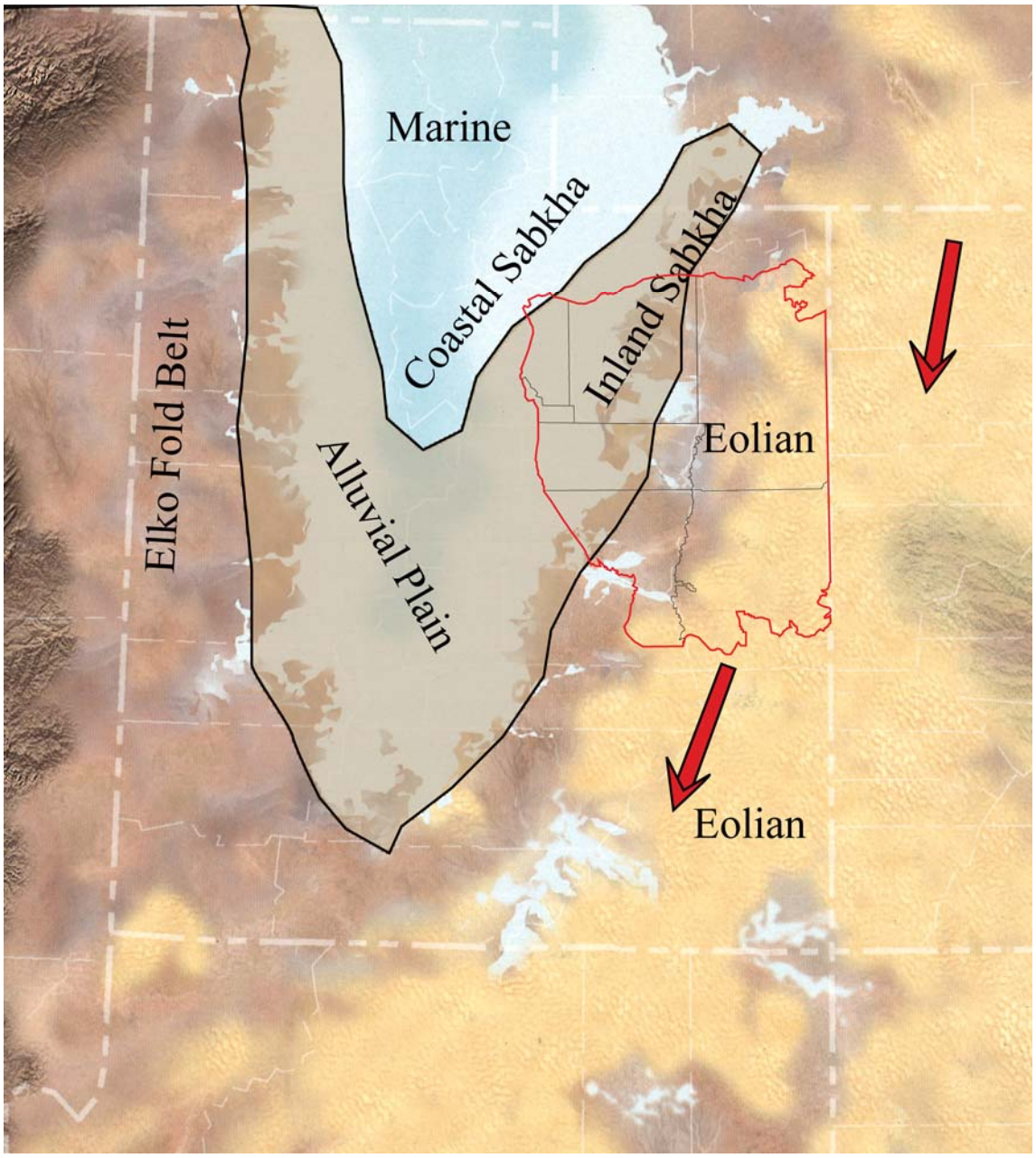

Figure 4.29. Paleogeographic interpretation of the Entrada Sandstone. Riggs and Blakey (1993) and Peterson (1994) refer to the Entrada deposits in central Utah as sand flats, also commonly referred to as red-bed or mud-rich facies. Jennings (2014) describes the Entrada in central Utah as dominantly alluvial plain deposits sourced from the Elko Fold Belt to the west. Red arrows indicate wind direction during the Early and Middle Jurassic. Modified from Blakey and Ranney, 2008.

A

B

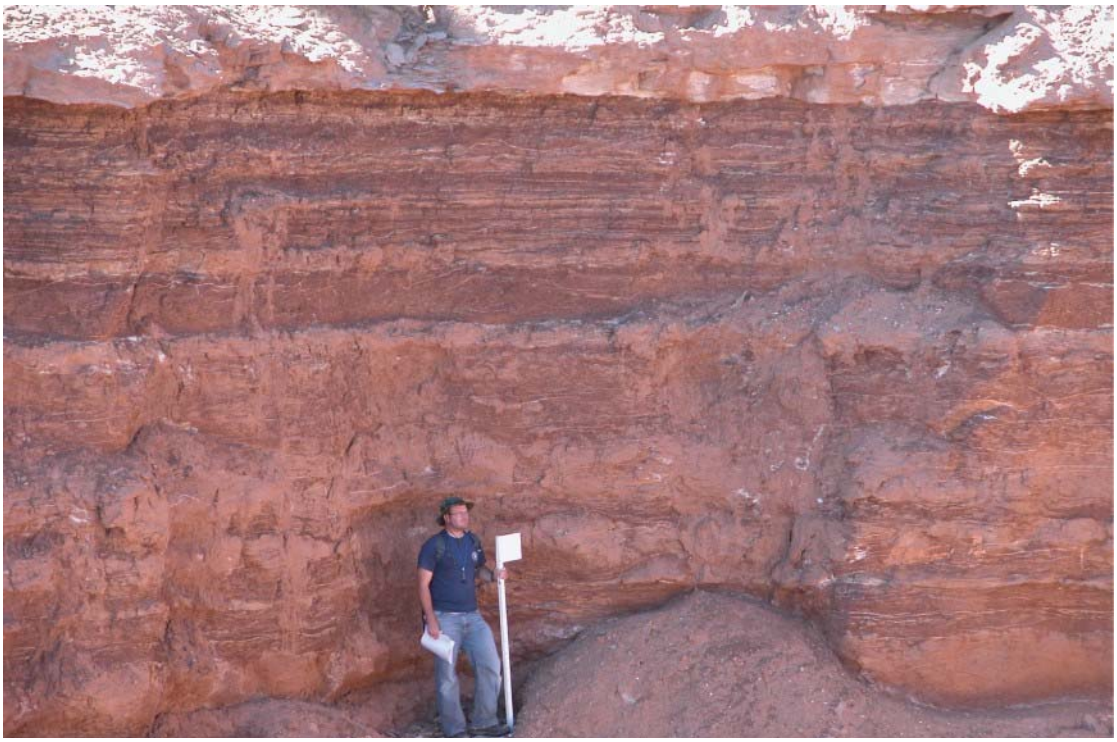

Figure 4.30. Entrada Sandstone dune facies (A) in Arches National Park near Moab and mud-rich facies (B) in the San Rafael Swell. Photograph B from Morris and Hicks, 2011.

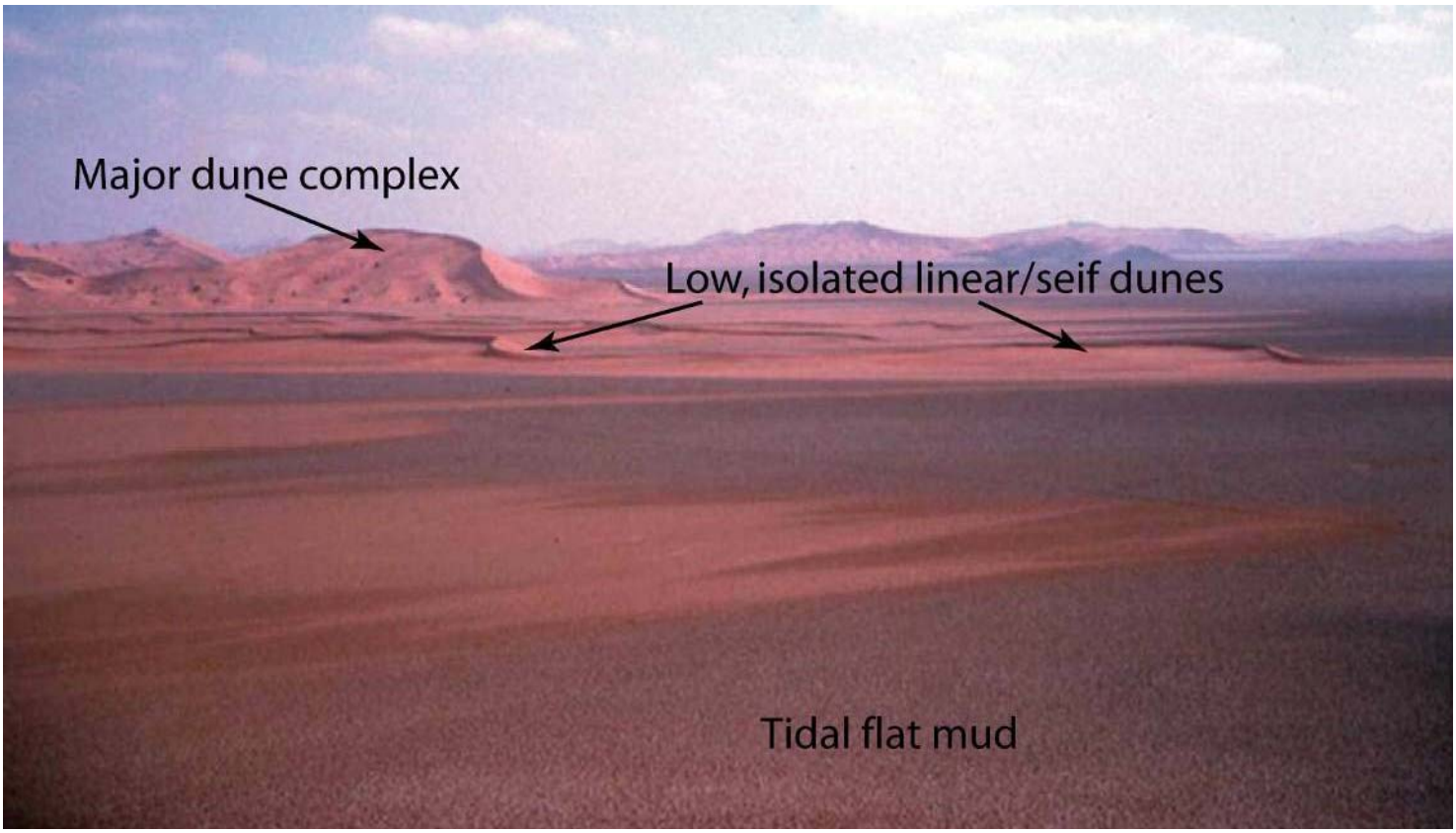

Figure 4.31. Working depositional model (Morris and others, 2005) with eolian dunes encroaching on a tidal flat, Namibia Desert.

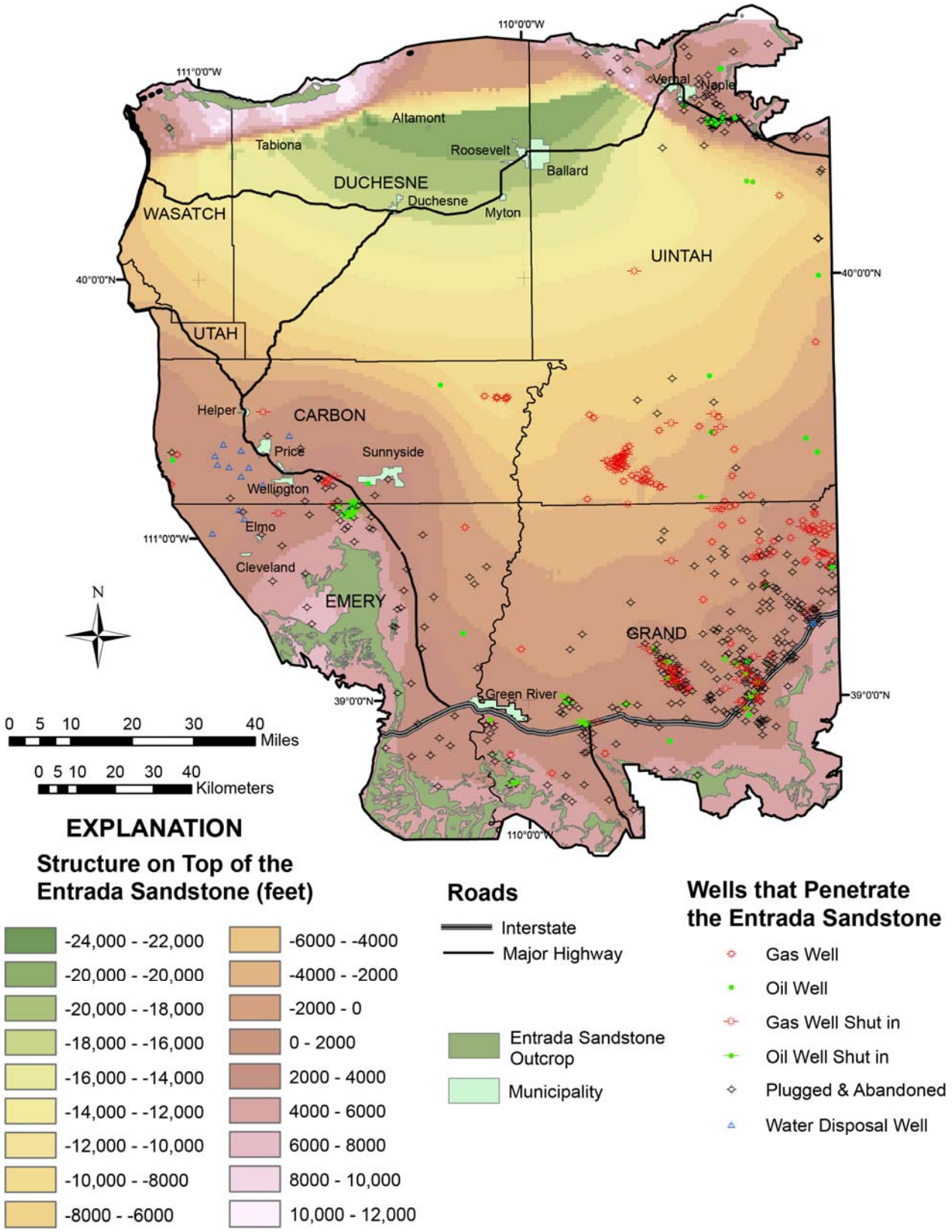

Figure 4.32. Structure on top of the Entrada Sandstone, Uinta Basin.

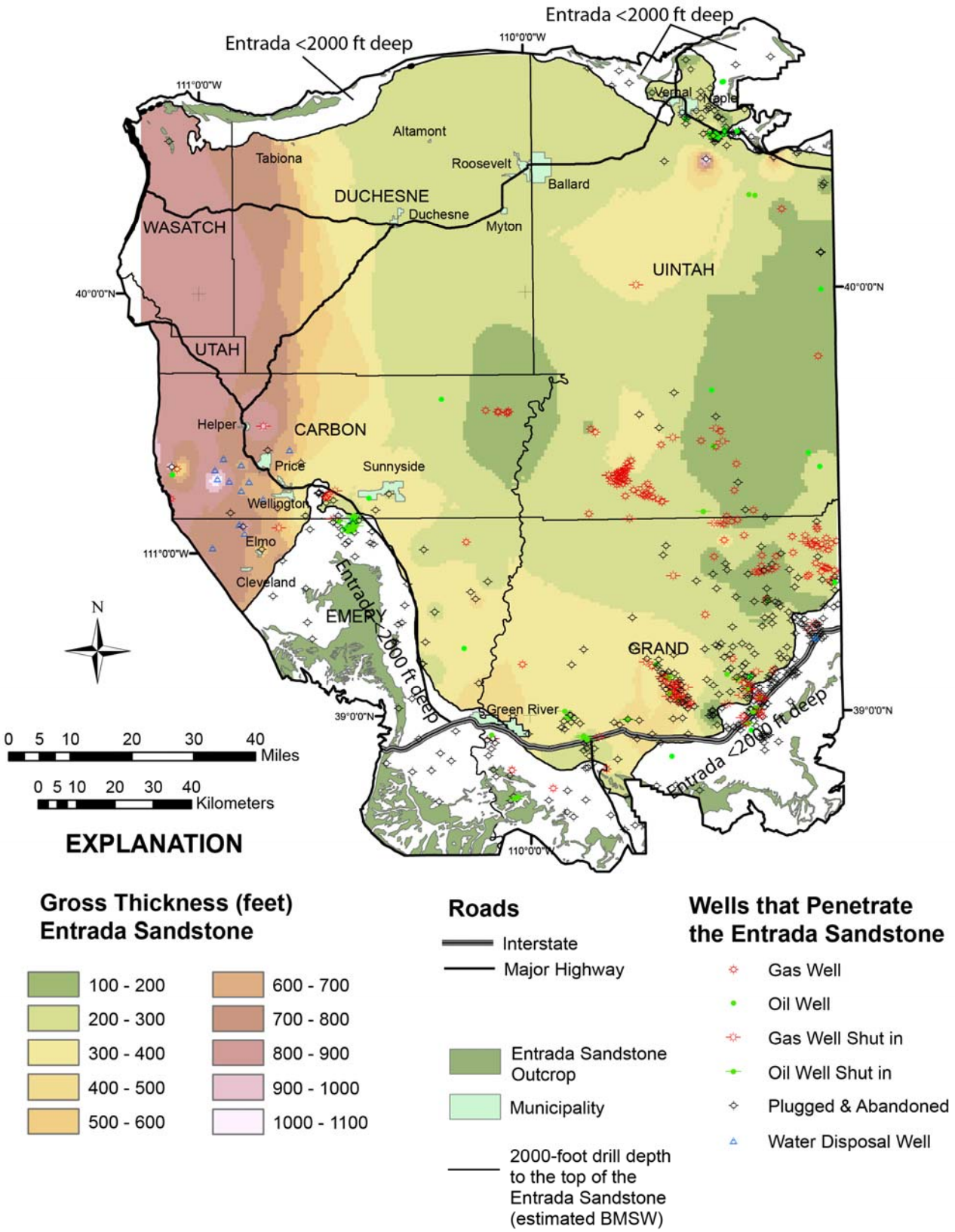

Figure 4.33. Gross thickness of the Entrada Sandstone for areas greater than 2000 feet (610 m) deep.

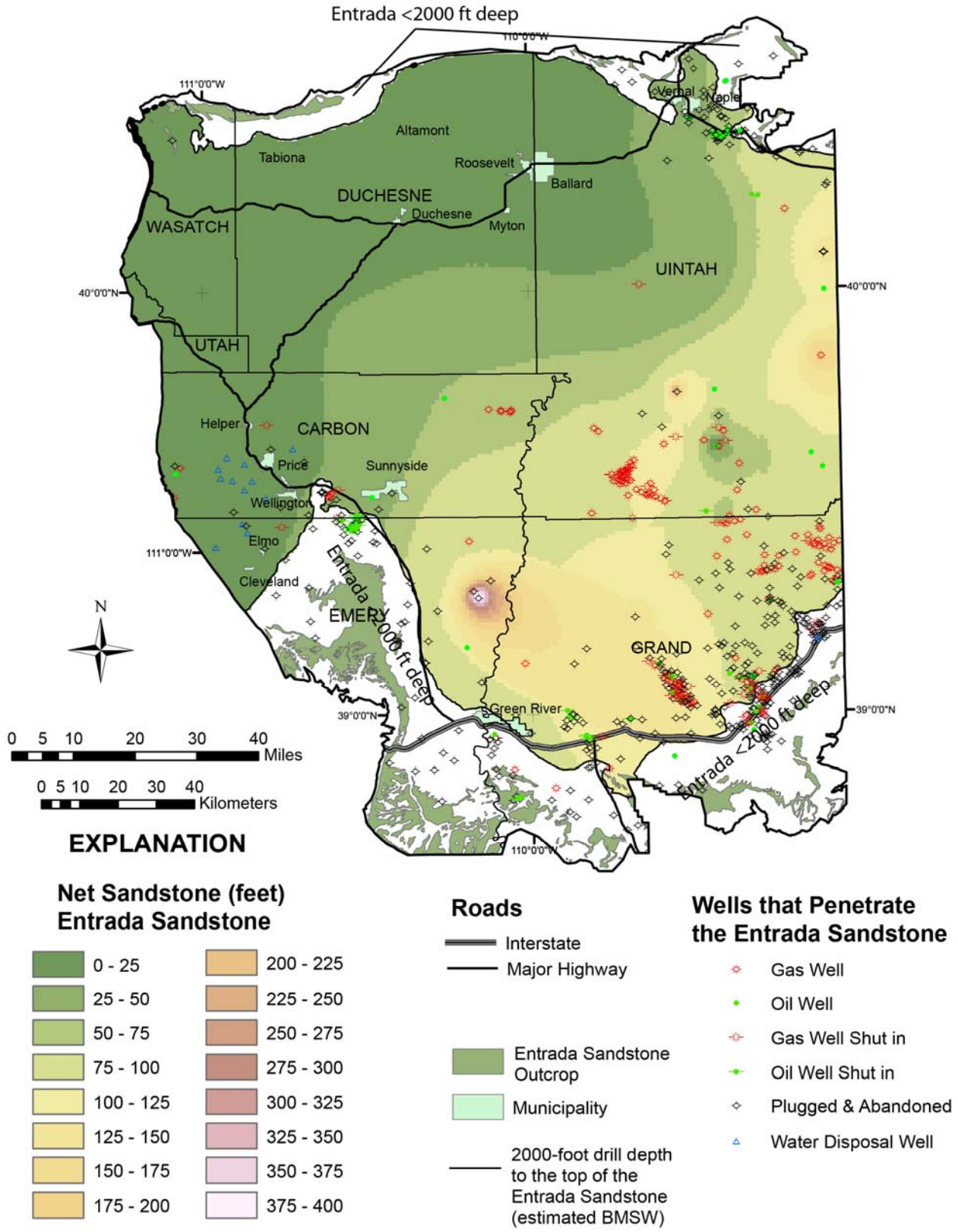

Figure 4.34. Net sandstone (gamma ray ≤ 60 API) in the Entrada Sandstone for areas greater than 2000 feet (610 m) deep.

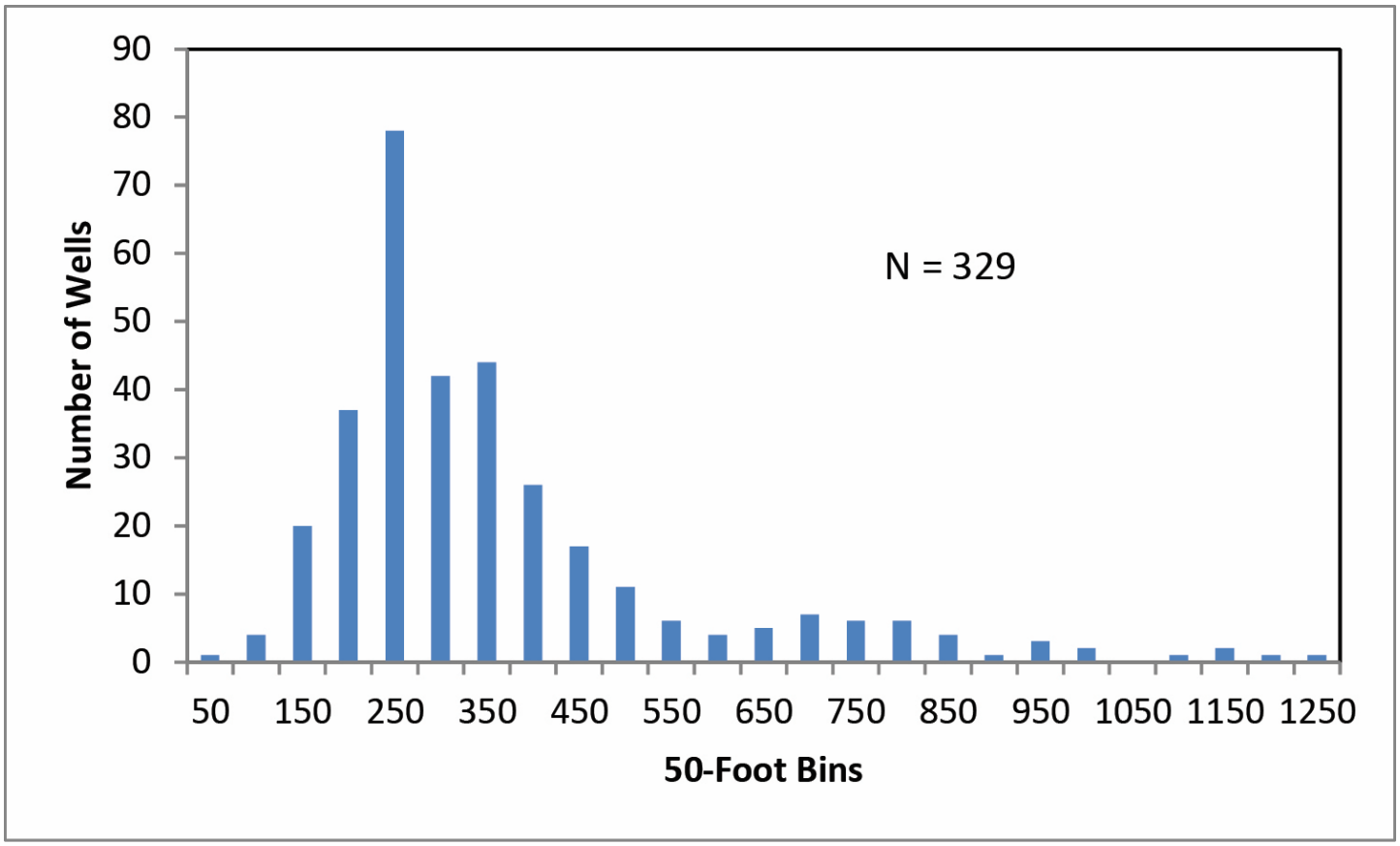

Figure 4.35. Frequency distribution of the gross thickness of the Entrada Sandstone in the geophysical well logs studied. The thickness ranges from 26 to 1210 feet (8-369 m), with an average of 340 feet (104 m) and a median of 273 feet (83 m).

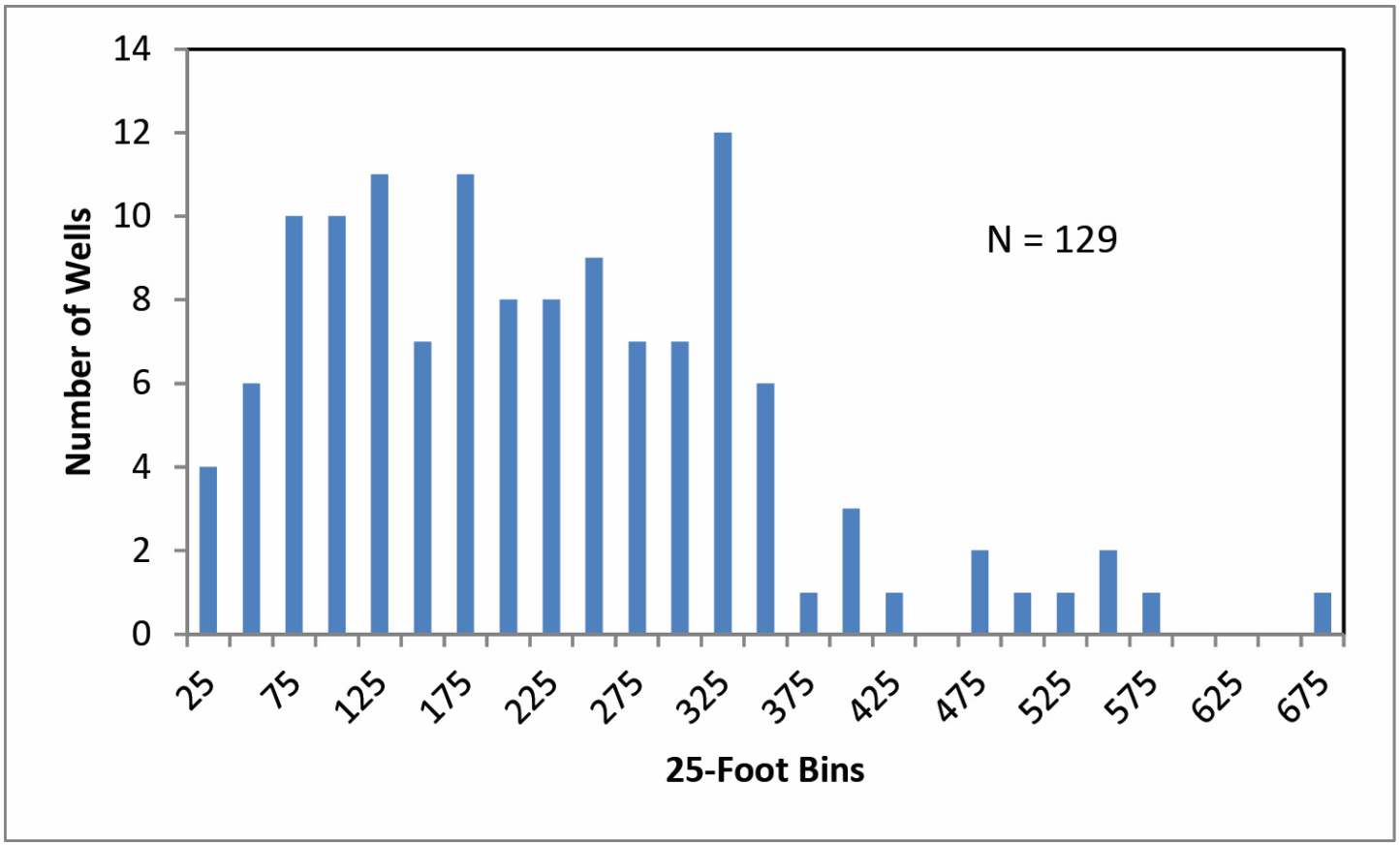

Figure 4.36. Frequency distribution of the net sandstone (≤ 60 API gamma ray) in the Entrada Sandstone in the geophysical well logs studied. The thickness ranges from 6 to 670 feet (2-204 m) with an average of 210 feet (64 m) and a median of 194 feet (59 m).

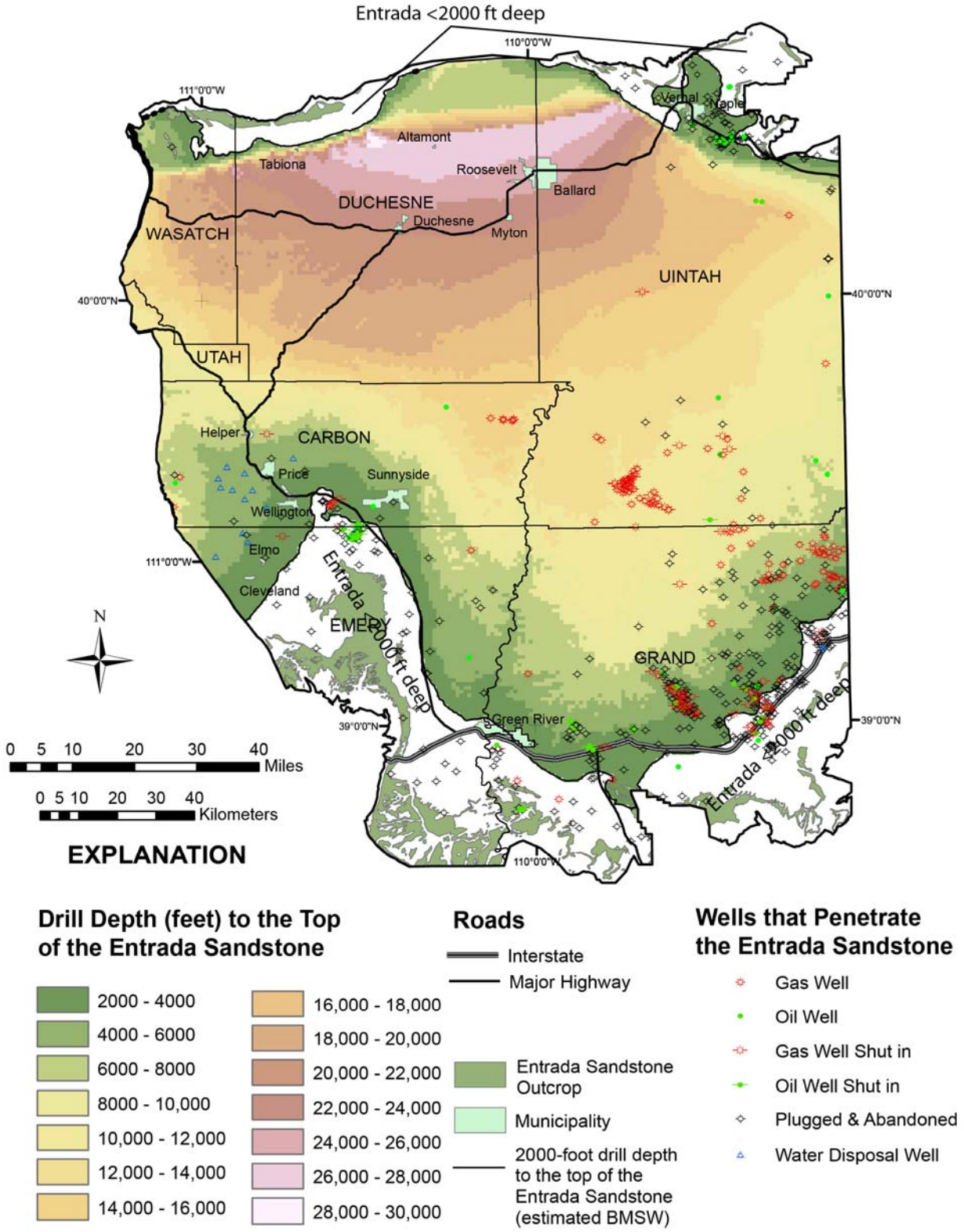

Figure 4.37. Drill depth to the top of the Entrada Sandstone for areas greater than 2000 feet (60 m) deep.

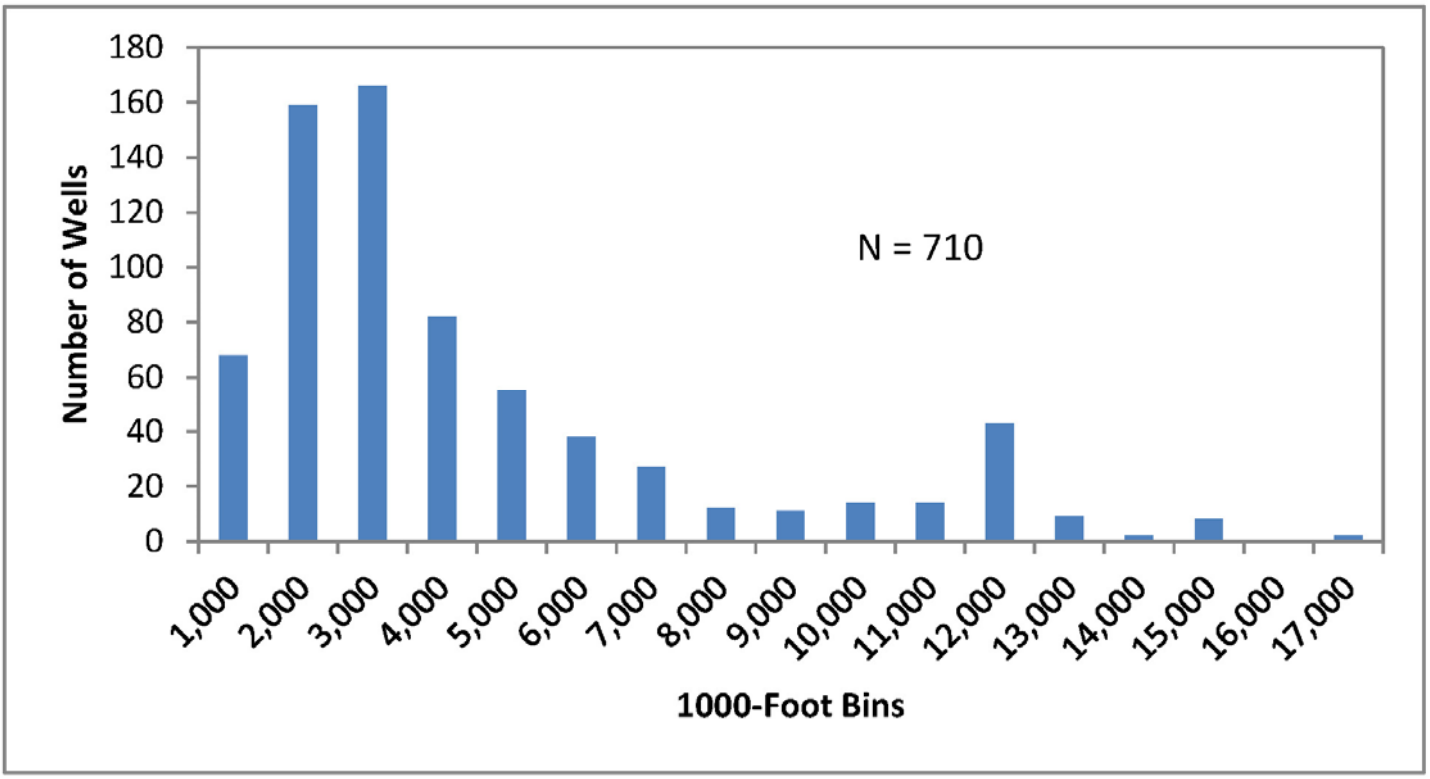

Figure 4.38. Frequency distribution of the drill depth in feet to the top of the Entrada Sandstone in the geophysical well logs studied. The drill depth ranges from 19 to 16,550 feet (6-5044 m) with an average of 3974 feet (1211 m) and median of 2684 feet (818 m).

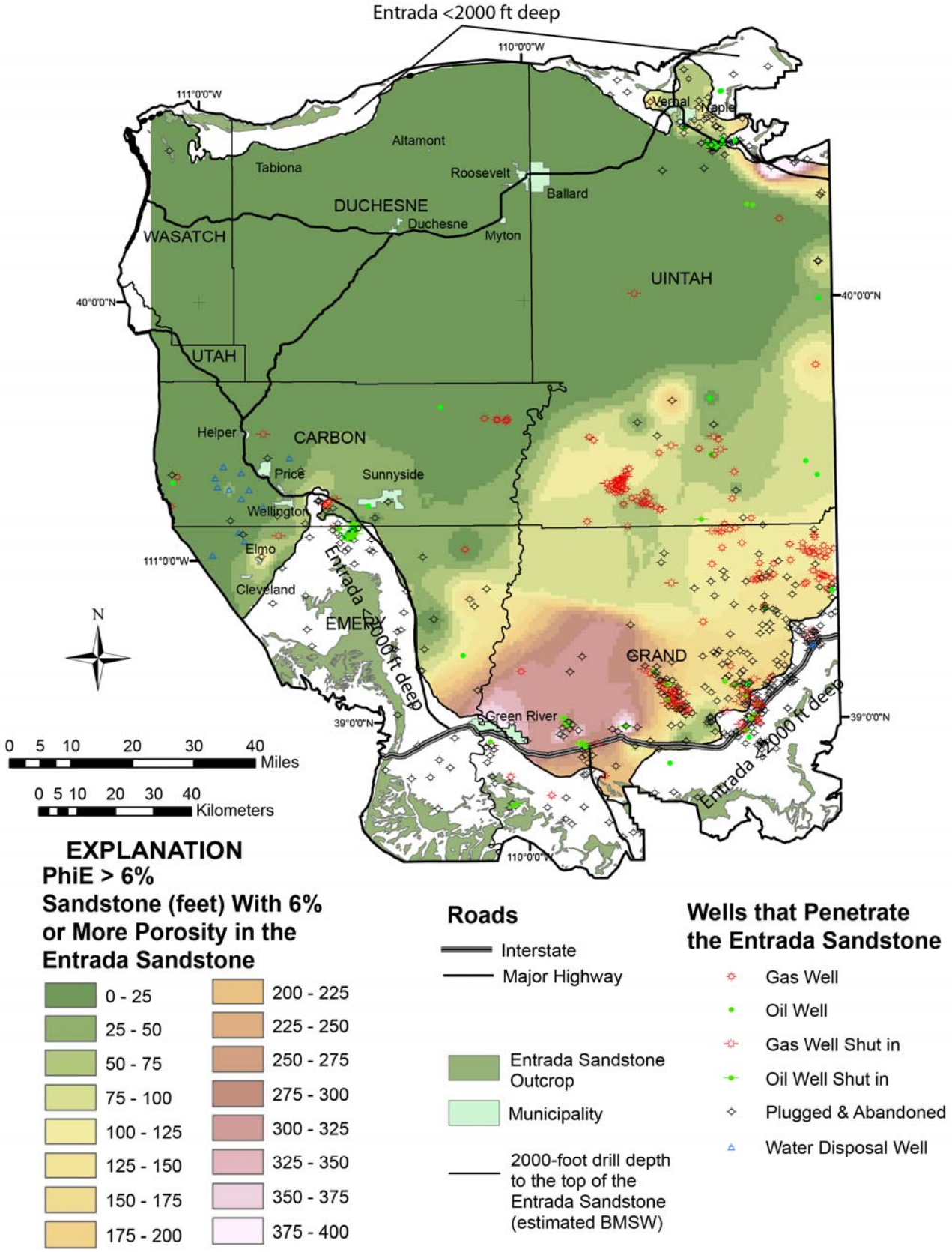

Figure 4.39. Feet of sandstone in the Entrada Sandstone with 6% or more porosity for areas greater than 2000 feet (210 m) deep. Porosity determined from density or sonic well logs.

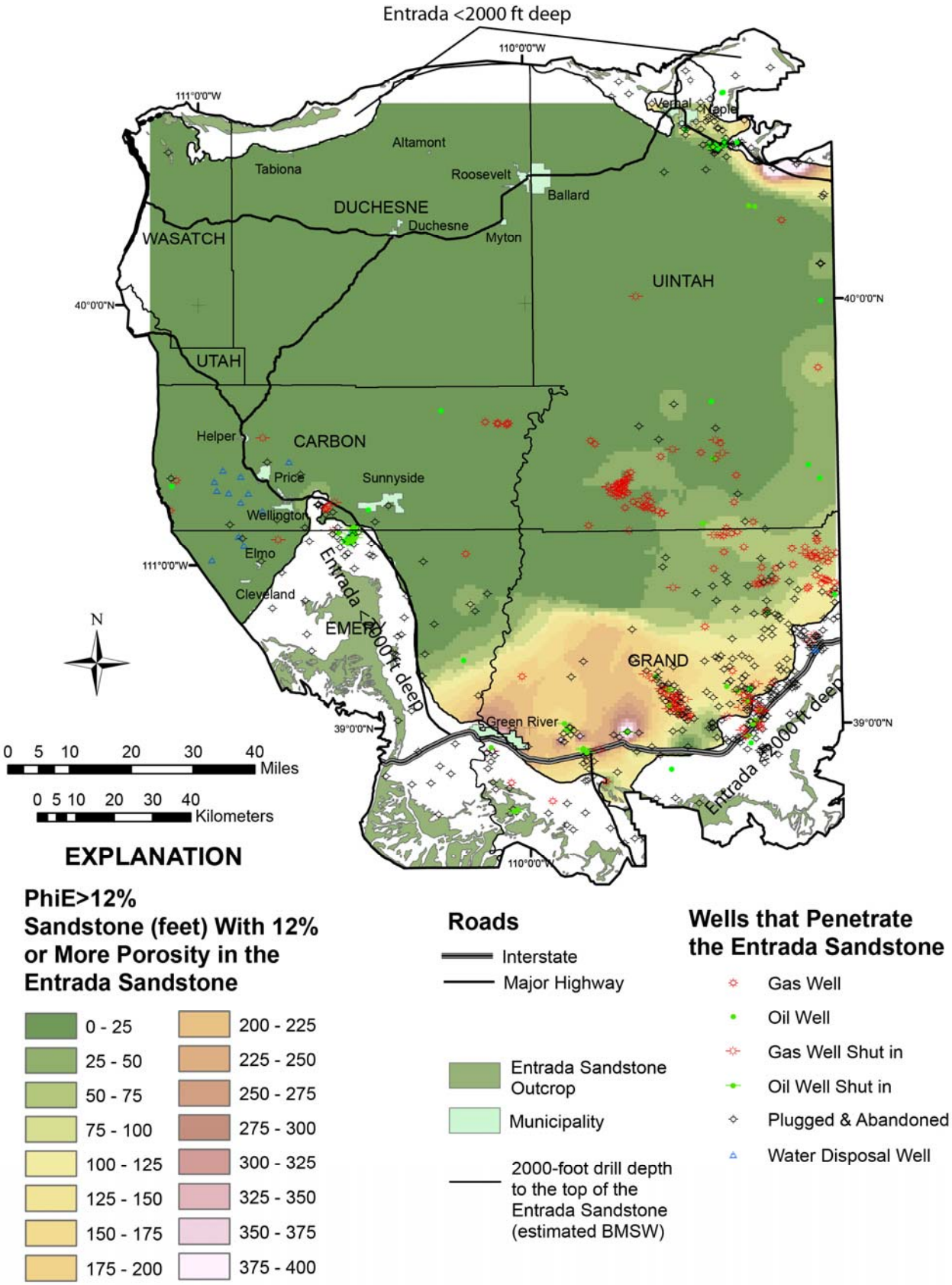

Figure 4.40. Feet of sandstone in the Entrada Sandstone with 12% or more porosity for areas greater than 2000 feet (210 m) deep. Porosity determined from density or sonic well logs.

A

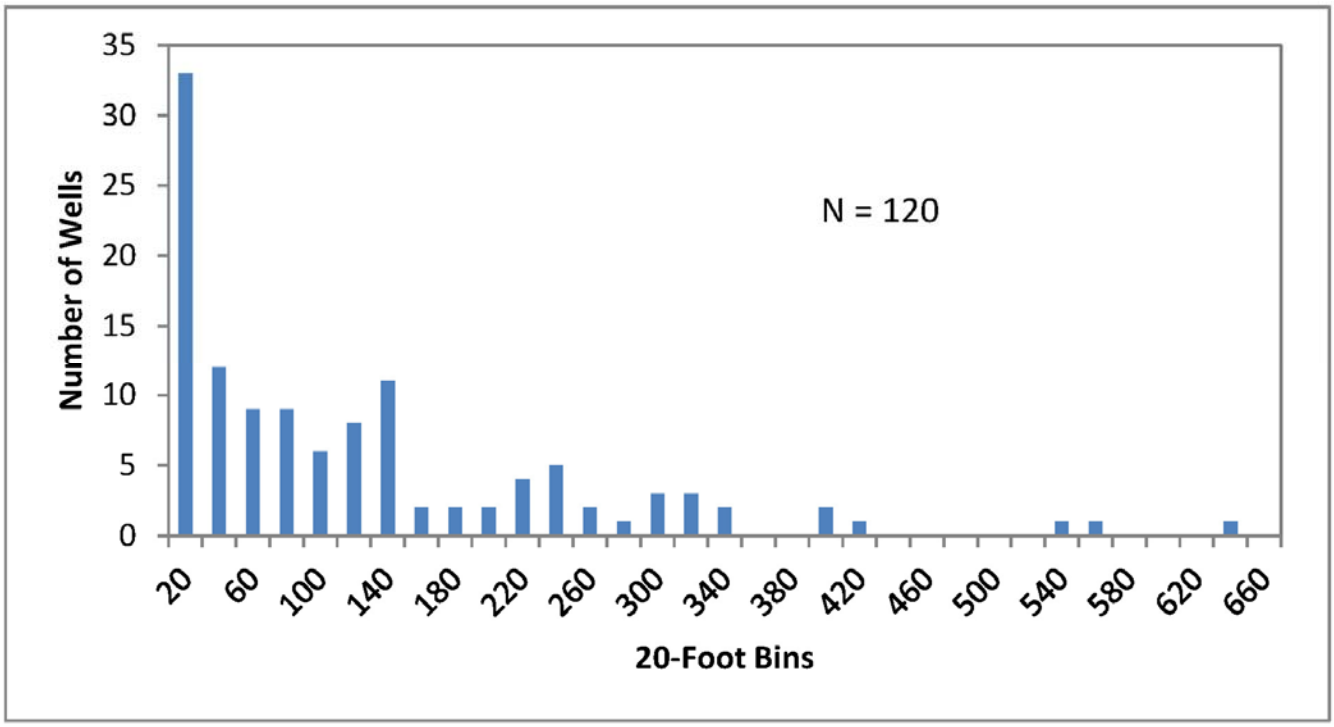

B

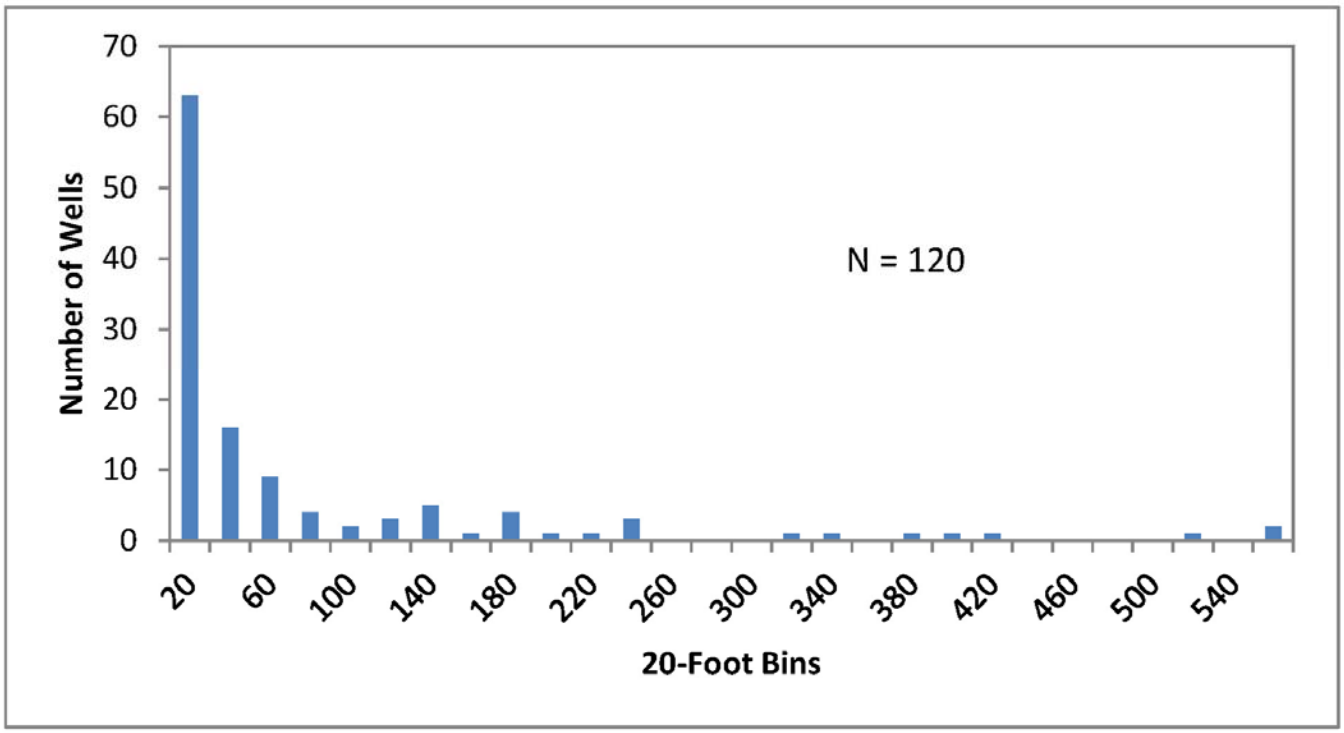

Figure 4.41. Frequency distribution graphs of the feet of sandstone with (A) ≥ 6% porosity (PhiE ≥ 6%) and (B) ≥ 12% porosity (PhiE ≥ 12%) in the Entrada Sandstone. PhiE ≥ 6% ranges from 0 to 640 feet (195 m) with an average of 114 feet (35 m) and a median of 72 feet (22 m). PhiE ≥ 12% ranges from 0 to 558 feet (0-170 m) with an average of 66 feet (20 m) and median of 17 feet (5 m).

A

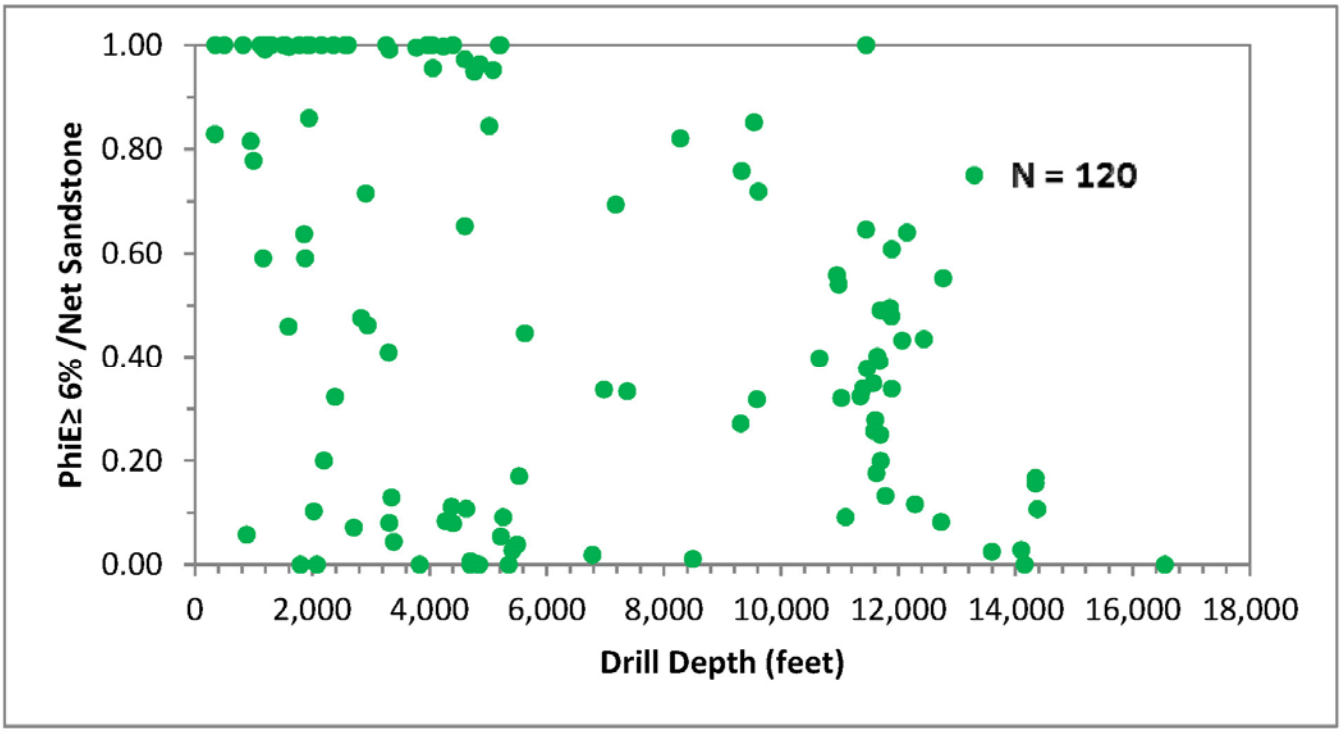

B

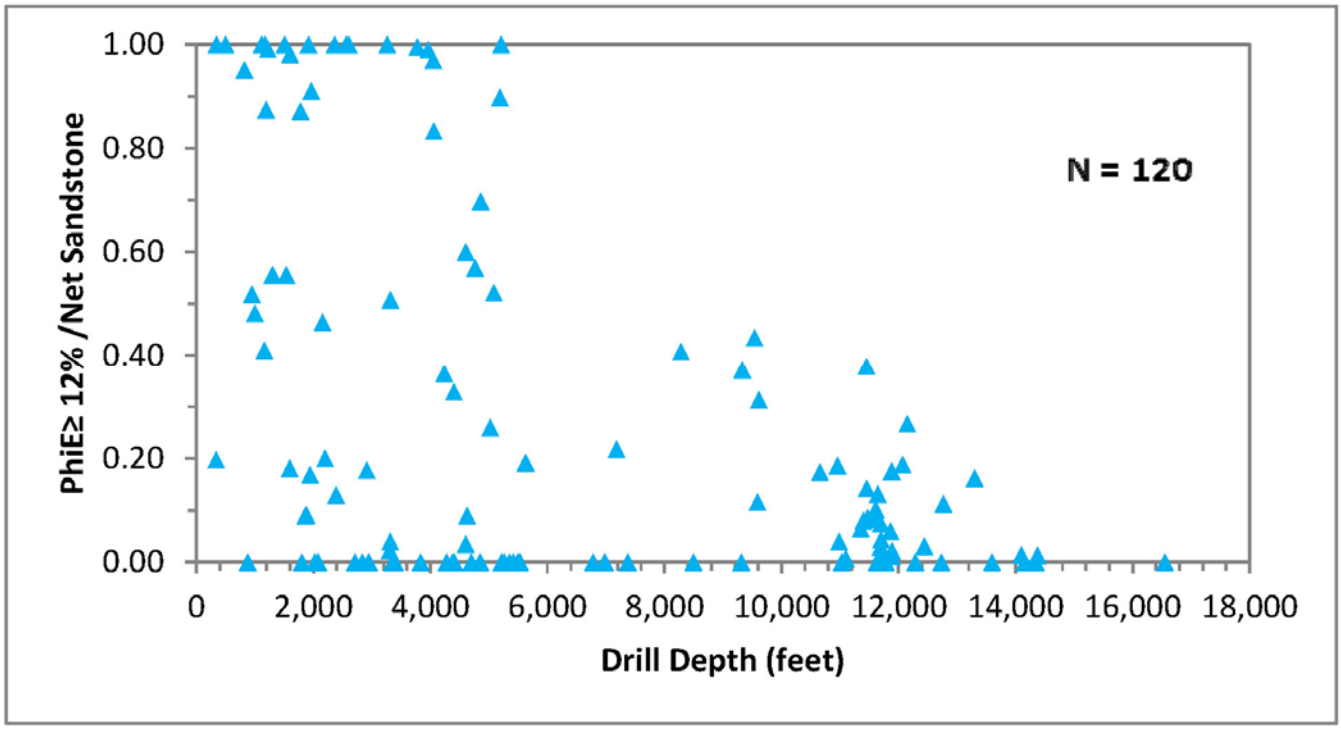

Figure 4.42. (A) Ratio of PhiE ≥ 6%/net sandstone versus drill depth, and (B) ratio of PhiE ≥ 12%/net sandstone versus drill depth in the Entrada Sandstone. Porosity calculated from density or sonic logs.

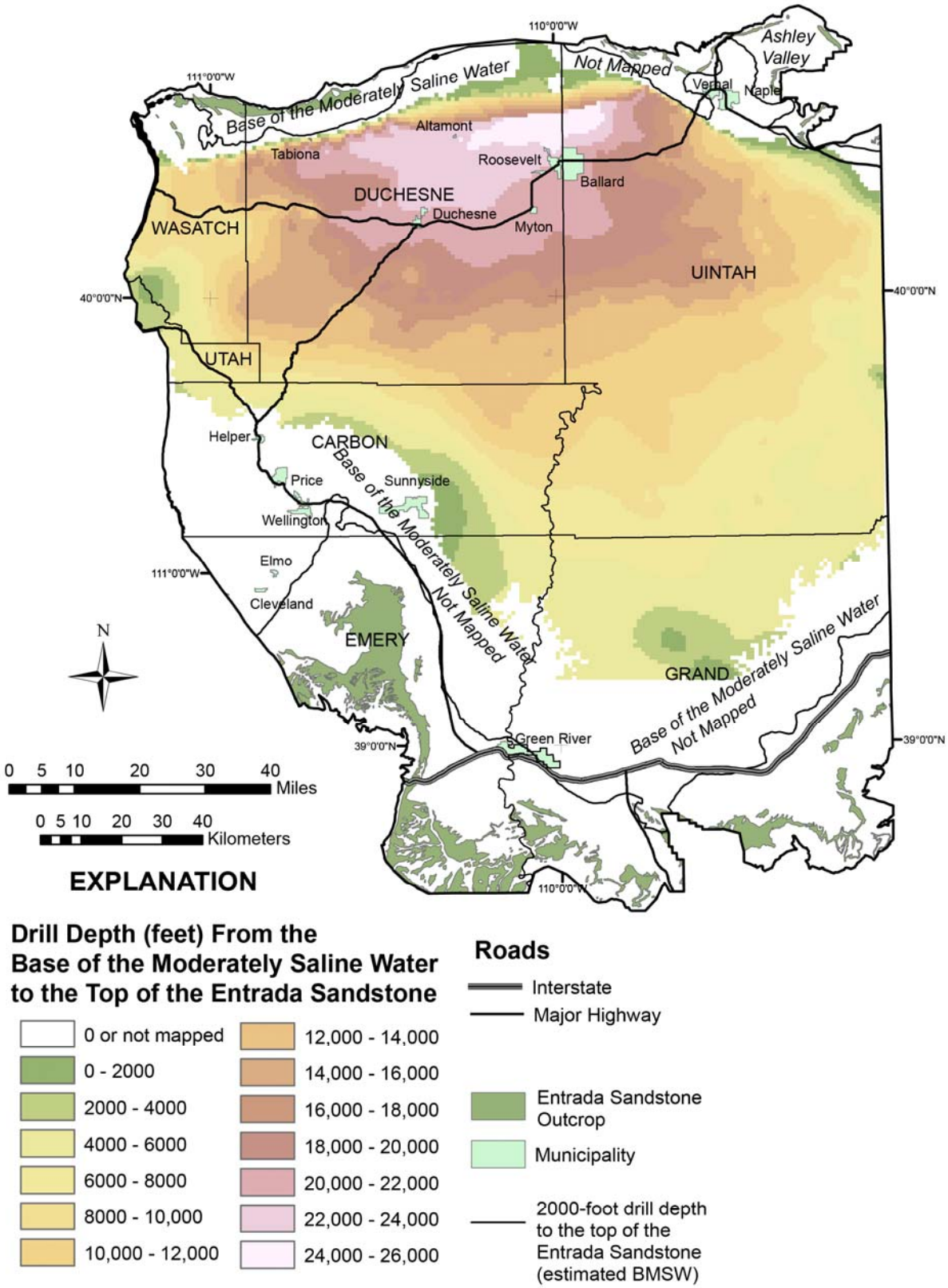

Figure 4.43. Drill depth (feet) from the base of the moderately saline water (BMSW) to the top of the Entrada Sandstone. The Entrada is above the BMSW in Ashley Valley (see figure 1.1 for field location). The map was created using ArcScene® by subtracting the drill depth map (figure 4.37) from the BMSA map of Anderson and others (2012).

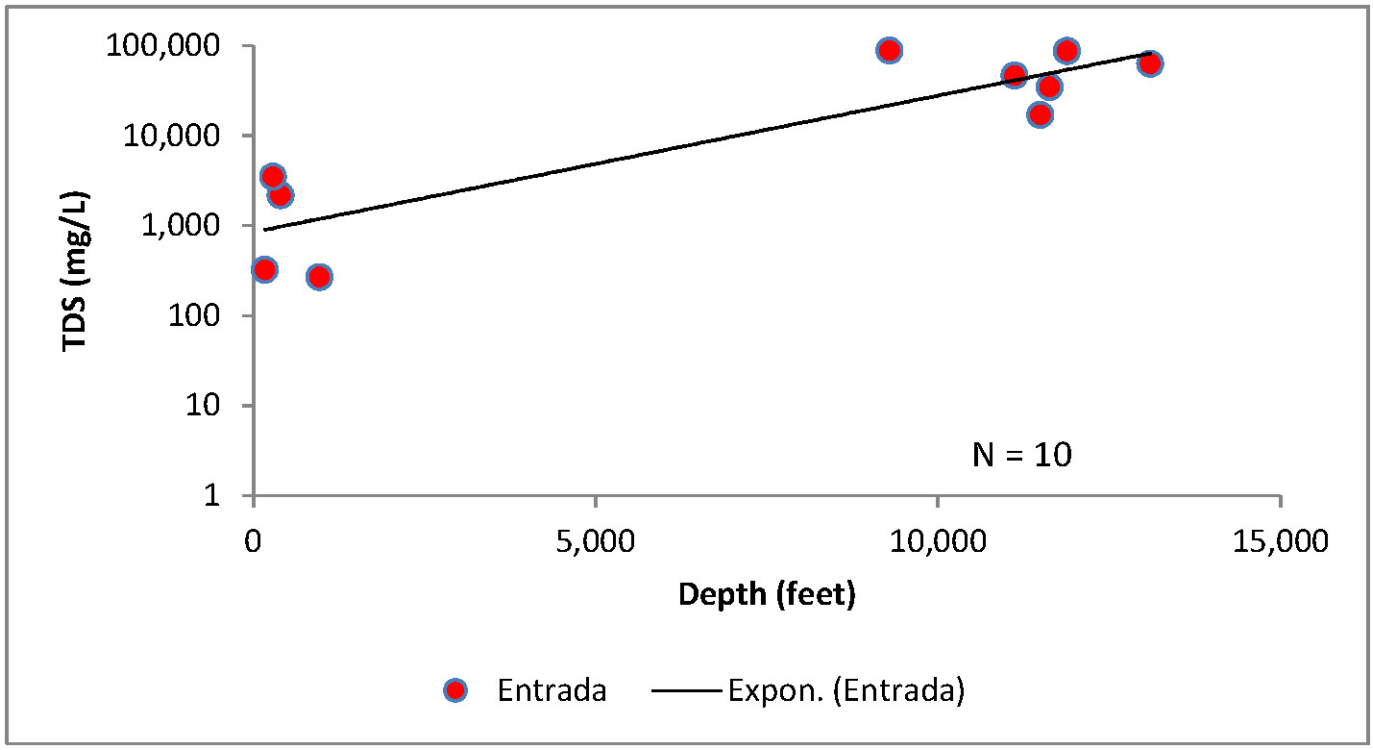

Figure 4.44. Total dissolved solids (mg/L) with depth (feet). The exponential trend line (Expon.) indicates less than 10,000 TDS to a depth of 7000 feet. The limited number of samples (10) is insufficient to be statistically significant for such a large area.

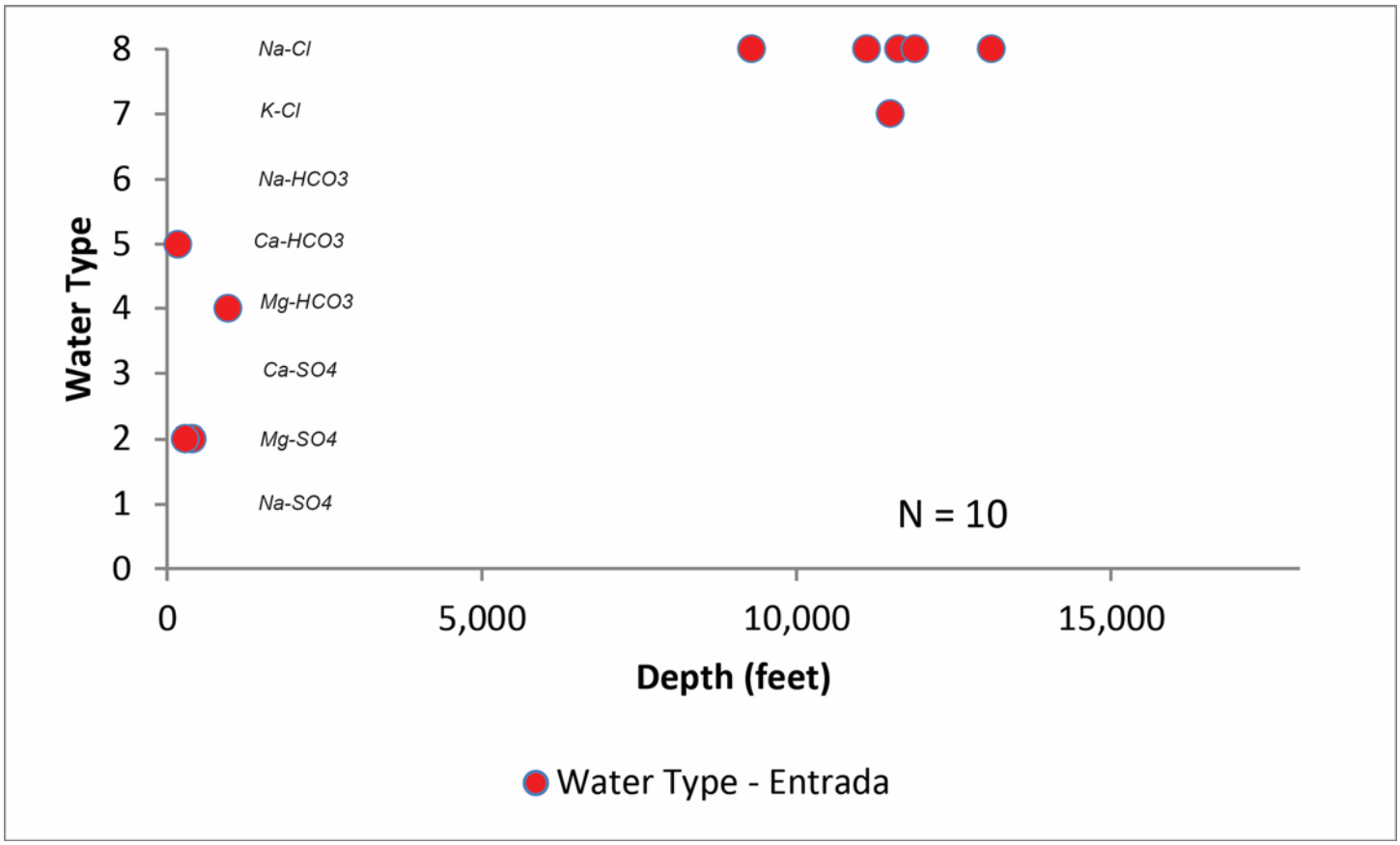

Figure 4.45. Water produced from the Entrada is mostly sodium chloride (Na-Cl) at depths greater than 7000 feet, and a mix of calcium bicarbonate (Ca-HCO_3), magnesium bicarbonate (Mg-HCO_3), and magnesium sulfate (Mg-SO_4), at shallower depths. The number of samples (10) is not statistically significant for such a large area.

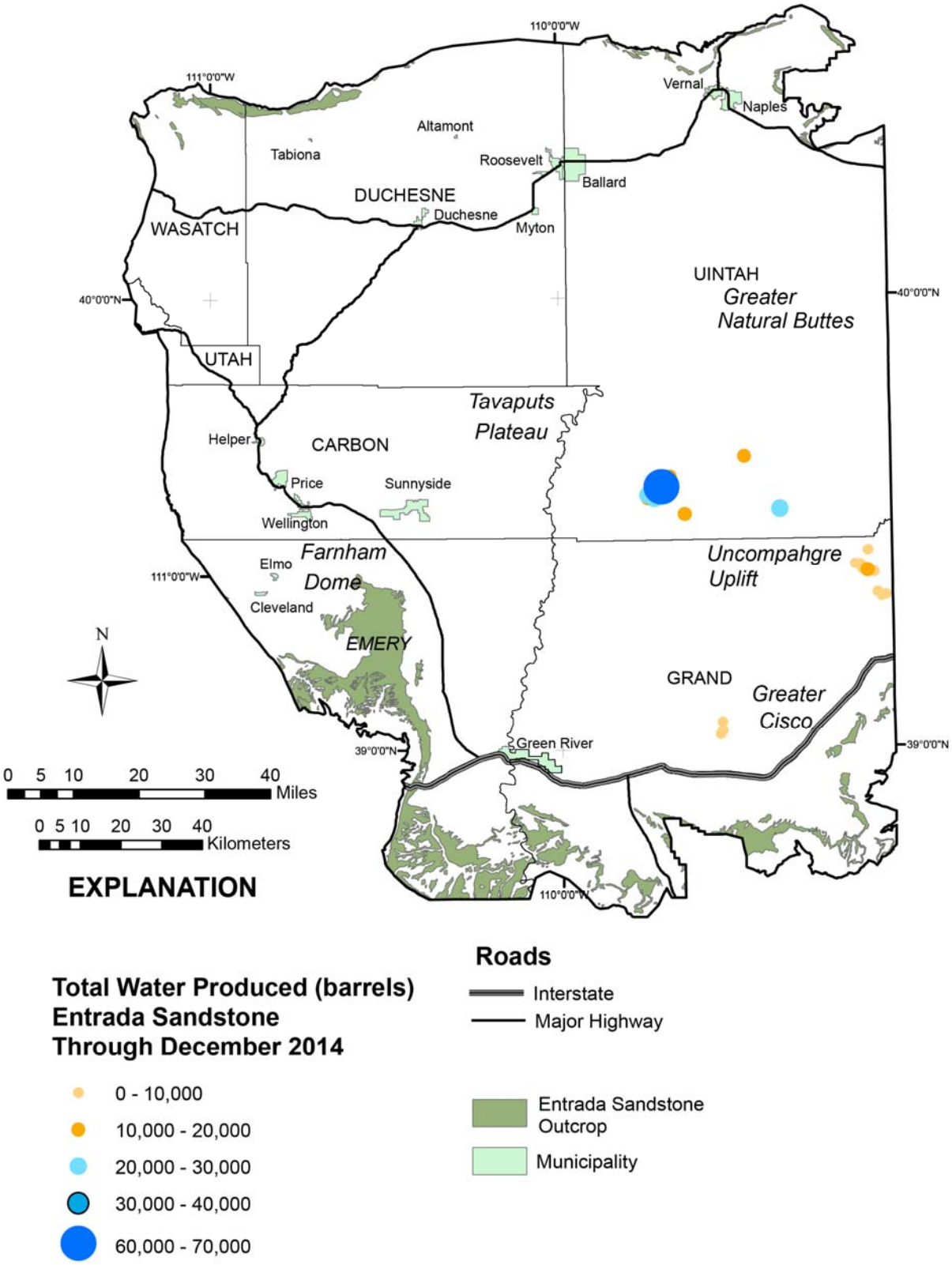

Figure 4.46. Total barrels of water produced from the Entrada Sandstone.

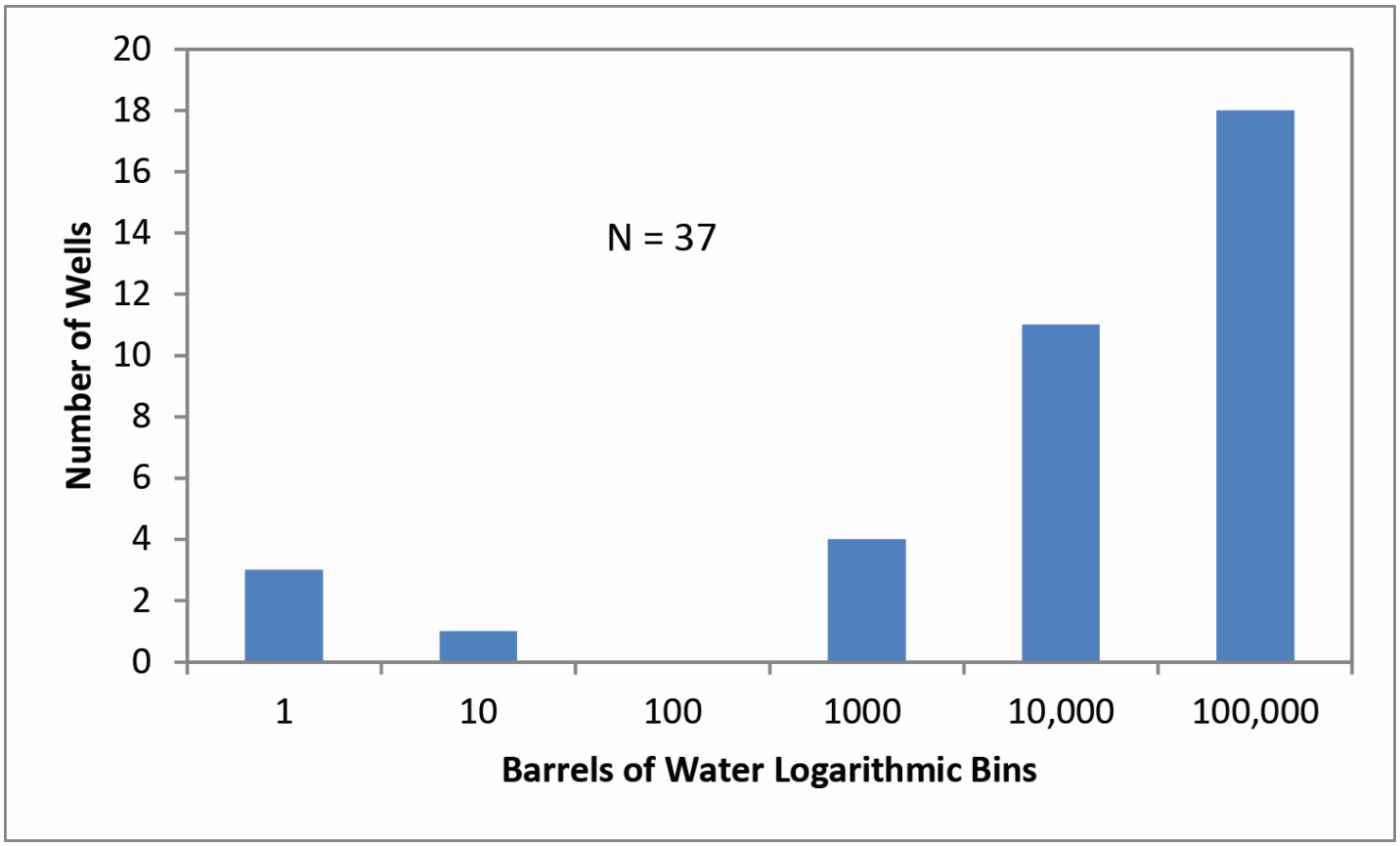

Figure 4.47. Frequency diagram of total water per well produced from the Entrada Sandstone. Water volumes range from 0 to 62,286 BW/well, the average is 12,118 BW with a median 9249 BW.

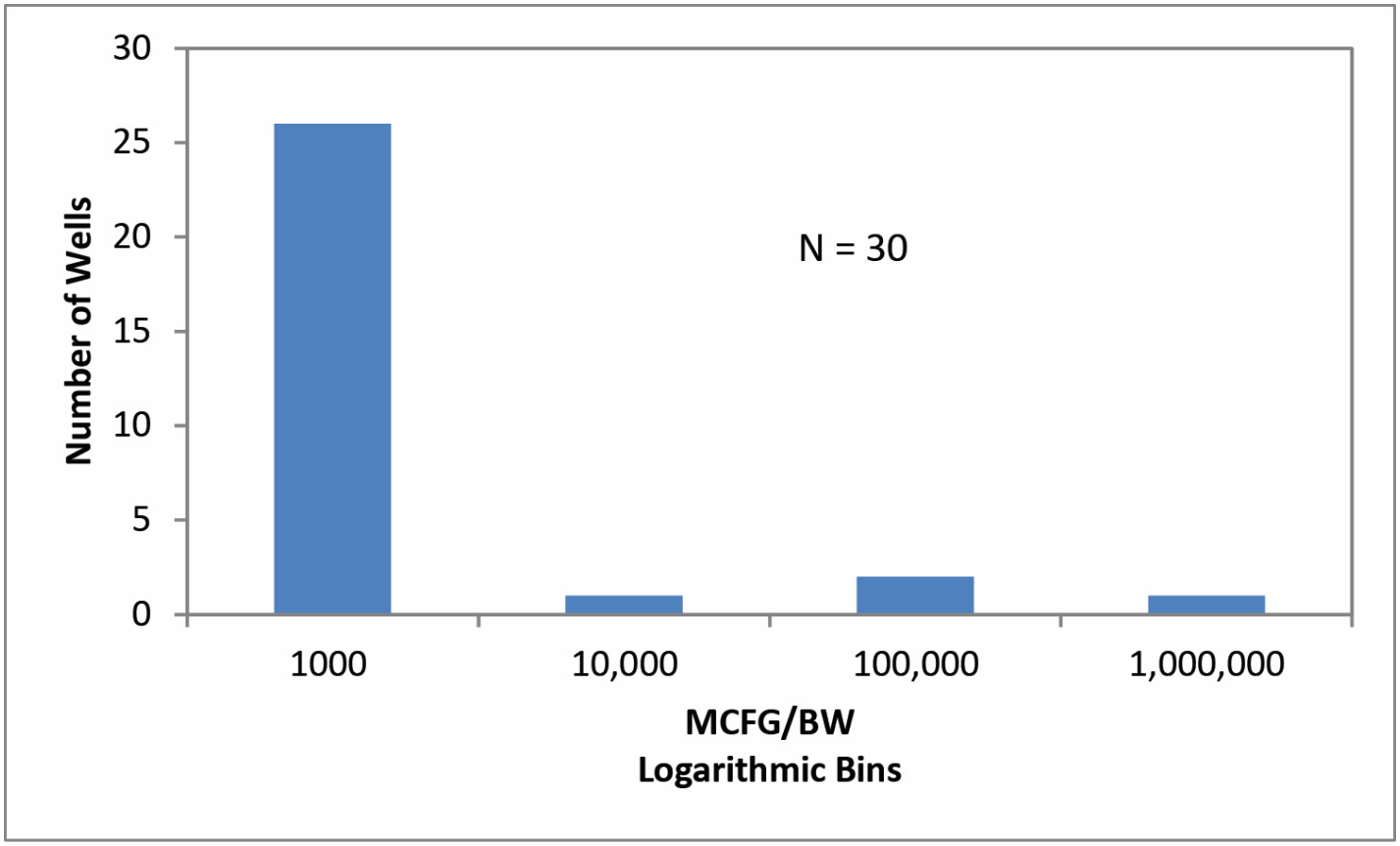

Figure 4.48. Frequency diagram of total gas produced per barrel of water (BW). Gas volumes are in thousand cubic feet (MCF). The range is from 7 to 134,536 MCFG/BW with an average of 5670 MCFG/BW and median of 200 MCFG/BW. Three wells not included in this data produced more than 9 BCF of gas and no water.

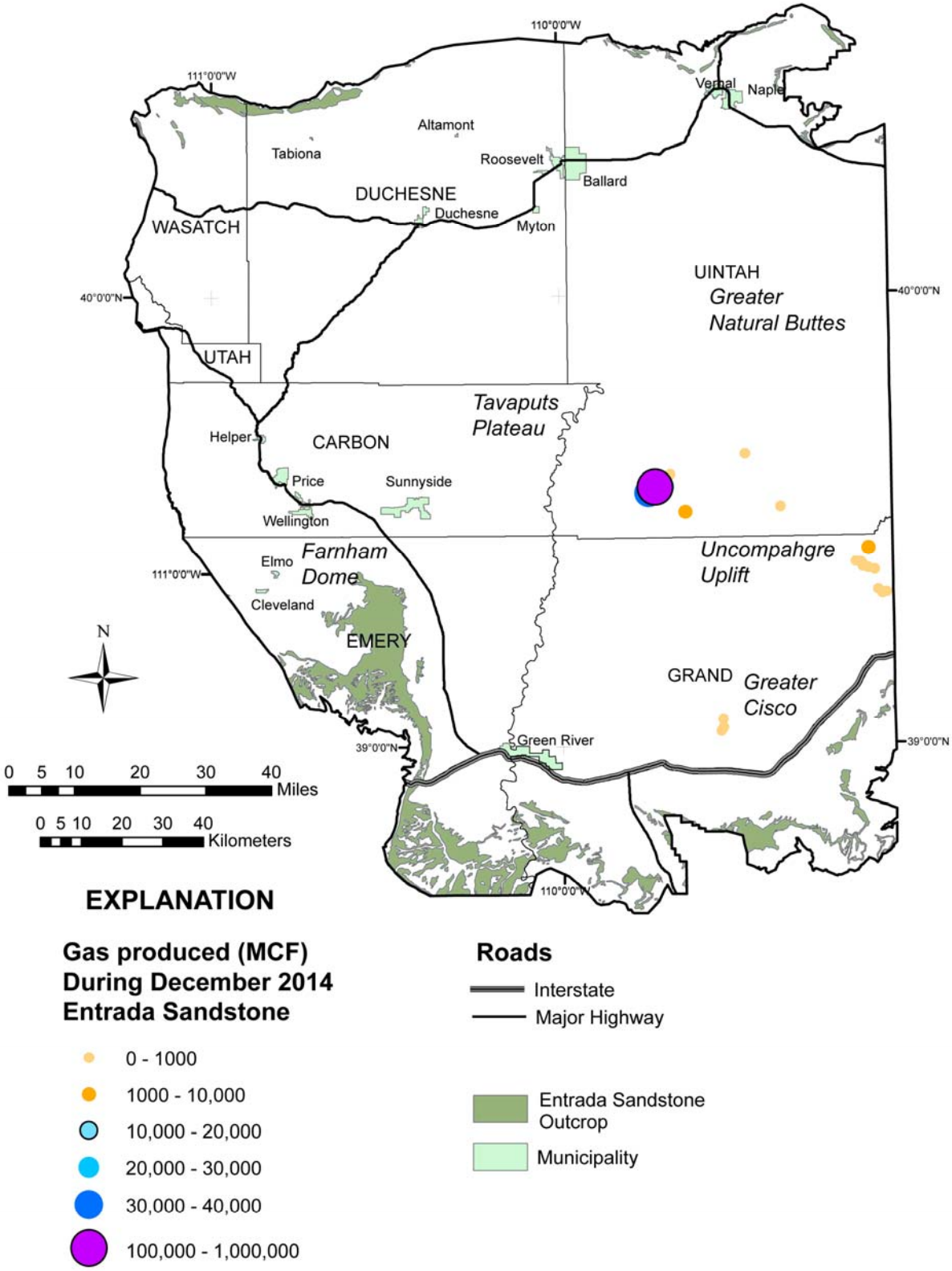

Figure 4.49. Gas produced from the Entrada Sandstone during the month of December 2014.

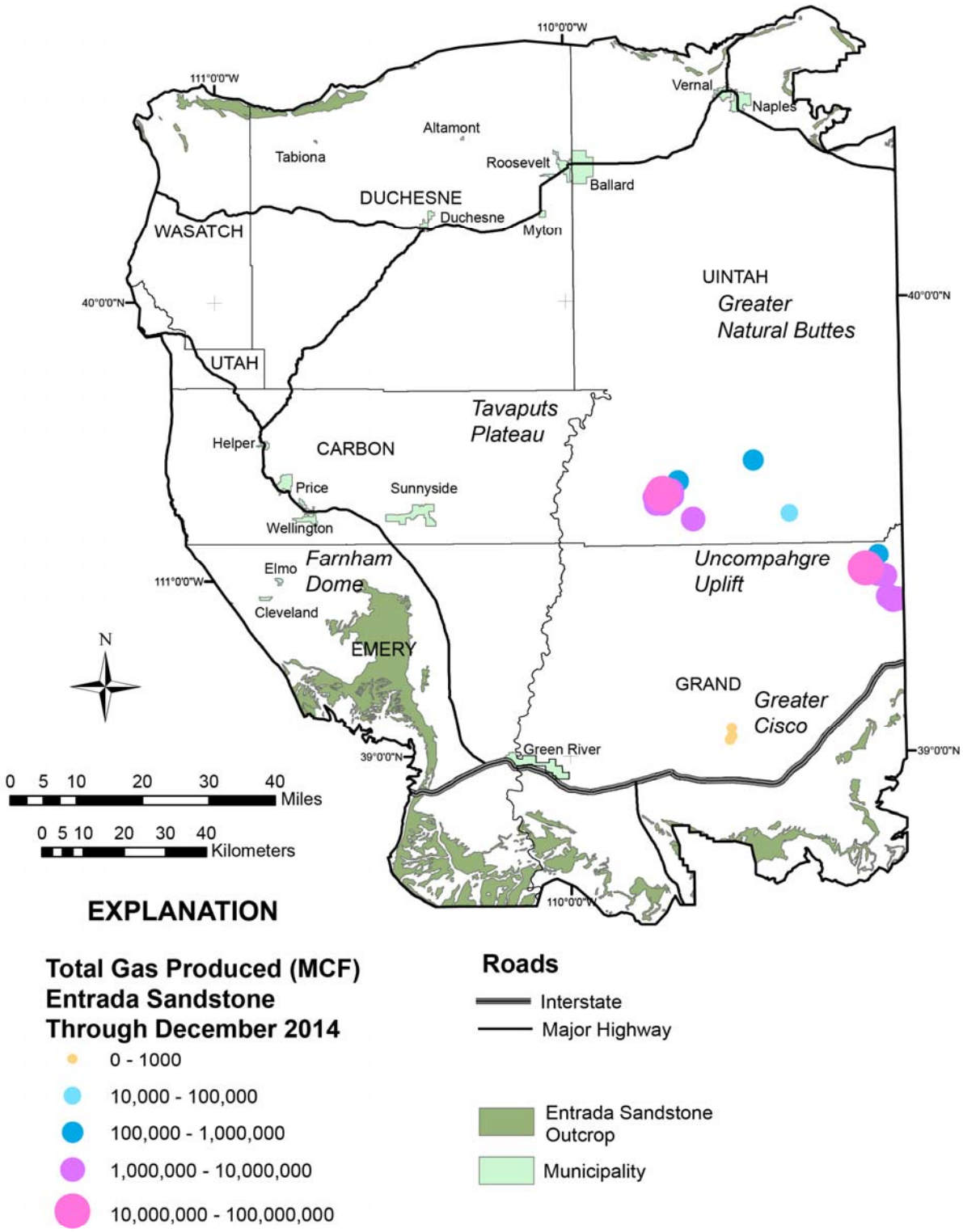

Figure 4.50. Total gas produced per well from the Entrada Sandstone through December 2014.

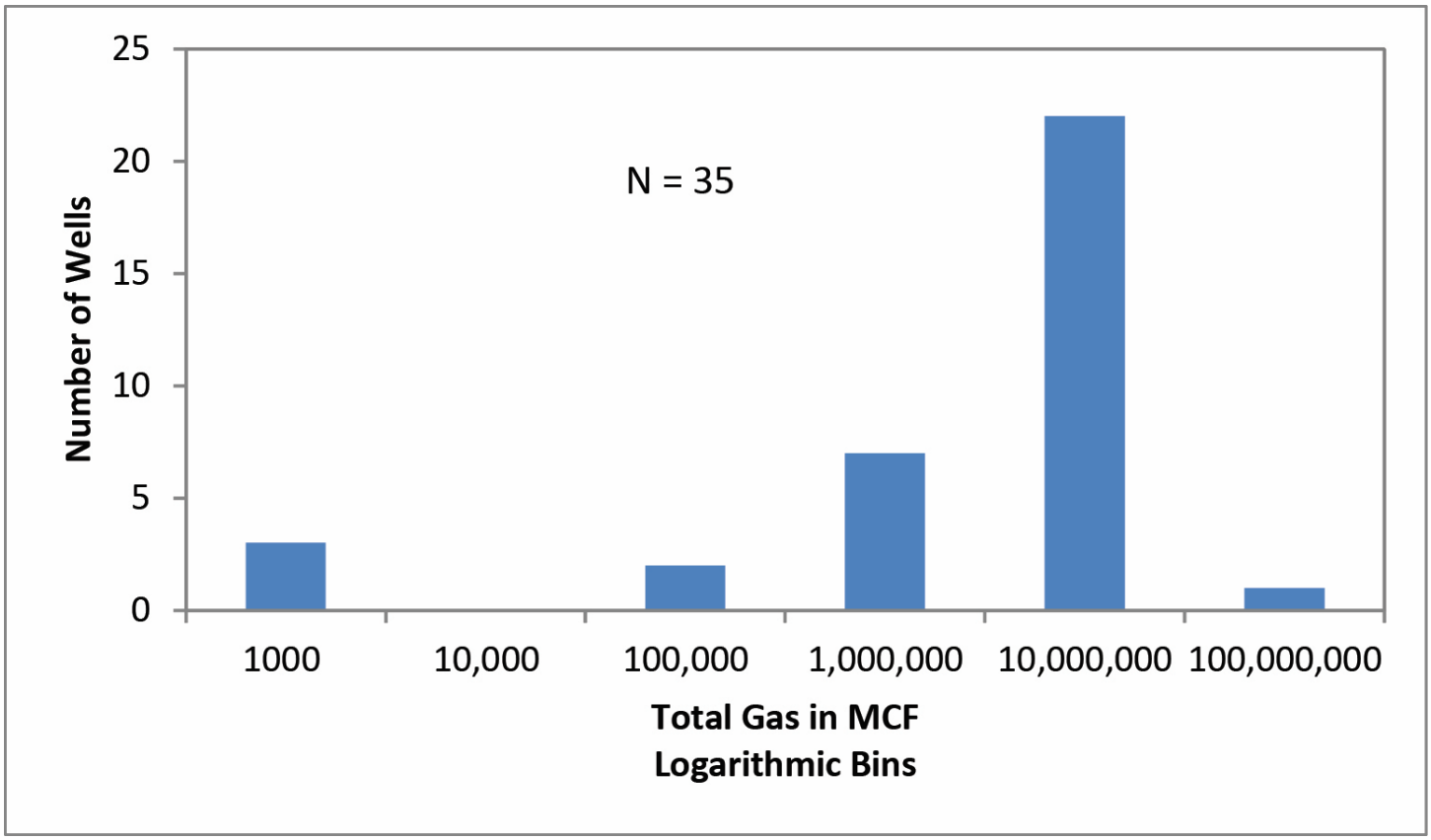

Figure 4.51. Frequency diagram of total gas produced per well from the Entrada Sandstone through December 2014. Gas volumes range from 14,878 to 12,276,656 MCFG/well with an average of 3,509,967 MCFG/well and median of 1,931,987 MCFG/well.

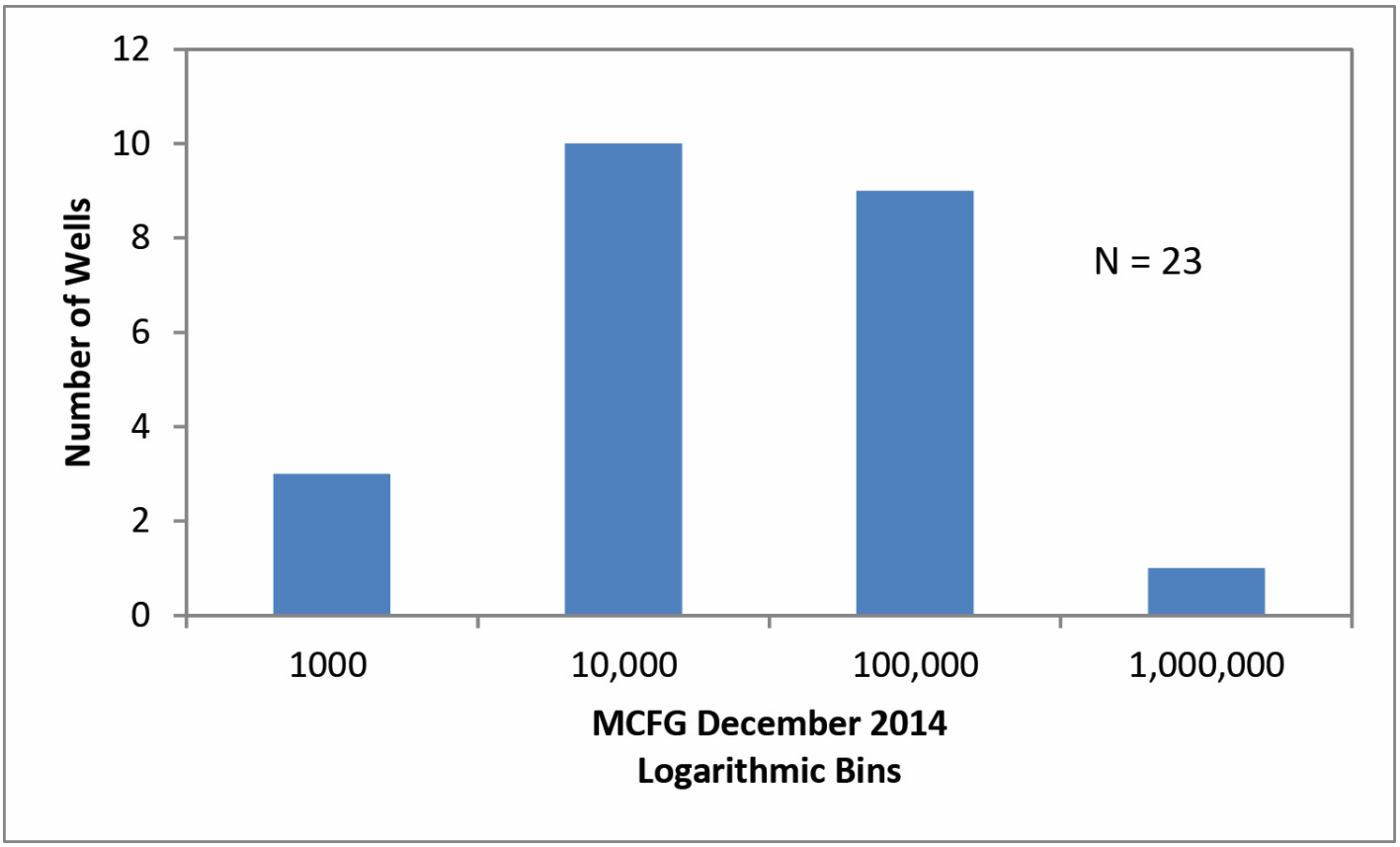

Figure 4.52. Frequency distribution diagram of gas produced per well from the Entrada Sandstone during December 2014. Production ranges from 118 to 181,310 MCFG/well with an average of 17,669 MCFG/ well and a median of 6954 MCFG/well.

A

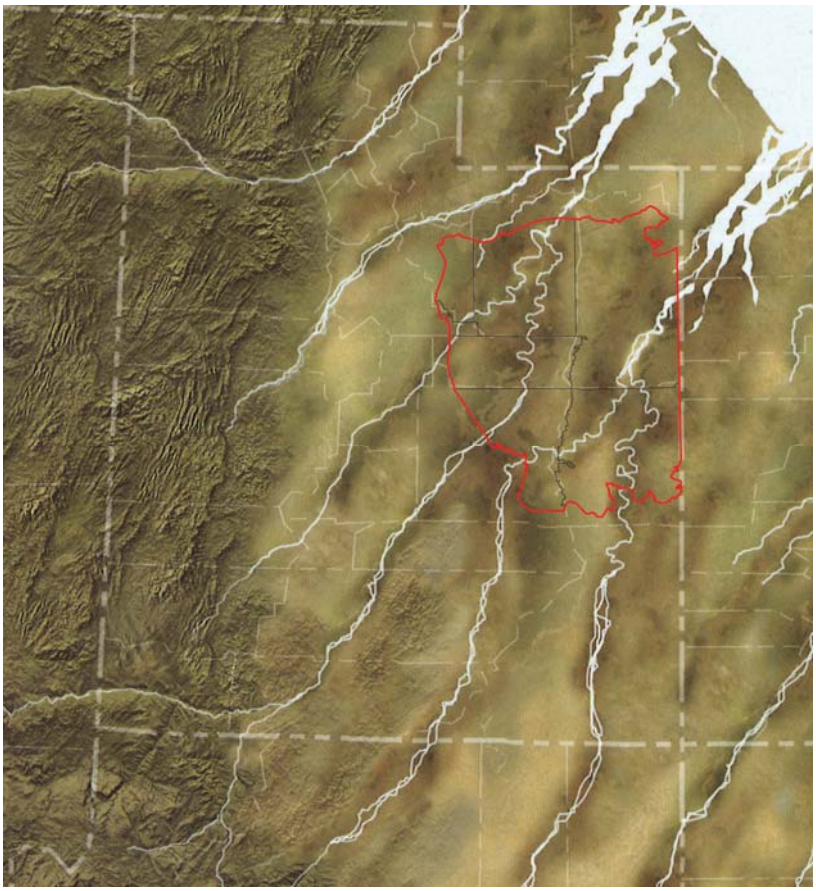

B

Figure 4.53. Early Cretaceous paleogeography. A – Cedar Mountain Formation, Early Cretaceous (125 Ma). B – Dakota Formation, Early Cretaceous (105 Ma). From Blakey and Ranney, 2008.

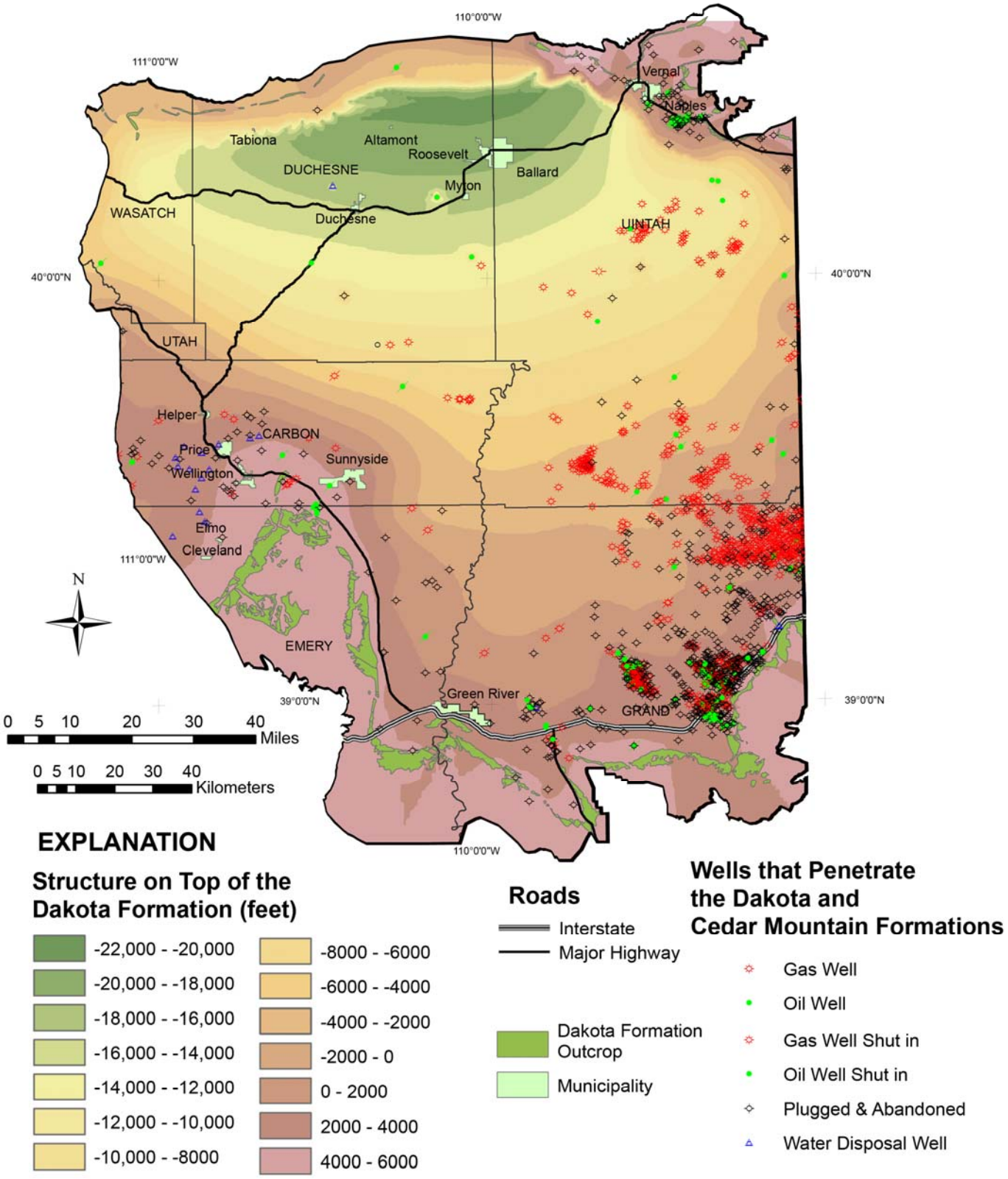

Figure 4.54. Structure on top of the Dakota Formation, Uinta Basin.

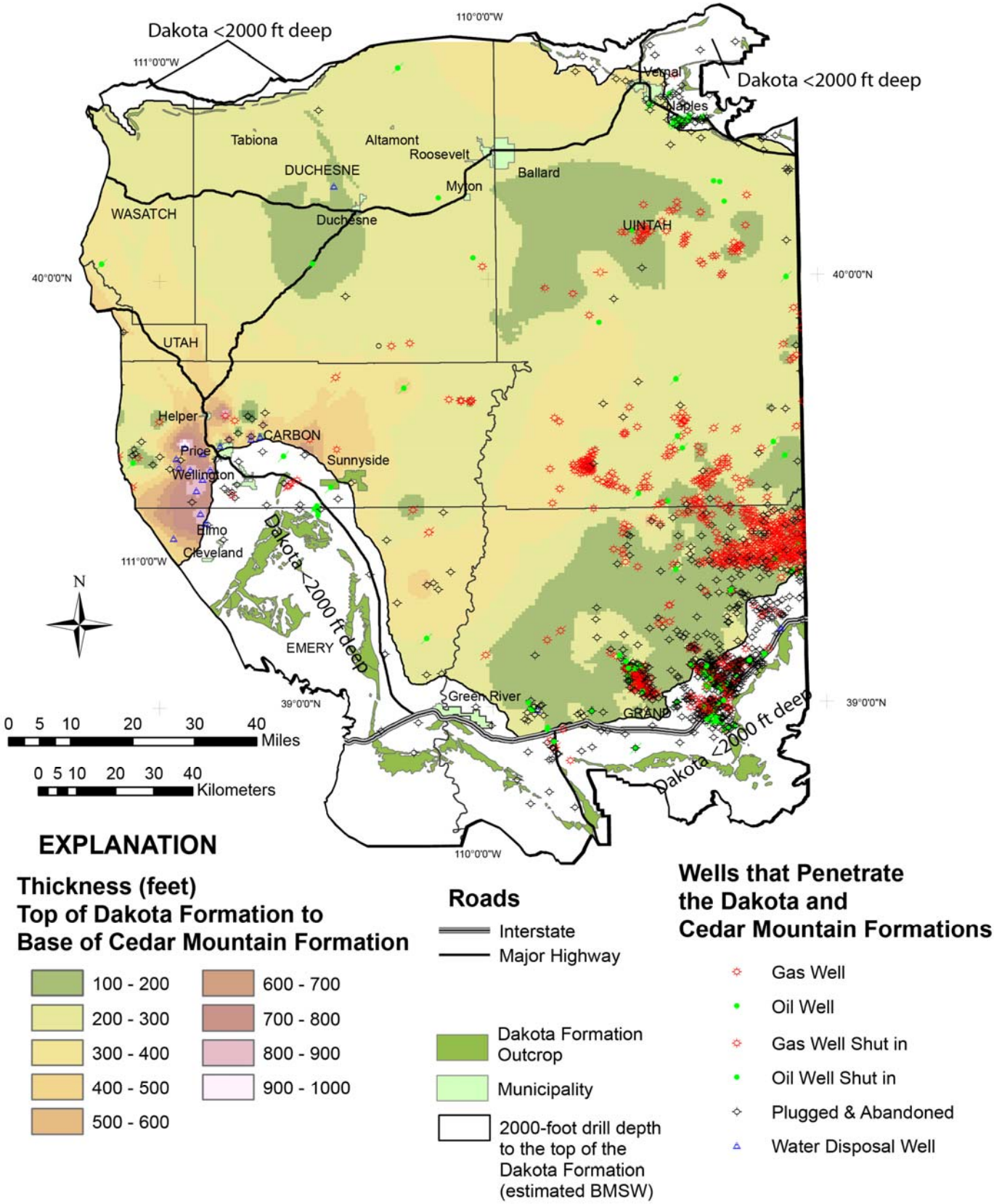

Figure 4.55. Gross thickness of the CMKD reservoir for areas greater than 2000 feet (610 m) deep.

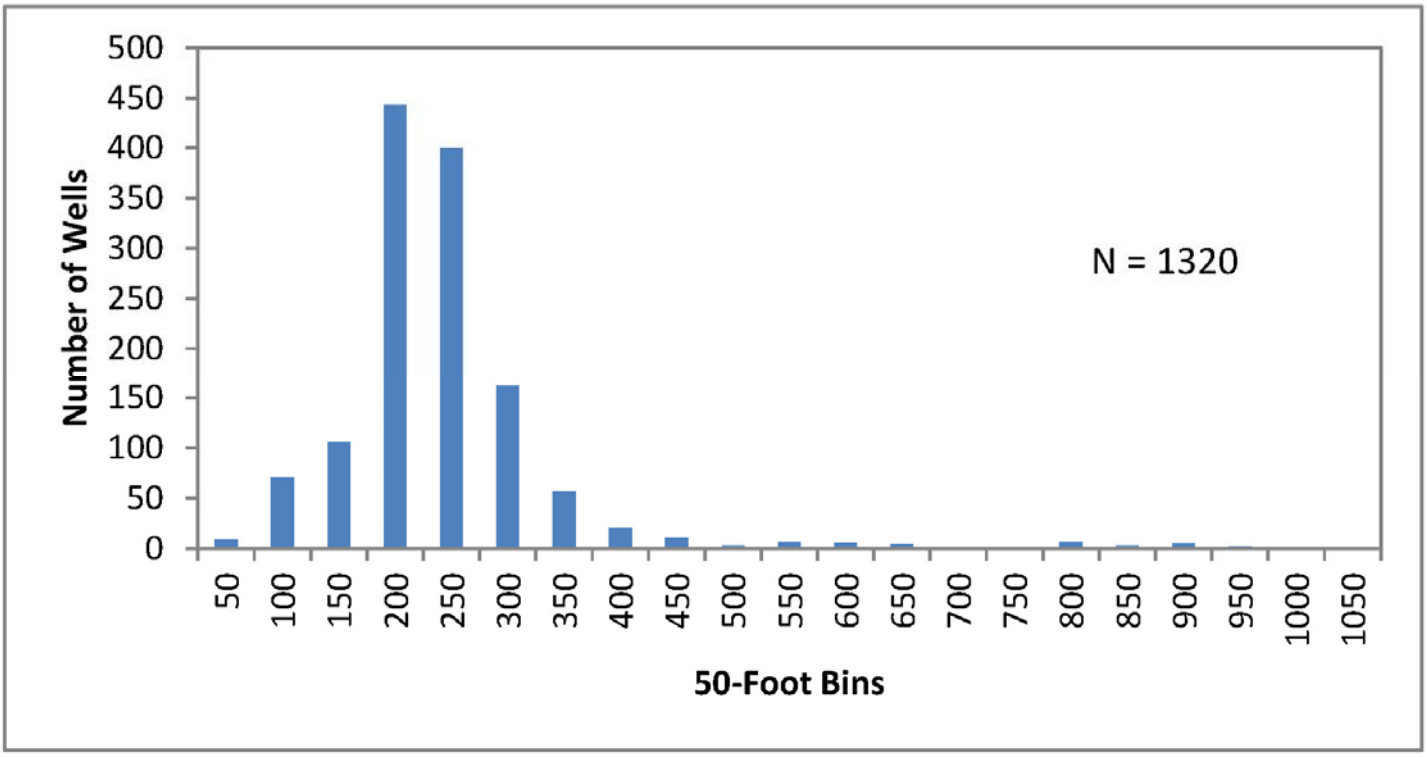

Figure 4.56. Frequency distribution of the gross thickness of CMKD reservoir in the geophysical well logs studied. The thickness ranges from 15 to 1048 feet (5-319 m), with an average of 220 feet (67 m) and a median 203 feet (62 m).

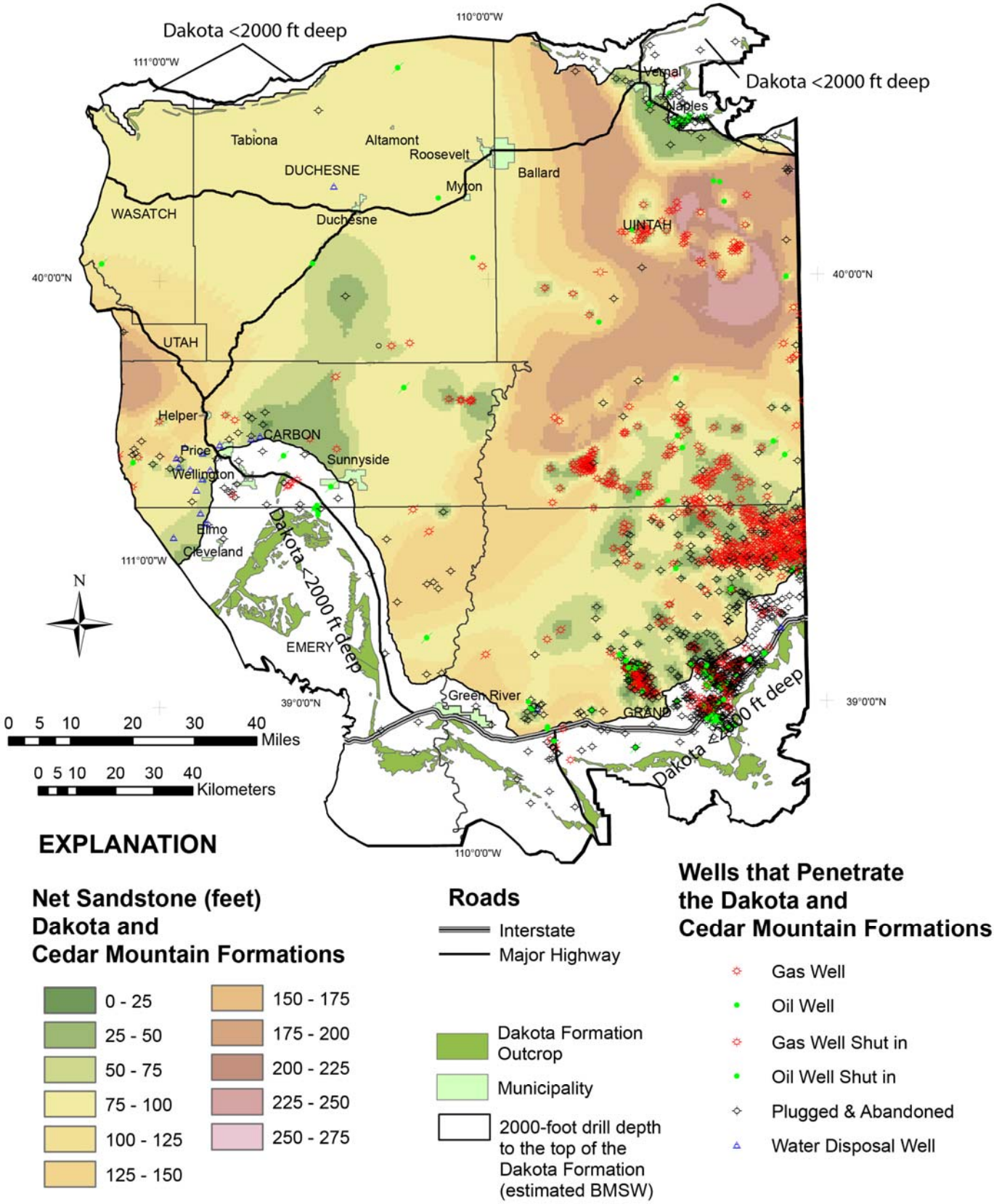

Figure 4.57. Net sandstone (gamma ray ≤ 60 API) thickness of the CMKD reservoir for areas greater than 2000 feet (210 m) deep.

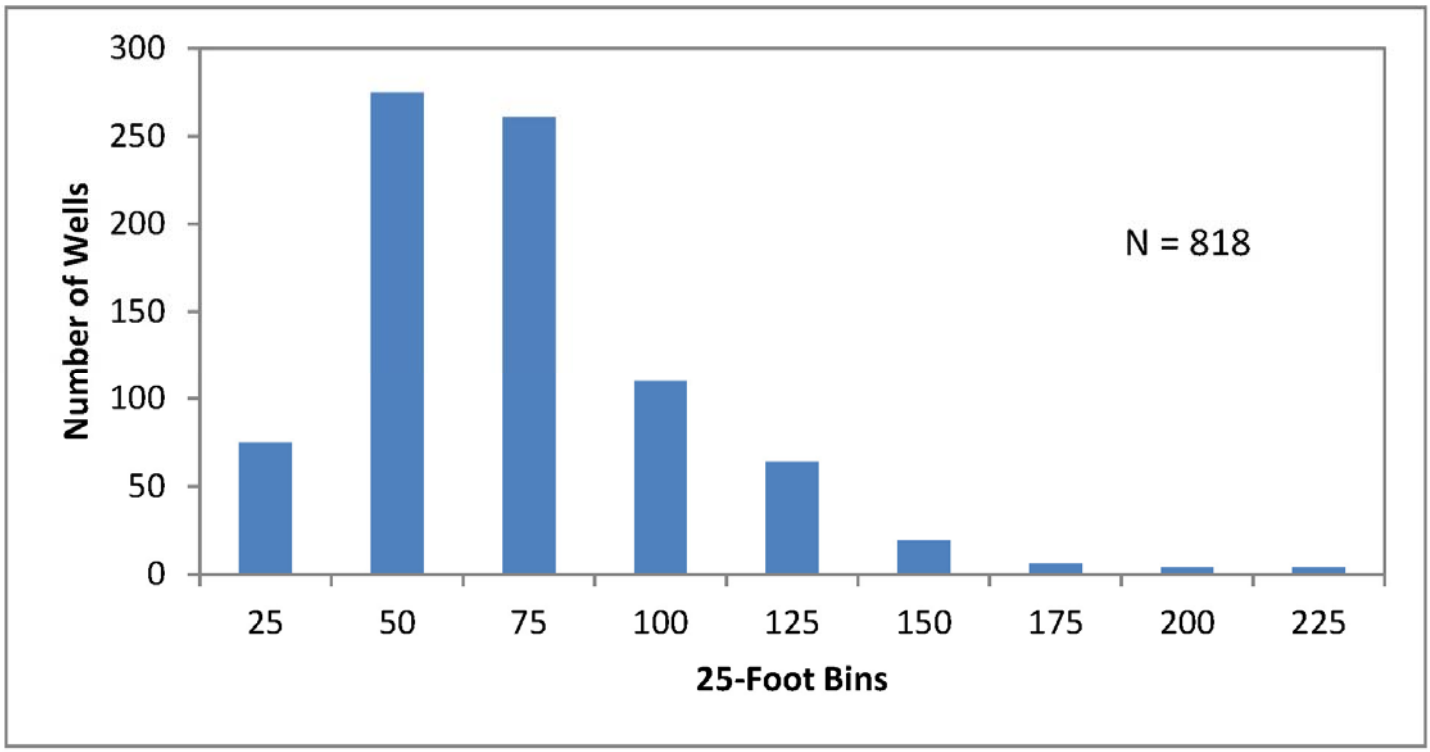

Figure 4.58. Frequency distribution of the net sandstone (≤60 API gamma ray) in the CMKD reservoir in the geophysical well logs studied. The thickness ranges from 0 to 218 feet (0-66 m), with an average of 61 feet (19 m) and a median of 56 feet (17 m).

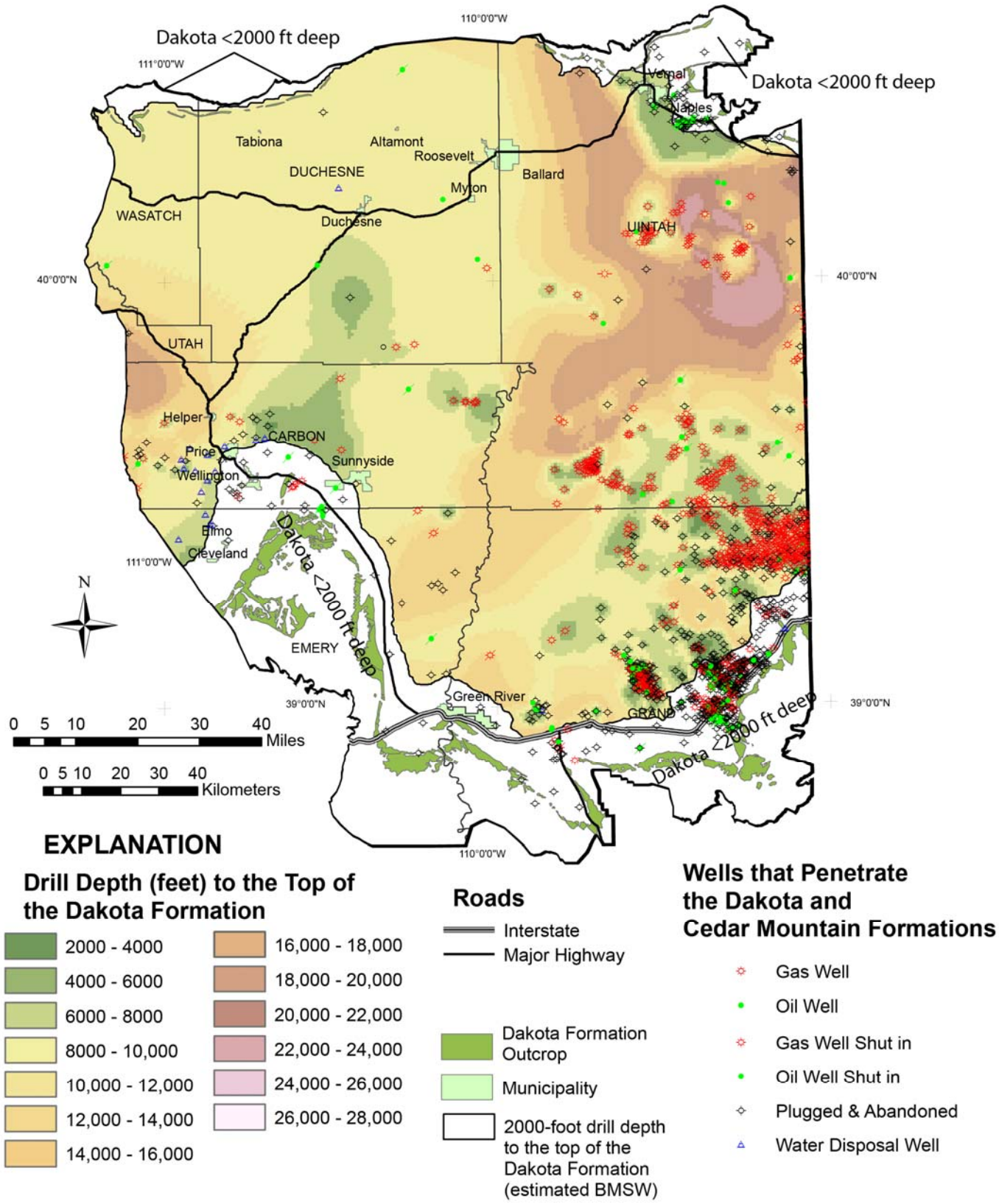

Figure 4.59. Drill depth to the top of the Dakota Formation for areas greater than 2000 feet (610 m) deep.

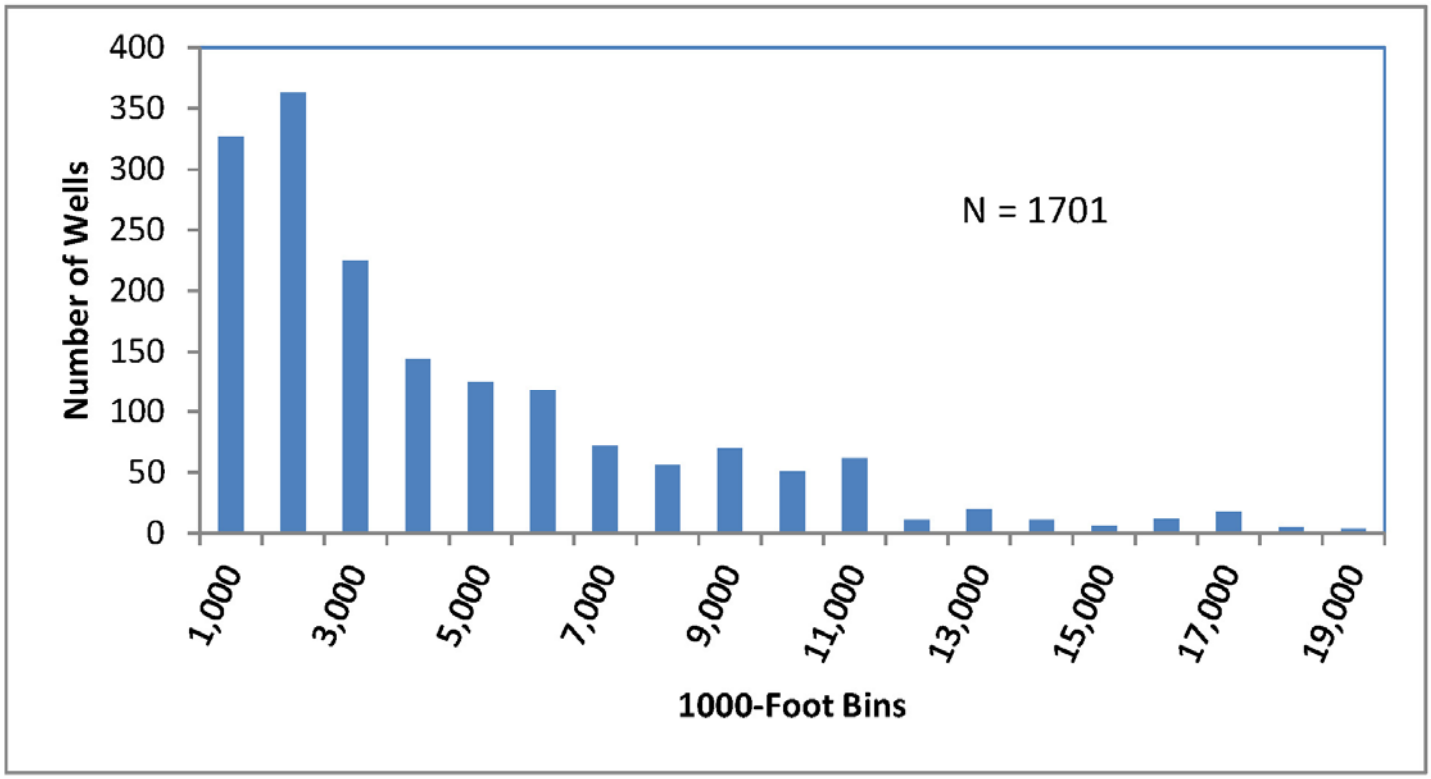

Figure 4.60. Frequency distribution of the drill depth to the top of the Dakota Formation. The drill depth ranges from 21 to 18,902 feet (6-5761 m) with an average depth of 4038 feet (1230 m) and a median of 2685 feet (818 m).

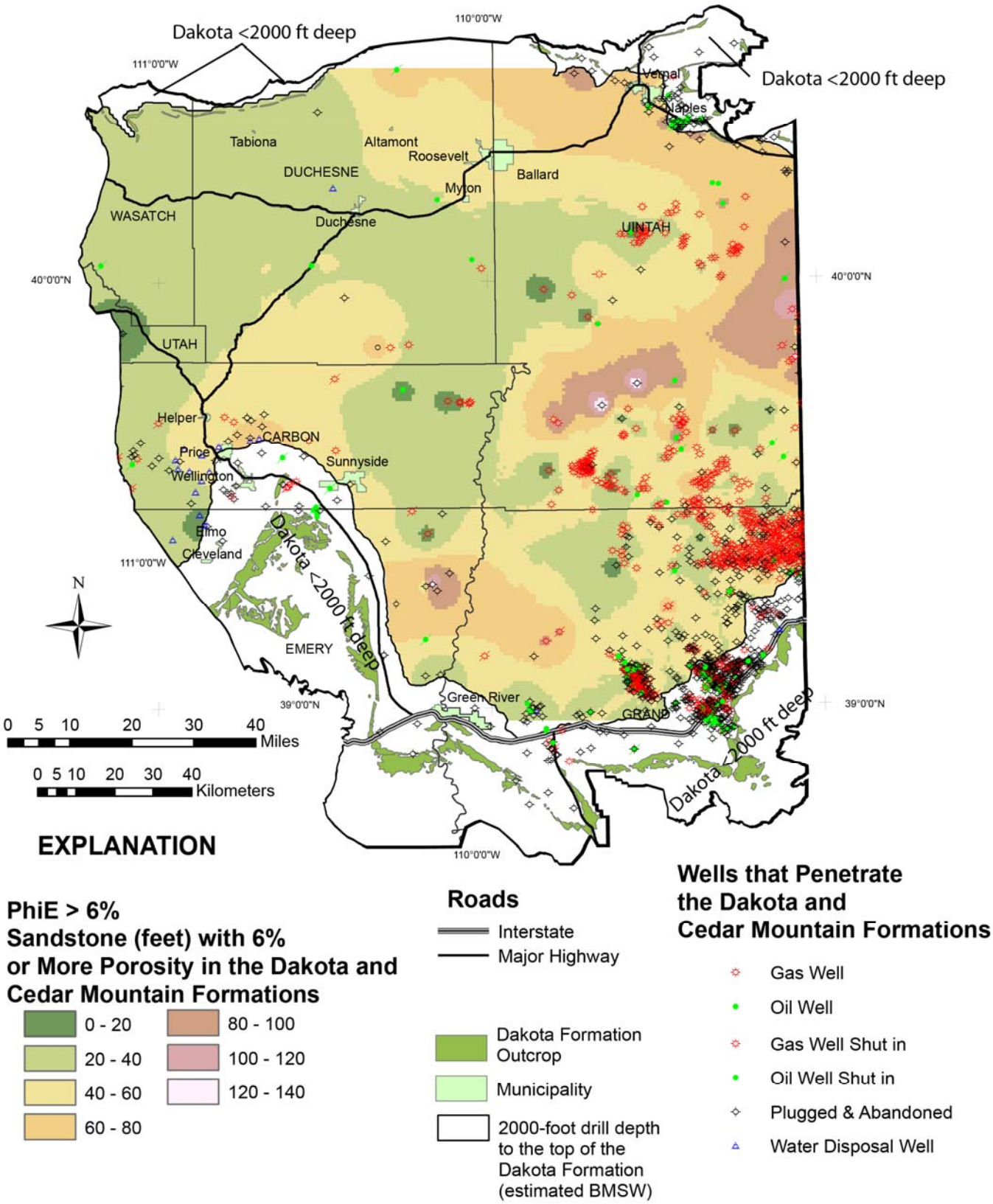

Figure 4.61. Feet of sandstone with porosity ≥ 6% in the CMKD reservoir for areas greater than 2000 feet (610 m) deep. Porosity derived from density or sonic geophysical well logs.

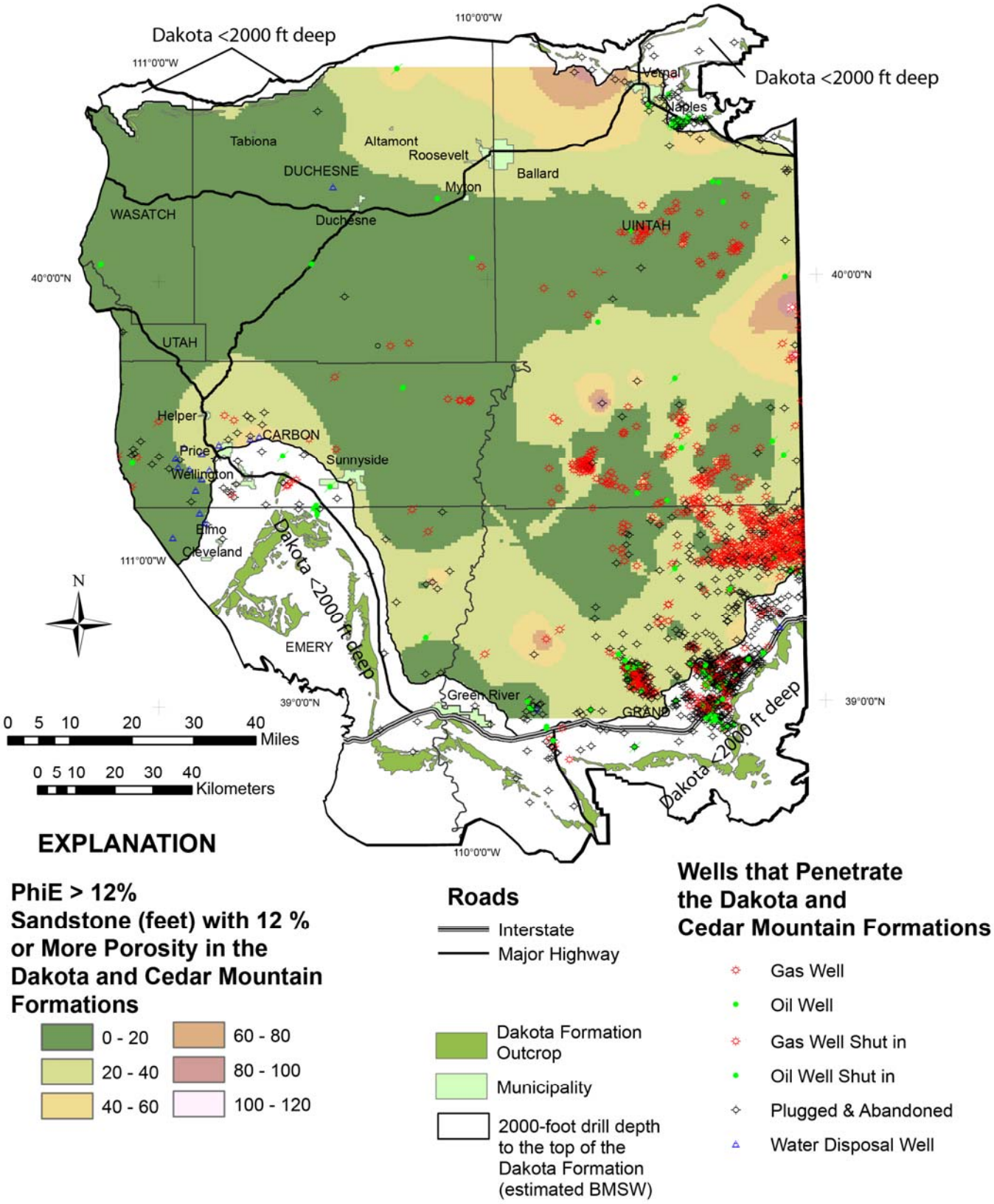

Figure 4.62. Feet of sandstone with porosity ≥ 12% in the CMKD reservoir for areas greater than 2000 feet (610 m) deep. Porosity derived from density or sonic geophysical well logs.

A

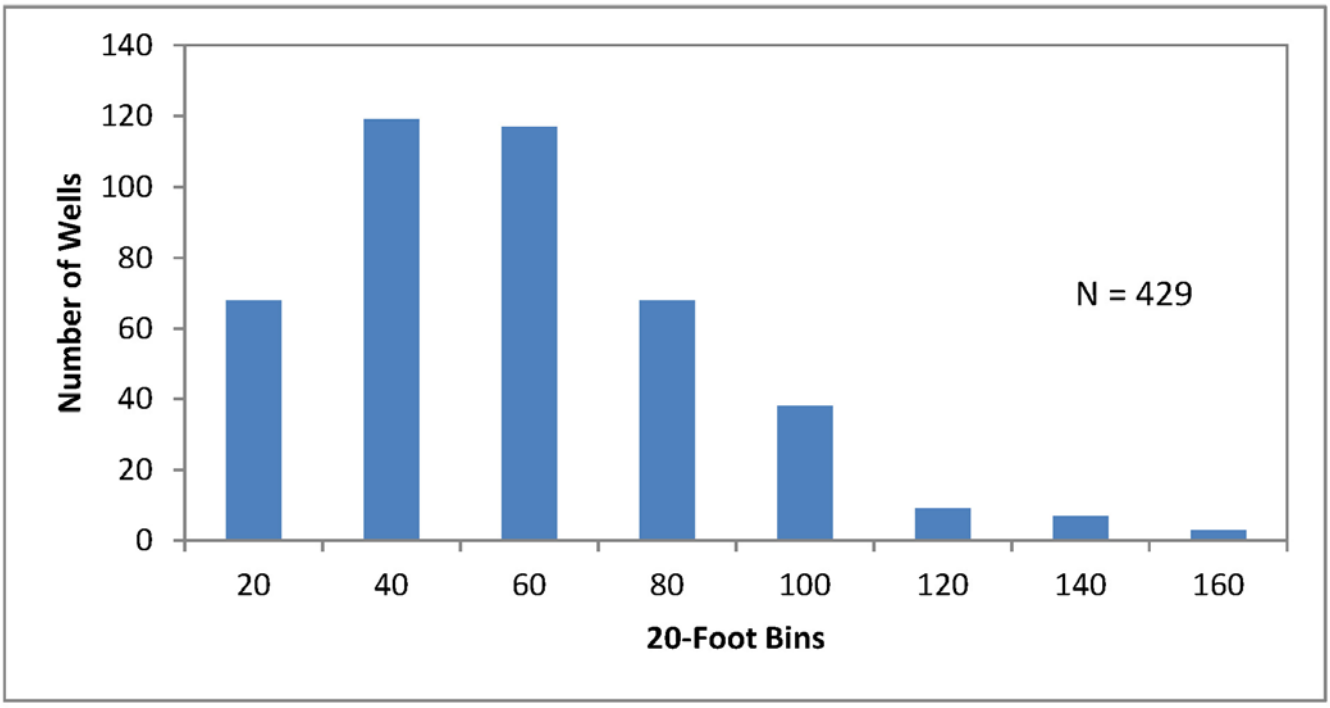

B

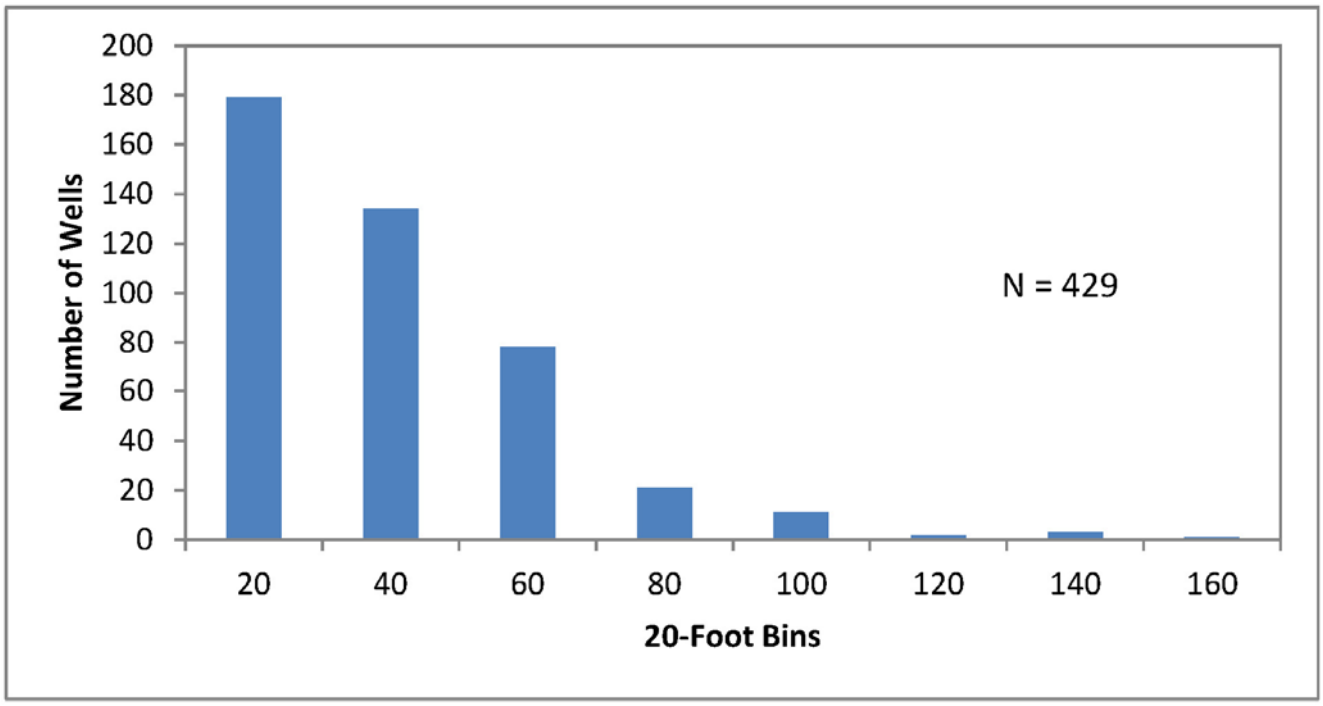

Figure 4.63. Frequency distribution graphs of the feet of sandstone with ≥ 6% porosity (A) and ≥ 12% porosity (B) in the CMKD reservoir. The feet of sandstone with ≥ 6% porosity ranges from 0 to 152 feet (0-46 m), with an average of 50 feet (15 m) and a median of 46 feet (14 m). The feet of sandstone with ≥ 12% porosity ranges from 0 to 144 feet (0-44 m) with an average of 30 feet (9 m) and a median of 26 feet (8 m).

A

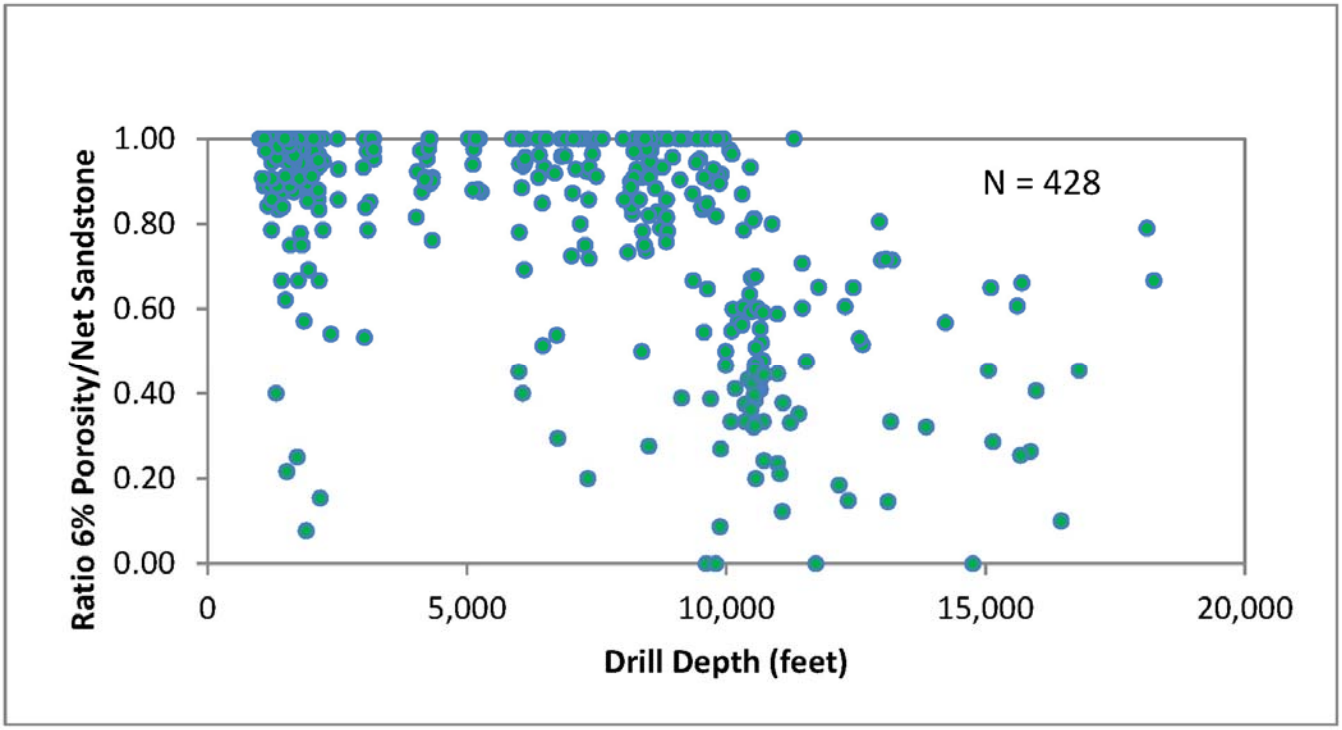

B

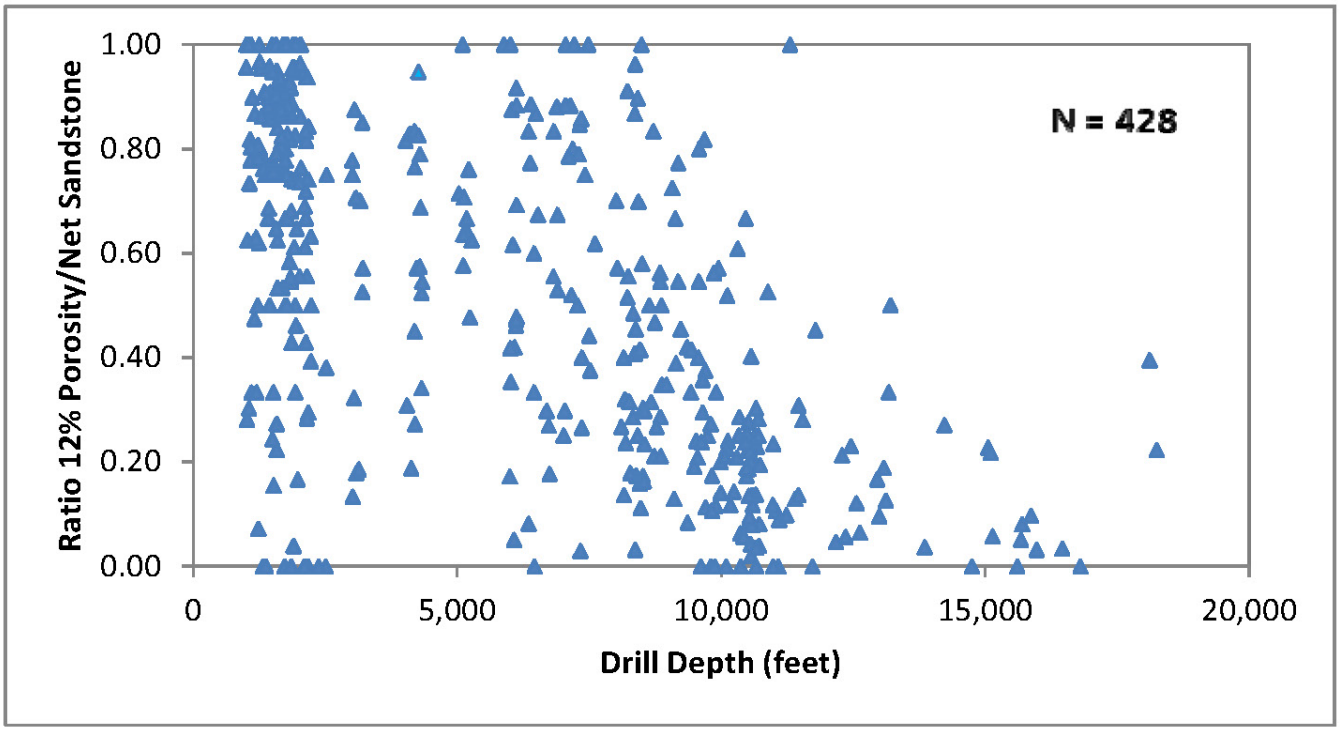

Figure 4.64. (A) Ratio of feet of sandstone with ≥ 6% porosity/net sandstone versus depth, and (B) ratio of ≥ 12% porosity/net sandstone, in the CMKD reservoir. Porosity calculated from density or sonic logs.

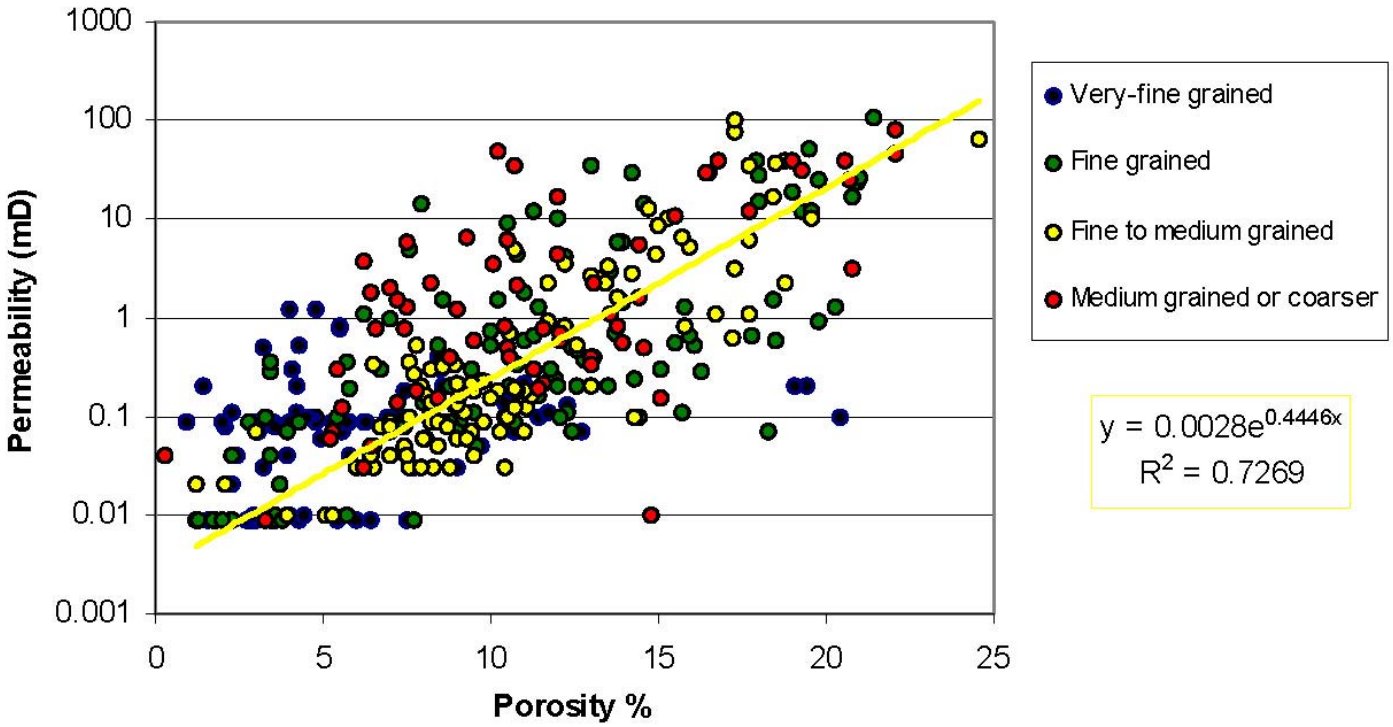

Figure 4.65. Plot of percent porosity versus permeability for 364 core data points. Values are color coded by grain size. From Currie and others, 2011.

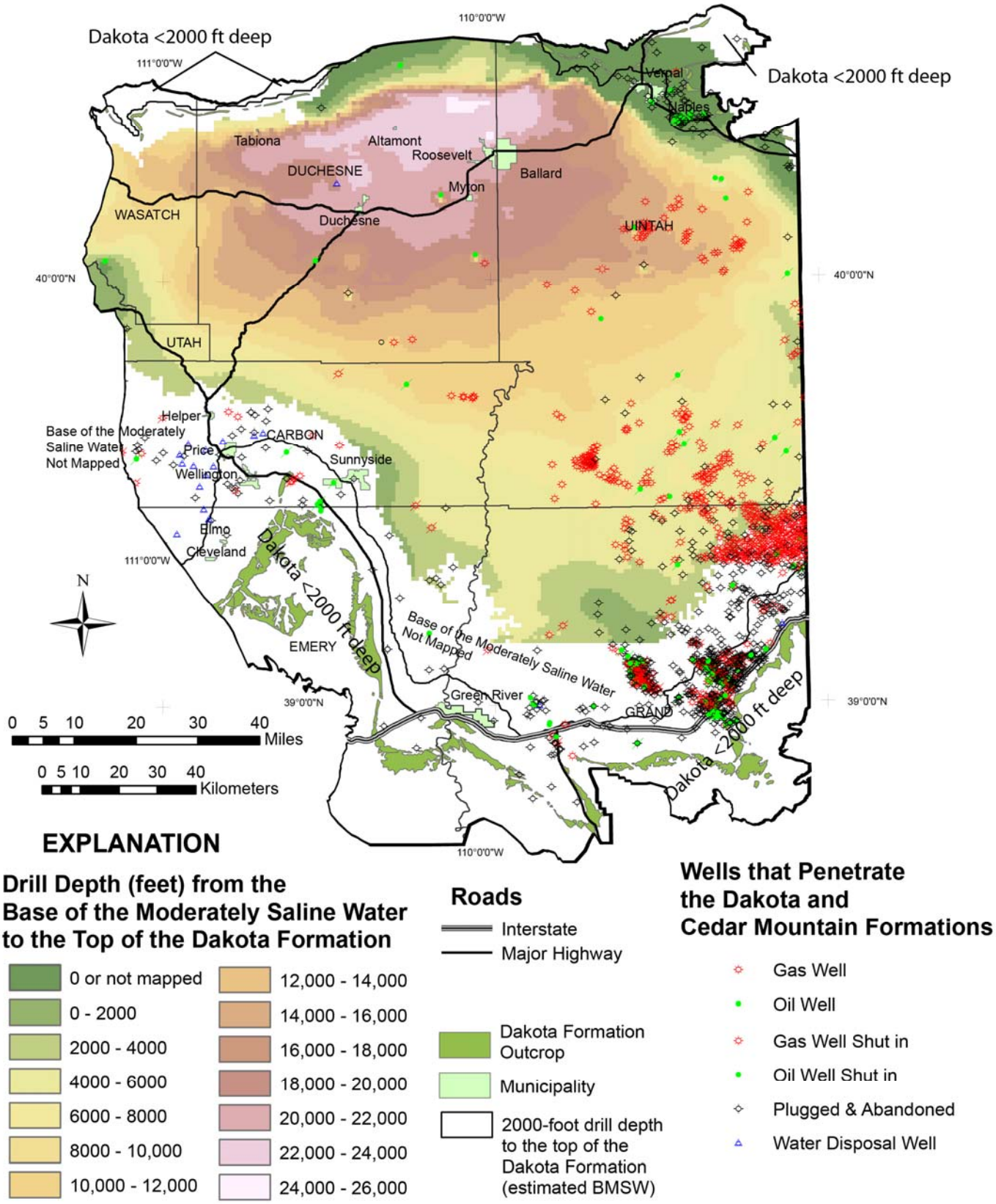

Figure 4.66. Drill depth (feet) from the base of the moderately saline water (BMSW) to the top of the Dakota Formation. The Dakota is above the BMSW in Ashley Valley field (see figure 1.1 for field location). The map was created using ArcScene® by subtracting the drill depth map (figure 4.59) from the BMSA map of Anderson and others (2012).

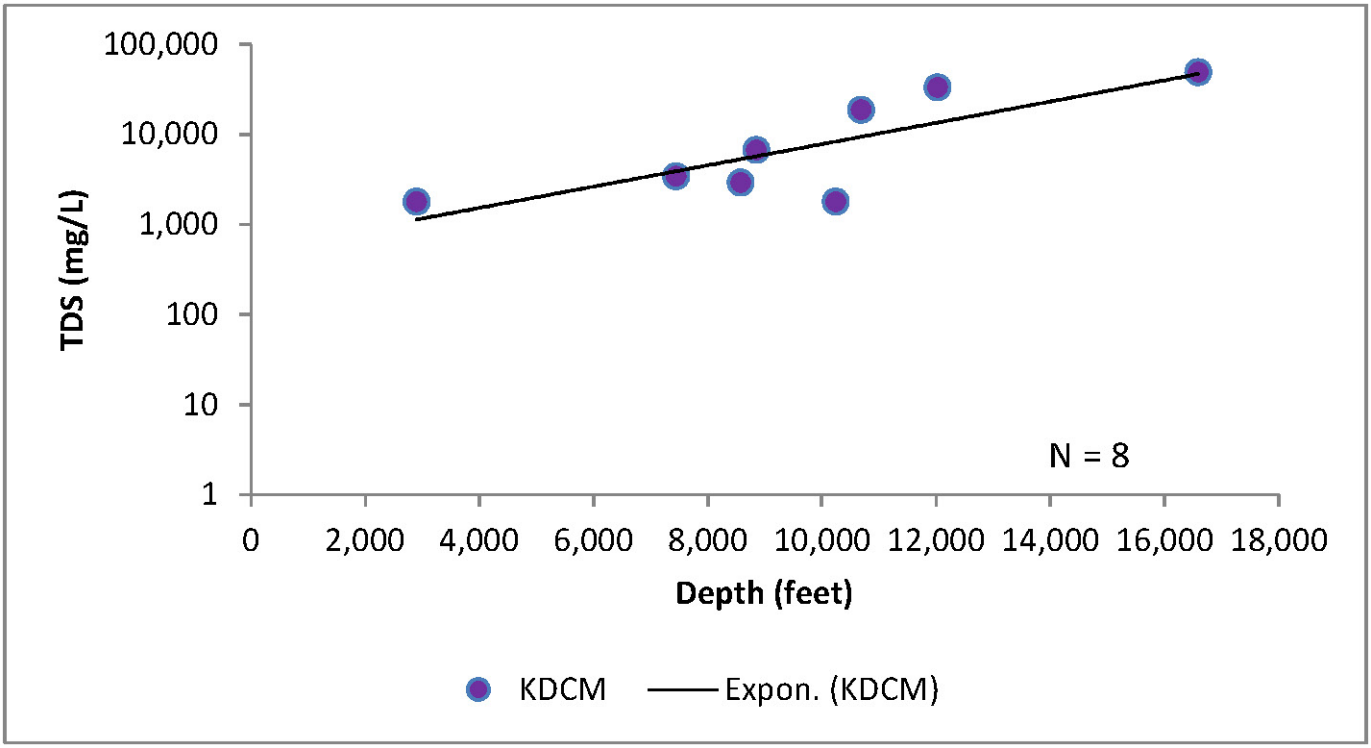

Figure 4.67. Total dissolved solids (mg/L) with depth (feet). The exponential trend line (Expon.) indicates less than 10,000 TDS to a depth of 10,000 feet (3000 m). The limited number of samples (eight) is insufficient to be statistically significant for such a large area.

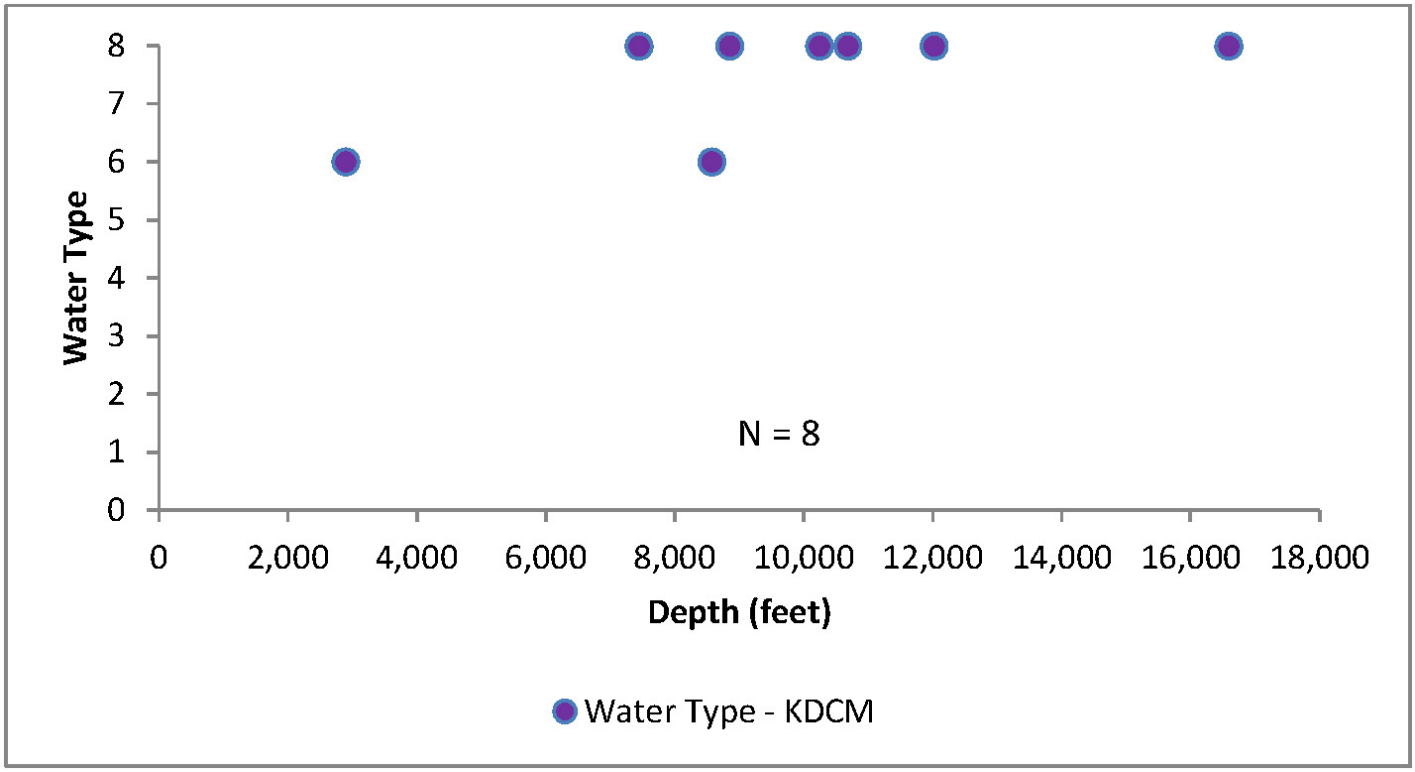

Figure 4.68. Water produced from the KDCM is mostly sodium chloride (Na-Cl) at depths greater than 5000 feet (1500 m) and sodium bicarbonate (Na-HCO_3) at shallower depth (one sample). The number of samples (eight) is not statistically significant for such a large area.

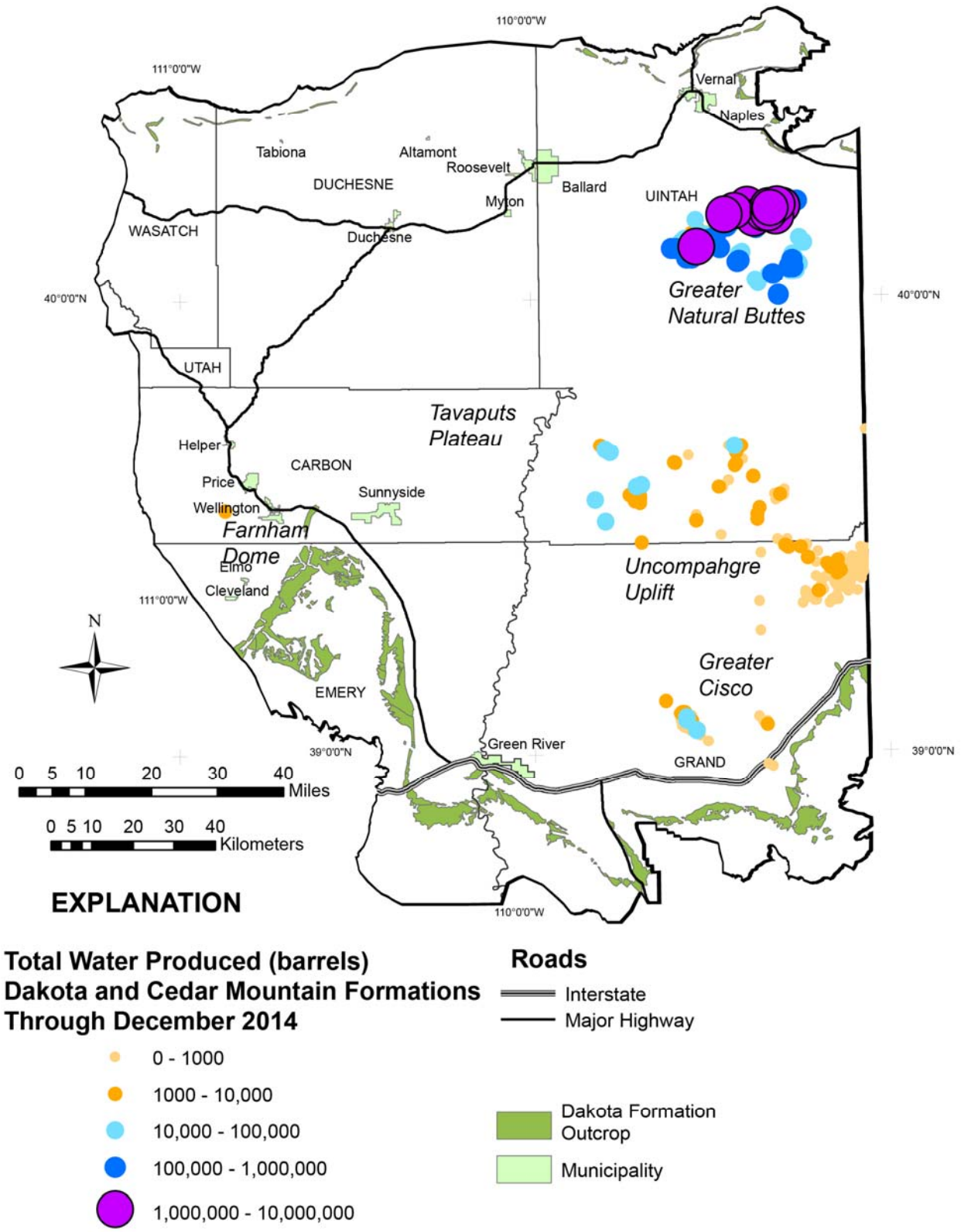

Figure 4.69. Total water produced from the CMKD reservoir through December 2015. Many wells are completed in more than just the CMKD. As a result, much of the water may be coming from other reservoirs.

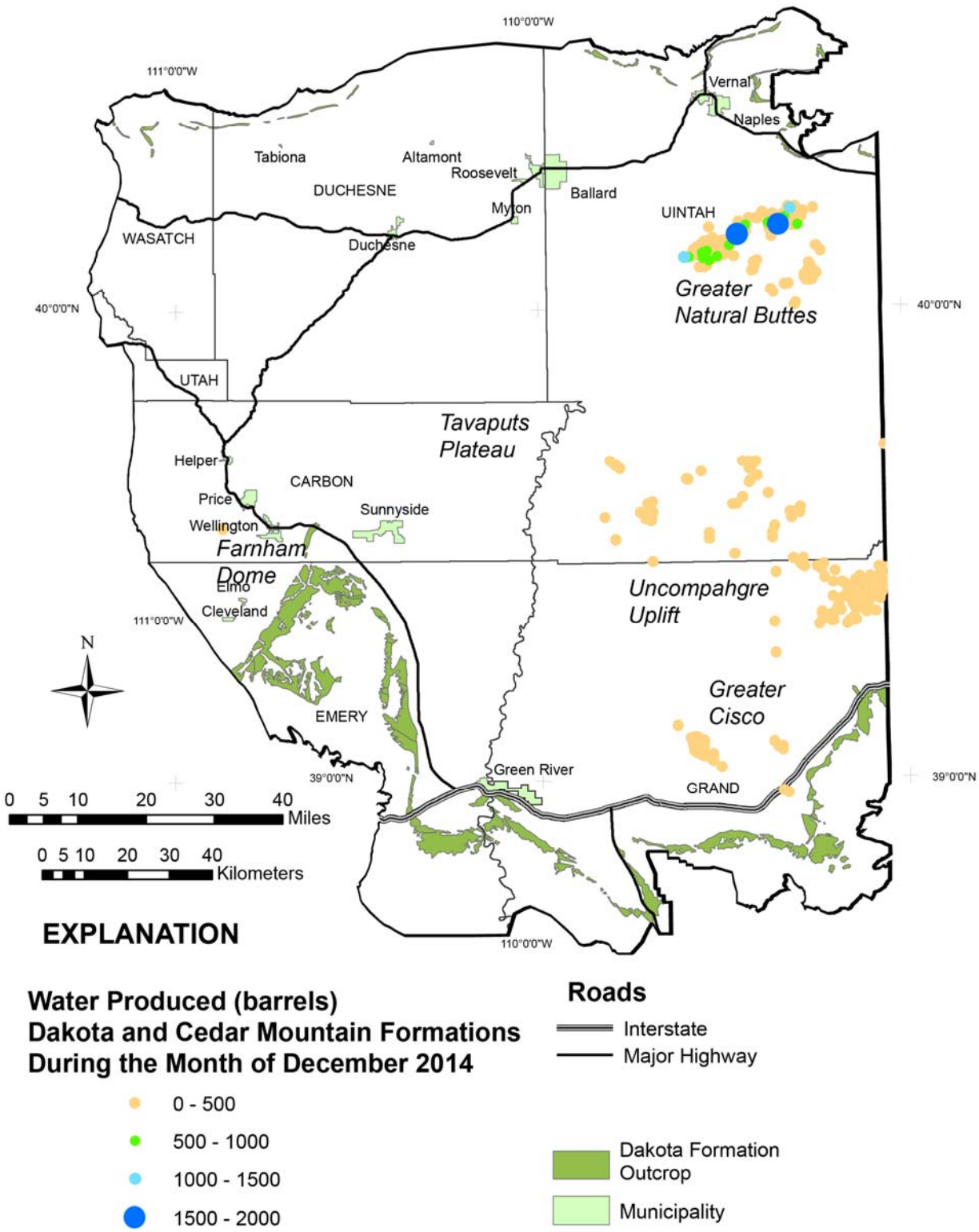

Figure 4.70. Water produced from the CMKD reservoir during December 2014. Many wells are commingled with other reservoirs and the majority of the produced water may not be from the CMKD.

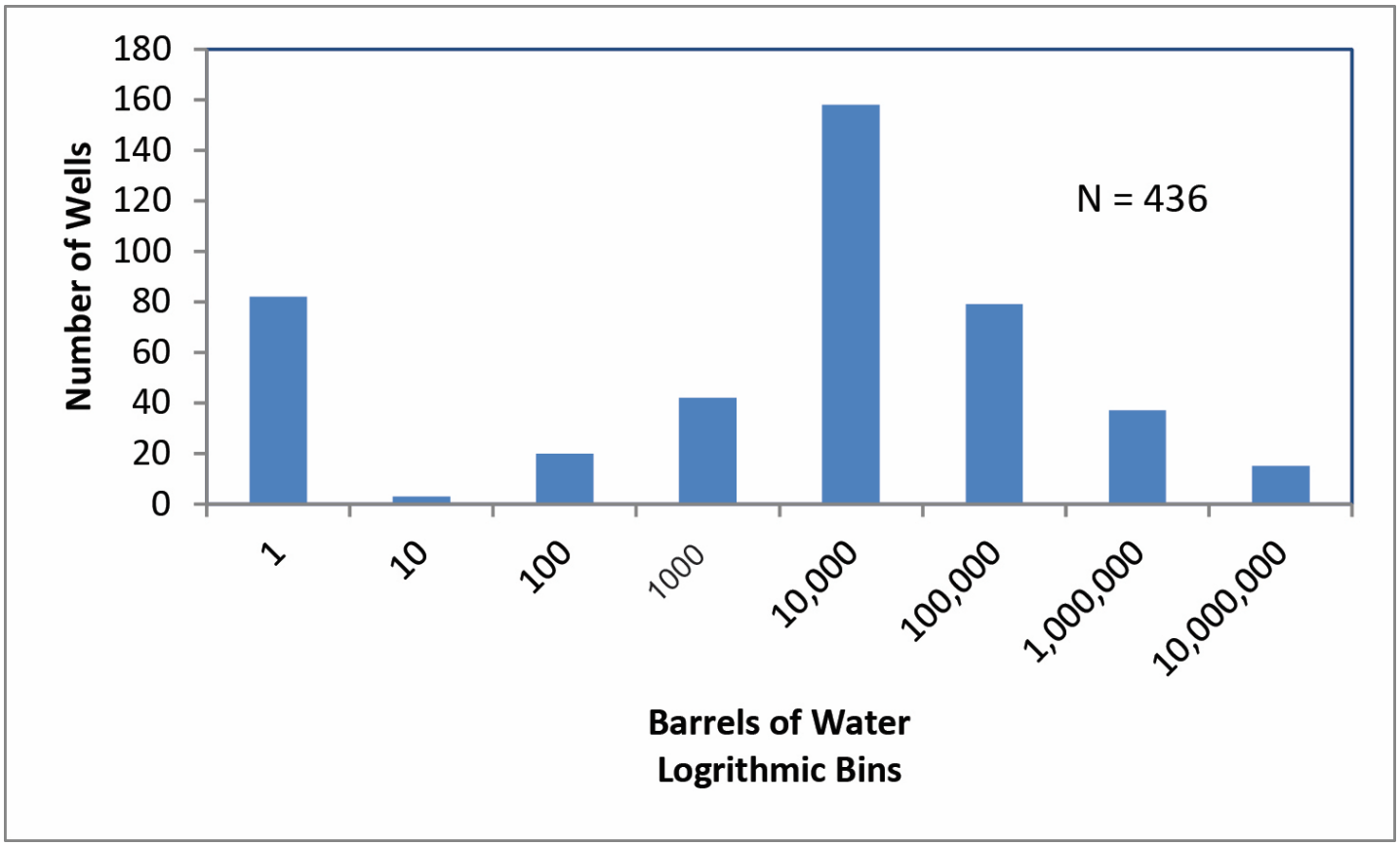

Figure 4.71. Frequency diagram of the total water produced from the CMKD reservoir. Water volumes range from 0 to 4,784,213 BW, the average is 121,730 BW with a median of 2908 BW. Many of the wells producing from the CMKD reservoir are comingled with shallower reservoirs such as Mancos, Mesaverde, and Wasatch. Production volumes cannot be separated from the numerous commingled reservoirs.

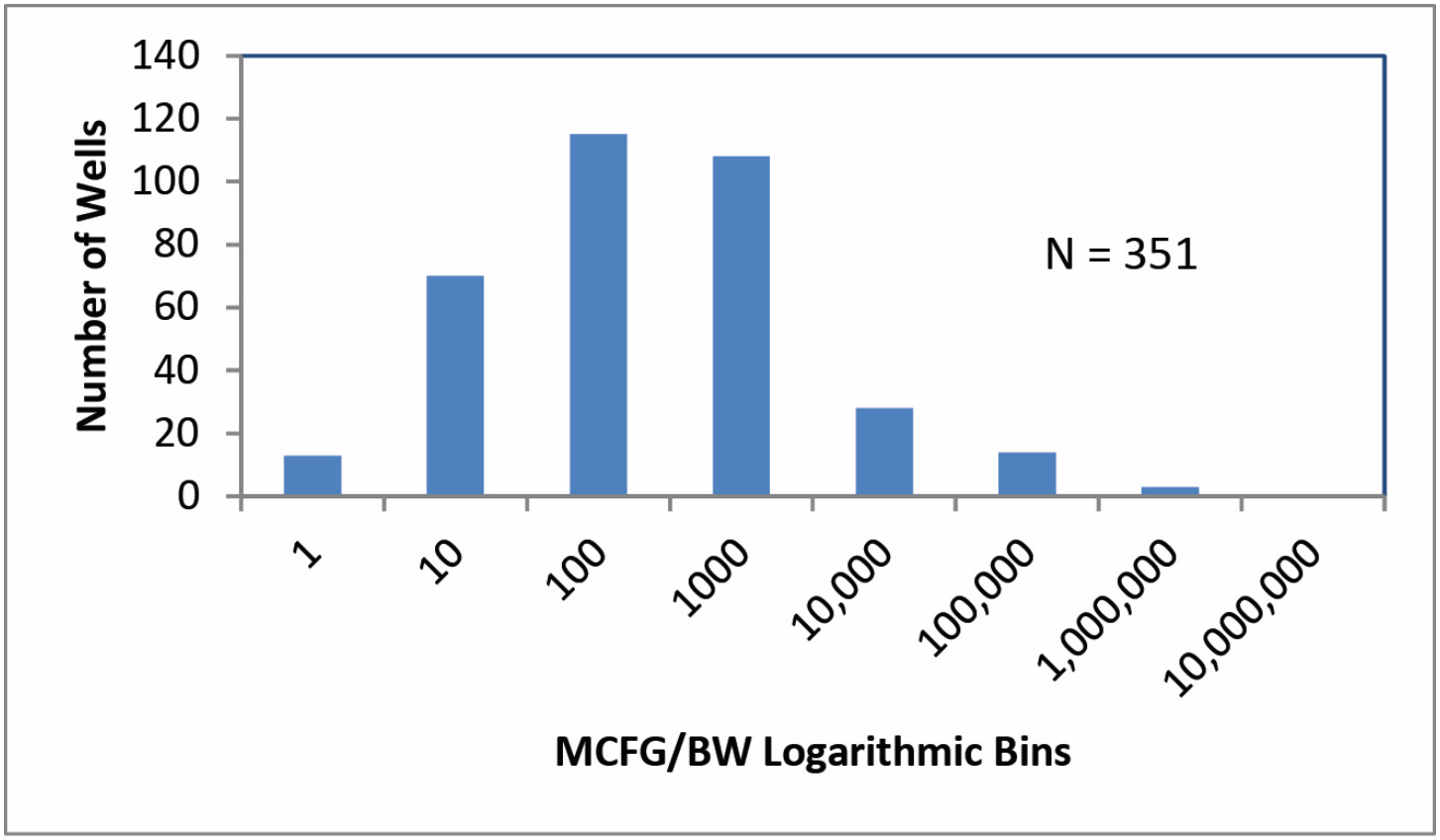

Figure 4.72. Frequency diagram of the gas per barrel of water produced per well (GWR). Gas volumes are in thousand cubic feet (MCFG). The range is from 0 to710,622 MCFG/BW with an average of 469 MCFG/BW and a median of 79 MCFG/BW.

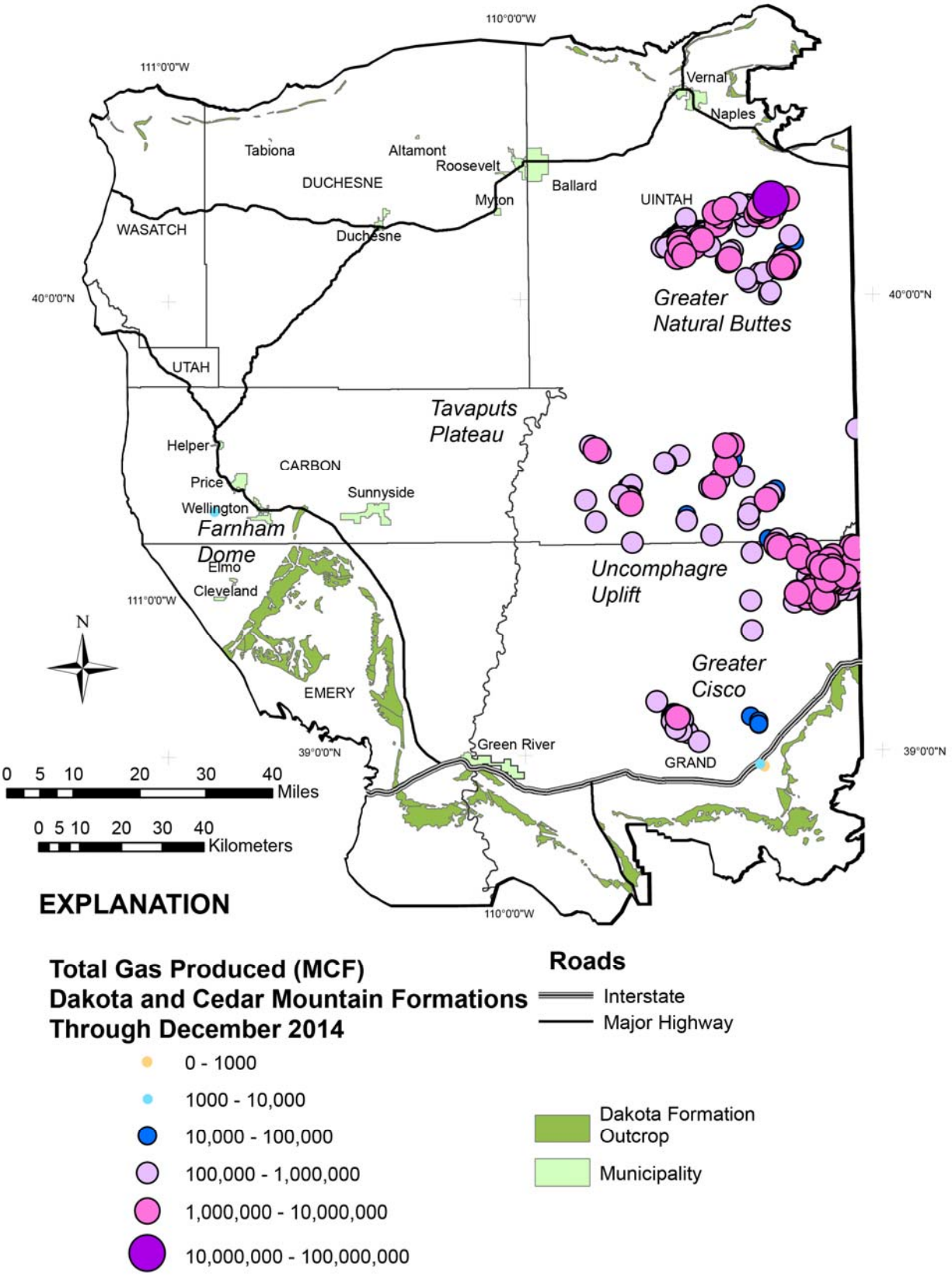

Figure 4.73. Total gas (MCFG) produced from the CMKD through the month of December 2014. Many of the wells producing from the CMKD reservoir are comingled with shallower reservoirs such as Mancos, Mesaverde, and Wasatch. Wells in the north are generally younger and commingled with Mancos and Mesaverde.

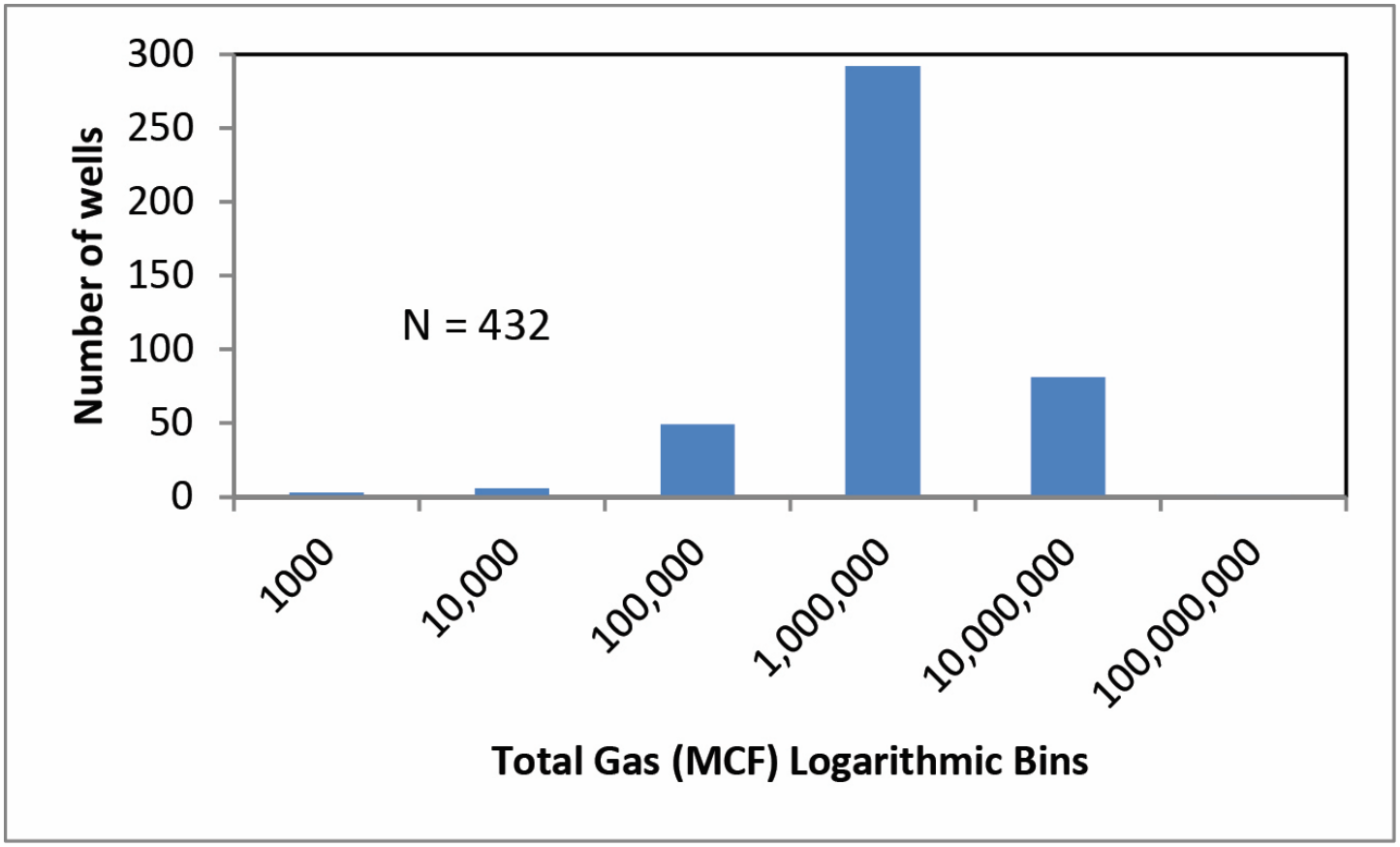

Figure 4.74. Frequency diagram of total gas (MCFG) produced from the CMKD reservoir through December 2014. Production ranges from 143 to 12,123,393 MCFG/month with an average of 737,753 MCFG and median of 422,803 MCFG. Many of the wells producing from the CMKD reservoir are commingled with shallower reservoirs such as Mancos, Mesaverde, and Wasatch.

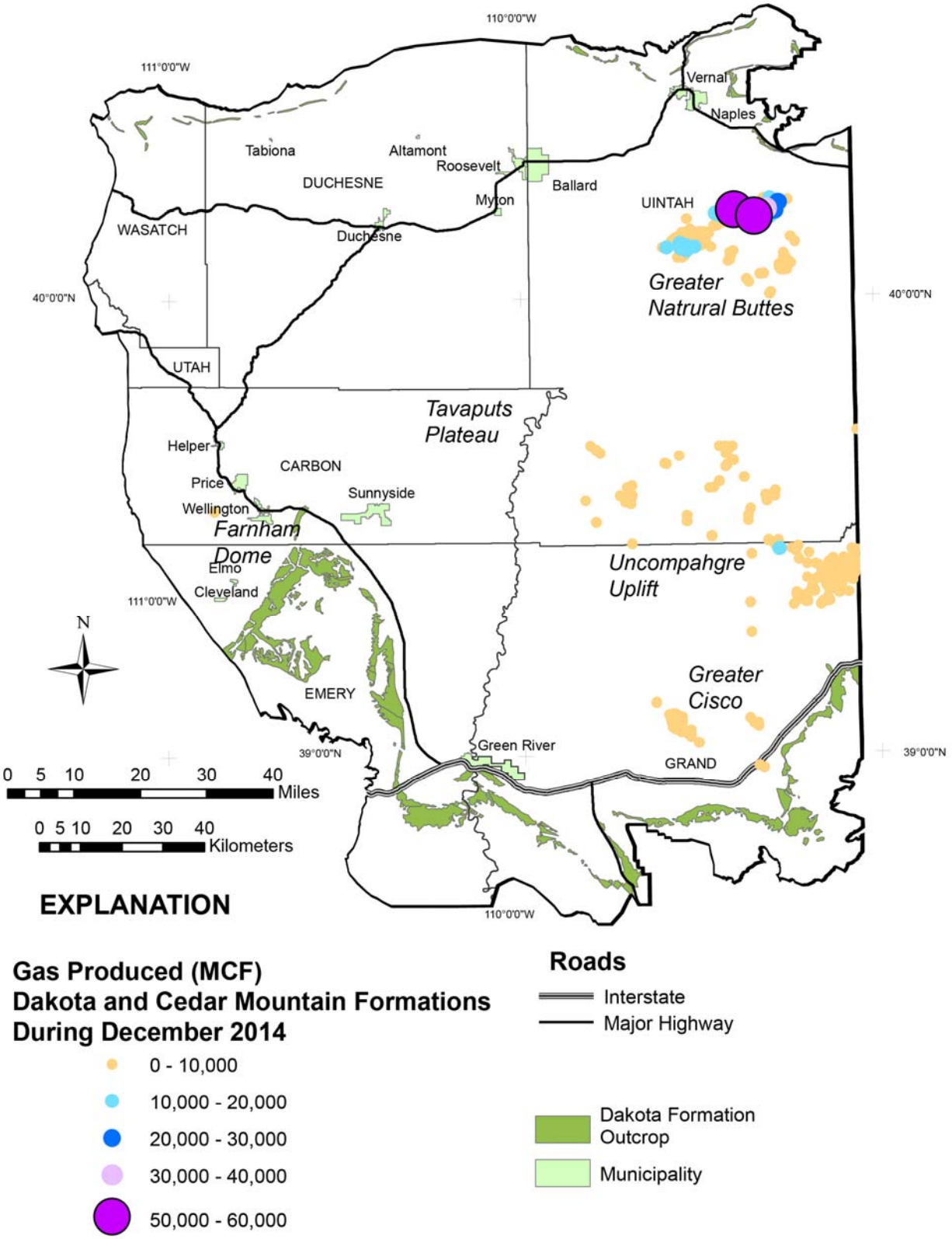

Figure 4.75. Gas production (MCFG) from the CMKD during the month of December 2014. Many of the wells producing from the CMKD reservoir are comingled with shallower reservoirs such as Mancos, Mesaverde, and Wasatch. Wells in the north are generally younger and commingled with Mancos and Mesaverde.

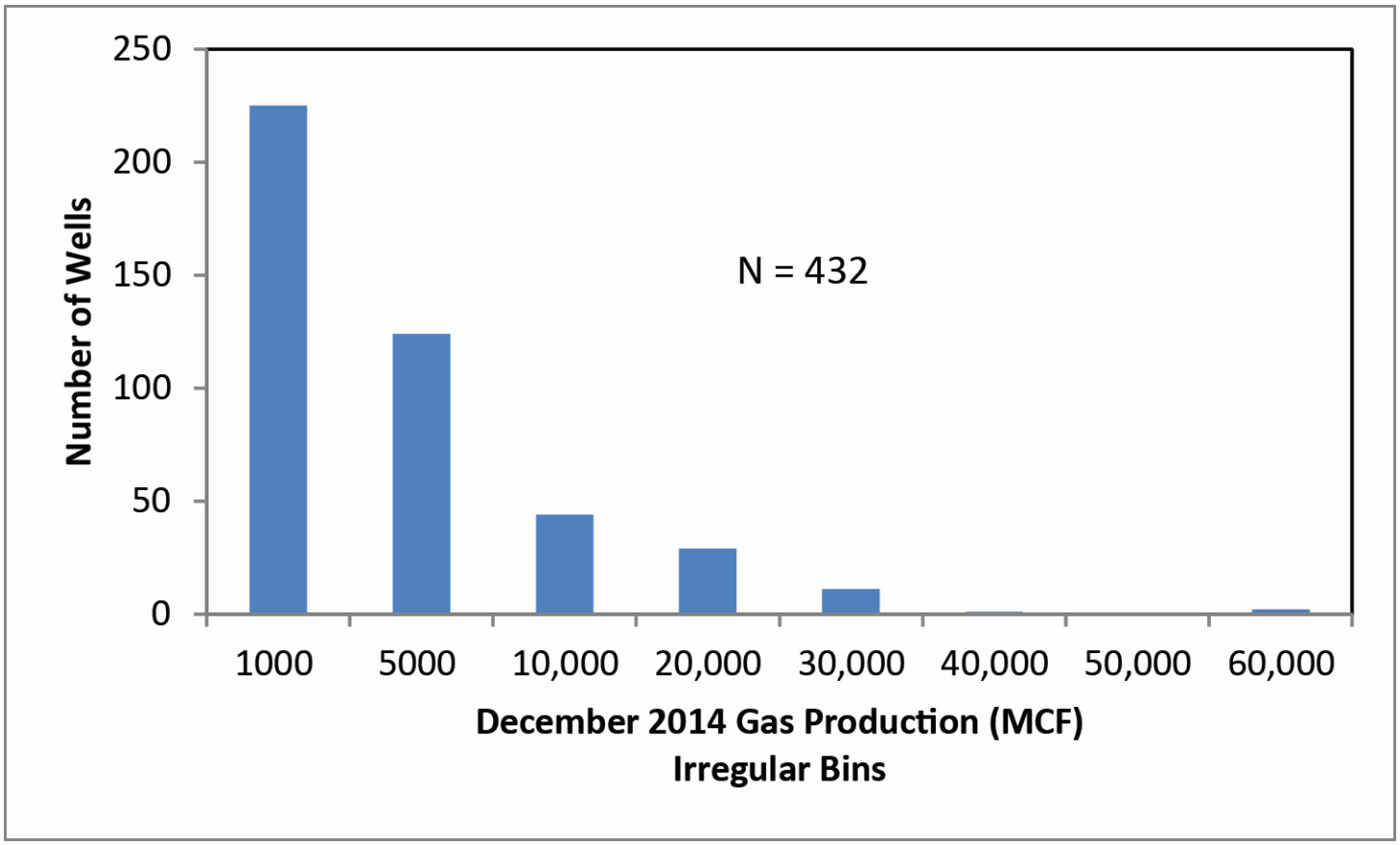

Figure 4.76. Frequency diagram of gas produced (MCFG) from the CMKD reservoir during December 2014. Production ranges from 0 to 59,485 MCFG/month with an average of 3383 MCFG and median of 958 MCFG. Many of the wells producing from the CMKD reservoir are commingled with shallower reservoirs such as Mancos, Mesaverde, and Wasatch.

CHAPTER V

UINTA BASIN RESERVOIRS/AQUIFERS: UPPER CRETACEOUS MANCOS SHALE

Robert Ressetar

With an average thickness of at least 4000 feet, the Upper Cretaceous Mancos Shale is among the thickest sedimentary formations in the UB, exceeded only by parts of the Eocene Green River Formation (see Hintze and Kowallis, 2009, pages 202–203). The Mancos also has wide lateral extent, occurring from Arizona and New Mexico northward to Wyoming. Thickness and extent, however, do not imply that the geology of the Mancos is thoroughly understood: although many studies include the Mancos, most focus either on a small part of it or treat it generally in the context of regional investigations. Notable examples of studies of subunits of the Mancos include work on its lower portion by Molenaar and Cobban (1991) and Anderson and Harris (2006), and on the upper portion by Cole and others (1997), Hettinger and Kirschbaum (2003), Gardner and others (2004), and Hampson (2010). These studies provide reasonably detailed correlations of the more heterogeneous parts of the Mancos, where it interfingers with relatively coarse-grained clastic sediments. However, the 2000 to 3000 feet of the middle Mancos has usually been treated as an undifferentiated marine mudstone (e.g., Johnson, 2003, plate 1).

METHODS

Recently the Research Partnership to Secure Energy for America (RPSEA) funded the UGS and the University of Utah (UU) to study the hydrocarbon potential of the Mancos in the UB and, in part, attempt to fill in some gaps in understanding Mancos geology (Ressetar and Birgenheier, in preparation). The results of that project, currently in review, are incorporated into this chapter. The project used digital well logs from approximately 300 oil and gas exploration wells as the principal data source. Correlations using the well logs resulted in the thickness and structural maps presented below, and calculations from the logs provide estimates of water saturation in the Mancos Shale. In addition, the project analyzed Mancos cores from five wells, one from the southwestern UB near Price, one from Main Canyon field in the southeastern basin, and three from Natural Buttes and Red Wash fields in the northeastern basin (figure 5.1 and appendix B). Core analysis included sedimentological description, geochemical and mineralogical analyses, and a variety of geomechanical tests. Unfortunately, only one of the wells in the UGS-UU project is represented in the 3000+ groundwater analyses in the UGS database.

UPPER CRETACEOUS MANCOS SHALE

The Mancos Shale is a widespread, thick, Upper Cretaceous, marine accumulation of largely siliciclastic sediments that were deposited in the Western Interior Seaway of North America. The Mancos consists, for the most part, of sediments that were eroded from the Sevier

orogenic belt and transported eastward into a foreland basin. Thus, the Mancos grades westward into more proximal, coarser grained terrigenous sediments, and into more distal, more carbonate-rich equivalents to the east. The carbonate-rich units include, notably, the Niobrara Member (or Formation), which is a significant hydrocarbon producer in Colorado and Kansas.

The Mancos Shale consists of several lower rank stratigraphic units (figure 5.2). In the UB of Utah these are, in approximately ascending stratigraphic order, the Tununk Shale Member (figure 2.14), the Coon Spring Sandstone Bed, the Juana Lopez Member, the Ferron Sandstone Member (figure 2.15), the lower part of the Blue Gate Shale Member, the Emery Sandstone Member, the Mancos B Member, and the upper part of the Blue Gate Shale Member. In the western UB, the Mancos B and the upper Blue Gate Shale Members grade into shallow marine to terrigenous deposits of the Star Point and Blackhawk Formations. The top of the Mancos B approximately correlates with the top of the Kenilworth Member of the Blackhawk (figure 5.2; Hettinger and Kirschbaum, 2003). The Blackhawk deltaic and shoreface sands prograded over the Mancos and cap the upper Blue Gate. Since several of these lesser units have limited geographic range, a vertical section or a wellbore at any given location is unlikely to encounter all of them.

The USGS includes the groundwater-bearing rocks of the UB within the Colorado Plateaus aquifers, which largely underlie the Colorado Plateaus Physiographic Province (U.S. Geological Survey, 2009). The Mancos confining unit, which includes most of the Mancos Shale stratigraphic unit, and the Chinle-Moenkopi are the thickest confining units in the Colorado Plateaus aquifers. The Mancos confining unit separates the underlying Dakota-Glen Canyon from the overlying Mesaverde aquifers. Some of the sandier members of the Mancos, particularly the Frontier and Ferron Sandstones (figures 2.12 and 2.15), are locally water-

producers, but generally the Mancos is a barrier to groundwater flow (U.S. Geological Survey, 2009).

Thickness

The maximum thickness of the Mancos Shale is about 5500 feet in the western UB, and it uniformly decreases in thickness to about 3400 feet to the southeast (figure 5.3). Note that due to the interfingering relationship between the Mancos Shale and Star Point or Blackhawk Formations, the top of the Mancos is rather arbitrarily defined. The top of the Mancos is time transgressive, becoming younger to the east. For this report the top of the Mancos is placed where normalized gamma-ray logs show a relatively uniform downward pattern of readings greater than 70 API units.

Depth

Structure maps were made for two stratigraphic surfaces: the tops of the Dakota Formation (base of the Mancos Shale) and the Mancos B Member (figures 5.4 and 5.5, respectively). The maps show essentially the same trends of decreasing elevation from the southern margin of the UB northward to the deepest part of the basin in northwestern Uintah County. Two northwest-trending structural highs are evident north of the Uintah-Grand County line. Also a minor northeast-trending high is near the Carbon-Emery County line in the area where the Mancos crops out. This feature is probably related to the Farnham dome, a subsidiary

structure of the San Rafael Swell, a Laramide uplift that mostly developed from the Late Cretaceous to early Tertiary.

Lithology

In general, the Mancos Shale consists of marine mudstone that grades into significant amounts of shallow-marine to deltaic sandstones in the Ferron and Emery Sandstone Members. In core, the lower Blue Gate Member consists primarily of siltstone with minor amounts of very fine grained sandstone (Horton, 2012). The rocks show a variety of sedimentary structures ranging from planar lamination to ripple cross-lamination and hummocky cross-stratification. In places they contain abundant trace fossils and shell debris; plant debris is comparatively rare. X-ray fluorescence analysis of the cores shows that the lower Blue Gate consists of 40% each clay and non-clay silicate grains, and 20% carbonate grains.

Apart from the western UB where the Mancos transitions into near-shore facies, the Mancos contains three relatively coarse-grained units: the Coon Spring Sandstone Bed and the Juana Lopez and Mancos B Members. These consist of heterolithic siltstone- and sandstone-rich bodies that represent gravity-flow deposits (Hampson, 2010) and distal, coarsening-upward equivalents of progradational shoreface sandstone. The sandstone content of the Mancos Shale, based on gamma-ray logs of less than 60 API units, show that sandstone constitutes less than 1% of the formation except where the Tununk and Blue Gate Shale Members interfinger with the Ferron and Emery Sandstone Members.

Reservoir Properties

Appendix B presents porosity and permeability measurements of the lower Blue Gate Shale Member obtained as part of the UGS-UU project on the five cored wells. The measurements on the Glen Bench and Red Wash wells were contributed by QEP Resources, and the RGU and Main Canyon measurements were made by a commercial laboratory. Porosities range rather narrowly from 3.5 to 8.7%, and do not appear to vary with depth or geographic location in the UB (figure 5.6). Permeabilities vary more widely, but are persistently low: the average permeabilities of the cores range from 0.03 to 164 nanodarcies (nD) (figure 5.7). These variations are at least partly related to burial depth. The samples with the highest permeabilities, from RGU and Main Canyon, are from depths of less than 1000 feet and about 7000 feet, respectively, whereas the Glen Bench and Red Wash samples are from depths of 9600 to 15,000 feet.

Water Quality

Of the more than 3000 groundwater analyses from the UB in the UGS files, only five have data that include groundwater from the Mancos Shale. Even these five wells did not sample the Mancos exclusively, but commingled samples from underlying (Dakota) and overlying (Mesaverde and Wasatch) units (table 5.1). Nonetheless, similarities among the five sample groups are consistent enough to provide a general picture of Mancos groundwater quality in the Ub. The water is mostly briny or saline and has TDS contents ranging from 22,000 to 67,000. Stiff diagrams (figure 5.8) show the water is predominately a sodium-chloride type with relatively less of the main ionic species.

Stoddard and McLennan (in preparation) applied standard log analyses to 25 wells in the UGS-UU project and calculated water saturations ranging from 35 to 95%. In general, water saturation increases with depth, and laterally to the north. For a large part of the Mancos Shale—the lower Blue Gate and the Mancos B Members—water saturation in the 8000- to 12,000-foot depth range was approximately 80 to 90%. However, at shallower depths for all units of the Mancos the water saturation is typically 35 to 60%. The high water saturation at depth, combined with the low permeability, likely rules out the deeper portions of the Mancos as a potential target for produced water disposal.

Water Production, Use, and Disposal

A moderate amount of water has been produced from oil and gas operations in the Mancos Shale. Between 1984 and 2015, a total of more than 422 MMBW were withdrawn from the Mancos (table 5.2). However, sorting this production total by time intervals and by producing unit within the Mancos suggests that the figure is not representative of the Mancos through the greater part of the UB. More than 99% of Mancos water production was from the Ferron Sandstone Member (table 5.2). Between 1984–1991 and 1992–2009, the annual rate of water production from the Ferron increased from 5.7 million barrels (bbls) to 14.5 million. Natural gas production from the Ferron increased by a comparable amount during this period, representing development of the CBM play along the southwest margin of the UB.

The Utah Division of Oil, Gas, and Mining website lists 89 produced-water disposal wells in the UB (broadly defined) as of the end of 2013. Nineteen of the wells, all located in the southwestern corner of the basin, inject water into the Mancos Shale (table 5.3). The Ferron

Sandstone Member is the only unit in the Mancos currently used for water disposal, and all but two of the wells are likely disposing water produced by CBM extraction from the Ferron. Apparently, no produced-water disposal into the Mancos is occurring in the main part of the UB.

Hydrocarbon Production

Oil production from the Mancos Shale began in 1902, and many shallow wells produced modest amounts of oil and gas from the eastern UB (Curtice, in preparation). Hydraulic stimulation of deep levels of the Mancos began in 1999 with the Ouray 34-79 well (section 34, T. 8 S., R. 21 E., SLB&M, Uintah County, API No. 43-047-33291). This well has been a successful producer but, as is typical, the contribution from the Mancos is commingled with units from the Dakota Formation to the Mesaverde Group. Table 5.2 shows the results of a search of the DOGM production records from the Mancos. As discussed above in the section on water production, hydrocarbon production is dominated by natural gas from the Ferron Sandstone Member since the 1990s. Excluding the Ferron CBM, hydrocarbon production from the Mancos is modest compared to other units in the UB. It continues to be a secondary drilling target for shale gas.

The UB contains 36 oil and gas fields, mainly in the southeastern part of the basin, identified by DOGM as hosting Mancos production or potential reservoirs (figure 5.1, table 5.4). However, a number of these fields are inactive, and in most of the active fields, Mancos production is commingled with production from lower reservoirs, commonly in the Dakota Formation, or overlying Cretaceous and Tertiary reservoirs, making it difficult to assess Mancos

productivity. Only Atchee Ridge and Black Horse Canyon fields are considered to produce exclusively from the Mancos.

As part of the UGS-UU project, Curtice (in preparation) reviewed production records from 1209 wells drilled since 1998 that had at least one stimulation record in the Mancos Shale. Screening to eliminate those wells that commingled Mancos production left only 26 wells that could be described as "Mancos only." The only horizontal well completed in the Mancos is XTO's HCU 1-30F (section 30, T. 10 S., R. 20 E., SLB&M, Uintah County, API 43-047-40396), drilled in 2010. Although this was the best performer of the "Mancos only" wells, it was not a commercial success.

Recently, Rose Petroleum reported producible oil and gas shows out of the Mancos Shale and visible oil in core from a single science well (State 1-34, section 34, T. 21 S., R. 23 E., SLB&M, Grand County, API 43-019-50067, currently shut-in) in the southeastern UB, in the Greater Cisco field area, where the lower Blue Gate Shale Member crops out (Rose Petroleum, 2015).

SUMMARY

The Upper Cretaceous Mancos Shale is a widespread, thick, marine accumulation of largely siliciclastic sediments that were eroded from the Sevier orogenic belt and transported eastward into a foreland basin in the Western Interior Seaway. The Mancos is one of the thickest, at least 4000 feet, confining units in the Colorado Plateaus aquifer, separating the Dakota-Glen Canyon and Mesaverde aquifers. It consists of marine mudstone that grades into

shallow-marine to deltaic sandstones. The sandstone content of the Mancos constitutes less than 1% of the formation except where the Tununk and Blue Gate Shale Members interfinger with the Ferron and Emery Sandstone Members. Structure maps show decreasing elevation from the southern margin of the UB northward to the deepest part of the basin in northwestern Uintah County. Porosities range from 3.5 to 8.7%, whereas permeabilities vary more widely, but are persistently low (0.05 to 160 nD). Although data are very sparse, groundwater in the Mancos appears to be saline to briny, dominated by sodium and chloride.

The only produced-water disposal into the Mancos Shale seems to be local injection of water from CBM operations in the Ferron Sandstone Member on the southwestern margin of the UB. Many shallow wells have produced modest amounts of oil and gas from the Mancos in the eastern UB, however, this production is usually commingled with production from other reservoirs. It continues to be a secondary drilling target for shale gas. A moderate amount of water has been produced from the Mancos in comparision to the major reservoirs in the basin such as the Upper Createaceous Mesaverde Group and Tertiary Wasatch and Green River Formations discussed in the next chapters. With very low permeability the Mancos is likely a poor candidate for produced-water disposal in most of the UB.

CHAPTER V FIGURE AND TABLE CAPTIONS

Figure 5.1. Oil and gas fields in the Uinta Basin identified by the Utah Division of Oil, Gas, and Mining with known or potential reservoirs in the Mancos Shale.

Figure 5.2. Stratigraphic relations of the Mancos Shale, its subunits and adjacent formations in the Uinta Basin. Members of the Blackhawk Formation are abbreviated – SC: Spring Canyon, A: Aberdeen, K: Kenilworth, S: Sunnyside, G: Grassy, D: Desert. From Birgenheier and others, in preparation.

Figure 5.3. Isopach of the Mancos Shale in the Uinta Basin. Contour interval equals 200 feet. From Ressetar and others, in preparation.

Figure 5.4. Structural map of the base of the Mancos Shale (top of the Dakota Formation) in the Uinta Basin. Elevations in feet relative to mean sea level, contour interval equals 1000 feet. From Ressetar and others, in preparation.

Figure 5.5. Structural map of the top of the Mancos B Member in the Uinta Basin. Elevations in feet relative to mean sea level, contour interval equals 1000 feet. From Ressetar and others, in preparation.

Figure 5.6. Average porosities (%) in cores from the lower Blue Gate Shale Member of the Mancos Shale. Well numbers (WSNs) are assigned by the log analysis software and are linked to well information in appendix B.

Figure 5.7. Average permeabilities (nanodarcies) in cores from the lower Blue Gate Shale Member of the Mancos Shale. Well numbers (WSNs) are assigned by the log analysis software and are linked to well information in appendix B.

Figure 5.8. Stiff diagrams of water samples from the Mancos Shale and adjacent units. See table 5.1 for well and chemical data.

Table 5.1. Water-chemistry data from five wells that sampled intervals including the Mancos Shale.

Table 5.2. Water, oil, and natural gas production from the Mancos Shale and adjacent units, 1984-2015.

Table 5.3. Produced-water disposal wells that inject into the Mancos Shale.

Table 5.4. Utah gas fields with reservoirs identified in the Mancos Shale. Gas production data from Utah Division of Oil, Gas, and Mining (http://oilgas.ogm.utah.gov/Statistics/PROD_Gas_field.cfm accessed January 2011); other data from Utah Division of Oil, Gas, and Mining (https://fs.ogm.utah.gov/PUB/Oil&Gas/Publications/Lists/field_list.pdf accessed January 2011).

Table 5.1. Water-chemistry data from five wells that sampled intervals including the Mancos Shale.

API No.	Well Name	UTM Northing	UTM Easting	Depth Top Mesaverde Group (ft)	Depth Top Mancos Shale (ft)	Depth Base Mancos Shale (ft)	Depth Top Sample Interval (ft)	Depth Base Sample Interval (ft)	Date	Total Depth (ft)	Depth BHT (ft)	BHT (ºF)	Corrected BHT (ºF)	Sample Temp (°F)
43-047-34753	Glen Bench 5M-9-8-22	4444327	631797	8970	~11,700	NR[1]	10,628	13,034	7/18/2005	13,039				
43-047-36260	Glen Bench 16D-28-8-21	4438654	623438	8765	11,508	16,282	10,454	16,412	5/25/2006	16,490	16,440	305.0	323.0	258.4
43-047-37295	Mustang 1320-11H	4395773	616643	4647	7347	NR[1]	6278	8120	7/25/2007	8376	8366	161.0	170.2	145.5
43-047-37298	Mustang 1320-24E	4392436	617061		7366	NR[1]	6796	7780	7/25/2007	8208	8195	159.0	168.0	146.9
43-047-37350	Red Wash 6D-5-9-24	4436686	650013	5678	8341	11,475	4581	12,806	7/19/2007	13,000	12,999	256.0	270.3	187.8

API No.	Well Name	pH	TDS (mg/L)	Water Type	HCO3 (meq/L)	Ca (meq/L)	Mg (meq/L)	Na (meq/L)	K (meq/L)	Cl (meq/L)	SO4 (meq/L)	Geologic Units
43-047-34753	Glen Bench 5M-9-8-22	7.7	27,493.6		5.2	6.9	6.7	59.0	316.2	363.6	9.7	Mesaverde-Mancos
43-047-36260	Glen Bench 16D-28-8-21	6.6	21,900.0	saline	8.36	38.92	6.17	305.14	12.79	354.69		Mesaverde-Mancos-Dakota
43-047-37295	Mustang 1320-11H	7.4	66,928.0	brine	12.14	98.23	22.21	1031.04	6.25	1086.99	35.57	Mesaverde-Mancos
43-047-37298	Mustang 1320-24E	7.3	45,546.0	brine	20.90	55.92	16.22	691.30	23.86	698.96	47.46	Mesaverde-Mancos
43-047-37350	Red Wash 6D-5-9-24	8.5	36,990.0		1.09	6.15	2.74	221.69	315.44	541.32	4.04	Wasatch-Mesaverde-Mancos-Dakota

[1] not reached

Table 5.2. Water, oil, and natural gas production from the Mancos Shale and adjacent units, 1984-2015.

Producing Formation/ Member	Total Oil (Barrels)	Total Gas (MCF*)	Total Water (Barrels)	Average Gas -to-Oil Ratio	Average Oil-to-Water Ratio	Average Gas -to-Water Ratio
2009-2015						
Mancos Shale	43,224	5,165,470	785,220	92,379	0.20	19,033.40
Mancos B	12,862	664,704	5,422	24,592	0.84	20,897.35
Ferron Sandstone Member	180	356,669,568	113,973,277	781	0.00	87,376.04
Frontier Sandstone	3,368	5,128,480	13,126	443,231	0.24	466,289.96
Tununk Shale Member	1,518	2,503	14,725	9	0.00	0.94
Tununk-Dakota	0	0	0	0	0.00	0.00
Production totals	61,152	367,630,725	114,791,770			
1992-2009						
Mancos Shale	62,059	3,299,530	301,029	128,072.35	0.59	59,043.64
Mancos B	15,091	868,318	17,746	163,517.27	1.07	88,389.93
Ferron Sandstone Member	4,162	835,804,971	261,062,072	1,307,742.70	0.00	63,058.43
Frontier Sandstone	14,819	12,668,028	43,385	1,413,230.20	1.30	1,198,778.24
Tununk Shale Member	159	123	0	549.32		
Tununk-Dakota	0	0	0			
Production totals	96,290	852,640,970	261,424,232			
1984-1991						
Mancos Shale	79,603	148,272	69	0.01	0.00	0.01
Mancos B	41	160,616	0	0.37	0.00	0.00
Ferron Sandstone Member	14,152	98,904,325	45,473,151	19.65	0.01	27.02
Frontier Sandstone	74,286	25,336,697	875,851	414.61	0.84	505.18
Tununk Shale Member	313	425	0	0.27	0.00	0.00
Tununk-Dakota	0	0	0	0.00	0.00	0.00
Production totals	168,395	124,550,335	46,349,071			
Combined production totals	**325,837**	**1,344,822,030**	**422,565,073**			

*MCF= thousand cubic feet

Table 5.3. Produced-water disposal wells that inject into the Mancos Shale.

Field	Type	County	Disposal unit	Number of wells
Clear Creek	Gas	Carbon/Emery	Ferron Sandstone	1
Drunkards Wash	Coalbed methane	Carbon/Emery	Ferron Sandstone	11
Helper	Coalbed methane	Carbon	Ferron Sandstone	6
Wildcat	Gas	Unknown	Ferron Sandstone	1

Table 5.4. Utah gas fields with reservoirs identified in the Mancos Shale. Gas production data from Utah Division of Oil, Gas, and Mining (http://oilgas.ogm.utah.gov/Statistics/PROD_Gas_field.cfm accessed January 2011); other data from Utah Division of Oil, Gas, and Mining (https://fs.ogm.utah.gov/PUB/Oil&Gas/Publications/Lists/field_list.pdf accessed January 2011).

Field Number	Field Name	Status	County	Discovery Date	Producing Stratigraphic Unit			Cumulative Natural Gas Production (MCF)	Discovery Well API Number
540	Agency Draw	Active	Uintah	1962	Wasatch	Mesaverde	Mancos	845,953	43-047-11120
543	Atchee Ridge	Active	Uintah	1996	Mancos B			144,547	43-047-32660
550	Black Horse Canyon	Active	Uintah	1979	Mancos			2,254,677	43-047-30765
555	Bonanza	Active	Uintah	1963	Wasatch	Mancos		751,285	43-047-15674
185	Bryson Canyon	Active	Grand	1928	Mancos B	Dakota		25,549,318	43-019-11306
167	Bushy	Active	Grand	1977	Mancos	Dakota		3,507	43-019-30361
13	Castlegate	Active	Carbon	1998	Blackhawk	Mancos		8,665,352	43-007-30119
580	Dry Burn	Inactive	Uintah	1978	Mancos			0	43-047-30331
600	Flat Rock	Active	Uintah	1963	Wasatch	Mancos		84,951,037	43-047-10577
792	Gate Canyon	Active	Duchesne	2006	Mesaverde	Mancos		1,366,208	43-013-32391
20	Gordon Creek	Active	Carbon	1948	Ferron	Mancos		4,395,517	43-007-16107
205	Greater Cisco	Active	Grand	1925	Mancos	Dakota	Cedar Mountain	27,090,501	43-019-11513
616	Hells Hole	Active	Uintah	1989	Mancos B	Dakota	Morrison	1,613,132	43-047-31802
18	Helper	Active	Carbon	1993	Ferron	Mancos		145,864,626	43-007-30189
617	Hill Creek	Active	Uintah	1984	Wasatch	Mesaverde	Mancos	13,427,057	43-047-31026
620	Horseshoe Bend	Active	Uintah	1984	Green River	Mesaverde	Mancos	27,861,916	43-047-15803
626	Lone Spring	Inactive	Uintah	1996	Mancos B			0	43-047-32705
625	Main Canyon	Active	Uintah	1979	Mancos	Dakota		5,560,308	43-047-30394
222	Mancos Flat	Inactive	Grand	1981	Mancos			0	43-019-30789
30	Miller Creek	Inactive	Carbon	1969	Ferron	Tununk	Dakota	0	43-007-30006
105	Monument Butte	Active	Duchesne	1964	Green River	Mesaverde	Mancos	107,400,856	43-013-30561
630	Natural Buttes	Active	Uintah	1972	Mesaverde	Wasatch	Mancos	2,222,560,556	43-047-10095
640	Pariette Bench	Active	Uintah	1962	Green River	Mesaverde	Mancos	29,934,362	43-047-10873
40	Peters Point	Active	Carbon	1953	Green River	Wasatch	Mancos	87,263,405	43-007-10216
645	Pine Springs	Active	Uintah	1979	Mancos B	Dakota		4,671,113	43-047-15923
660	Rat Hole Canyon	Inactive	Uintah	1977	Mancos			0	43-047-30325
665	Red Wash	Active	Uintah	1951	Green River	Mesaverde	Mancos	356,058,630	43-047-15135
636	South Canyon	Inactive	Uintah	1981	Mancos B			0	43-047-31104
685	Sweetwater Canyon	Inactive	Uintah	1978	Mancos			57	43-047-30332
686	Sweetwater Ridge	Inactive	Uintah	1996	Mancos B			0	43-047-32593
695	Uteland Butte	Active	Uintah	1962	Wasatch	Mesaverde	Mancos	5,985,489	43-047-15642
265	Westwater	Active	Grand	1957	Mancos B	Dakota		38,631,566	43-019-10780
717	Whiskey Creek	Inactive	Uintah	1996	Mancos B			0	43-047-32602
705	White River	Active	Uintah	1961	Green River	Mancos B		13,362,827	43-047-15080
707	Wolf Point	Active	Uintah	1984	Mancos	Dakota	Morrison	793,564	43-047-30622
710	Wonsits Valley	Active	Uintah	1959	Green River	Mesaverde	Mancos	119,092,004	43-047-16509

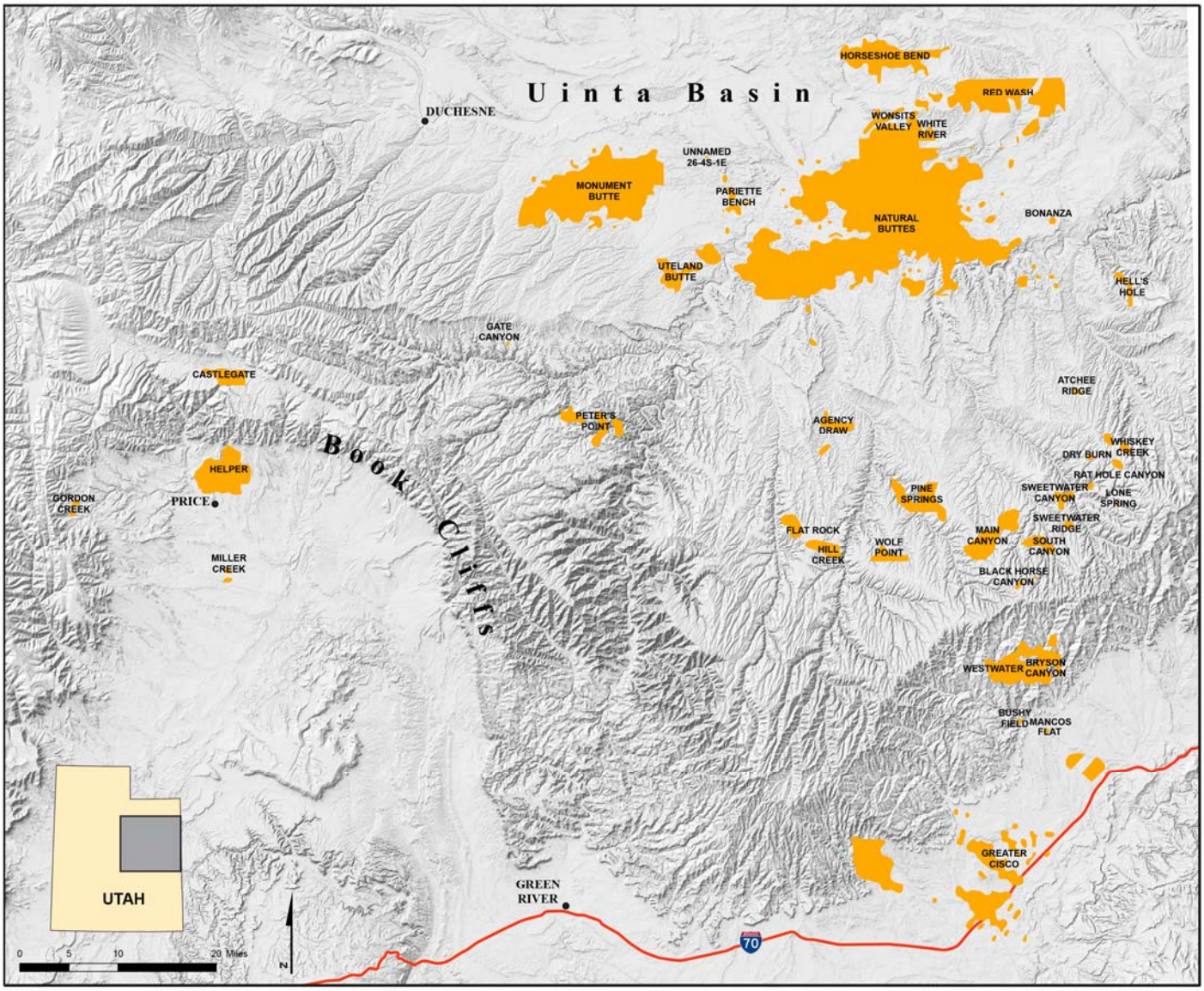

Figure 5.1. Oil and gas fields in the Uinta Basin identified by the Utah Division of Oil, Gas, and Mining with known or potential reservoirs in the Mancos Shale.

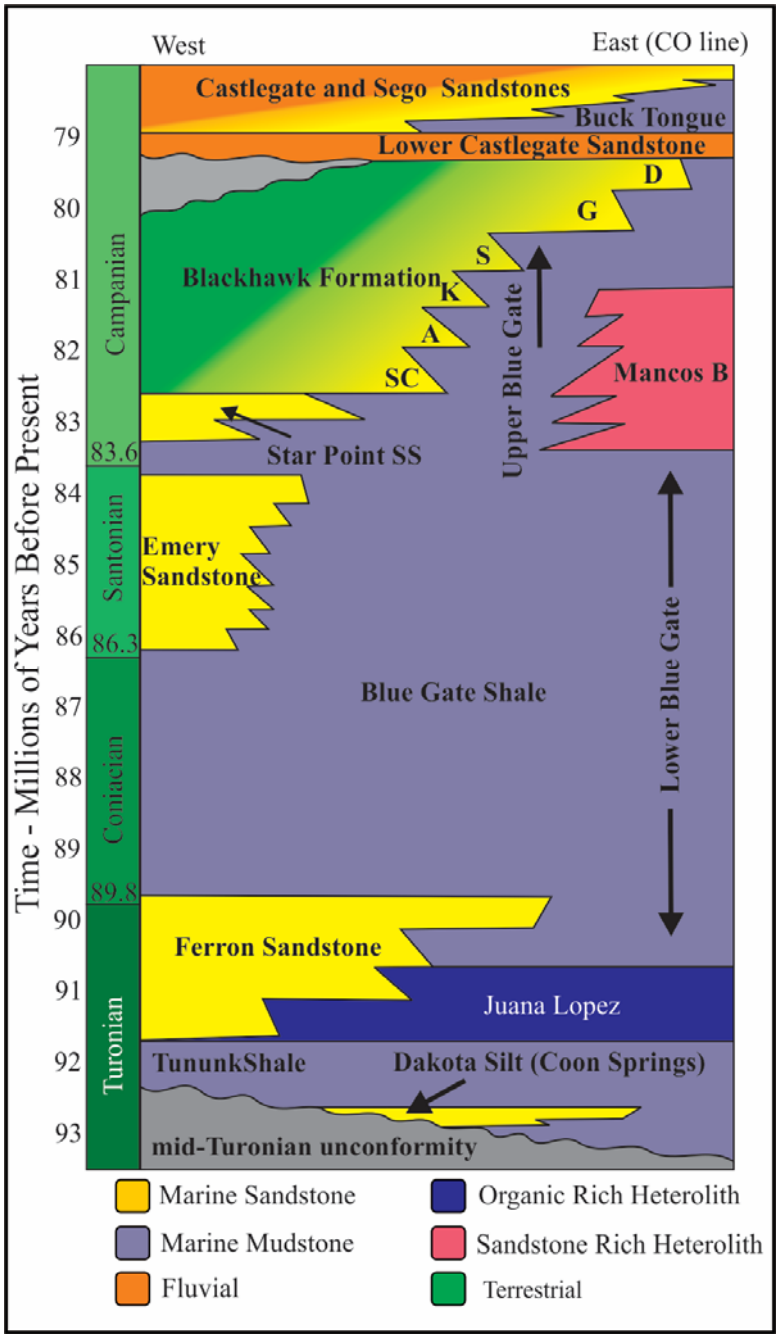

Figure 5.2. Stratigraphic relations of the Mancos Shale, its subunits and adjacent formations in the Uinta Basin. Members of the Blackhawk Formation are abbreviated – SC: Spring Canyon, A: Aberdeen, K: Kenilworth, S: Sunnyside, G: Grassy, D: Desert. From Birgenheier and others, in preparation.

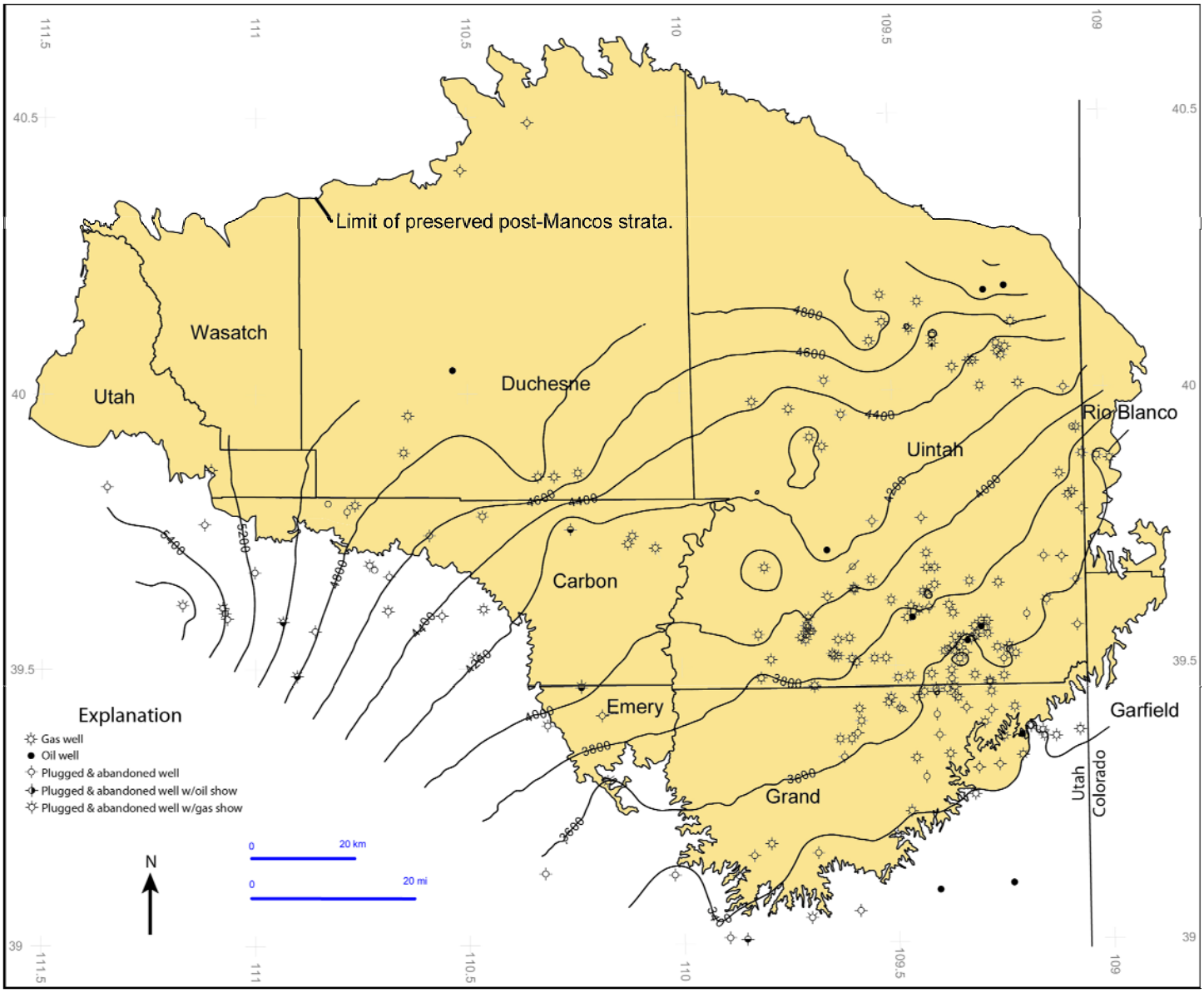

Figure 5.3. Isopach of the Mancos Shale in the Uinta Basin. Contour interval equals 200 feet. From Ressetar and others, in preparation.

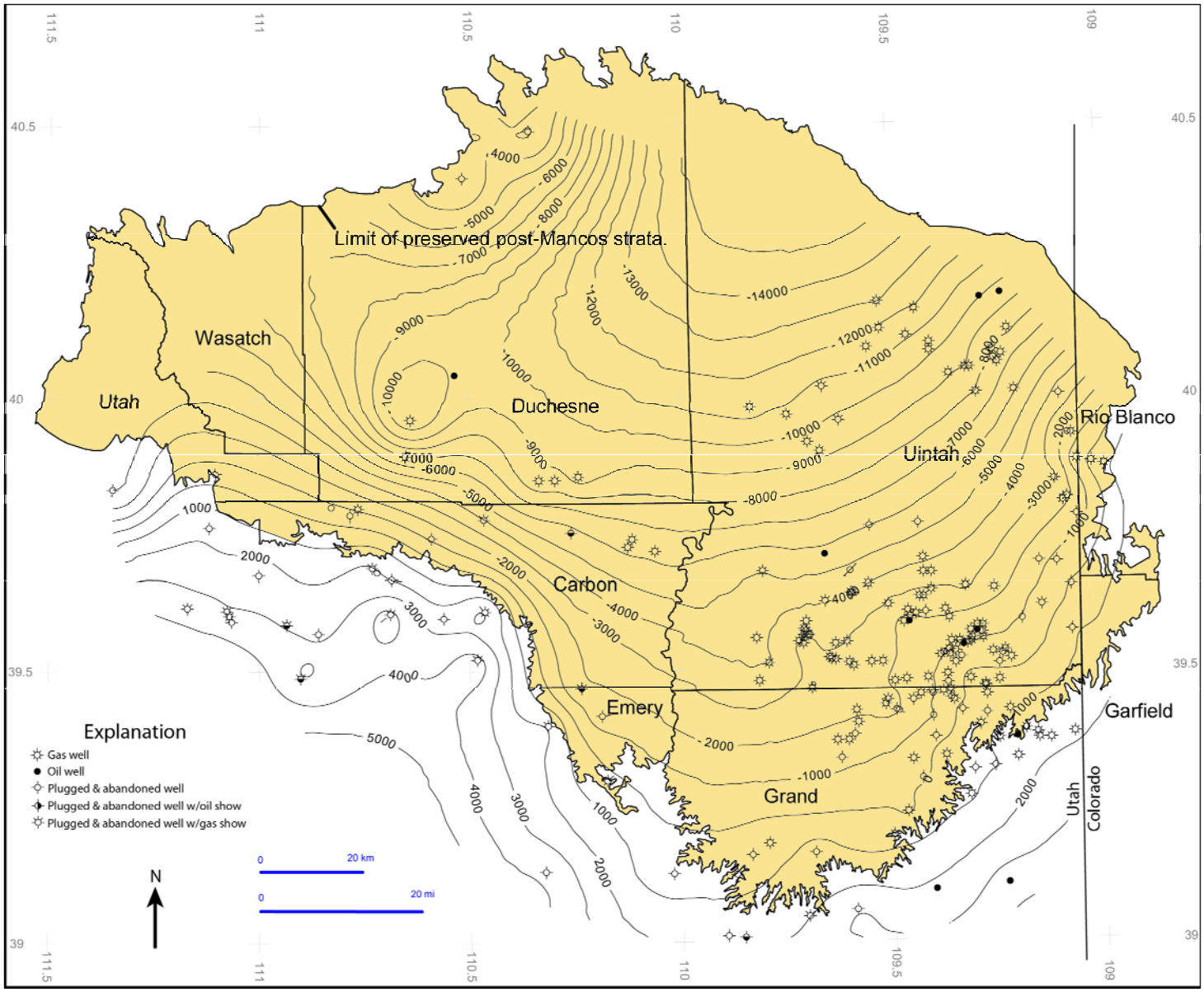

Figure 5.4. Structural map of the base of the Mancos Shale (top of the Dakota Formation) in the Uinta Basin. Elevations in feet relative to mean sea level, contour interval equals 1000 feet. From Ressetar and others, in preparation.

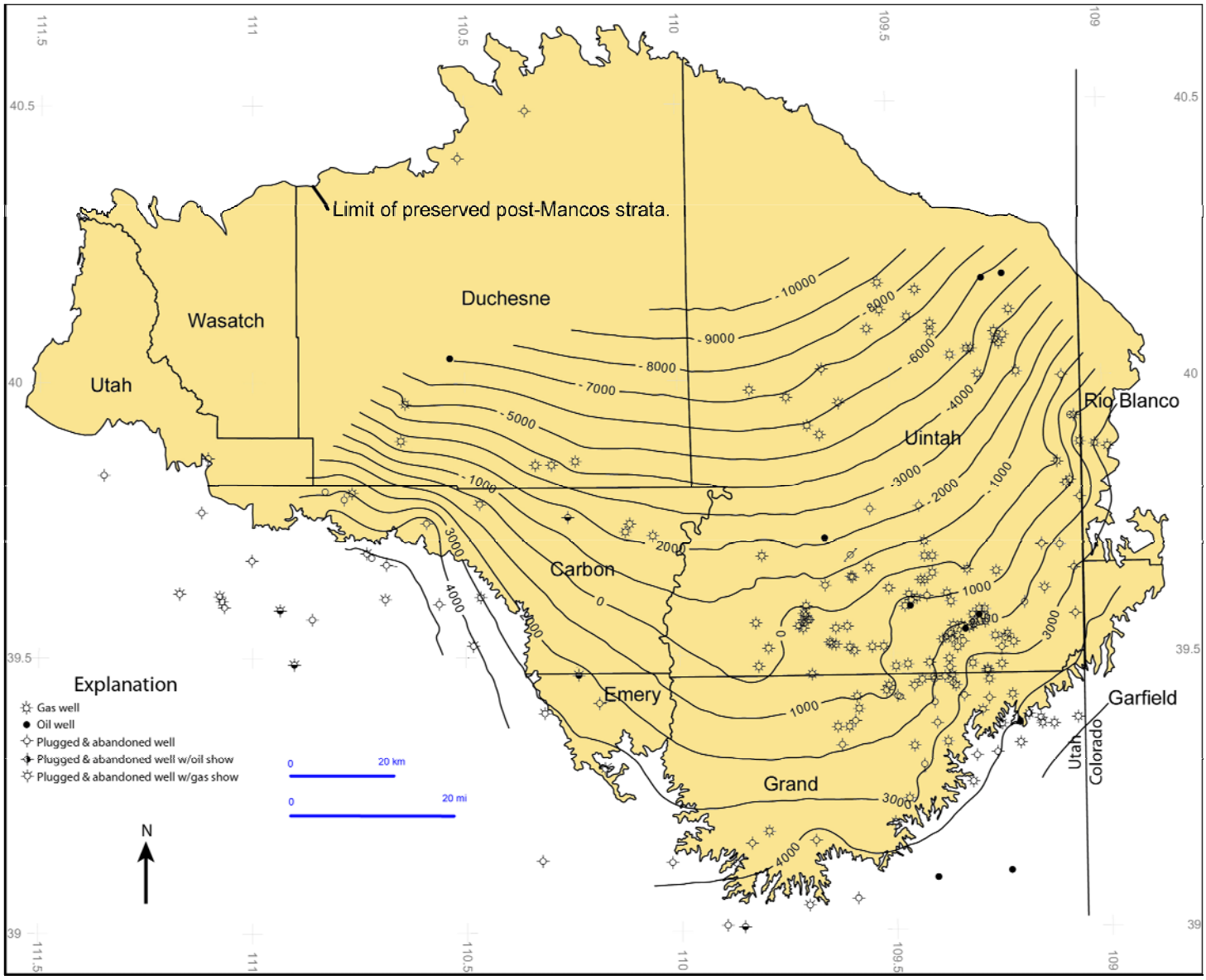

Figure 5.5. Structural map of the top of the Mancos B Member in the Uinta Basin. Elevations in feet relative to mean sea level, contour interval equals 1000 feet. From Ressetar and others, in preparation.

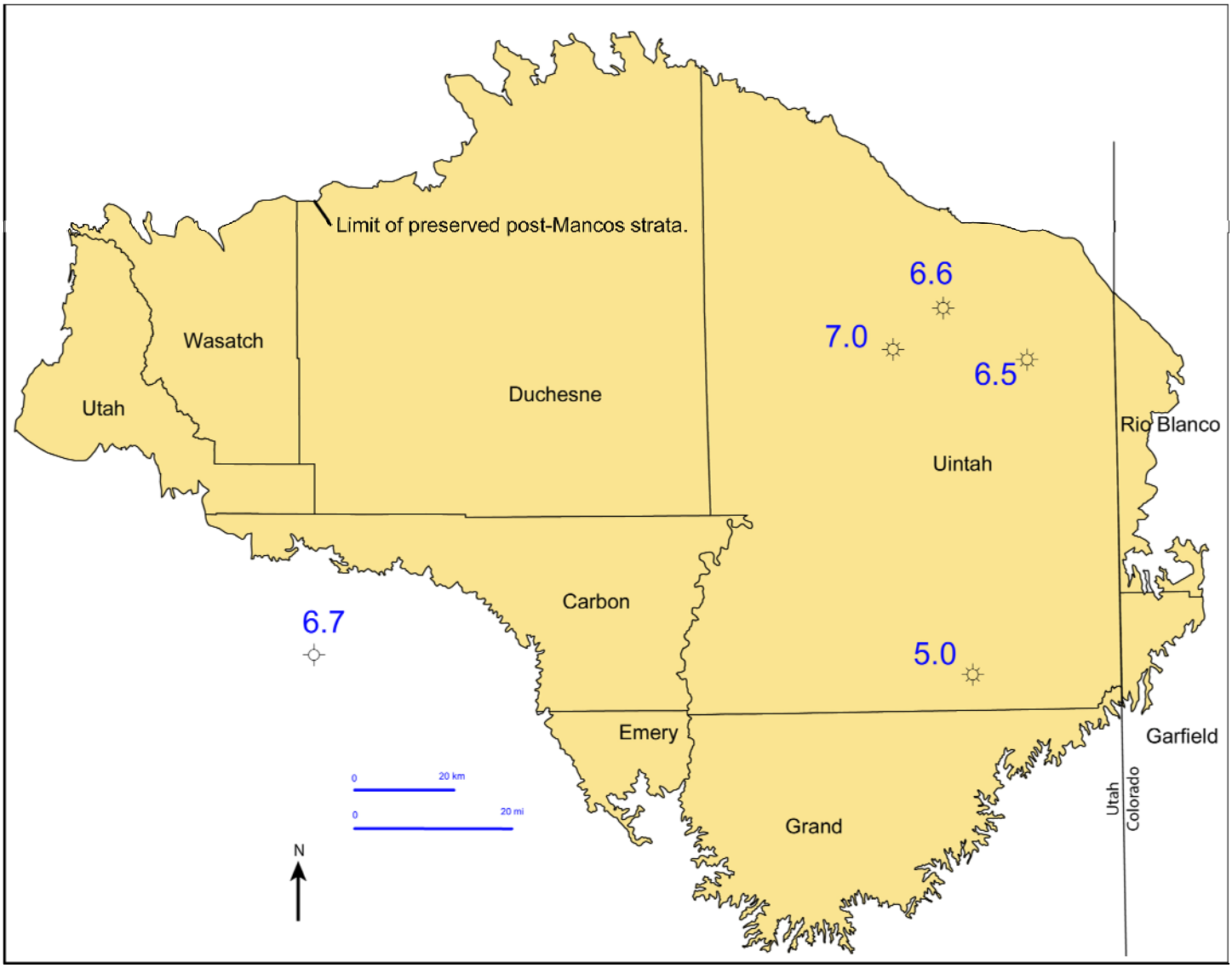

Figure 5.6. Average porosities (%) in cores from the lower Blue Gate Shale Member of the Mancos Shale. Well numbers (WSNs) are assigned by the log analysis software and are linked to well information in appendix B.

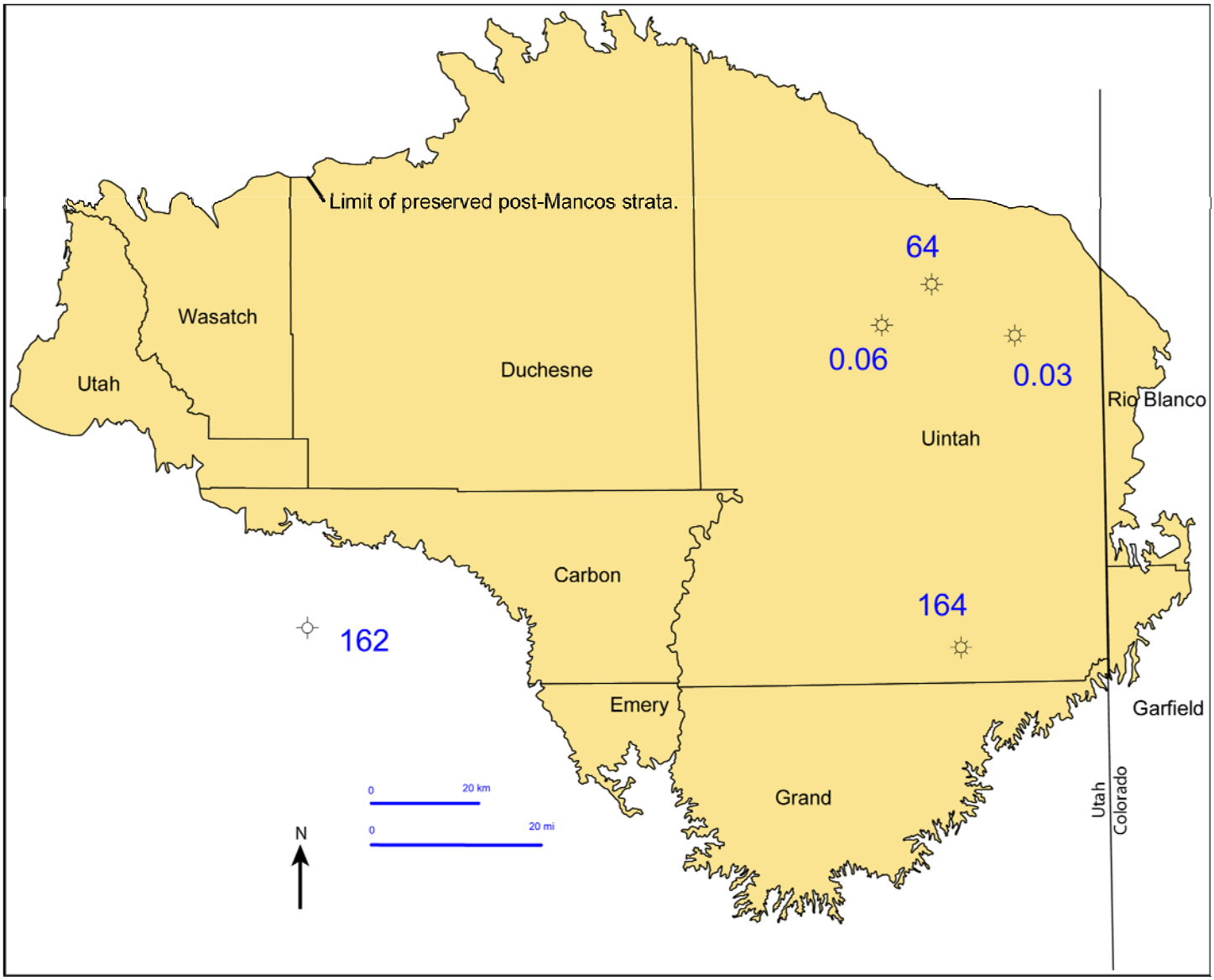

Figure 5.7. Average permeabilities (nanodarcies) in cores from the lower Blue Gate Shale Member of the Mancos Shale. Well numbers (WSNs) are assigned by the log analysis software and are linked to well information in appendix B.

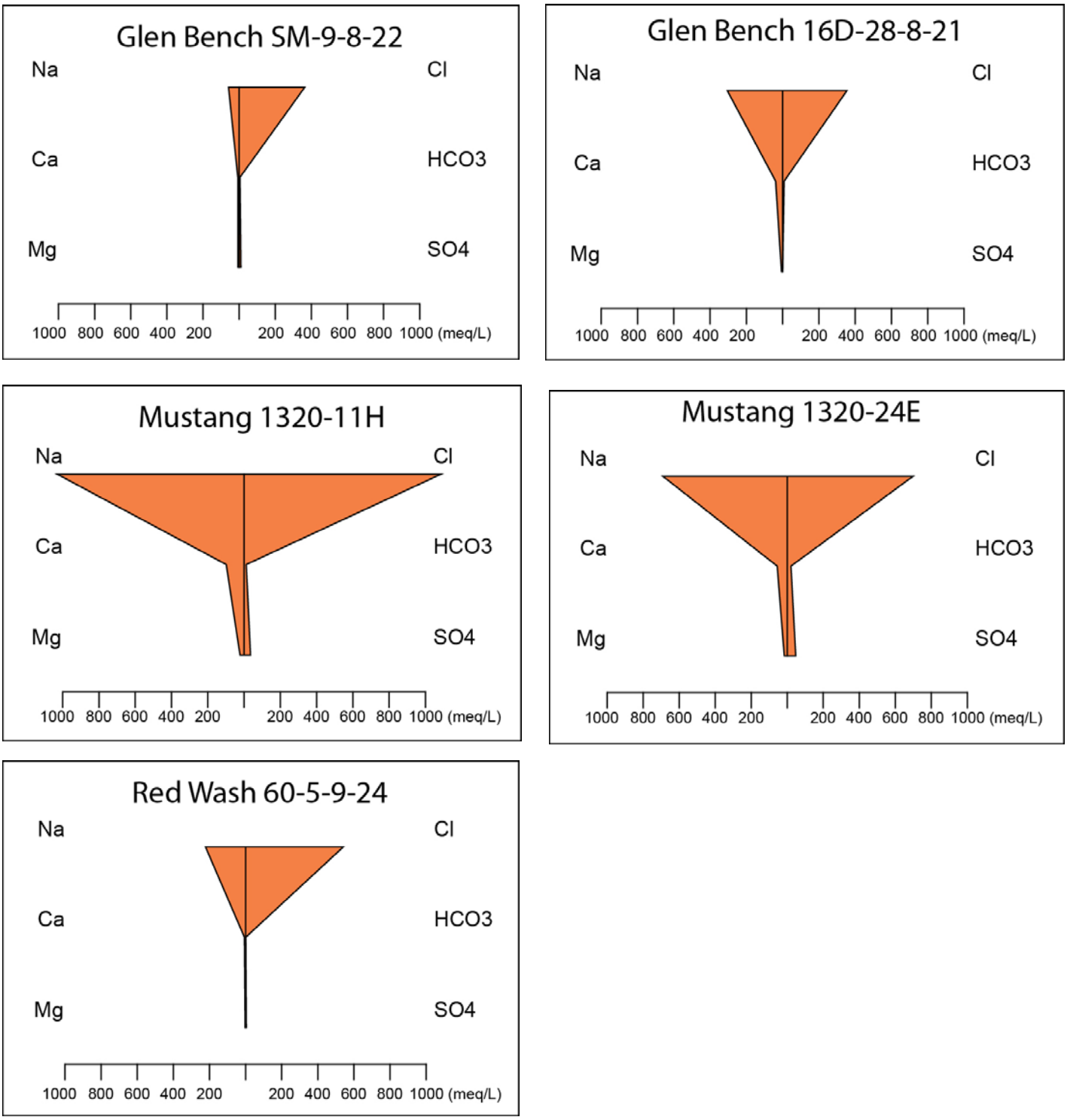

Figure 5.8. Stiff diagrams of water samples from the Mancos Shale and adjacent units. See table 5.1 for well and chemical data.

CHAPTER VI

UINTA BASIN RESERVOIRS/AQUIFERS: UPPER CRETACEOUS MESAVERDE GROUP AND UPPER PALEOCENE TO LOWER EOCENE WASATCH/COLTON FORMATION

Peter J Nielsen and Rebekah W. Stimpson

The asymmetrical UB formed structurally during the Late Cretaceous to Eocene from uplift and tectonism in Sevier Highlands to the west and Laramide uplifts, including the Uinta Uplift to the north, San Rafael Swell to the southwest, and the Douglas Creek arch in the east, which separates the UB from the Piceance Basin in Colorado (Johnson, 1985; Dickinson and others, 1988; Bader, 2009; Dickinson and others, 2012). In this part of the study we focus on the Upper Cretaceous Mesaverde Group and the upper Paleocene to lower Eocene Wasatch/Colton Formation deposited within the UB via fluvial, coastal plain, coal swamp, delta, and marine environments (figure 6.1). Both the Mesaverde Group and the Wasatch/Colton Formation are reservoirs for oil and gas, predominantly natural gas trapped in tight-gas sandstones (Nelson and Hoffman, 2009), which, in this study, are isolated, filled fluvial channels with low permeability.

Significant saline water is often associated with the hydrocarbon production from these formations requiring a produced water disposal solution—the primary overall objective of this project. The produced water is typically very poor quality and unfit for beneficial use (unless

treated), and the current optimal strategy for dealing with produced water is to reinject it into deep underground reservoirs. This report provides an analysis of the current water quality, as well as potential disposal reservoirs within these formations, in addition to the general stratigraphy, thickness, depth, reservoir properties, porosity and permeability, and hydrocarbon production of the Mesaverde Group and the Wasatch/Colton Formation.

METHODS

Data for this project came from several sources (figure 6.2). There are approximately 22,000 wells within the UB that can be used for subsurface analysis. We selected 59 wells from Anderson's (2005) study of hydrocarbon potential of the Mesaverde Group in the southeastern UB. The database from that study consisted of formation tops for the Wasatch/Colton and Mesaverde Group formations. We also used raster gamma logs and a few formation resistivity logs from 55 wells to identify the formation tops. For our more regional study, we expanded our search to find additional wells that penetrated the Wasatch/Colton Formation and Mesaverde Group, as well as those that had a full suite of raster log images or digital log files. Many wells penetrated to depths below the lower Castlegate Sandstone and into the Blackhawk Formation and Mancos Shale, but logging was often incomplete or the images were poor quality. Nonetheless, we identified 55 additional wells that were distributed throughout the UB study area and had usable and legible well logs through the formations of interest (appendix C). We have assembled data and logs from 114 wells for this study.

Gamma-ray (GR) logs were available for nearly all the wells selected for this study. Most wells had a series of sonic and resistivity logs and approximately one-third had density and porosity logs. We digitized approximately 50 GR, sonic (DT), spontaneous potential (SP), and resistivity (RES) logs for use in this study.

Formation tops and lithology can be identified from the general curve trends; however, calculating rock properties from the GR and SP curves requires the curves to be normalized. Errors are often introduced into GR and SP curves because of scale problems, different hardware configurations between companies, and different calibrations between downhole runs with different logging tools. Several studies indicate that over 90% of GR and SP logs require some sort of normalization while DT and RES logs only require occasional normalization (Shier, 2004; Robert Cluff, Discovery Group, written communication, 2014). The GR curves should be normalized to calculate accurate V-shale (Vsh) and net-to-gross ratios (NGR) for the different formations.

We prepared several west-to-east and north-to-south GR and SP well log cross sections through the UB to evaluate curve anomalies between wells in the same formations. The sections consisted of 25 to 30 closely spaced wells showing unprocessed GR or SP curves. The large number of well curves allows identification of anomalous curves, shifted curves, and other scale problems (Robert Cluff, Discovery Group, written communication, 2014). The largest, observed problem with the GR curves is different instrument response between various logging companies. The unprocessed GR curves generally have similar formation responses, meaning that one can pick formation tops and general lithology. However, one can see equipment response or instrument gain is different between wells. This means that all wells, where the same equipment is used, should have the same gamma ray measurements (gamma ray in

American Petroleum Institute units [GAPI]) response for a clean sand or shale interval. Different logging equipment, set at a higher or lower gain for instance, will have a different GAPI for a similar clean sand or shale interval. Normalizing GR curves involves determining what a clean sand and shale response should be for a particular area or zone and then normalizing all GR curves in that defined area to that GAPI response range.

We calculated the mean GR and standard deviation for the Wasatch/Colton Formation and Mesaverde Group for each of the 50 selected wells. We also prepared a trend surface using the mean GR for the Mesaverde and Wasatch/Colton (figure 6.3). The shale content of both units increases from west to east matching the observed stratigraphy. A standard normalization of the GR curves would shift the data so that those on the western side of the basin would become siltier than they should be, and GR curves on the eastern part would become sandier. We divided the study area into three areas reflecting the eastward increasing shale trend, and identified a type well in each area that represents each area's regional curve response (Shier, 2004). The three north-south demarcated zones dividing the basin are as follows: Zone 1 is the western third of the basin; Zone 2 is the central third; and Zone 3 is the eastern third. The method selected for GR logs in the study was to normalize high and low GR curve responses to the high and low regional type well curve GR responses. The type wells selected were Reservation Ridge State No. 42-2 (section 2, T. 11 S., R. 11 E., SLB&M, Duchesne County, API No. 43-013-33758) for Zone 1, Pete's Wash No. 23-12-1 (section 12, T. 10 S., R. 17 E., SLB&M, Uintah County, API No. 43-047-34286) for Zone 2, and Over-Under Sage GR No. 10W-15-8-22 (section 15, T. 8 S., R. 22 E., SLB&M, Uintah County, API No. 43-047-34719) for Zone 3. Each type well log penetrates both the Wasatch/Colton and the Mesaverde. The GR curves for the type wells were normalized using representative shale (highest) and sand (lowest)

parts of the curve and the 10th and 90th percentile values from the curve. This essentially stretches the curves to match the expected response that a shale horizon and a sand body should have in each zone. After the GR curves were normalized for the type wells, the high and low GR parts of the curve were selected and used for the regional high and low for the remaining wells in each individual zone. GR histograms were generated and the GR high and low picks were made for each well. Each well within a zone was normalized to the zone type well with the regional patterns (Robert Cluff, Discovery Group, written communication, 2014). Below is the standard, regional equation for normalization used to prepare a normalized GR curve for each well (Shier, 2004):

$$Vnorm = Rmin + \frac{(Rmax - Rmin)\,(Vlog - Wmin)}{(Wmax - Wmin)} \tag{6.1}$$

where:

Vnorm = new normalized curve value,

Rmin = regional curve minimum (lowest picked value from type well),

Rmax = regional curve maximum (highest picked value from type well),

Vlog = curve values,

Wmin = well curve minimum (lowest picked value from well), and

Wmax = well curve maximum (highest picked value from well).

SP curves typically show good negative or positive trends but require scale shifts to be removed from the curve. The raster well logs were reviewed for each well and any shifts in the curve were noted. Individual sections of each curve were shifted by depth. SP curve histograms were prepared and the shale baseline and static spontaneous potential (SSP) was selected for each well. The shale baseline is observed in shaly zones in the wells and the value selected for the water resistivity (Rw) calculation (Rider and Kennedy, 2011). The expected SP response would be a more negative SP with increasing depth, indicating that the salinity of the deeper formation water is greater than the drilling mud. A positive SP trend in the curve indicates that the formation water has a lower salinity that the drilling mud. A review of SP curves throughout the basin showed SP curves in the middle of the basin generally show a negative shift, and SP curves around the margins have zones of positive SP shift suggesting zones of less saline water. Several positive SP shifts were identified and associated with sandy intervals possibly indicating lower salinity or the presence of hydrocarbons. These lower salinity zones were distributed throughout the Mesaverde Group interval and may be related to recharge areas or conduits.

V-shale curves were calculated using both the normalized GR curves and the corrected SP curves. Vsh gives an indication of how the formation responds to electrical current and will impact the water saturation and bound volume of water calculations. Clay minerals in rocks lower the matrix resistivity because they conduct electrical current between their layers (Tiab and Donaldson, 2012). Vsh from GR curves are calculated using the GR index and the Larionov

nonlinear equation for rocks older than Tertiary (Asquith and Krygowski, 2004). The GR index equation is:

$$Igr = \frac{(GRlog - GRmin)}{(GRmax - GRmin)} \tag{6.2}$$

The nonlinear Larionov equation is:

$$Vsh = 0.33 * (2^{2*Igr} - 1) \tag{6.3}$$

where:

Igr = gamma ray index,

GRlog = formation gamma ray reading,

GRmin = minimum gamma ray or clean sand gamma ray, and

GRmax = maximum gamma ray or clean sand gamma ray.

Vsh curves calculated from the SP tend to be more optimistic than those calculated using GR curves because the relationship is a linear equation and clay minerals in shale can lower the formation resistivity, thereby shifting the shale baseline more negative. The equation for Vsh from the SP curve is:

$$Vsh = 1 - \frac{PSP}{SSP} \tag{6.4}$$

where:

Vsh = volume of shale in formation as a fraction,

PSP = pseudo-static spontaneous potential or the SP reading in a shaly zone, and

SSP = static spontaneous potential or maximum value in a clean sand zone.

The calculation of water saturation (Sw) and the bulk volume of water (BVW) for a formation requires knowing the resistivity of formation water and the porosity. Two methods were used to calculate the formation water resistivity: (1) calculation of TDS, NaCl equivalent concentration, and water salinity using several water analyses from the Wasatch/Colton interval and the Mesaverde Group; and (2) calculation of Rw from SP readings using resistivity of the borehole mud cake and formation temperatures.

The cations, anions, and TDS values are presented in appendix D. There is some uncertainty regarding the exact depth of the samples collected, and some of the samples represent mixed water from several perforated intervals. We reviewed the water chemistry database extensively and believe that we have used the best and most representative samples for the various formations. Three equations were used to estimate water resistivity using laboratory analyses and essentially converted measured components into NaCl equivalent solutions. The

equations and multipliers are found in Tiab and Donaldson (2011) and in Schlumberger (2009). The three equations for NaCl equivalent resistivity are:

$$Csp = \Sigma_{i=1}^{n} Mi * Csii \tag{6.5}$$

$$Rw75 = \frac{1}{2.74 * 10^{-4 * Csp^{0.955}}} + 0.0123 \tag{6.6}$$

and Arps equation:

$$RwFT = Rw75 * \frac{75 + 6.77}{FT + 6.77} \tag{6.7}$$

where:

Mi = weighting multiplier for each component at a concentration range,

Csii = concentration of each ion in parts per million (ppm) or mg/L,

n = number of ions,

Csp = equivalent NaCl concentration,

Rw75 = resistivity of equivalent NaCl concentration at 75 °F,

RwFT = resistivity at formation temperature, and

FT = formation temperature (°F).

Another method for calculating formation water resistivity (Rw) uses the SP curve values (Asquith and Krygowski, 2004), the formation temperature estimated using a temperature gradient equation and the bottom-hole temperature (BHT), and the resistivity of the mud filtrate (RmfFT) at the formation temperature calculated using the Arps equation shown above. Formation temperature for each well is calculated using either a basin-wide temperature gradient or by using the annual mean surface temperature for the area and the BHT. A mud filtrate resistivity (Rmf) curve is then calculated using the Arps equation and the estimated formation temperature. An equivalent formation water resistivity (Rwe) curve is calculated using:

$$Rwe = RmfFT * 10^{\left(\frac{\mathrm{SP}}{61 + 0.133 * \mathrm{BHT}}\right)} \tag{6.8}$$

and an Rw curve or value by:

$$Rw = \frac{Rwe = 0.131 * 10^{\left(\frac{1}{\log\left(\frac{\mathrm{BHT}}{19.9}\right)}\right)^{-2}}}{-0.5 * Rwe + 10^{\frac{0.0426}{\log\left(\frac{BHT}{50.8}\right)}}} \tag{6.9}$$

where:

Rwe = equivalent water resistivity at formation temperature,

Rmfft = resistivity of mud filtrate at formation temperature,

SP = SP curve readings,

BHT = bottom-hole temperature in °F, and

Rw = resistivity of formation water at depth.

Most wells in the project had a Delta T (DT) curve, a *SPHI* curve, or both. Wells with SPHI curves were only were back-calculated to DT using DTma and DTfl values from the well logs. DT is calculated by a derivation of the Wyllie equation (Wyllie and others, 1958).

$$SPHI\ (DTfl - DTma) + DTma = DT \tag{6.10}$$

where:

SPHI = sonic porosity readings or curve values,

DTfl = interval transit time of the fluid in the formation in µS/ft,

DTma = interval transit time of the formation matrix in µS/ft, and

DT = combined interval transit time of the formation in µS/ft.

SPHI is calculated from the acoustic velocity curve using standard rock matrix and fluid values specified by the geologist at the well site. We reviewed the well logs and found that most of the SPHI values had DTma values of 51.3 µS/ft, a typical sandstone matrix. However, several wells had limestone SPHI values using a limestone matrix value of 47.6 µS/ft. Fluid values were all for fresh water or 189 µS/ft. To standardize the SPHI curves, we calculated a DT curve using Equation 6.10. After DT was calculated, sonic porosity – sandstone (SPHIS) curves were generated with the 51.3 µS/ft sandstone matrix and 189 µS/ft fresh water values using the standard Wyllie equation. SPHIS should indicate corrected sandstone porosities. Several wells, particularly in the eastern portion of the basin, had neutron and density porosity logs. A review of several of them showed gas crossover, particularly in the Sego and Castlegate Sandstones. A sonic porosity curve adjusted for gas (SPHIS_GAS) was prepared for each well (Hilchie, 1978). In sandstone units without a neutron porosity crossover, the SPHIS_GAS porosity will be too low. The two curves, SPHIS and SPHIS_GAS, should bracket the formation porosities.

After calculating water resistivity using lab samples and SP curves, formation water saturation (Sw) was estimated using the standard Archie equation (Archie, 1942, Asquith and Krygowski, 2004).

$$Sw = \left(\frac{a * Rw}{Rt * SPHIS^{m}}\right)^{\frac{1}{n}} \tag{6.11}$$

where:

Sw = formation water saturation as a fraction,

Rw = formation water resistivity,

Rt = formation resistivity or deep resistivity (RESD),

SPHIS = sonic porosity for sandstone,

a = tortuosity factor or 0.81 for consolidated sands,

m = cementation exponent or 2.0 for consolidated sands, and

n = saturation exponent or 2.0 for consolidated sands.

Formation water saturation was calculated using the water resistivity from lab analyses and from the Archie equation, and there is good agreement between the results. We therefore concluded the Rw and Sw values calculated from SP curves are representative of the formations and give a good distribution of Rw and Sw for the study area.

Finally, the bulk volume of water (BVW) is calculated by the following equation (Asquith and Krygowski, 2004):

$$BVW = SPHIS * Sw \tag{6.12}$$

where:

BVW	=	bulk volume of water or water available to flow,
SPHIS	=	Sonic porosity for sandstone, and
Sw	=	Formation water saturation.

The BVW indicates how much water is available to flow to the well. As the BVW approaches 0, the number approaches the irreducible water saturation number that is essentially water bound to the pore surface or clay particles.

The NGR for each formation have been calculated using the normalized GR and calculated SPHI curves. A ≥60 GAPI cutoff was applied to the normalized GR curve. The SPHI curve was used to limit the sandstone summation to a minimum porosity of 6%. All footages are in feet and porosities are in fractional volume.

Water samples sourced from well files curated at the DOGM and company donations were compiled in a comprehensive water chemistry database by the UGS (appendix E). The structure and isopach maps of the Mesaverde Group were created in IHS Petra™ using formation tops data for the 114 wells recorded in appendix D. Sonic logs were used to calculate average formation porosity and bulk density logs were used for average formation density.

UPPER CRETACEOUS MESAVERDE GROUP

The Upper Cretaceous Mesaverde Group in the UB comprises the sedimentary units overlying the Mancos Shale and underlying the Upper Cretaceous to Paleogene North Horn, and Colton and Wasatch Formations (figures 1.5 and 2.13). Deposition occurred as the Cretaceous Western Interior Seaway regressed to the east and rivers and streams flowed eastward from the Sevier highlands in western Utah to the sea (figure 6.1A and 6.1B). In the western half of the Uinta Basin, the Mesaverde Group, from oldest to youngest, is composed of the Blackhawk Formation, Castlegate Sandstone (lower, middle Bluecastle Sandstone members), and Price River Formation, all resultant from landward deposition, whereas in the eastern seaward portion of the UB, the group comprises lower Castlegate, Buck Tongue of the Mancos Shale, Sego, Neslen, Farrer, and Tuscher Formations (figure 2.13; plate 2). The group thins to the north and south from the basin middle (plate 3 and figure 6.4). Depositional environments for these formations include fluvial, coastal plain, coal swamp, delta, and marine, and lithologies vary from shale to siltstone to sandstone. Several of these formations contain thick sandstone packages that provide reservoirs for hydrocarbons and water.

Thickness

Thickness of the Mesaverde Group ranges from less than 500 to ~3500 feet (figure 6.5). At the group's exposure along the Book Cliffs, the strata range from approximately 160 to 2290 feet thick, based on geologic mapping (Gualtieri, 1988; Weiss and others, 1990), and our data (figure 6.4) show a range of less than 500 feet to over 2000 feet along the southern margin of the UB. Overall, the group is thickest in an east-west trending band along the middle of the UB and

thins toward the northern and southern margins and toward the Douglas Creek arch (Johnson and Roberts, 2003).

Depth

The Laramide-aged UB is bounded by the SRS and Uncompahgre uplift to the south and the Uinta Mountains along the north (Potter and others, 1991). Stratigraphic units filling the basin gently dip north along the Book Cliffs in the south and outcrops along the northern margin of the basin steeply dip south (figure 6.5) (Morgan and others, 2002). Outcrops along the Book Cliffs provide a view of the intertonguing and lateral transitions of the vertical succession of sedimentary units that extend throughout the basin (figure 6.6). The deepest showing of the Mesaverde Group is greater than 19,000 feet (Johnson and Roberts, 2003).

Lithology

The Blackhawk Formation is composed of interbedded sandstone, siltstone, shale, and coal (figure 6.7A). The formation has been interpreted as a wave-dominated delta deposit in some places reaching thicknesses of more than 1000 feet (Franczyk and others, 1990a; Dubiel, 2000; Howell and Flint, 2005). Coal found within the Blackhawk formed from widespread marshes and swamps overlying sands along the shoreface of the Western Interior Seaway (Maberry, 1971; Franczyk and others, 1990a). The lower Blackhawk hosts thick and laterally continuous coal beds, whereas upper Blackhawk coals are thin and discontinuous (Dubiel and others, 2000). Sedimentation gradually changed laterally and vertically from non-marine as

meandering streams flowed eastward, their channels cross-cutting peat deposits, into delta front deposits that prograded into the sea (Maberry, 1971; Howell and Flint, 2005).

The Castlegate Sandstone sharply overlies the meandering stream and coastal plain deposits of the Blackhawk Formation or, in the eastern Uinta Basin, the marine Mancos Shale (figure 6.7A and 6.7B) (Howell and Flint, 2005). The lower member ranges in thickness from ~10 to 800 feet thick but is on average ~300 feet thick (figure 6.9) and is composed of massive sandstones that formed in an east to southeast-flowing, braided, sand-rich stream environment (figures 6.7B and 6.9). The upper member contains interbedded mudstone and sandstone from a meandering stream system (Lawton, 1983; Hettinger and Kirschbaum, 2002). The upper unit is thickest (up to 500 feet) in the west and thins to about 10 feet in the east (figure 6.10). Coarse-grained sandstone zones are interpreted to be linked to thrusting during the Sevier orogeny (Chan and Pfaff, 1991).

The Bluecastle Sandstone Member (uppermost member) of the Castlegate Sandstone was deposited in an evolving meandering stream environment within an alluvial plain and contains stacked, fine to coarse-grained sandstone channels with trough cross-stratification (Franczyk and others, 1990b). Paleocurrent data exhibit northeast and southeast flow from the Sevier highlands to the eastern sea (Franczyk and others, 1990a). The unit preserves the last major sediment body resulting from thrusting associated with the Sevier orogeny (Franczyk and others, 1990a), and it pinches out eastward above the Neslen Formation (figure 6.11 and plate 2) (Hettinger and Kirschbaum, 2002).

The Price River Formation consists of approximately 600 to 1600 feet of poorly sorted siltstone and ledge-forming sandstone beds deposited within an eastward-flowing meandering fluvial system (figure 6.7C) (Lawton, 1983; Hettinger and Kirschbaum, 2002). The formation

changes laterally into the Tuscher and Farrer Formations in the eastern part of the UB (figure 6.12; plate 2). Sandstones in the upper Price River are thicker and more laterally continuous than those in the lower section (Lawton, 1983). The Price River and the Farrer contain numerous thin, isolated, heterolithic sandstone bodies from meandering and tidally influenced fluvial channels, which provide small hydrocarbon reservoirs, though the sand bodies become thicker and more interconnected up-section in the Tuscher (figure 6.12) (Aschoff, 2010).

The Buck Tongue of the Mancos Shale underlies the Sego Sandstone in the eastern half of the UB (figure 6.13A) and consists of interbedded, gray sandstone, siltstone, and mudstone interfingering with the Mesaverde Group (Franczyk and others, 1990a). The unit records a marine transgression that thickens to the east and gradually transitions upward into the Sego as sediments become increasingly coarse grained (Franczyk and others, 1990a; Anderson, 2005). The unit is thickest in the easternmost portion of the study area and pinches out slightly west of the present day Green River (figure 6.14).

The Sego Sandstone is composed of stacked, cross-stratified sandstone packages with parallel laminations in its uppermost package, and has a sharp, conformable contact with the overlying Neslen Formation (figure 6.13A and 2.13B) (Franczyk and others, 1990a). The Buck Tongue of the Mancos Shale and the Sego Sandstone record the final transgression and regression of the Cretaceous Western Interior Seaway in the UB and east-central Utah (Franczyk and others, 1990a). Sandstone thickness is on average ~180 feet (Hettinger and Kirschbaum, 2002). The upper Castlegate Sandstone member is a western equivalent of the Sego Sandstone and Neslen Formation of the eastern UB (figure 6.15).

Deposited by eastward-flowing rivers in a coastal plain (figure 6.1B) behind the shorelines of the Sego Sandstone, the Neslen Formation contains carbonaceous mudstone, coal,

and channelized sandstone beds that increase in abundance toward the top of the unit (figure 6.13) (Franczyk and others, 1990a; Cole and others, 2008). The Neslen is the eastern lateral equivalent of the upper Castlegate Sandstone of the western Uinta Basin (Lawton, 1983). Franczyk and others (1990a) report total thickness of these units ranges from 175 to 670 feet, and Anderson (2005) reports the average thickness is ~250 feet (figure 6.15). In outcrop, the Thompson Canyon Sandstone, approximately in the middle of the Neslen Formation, forms a continuous sandstone ledge up to 15 feet thick (figure 6.13A) (Fisher, 1936). The coal beds are discontinuous and range from 1 to 7 feet thick (figure 6.13C) (Franczyk and others, 1990a; Hettinger and Kirschbaum, 2002).

Like the equivalent Price River Formation, the Farrer Formation was deposited by an east and northeast-flowing, straight to sinuous river system that crossed a coastal plain (figure 6.1B) (Cole and others, 2008). The sandstone bodies preserve anastomosing channels, and as the sandstones become thicker up section, the Farrer Formation transitions into the Tuscher Formation (figure 6.12) (Keighin and Fouch, 1981). The sandstone is very fine to medium-grained with interbedded mudstone resultant from floodplain deposits (Hettinger and Kirschbaum, 2002). The Farrer contains significantly more sandstone and less carbonaceous material than the underlying Neslen (Franczyk and others, 1990a). The maximum thickness of the Farrer Formation is 950 feet in Tusher Canyon and it thins westward to 130 feet in Soldier Canyon (figure 6.16) (Lawton, 1983).

The eastern UB's Tuscher Formation is correlative to the west with the upper Price River Formation (Lawton, 1983). The Tuscher is approximately 250 feet thick, comprising multi-story, thick, sandstone bodies overlying the Farrer Formation, and was also deposited within a northeast-flowing fluvial environment (figures 6.1B and 6.12b) (Lawton, 1983; Hettinger and

Kirschbaum, 2002; Cole and others, 2008). Excellent outcrops of the Neslen, Farrer, and Tuscher Formations can be found in Sego and Tuscher Canyons along the southeastern Book Cliffs in Grand County (figure 6.12a and 6.17). Contacts between the Neslen, Farrer, and Tuscher are gradational, but the Tuscher can be identified from the Farrer Formation by the presence of lighter-colored and more massive sandstones (Franczyk and others, 1990ba Anderson, 2005). As the coastal plain prograded and the Western Interior Seaway regressed to the east, the Farrer and Tuscher were deposited in the alluvial plain that also migrated eastward (Keighin and Fouch, 1981).

Reservoir Properties

We compared the net sand with greater than 6% porosity to the gross thickness of sand in some individual formations as well as for the full Mesaverde Group. A discussion of the reservoir properties for the Mesaverde Group follows.

Appendix F shows the NGR and average porosity (PHIA) calculations for the combined Mesaverde Group. The NGR calculation used a minimum 6% SPHI and a maximum 60 GAPI GR cutoff to arrive at the net sand thickness. The average PHIA of all wells is 21%, and the values range from 13% to a high of 35% (appendix F), which is lower than the Wasatch/Colton interval (discussed later). The NGR is generally lower in the Mesaverde than the Wasatch/Colton Formation, reflecting an overall higher shale component, particularly on the eastern side of the basin (figure 6.18). However, there are very thick sequences of Mesaverde sandstone with porosity greater than 6%. We suggest the sandy formations in the upper part of

the Mesaverde could make favorable injection units, particularly around the margins of the basin where their water saturation is lower.

The Price River Formation is the youngest formation in the western Mesaverde Group, and it is chronostratigraphically equivalent with the Tuscher and Farrer Formations on the eastern side of the basin. NGR, gross sand, and PHIA averages for wells that penetrate the Price River Formation are recorded in appendix F. The average NGR is 0.68, gross sand is 435 feet, and the PHIA is 15%. However, the Price River has much thinner stacked sequences of sandstone. Well logs through the interval show interbedded sandstone and silty or shaly sandstone. Two wells, Yellowstone River Tribal No. 1 (section 17, T. 1 N., R. 4 W., UBL&M, Duchesne County, API No. 43-013-30047) and Skyline Govt No. 1 (section 10, T. 11 S., R. 7 E., SLB&M, Utah County, API No. 43-049-30003), have gross sand thicknesses of 1652 and 1115 feet, respectively, reflecting an area of the basin with a higher concentration of fluvial channels. The net sand in these two wells is higher than other wells, but the NGR ratio is generally lower because of the high gross sand thickness. Injecting high volumes of produced water into this formation would require either a long perforated interval through the extent of the formation, or many very detailed perforations targeting clean sands.

The Tuscher Formation is located on the eastern side of the UB. The formation is generally sandy, and well logs of Tuscher show several thick, blocky sandstone intervals, which likely represent thick meandering fluvial channels. The channels are bounded vertically by silty to shaly sandstones. The blocky channels in the Tuscher do not show a fining upward trend and the contacts appear to be sharp. The lateral continuity of the channels has not been established as part of this study. However, two nearby wells typically show similar, blocky, sandy channels in GR logs. This suggests that the channel sands may be continuous laterally over a larger area.

The average PHIS in the Tuscher is 16%. The average gross sand thickness is 150 feet. The average NGR of 0.79 is slightly higher than for the Price River Formation, suggesting that a greater percentage of the gross sand has high porosity (appendix F). This implies that the sands are cleaner and sharply contrast the silty and shaly sands above and below. This could make the channel sandstones in the Tuscher on the eastern side of the basin favorable injection locations for disposal of produced water.

GR curves from the Farrer Formation show several thick, interbedded sand-silt channel sandstone sequences. The Farrer has an average gross sand thickness of 211 feet, which is higher than the Tuscher Formation above and one half of the gross sand thickness in the Price River Formation. The average NGR is 0.74, nearly matching the Tuscher NGR above. The Farrer has significant sandstone channels, but they have more finer-grained interbeds and are less massive compared to the Tuscher channels. The Farrer could also provide some good candidate sandstones for water injection, similar to the Tuscher.

Porosity values in the Mesaverde Group are linked to the thermal maturity and depositional environments; values range from 5 to 8%, and the highest likely porosity is 13% (Schmoker and others, 1992). Calculated average porosity values, using sonic logs, for each formation within the Mesaverde are presented in table 6.1. According to the data, the overall average porosity for the sandstones in the Mesaverde, unadjusted for the presence of hydrocarbons, is 15%. The highest calculated porosity is within the Tuscher Formation (16.2%), followed by the Neslen and Farrer (15.6% and 15.5%, respectively). When adjusted for the presence of oil or gas, the average porosity value for the group decreases to 10% (gas) and 13% (oil). Further subdivision into units or facies would provide a more accurate representation of high and low porosity zones within each formation, but this level of detail was beyond the scope

of this project. Tables 6.2 and 6.3 display porosity and permeability data from two cores within Greater Natural Buttes field area. As expected, permeability values from the tight sand bodies in the study interval are extremely low. One value of 162.33 mD from 10,532 feet in the NBU No. 253 (section 10, T. 9 S., R. 21 E., SLB&M, Utah County, API No. 43-047-32917), core is higher and reflects fracture permeability.

Water Quality

Water samples sourced from the Mesaverde Group vary considerably with regard to TDS. The TDS from Mesaverde water samples range from fresh to brine, with most of the samples falling in the saline category (figures 6.19 and 6.20; table 6.4). Stiff diagrams displayed geographically in figure 6.21 show water samples near the southwestern border of the UB are fresher than the saline found deeper to the east-northeast. A study from the U.S. Environmental (2004) proposes recharge occurs around the basin edges and most is sourced from the Uinta Mountains along the northern basin margin.

Appendix B contains calculated Mesaverde Group Rw, which is inversely related to TDS values. As with the Wasatch/Colton Formation, the Mesaverde has higher Rw values along the southern Book Cliffs and along the north and northeastern portions of the basin. This is expected since the residence time of the water in the formation has not been sufficient to concentrate dissolved solids. Higher Rw values are observed in the Mesaverde in the central part of the basin (eastern Duchesne County) and could possibly be associated with the east-west-trending Duchesne fault zone (figure 2.1, plate 1) that might be allowing downward percolation of fresher water to the strata at that location. Higher water resistivity is also observed parallel to northwest

trending gilsonite dike swarms (figures 2.1 and 3.1, plate 1). Fresher waters are found along the eastern edge of the UB southeast of Bonanza, possibly resultant from fresh water recharge to exposures along the Douglas Creek arch. Groundwater leached from the overlying Flagstaff Limestone into the Mesaverde Group in the western UB leaves a carbonate signature in the calcium-sodium (Ca/Na) ratio (figure 6.23).

Water saturation values in the Mesaverde Group and Wasatch/Colton Formation have similar trends. Sw values are lower in the southern and southeastern area near Book Cliff outcrops. Lower Sw values possibly reflect the presence of hydrocarbons and/or the generally higher silt and shale content in the Mesaverde in the central and eastern parts of the basin. Water saturation values increase to 100% on the western and northern sides of the basin. The reason for this is unknown but may be related to coarse grain size and a higher recharge rate in those areas. BVW values are generally above 20% in the Mesaverde, meaning there is available water to flow in the pores.

The Rw values in the Mesaverde Group suggest variably salt-saturated water will be produced from its formations. Western and near outcrop areas of the UB could produce water in the lower saline range. Where Rw values approach 0.1 to 0.3, either saline or brine solutions could be produced with hydrocarbons. Sw and BVW values indicate the presence of hydrocarbons and water and that pore water is available to flow in the wells. Further studies should be conducted to correlate TDS and NaCl waters from laboratory analyses to formation water resistivity from logs.

Water Production, Use, and Disposal

Significant water production occurs from oil and gas fields producing from the Mesaverde Group (figure 6.23). These fields include Big Valley, Devil's Playground, Gate Canyon, Natural Buttes, Nine Mile Canyon, Pariette Bench, Peter's Point, Red Wash, and Rock House (figure 1.1) (Wood and Chidsey, 2015). Cumulative water production from all of the fields producing from the Mesaverde Group from first production to January 1, 2015, was nearly 700 million bbls (table 6.5); note that production is commonly commingled with additional formations (Utah Division of Oil, Gas, and Mining, 2015).

Figure 6.24 shows the water disposal well locations and water volumes for wells perforated in the Mesaverde Group. As of March 2015, there was only one Mesaverde disposal well, Jack Cyn U ST 14-32 (section 32, T. 12 S., R. 16 E., SLB&M, Carbon County, API No. 43-007-30913), originally a gas well completed in the Castlegate Sandstone, that was converted into an injection well in 2010. It has injected 710,626 BW since completion with an injection rate of approximately 431 barrels per day (BPD). The well is located in an area with a NGR between 0.61 and 0.70, suggesting good porosity sandstone, and where we map 25,000 to 30,000 TDS water.

Hydrocarbon Production

The Mesaverde Group is a primary hydrocarbon producer in the UB, along with the Green River and Wasatch/Colton Formations. Natural gas is produced primarily from non-marine, lenticular, fluvial tight-gas sandstone packages within the Neslen, Farrer, and Tuscher Formations in the central and eastern UB, true to basin-centered gas systems, a model for deep, tight gas systems versus unconventional shale gas or coalbed methane systems (figure 6.25)

(Keighin and Fouch, 1981; Anderson, 2005; Wood and Chidsey, 2015). Sandstone reservoirs in the Mesaverde are generally discontinuous, isolated, lenticular bodies of fluvial origin deposited when rivers carried sediment from the west (landward) to the eastward-regressing Cretaceous Western Interior Seaway (Johnson and Roberts, 2003). Production from the Mesaverde Group is typically commingled with the Wasatch/Colton Formation. Though not as prevalent as natural gas, oil produced from the Mesaverde Group is waxy and has the characteristics of oils sourced from coal or coal-rich organic matter; the source may be from the lower Mesaverde (figure 6.27) (Lillis and others, 2003).

The Mesaverde Group (Mesaverde in table 6.6) between January 2009 and March 2015 produced approximately 4.5 thousand barrels of oil (MBO), 258.6 million cubic feet of gas (MMCFG), and 35.3 thousand barrels of water (MBW), and has an average gas-oil ratio (GOR) of 115,189 and an average oil-water ratio (OWR) of 0.20. Commingled Mesaverde production increases to approximately 4.7 MBO, 284 MMCFG, and 38 MBW, and has an average GOR of 213,372 and an average OWR of 0.12. The GOR and OWR from table 6.6 indicate that Mesaverde production will produce more water for disposal than Wasatch/Colton production in the UB.

UPPER PALEOCENE TO LOWER EOCENE WASATCH/COLTON FORMATION

Much of the Wasatch/Colton Formation formed when the paleo California River transported sediment from as far south as the Mojave region in present day California to the UB

and lapped onto the Douglas Creek arch (Dickinson and others, 2012). Previous studies (Osmond, 1964; Dickinson and others, 1986; Estes-Jackson and others, 2008) proposed the Wasatch/Colton formed as a result of erosion from nearby Laramide uplifts, or from recycled material from Laramide uplifts deposited by the California River (Wernicke, 2011), but detrital zircon ages, paleocurrents, and sandstone petrofacies indicate the southern portion, at least, had a more distant, southwestern source (Davis and others, 2010; Dickinson and others, 2012), and the northern portion of the formation may have formed from erosion of the Uinta Uplift (Franczyk and others, 1990b; Jones and Plink-Björklund, 2015). The Colton Formation was previously known as the upper member of the Wasatch Formation but gained formation status and comprises the beds between the Flagstaff Limestone and the Green River Formation (Spieker, 1946). The Wasatch is the section of rock between the Mesaverde and the Green River where the Flagstaff Limestone is not present (figure 2.13). We aggregate the Colton and Wasatch Formations for this study because they are time equivalent (Sendziak, 2012), their fauna are the same, both formed in a fluvial depositional environment (figure 6.1C and 6.1D), they have similar lithologies (Spieker, 1946), and the production as reported by DOGM is not separated.

Thickness

The Wasatch/Colton Formation is exposed along the Roan Cliffs. Mapped thicknesses range from 400 to over 4000 feet (figure 6.27). The unit is thickest in a northeasterly trending band starting north of Helper and extending toward Jensen in the northeastern UB and thins away from this curved band (figure 6.27). At depth, Nelson and Hoffman (2009) report the formation to be 3000 feet thick in the west and 2000 feet thick in the eastern UB.

Depth

The Wasatch/Colton Formation is exposed along the southern margin of the UB along the Roan and Book Cliffs (Witkind, 1988) and along a thin strip of the northeastern margin of the basin along Raven Ridge (Sprinkel, 2007). The UB is an asymmetrical syncline and, as mentioned above, units within the southern and central portions of the basin gently dip northwest whereas outcrops along the northern margin dip steeply to the south (figure 6.29) (Keighley, 2015). In the deepest area of the UB, the Wasatch/Colton reaches depths greater than 16,000 feet.

Lithology

The Wasatch/Colton Formation contains discontinuous, lenticular, fluvial, red to tan channel sandstones and variegated shale floodplain sediments that were deposited adjacent to Lake Uinta (figures 1.3 and 6.29) (Bredehoeft and others, 1994; Johnson and Roberts, 2003; Estes-Jackson and others, 2008; Nelson and Hoffman, 2009). Jones and Plink-Björklund (2013) divide the Wasatch/Colton into three packages: (1) a lower package containing isolated, filled, fluvial channels up to ~30 feet thick, interpreted to have been rapidly deposited; (2) a middle package composed of amalgamated, filled, fluvial channels up to ~100 feet thick, deposited in a system with a high depositional rate; and (3) an upper package with isolated sandstone channels up to ~50 feet thick, deposited at a moderate rate in a fluvial environment. The formation is thickest in the south-central UB (figure 6.27) and thins towards the margins of the basin

(Johnson, 2002). The thickest region curves from the Uinta Uplift in the northwest through the center of the basin and ends near Jensen, Utah (Franczyk and others, 1990b). Sandstones in the Wasatch/Colton record the progradational deltas marking the transition from the shallow Lake Flagstaff to Lake Uinta (Morris and others, 1991). Thick channel sandstones of the Wasatch Formation interfinger, and are equivalent to, the middle Green River Formation (Morgan, 2003a).

Reservoir Properties

We calculated several reservoir properties for the Wasatch/Colton interval. Two reservoir properties suggest the amount of sand and porous sand in a defined interval. Gross sand indicates the thickness of sand (in a particular well or interval) that means a particular GAPI classification. In our study, gross sand was defined as sand intervals with normalized GR values of <60 GAPI regardless of other parameters. Net sand is further defined as having a porosity value greater than or equal to a defined value. Correctly adjusted or calculated porosity from acoustic, density, or resistivity logs is used for the porosity comparison. In our study, net sand is defined as having a GR value less than or equal to 60 GAPI and acoustic (sonic) sandstone porosity greater than or equal to 6%.

The Colton area is a smaller percentage of the combined reservoir area. Appendix F lists the NGR sand parameters from GR and SPHI curves in the Wasatch/Colton Formation. The NGR was calculated using a minimum 6% porosity and a maximum 60 GAPI cutoff the net sand portion. The Wasatch/Colton interval has great thicknesses of sandstone and the NGR is generally over 50% (figure 6.31). The average porosity of the Wasatch/Colton Formation for the

entire UB area is 24%. Sixteen out of 44 wells have PHIA values less than 20%. The generally higher NGR and PHIA in this interval suggest favorable conditions for water disposal. Since the Wasatch is an oil reservoir in the central parts of the basin, it would lend itself to water flooding or injection for disposal.

Permeability of Wasatch Formation sandstones in the Greater Natural Buttes field area ranges from less than 0.1 mD to 0.1 mD with a median average permeability of 0.1 mD (Stancel and others, 2008). Estes-Jackson and others (2008) report Wasatch permeability values from 0.22 to 37 mD. Using values from the representative sonic logs, the average porosity for sandstones in the Wasatch and Colton equals about 16% and 15%, respectively (table 6.7),but these values decrease when adjusted for the presence of hydrocarbons. Porosity values within the Wasatch/Colton Formation have a wider range of values and higher average compared to the Mesaverde Group.

Water Quality

Water quality data from the Wasatch/Colton Formation predominantly range from brackish to brine (table 6.4; figures 6.31 and 6.33). We attempted to determine if Rw, Sw, and BVW data could be determined from SPHI, SP, and RESD logs and if they correlate to several water samples identified from the water sample database in appendix E. Appendix F shows Rw values for the Wasatch/Colton Formation. Higher Rw values, indicating fresher water, are found around the margins of the basin, likely directly related to recharge at the southern, eastern, and northern outcrops (figure 2.1). There is also a high Rw location at the approximate Three Rivers location north of Ouray and contiguous with the trend of the gilsonite dikes (figures 2.1, 3.1, and

3.7, plate 1). The Rw values calculated from well logs generally match those values calculated from laboratory samples. We predict however, that formation water from the Wasatch/Colton will have very low resistivity values indicating at least a saline and likely a brine water to treat. Calcium-sodium ratios from water in the Wasatch/Colton are higher in the western UB, possibly due to recharge from the Wasatch Plateau (figure 6.33). The Rw calculated from well logs and TDS from water samples appear to correlate. An Rw contour map from the Wasatch/Colton would reflect the TDS map presented in figure 6.32.

Water saturation was calculated using SPHI and SP curves from several wells. The Wasatch/Colton interval generally has 20 to 40% water saturation with pockets of 60 to 100% saturation. Higher (> 20%) saturations occur near regional features such as the gilsonite dikes (figure 2.1, plate 1) and along northern outcrops. Southern outcrop locations have a water saturation of approximately 20%. Although Sw data are sparse in the northern part of the basin, the closest available wells with data show high water saturation, and it is very likely that water saturation approaches 100% on the northwestern side of the basin, reflecting lower hydrocarbon concentration. However, the predicted Sw and BVW values could change if more data were available in the northwestern part of the UB. BVW values generally vary in the interval and are between 0.2% and 11%. A BVW approaching zero indicates irreducible water that is not available for flow. The existing BVW and Sw data suggest that water will flow from the formation and that the Wasatch/Colton possibly has pore space available for water disposal. As noted earlier, the Wasatch/Colton strata are highly interbedded sandstone and shale, but sandstone beds should be injectable and available for water flooding disposal purposes.

Water Production, Use, and Disposal

Significant water production occurs within oil and gas fields producing from the Wasatch/Colton Formation. These fields include Altamont, Antelope Creek, Big Valley, Bluebell, Buck Canyon, Cedar Rim, Devils Playground, Duchesne, Moffat Canal, Natural Buttes, Nine Mile Canyon, Peter's Point, Rock House, and Wonsits Valley (figures 1.1 and 6.23) (Wood and Chidsey, 2015). Cumulative water production from all fields producing from the Wasatch/Colton Formation from first production to January 1, 2015, totals nearly 1.2 billion barrels (table 6.5); again, production is commingled with additional producing formations in each field (Utah Division of Oil, Gas, and Mining, 2015c).

Figure 6.24 shows seven water disposal wells completed into either the Wasatch/Colton Formation, or a combination of North Horn and Wasatch/Colton Formations, or lower Green River and Wasatch/Colton Formations. Over 663 million barrels has been injected into the Wasatch/Colton Formation since the first completion in 1986 and up to March 2015. One water disposal well located in Bluebell field (figure 6.23) has been injecting since 1986. Figure 6.24 shows the injection volumes in red for the Wasatch/Colton disposal wells. Two wells, Lake Fork 2-23B4 (section 23, T. 2 S., R. 4 W., UBL&M, Duchesne County, API No. 43-013-30038) and Central Bluebell 2-26A (section 26, T. 1 S., R. 2 W., UBL&M, Duchesne County, API No. 43-013-30389) are private, fee-based disposal wells and have the highest injection rates of 2483 and 1103 BPD, respectively. The water injection rates into the private wells are two to three times higher than the injection rates for other wells in the same formations. The private wells are in an area with NGR values of 0.51 to 0.60, so they should have over 50% sand with high porosity. Typically, the injection rates in the Wasatch/Colton Formation are lower than the single Mesaverde Group disposal well rate of 431 BPD. This implies an overall lower NGR exists for

the disposal wells completed in the Wasatch/Colton. It may be difficult to locate and complete high porosity zones in the Wasatch/Colton that are not already producing hydrocarbons.

Produced water from the Wasatch/Colton Formation and Mesaverde Group presents challenges for disposal. The high salt concentration precludes surface disposal into river and stream drainage systems, it cannot be used for irrigation water without treatment, and it is expensive to evaporate. We believe that there are two options for disposing of produced water from the Mesaverde Group and the Wasatch/Colton Formation.

One treatment option would desalinate produced water to decrease the total dissolved solids to a level where the water can be used in hydraulic fracturing operations, possibly for irrigation water, or for other surface uses. We suggest that injection into sandstones of the Mesaverde Group or into the Wasatch/Colton Formation is a good second option, either as disposal or water flooding.

During our review and selection of formation tops for this project, we looked at numerous wells, and found several candidate sandstones for injection throughout the UB. For example, NBU No. 921-21L (section 21, T. 9 S., R. 21 E., SLB&M, Uintah County, API No. 43-047-39256) in Natural Buttes field was drilled and completed in 2008, has good logs, and available core data. Figure 6.34 is the NBU No. 921-21L well log from 8200 to 8500 feet measured depth started 60 feet above the top of the Tuscher Formation and extending approximately 240 feet below the upper contact. The zone was selected because it has three prominent, thick sandstone channels that can be traced laterally in several wells. Figure 6.34 shows the three identified sandstone channels, labeled S1, S2, and S3, with their measured depths and thickness. The GR log indicates they are essentially clean sands, and the NPHI and DPHI logs show gas crossover and an average porosity of 10 to 11%. Although these are gas

producing units, we calculated the radial volumetric storage potential of the three sandstones and present our results in table 6.8. The table presents 10-foot radial increments from the 8200- to 8500-foot interval. At radial distances of 100 and 1000 feet from the well, we estimate storage of 42,375 and 4.2 MMBW, respectively, in the three sandstone channels. We did not attempt to calculate the radial flow rate using the Darcy equation as part of this study so the time involved in injecting this amount of water is unknown. There are likely hundreds of candidate sandstone channels in the Mesaverde Group formations. We believe other suitable sandstone channels exist in the Wasatch/Colton Formation interval as well; however, we think water disposal there will be less favorable since the sandstones are typically interbedded with siltstone. We believe the Mesaverde Group can provide good injection zones for water disposal in areas where they are not gas productive.

Hydrocarbon Production

Hydrocarbons produced from the Wasatch/Colton Formation are primarily found in channel sandstones and are interpreted to have been sourced from coals and carbonaceous shales in the Mesaverde Group (Lillis and others, 2003; Nelson and Hoffman, 2009). Production from the Wasatch/Colton is often commingled with the Mesaverde Group, and the Green River Formation, North Horn Formation, and Flagstaff Limestone. Table 6.6 shows the oil, gas, and water production since January 2009 through March 2015 from wells producing from the Wasatch and Mesaverde. Graphical production reports are presented in figures 6.25 and 6.26. In many parts of the UB, the Wasatch/Colton is overlain by the Uteland Butte Limestone member of the lower Green River Formation, which currently produces oil.

The Wasatch/Colton Formation produces oil from over 4500 feet of strata, up to 16,000 feet deep, and first become a target for horizontal drilling in the early 1990s (Chidsey and Laine, 1992). As observed in table 6.6, the Wasatch/Colton Formation interval produced 13.3 MMBO, 156 BCFG, and over 36 MMBW. The average GOR is 135,215 while the average OWR is 0.32. If commingled Wasatch production (Wasatch in table 6.6) is taken into account, approximately 21.9 MBO, 1655 MMCFG, and 161 MBW have been produced with a GOR of 139,730 and an OWR of 0.17.

SUMMARY

The Cretaceous Mesaverde Group, and major producer of gas from tight-sand reservoirs, is more than 2000 feet thick in much of the UB; the upper formations of the Group may provide favorable locations for water disposal. Drilling depths for the Mesaverde Group may exceed 19,000 feet. Much of the Mesaverde was deposited in a fluvial environment, and lithologies are variable. Water types range from brackish to brine, and the freshest samples occur along the margins of the Uinta Basin. Hydrocarbons and associated water from the Mesaverde Group are predominantly produced in the eastern and southern Uinta Basin.

GR and SP curves for 115 wells were normalized and corrected to regional high and low response. Porosities from acoustic and density curves were recalculated to sandstone porosity. The average sandstone porosity in the Mesaverde Group is 21%, ranging between 13 and 35%. A few permeability values were obtained from DST test and a few core tests and range between 0.1 mD on the high end to 0.001 mD on the low side. The Mesaverde NGR is 0.76 indicating significant sand with porosity greater than 6%. The Bluecastle Tongue and lower members of

the Castlegate Sandstone have the lowest NGR in the group at 0.58 and 0.61, respectively. They have typically less gross sand and lower porosities in the sand. The Sego, Farrer, and Tuscher Formations of the Mesaverde Group have the highest NGR values at 0.79, 0.74, and 0.83, respectively. However, the Sego Sandstone has the lowest average gross sand thickness at 79 feet. The Farrer and Tuscher Formations have average gross sand thicknesses of 150 and 211 feet. We believe that the Farrer and Tuscher are good candidates for disposal wells. Both formations, particularly the Tuscher Formation, have thick-blocky sandstones that have good porosity. We calculated that three sandstone channels, or approximately 40 feet of sandstone, would be able to dispose of 4.2 MMBW in a 1000-foot radius around a well.

The Paleocene to Eocene Wasatch/Colton Formation, the other major producer of gas from tight-sand reservoirs in the UB, ranges in thickness from 400 to over 4000 feet and may provide locations suitable for waste water disposal. Drilling depths to the Wasatch/Colton Formation may exceed 16,000 feet. Most of the water samples from the formations range from brackish to brine. Hydrocarbons and associated water from the Wasatch/Colton are produced throughout the central UB.

The Wasatch/Colton Formation has an average sandstone porosity of 24%, and the average permeability is 0.1 mD (table 6.9). The average NGR is 0.67, significantly less than typical Mesaverde Group. The Wasatch/Colton has a higher average gross sand thickness at 2232 feet but less sand with porosities greater than 6%. The Wasatch/Colton is typically siltier and has thinner sandstone beds. We believe there are probably areas of the Wasatch/Colton where sufficient thicknesses of sand are available for water disposal. However, disposal would require long perforated zone or very targeted zones.

Many water quality samples were identified from the Wasatch and commingled Wasatch. The common case is that water samples are collected from large perforated zones crossing formation boundaries. However, many were identified within the Wasatch/Colton Formation. Fresh to brackish water is typically found up to several miles from the southern outcrop locations of the Wasatch/Colton Formation. Water in the interior of the basin is saline and marginally briny. Several areas with fresher water or higher Rw values (0.3 to 0.5), near Ouray suggest possible connection to shallower, lower-TDS surface water. Ca–Na ratios show that surface recharge is dissolving the Paleocene Flagstaff Limestone and flowing into the lower Wasatch Formation. Water samples from the Mesaverde Group in very close proximity to the southern Roan and Book Cliffs outcrops and along the north and northeastern outcrops are fresh. However, within a short distance into the basin, the water samples are saline to brine in almost all of the Mesaverde. Rw values are typically 0.1 to 0.3 indicating very low resistance. Ca–Na values in the Mesaverde also show mixing with carbonate waters from the Flagstaff. This suggests likely hydrologic connections between the Wasatch and underlying formations and/or updip carbonaceous formations in the UB.

One water disposal well currently injects into the Castlegate Sandstone. The average disposal rate is 431 BPD, which is significantly lower than the production rate. Seven disposal wells inject into the Wasatch/Colton intervals. Approximately 663 million barrels of produced water has been disposed in the interval by the seven wells. The average injection rate is similar to or lower than the Castlegate well except for two private disposal sites with rates of 2483 and 1103 BPD. The private wells are likely injecting into much longer perforated zones or at higher pressure.

We believe there are sandstones in the Wasatch/Colton interval that are candidates for water disposal. However, they will require targeting very specific sandstones or need long perforated zones, both costly to perform. The Mesaverde Group does have candidate sandstone for water disposal. The Farrer and particularly the Tuscher Formations, in the middle to eastern side of the basin, have thick, stacked sandstone channels with good porosity that can accommodate produced water.

CHAPTER VI FIGURES

Figure 6.1. Paleogeographic maps show the Sevier highlands west of the Uinta Basin area, Laramide uplifts including the Uinta Mountains and the San Rafael Swell, and the eastward regression of the Cretaceous Western Interior Seaway (A and B). Rivers flowed across the coastal and alluvial plain from the Sevier highlands, north from the distant Mojave region, and south from the Uinta uplift during deposition of the formations discussed in this study (C and D). Figures modified from Blakey and Ranney (2008).

Figure 6.2. Index map of the Wasatch/Colton Formation and Mesaverde Group. Index map indicates the different sources of data for geology and chemistry and cross sections.

Figure 6.3. Gamma-ray trend across the Uinta Basin based on normalizing GR curves. Zone 1 is the western third of the basin; Zone 2 is the central third, and Zone 3 is the eastern third. The

type well for each zone penetrates the formations addressed in this study and has a complete suite of well logs.

Figure 6.4. Isopach of the entire Mesaverde Group. The contour range is 0 to 3500 feet, and the contour interval is 500 feet. Tops data are from Anderson (2005), Hettinger and Kirschbaum (2002), and selected from well logs as part of this study.

Figure 6.5. Structure of the top of the Mesaverde Group. The contour range is -7000 to 8500 feet, and the contour interval is 1000 feet. The Mesaverde is exposed along the southern boundary of the Uinta Basin in the Book Cliffs and dips gently to the north. Mesaverde Group rocks are also exposed on the north and northeast portion of the basin. Tops data are from Anderson (2005), Hettinger and Kirschbaum (2002), and selected from well logs as part of this study.

Figure 6.6. Classic Mesaverde Group along the Book Cliffs northwest of Green River.

Figure 6.7. Representative Mesaverde Group outcrops of the Blackhawk, Castlegate, and Price River Formations in the eastern half of the Uinta Basin. A – The Blackhawk Formation underlies the Castlegate Sandstone and is composed of interbedded sandstone, siltstone, shale, and coal. B – The Castlegate Sandstone is composed of massive sandstones deposited in a braided stream environment. C – The Price River Formation overlies the Castlegate Sandstone and is composed of poorly sorted siltstone and ledge-forming sandstone beds deposited in a fluvial environment.

Figure 6.8. Isopach of the lower Castlegate Sandstone. The contour range is 0 to 1000 feet, and the contour interval is 50 feet. Tops data are from Anderson (2005), Hettinger and Kirschbaum (2002), and picks from well logs from additional wells as part of this study.

Figure 6.9. Schematic block diagram of a braided stream environment (modified from Howell and Flint, 2005). Castlegate Sandstone was deposited in a braided stream environment as sediments were eroded from the Sevier highlands in western Utah and transported eastward to the Cretaceous Western Interior Seaway.

Figure 6.10. Castlegate Sandstone overlying the Desert Member of the Blackhawk Formation and the Mancos Shale at the mouth of Thompson Canyon, east of Green River.

Figure 6.11. Isopach of the Bluecastle Sandstone Member of the Castlegate Sandstone. The contour range is 0 to 750 feet, and the contour interval is 50 feet. The coarse-grained, pebbly unit is thickest in the northwestern region of the Uinta Basin and pinches out into the Neslen Formation in Sego Canyon to the southeast (Hettinger and Kirschbaum, 2002). Tops data are from Anderson (2005), Hettinger and Kirschbaum (2002), and from well logs used as part of this study.

Figure 6.12. Typical outcrops of the (A) Farrer Formation and (B) the overlying Tuscher Formation; Sego Canyon.

Figure 6.13. Excellent outcrops of the Mesaverde Group in Sego Canyon. A – The Buck Tongue of the Mancos Shale underlies the Sego Sandstone, above which are the Neslen and Farrer Formations. B – The Sego Sandstone is overlain by the heterogeneous Neslen Formation. C – The Neslen Formation contains several coal-bearing layers deposited in a coastal plain (Franczyk and others, 1990a).

Figure 6.14. Isopach of the Buck Tongue of the Mancos Shale. The contour range is 0 to 500 feet, and the contour interval is 50 feet. The Buck Tongue is thickest in the eastern Uinta Basin (seaward) and thins to the west (landward). Tops data are from Anderson (2005), Hettinger and Kirschbaum (2002), and picked from well logs as part of this study.

Figure 6.15. Combined isopach of the middle Castlegate Sandstone in the west and Sego Sandstone and Neslen Formation in the east. The contour range is 100 to 1000 feet, and the contour interval is 100 feet. The Castlegate is thickest in the western portion of the Uinta Basin and thins to the east. Tops data are from Anderson (2005), Hettinger and Kirschbaum (2002), and picks from well logs from additional wells as part of this study.

Figure 6.16. Combined isopach of the Price River Formation in the west and the Tuscher and Farrer Formations in the east. The contour range is 4386 to 1800 feet, and the contour interval is 200 feet. The Price River is thickest in the northwestern region of the Uinta Basin, thins in the middle of the basin, and splits into the thick-again Tuscher and Farrer Formations in the eastern portion of the basin. Tops data are from Anderson (2005), Hettinger and Kirschbaum (2002), and picked from well logs as part of this study.

Figure 6.17. Buck Tongue of the Mancos Shale, overlain by the Sego Sandstone and the coal-bearing Neslen Formation, Tusher Canyon.

Figure 6.18. Net to gross ratio of sands within the Mesaverde Group.

Figure 6.19. Calculated TDS with depth in the Mesaverde Group (number of samples: fresh – 13, brackish – 20, saline – 34, brine – 33).

Figure 6.20. TDS map of the Mesaverde Group. Contour intervals are 5000 mg/L. Data is from water samples from wells perforated in the Mesaverde and do not correspond to the wells used for the formation tops and thicknesses.

Figure 6.21. Stiff diagrams from water samples sourced from the Mesaverde Group. Samples are freshest along the edges of the Uinta Basin and become saline in the basin interior.

Figure 6.22. Calcium/sodium ratio map for Mesaverde Group water. The Ca–Na ratio reveals the location and extent of the Paleocene Flagstaff Limestone as groundwater leaches calcium-rich fluids into the Mesaverde from the overlying carbonate.

Figure 6.23. Cumulative water production from Mesaverde Group and/or the Wasatch/Colton Formation gas reservoirs in Uinta Basin fields. Production from a particular formation is not

reported separately so data used in this map combine production from all producing formations in the field.

Figure 6.24. Locations and volumes for water disposal wells into the Mesaverde Group and Wasatch/Colton Formation.

Figure 6.25. Cumulative natural gas production (in MCF) from Mesaverde Group and/or the Wasatch/Colton Formation reservoirs in Uinta Basin fields. Production from a particular formation is not reported separately so data used in this map combine production from all producing formations in the field. Names in red denote field that produce(d) primarily nonassociated natural gas whereas those in green primarily produce(d) oil. The field areas are color-coded by geologic age of the producing reservoirs; symbols of the producing reservoirs are listed under the field names (see figure 2.1 for age and formation names). Field designations are also listed under the field names: (A) = abandoned, (CBM) = coalbed methane, (D) = produced water disposal project, (HD) = horizontal drilling, (SI) = shut-in field, (WF) = waterflood project. Modified from Wood and Chidsey, 2015.

Figure 6.26. Cumulative crude oil production (in barrels [bbls]) from Mesaverde Group and/or the Wasatch/Colton Formation reservoirs in Uinta Basin fields. Production from a particular formation is not reported separately so data used in this map combine production from all producing formations in the field. Names in red denote field that produce(d) primarily nonassociated natural gas whereas those in green primarily produce(d) oil. The field areas are color-coded by geologic age of the producing reservoirs; symbols of the producing reservoirs are

listed under the field names (see figure 2.1 for age and formation names). Field designations are also listed under the field names: (A) = abandoned, (CBM) = coalbed methane, (D) = produced water disposal project, (HD) = horizontal drilling, (SI) = shut-in field, (WF) = waterflood project. Modified from Wood and Chidsey, 2015.

Figure 6.27. Isopach for the Colton/Wasatch Formation. The contour range is 0 to 5000 feet, and the contour interval is 500 feet. Tops data are from Anderson (2005), Hettinger and Kirschbaum (2002), and selected from well logs as part of this study.

Figure 6.28. Structure of the top of the Wasatch/Colton combined formations. Contour interval is 500 feet. Tops data are from Anderson (2005), Hettinger and Kirschbaum (2002), and selected from well logs as part of this study.

Figure 6.29. Representative outcrops of the Wasatch/Colton Formation. A – Outcrop of the Wasatch/Colton Formation at Whitmore Park along the western Roan Cliffs. The formation in this locality is composed of red to tan silty slopes and cliff-forming channel sandstone that pinch out laterally. B – A closer view of the Wasatch/Colton Formation at along the Green River in Desolation Canyon, southern Uinta Basin. Photos courtesy of Craig D. Morgan, UGS.

Figure 6.30. Net to gross ratio of sands within the Wasatch/Colton Formation.

Figure 6.31. Calculated TDS with depth in the Wasatch/Colton Formation (number of samples: fresh – 5, brackish – 129, saline – 178, brine – 45).

Figure 6.32. TDS map of the Wasatch/Colton Formation. Contour intervals are 5000 mg/L.

Figure 6.33. Calcium–sodium ratio map for the Wasatch/Colton Formation water. The Ca–Na ratio values from the Wasatch/Colton are highest in the western Uinta Basin.

Figure 6.34. Wells log for NBU No. 921-21L, Natural Buttes field, revealing three large sandstone packages in the upper Tuscher Formation. Modeled sandstones have been identified as S1, S2, and S3 on the left side of illustration. Sandstone thickness is presented on the right side of the graphic.

CHAPTER VI TABLES

Table 6.1. Porosity values from sonic logs within the Mesaverde Group.

Table 6.2. Porosity and permeability from the NBU No. 253 core, Natural Buttes field.

Table 6.3. Porosity and permeability from the NBU No. 921-21L core, Natural Buttes field.

Table 6.4. Water classification based on total dissolved solids (Masters and Ela, 2007).

Table 6.5. Cumulative production through December 2014 from the Utah Division of Oil, Gas, and Mining (2015c); several fields produce from both the Wasatch Formation and the Mesaverde Group, and their water production is commingled.

Table 6.6. Total oil, gas, and produced water between January 2009 and March 2015 for producing zones in the Wasatch and Mesaverde Group. The formations generally show combined perforations. Wasatch and Mesaverde production is summarized at the bottom of the table.

Table 6.7. Porosity values from sonic logs within the Wasatch/Colton Formation.

Table 6.8. Calculated volume of water storage per radial foot in three Tuscher Formation channel sandstones from the NBU No. 921-12L gas well, Natural Buttes field.

Table 6.9. Reservoir properties Wasatch/Colton Formation and Mesaverde Group. The Colton/Wasatch values are combined values. The Mesaverde values were calculated for the entire thickness from the top of the Price River Formation – Tuscher Formation to the base of the lower Castlegate Sandstone. The Castlegate values are inclusive of Bluecastle Sandstone Member, and middle and lower members.

Table 6.1. Porosity values from sonic logs within the Mesaverde Group.

Producing Reservoir	Count	PHIS[1] (average)	Gas Adjustment[2]	Oil Adjustment[2]
Mesaverde Group	33	0.146	0.102	0.131
Price River Formation	35	0.154	0.108	0.139
Tuscher Formation	26	0.162	0.113	0.146
Farrer Formation	28	0.155	0.109	0.140
Castlegate Sandstone	35	0.131	0.092	0.118
Bluecastle Sandstone Member, Castlegate Sandstone	25	0.115	0.081	0.104
Middle Castlegate Sandstone	34	0.153	0.107	0.138
Neslen Formation	25	0.156	0.109	0.140
Sego Sandstone	25	0.150	0.105	0.135
Lower Castlegate Sandstone	34	0.114	0.080	0.103

[1]PHIS is the sandstone matrix porosity and not reflective of the entire formation.

[2]Gas adjustment is 70% of the PHIS and oil adjustment is 90% of the PHIS.

Table 6.2. Porosity and permeability from the NBU No. 253 core, Natural Buttes field.

Depth (ft)	Permeability (mD)	Porosity (%)
10,532	162.330	2.06
10,572	0.068	5.69
10,580	0.007	5.13
10,612	0.042	5.74
10,651	0.007	3.88
10,677	0.007	5.43
10,700	0.007	5.72

Table 6.3. Porosity and permeability from the NBU No. 921-21L core, Natural Buttes field.

Depth (ft)	Permeability (mD)	Porosity (%)
9325.8	0.011	5.79
9326.8	0.002	4.22
9333.8	0.001	3.33
9340.8	0.001	2.53
9342.8	0.001	2.03
9348.8	0.001	2.30
9352.8	0.005	2.15
9354.8	0.002	1.62
9356.8	0.001	2.26
9358.8	0.005	5.29
9360.8	0.002	4.13
9362.8	0.014	4.07
9364.8	0.003	4.04
9366.8	0.001	0.57
9368.8	0.001	1.04
9372.8	0.003	2.84
9374.8	0.002	2.68
9376.8	0.004	2.39
9378.8	0.009	2.90
9379.8	0.002	1.94
9382.8	0.001	2.51
9384.8	0.005	3.13
9387.8	0.007	5.29
9390.8	0.002	4.37
9394.8	0.001	3.73
9396.8	0.004	5.59
9398.8	0.002	4.58
9399.8	0.002	2.25
9401.8	0.003	2.95
9403.8	0.008	5.55
9405.8	0.014	7.65
9406.8	0.020	8.64
9407.8	0.019	8.36
9409.8	0.009	6.11
9411.8	0.031	3.46
9413.8	0.001	1.85
9424.8	0.000	0.43
9427.8	0.000	2.27
9429.8	0.000	1.83

Table 6.4. Water classification based on total dissolved solids (Masters and Ela, 2007).

Water Classification	Total Dissolved Solids (mg/L)
Fresh water	<1000
Brackish water	1000-10,000
Saline water	10,000-30,000
Brine	>30,000

Table 6.5. Cumulative production through December 2014 from the Utah Division of Oil, Gas and Mining (2015c); several fields produce from both the Wasatch Formation and the Mesaverde Group, and their water production is commingled.

Producing Reservoir	Cumulative Oil (bbls)	Cumulative Gas (MCF)	Cumulative Water (bbls)
Wasatch	451,040,245	4,782,087,711	1,179,713,835
Mesaverde	151,041,333	4,540,565,692	668,422,168

Table 6.6. Total oil, gas, and produced water between January 2009 and March 2015 for producing zones in the Wasatch and Mesaverde Group. The formations generally show combined perforations. Wasatch and Mesaverde production is summarized at the bottom of the table.

Producing Reservoir	Total Oil (bbls)	Total Gas (MCF)	Total Produced Water (bbls)	Average Gas-Oil Ratio	Average Oil-Water Ratio	Average Gas-Water Ratio
Mesaverde - Lower Douglas Creek Member, Green River Formation	-	220,692	95,186	-	0.00	3600
Mesaverde - Middle Douglas Creek Member, Green River Formation	-	139,642	75	-	0.00	333
Mesaverde - Mancos Shale	183,884	24,854,696	2,597,971	363,125	0.21	16,746
Mesaverde	4,534,438	258,675,908	35,383,530	115,189	0.20	15,560
Mesaverde - North Horn	589	392,231	6033	588,548	0.19	151,043
Mesaverde - Flagstaff	5028	7987	32,922	534	0.09	102
Wasatch - North Horn	255	107,574	2283	45,925	0.03	10,894
Wasatch - Mesaverde	8,344,623	1,483,576,425	123,247,961	378,615	0.15	42,721
Wasatch - Middle Mesaverde	249,077	15,756,764	1,971,082	138,363	0.24	22,114
Wasatch - Colton	13,336,887	156,082,095	36,037,750	135,215	0.32	56,204
Wasatch	21,935,870	1,655,530,845	161,291,998	139,730	0.17	26,407
Mesaverde	4,718,911	284,283,169	38,082,795	213,372	0.12	37,456

Table 6.7. Porosity values from sonic logs within the Wasatch/Colton Formation.

Formation	Count	PHIS (average)	Gas Adjustment	Oil Adjustment
Wasatch	24	0.16	0.112	0.144
Colton	32	0.15	0.105	0.135

Table 6.8. Calculated volume of water storage per radial foot in three Tuscher Formation channel sandstones from the NBU No. 921-12L gas well, Natural Buttes field.

		Radial Distance from Well (ft)														
		10	20	30	40	50	60	70	80	90	100	200	400	600	800	1000
Sandstone	**S1**															
Top (ft)	8263								Hydrostatic Head in Well: 3801 psi							
Bottom (ft)	8282															
Thickness (ft)	19															
Porosity (v/v)	0.11															
Volume (ft^3)		5969	23,876	53,721	95,504	149,226	214,885	292,482	382,018	483,491	596,903	2,387,610	9,550,442	21,488,493	38,201,766	59,690,259
Barrels of Water		156	624	1403	2495	3898	5613	7640	9979	12,630	15,592	62,368	249,474	561,316	997,895	1,559,211
Sandstone	**S2**															
Top (ft)	8321								Hydrostatic Head in Well: 3828 psi							
Bottom (ft)	8336															
Thickness (ft)	15															
Porosity (v/v)	0.10															
Volume (ft^3)		4712	18,850	42,412	75,398	117,810	169,646	230,907	301,593	381,704	471,239	1,884,956	7,539,822	16,964,600	30,159,289	47,123,889
Barrels of Water		112	448	1007	1790	2798	4029	5483	7162	9064	11,191	44,762	179,048	402,858	716,193	1,119,051
Sandstone	**S3**															
Top (ft)	8340								Hydrostatic Head in Well: 3836 psi							
Bottom (ft)	8359															
Thickness (ft)	19															
Porosity (v/v)	0.11															
Volume (ft^3)		5969	23,876	53,721	95,504	149,226	214,885	292,482	382,018	483,491	596,903	2,187,610	9,550,442	21,488,493	38,201,766	59,690,259
Barrels of Water		156	624	1403	2495	3898	5613	7640	9979	12,630	15,592	62,368	249,474	561,316	997,895	1,559,211
Barrels of Water		424	1695	3814	6780	10,594	15,255	20,763	27,120	34,324	42,375	169,498	677,996	1,525,490	2,711,983	4,237,473
Gallons of Water (42 gal/bbl)		17,797	71,190	160,176	284,758	444,935	640,706	872,072	1,139,033	1,441,588	1,779,739	7,118,955	28,475,819	64,070,593	113,903,277	177,973,870

Note: The top, bottom, and porosity (v/v = volume/volume) of the S1, S2, and S3 sandstone channels in the Tuscher Formation were picked from the well log of the NBU No. 921-21L. The well log is shown in figure 6.34. Hydrostatic head (pounds per square inch [psi]) at the top of the zone is provided for a column of saline water. Volume (ft^3) is the pore volume at the radial distance from the well. The barrels of water are storage volumes and do not indicate radial flow from the well.

Table 6.9. Reservoir properties Wasatch/Colton Formation and Mesaverde Group. The Colton/Wasatch values are combined values. The Mesaverde values were calculated for the entire thickness from the top of the Price River Formation – Tuscher Formation to the base of the lower Castlegate Sandstone. The Castlegate values are inclusive of Bluecastle Sandstone Member, and middle and lower members.

Producing Reservoirs	Average Net Sand >6% Porosity (ft)	Average Gross Sand (ft)	Average Net to Gross Sand (NGR)	Average Porosity (PHIA, %)	Average Unit Thickness (ft)	Minimum Thickness (ft)	Maximum Thickness (ft)
Colton/Wasatch	1340	2232	0.67	24	2312	330	4677
Mesaverde Group	1528	2042	0.76	21	2121	894	3089
Price River Formation	283	435	0.68	15	1255	490	1702
Tuscher Formation	116	150	0.79	16	504	193	783
Farrer Formation	167	211	0.74	15	777	255	1296
Bluecastle Sandstone Member, Castlegate Sandstone	53	108	0.58	13	193	24	725
Middle Castlegate Sandstone	85	125	0.69	14	445	145	814
Neslen Formation	87	110	0.78	15	475	169	814
Sego Sandstone	59	79	0.83	15	182	83	287
Lower Castlegate Sandstone	77	143	0.61	12	157	8	370
Castlegate Sandstone	201	342	0.64	13	727	8	2382

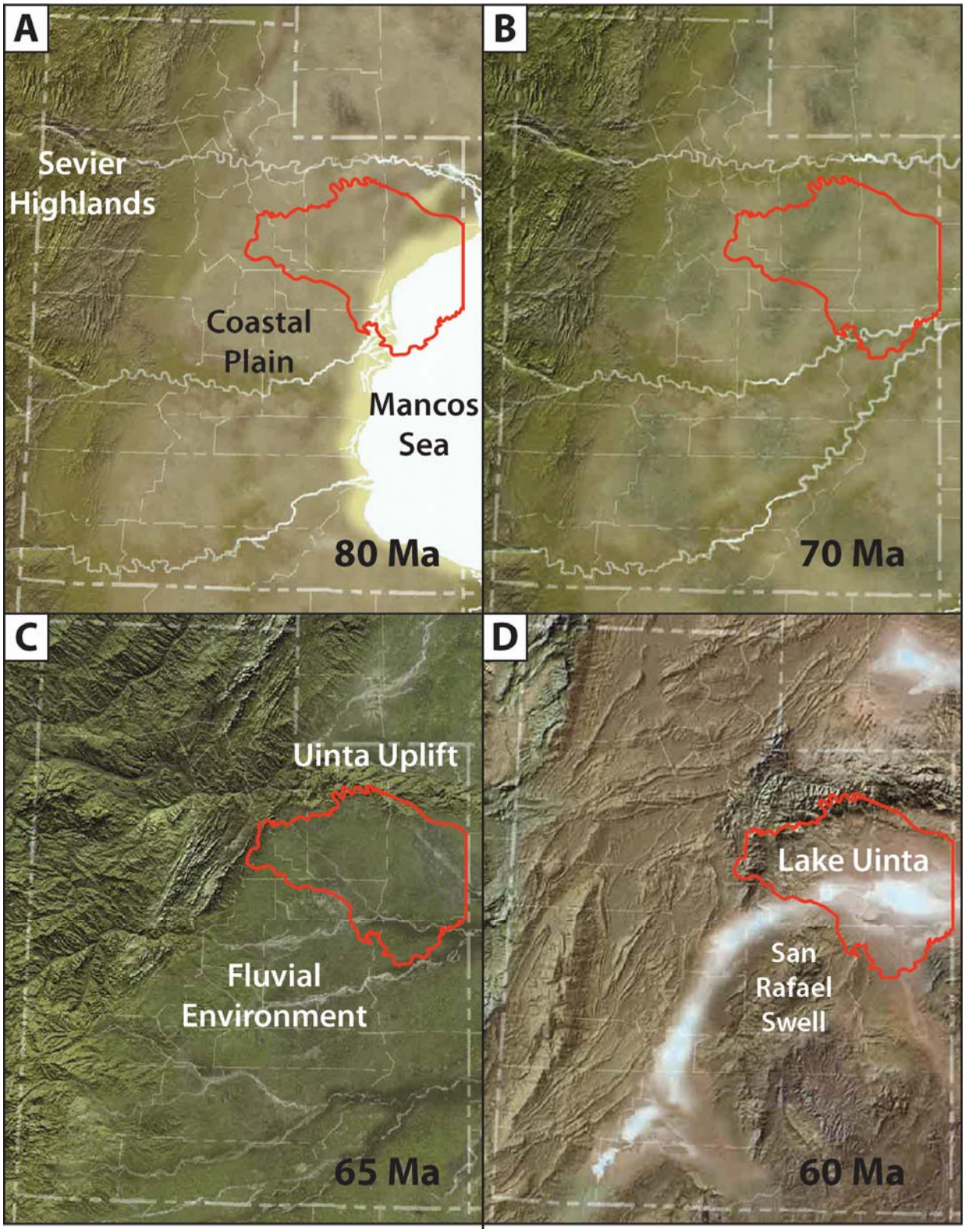

Figure 6.1. Paleogeographic maps show the Sevier highlands west of the Uinta Basin area, Laramide uplifts including the Uinta Mountains and the San Rafael Swell, and the eastward regression of the Cretaceous Western Interior Seaway (A and B). Rivers flowed across the coastal and alluvial plain from the Sevier highlands, north from the distant Mojave region, and south from the Uinta uplift during deposition of the formations discussed in this study (C and D). Figures modified from Blakey and Ranney (2008).

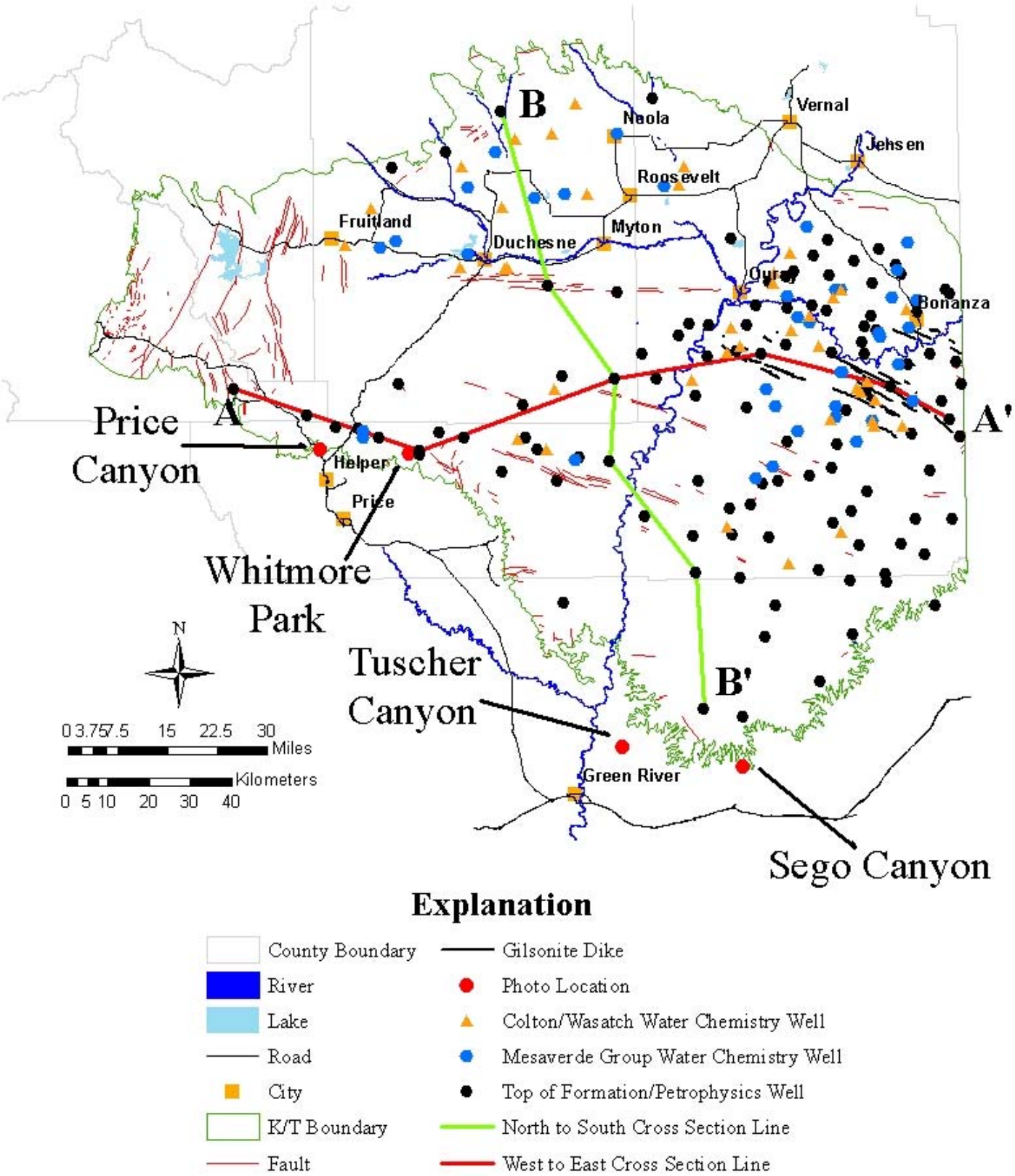

Figure 6.2. Index map of the Wasatch/Colton Formation and Mesaverde Group. Index map indicates the different sources of data for geology and chemistry and cross sections.

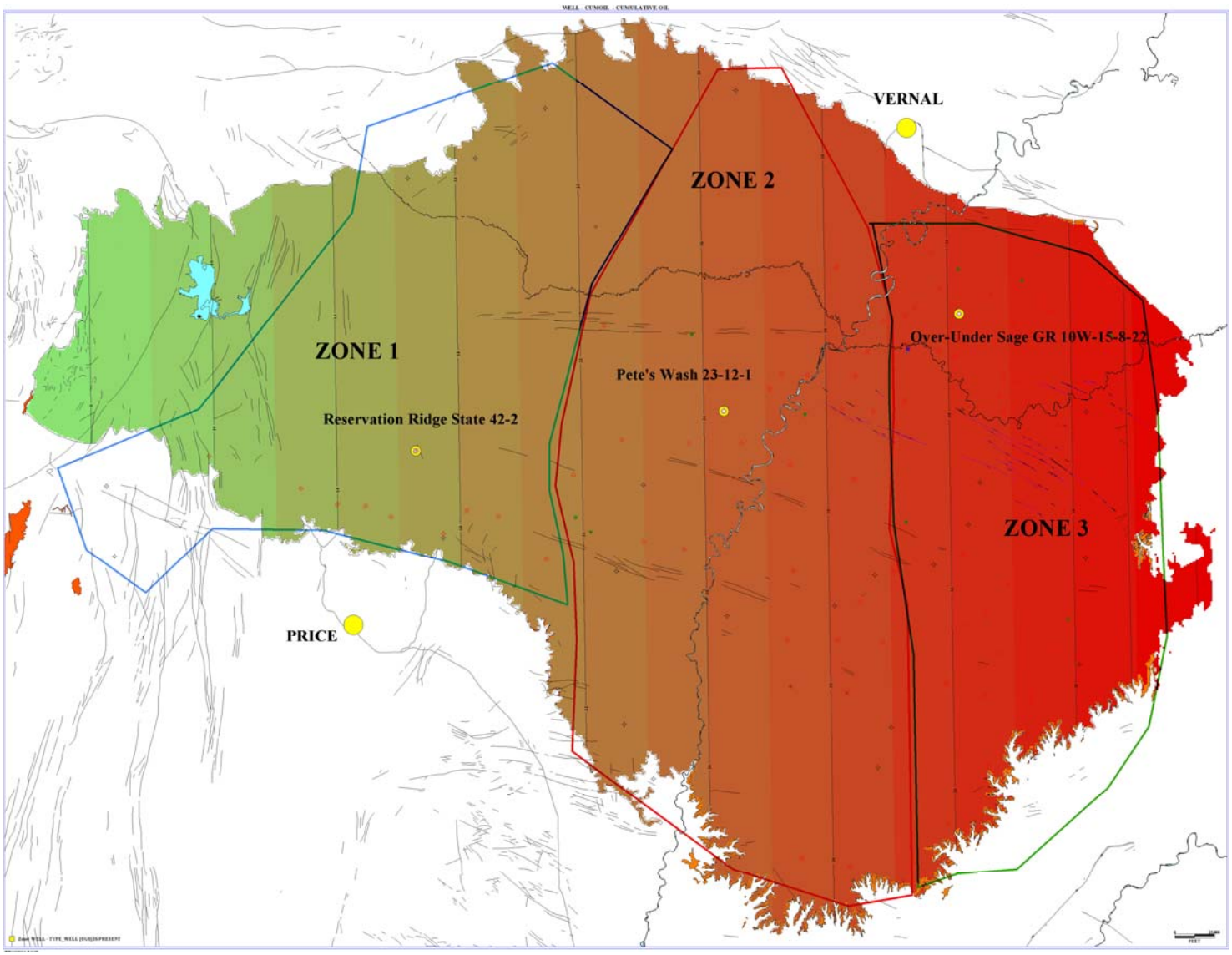

Figure 6.3. Gamma-ray trend across the Uinta Basin based on normalizing GR curves. Zone 1 is the western third of the basin; Zone 2 is the central third, and Zone 3 is the eastern third. The type well for each zone penetrates the formations addressed in this study and has a complete suite of well logs.

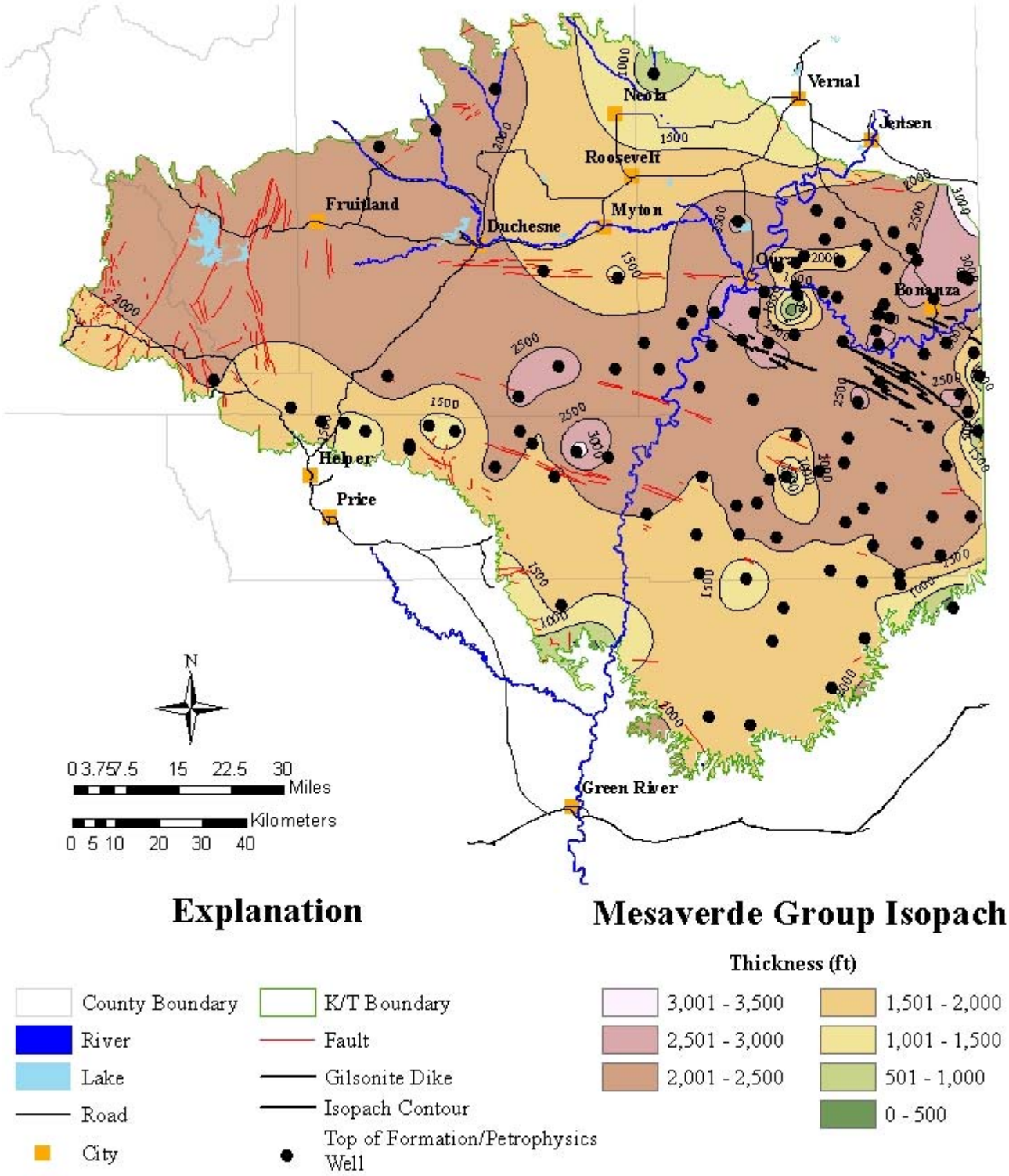

Figure 6.4. Isopach of the entire Mesaverde Group. The contour range is 0 to 3500 feet, and the contour interval is 500 feet. Tops data are from Anderson (2005), Hettinger and Kirschbaum (2002), and selected from well logs as part of this study.

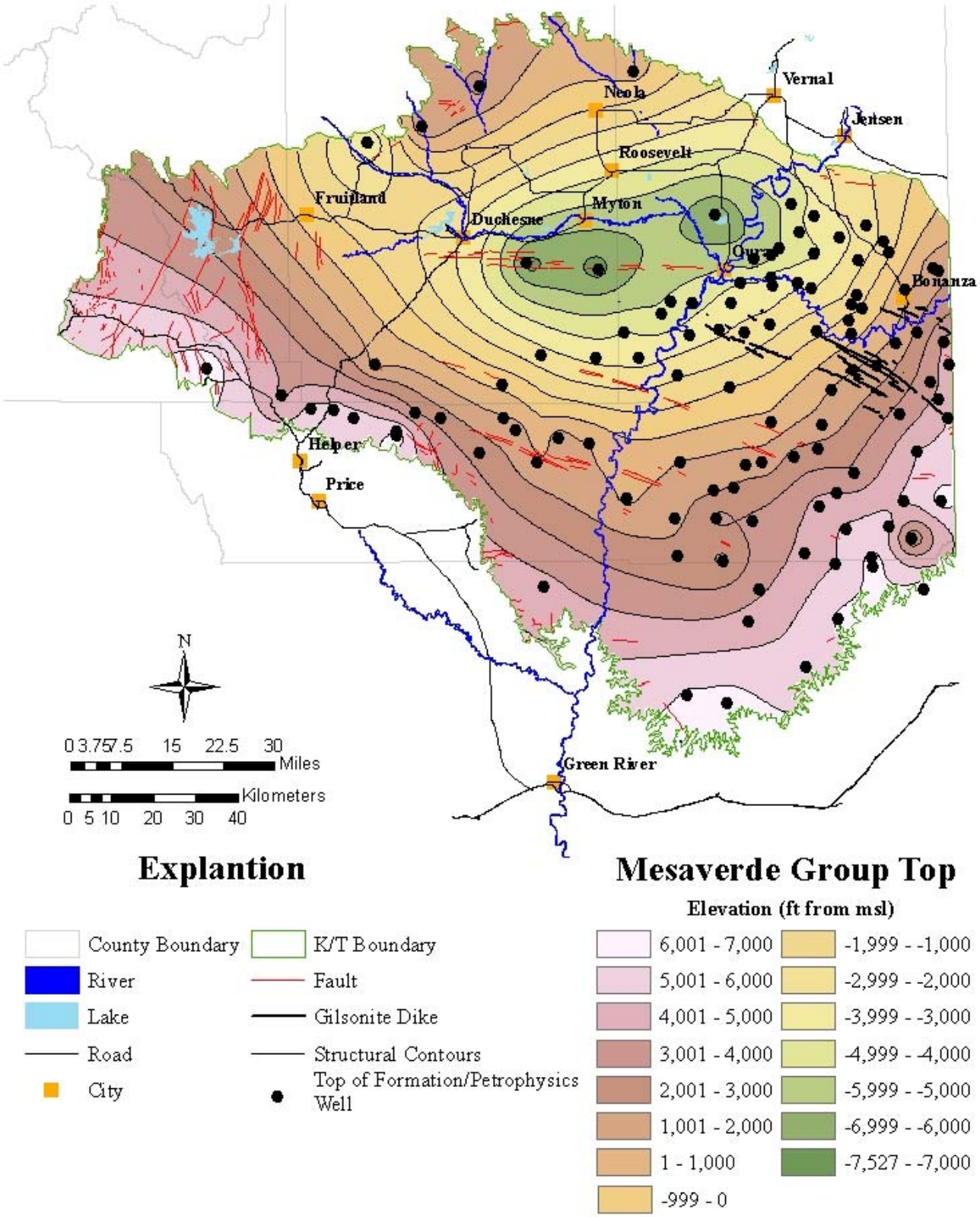

Figure 6.5. Structure of the top of the Mesaverde Group. The contour range is -7000 to 8500 feet, and the contour interval is 1000 feet. The Mesaverde is exposed along the southern boundary of the Uinta Basin in the Book Cliffs and dips gently to the north. Mesaverde Group rocks are also exposed on the north and northeast portion of the basin. Tops data are from Anderson (2005), Hettinger and Kirschbaum (2002), and selected from well logs as part of this study.

Figure 6.6. Classic Mesaverde Group along the Book Cliffs northwest of Green River.

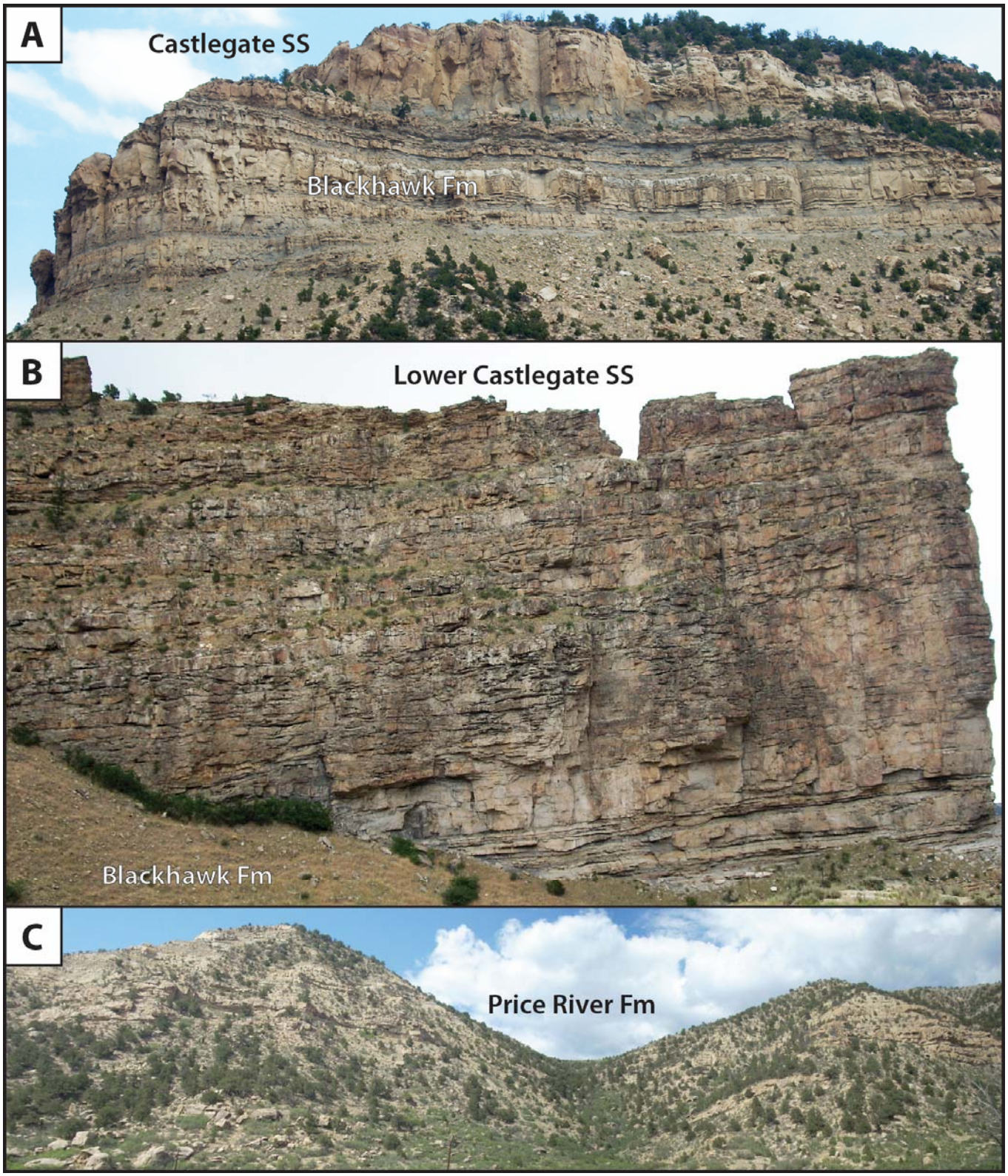

Figure 6.7. Representative Mesaverde Group outcrops of the Blackhawk, Castlegate, and Price River Formations in the eastern half of the Uinta Basin. A – The Blackhawk Formation underlies the Castlegate Sandstone and is composed of interbedded sandstone, siltstone, shale, and coal. B – The Castlegate Sandstone is composed of massive sandstones deposited in a braided stream environment. C – The Price River Formation overlies the Castlegate Sandstone and is composed of poorly sorted siltstone and ledge-forming sandstone beds deposited in a fluvial environment.

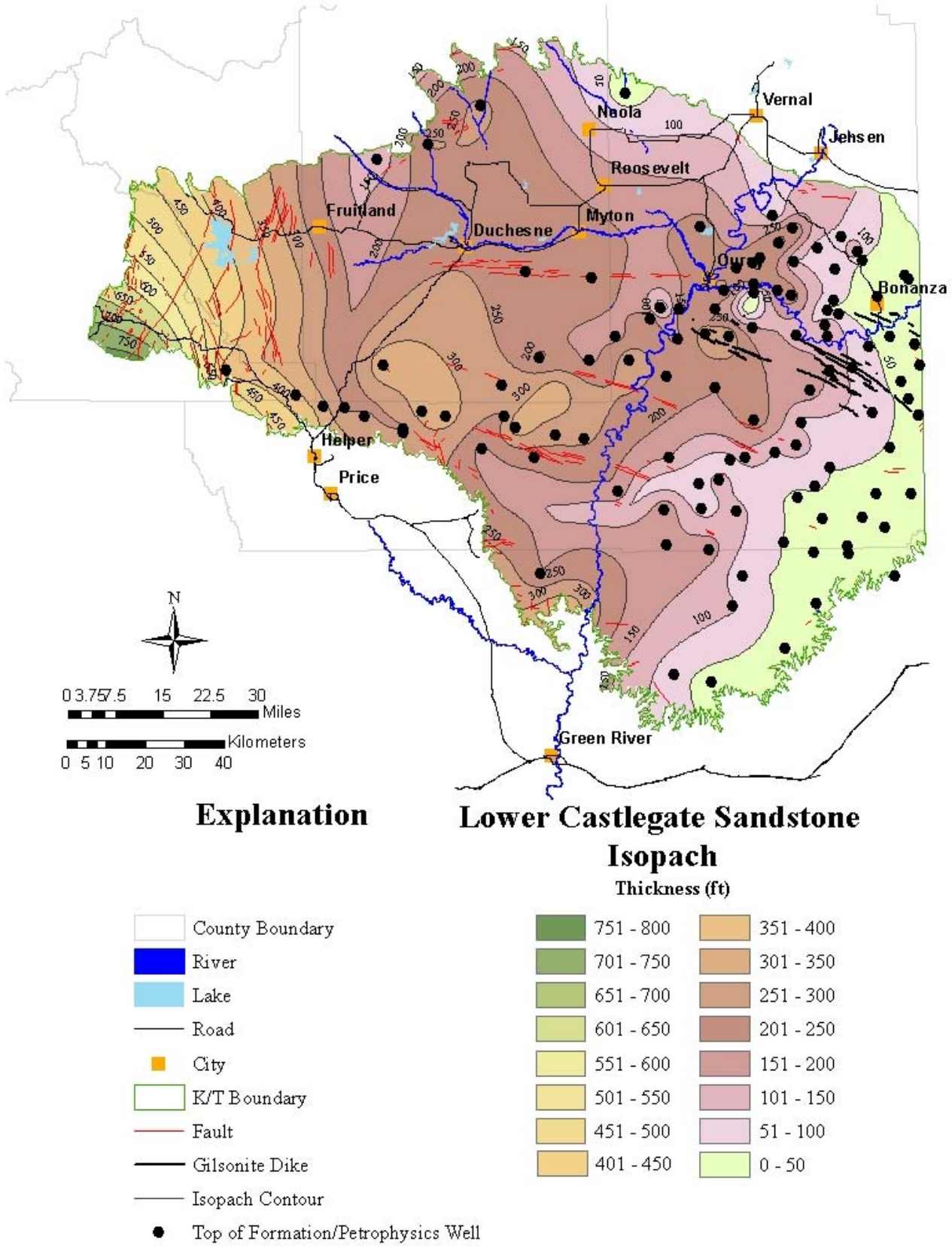

Figure 6.8. Isopach of the lower Castlegate Sandstone. The contour range is 0 to 1000 feet, and the contour interval is 50 feet. Tops data are from Anderson (2005), Hettinger and Kirschbaum (2002), and picks from well logs from additional wells as part of this study.

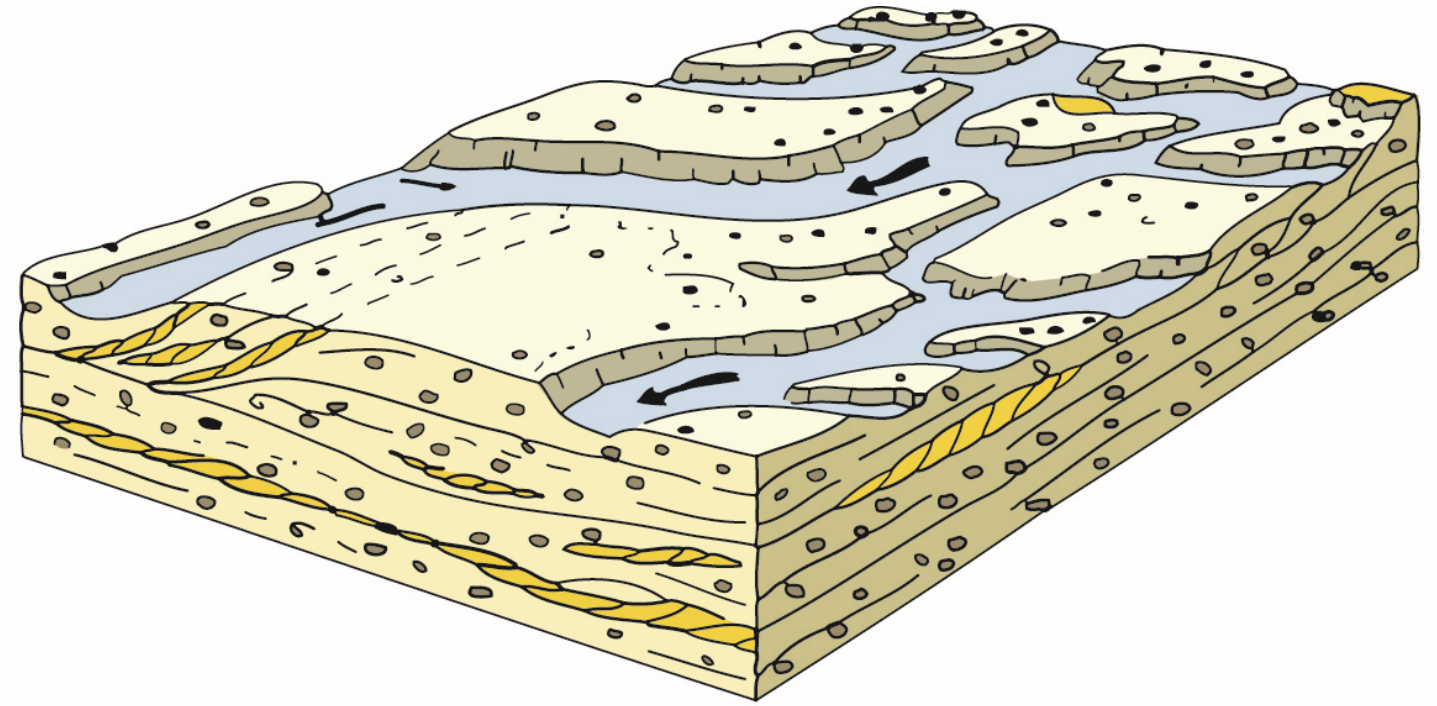

Figure 6.9. Schematic block diagram of a braided stream environment (modified from Howell and Flint, 2005). Castlegate Sandstone was deposited in a braided stream environment as sediments were eroded from the Sevier highlands in western Utah and transported eastward to the Cretaceous Western Interior Seaway.

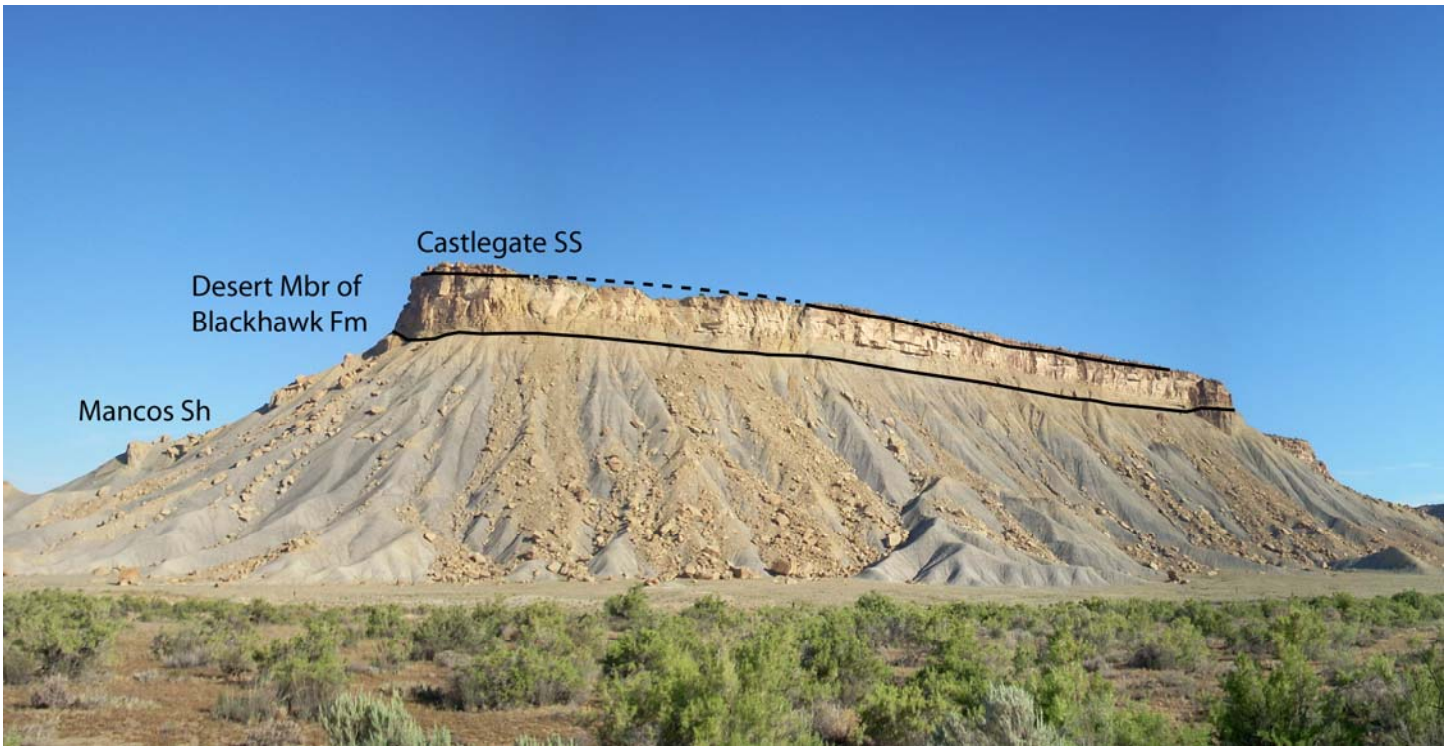

Figure 6.10. Castlegate Sandstone overlying the Desert Member of the Blackhawk Formation and the Mancos Shale at the mouth of Thompson Canyon, east of Green River.

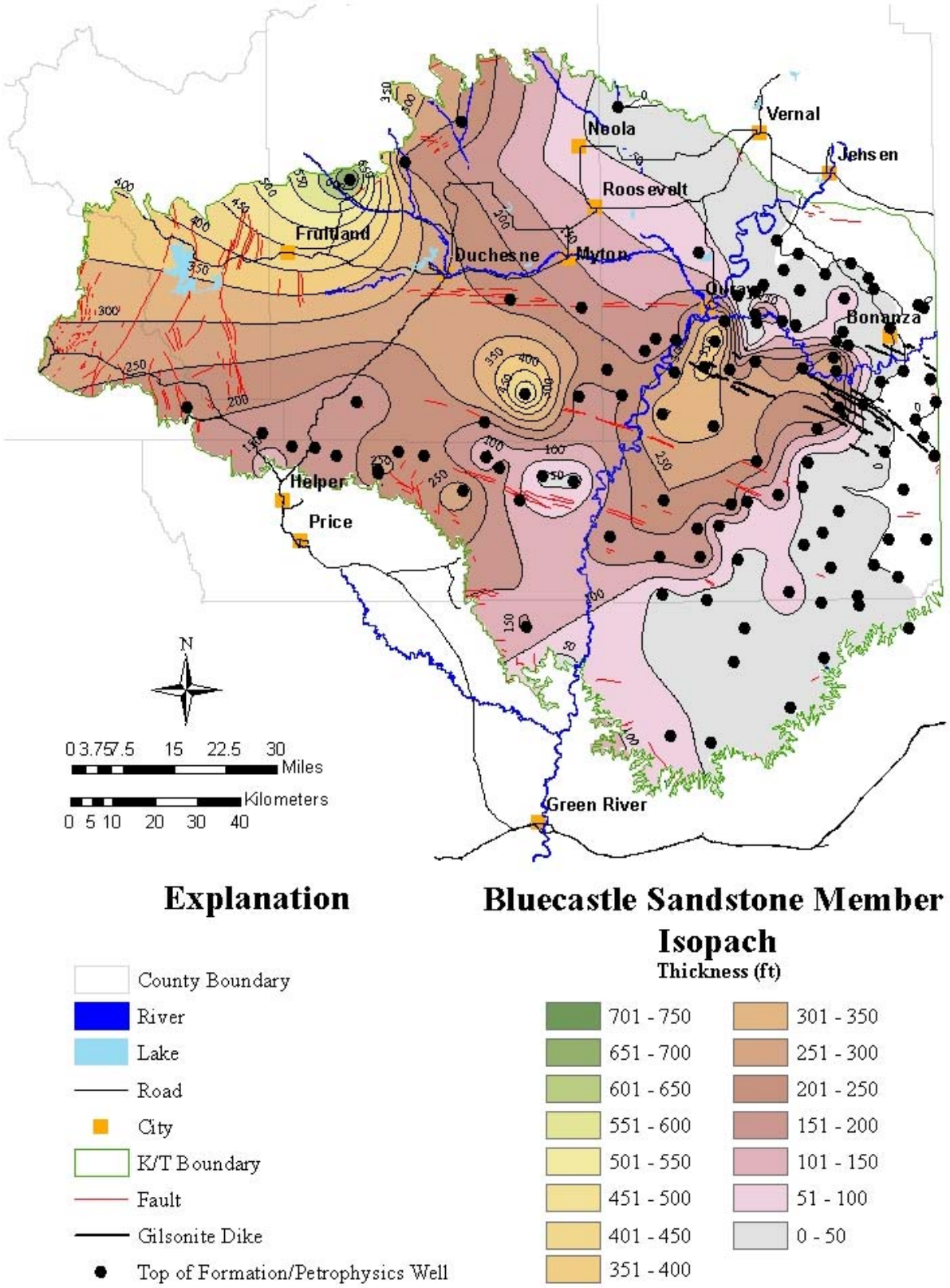

Figure 6.11. Isopach of the Bluecastle Sandstone Member of the Castlegate Sandstone. The contour range is 0 to 750 feet, and the contour interval is 50 feet. The coarse-grained, pebbly unit is thickest in the northwestern region of the Uinta Basin and pinches out into the Neslen Formation in Sego Canyon to the southeast (Hettinger and Kirschbaum, 2002). Tops data are from Anderson (2005), Hettinger and Kirschbaum (2002), and from well logs used as part of this study.

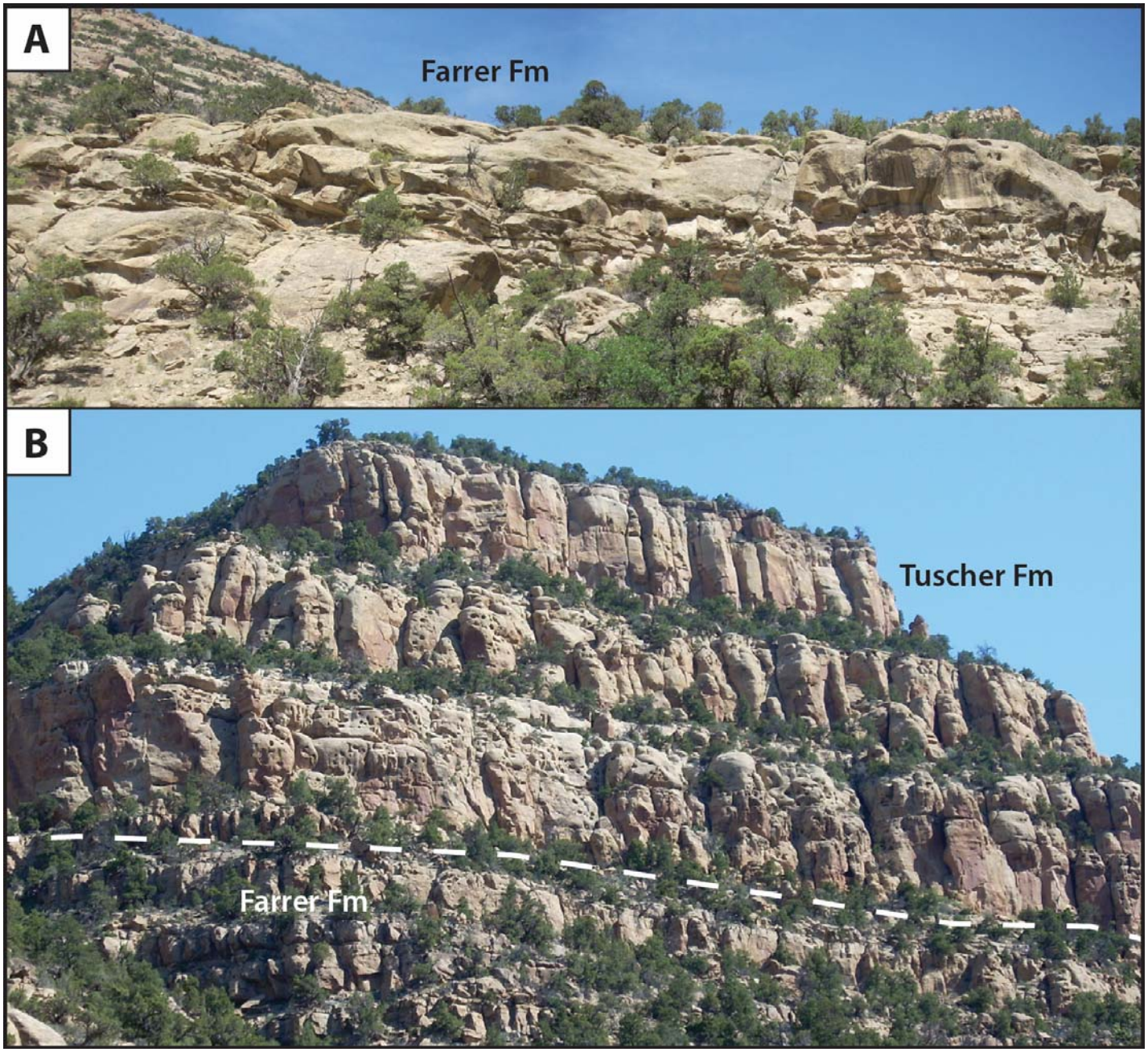

Figure 6.12. Typical outcrops of the (A) Farrer Formation and (B) the overlying Tuscher Formation; Sego Canyon.

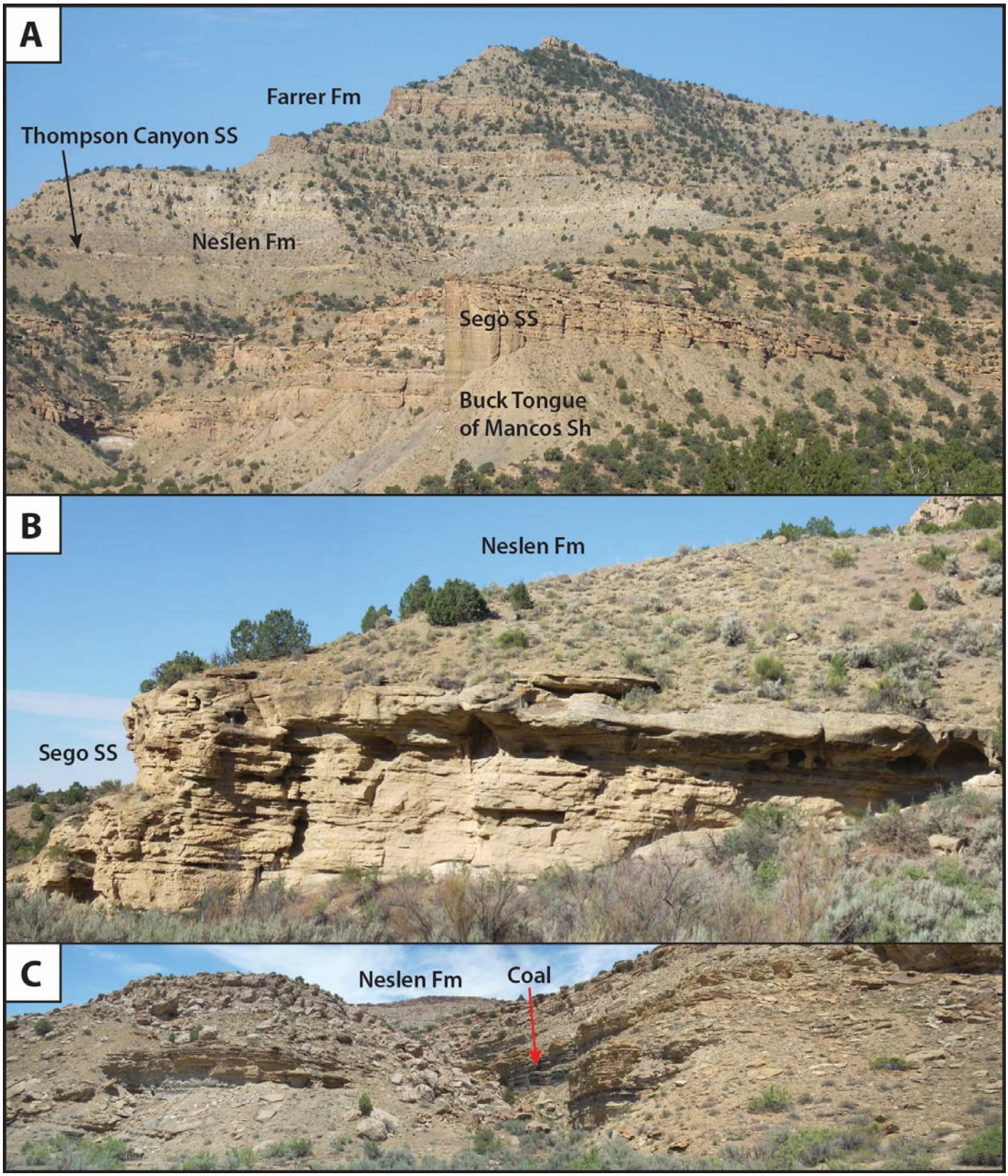

Figure 6.13. Excellent outcrops of the Mesaverde Group in Sego Canyon. A – The Buck Tongue of the Mancos Shale underlies the Sego Sandstone, above which are the Neslen and Farrer Formations. B – The Sego Sandstone is overlain by the heterogeneous Neslen Formation. C – The Neslen Formation contains several coal-bearing layers deposited in a coastal plain (Franczyk and others, 1990b).

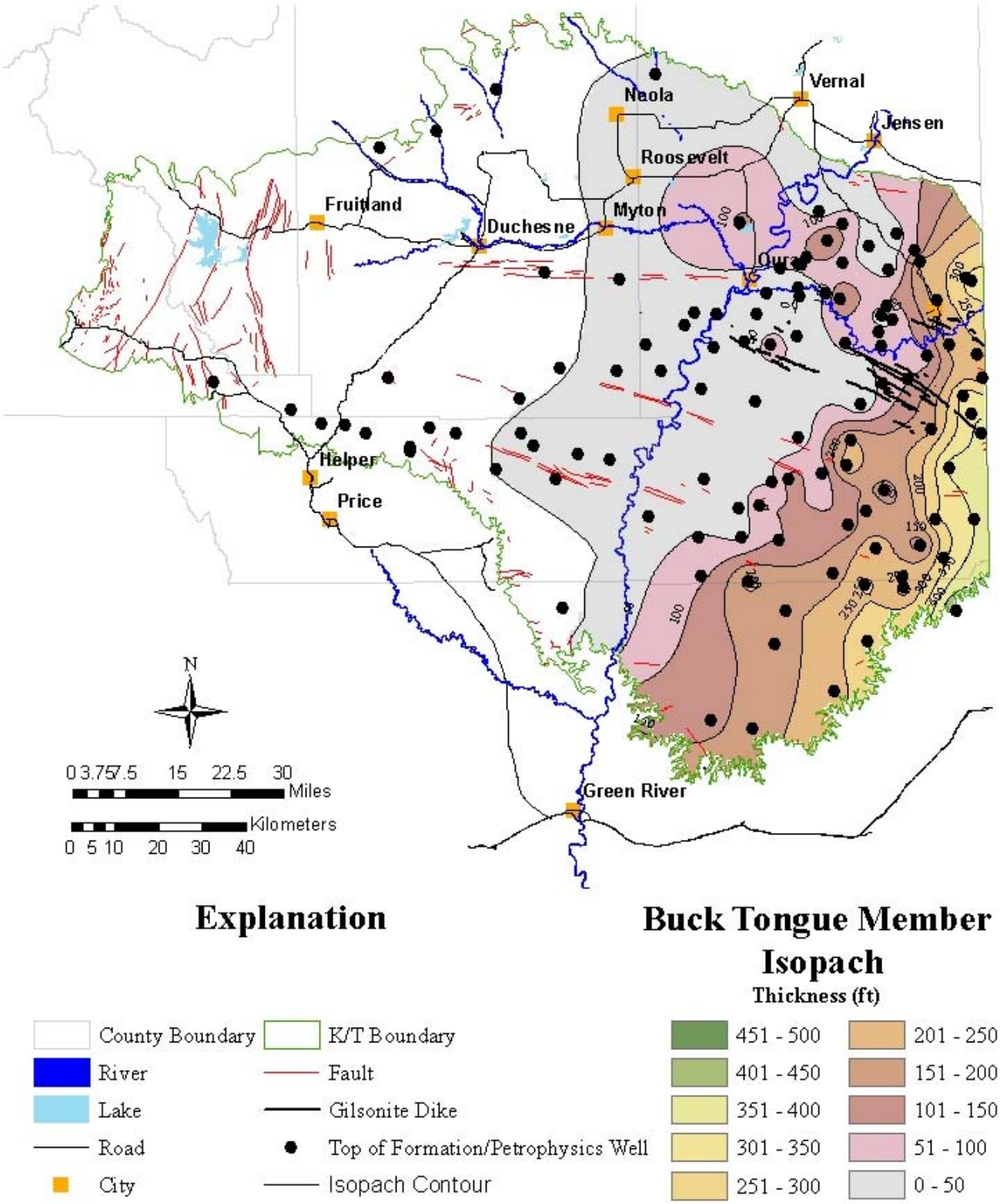

Figure 6.14. Isopach of the Buck Tongue of the Mancos Shale. The contour range is 0 to 500 feet, and the contour interval is 50 feet. The Buck Tongue is thickest in the eastern Uinta Basin (seaward) and thins to the west (landward). Tops data are from Anderson (2005), Hettinger and Kirschbaum (2002), and picked from well logs as part of this study.

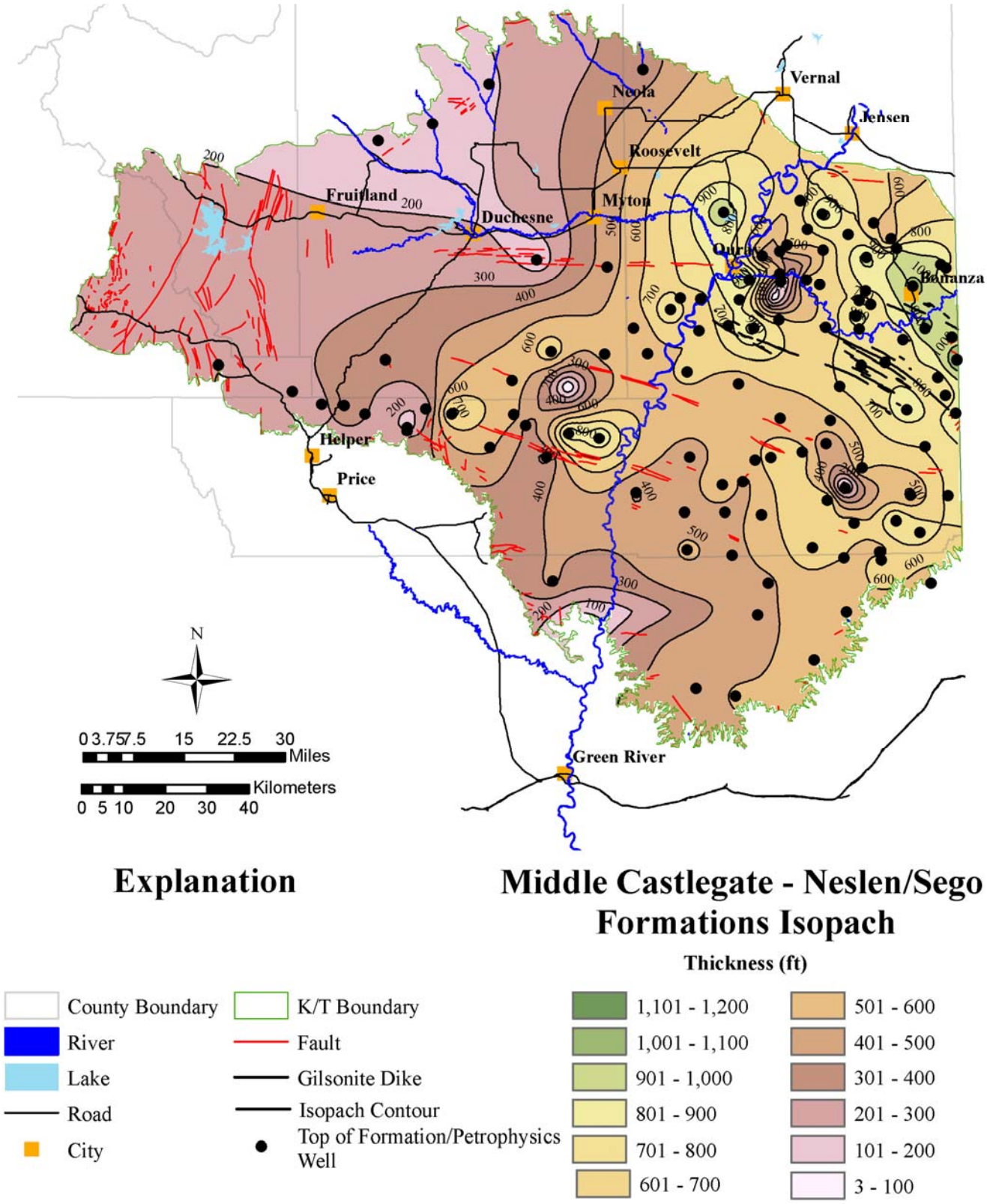

Figure 6.15. Combined isopach of the middle Castlegate Sandstone in the west and Sego Sandstone and Neslen Formation in the east. The contour range is 100 to 1000 feet, and the contour interval is 100 feet. The Castlegate is thickest in the western portion of the Uinta Basin and thins to the east. Tops data are from Anderson (2005), Hettinger and Kirschbaum (2002), and picks from well logs from additional wells as part of this study.

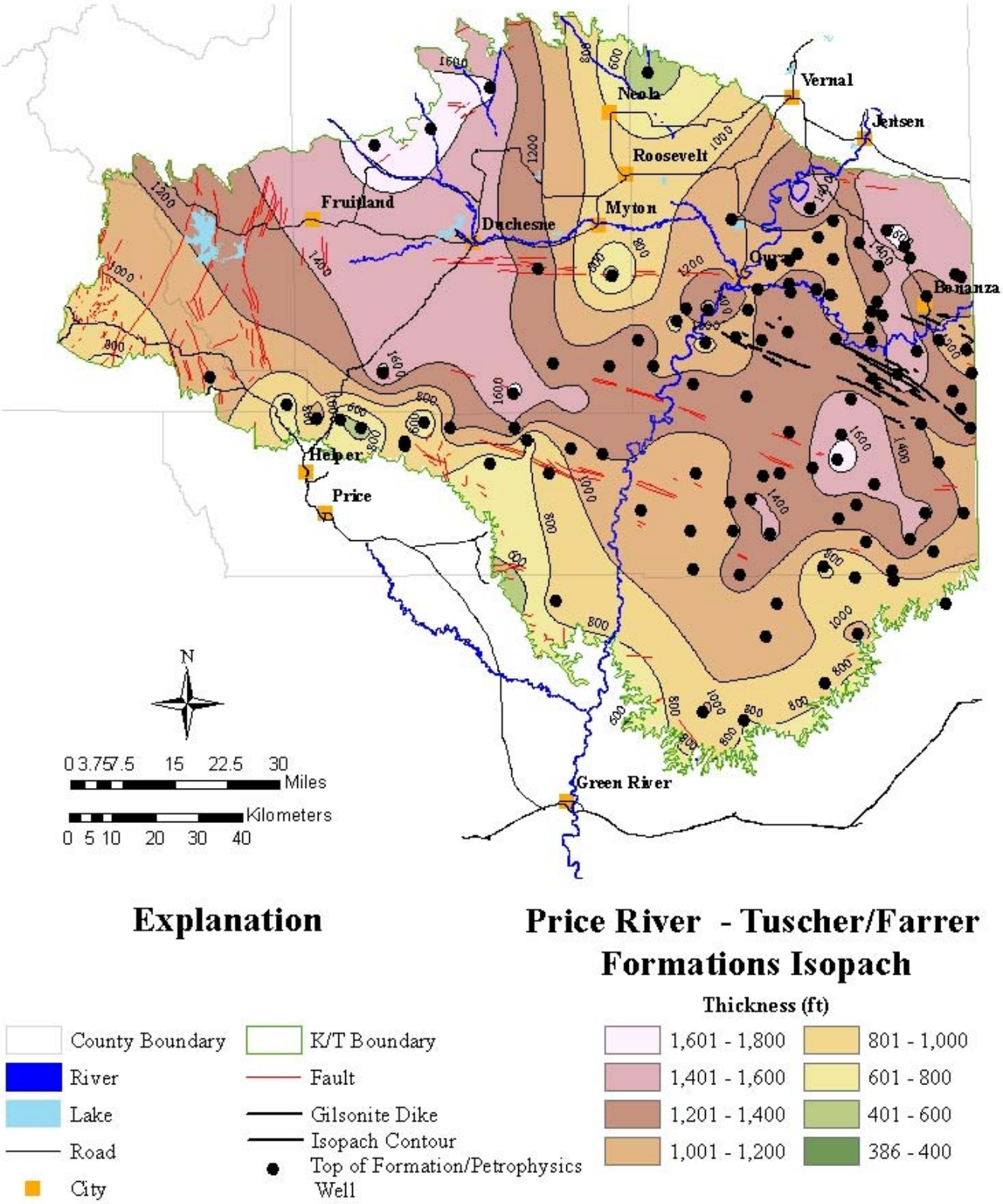

Figure 6.16. Combined isopach of the Price River Formation in the west and the Tuscher and Farrer Formations in the east. The contour range is 4386 to 1800 feet, and the contour interval is 200 feet. The Price River is thickest in the northwestern region of the Uinta Basin, thins in the middle of the basin, and splits into the thick-again Tuscher and Farrer Formations in the eastern portion of the basin. Tops data are from Anderson (2005), Hettinger and Kirschbaum (2002), and picked from well logs as part of this study.

Figure 6.17. Buck Tongue of the Mancos Shale, overlain by the Sego Sandstone and the coal-bearing Neslen Formation, Tusher Canyon.

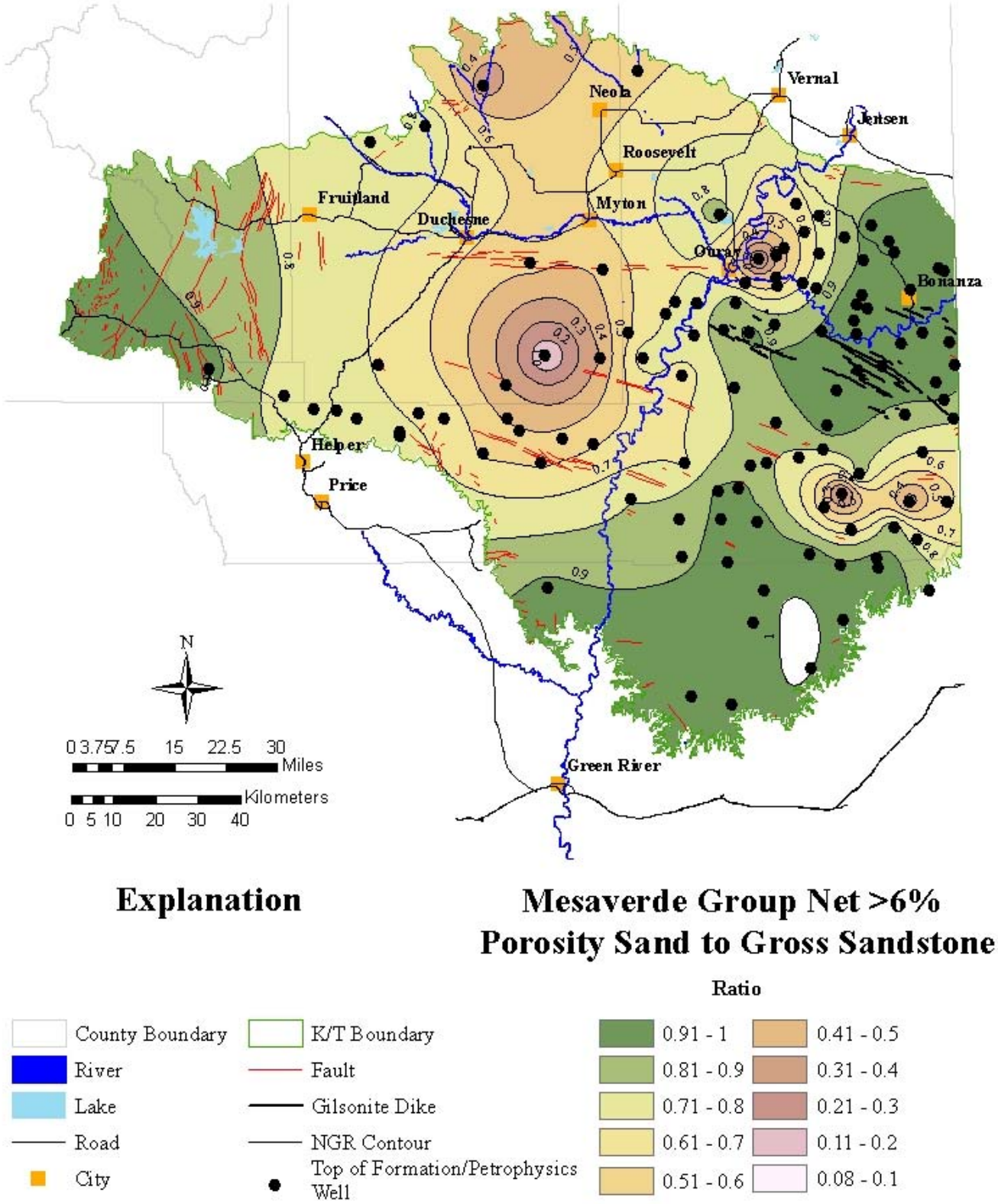

Figure 6.18. Net to gross ratio of sands within the Mesaverde Group.

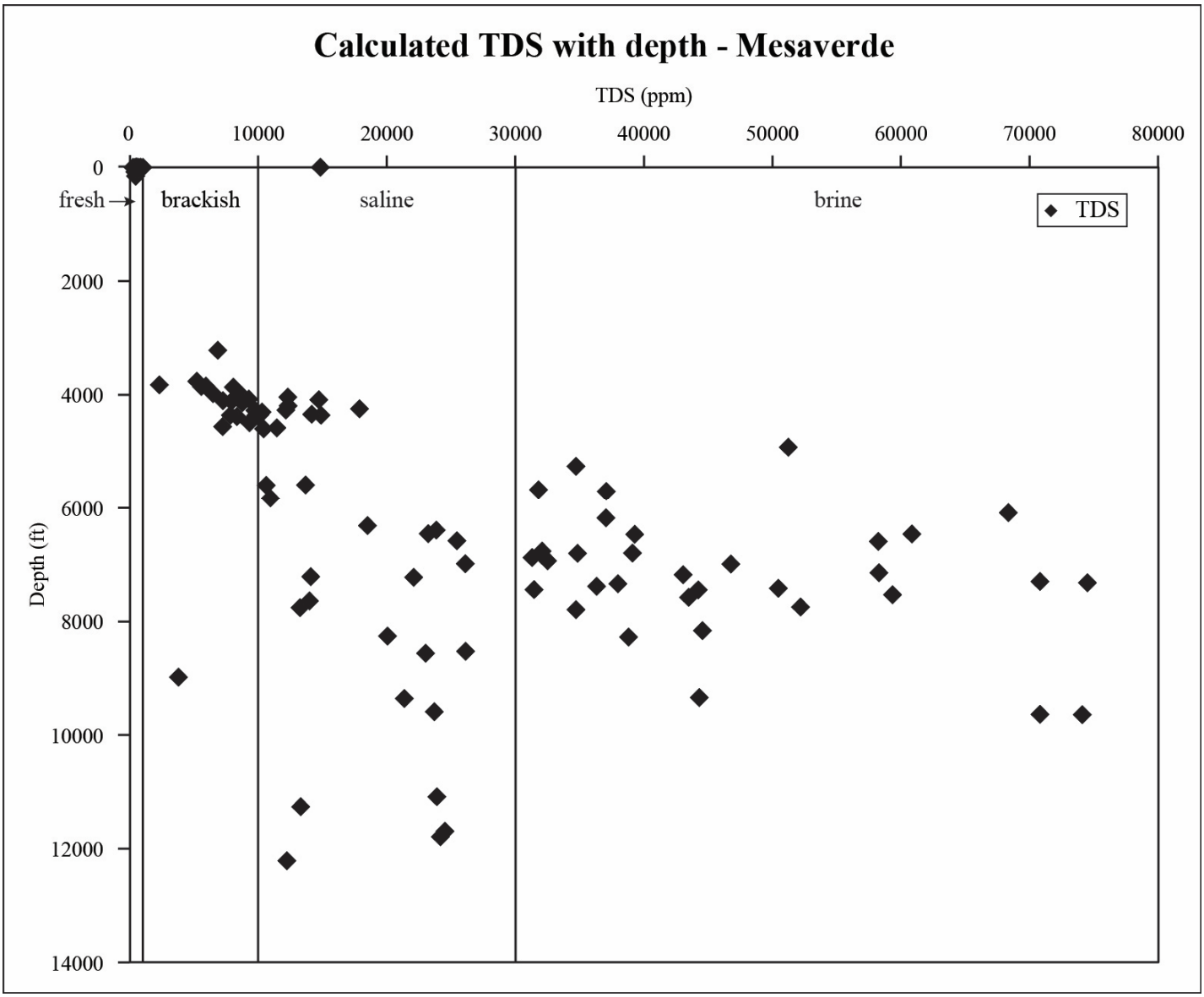

Figure 6.19. Calculated TDS with depth in the Mesaverde Group (number of samples: fresh – 13, brackish – 20, saline – 34, brine – 33).

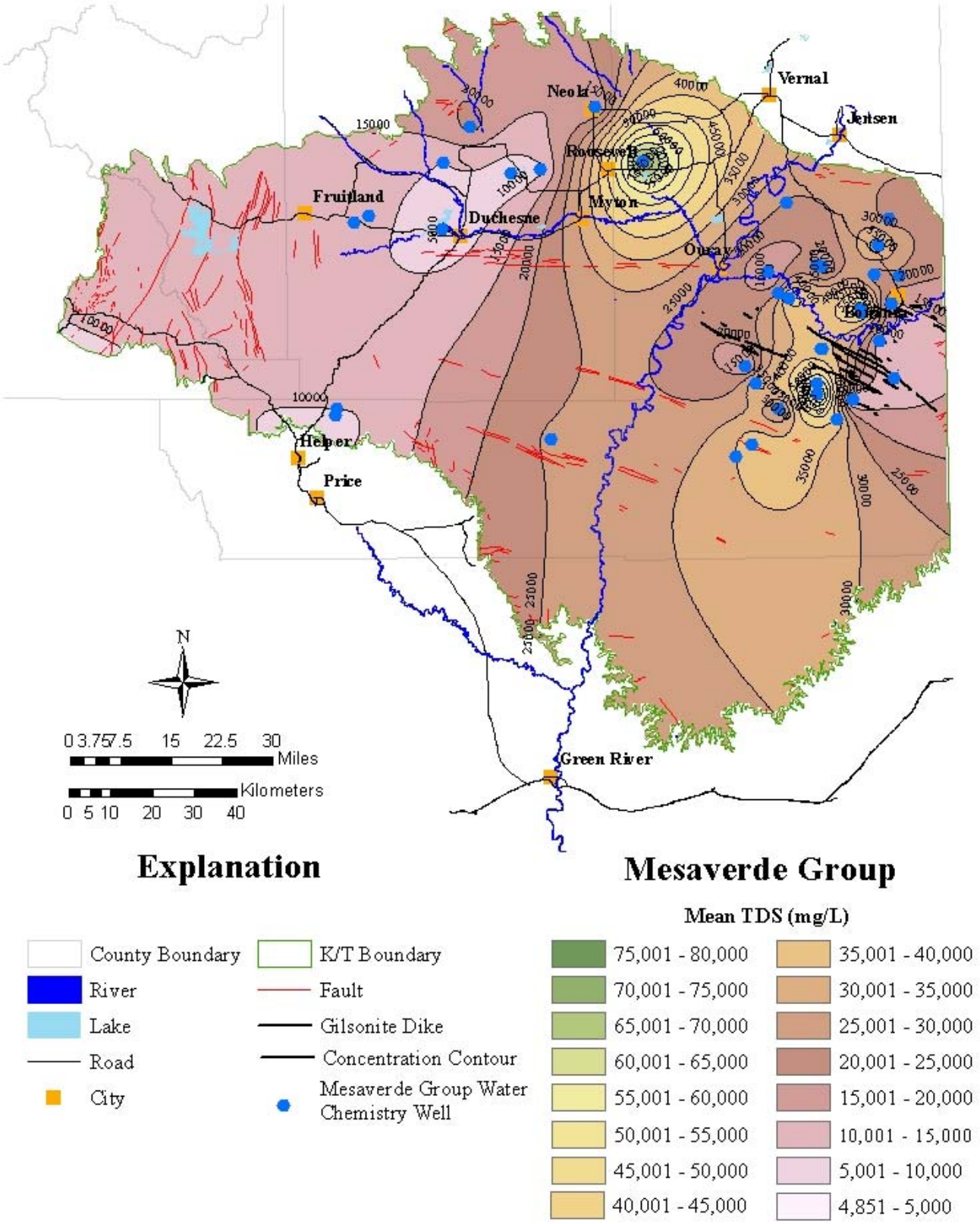

Figure 6.20. TDS map of the Mesaverde Group. Contour intervals are 5000 mg/L. Data is from water samples from wells perforated in the Mesaverde and do not correspond to the wells used for the formation tops and thicknesses.

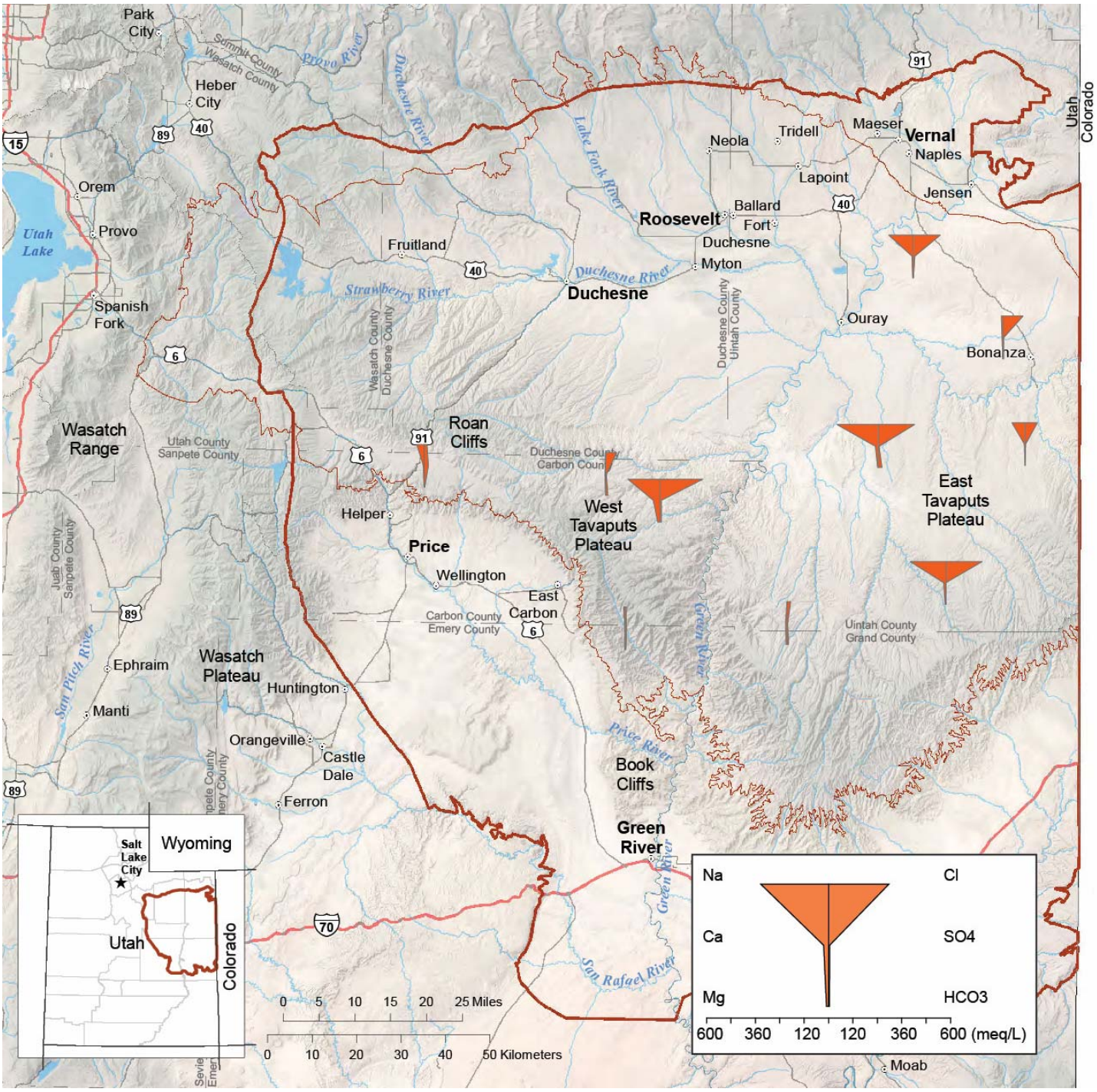

Figure 6.21. Stiff diagrams from water samples sourced from the Mesaverde Group. Samples are freshest along the edges of the Uinta Basin and become saline in the basin interior.

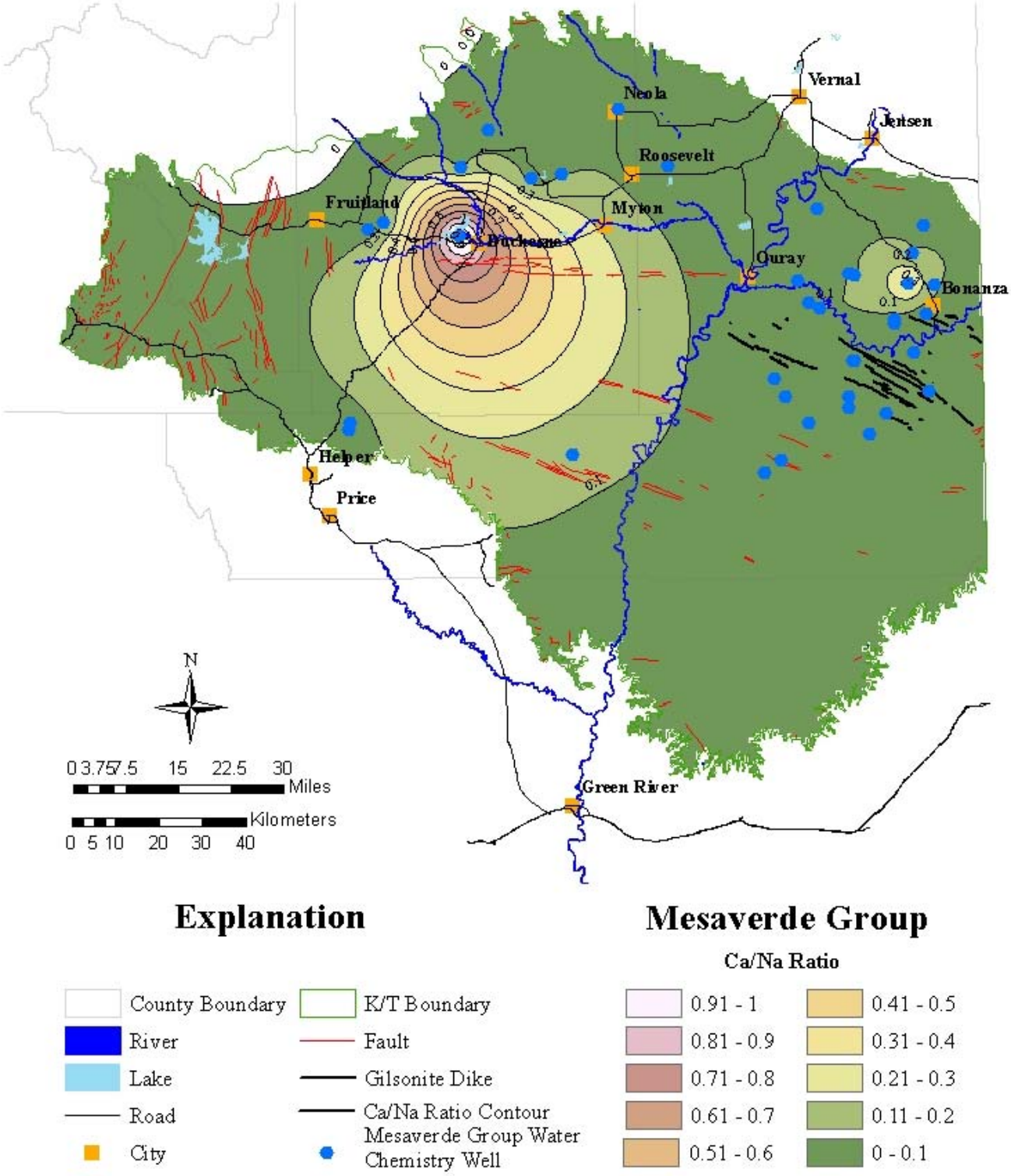

Figure 6.22. Calcium/sodium ratio map for Mesaverde Group water. The Ca/Na ratio reveals the location and extent of the Paleocene Flagstaff Limestone as groundwater leaches calcium-rich fluids into the Mesaverde from the overlying carbonate.

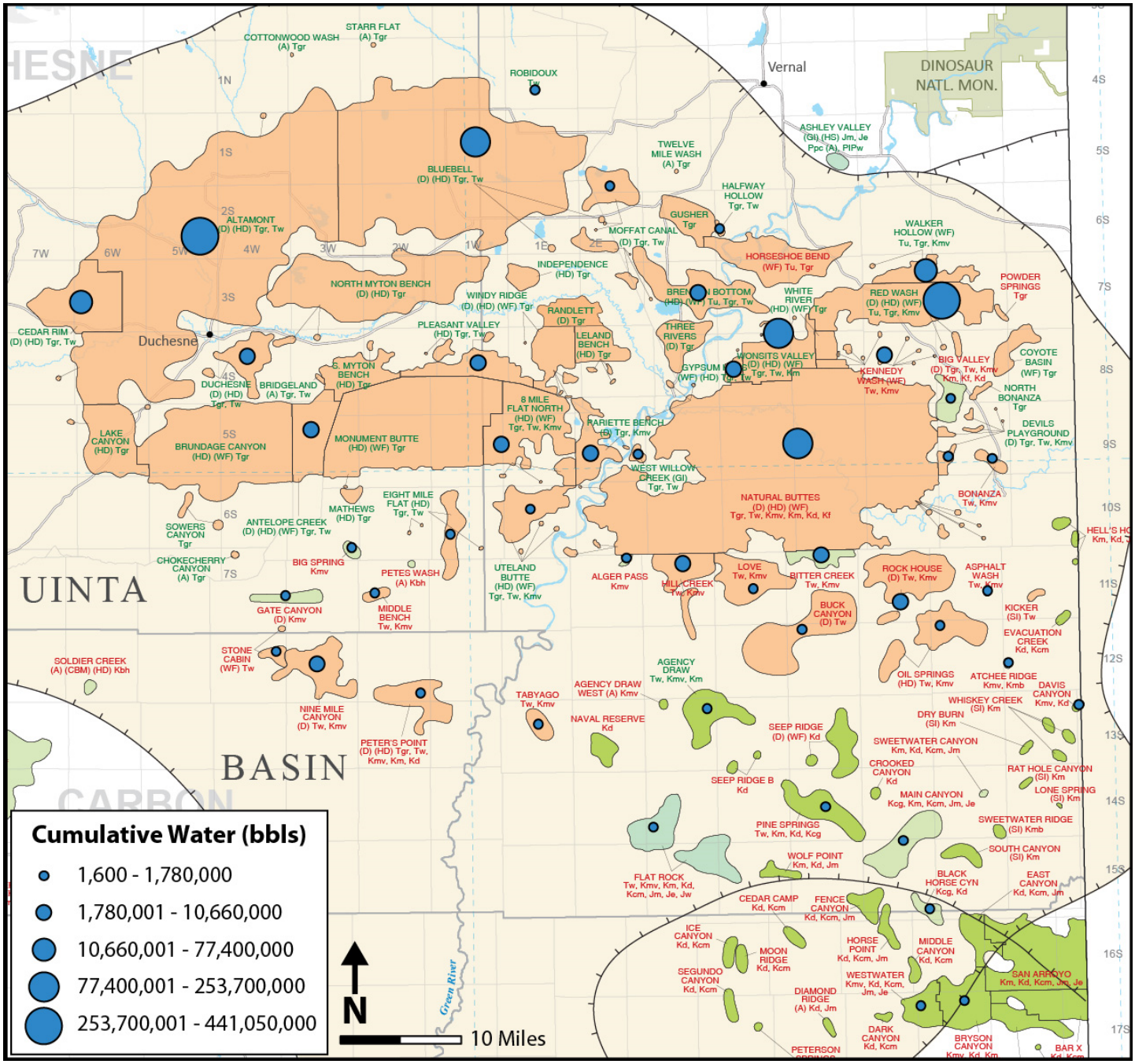

Figure 6.23. Cumulative water production from Mesaverde Group and/or the Wasatch/Colton Formation gas reservoirs in Uinta Basin fields. Production from a particular formation is not reported separately so data used in this map combine production from all producing formations in the field.

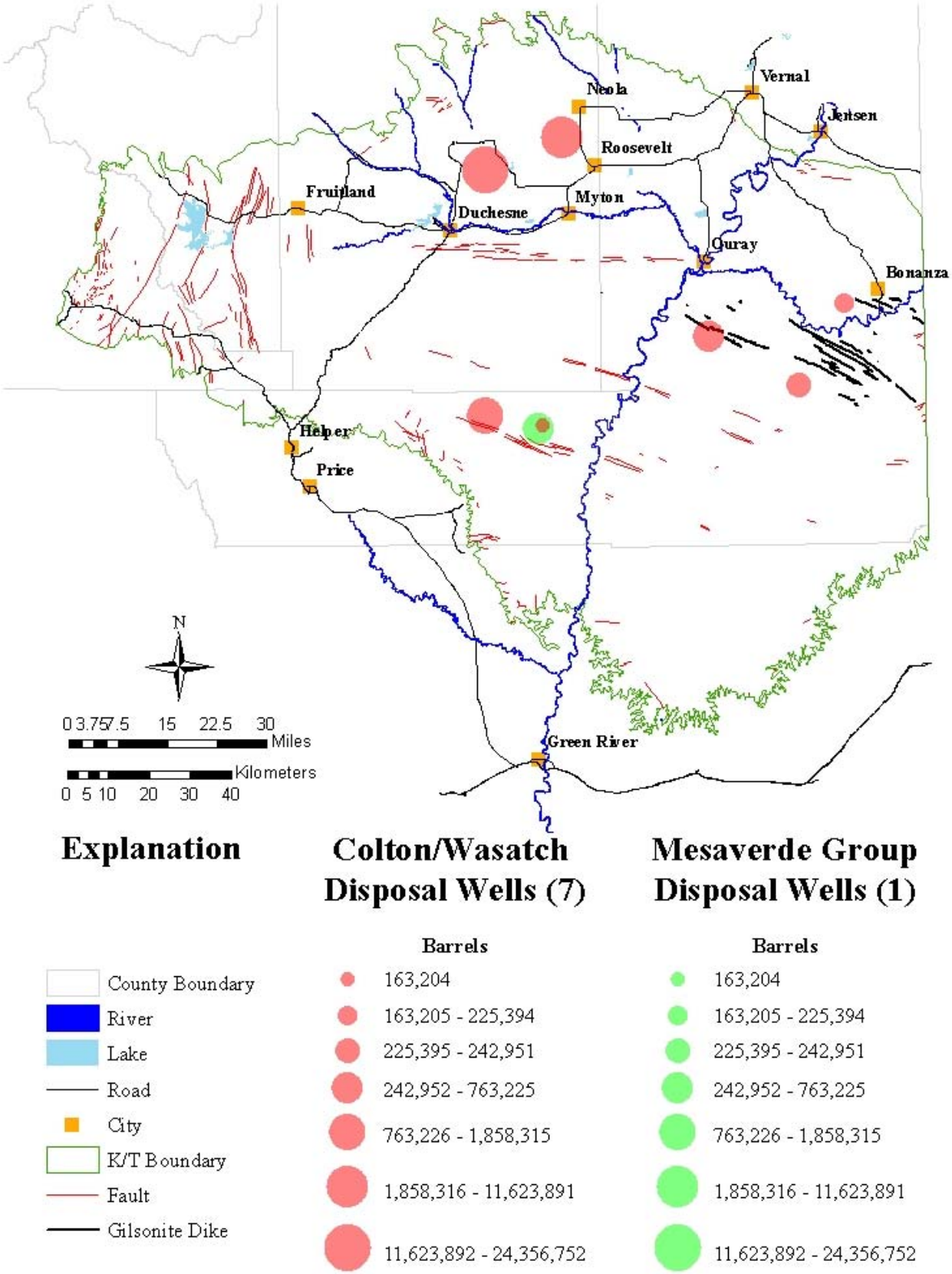

Figure 6.24. Locations and volumes for water disposal wells into the Mesaverde Group and Wasatch/ Colton Formation.

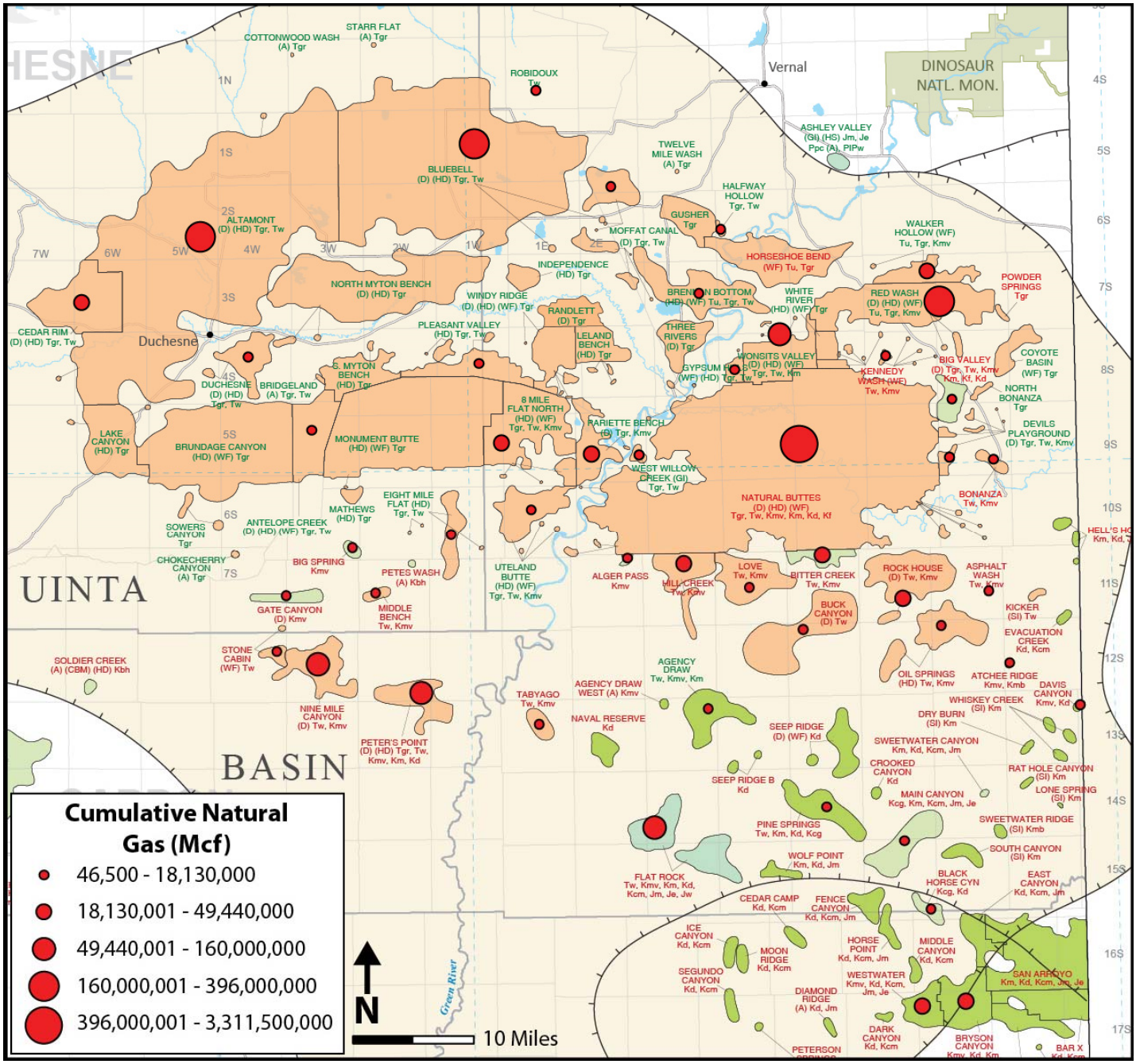

Figure 6.25. Cumulative natural gas production (in MCF) from Mesaverde Group and/or the Wasatch/ Colton Formation reservoirs in Uinta Basin fields. Production from a particular formation is not reported separately so data used in this map combine production from all producing formations in the field. Names in red denote field that produce(d) primarily nonassociated natural gas whereas those in green primarily produce(d) oil. The field areas are color-coded by geologic age of the producing reservoirs; symbols of the producing reservoirs are listed under the field names (see figure 2.1 for age and formation names). Field designations are also listed under the field names: (A) = abandoned, (CBM) = coalbed methane, (D) = produced water disposal project, (HD) = horizontal drilling, (SI) = shut-in field, (WF) = waterflood project. Modified from Wood and Chidsey, 2015.

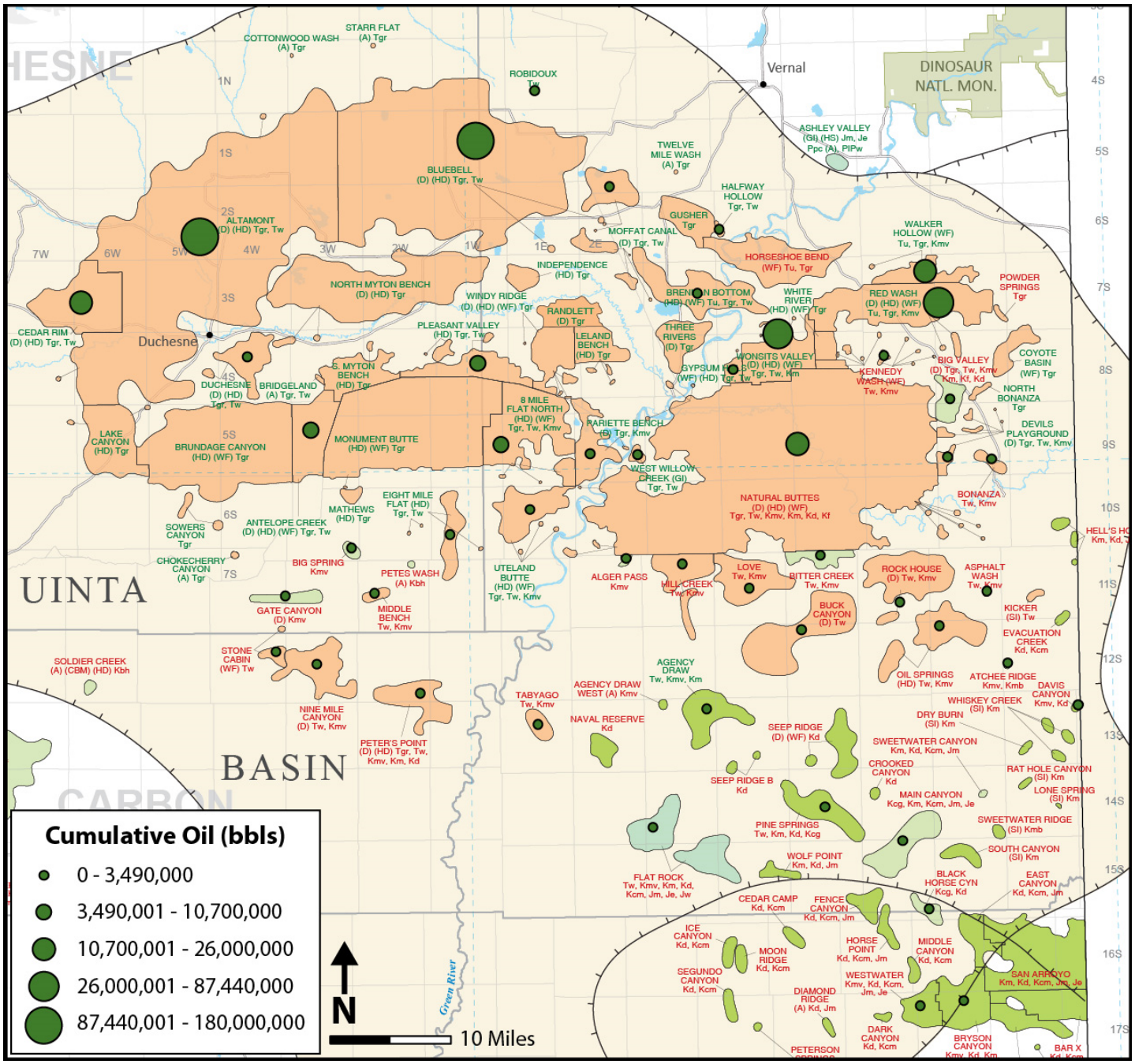

Figure 6.26. Cumulative crude oil production (in barrels [bbls]) from Mesaverde Group and/or the Wasatch/Colton Formation reservoirs in Uinta Basin fields. Production from a particular formation is not reported separately so data used in this map combine production from all producing formations in the field. Names in red denote field that produce(d) primarily nonassociated natural gas whereas those in green primarily produce(d) oil. The field areas are color-coded by geologic age of the producing reservoirs; symbols of the producing reservoirs are listed under the field names (see figure 2.1 for age and formation names). Field designations are also listed under the field names: (A) = abandoned, (CBM) = coalbed methane, (D) = produced water disposal project, (HD) = horizontal drilling, (SI) = shut-in field, (WF) = waterflood project. Modified from Wood and Chidsey, 2015.

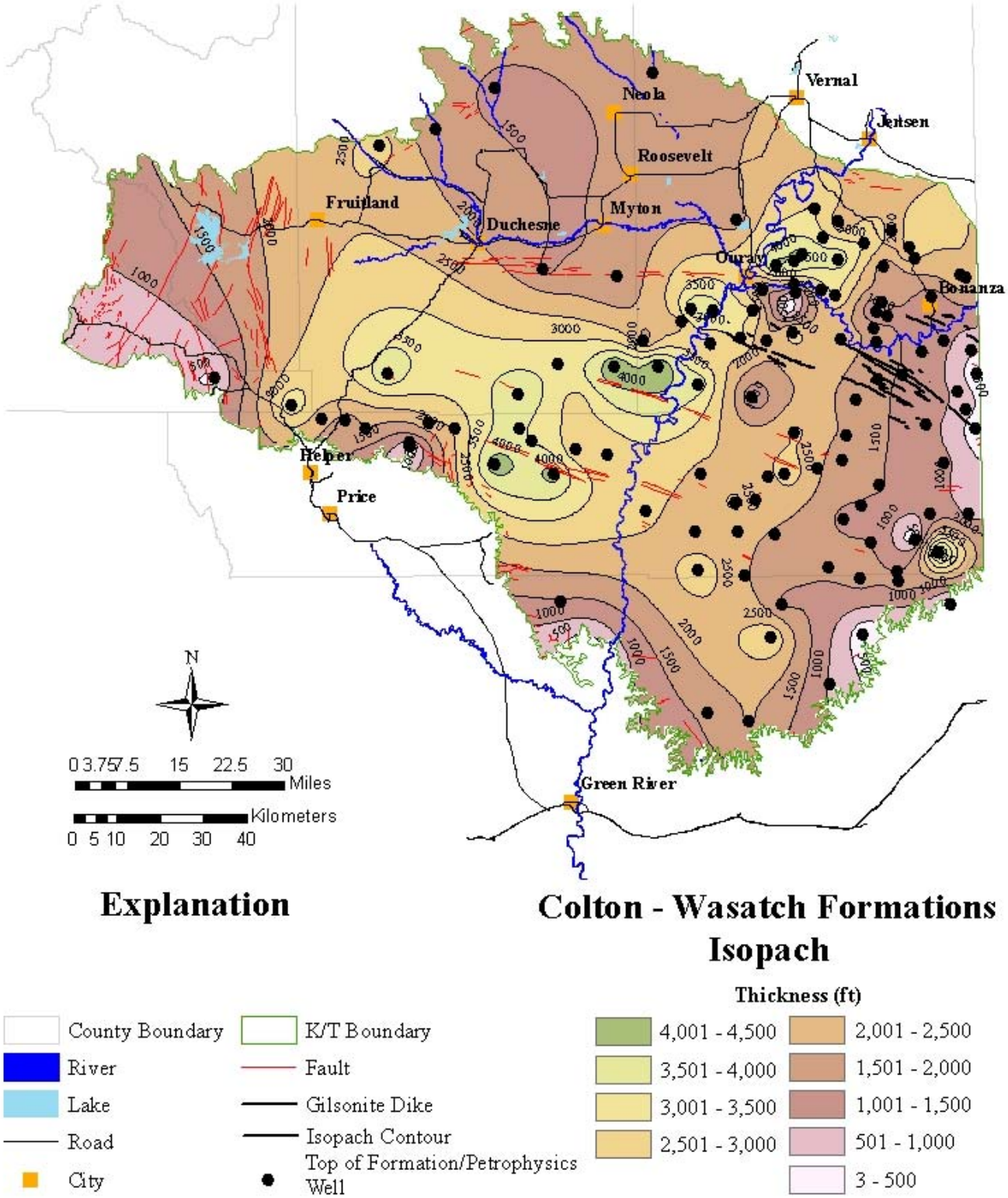

Figure 6.27. Isopach for the Colton/Wasatch Formation. The contour range is 0 to 5000 feet, and the contour interval is 500 feet. Tops data are from Anderson (2005), Hettinger and Kirschbaum (2002), and selected from well logs as part of this study.

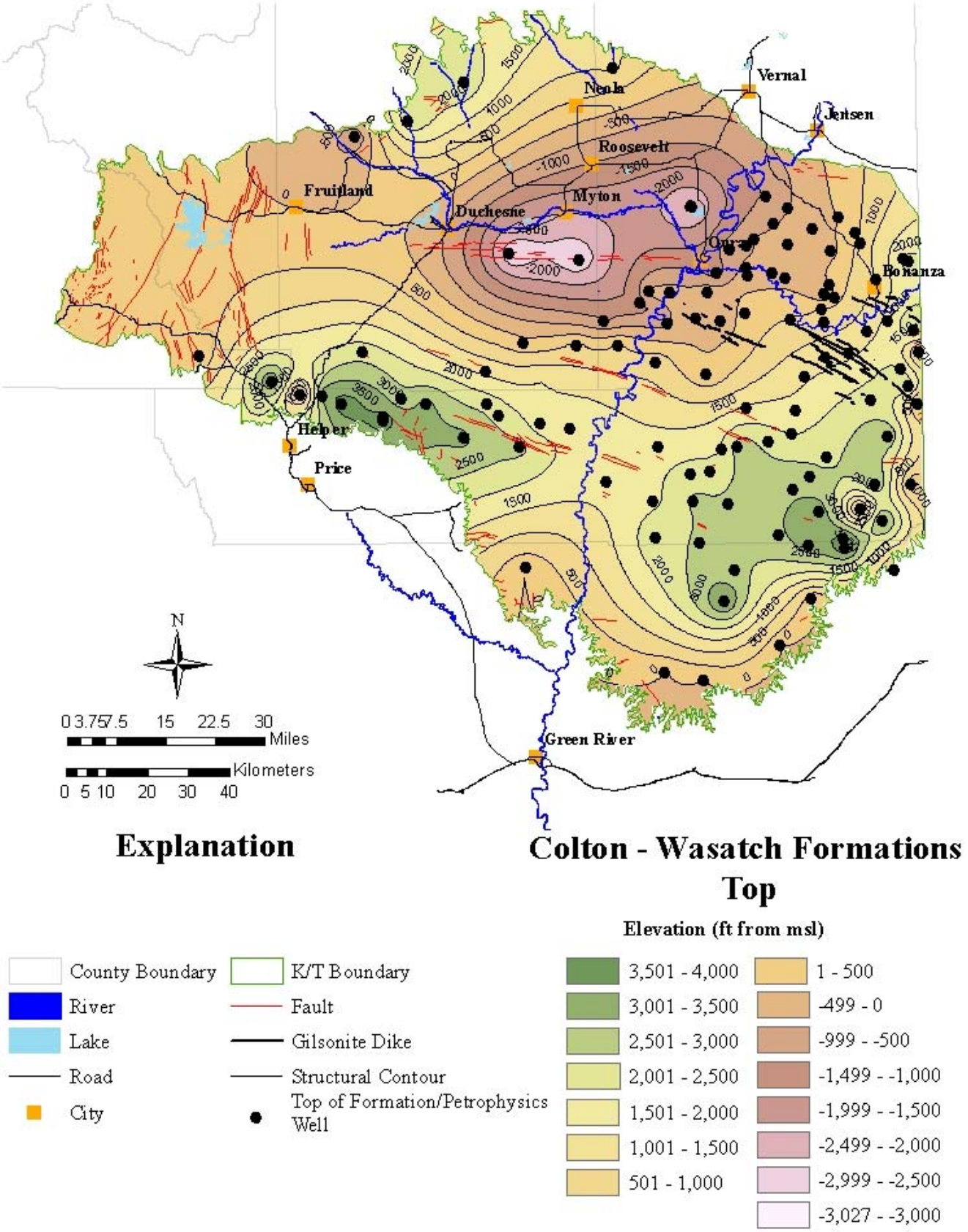

Figure 6.28. Structure of the top of the Wasatch/Colton combined formations. Contour interval is 500 feet. Tops data are from Anderson (2005), Hettinger and Kirschbaum (2002), and selected from well logs as part of this study.

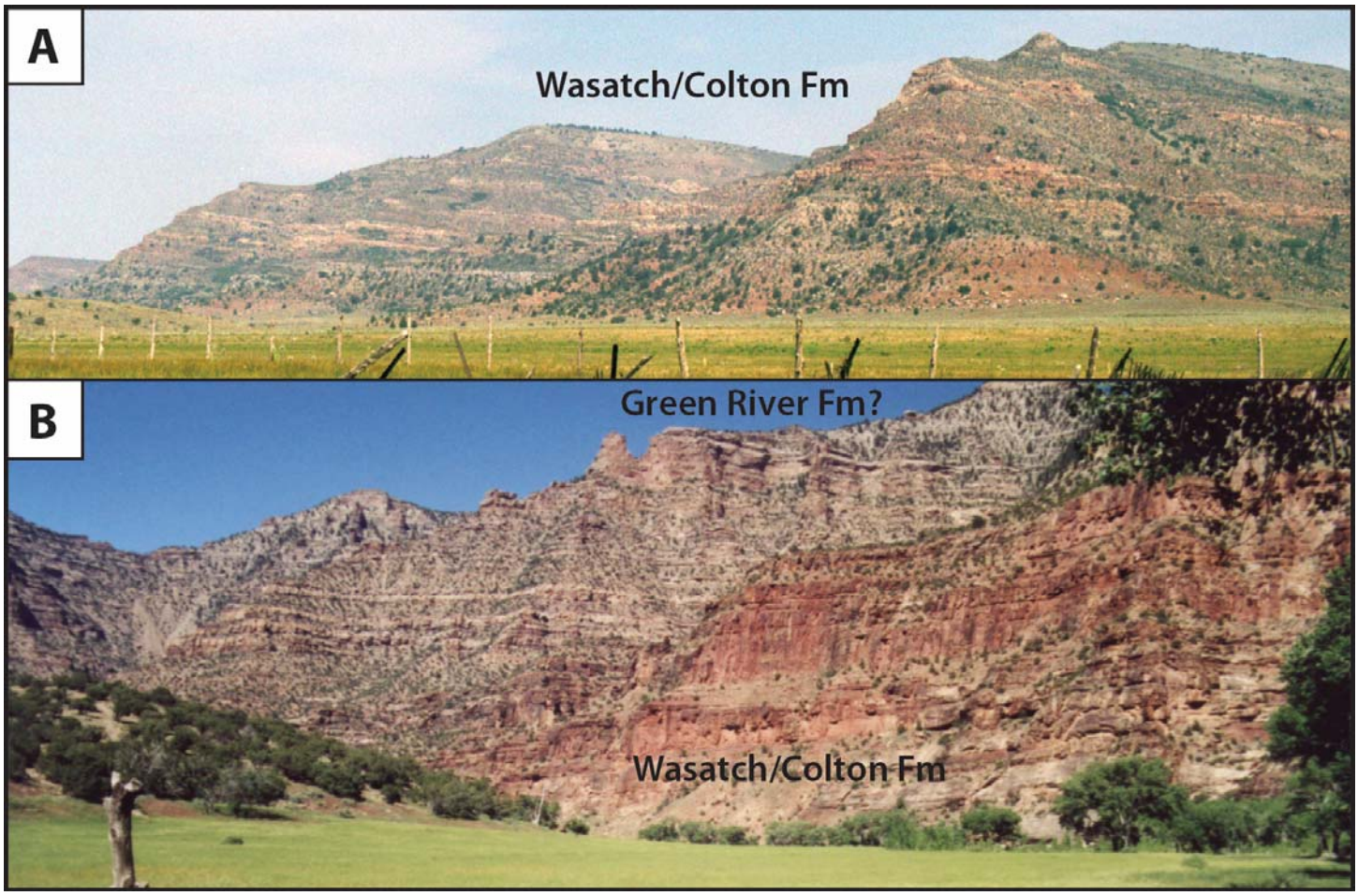

Figure 6.29. Representative outcrops of the Wasatch/Colton Formation. A – Outcrop of the Wasatch/ Colton Formation at Whitmore Park along the western Roan Cliffs. The formation in this locality is composed of red to tan silty slopes and cliff-forming channel sandstone that pinch out laterally. B – A closer view of the Wasatch/Colton Formation at along the Green River in Desolation Canyon, southern Uinta Basin. Photos courtesy of Craig D. Morgan, UGS.

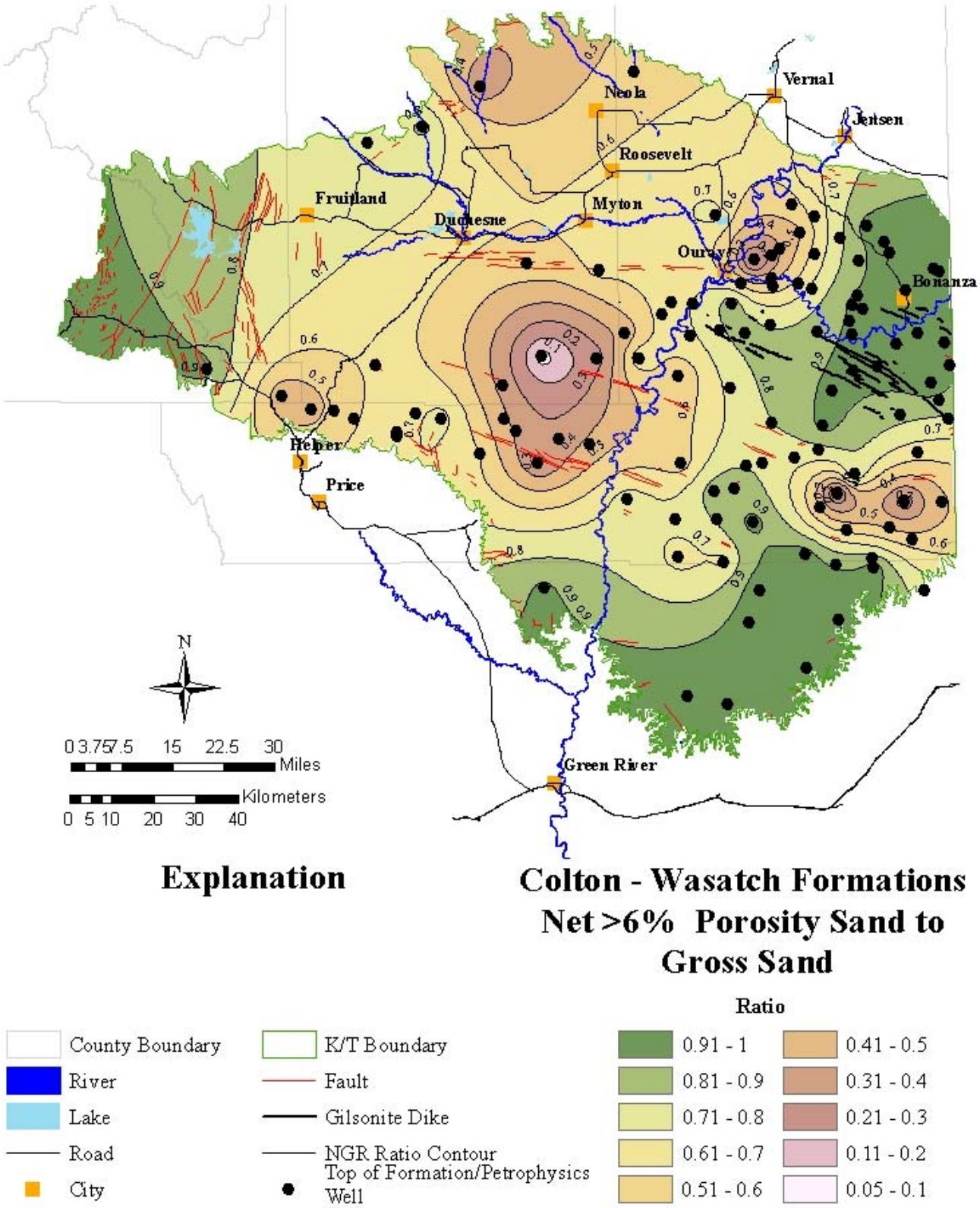

Figure 6.30. Net to gross ratio of sands within the Wasatch/Colton Formation.

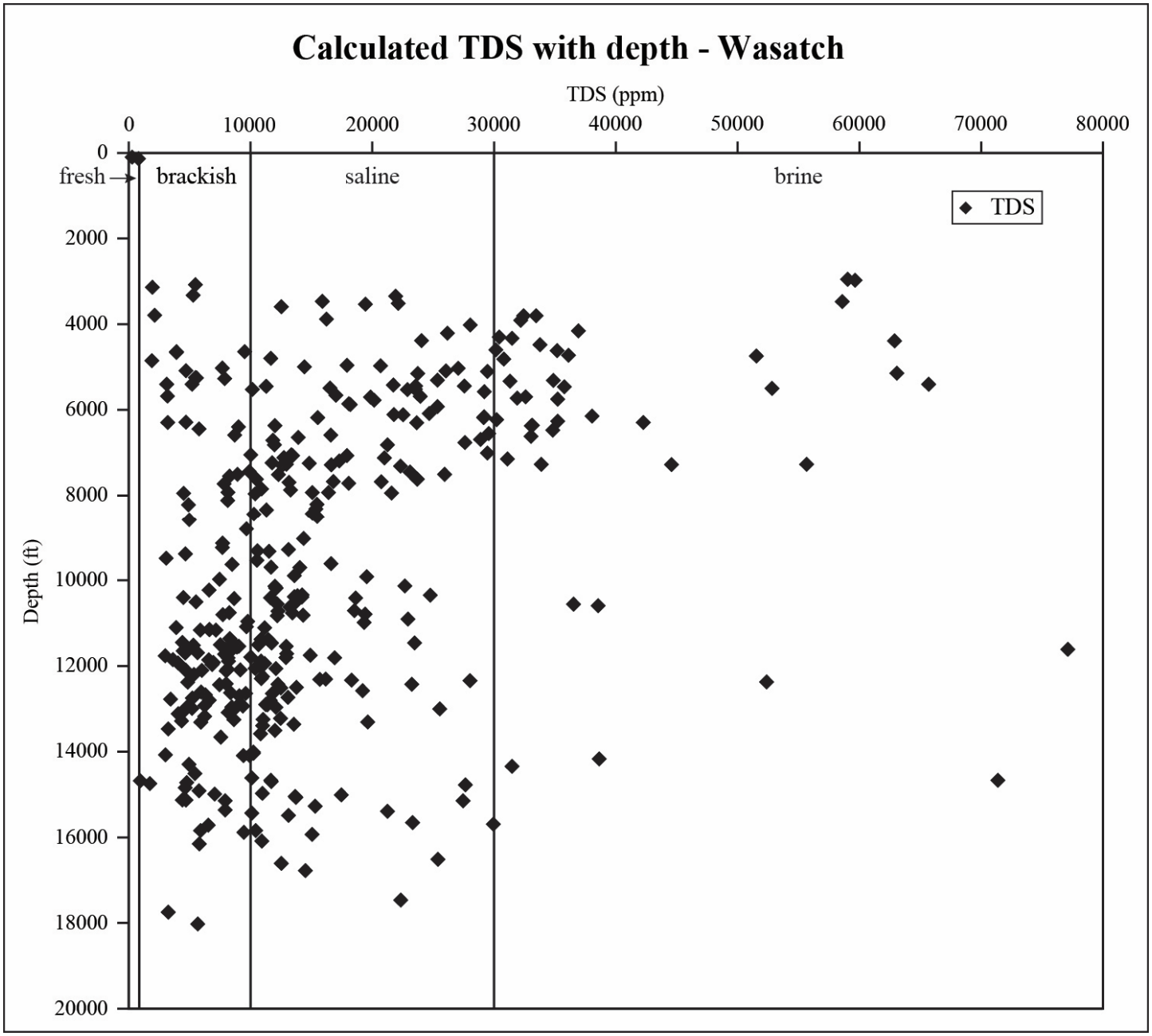

Figure 6.31. Calculated TDS with depth in the Wasatch/Colton Formation (number of samples: fresh – 5, brackish – 129, saline – 178, brine – 45).

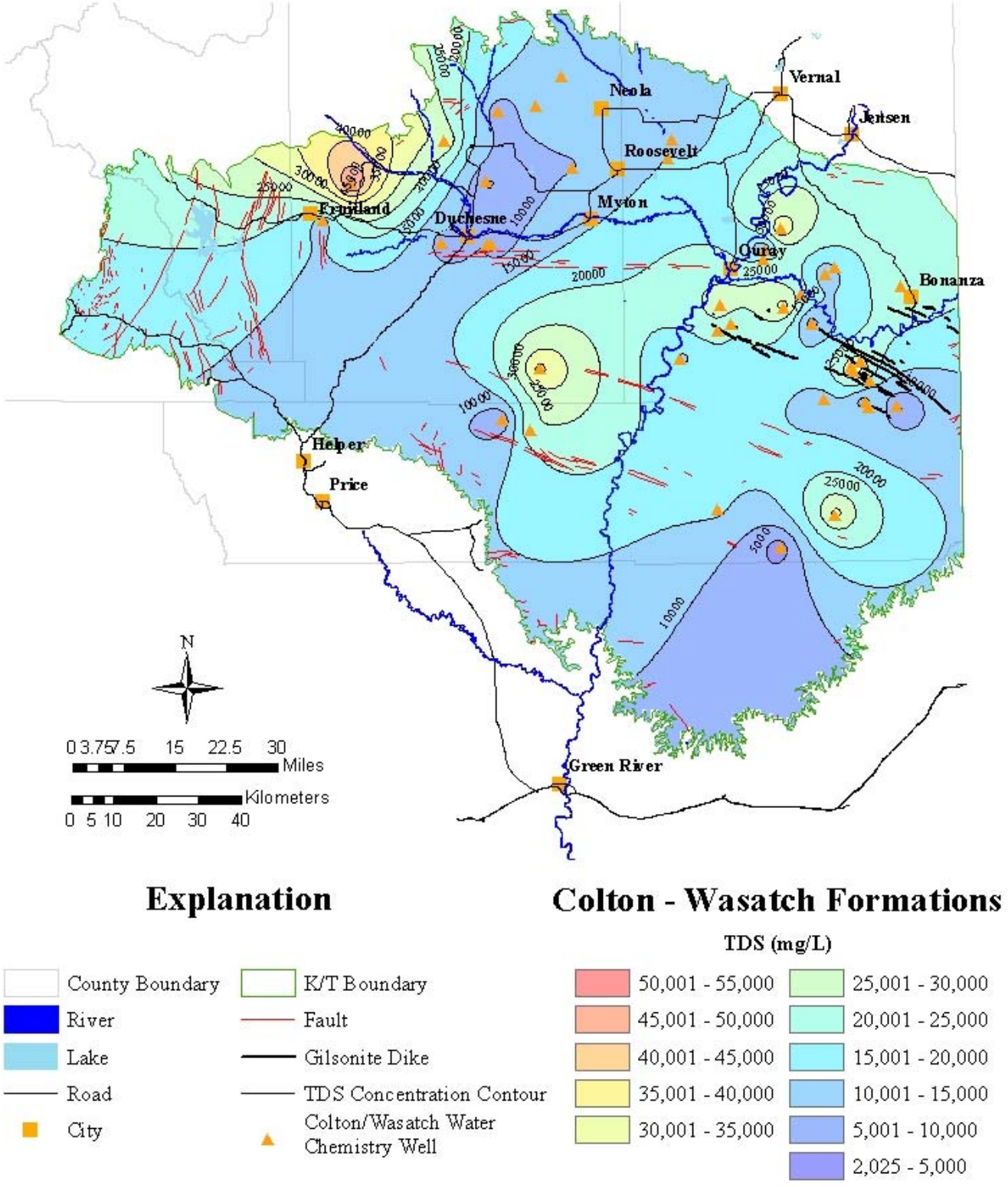

Figure 6.32. TDS map of the Wasatch/Colton Formation. Contour intervals are 5000 mg/L.

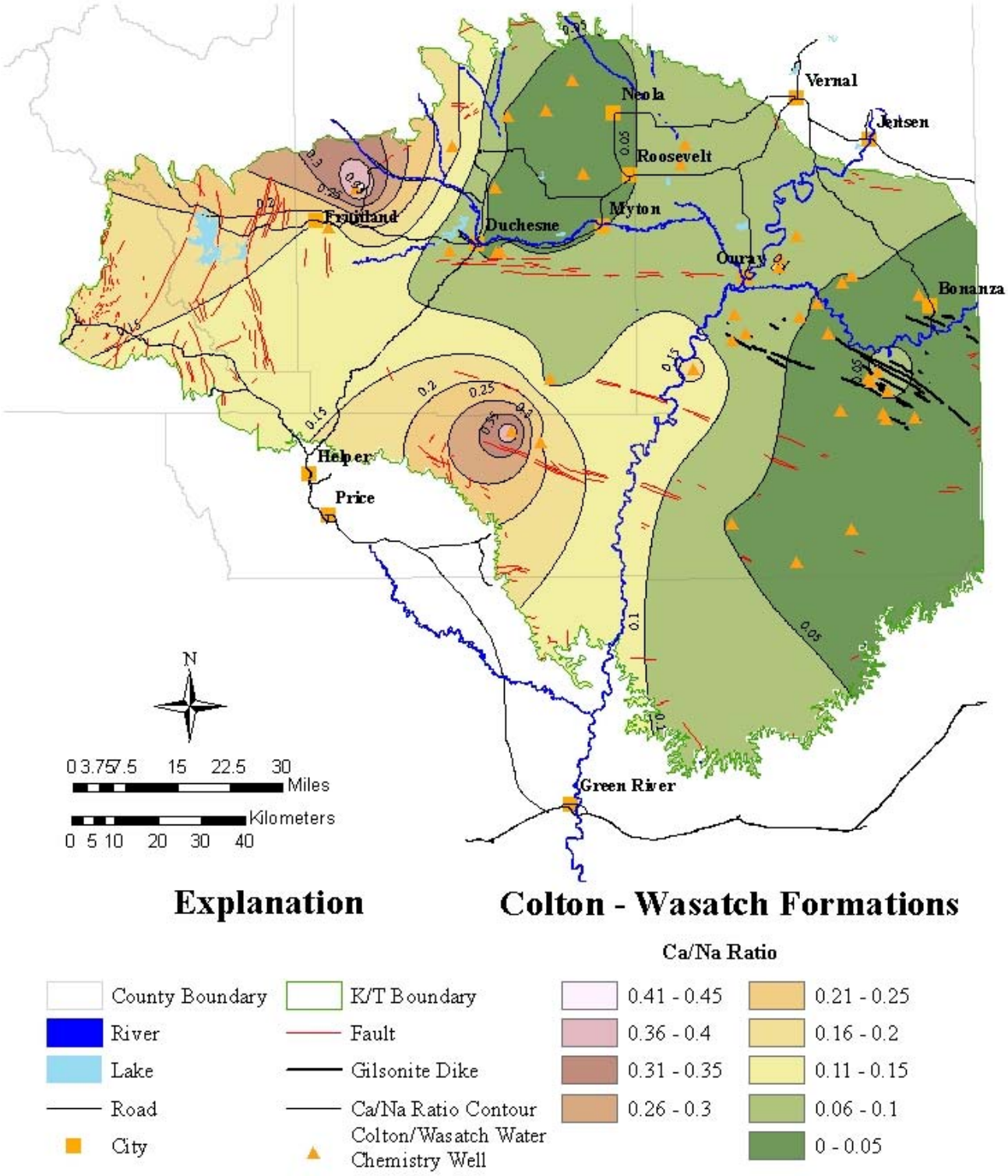

Figure 6.33. Calcium/sodium ratio map for the Wasatch/Colton Formation water. The Ca/Na ratio values from the Wasatch/Colton are highest in the western Uinta Basin.

NATURAL BUTTES UNIT 921-21L
T. 9 S. R. 21 E. Section 21
Uintah County
API: 43-047-39256

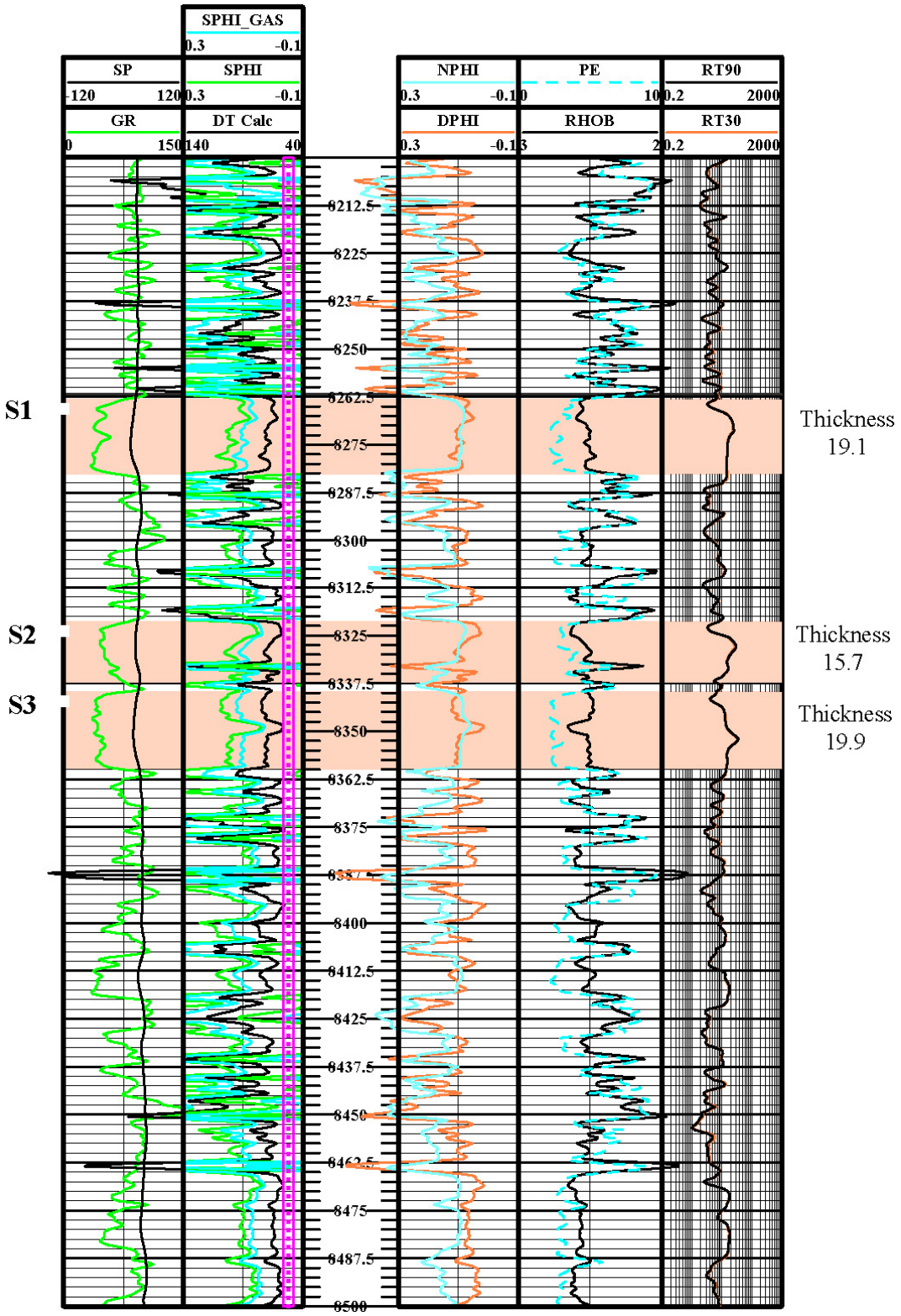

Figure 6.34. Wells log for NBU No. 921-21L, Natural Buttes field, revealing three large sandstone packages in the upper Tuscher Formation. Modeled sandstones have been identified as S1, S2, and S3 on the left side of illustration. Sandstone thickness is presented on the right side of the graphic.

CHAPTER VII

UINTA BASIN RESERVOIRS/AQUIFERS: EOCENE GREEN RIVER FORMATION

Stephanie M. Carney and Michael D. Vanden Berg

Paleocene and Eocene sedimentary rocks make up more than half (>16,000 feet) of the sedimentary sequence within the UB (Anders and other, 1992; Morgan, 2003b), and the Eocene Green River Formation (GRF) constitutes up to 7000 feet of that total (Hintze and Kowallis, 2009; Sprinkel, 2009). As briefly described in Chapter II, the GRF was deposited in marginal lacustrine and lacustrine environments associated with an areally extensive, shallow, saline to freshwater lake—Lake Uinta—in the subsiding UB (figures 1.3 and 2.30). The formation is present throughout the UB; the base is exposed in outcrop along the southern basin boundary and dips to the north-northwest where it is buried over 10,000 feet (figure 7.1). The GRF is an important conventional and unconventional oil play and gas source; the amount of hydrocarbons produced per year solely from the formation accounts for approximately 20% of the state's total oil and 5% of the state's total gas (Utah Division of Oil, Gas, and Mining, 2015e).

Previous water chemistry studies show that salinity of groundwater significantly varies laterally and vertically throughout the UB (Wanty and others, 1991; Anderson and others, 2012). This study was conducted to further define water chemistry trends specifically in the GRF. An extensive water chemistry database, part of a larger groundwater study, was created (appendix G) that contains data from all producing formations within the basin. This database was

compiled from several sources: Howells and others (1987), Gwynn (1992, 1995), Zhang and others (2009), and Anderson and others (2012), as well as previously unpublished USGS data, UGS data, and several company reports. Information from this water chemistry database was used to create regional maps displaying the distribution of TDS concentrations (mg/L) in the GRF. In addition, updated structure contour and isopach maps were generated for the GRF, as well as tabulations of formation-specific hydrocarbon and water production, and water injection volumes.

METHODS

Ancient Lake Uinta started as a fresh water system (Uteland Butte member of the lower GRF), but quickly turned saline (above the Long Point bed within the Carbonate Marker Unit); however, the lake did not become hypersaline until late in its existence (upper GRF). Therefore, saline mineral deposition and preservation only occurred at and above the Mahogany bed, as the lake began to shrink and disappear (Vanden Berg, in preparation). This scenario created a natural divide between the characteristics of the groundwater within the upper GRF, above the Mahogany bed, and the characteristics of the groundwater within the lower GRF, below the Mahogany bed (figure 2.28). Subsequent analyses and interpretations will focus on these two broad intervals.

Formation tops were compiled from several previous studies, the DOGM online database, company reports, and internal UGS files. This dataset includes tops for the Wasatch Formation and GRF, including the Mahogany bed. From this data, structure contour and various isopach

maps were created. Maps were made using the Inverse Distance Weighting (IDW) method within ArcGIS™.

In addition, maps displaying TDS concentrations for water within the GRF were created using the compiled water chemistry database (appendix G). The chemistry data were identified as being from either the upper or lower GRF based on the sample depth relative to the Mahogany bed. Because the upper GRF interfingers with the Uinta Formation above (figure 1.5), the boundary between the two formations is often difficult to identify. Several samples obtained from this transition zone were included in the evaluation of the upper GRF. Most of these samples were collected from the northwest portion of the basin and have high TDS values due to saline mineral dissolution from sediments laid down during the hypersaline last remnant of ancient Lake Uinta.

In most cases, the water chemistry analyses were obtained from samples taken during oil and gas well drilling. A single well commonly had samples taken from multiple depths within the formation or multiple samples taken from the same depth (table 7.1). The sample interval can be less than tens of feet or up to hundreds or thousands of feet. For example, the Red Wash Unit No. 32-27AG well (section 27, T. 7 S., R. 22 E., SLBL&M, Uintah County, API No. 43-047-35670) has water chemistry data from four water samples; two samples from a depth of 5535 to 5539 feet, one sample from 5745 to 5749 feet, and a final sample from 5922 to 5928 feet. In contrast, the Fenceline Federal No. 3-24-8-16 well (section 24, T. 8 S., R. 16 E., SLBL&M, Duchesne County, API No. 43-013-32363) has only one water sample that represents over 1500 feet of strata from 4736 to 6461 feet. Furthermore, some wells with several water samples taken from the same depth were sampled during different years. An example is the Natural Duck No. 1-15 well (section 15, T. 9 S., R. 20 E., SLBL&M, Uintah County, API No.

43-047-30393), which had a water sample taken from 4788 to 4796 feet in 1978 and then a second sample taken from the same interval in 1987. In some cases, wells had multiple water samples taken at different depths over different years.

Fully analyzing the extreme complexity of the groundwater in the GRF, stratigraphically and through time, was beyond the scope of this project. This study focuses on overall averages and trends. To this end, the data were culled, filtered, and averaged so that each well had one representative data point for the upper and/or lower GRF. A sample that was "balanced" (sum of ions equal to measured TDS) and had the most recent sample date was usually selected to represent the well in the final dataset. Samples that were "out of balance" were only used for areas in the basin with sparse data. For samples taken over multiple depths, the most recent sample closest to the median depth was selected.

EOCENE GREEN RIVER FORMATION

The UB formed in the early Cenozoic in response to tectonic activity of the Laramide Orogeny (Hintze and Kowallis, 2009) and was surrounded by several Laramide uplifts: the Uinta, Uncompaghre, and San Rafael to the north, southeast, and southwest, respectively, and the relict Sevier orogenic belt to the west. Structural asymmetry, coupled with the surrounding highlands, created an internally drained basin and lake system—Lake Uinta, which existed throughout the Eocene epoch (figure 7.2). The GRF is a synorogenic deposit of this lake system (Keighley and Flint, 2008). The depocenter of the lake was focused in the northern part of the basin, parallel to the synclinal axis of the UB, but the location shifted from west to east, then

west again, over the lifespan of the lake. Lake Uinta was fringed by alluvial fans and delta complexes, which supplied sediment to the basin from the surrounding highlands (Ryder and others, 1976). In the northwest, deposition of sediments occurred along the deep lake margin, and sandbodies are interpreted to be thin, gravity-flow and shoreface deposits dominated by quartz-rich sediment (Castle, 1990; Remy, 1992; Borer, 2003). Along the northeast margin, sediments were deposited in wave-dominated lacustrine and alluvial fan environments (Borer and McPherson, 1998). Along the south and southwest margins of the lake, fluvial and deltaic deposits dominate due to slower depositional rates and a shallow topographic gradient (Ryder and others, 1976). A large fluvial-deltaic complex, termed the Sunnyside delta, developed along the southern shore of Lake Uinta and extended into the center of the basin (Remy, 1992). The delta consists of fluvial-deltaic, feldspar-rich sandstone, mudstone, and carbonate, and serves as an oil and gas reservoir for many fields in the basin (Fouch, 1975). Over time, lake level fluctuated due to tectonic and climatic changes, and organic-rich lacustrine carbonate and shale were interbedded with alluvial and fluvial sandstone, creating source/reservoir packages (Keighley and others, 2002; Keighley and Flint, 2008).

Thickness

An isopach map representing the entire GRF shows that the thickest section of the formation (~6900 feet) occurs in the western part of the UB, with the formation thinning to the east (~1700 feet) (figure 7.3). The lake generally covered the entire basin soon after its formation, with a depocenter, and thicker strata, centered to the west-northwest during lower GRF time. Figure 7.4 displays an isopach map of the lower GRF (below the Mahogany bed)

with strata up to 3900 feet thick to the west and only 1700 feet thick in the marginal lacustrine areas to the east. Deposits in the central and western parts of the basin are also thicker due to the Sunnyside delta sands coming into the basin in this area. As the lake dried and disappeared, it shrunk from east to west (Vanden Berg and Birgenheier, 2014). Therefore the lake was much longer lived in the west and deposited a much thicker section of upper GRF. This is illustrated in the upper GRF isopach showing sediments to the east at only about 200 feet thick whereas sediments to the west reach 3200 feet in thickness (figure 7.5).

Depth

A structure contour map of the GRF shows the top is at an elevation of ~2000 feet below sea level in the north-central area of the basin and 6700 feet above sea level in the south, which reflects the UB's asymmetrical shape (figure 7.6). An approximate GRF top was picked in roughly 250 wells across the basin. Due to complex interfingering with the Uinta Formation above, the top of the GRF is difficult to pick consistently using geophysical well logs.

Lithology and Stratigraphy

The GRF is a complex sedimentary deposit. In general, the lower portion is characterized by fluvial-deltaic sand interbedded with lacustrine organic-rich mud and carbonate. The upper GRF is dominated by alternating organic-rich and organic-lean marlstone with distinct stages of saline mineral deposition (Vanden Berg, 2008; Vanden Berg and others, 2013). The formation interfingers with the Colton/Wasatch Formation below and the Uinta Formation above (figure

7.7). Because of its depositional complexity, stratigraphic nomenclature for the GRF varies from west to east and has been defined and re-defined by several previous researchers such as Bradley (1931), Fouch (1975), Ryder and others (1976), Weiss and others (1990), Fouch and others (1994), Ruble (1996), and Morgan (2003). Nomenclature is often based on facies that tend to interfinger and change laterally within the basin. Three marker beds, deposited during maximum flooding events of Lake Uinta, can be helpful for regional correlation. These beds are the carbonate marker, middle marker, and Mahogany bed. Figure 7.8 shows how several researchers have divided the GRF over the years (Morgan, 2003b).

Sediments in the lower GRF were deposited in marginal- to open-lacustrine environments during the early, expansive rise in lake level and subsequent fluctuations. Nearly all oil and gas, and associated water, are produced out of reservoirs in the lower GRF. The dominant reservoirs are fluvial and deltaic sands from the Sunnyside delta in the south (e.g., Monument Butte field), alluvial and wave-dominated shoreline sands in the northeast (e.g., Red Wash and Wonsits field), and deltaic/alluvial sands shed off the Uinta Mountains to the north-northwest (e.g., Altamont and Bluebell fields) (see figure 1.1 for field locations). These sands, as well as associated carbonate grainstone reservoirs, are typically lenticular in geometry and are interbedded with open-lacustrine limestones and shales, reducing the connectivity between individual reservoirs. This also creates a situation where groundwater chemistry can vary significantly laterally and vertically. Some carbonate deposits, such as the dolomite intervals within the basal Uteland Butte member of the lower GRF, create a more laterally consistent reservoir, but despite the high porosity (up to 30%), permeability is very low (Vanden Berg and others, 2014).

For this study, the base of the upper GRF is marked by the Mahogany bed, which is a very organic-rich (up to 40% TOC) marlstone deposited during the maximum high-stand of Lake

Uinta (U.S. Geological Survey, 2010b; Tänavsuu-Milkeviciene and Sarg, 2012). The Mahogany interval and younger strata in the upper GRF record three phases of hypersaline conditions and saline mineral deposition (Vanden Berg and others, 2013; Vanden Berg and Birgenheier, 2014; Vanden Berg, in preparation). These saline intervals greatly influence groundwater chemistry within this interval.

The phase 1 saline zone occurred during Lake Uinta's maximum lake transgression (Mahogany bed) and was restricted to the paleo-depocenter in the northeast part of the basin (figure 7.9). Saline mineral deposition covers an area of approximately 203 square miles and is characterized by large nahcolite ($NaHCO_3$) nodules and minor associated small saline mineral crystals that formed within or near the Mahogany zone (Vanden Berg, in preparation). Evidence of these large nodules in core indicates that no post-deposition dissolution has taken place within the phase 1 saline zone (figure 7.9), thus these saline minerals will have little influence on groundwater salinity.

The phase 2 saline zone has previously been identified and studied as the Birds Nest aquifer interval or Birds Nest saline interval, historically by Cashion (1967) and Dyni (1996). Most recently, Vanden Berg and others (2013) completed a very extensive report on the Birds nest aquifer, which includes a detailed discussion of its origin, properties, and groundwater characteristics. The beginning of this saline interval is related to a strongly regressive phase of Lake Uinta and is correlative to the Horse Bench Sandstone, which was deposited in the southwest portion of the Uinta Basin (Dyni, 1996; Toms, 2014).

The phase 2 saline zone is separated into two distinct facies, the large-saline-nodule (LSN) facies and the small-saline-crystal (SSC) facies. Two distinct intervals, a lower and an upper zone, of the LSN facies occur within an overall, more regionally extensive SSC facies

zone (figure 7.10). The more extensive lower LSN facies represents the first phase 2 deposition of large nahcolite nodules in the basin's paleo-depocenter (figure 7.11). This interval is overlain by a thick sequence of organic-lean marlstone (oil shale) with only minor saline mineral deposition—mostly small crystals and shortite ($Na_2Ca(CO_3)_2$) (SSC facies). A more aerially restricted upper large nodule zone records a second period of nahcolite nodule deposition followed again by a sequence of organic-lean marlstone with only minor small saline crystals (figure 7.11). Similar to the phase 1 saline zone, the large saline nodules found in phase 2 correlate well with the area in the UB of highest oil yield within the middle R-8 oil shale interval (Bed 44 to Bed 76) measured in barrels per acre (U.S. Geological Survey, 2010b) (figure 7.11). Again, this area of high organic matter accumulation is recognized as the paleo-depocenter of the basin and would be the same place large nahcolite nodules might form. Extending away from the basin's paleo-depocenter and the area with the LSN facies, the overall phase 2 saline zone thins and contains only deposition of small saline crystals (figure 7.11). This transition is confirmed in the southern part of the basin where cores and outcrop exposures are present, and it is presumed that the same transition to small saline crystals exists to the north, but no cores exist to confirm this hypothesis. The 16X-23D-36 core (section 23, T. 3 S., R. 6 W., USBL&M, Duchesne County, API No. 43-013-50623), on the far western side of the basin, captured a small portion from the same stratigraphic interval that displays small saline crystals, confirming that the SSC facies extend nearly basin wide.

After defining the areal extent of the LSN zones, the tops database could be used to create isopach maps of the upper and lower zones. The lower LSN zone, as defined by 217 wells, covers 719 square miles and averages 84 feet thick (figure 7.12). The lower zone has the shape of an elongated oval and is thickest in the center (between 100 and 110 feet thick), and

gradually thins toward the north and south (between 33 and 40 feet thick). The upper LSN zone, as defined by 150 wells, covers 410 square miles and averages 79 feet thick (figure 7.12). The interval is thickest near its center (between 100 and 110 feet thick) and gradually thins toward its edges (between 33 and 40 feet thick) defining the bowl-like structure of the ancient lake's depocenter.

The phase 3 saline zone has been previously recognized as the "saline facies" of Bradley (1931), Dane (1954), Dyni (1976), and Dyni and others (1985). This interval is well exposed in Indian Canyon on the southwestern side of the UB and measures about 1100 feet thick. Similar to the other saline intervals, there is an area within the interpreted paleo-depocenter of the basin that contains a greater concentration of evaporative minerals. However, instead of large nodules of nahcolite, which define the former two phases, the third phase is characterized by deposition of bedded halite (first appearance in the UB) mixed with beds/crystals of other obscure sodium-rich minerals such as trona ($Na_2CO_3 \bullet NaHCO_3 \bullet 2H_2O$), wegscheiderite ($Na_2CO_3 \bullet NaHCO_3$), leucosphenite ($Na_2Ca,Ba)10B_2Ti_5Si_{19}O_{15}$), reedmergnerite ($Na_2B_2SiO_6$), searlesite ($Na_2B_2Si_4O_6 \bullet 2H_2O$), and eitelite ($Na_2CO_3 \bullet MgCO_3$), as well as nahcolite and shortite (Milton and others, 1954a, 1954b; Dyni and others, 1985).

The Shrine Hospital No. 1 core (section 10, T. 3 S., R. 5 W., USBL&M, Duchesne County, API No. 43-013-30393) is the only core that captured the bedded evaporites found in the phase 3 saline zone (figure 7.13). This core was extensively studied by Dyni and others (1985) so only a brief description will be included here. Between 4165 and 4251 feet, three prominent evaporative beds occur that are 2, 6, and 12 feet thick and are composed of primarily halite with lesser amounts of wegscheiderite (figure 7.13). There are an additional six thinner beds of mixed sodium carbonate minerals (nahcolite, trona, wegscheiderite, and eitelite) that range from 0.3 to

1.5 feet in thickness. These saline mineral sequences are interbedded with brown dolomitic marlstone that contains scattered crystals and thin layers of shortite, nacholite, northupite ($Na_2CO_3 \bullet MgCO_3 \bullet NaCl$), and eitelite (small crystal facies) (Dyni and others, 1985). In the lower part of the core is a light bluish-gray tuff bed (Fat tuff), 6.2 feet thick, that can be correlated to several other cores in the area.

The bedded saline minerals found in the Shrine Hospital No. 1 core can be readily identified using geophysical logs, in particular the density logs and washouts in the caliper log. By analyzing logs from oil and gas wells in the surrounding area, it is possible to estimate the regional extent of the saline mineral beds. The phase 3 saline zone covers an estimated area of 117 square miles (figure 7.14) (Vanden Berg, in preparation). The area correlates well with the area in the UB with the thickest interval of GRF, indicating the area where the lake was longest lived.

Again, similar to phase 1 and 2, the area of bedded evaporative minerals seems to be surrounded by an area containing only smaller saline mineral crystals (SSC facies) with a more expansive area to the west (figure 7.14). The extent of the SSC facies is roughly defined to the south by the presence of saline minerals captured in several cores: Half Moon Canyon 1, Sams Canyon 1, Marine Minerals Core hole 1, and Marine Minerals Core hole 2, all of which can be correlated with the Fat tuff. This interval is also exposed in outcrop, but only the Indian Canyon exposures have been thoroughly studied (Dyni and others, 1985). The western extent can be approximated based on previous field-based studies that indicate small saline mineral crystals in the “saline facies” in outcrops 15 miles west of Indian Canyon along the Walker Hollow road (Dane, 1954) and as far away as 40 miles west of Indian Canyon, southwest of Strawberry Reservoir, in sections 10 and 15, T. 5 S., R. 12 W., USBL&M, Duchesne County (Dyni and

others, 1985). The northern boundary of the phase 3 SSC facies cannot be accurately defined due to a lack of core or exposures in the area, but is presumed to pinch out or interfinger with Uinta Formation sands coming off the Uinta Uplift not far north of the bedded saline zone (figure 7.14).

Reservoir Properties

Porosity in GRF reservoirs generally ranges from 5 to 30%, but is highly variable depending on reservoir and porosity type, and location (Lucas and Drexler, 1975; Osmond, 1985; Fouch and others, 1992a, 1992b; Kelly and Castle, 1992; Vanden Berg and others, 2014; Schamel, 2015). Permeability typically ranges from 0.1 to 42 mD, and is similarly highly variable (Fouch and others, 1992a; Kelley and Castle, 1992). Reservoir porosity and permeability are greatly affected by diagenetic processes. For example, compaction (extreme in the Altamont-Bluebell field area), quartz overgrowths, extensive carbonate cementation, and authigenic clay formation (illite [Altamont-Bluebell], kaolinite [Monument Butte-Natural Buttes], chlorite, and smectite) have all reduced reservoir porosity and permeability in the GRF (Pitman and others, 1982; Colburn and others, 1985; Fouch and others, 1992b; Kelly and Castle, 1992). Whereas, secondary dissolution of both framework grains and carbonate cement has increased reservoir porosity and permeability as much as 25% in some areas (Kelly and Castle, 1992). Natural, open fractures greatly enhance permeability in reservoirs, especially in the northern part of the basin in the Cedar Rim, Altamont, and Bluebell fields (Narr and Currie, 1982; Morgan, 2003b).

Water Quality

Groundwater movement in the UB generally follows the slope and direction of major streams and rivers (Price and Miller, 1975; Wallace, 2012a). For the southeastern part of the basin, flow direction is from the southeast to the northwest, and for the north, groundwater generally flows from northwest to southeast. Recharge to the basin mostly occurs from the Uinta Mountains to the north, with a smaller amount coming from outcrops along the southern and eastern margins of the basin (Zhang and others, 2009). However, the complexity of the GRF reservoirs, their lenticular morphology, and often being surrounded by low permeability facies such as lacustrine limestone and shale, creates significant heterogeneity in overall groundwater characteristics.

In general, water quality in the lower GRF tends to have an overall TDS concentration greater than 10,000 mg/L (416 out of 532 wells/samples), but values range from 650 to 112,000 mg/L (figure 7.15). Areas of lowest TDS concentration are coincident with areas of recharge along outcrops near the Douglas Creek arch to the east-southeast and along the Wasatch Plateau to the west. In addition, an area to the north seems to record low TDS water, indicating recharge from the Uinta Mountains, but data are sparse. An area of high TDS concentration occurs in a northeast-southwest-trending zone in the central part of the basin and is roughly coincident with the surface location of the Green River. Within this zone, the highest TDS values (>60,000 mg/L) occur in water located between 300 and 800 feet of elevation and 1200 to 2000 feet below the Mahogany bed. The dominant cations and anions are sodium (Na), chloride (Cl), and sulfate (SO_4); bicarbonate (HCO_3), calcium (Ca), and magnesium (Mg) occur in minor amounts. As stated above, the general groundwater flow direction is towards the major river systems (i.e., the

Green River). This area of higher TDS could represent long-residence time water funneling towards the Green River from outcrop areas to the east and west, picking up solutes as it travels.

TDS values for the upper GRF range from 600 mg/L to over 300,000 mg/L and are heavily influenced by the existence of saline minerals in certain areas of the basin (saline phases as identified above) (figure 7.16). The isolated and few nahcolite nodules found within the phase 1 saline zone, located within the Mahogany zone, do not influence groundwater salinity and therefore this interval is not displayed on figure 7.16.

Groundwater related to the phase 2 saline interval (Birds Nest aquifer) varies significantly from southeast to northwest. Using data compiled during this study and from Vanden Berg and others (2013), it was possible to delineate a southeast to northwest transition from low to higher TDS water within the Birds Nest aquifer (figure 7.17). Chemistry of water to the northwest of the boundary (averaging >10,000 mg/L TDS and as high as 100,000 mg/L TDS) is distinct from that in the southeast (averaging <10,000 mg/L TDS and down to near 1000 mg/L TDS). The observed variations in Birds Nest aquifer salinity are most likely due to differing amounts of saline mineral dissolution. Areas where Birds Nest aquifer TDS values are <10,000 mg/L are located near and immediately downdip from areas of aquifer recharge such as Evacuation Creek, the White River, and outcrops to the east and south. In these areas, continuous freshwater recharge and flushing over time have likely removed all of the original natural saline minerals. Areas where the Birds Nest aquifer salinity is known to exceed 10,000 mg/L TDS are located away from active aquifer recharge and flushing, so the original saline minerals are still present and possibly undergoing active dissolution. Wells with high TDS concentrations have water chemistry with abundant sodium (Na) and bicarbonate (HCO_3), as expected from the dissolution of nacholite (Na_2HCO_3). For example, water analyses from this

interval in the Hoss No. 904-36 well (section 36, T. 8 S., R. 22 E., SLBL&M, Uintah County, API No. 43-047-50304) has 62,537 mg/L of HCO_3 and 27,800 mg/L of Na. In contrast, water from the same interval from a well farther south, the Bonanza No. 1023-14C (section 14, T. 10 S., R. 23 E., SLBL&M, Uintah County, API No. 43-047-38299) contains only 585 mg/L of HCO_3 and 1059 mg/L of Na.

High TDS areas in the upper GRF in the northwest and central portion of the basin are likely due to the presence of disseminated and bedded saline minerals of the phase 3 saline zone, stratigraphically higher than the Birds Nest aquifer. Several sample sites, indicated as red triangles on figure 7.16, are from the GRF-Uinta Formation transition zone. Two wells within the phase 3 bedded saline zone have water chemistry strongly reflective of the mineral halite. The Altamont No. 1 salt water disposal well (section 24, T. 2 S., R. 6 W., USBL&M, Duchesne County, API No. 43-013-30372) has 120,000 mg/L of Na and 180,000 mg/L of Cl, and the Ute 1-14C6 (section 14, T. 2 S., R. 6 W., USBL&M, Duchesne County, API No. 43-013-30056) has 122,443 mg/L of Na and 141,600 mg/L of Cl, but also has significant HCO_3 (12,200 mg/L), indicating the presence of nahcolite. All other wells in the phase 3 saline zone have water with varying concentrations of Na, Cl, and HCO_3, as well as varying amounts of minor constituents including Mg, SO_4, and Ca. As shown on the TDS map of the upper GRF (figure 7.16), not only do the bedded salts influence groundwater chemistry, but the larger area of SSC has a significant impact on overall water quality.

Anderson and others' (2012) study of water quality in the UB produced a map of the BMSW (TDS of 10,000 mg/L). Using the newly updated structure contour map of the GRF, a map was created to show where the top of the GRF is relative to the BMSW (figure 7.18). The map shows that the top of the GRF is up to 6000 feet below the BMSW in the north, whereas the

top of the formation is above the BMSW (up to 5300 feet) in the southern, western, and eastern parts of the basin.

Water Production, Use, and Disposal

Total cumulative water production from the GRF varies across the basin from 15 bbls at Oil Springs field in the southeast, where the only well to produce from the GRF is now plugged and abandoned, to over 347 million bbls at Red Wash field in the northeast (figure 7.19). The cumulative total of water produced from the GRF is over 754 million bbls (MMB) from 5355 wells in 46 named fields, 3 wildcats, and 3 undesignated fields, as of December 2014. The average cumulative water volume produced per well equals about 140,000 bbls (MB), but this average is skewed high due to a minority of wells with greater than 1 MMB of production. The vast majority of wells (4400 out of 5310) have cumulative production between 1000 and 100,000 BW (figure 7.20A) and daily production between 1 and 5 bbls (figure 7.20B). A word of caution, several thousand wells in the UB produced from both the GRF and the underlying Wasatch Formation. This production is commingled and there is no way to distinguish production between the formations. This commingled data is not included in this study.

At Monument Butte field (figure 1.1) and several other UB fields, produced water from the GRF reservoirs is treated and used for major EOR waterflood programs. In 2012, for example, 8.2 MMBW were produced at Monument Butte and 22 MMBW were injected for waterflooding.

Elsewhere, water produced from the GRF, and other formations, is currently disposed using injection wells and evaporation ponds. There are currently 51 salt water disposal wells

active in the GRF as of May 2015 (figures 7.21 and 7.22) (Utah Division of Oil, Gas, and Mining, 2015e). Eighteen of these wells are in the western part of the basin and 32 are in the east, where more than half inject into the Birds Nest aquifer (denoted by star shape on figure 7.21). The total volume of water injected as of May 2015 is 356 MMB (Utah Division of Oil, Gas, and Mining, 2015e), with most wells injecting between 1 million and 10 million total bbls or 1000 to 2500 BPD (figure 7.23). Of the total water volume injected, 137 MMB has been injected into the lower GRF and 219 MMB in the upper GRF, of which 121 MMB went into the Birds Nest aquifer.

The Birds Nest aquifer (phase 2 saline zone) has significant potential for water disposal as discussed in detail in Vanden Berg and other (2013). In an area of known saline mineral dissolution, the upper Birds Nest zone has an area of ~359 square miles (mi^2) and a mean thickness of 81.7 feet, which equals a total volume of 8.2×10^{11} cubic feet (ft^3). Vanden Berg and others (2013) calculated a macro pore volume (at 2.5%) of 20.4 billion ft^3 (469,157 acre feet) for saline water storage/disposal. For the lower Birds Nest, they estimated an area of 498.6 mi^2, a mean thickness of 85.2 feet, a total volume of 1.2×10^{12} ft^3, and a macro pore volume (at 2.5%) of 29.6 billion ft^3 (679,908 acre feet). However, several assumptions were made to derive these numbers, actual reservoir storage could vary significantly (see Vanden Berg and others [2013] for a detailed discussion of the Birds Nest aquifer and its disposal potential).

Hydrocarbon Production

Cumulative production from the GRF totals over 315 MMBO and 900 BCFG, as of December 2014. The producing reservoirs are stratigraphic and fracture-enhanced structural

traps composed of lenticular sandstone beds, carbonate beds, and shale (Morgan, 2003b). Production of oil and gas from the GRF is largely focused in the north-central, south-central, and northeast portions of the basin (figure 7.24 and 7.25). The fields with highest cumulative oil production are Red Wash (85 MMBO), Monument Butte (65 MMBO), and Wonsits Valley (48 MMBO) and fields with highest cumulative gas production are Red Wash (373 BCF), Monument Butte (129 BCF), and Brundage Canyon (113 BCF). Total oil production from the GRF averages about 60,000 bbls per well, with the best producer reaching 2.7 MMBO (Woodward No. 1-21A2 well, section 21, T. 1 S., R. 2 W., USBL&M, Duchesne County, API No. 43-013-30130, Bluebell field, figures 7.24 and 7.25). However, most wells have produced between 10,000 and 100,000 bbls of oil (BO) (3528 out of 5306 wells) and between 1 and 25 BO per day (4017 out of 5257 wells) (figure 7.26A and C). Total gas production from the GRF is much more variable and averages about 170 MMCF per well, with the best producer reaching a very high 45 BCF (RW No. 32-33C, section 33, T. 7 S., R. 24 E., SLBL&M, Uintah County, API No. 43-047-15171, Red Wash field, figures 7.24 and 7.25). However, most wells have cumulatively produced between 10 MMCFG and 1 BCFG (4223 out of 5304 wells) with daily production between 10 and 50 MCF (2946 out of 5263 wells) (figure 7.26B and D). As stated above, several thousand wells in the UB produced from both the GRF and the underlying Wasatch Formation. This commingled data is not included in this study.

SUMMARY

The GRF is a complex lacustrine sedimentary deposit that is up to 7000 feet thick. The lower GRF, defined as below the Mahogany bed in this study, is mostly lacustrine organic-rich mud and limestone (main source rocks) interbedded with fluvial-deltaic sand and carbonate grainstones (main reservoir rock). The upper GRF, defined as above the Mahogany bed, consists of alternating organic-rich and organic-lean marlstone with three distinct stages of saline mineral deposition, the second of which includes the Birds Nest aquifer. Production from the GRF has totaled 315 MMBO, 900 BCFG, and 754 MMBW as of December 2014.

Water quality in the complex lower GRF varies widely from 650 to 112,000 mg/L of TDS. Groundwater movement in the UB generally follows the slope and direction of major streams and rivers, with recharge mostly from the Wasatch Range to the west, the Douglas Creek arch and Uncompahgre uplift to the east-southeast, and the Uinta Mountains to the north. Groundwater in the lower GRF seems to travel toward the Green River in the central portion of the basin and coincides with an area of higher TDS water.

Water quality in the upper GRF also varies widely from 600 to over 200,000 mg/L TDS. Groundwater in the upper GRF is highly influenced by the location of saline mineral deposition, which occurs in three distinct phases and locations.

The unique Birds Nest aquifer (phase 2 saline zone) in the upper GRF in the eastern part of the UB and the area located around the phase 3 saline interval in the western part of the basin, as well as select areas in the lower GRF, serve as excellent produced water disposal zones since reservoir water already exceeds 10,000 TDS (mg/L). In fact, over 356 MMB of produced water have already been disposed of into GRF reservoirs.

CHAPTER VII FIGURE AND TABLE CAPTIONS

Figure 7.1. Overview map showing location of study area, the outcrop of the top and base of the Green River Formation, and the outcrop of the Mahogany bed.

Figure 7.2. Paleogeographic reconstruction of the Uinta Basin during the Eocene epoch (from Blakey and Ranney, 2008).

Figure 7.3. Isopach map of entire Green River Formation.

Figure 7.4. Isopach map of lower Green River Formation, below the Mahogany bed.

Figure 7.5. Isopach map of upper Green River Formation, above the Mahogany bed.

Figure 7.6. Structure contour map of the top of the Green River Formation, illustrating the northerly dip of the beds.

Figure 7.7. General stratigraphic columns of the Green River Formation (from Hintze and Kowallis, 2009).

Figure 7.8. A compilation of the various stratigraphic nomenclature used for the Green River Formation throughout the years and across the basin. CM = Carbonate marker; MM = Middle marker; MS = Mahogany shale (bed) (from Morgan, 2003b).

Figure 7.9. Extent of the phase 1 saline interval in the upper Green River Formation. Saline mineral deposition occurs within the paleo-depocenter of the lake during Mahogany zone time, as illustrated by organic-richness (oil yield) in barrels per acre (U.S. Geological Survey, 2010b). The extent was identified by examining core and "gas-plus-loss" measurements from Fischer assay analyses. During the heating of rock samples for Fischer assay analysis, nahcolite within a sample will decompose, giving off large amounts of carbon dioxide recorded as "gas plus loss." Therefore, a high weight percent of "gas plus loss" indicates the presence of significant saline minerals. This phenomenon is discussed in detail by the U.S. Geological Survey (2010a). The inset photo displays intact nacholite nodules within the Red Wash No. 1 core.

Figure 7.10. The Utah State No. 13X-2 core represents a typical phase 2 saline zone section from the basin's paleo-depocenter. The phase 2 saline zone in this area is nearly 400 feet thick and contains two intervals with large saline mineral nodules/beds. The upper large-saline-nodule zone is 94 feet thick (1476 to 1570 feet) and the lower zone is 99 feet thick (1690 to 1789 feet). A – Nahcolite beds, 1760 to 1769 feet. B – Dissolved nahcolite nodule, 1528 feet. C – Dissolved nahcolite nodule lined with pyrite, 1774 feet. D – Dissolved nahcolite nodules, 1769 to 1776 feet. E – Shortite fracture fill, 1580 feet.

Figure 7.11. Extent of the phase 2 saline interval (Birds Nest aquifer) in the upper Green River Formation. The most abundant saline mineral deposition occurs within the paleo-depocenter of the lake during middle R-8 time, as illustrated by organic-richness (oil yield) in barrels per acre (U.S. Geological Survey, 2010b). Saline mineral distribution is influenced by two significant

siliciclastic deposits, the Horse Bench Sandstone on the west side of the basin and volcaniclastic debris flows on the east side.

Figure 7.12. Isopach maps, with depth contours, of the upper and lower "large-saline-nodule" facies (upper and lower Birds Nest aquifers) from the phase 2 saline zone.

Figure 7.13. Shrine Hospital No. 1 core representative of the phase 3 saline zone section. A – Generalized lithologic description of the Shrine Hospital No. 1 core, showing bedded saline minerals from the phase 3 saline zone (from Brownfield and others, 2010). B – Several feet of bedded halite with smaller wegscheiderite crystals and other sodium-rich saline minerals (between red lines) from 4180.3 to 4192.5 feet (mineral identification from Dyni and others, 1985). C – Large subhedral crystals of eitelite in marlstone (oil shale), 4248.4 feet (mineral identification from Dyni and others, 1985). Yellow bar equal one-tenth foot. D – Bedded halite (darker gray, glassy, partially dissolved) with wegscheiderite crystals (light gray, more resistant), 4187.1 feet (mineral identification from Dyni and others, 1985). Yellow bar equal one-tenth foot.

Figure 7.14. Extent of the phase 3 saline interval in the upper Green River Formation. The area with bedded salt deposition occurs within the area of thickest sediment accumulation in the Green River, representing the paleo-depocenter of the lake during its final phase of existence.

Figure 7.15. Map displaying available total dissolved solids concentrations (mg/L) from water samples taken within the lower Green River Formation.

Figure 7.16. Map displaying available total dissolved solids concentrations (mg/L) from water samples taken within the upper Green River Formation.

Figure 7.17. Map displaying available total dissolved solids concentrations (mg/L) from water samples taken within the Birds Nest aquifer (phase 2 saline zone) (from Vanden Berg and others, 2013).

Figure 7.18. Map showing the depth from the base of the moderately saline water (BMSW) to the top of the Green River Formation (Anderson and others, 2012).

Figure 7.19. Bubble map showing cumulative produced water (barrels) from the Green River Formation by oil or gas fields (through December 2014) (Utah Division of Oil, Gas, and Mining, 2015e).

Figure 7.20. Histogram displaying total water production (barrels) by well from the Green River Formation (through December 2014) (Utah Division of Oil, Gas, and Mining, 2015e). A – Cumulative water production. B – Water production per day.

Figure 7.21. Location of injection wells currently disposing produced water (barrels) into the Green River Formation (Utah Division of Oil, Gas, and Mining, 2015e).

Figure 7.22. Bubble map showing the volume of water (barrels) that has been injected into the Green River Formation from each injection well (Utah Division of Oil, Gas, and Mining, 2015e).

Figure 7.23. Histograms displaying water (barrels) injected into the Green River Formation via disposal wells (through March 2015) (Utah Division of Oil, Gas, and Mining, 2015e). A – Cumulative water injection per well. B – Water injection per day per well.

Figure 7.24. Bubble map showing the volume of oil (barrels) produced from the Green River Formation by field (Utah Division of Oil, Gas, and Mining, 2015e).

Figure 7.25. Bubble map showing the volume of gas (MCF) produced from the Green River Formation by field (Utah Division of Oil, Gas, and Mining, 2015e).

Figure 7.26. Histograms displaying cumulative (A) oil (barrels) and (B) gas (MCF) and daily production of (C) oil (barrels) and (D) gas (MCF) by well from the Green River Formation (through December 2014) (Utah Division of Oil, Gas, and Mining, 2015e).

Table 7.1. Examples of wells with varied water sample depths, dates, and total dissolved solid concentrations.

Table 7.1. Examples of wells with varied water sample depths, dates, and total dissolved solid concentrations.

Well Name	Sample Depth (ft)	Date Sampled	TDS (mg/L)	Balanced	Upper or Lower	Sample selected
Red Wash Unit 32-27AG	5535-5539	2/7/2005	25,720	Yes	Lower	Chose sample at 5745-5749 ft depth, which had more recent sample date and TDS value closest to average value of all three 2005 samples
	5535-5539	2/9/2005	42,005	Yes	Lower	
	5745-5749	1/20/2005	29,220	Yes	Lower	
	5922-5928	12/10/2004	37,835	Yes	Lower	
Fenceline Federal 3-24-8-16	4736-6461	11/21/2006	24,478	Yes	Lower	Only sample for this well
Natural Duck 1-15	4788-4796	5/13/1987	72,962	Yes	Lower	Chose most recent sample
	4788-4796	8/18/1978	18,399	Yes	Lower	
Lake Fork 2-23B4	4204-4645	11/3/1987	65,371	Yes	Upper	Chose both samples since one represented upper GRF and one
	11050-11220	6/7/1973	6693	Yes	Lower	
Red Wash Unit 41-9F	1818-1836	5/1/1956	2390	Yes	Upper	Used an average TDS value
	1818-1836	5/23/1956	2394	Yes	Upper	
Windmill	1382	7/15/2009	2394	No	Upper	Chose most recent, balanced sample
	1382	9/21/2010	2106	Yes	Upper	
Island Unit 3	3310-3337	10/21/1960	2490	No	Lower	Chose most recent, balanced sample (TDS = 31,000)
	3488-3514	Unknown	28,490	Yes	Lower	
	3488-3514	7/12/1962	31,000	Yes	Lower	
	3488-3514	7/12/1962	31,008	Yes	Lower	

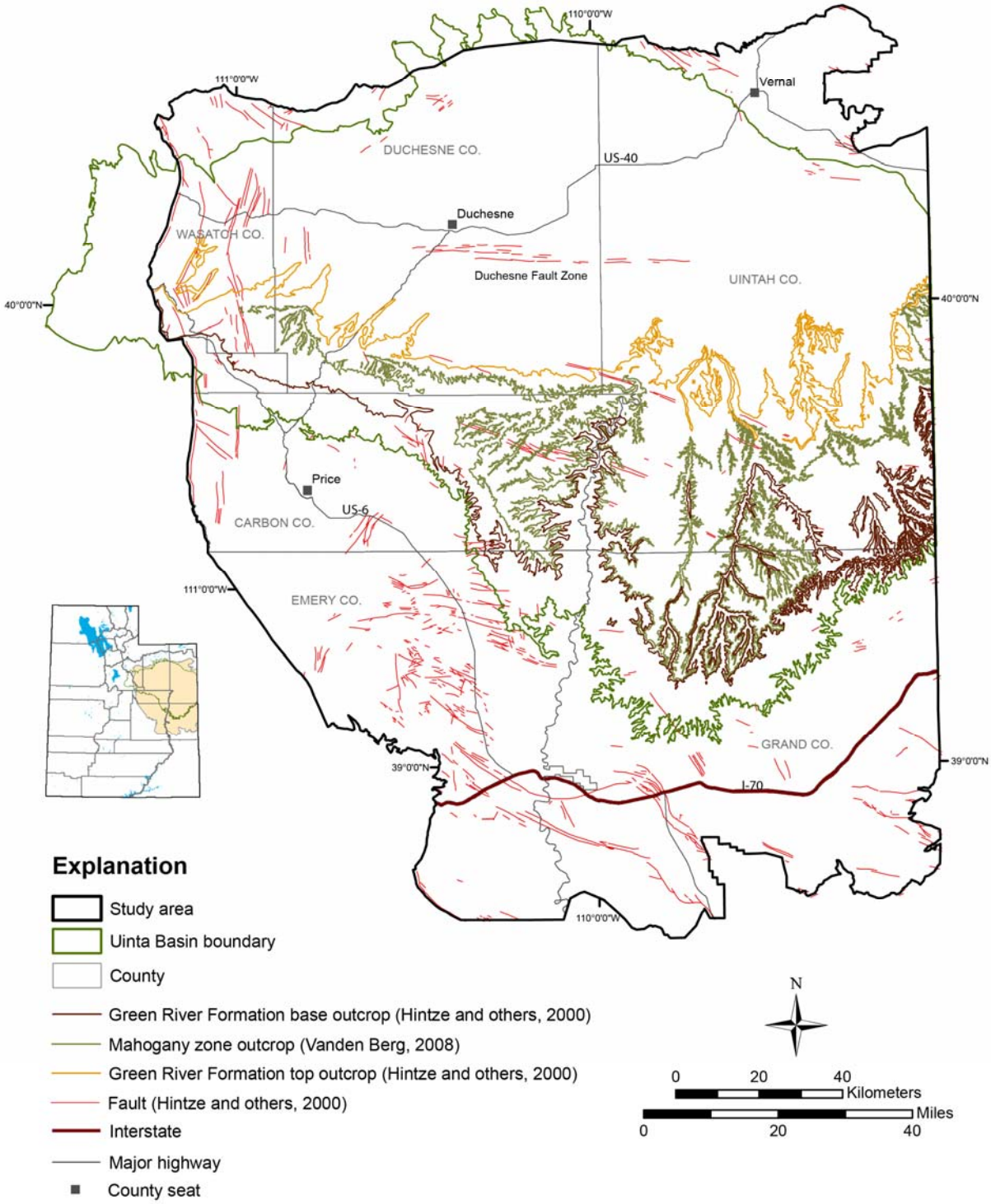

Figure 7.1. Overview map showing location of study area, the outcrop of the top and base of the Green River Formation, and the outcrop of the Mahogany bed.

Figure 7.2. Paleogeographic reconstruction of the Uinta Basin during the Eocene epoch (from Blakey and Ranney, 2008).

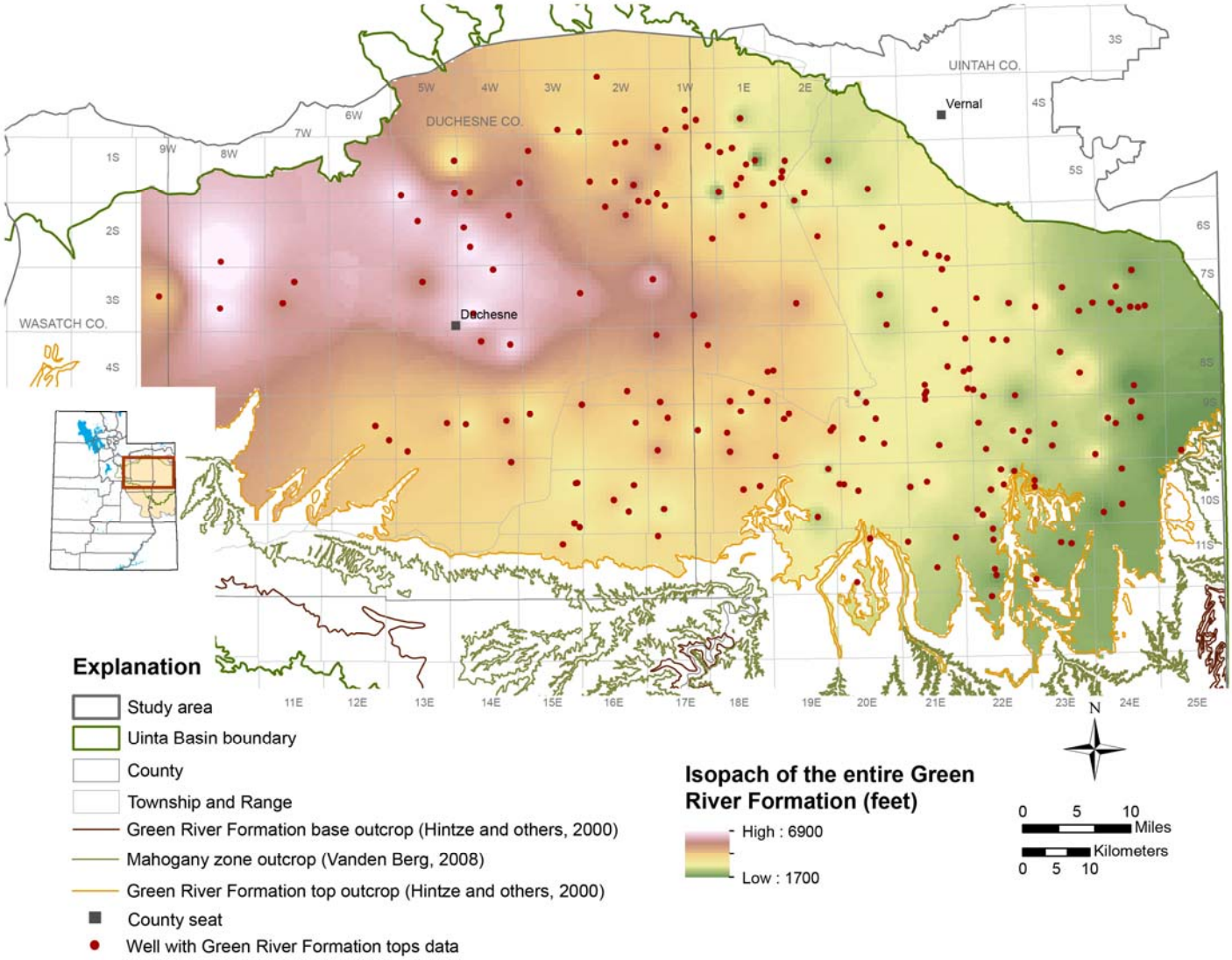

Figure 7.3. Isopach map of entire Green River Formation.

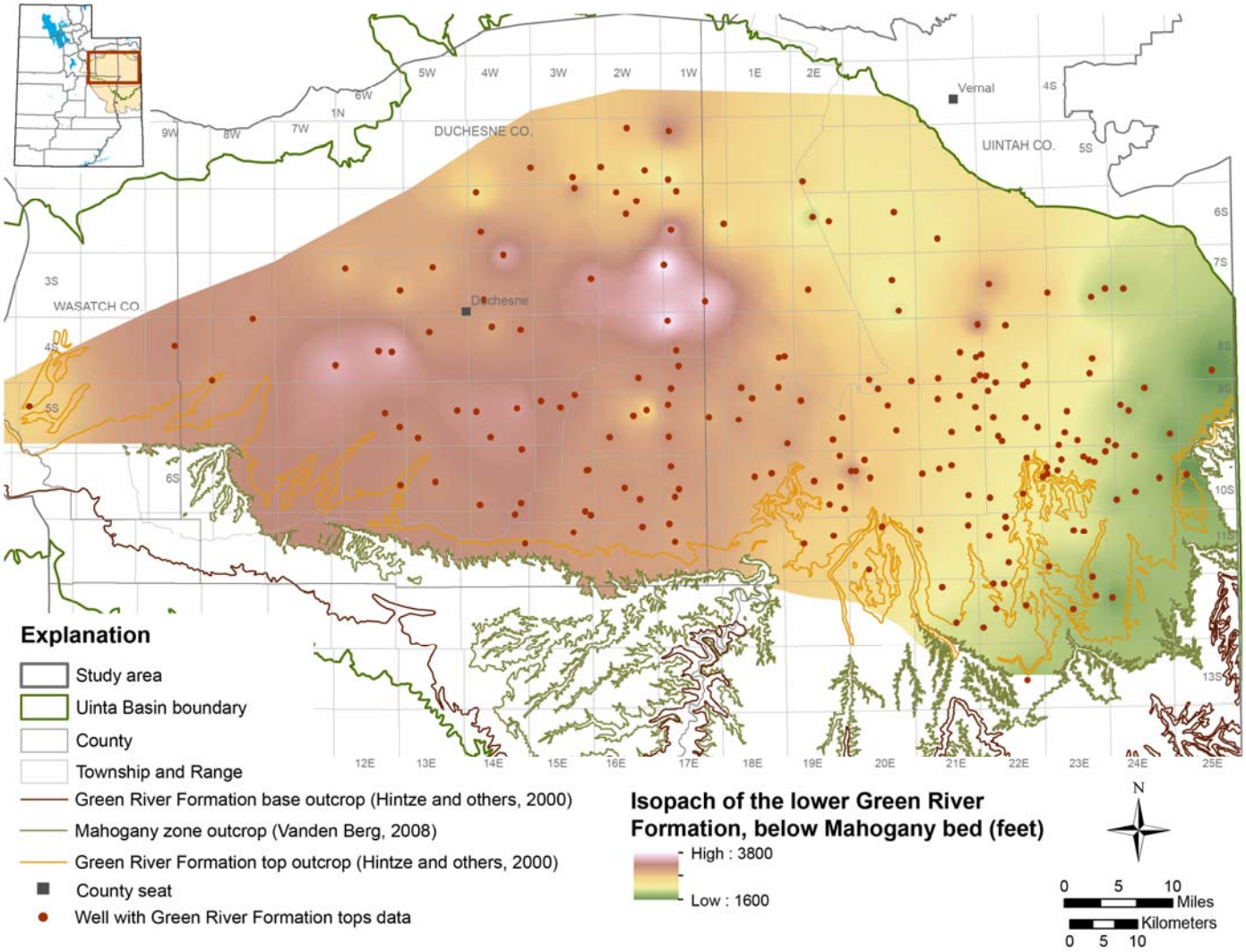

Figure 7.4. Isopach map of lower Green River Formation, below the Mahogany bed.

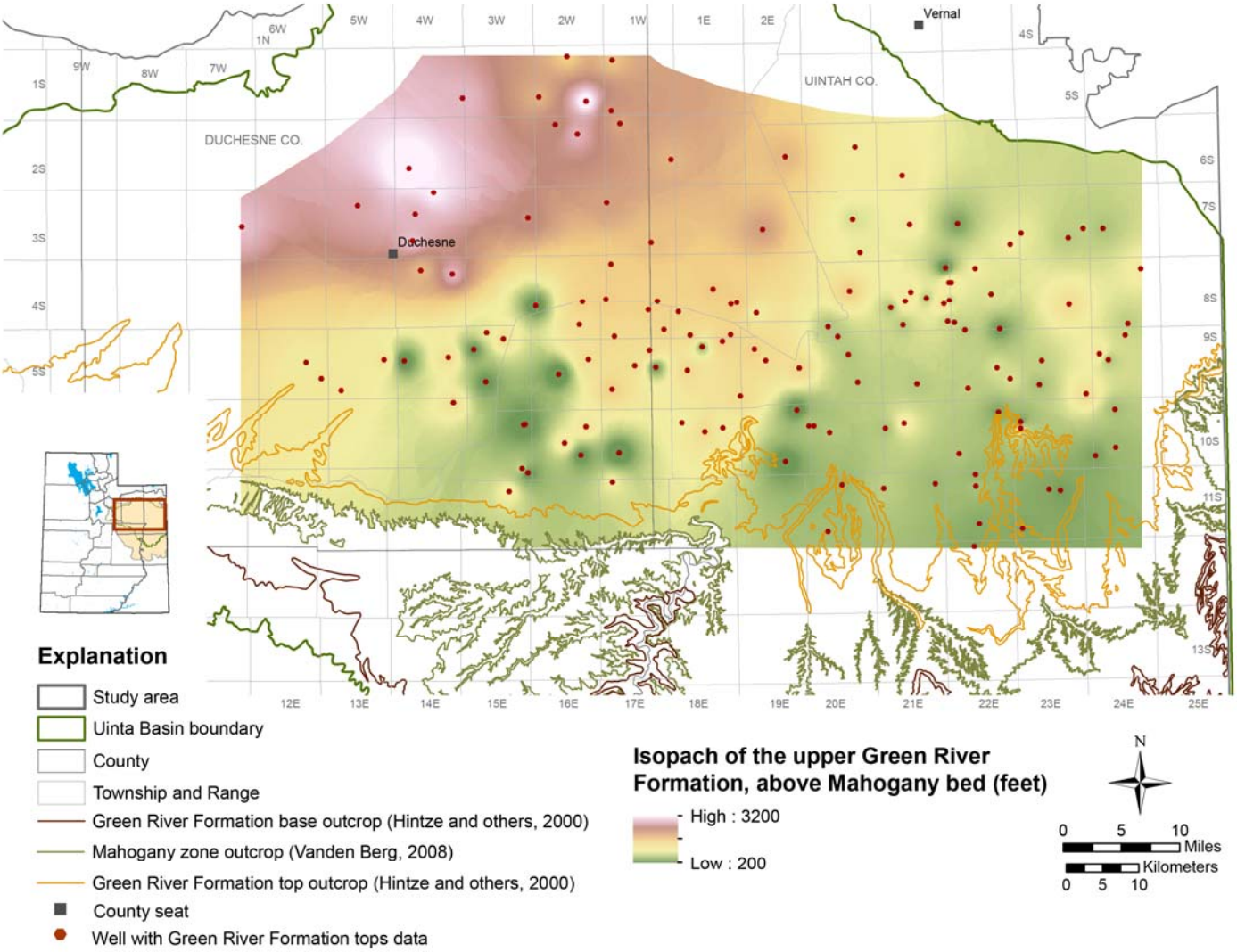

Figure 7.5. Isopach map of upper Green River Formation, above the Mahogany bed.

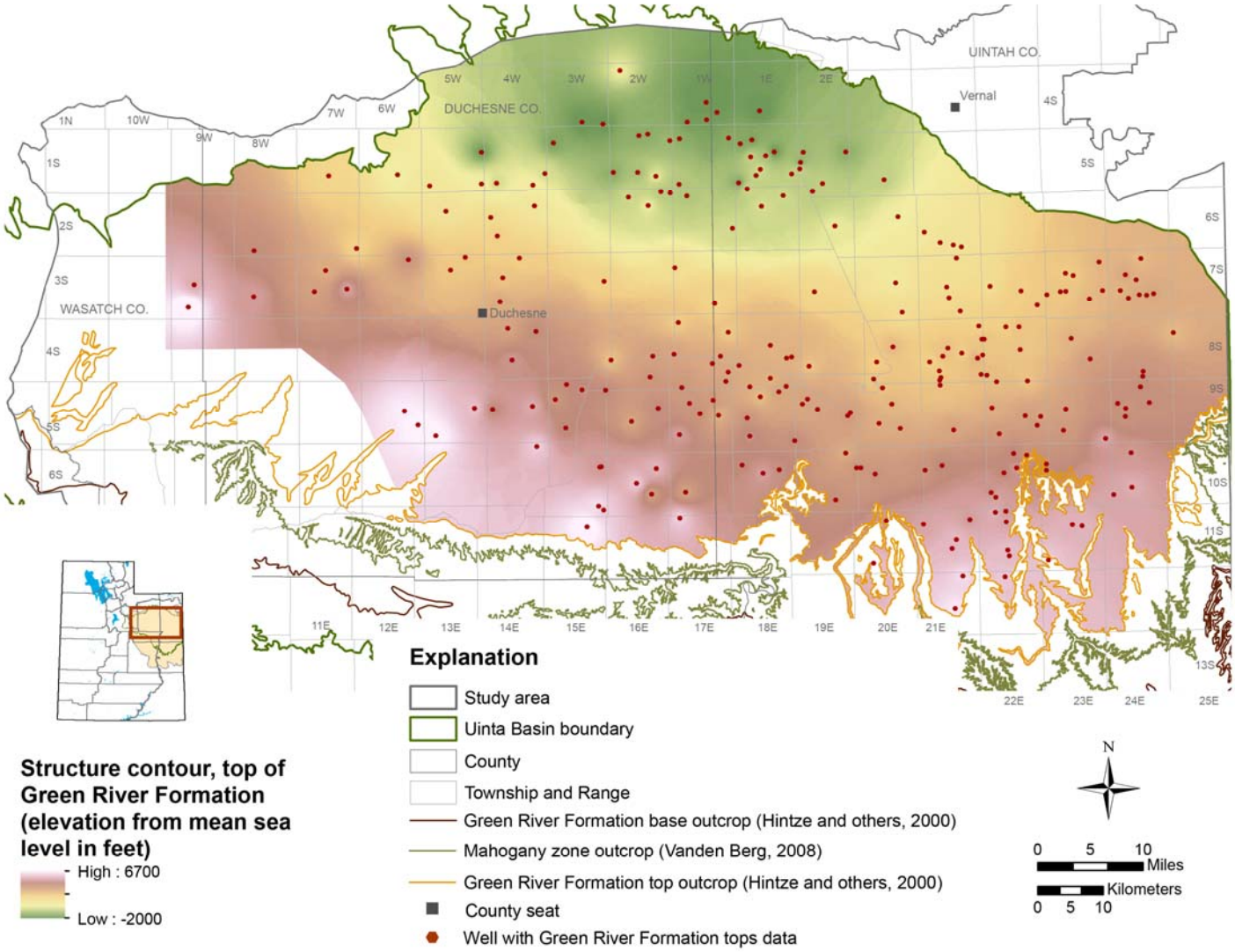

Figure 7.6. Structure contour map of the top of the Green River Formation, illustrating the northerly dip of the beds.

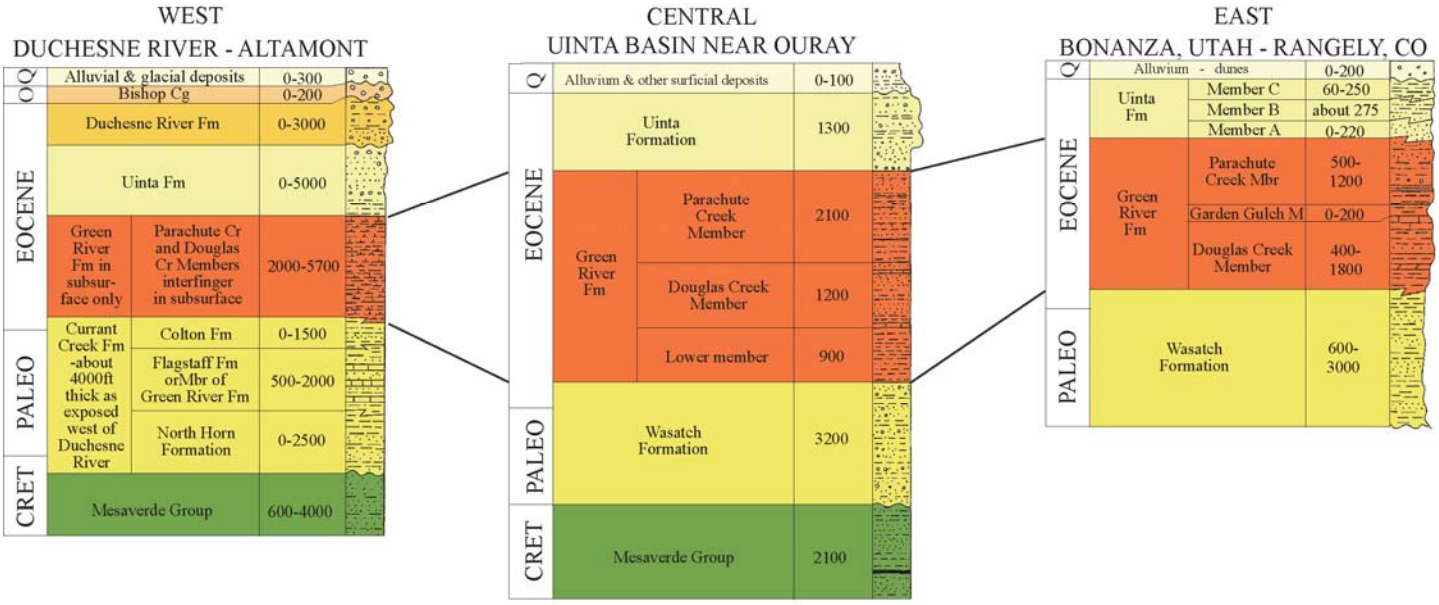

Figure 7.7. General stratigraphic columns of the Green River Formation (from Hintze and Kowallis, 2009).

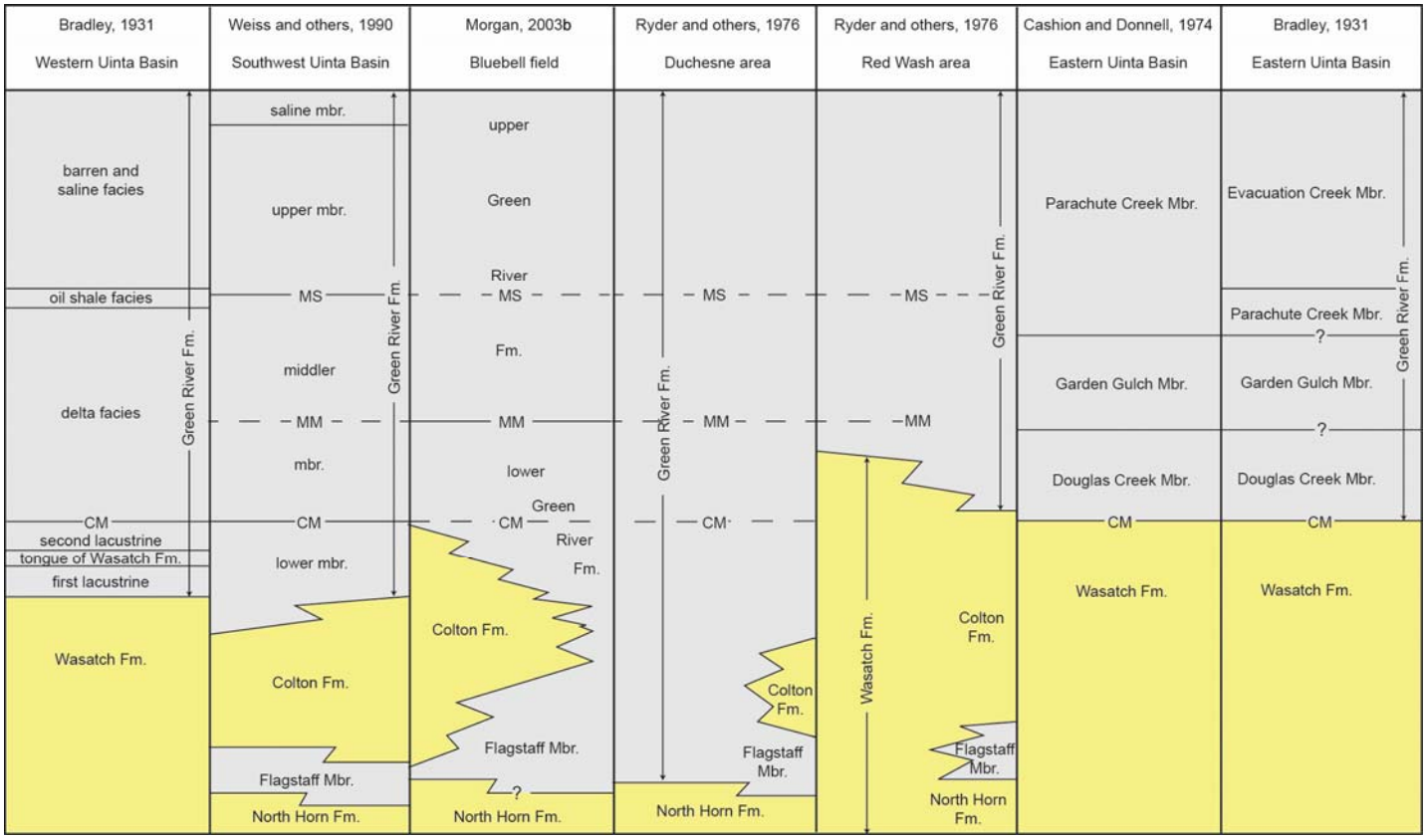

Figure 7.8. A compilation of the various stratigraphic nomenclature used for the Green River Formation throughout the years and across the basin. CM = Carbonate marker; MM = Middle marker; MS = Mahogany shale (bed) (from Morgan, 2003b).

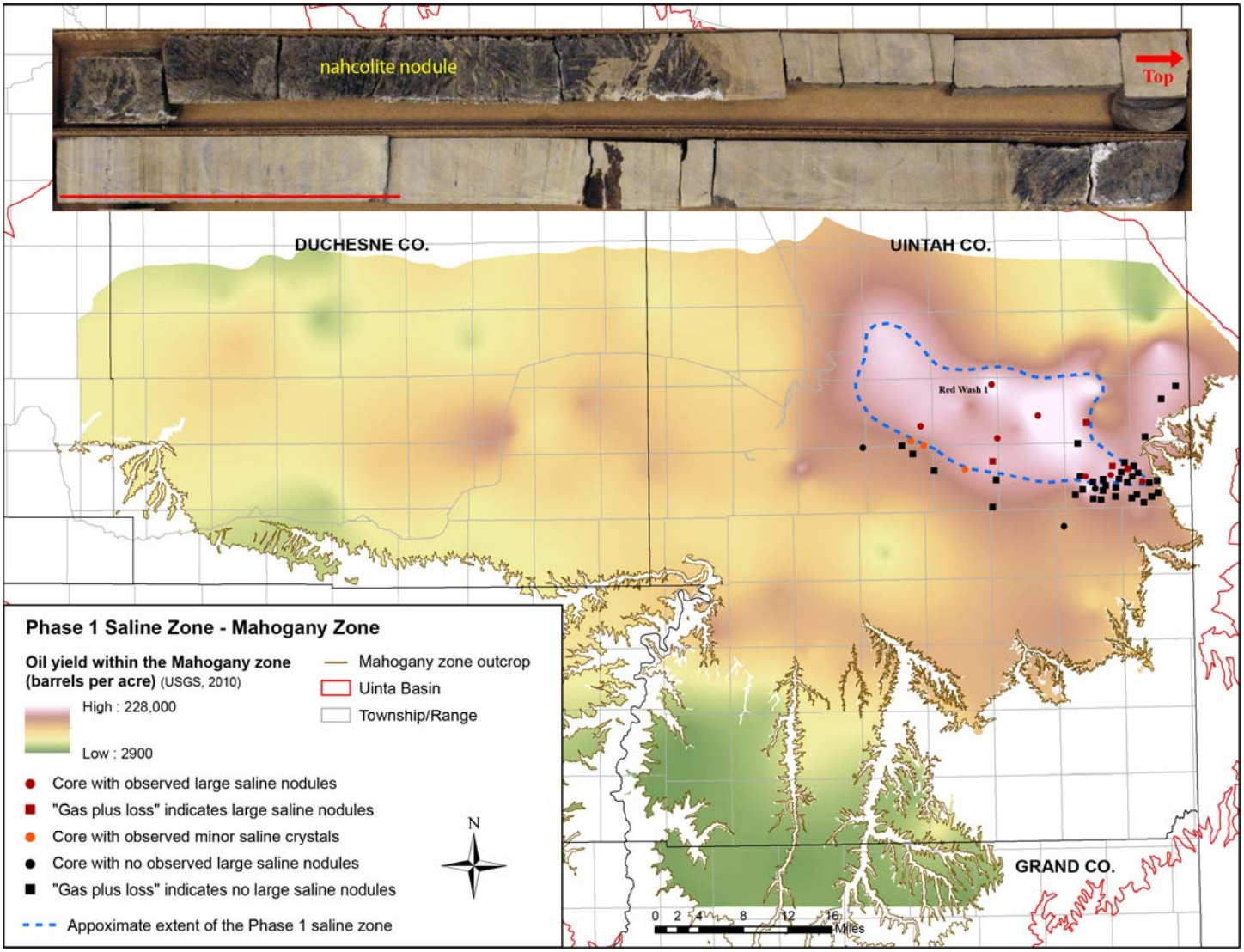

Figure 7.9. Extent of the phase 1 saline interval in the upper Green River Formation. Saline mineral deposition occurs within the paleo-depocenter of the lake during Mahogany zone time, as illustrated by organic-richness (oil yield) in barrels per acre (U.S. Geological Survey, 2010b). The extent was identified by examining core and "gas-plus-loss" measurements from Fischer assay analyses. During the heating of rock samples for Fischer assay analysis, nahcolite within a sample will decompose, giving off large amounts of carbon dioxide recorded as "gas plus loss." Therefore, a high weight percent of "gas plus loss" indicates the presence of significant saline minerals. This phenomenon is discussed in detail by the U.S. Geological Survey (2010a). The inset photo displays intact nacholite nodules within the Red Wash No. 1 core.

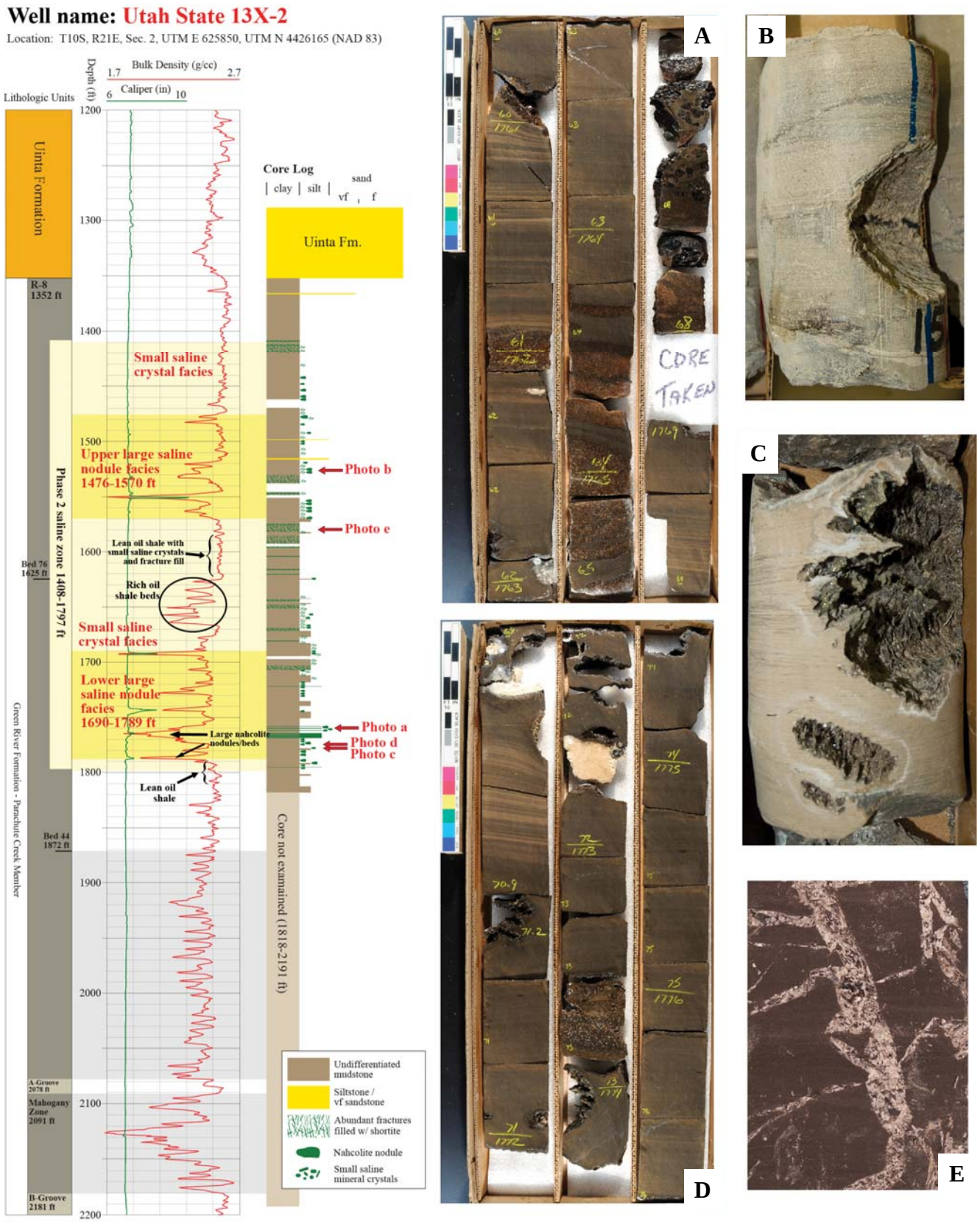

Figure 7.10. The Utah State No. 13X-2 core represents a typical phase 2 saline zone section from the basin's paleo-depocenter. The phase 2 saline zone in this area is nearly 400 feet thick and contains two intervals with large saline mineral nodules/beds. The upper large-saline-nodule zone is 94 feet thick (1476 to 1570 feet) and the lower zone is 99 feet thick (1690 to 1789 feet). A – Nahcolite beds, 1760 to 1769 feet. B – Dissolved nahcolite nodule, 1528 feet. C – Dissolved nahcolite nodule lined with pyrite, 1774 feet. D – Dissolved nahcolite nodules, 1769 to 1776 feet. E – Shortite fracture fill, 1580 feet.

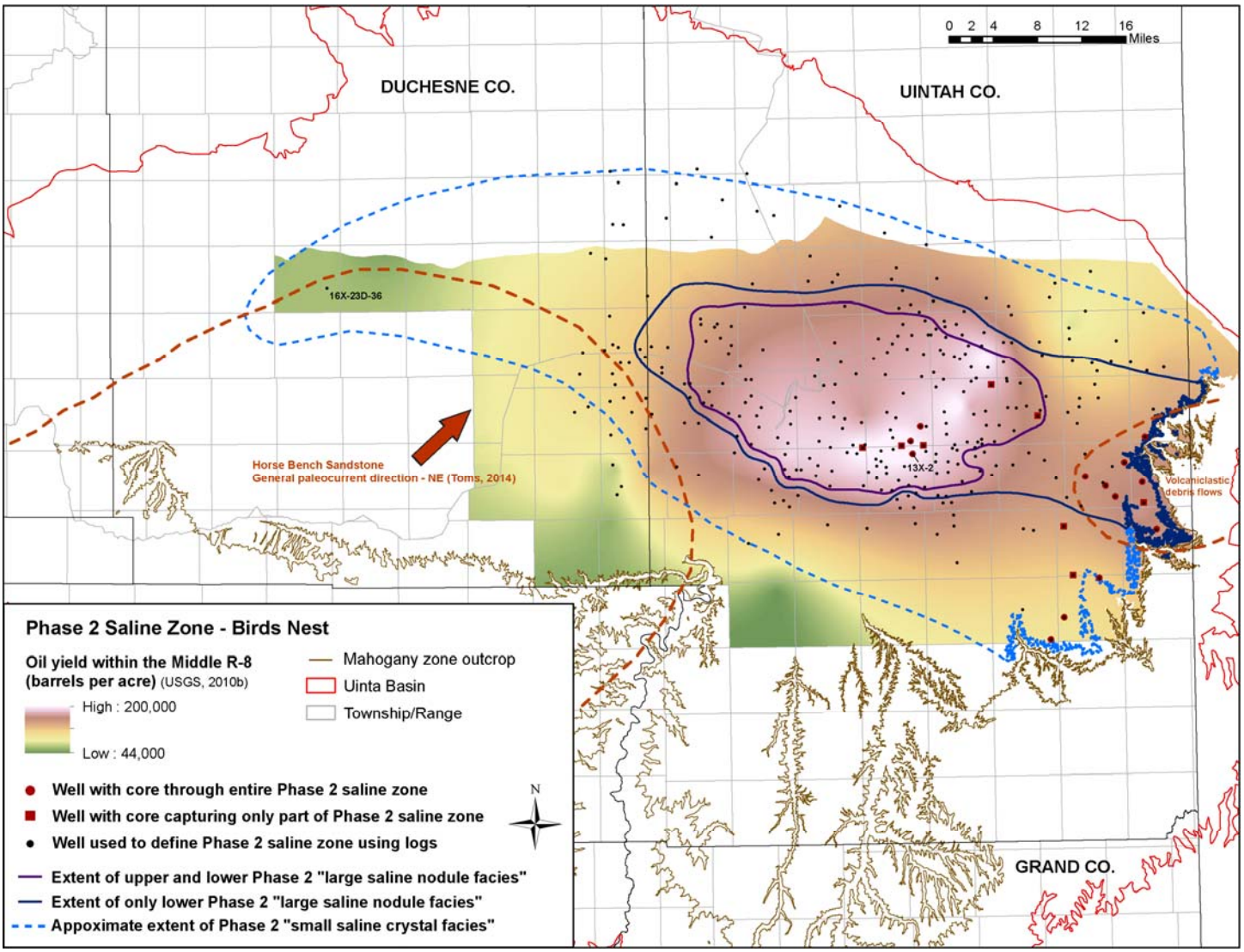

Figure 7.11. Extent of the phase 2 saline interval (Birds Nest aquifer) in the upper Green River Formation. The most abundant saline mineral deposition occurs within the paleo-depocenter of the lake during middle R-8 time, as illustrated by organic-richness (oil yield) in barrels per acre (U.S. Geological Survey, 2010b). Saline mineral distribution is influenced by two significant siliciclastic deposits, the Horse Bench Sandstone on the west side of the basin and volcaniclastic debris flows on the east side.

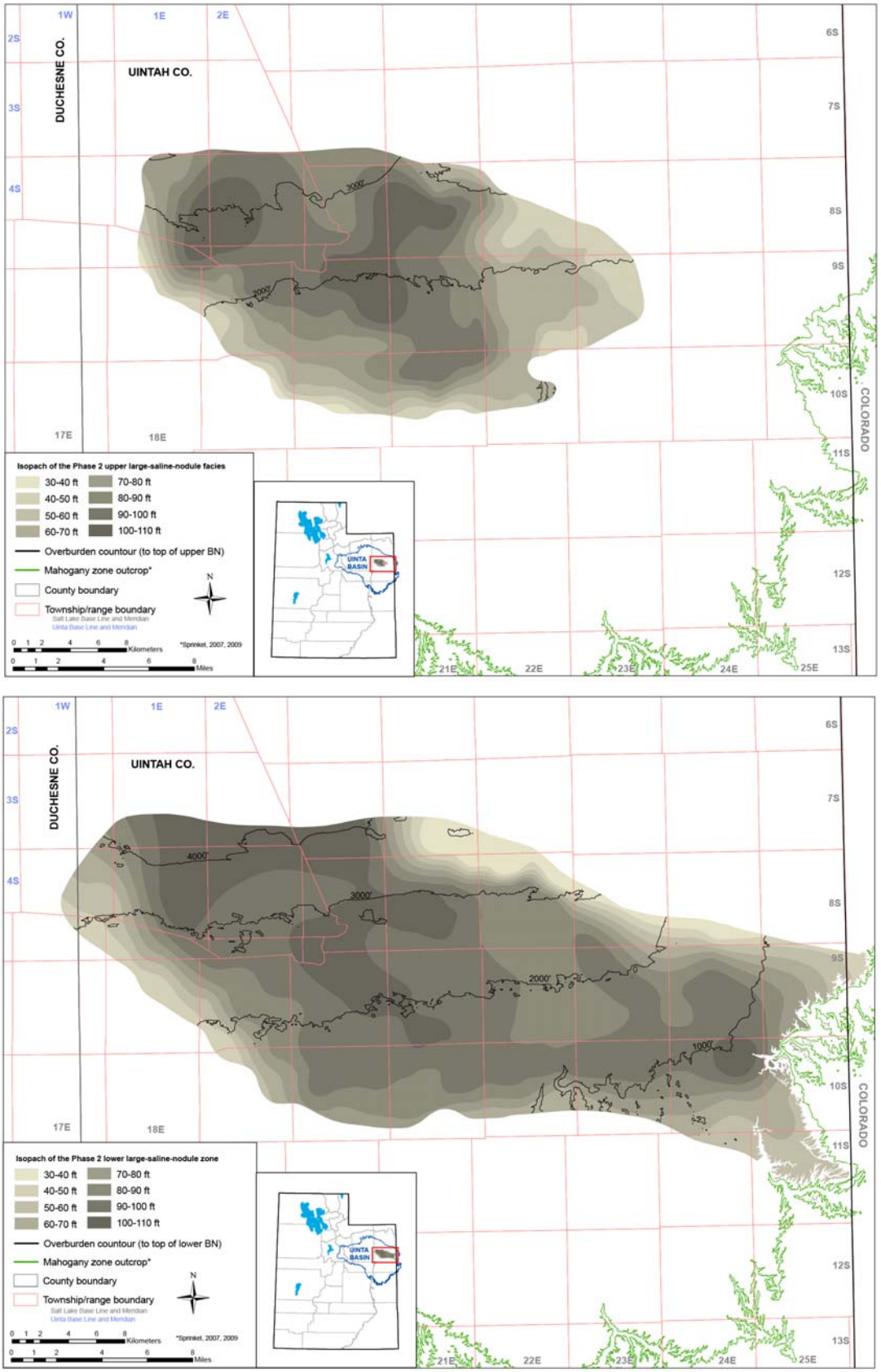

Figure 7.12. Isopach maps, with depth contours, of the upper and lower "large-saline-nodule" facies (upper and lower Birds Nest aquifers) from the phase 2 saline zone.

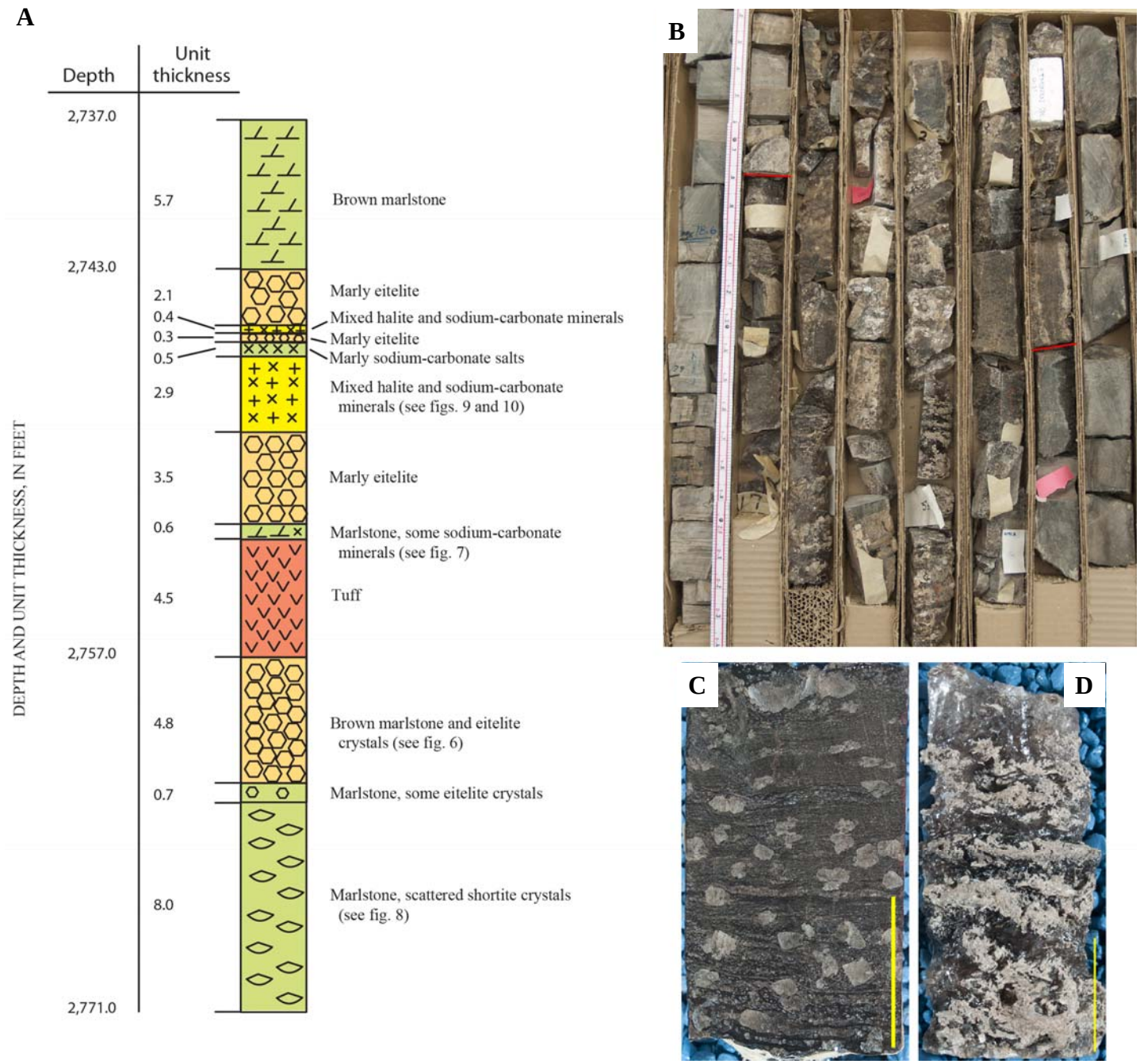

Figure 7.13. Shrine Hospital No. 1 core representative of the phase 3 saline zone section. A – Generalized lithologic description of the Shrine Hospital No. 1 core, showing bedded saline minerals from the phase 3 saline zone (from Brownfield and others, 2010). B – Several feet of bedded halite with smaller wegscheiderite crystals and other sodium-rich saline minerals (between red lines) from 4180.3 to 4192.5 feet (mineral identification from Dyni and others, 1985). C – Large subhedral crystals of eitelite in marlstone (oil shale), 4248.4 feet (mineral identification from Dyni and others, 1985). Yellow bar equal one-tenth foot. D – Bedded halite (darker gray, glassy, partially dissolved) with wegscheiderite crystals (light gray, more resistant), 4187.1 feet (mineral identification from Dyni and others, 1985). Yellow bar equal one-tenth foot.

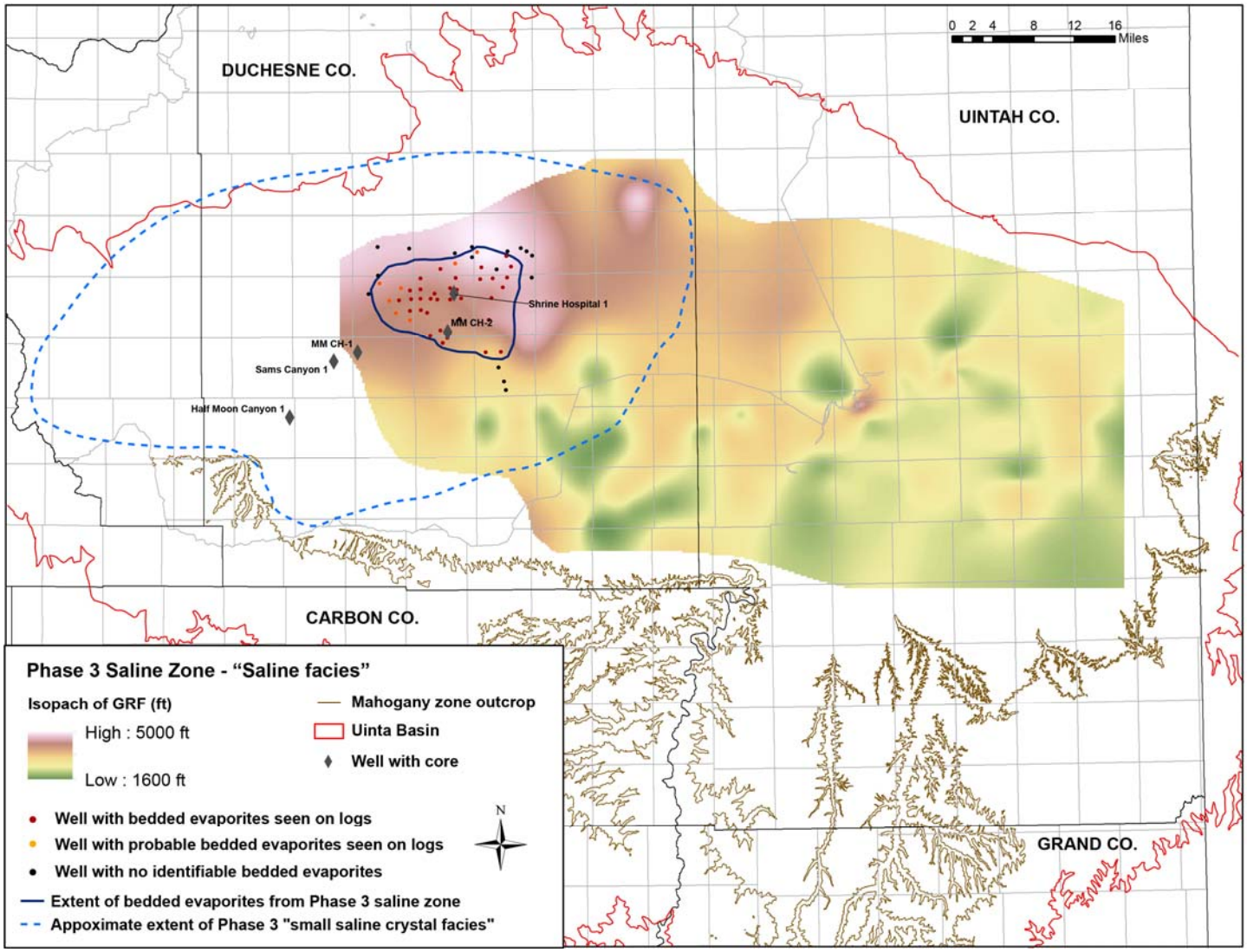

Figure 7.14. Extent of the phase 3 saline interval in the upper Green River Formation. The area with bedded salt deposition occurs within the area of thickest sediment accumulation in the Green River, representing the paleo-depocenter of the lake during its final phase of existence.

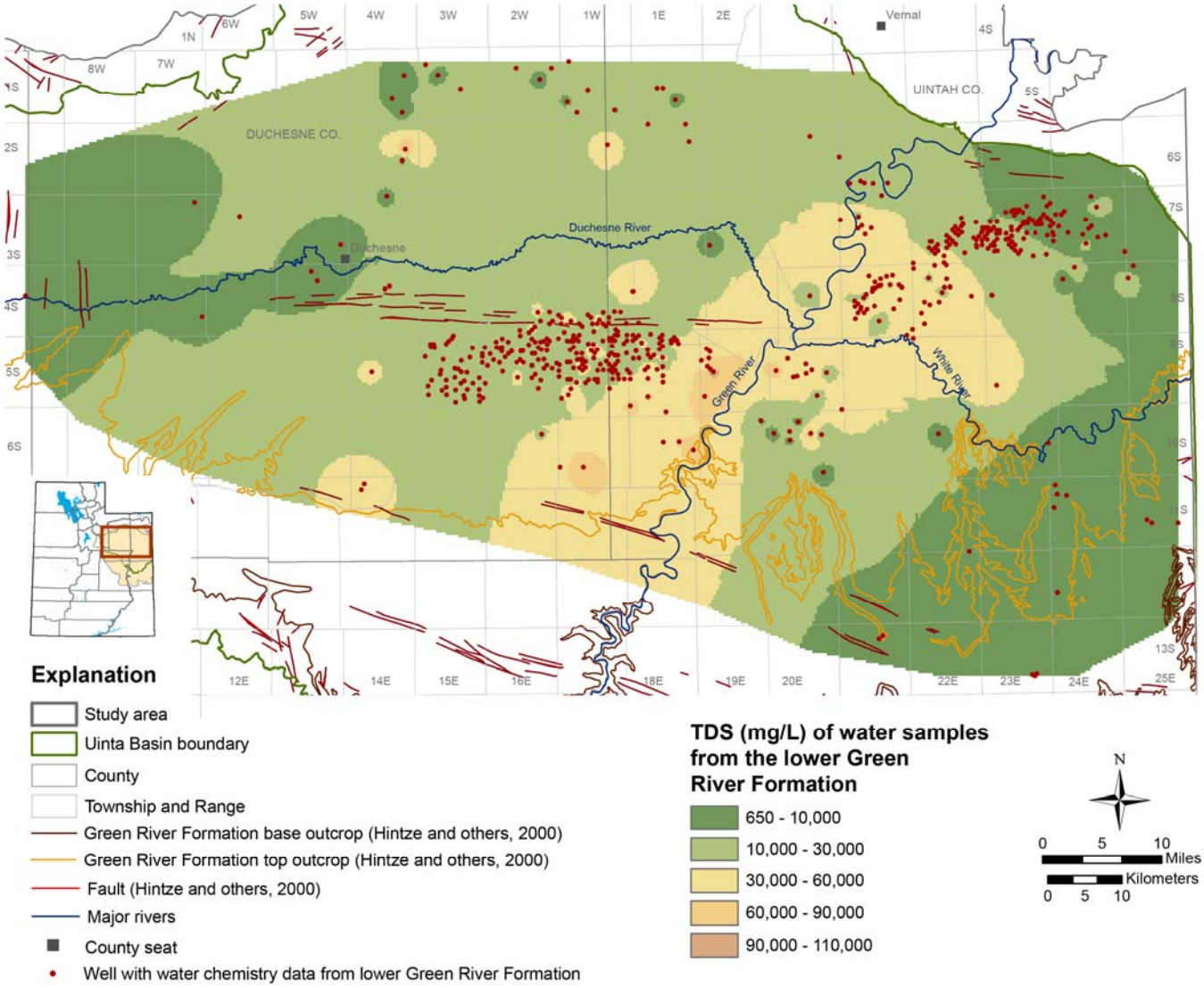

Figure 7.15. Map displaying available total dissolved solids concentrations (mg/L) from water samples taken within the lower Green River Formation.

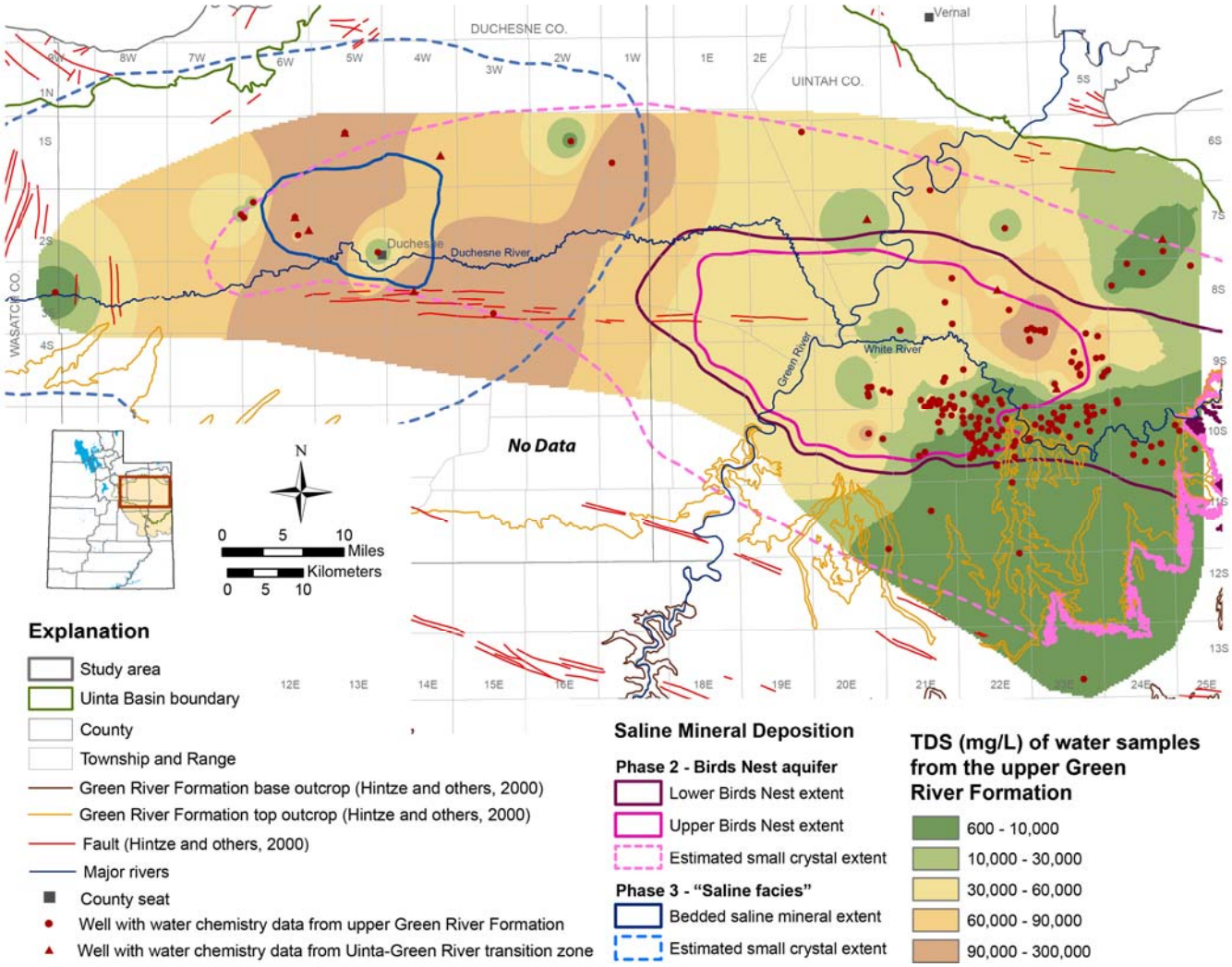

Figure 7.16. Map displaying available total dissolved solids concentrations (mg/L) from water samples taken within the upper Green River Formation.

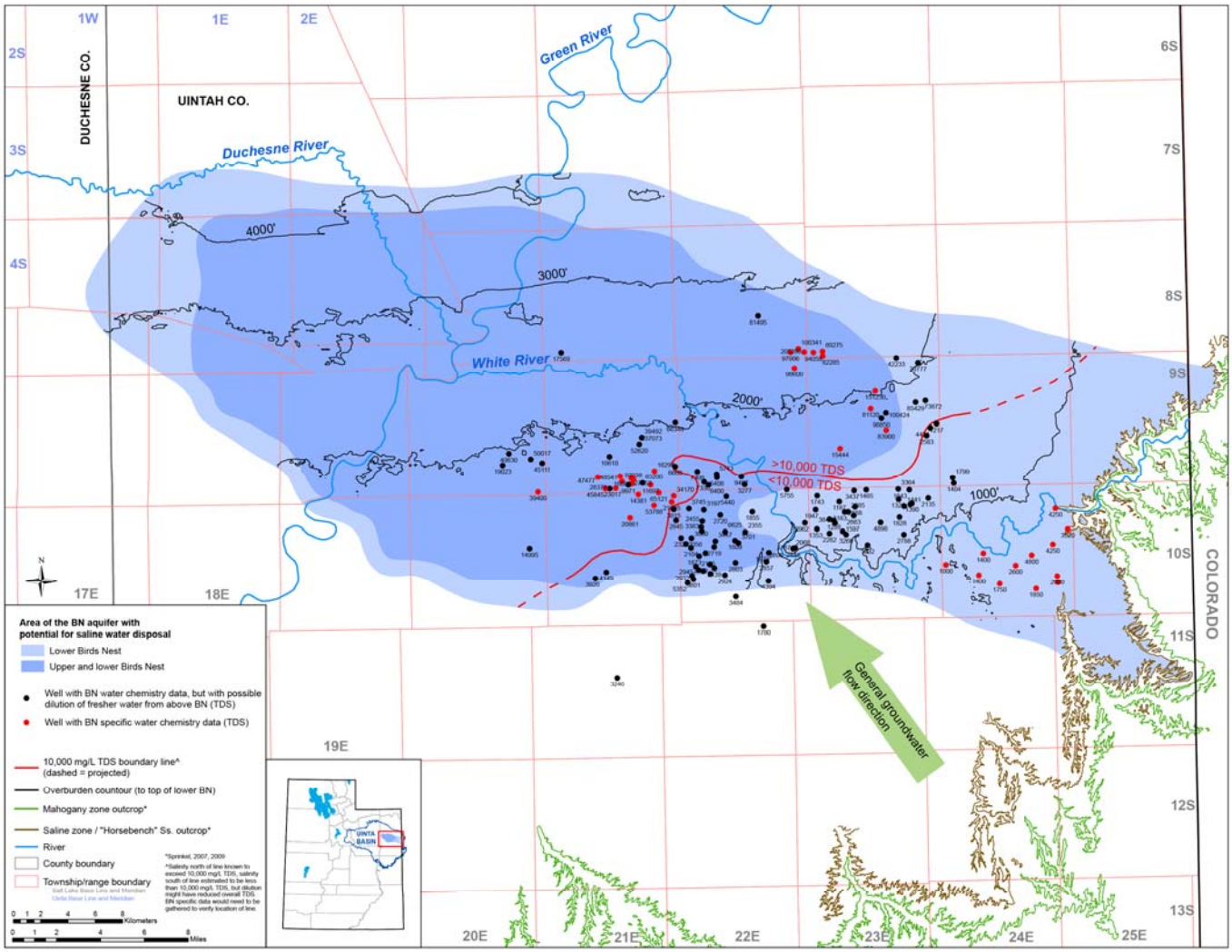

Figure 7.17. Map displaying available total dissolved solids concentrations (mg/L) from water samples taken within the Birds Nest aquifer (phase 2 saline zone) (from Vanden Berg and others, 2013).

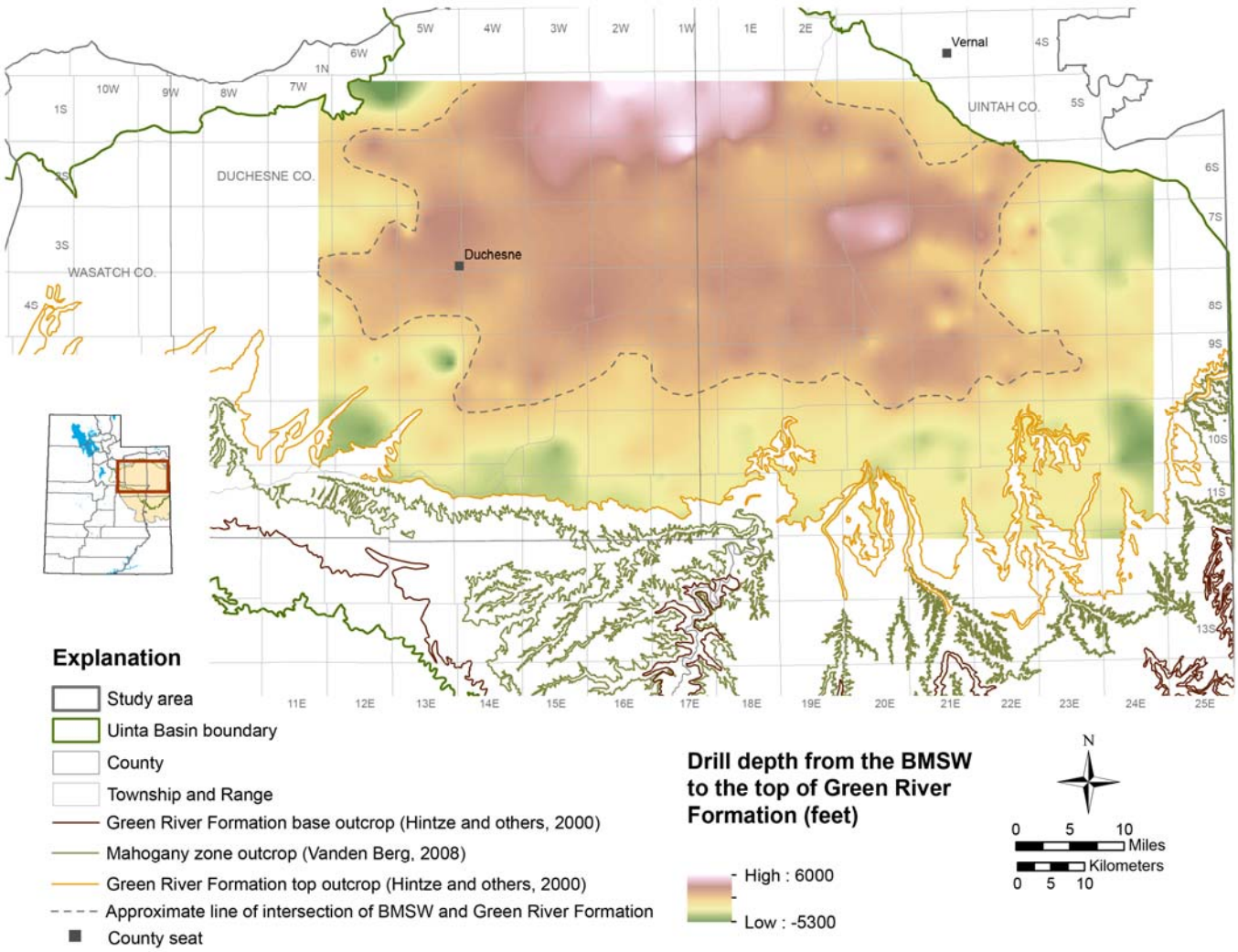

Figure 7.18. Map showing the depth from the base of the moderately saline water (BMSW) to the top of the Green River Formation (Anderson and others, 2012).

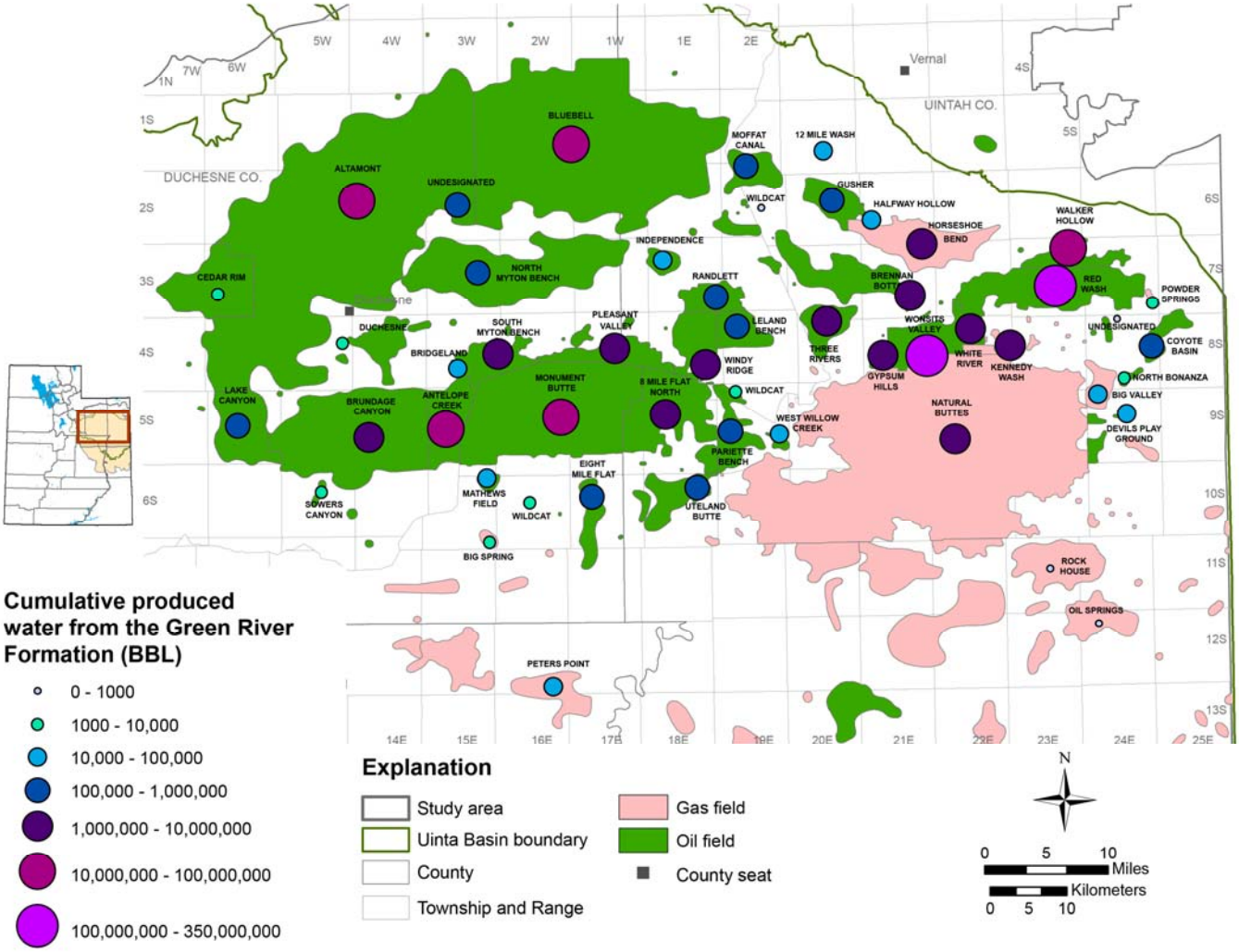

Figure 7.19. Bubble map showing cumulative produced water (barrels) from the Green River Formation by oil or gas fields (through December 2014) (Utah Division of Oil, Gas, and Mining, 2015).

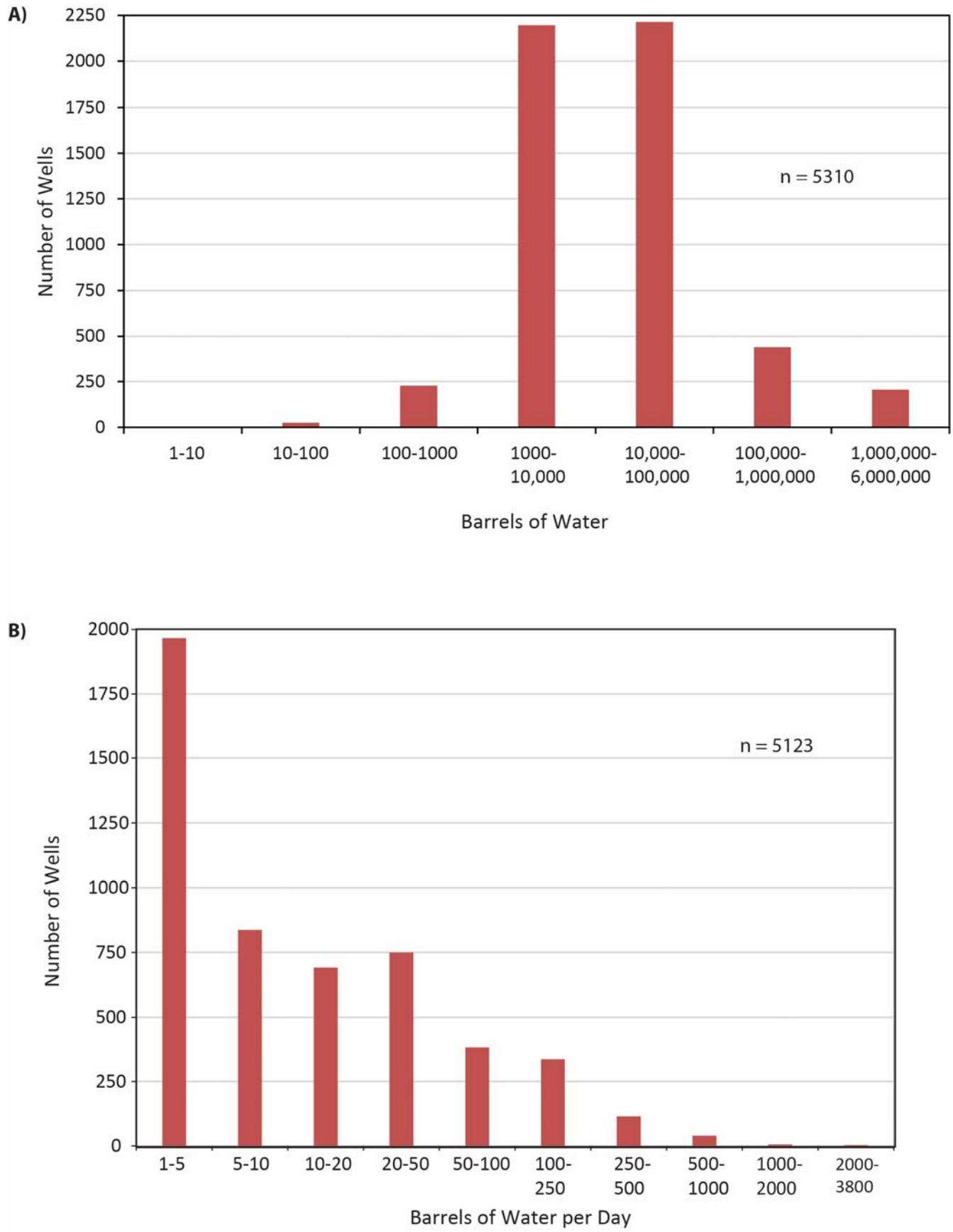

Figure 7.20. Histogram displaying total water production (barrels) by well from the Green River Formation (through December 2014) (Utah Division of Oil, Gas, and Mining, 2015e). A – Cumulative water production. B – Water production per day.

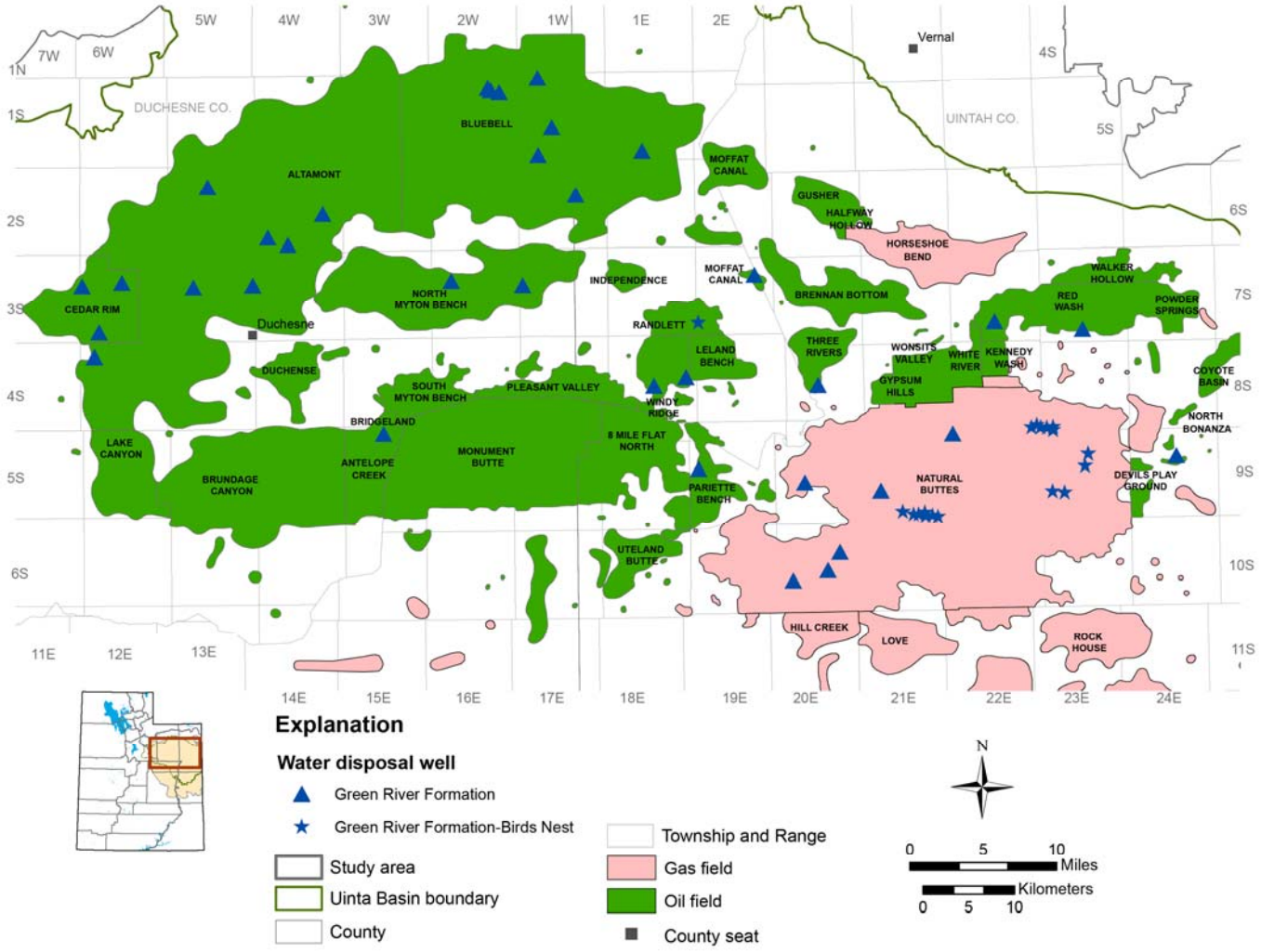

Figure 7.21. Location of injection wells currently disposing produced water (barrels) into the Green River Formation (Utah Division of Oil, Gas, and Mining, 2015).

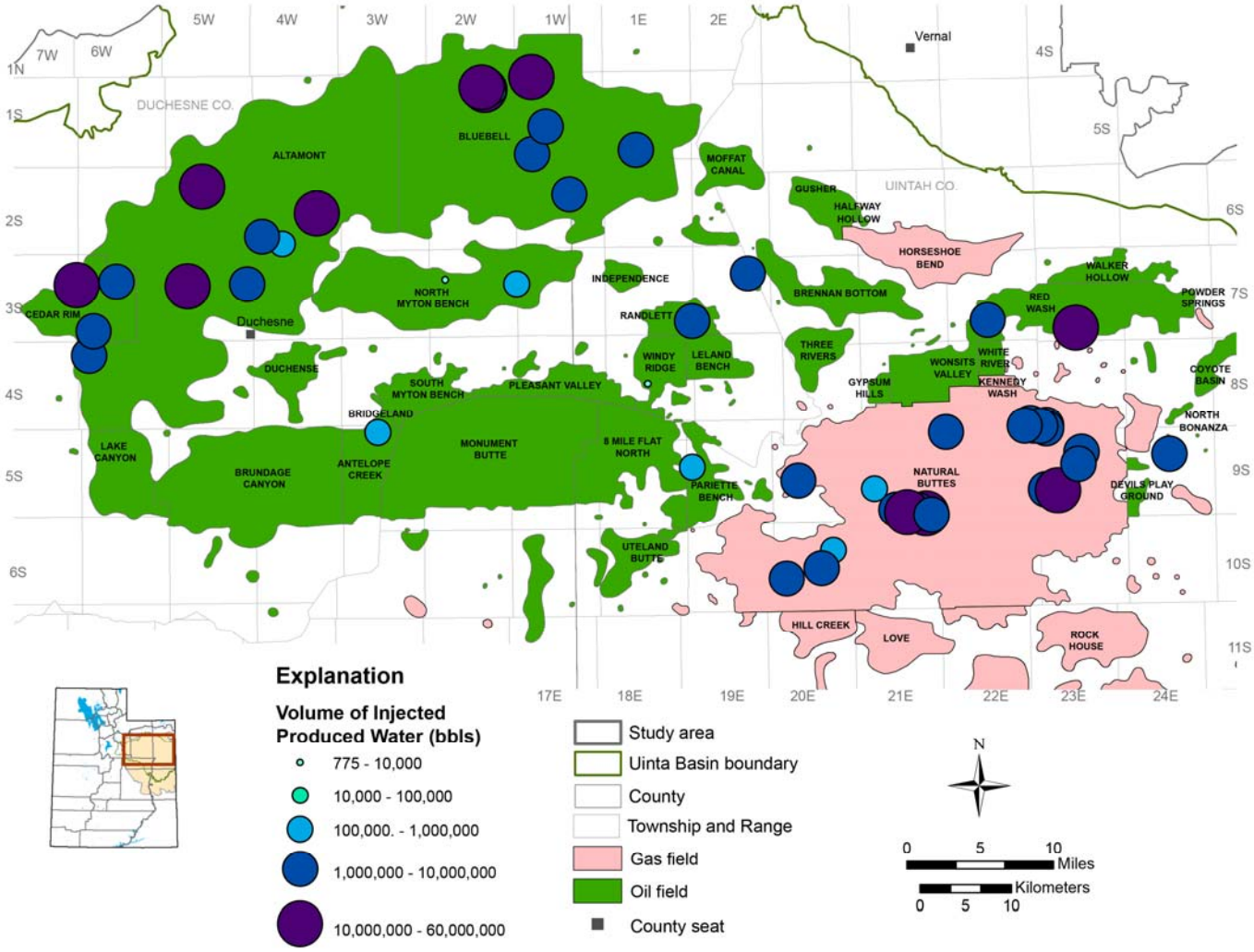

Figure 7.22. Bubble map showing the volume of water (barrels) that has been injected into the Green River Formation from each injection well (Utah Division of Oil, Gas, and Mining, 2015).

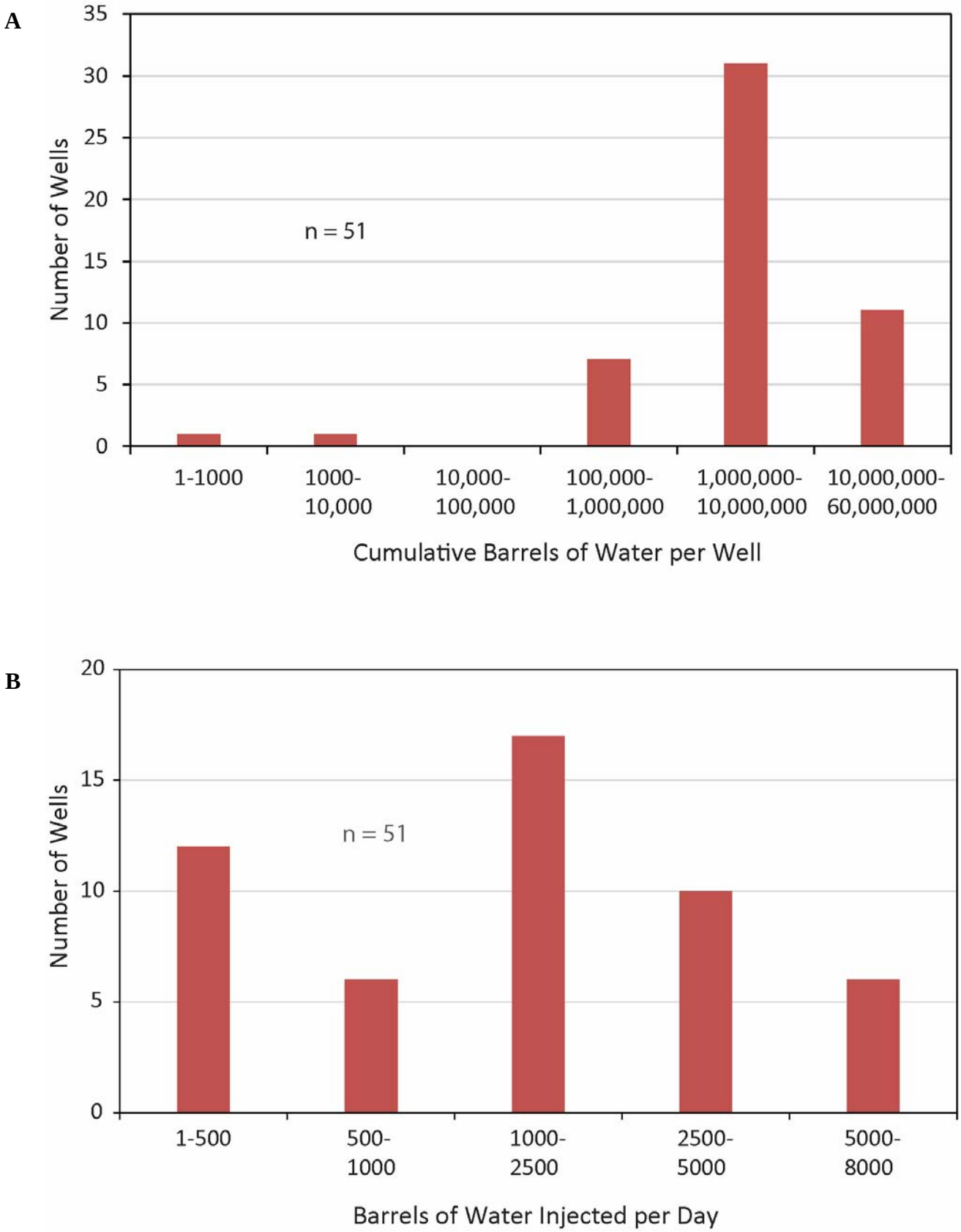

Figure 7.23. Histograms displaying water (barrels) injected into the Green River Formation via disposal wells (through March 2015) (Utah Division of Oil, Gas, and Mining, 2015). A – Cumulative water injection per well. B – Water injection per day per well.

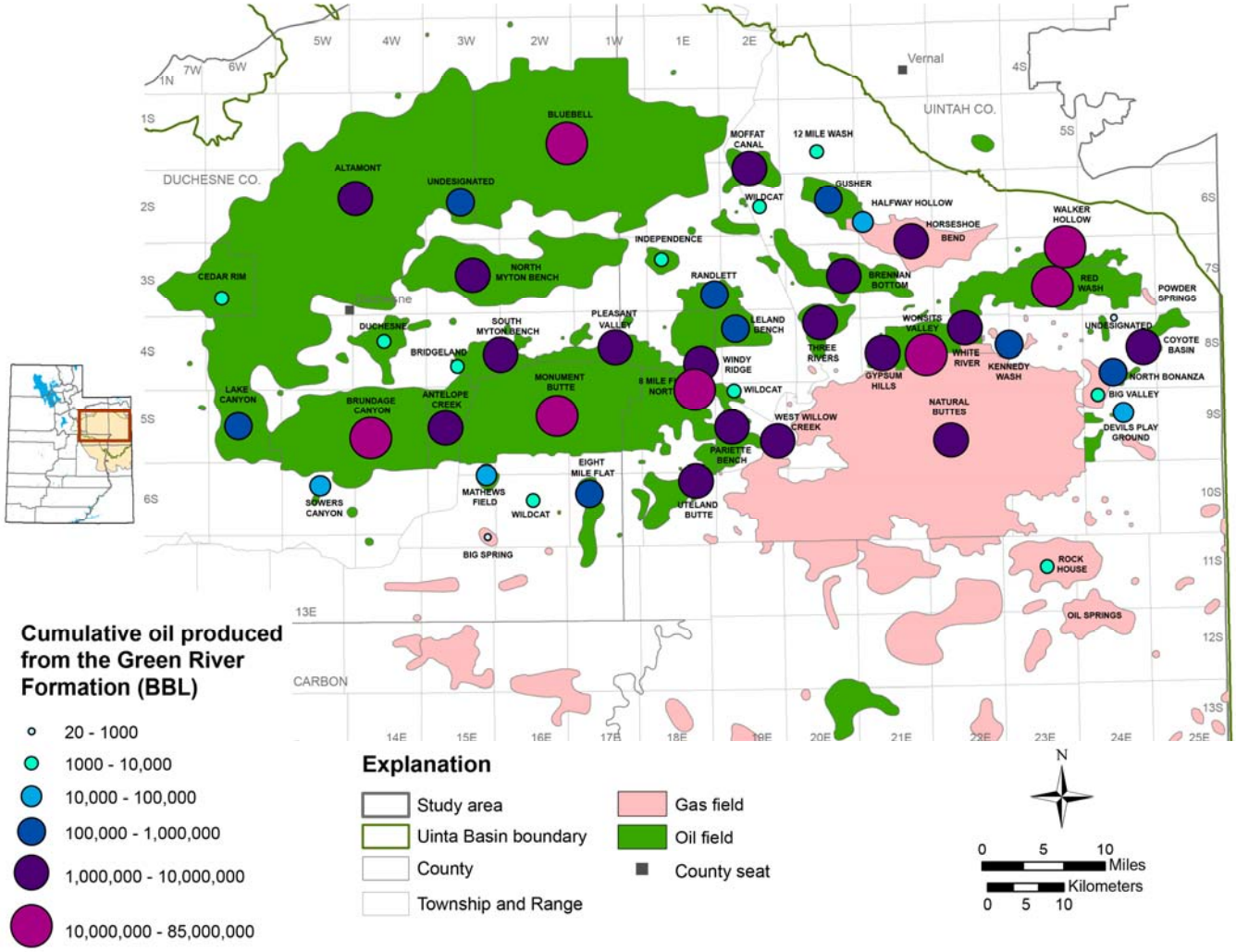

Figure 7.24. Bubble map showing the volume of oil (barrels) produced from the Green River Formation by field (Utah Division of Oil, Gas, and Mining, 2015).

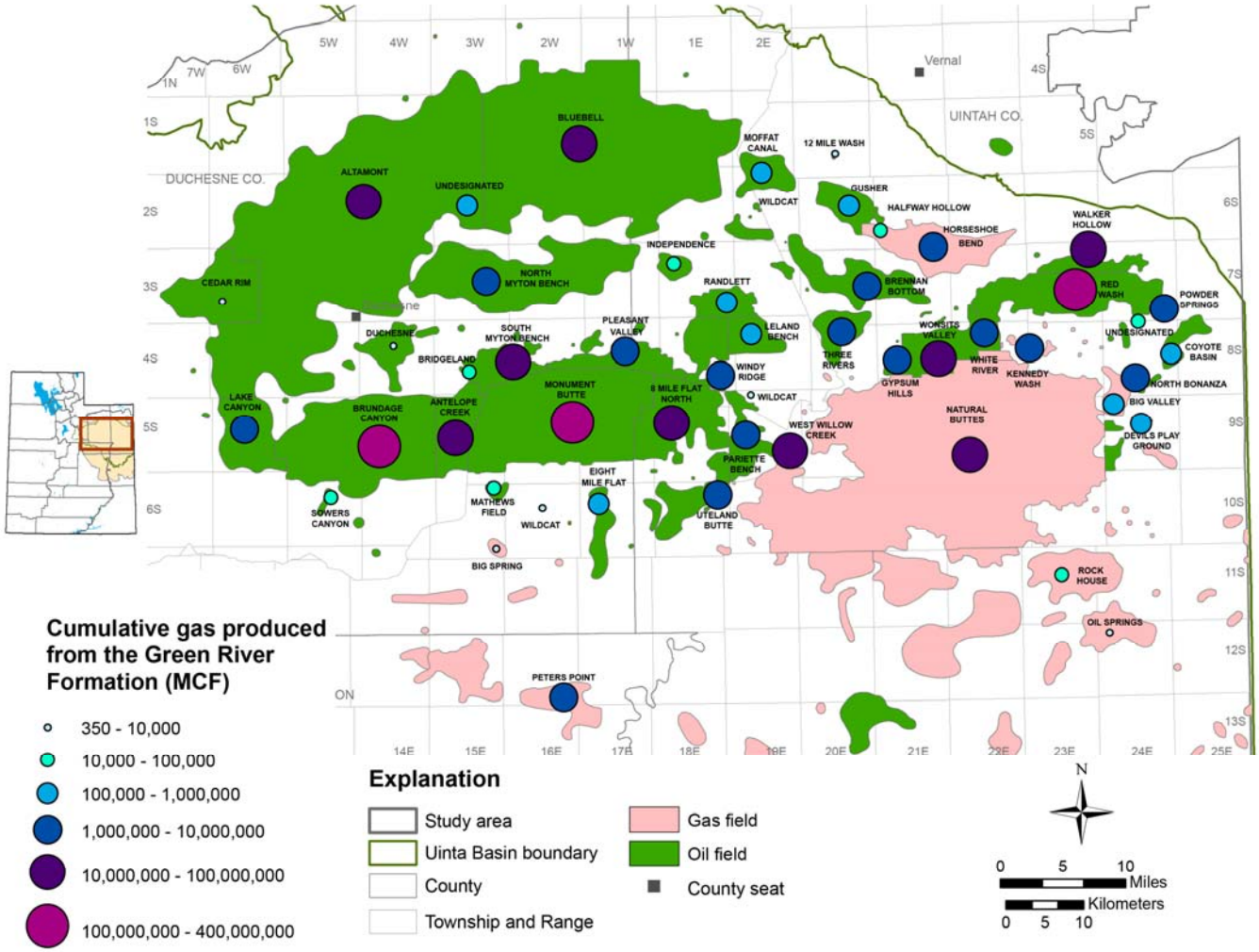

Figure 7.25. Bubble map showing the volume of gas (MCF) produced from the Green River Formation by field (Utah Division of Oil, Gas, and Mining, 2015).

A

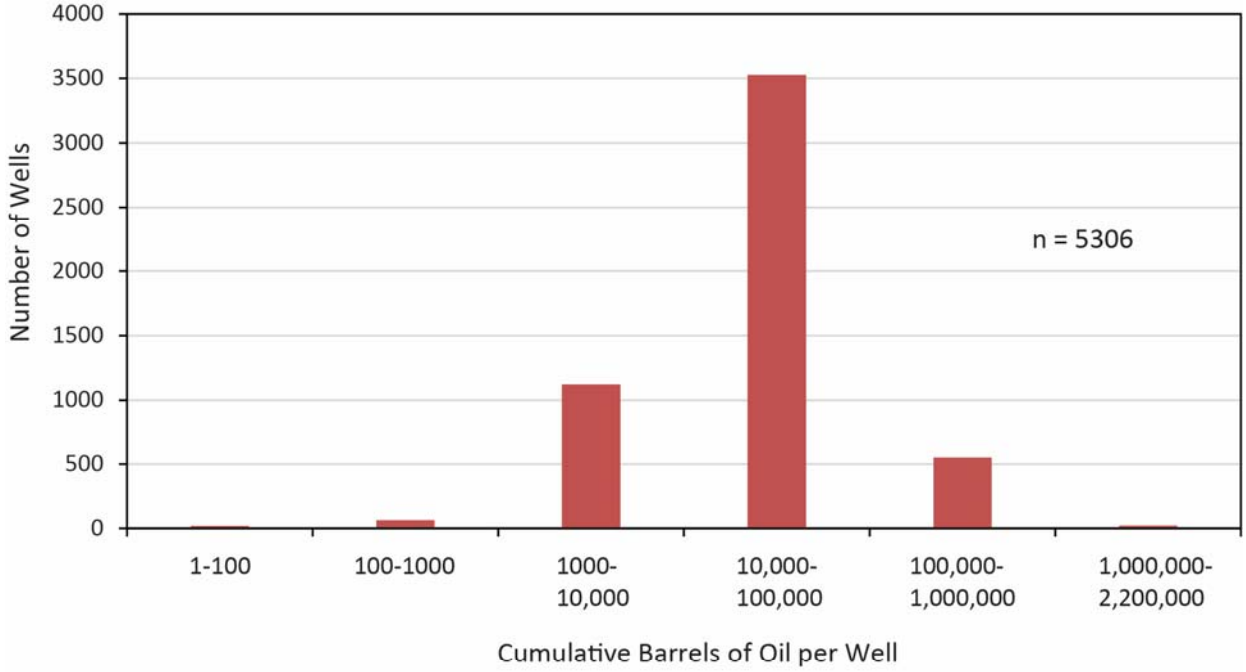

B

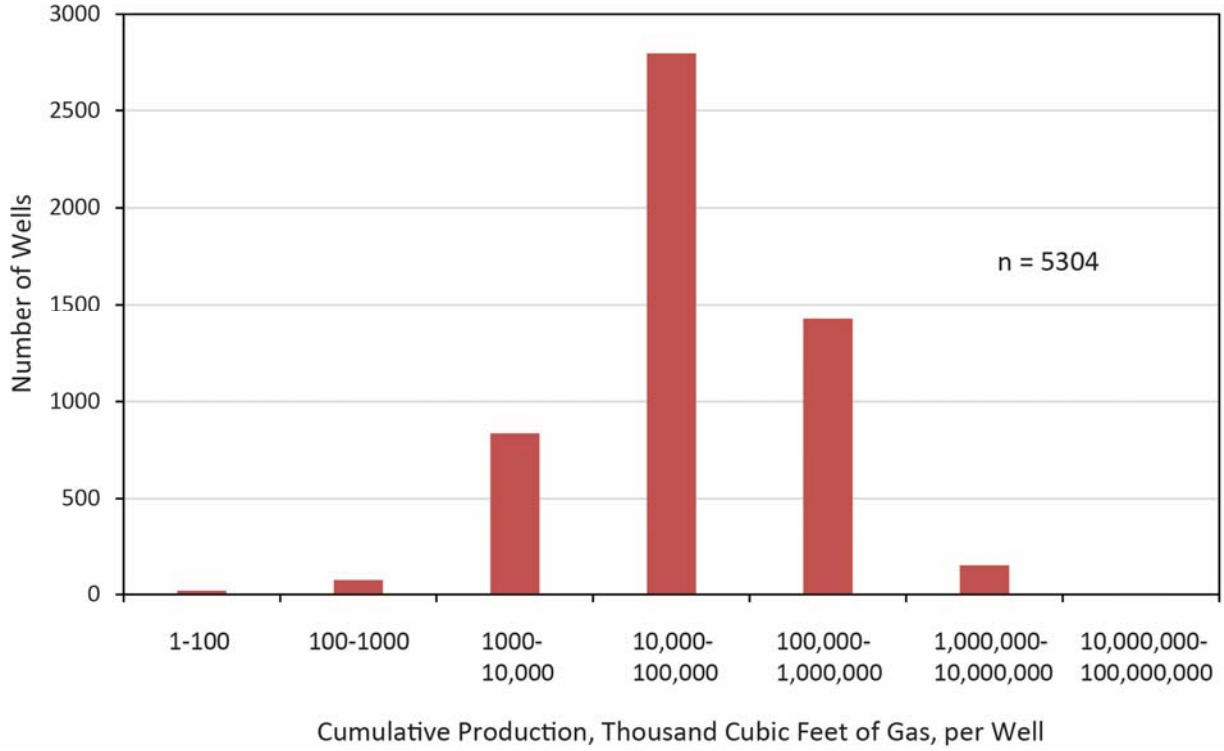

Figure 7.26. Histograms displaying cumulative (A) oil (barrels) and (B) gas (MCF) and daily production of (C) oil (barrels) and (D) gas (MCF) by well from the Green River Formation (through December 2014) (Utah Division of Oil, Gas, and Mining, 2015e).

C

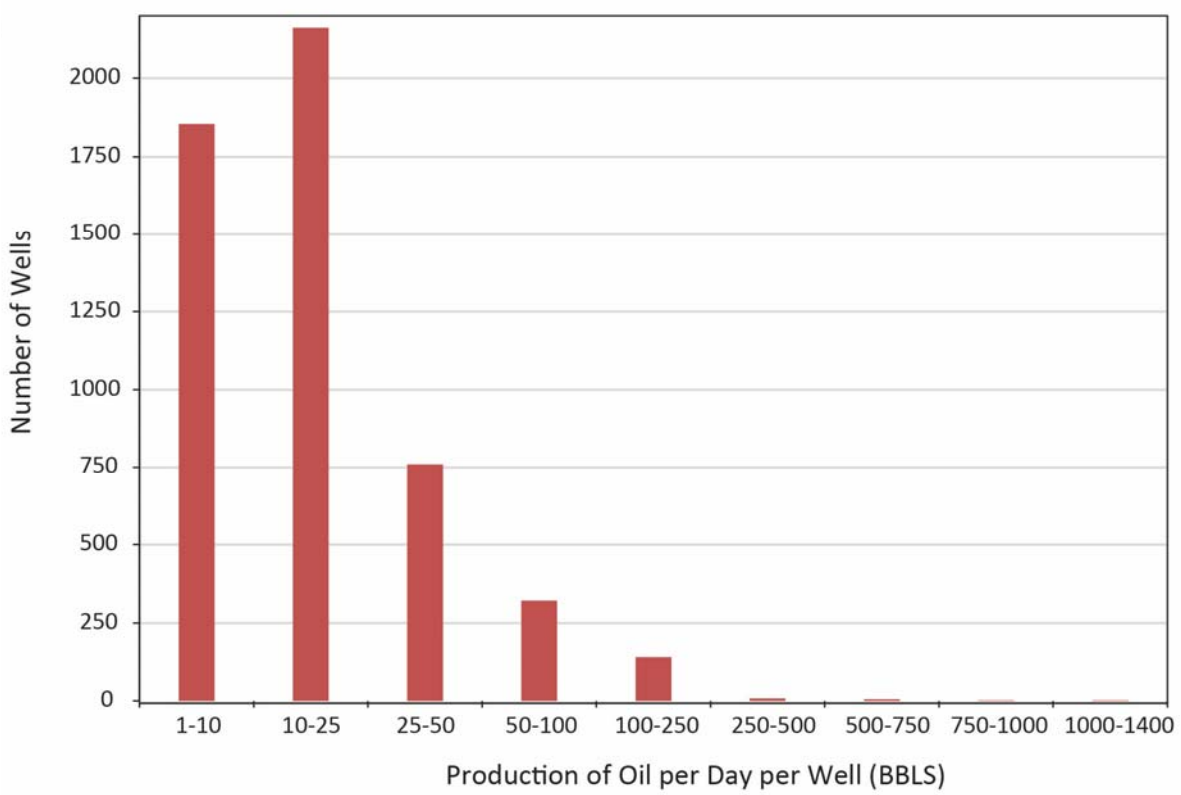

D

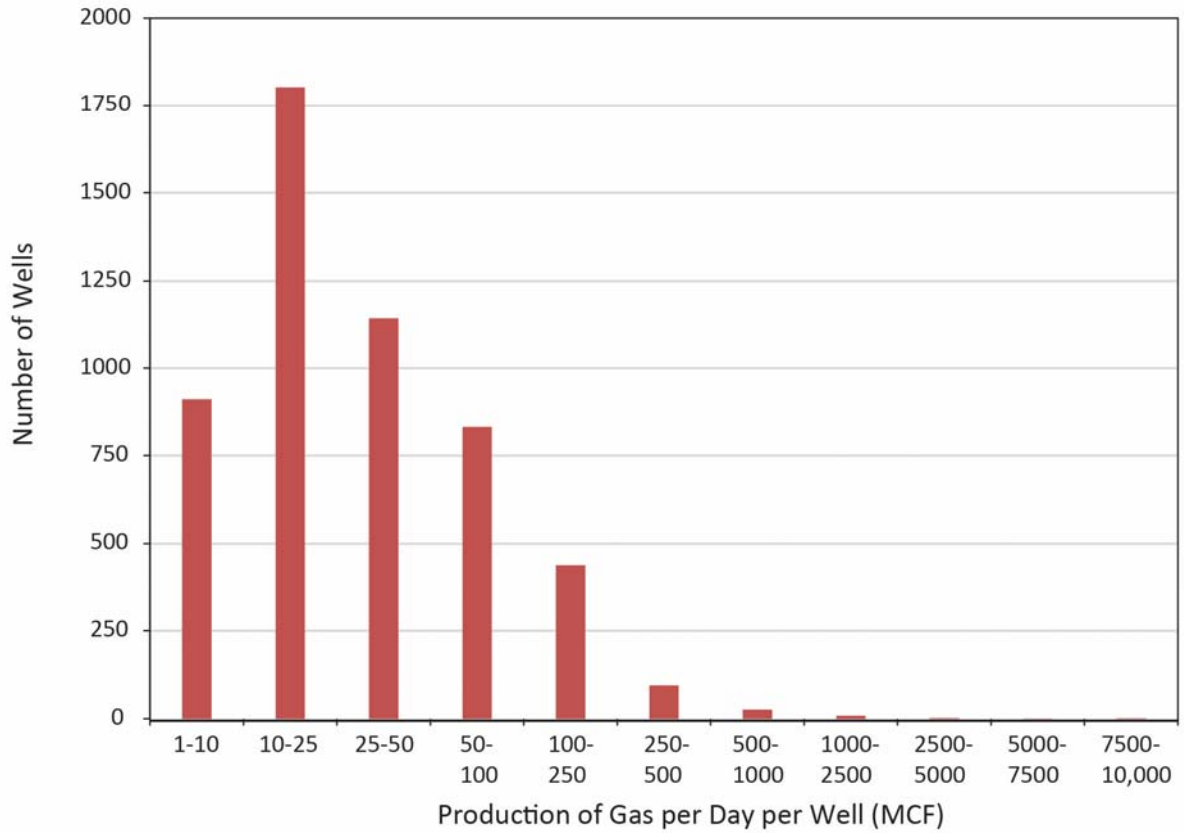

Figure 7.26 continued. Histograms displaying cumulative (A) oil (barrels) and (B) gas (MCF) and daily production of (C) oil (barrels) and (D) gas (MCF) by well from the Green River Formation (through December 2014) (Utah Division of Oil, Gas, and Mining, 2015e).

CHAPTER VIII

SUMMARY OF THE COMPILED FLUID GEOCHEMISTRY DATABASE FOR THE UINTA BASIN

Stefan M. Kirby

Fluid chemistry of groundwater and produced water places basic constraints on oil and gas operations and development. In the UB significant quantities of both produced water and groundwater are used for various phases of oil and gas development and rural agricultural and domestic water supply. The basic chemistry of these fluids controls their ultimate use and value.

The database presented in this chapter is a compilation of available major ion chemistry for both produced water and groundwater in the larger UB area. These data include time series and other samples from a variety of geologic units and depths that provide both a record of geochemistry through time and baseline chemistry for the UB of eastern Utah.

BACKGROUND

This chapter presents a compiled database of fluid chemistry for the UB area. The database covers an area that includes the UB and adjoining areas to the south and west. Sample

locations range from approximately 38° 30′ south to 40° 30′ north latitude and from 111° 30′ west to 109° east longitude. The database forms the basis for water chemistry used for various sections of the larger UB produced water study (appendix G).

The database includes fluid geochemical analyses for groundwater from springs and wells as well as produced water collected as part of oil and gas exploration and production. The data is taken from four primary sources that include (1) the National Water Information System (NWIS) database (U.S. Geological Survey, 2014), (2) the chemistry database included in Utah Geological Survey Special Study 144 (Anderson and others, 2012), (3) samples compiled from DOGM (Utah Division of Oil, Gas, and Mining, 2014), and (4) new samples collected as part of this study. The database contains 4184 samples that includes a mix of unique samples for given location and depth as well as samples that represent a time series of multiple samples from a given location and depth.

Each sample in the database includes data source, basic location information, and a unique identifier. All other data fields are populated when the data is available. General data fields include a site name, site number, altitude, depth of sample, and date of sampling. Site name includes a general name of the sample site when known. The site number field includes the API number for samples from oil and gas wells or the NWIS number for groundwater samples compiled from the USGS database (U.S. Geological Survey, 2014). The altitude is the land surface elevation in feet derived from the 5 meter (16.4 feet) digital elevation model for Utah for a given location. The depth of the sample is listed as a discrete value in feet below land surface. The source databases contain depth of sample information as either a single discrete depth or an open or screened interval. Depth was calculated as the midpoint of the open interval for samples that list screened or open interval.

Sample chemistry fields in the database include temperature, pH, conductivity, TDS, and chemical concentration values. Solute concentrations for CO_2, HCO_3, Ca, Mg, Na, K, SO_4, F, SiO_2, and NO_3 are in mg/L. The concentration of As is µg/L. The sources from which the data are compiled overlap in part and duplicate measurements indicated by indentical chemistry and location information were removed.

The milliequivalent concentration of each major solute concentration in the database was calculated using standard methods with the AquaCHEM™ software. Milliequivalent concentrations were used to calculate charge balance of the percent difference between the sum of charge equivalents for major anions and cations. Samples were given a qualitative balance field indicating whether a sample has charge balance plus or minus 5%, between 5 and 10%, and greater than 10%.

Geochemical samples were subdivided based on calculated water type or hydrochemical facies. Water type was calculated for all samples using AquaCHEM™ geochemical software based on standard methodologies presented by Kehew (2000). Water type is listed in both long and short forms in separate database fields. The long water type includes the two or three major anions and cations for a given sample, and the short water type includes only the single anion and cation with greatest relative concentration.

Five standard scaling and corrosion indices were calculated for samples that included sufficient data using the AquaCHEM™ software. These indices include (1) Puckorius, (2) Larson-Skold, (3) Residual-Ca, (4) Ryznar, and (5) LSI. The Puckorius, Ryznar, Residual-Ca, and LSI scaling indices give estimates of the propensity for the formation of calcium carbonate scale based on measured water chemistry. Lower values of these scaling indices indicate a greater tendency for calcium carbonate scaling. These scaling indicators do not give absolute

scaling potential but are instead intended to show relative scaling potential based on water chemistry. The Larson-Skold indice is an estimate of the corrosive potential of moderate alkaline waters (Larson and Skold, 1958). Larson-Skold values greater than 1.2 indicate a tendency towards high corrosion rates. Values less than 0.8 indicate a low tendency for corrosion and values between 1.2 and 0.8 indicate a moderate tendency for corrosion.

Samples are categorized into 12 simplified geologic units based on geologic unit information in the original data source. Compiled samples without geologic unit information were categorized based on depth information when possible. The simplified geologic units include Unconsolidated, Uinta-Duchesne River, upper Green River, lower Green River, Green River (undivided), North Horn, Wasatch-Colton, Mancos, Mesaverde, Dakota-Cedar Mountain, Entrada, and Glen Canyon. Geologic units other than these are categorized as other. Samples collected from multiple open intervals in different geologic units or open intervals that span geologic unit boundaries are classified as mix. More detailed geologic unit information and geologic unit name from the source database is included in the geo notes field of the database.

Many samples contain partially complete data and/or have a poor geochemical balance. Many other samples represent repeat sampling of discrete locations and depths. To summarize the geochemistry and facilitate analysis of fluid geochemistry by geologic unit a subset of samples that include the highest quality geochemical analyses and/or most recent and relevant samples was chosen from the larger database. Chosen samples are indicated by a value of 1 in the pick field. Individual chapters in this report discuss the fluid geochemistry for many of the simplified geologic units in greater detail. These chapters also depict the spatial distribution of water chemistry for the various geologic units.

DATA ANALYSIS

Samples were selected from the database to analyze trends in water quality. Samples were chosen for each simplified geologic unit based on electrolytic charge balance, location, depth, date of sampling, and completeness of the data. For locations with multiple samples, the most recent sample with charge balance nearest zero was chosen. The geochemical trends of the selected samples are summarized in this section. The selected samples are subsequently referred to as the select samples. Detailed discussion of the geochemistry specific to many of the geologic units is presented in other chapters of this report.

A total of 1377 samples were chosen from the larger database to summarize trends in fluid geochemistry (figure 8.1). Just more than half of the samples (728) come from either the upper or lower Green River Formation. Nearly a quarter (318) of the select samples are from the Wasatch-Colton. The remainder of the select samples come from Unconsolidated (106), Mesaverde (83), Uinta-Duchesne River (53), Mancos (41), Glen Canyon (19), Entrada (12), North Horn (9), and the Dakota-Cedar Mountain (8) geologic units.

A map of the select samples shows that most samples lie within the UB and immediately to the south in eastern Utah (figure 8.2). Sample distribution by geologic unit is tightly clustered by the distribution of oil and gas wells in the UB and water wells elsewhere. Unconsolidated samples are limited to areas of valley fill in the southeast part of the study area and along major drainages in the UB. Samples from the Uinta-Duchesne River unit are scattered across the northwest part of the basin where these rocks are exposed (figure 2.1 and plate 1). Samples from the upper and lower Green River units are densely clustered in areas of oil and gas production

within the UB. North Horn samples are clustered primarily southwest of the UB along the east flank of the Wasatch Plateau. Most Wasatch-Colton samples are located in the northern and eastern parts of the UB where this unit is a significant oil and gas reservoir. Mesaverde samples are primarily found in areas where this unit produces gas in the southeast part of the basin. Most Mancos samples are located to the southeast of the Uinta Basin just east of the Wasatch Plateau. Several Mancos samples are from the eastern part of the UB. Dakota-Cedar Mountain samples are scattered across the eastern half of the basin. Both the Entrada and Glen Canyon samples are widely scattered across the map area. Notable samples from Entrada and Glen Canyon units occur in the northeast and east parts of the UB and south of the basin where these units are important aquifers.

The depth of select samples ranges from zero in the case of several spring samples from the Green River and Unconsolidated units to just over 18,000 feet for samples of produced water from the Wasatch-Colton unit (figure 8.3). Sample data was binned by depth range to show depth trends for the geologic units (table 8.1, figure 8.4). The samples cluster in depth ranges depending on the geologic unit. Nearly all samples for the Unconsolidated and Uinta-Duchesne River units are from depths of 500 feet or less and represent groundwater supply wells. Nearly all samples from the upper Green River are from depths between 1000 and 2500 feet. Samples from the lower Green River range in depth from 2500 to 15,000 feet, with most samples between 5000 and 10,000 feet in depth. Samples from the Wasatch-Colton unit cluster between 5000 to 15,000 feet in depth. Samples from the North Horn unit range from several thousand to greater than 15,000 feet in depth. Most samples from the Mancos unit occur at depths less than 500 feet. These Mancos wells represent shallow CBM dewatering wells located southwest of the UB. Samples from the Mesaverde and Dakota-Cedar Mountain units come from depths between

several thousand and 15,000 feet. Nearly two thirds of the samples from the Glen Canyon unit are from depths less than 1000 feet, a few additional samples also exist for the Glen Canyon up to 15,000 feet. The greatest percentage of Entrada samples occurs between depths of 10,000 and 15,000 feet.

Figure 8.3 also shows TDS versus depth for select samples. TDS for various geologic units increases with depth from 0 to 2000 feet but is generally below 10,000 mg/L. Below 2000 feet TDS concentrations span a large range from several thousand up to 100,000 mg/L. The select samples for the Mesaverde show a general trend of increasing TDS with increasing depth. Other units including upper and lower Green River, and the Wasatch-Colton show little correlation between TDS and the depth of sample. Several deep (>9,000 ft) samples from the Entrada and the Glen Canyon unit have relatively high TDS values between 10,000 and 100,000 mg/L.

TDS values are binned by concentration range to explore trends in the TDS concentration for each of the simplified geologic units (table 8.2, figure 8.5). All select samples from the Unconsolidated unit have TDS values less than 10,000 mg/L, with nearly half of the samples having a concentration between 1000 and 5000 mg/L. Most samples from the Uinta-Duchesne River unit have TDS concentrations less than 10,000 mg/L and nearly 40% of these samples have TDS less 500 mg/L. The Uinta-Duchesne River unit also contains small percentages (<10%) of samples with TDS concentrations greater than 25,000 mg/L. Early Tertiary age geologic units including the upper and lower Green River, North Horn, and Wasatch-Colton units have samples with much higher TDS values. More than 40% of the samples in the lower Green River and Wasatch-Colton units have TDS between 10,000 and 25,000 mg/L. The upper Green River unit has 50% of its samples with TDS between 1000 and 5000 mg/L. Most North

Horn samples have TDS less than 500 mg/L. Samples from Cretaceous age geologic units including the Mancos, Mesaverde, and Dakota-Cedar Mountain have TDS distributions similar to those of the early Tertiary age units. Nearly 50% of the samples from both the Mancos and Dakota-Cedar Mountain units have TDS concentrations between 1000 and 5000 mg/L. The Mancos unit has 20% of samples with TDS between 500 and 1000 mg/L, and the remainder of the Mancos samples have TDS greater than 5000 mg/L. More than 20% of samples from the Dakota-Cedar Mountain unit have TDS between 25,000 and 50,000 mg/L. Approximately 30% of the Mesaverde unit samples are in the 10,000 to 25,000 mg/L range. A smaller percentage of Mesaverde samples are in the 5000 to 10,000 mg/L or 25,000 to 50,000 mg/L concentration ranges. No Mesaverde samples have TDS less than 5000 mg/L. Samples from the Glen Canyon and Entrada units have more evenly distributed TDS concentrations than the other units. The samples for the Entrada unit include TDS concentrations that range from less than 500 to more than 50,000 mg/L; most Entrada samples are in the 1000 to 5000 or the greater than 50,000 mg/L TDS concentration ranges. The majority of Glen Canyon samples have TDS concentrations less than 5000 mg/L and smaller percentages of samples in the 10,000 to 25,000 and greater 50,000 mg/L TDS ranges.

Major ion chemistry is both a product and driver of water rock interaction, scaling, and corrosion and ultimately the use of a fluid. The select samples for each geologic unit were subdivided into groups based on the major ion water type (table 8.3, figure 8.6). The total number water types include nine major ion combinations of NaCl, $NaSO_4$, $NaHCO_3$, CaCl, $CaSO_4$, $CaHCO_3$, MgCl, $MgSO_4$, and $MgHCO_3$. Potassium water types are only found in only three samples and are excluded from the water type percentage calculations in table 8.3 and the bar graphs on figure 8.6. Major ion chemistry is variable across the geologic units with oil and

gas producing geologic units such as the upper and lower Green River, Wasatch-Colton, Mesaverde, Mancos, and Dakota-Cedar Mountain having sodium chloride- or sodium bicarbonate- dominated water types. The Unconsolidated, Uinta-Duchesne River, Entrada, and Glen Canyon units have a greater diversity of water types and include a significant fraction of calcium bicarbonate and calcium sulfate samples. Samples from the Unconsolidated and Uinta-Duchesne River units are primarily bicarbonate water types that include either sodium or calcium as the major cation. Both these units have a small fraction of samples (less than 10%) of magnesium water types. Two thirds of the North Horn samples are calcium bicarbonate water type and the remainder is sodium chloride water type. Nearly half of the Entrada samples are sodium chloride water type. Just more than half of the Glen Canyon samples are calcium bicarbonate and calcium sulfate waters.

A plot of TDS versus major ion chemistry indicates the solutes that are the source of dissolved solids (figure 8.7). Samples with TDS greater than 10,000 mg/L are dominated by sodium chloride, sodium bicarbonate, and sodium sulfate water types. Samples from the lower Green River include calcium chloride and magnesium chloride water types with TDS greater than 10,000 mg/L. Most samples with TDS less than 1000 mg/L are bicarbonate water types and the samples with the lowest TDS concentrations are calcium bicarbonate type. TDS concentrations between 1000 and 10,000 mg/L have mostly sodium water types.

A piper diagram of all select samples is shown in figure 8.8. Water chemistry spans a great range from waters that are dominated by calcium and bicarbonate to waters dominated by sodium and chloride. These chemistry differences are most prominent between geologic units that are oil and gas producers (upper and lower Green River, Wasatch-Colton, and Mesaverde) and geologic units that are groundwater aquifers (Unconsolidated, Uinta-Duchesne River, and

Glen Canyon). The chemistry of samples from the upper and lower Green River, Wasatch-Colton, and Mesaverde geologic units are tightly clustered due to consistently high concentrations of sodium and chloride. Variation in chemistry in these units is related to variation in sulfate concentrations. The chemistry of samples from the Unconsolidated and Uinta-Duchesne River units spans a large range that overlaps chemistry of many of the other units.

A statistical summary of the major ion concentrations of select samples for each geologic unit is presented in appendix H. This summary includes a geometric mean, median, maximum and minimum, and a standard deviation for the major ions of calcium, magnesium, sodium, potassium, bicarbonate, chloride, sulfate, and TDS.

SUMMARY

The database compiled as part of this report includes fluid chemistry for groundwater and produced water from the UB and surrounding areas in eastern Utah. These samples come from either groundwater from springs and water wells or produced water collected as part of oil and gas exploration and production. The database contains 4184 samples that includes a mix of unique samples for given location and depth as well as samples that represent a time series of multiple samples from a given location and depth. Each sample in the database includes data source, basic location information, and a unique identifier. All other data fields are populated when the data is available. Samples are categorized into 12 simplified geologic units based on geologic unit information in the original data source or depths. Sample chemistry fields in the

database include temperature, pH, conductivity, TDS, and chemical concentration values. AquaCHEM™ software was used to calculate charge balance of the major anions and to delineate a water type for each sample. Five scaling and corrosion indices were calculated for the compiled samples with sufficient data using the AquaCHEM™ software. The resulting dataset was cleaned for duplicates based on samples with identical sample information.

Samples were selected from the larger database to analyze general trends in water chemistry. Samples were chosen for each simplified geologic unit based on electrolytic charge balance, location, depth, date of sampling, and completeness of the data. For locations with multiple samples, the most recent sample with charge balance nearest zero was chosen. Based on these criteria a total 1377 samples were chosen from the database to represent chemistry trends in the various geologic units.

The spatial distribution of samples is controlled by the distribution of oil and gas wells in the UB and water wells elsewhere. The depth of collection for the select samples range from the surface to just over 18,000 feet. The depth of samples is generally less 500 feet for samples taken from important regional aquifers that include the Unconsolidated, Uinta-Duchesne River, and Glen Canyon geologic units. The depth of samples is generally between 2500 and 15,000 feet for the upper and lower Green River, Wasatch-Colton, Mesaverde, and Dakota-Cedar Mountain. Both the spatial and depth distribution of select samples tends to be clustered due to the origin of samples; either from oil and gas wells or from more typical groundwater samples. This clustering may limit the validity of generalized chemical trends applied over areas or depths not represented in the database.

TDS is variable across the select database. Highest TDS tends to correlate with sodium chloride or sodium bicarbonate water types that are typical of the upper and lower Green River,

Wasatch-Colton, and Mesaverde units. These samples are predominately produced water and the high TDS may be the result of oil and gas generation processes, long residence time, and or increased water rock interaction within these units. Lower TDS values and bicarbonate water types are typical of the Unconsolidated, Uinta-Duchesne River, Glen Canyon units. These chemistries likely result from a relatively active meteoric groundwater system within these units where they are near surface. Little data exists for any of the units at significant depths (>1000 feet) away from areas of oil and gas development.

The dataset contains many samples that represent repeat measurements of discrete locations and intervals through time. These time series samples were not analyzed in this report because of the project scope. Future work on the time series samples could yield unique perspectives on large scale geochemical changes resulting from oil and gas development activities. The select samples in this database may also be used for important baseline chemistry over large areas of eastern Utah.

The samples in this database represent a unique regional scale snapshot of fluid geochemistry across an active petroleum province including both the shallow meteoric groundwater system and the deeper basin fluid system. Further study and geochemical analysis of these data could yield insight into large scale fluid evolution in both active petroleum provinces and similar geographic setting elsewhere.

CHAPTER VIII FIGURE AND TABLE CAPTIONS

Figure 8.1. Pie graph of the number of samples for each geologic unit.

Figure 8.2. Location of select fluid geochemical samples. Samples in this subset of the database were selected to represent geochemistry of simplified geologic units.

Figure 8.3. Total dissolved solids versus depth for select samples.

Figure 8.4. Summary of depths of samples by geologic unit. Data correlates with that in table 8.1.

Figure 8.5. Summary of total dissolved solids by geologic unit. Data correlates with that in table 8.2.

Figure 8.6. Summary of water types by geologic unit. Data correlates with that in table 8.3.

Figure 8.7. Major ion chemistry versus total dissolved solids.

Figure 8.8. Piper diagram of select samples.

Table 8.1. Summary of depth distribution of select water chemistry samples.

Table 8.2. Summary of total dissolved solids distributions for select water chemistry samples.

Table 8.3. Water type distribution for select samples.

Table 8.1. Summary of depth distribution of select water chemistry samples.

Depth (ft)	Geologic Unit											
	Unconsolidated	Uinta-Duchesne River	upper Green River	lower Green River	North Horn	Wasatch-Colton	Mesaverde	Mancos	Dakota-Cedar Mountain	Entrada	Glen Canyon	All Units
<500	84	39	9	0	0	0	0	22	0	3	7	164
500-1000	0	9	11	5	0	0	0	2	0	1	6	34
1000-2500	0	0	141	13	0	0	0	2	0	0	1	157
2500-5000	0	5	21	159	1	31	30	0	1	0	1	249
5000-10,000	0	0	8	338	0	116	48	2	3	1	0	516
10,000-15,000	0	0	0	14	1	145	4	4	3	5	1	177
>15,000	0	0	0	1	1	26	0	0	1	0	0	29
total obs	84	53	190	530	3	318	82	32	8	10	16	1326
<500	100%	74%	5%	0%	0%	0%	0%	69%	0%	30%	44%	12%
500-1000	0%	17%	6%	1%	0%	0%	0%	6%	0%	10%	38%	3%
1000-5000	0%	0%	74%	2%	0%	0%	0%	6%	0%	0%	6%	12%
5000-10,000	0%	9%	11%	30%	33%	10%	37%	0%	13%	0%	6%	19%
10,000-25,000	0%	0%	4%	64%	0%	36%	59%	6%	38%	10%	0%	39%
25,000-50,000	0%	0%	0%	3%	33%	46%	5%	13%	38%	50%	6%	13%
>50,000	0%	0%	0%	0%	33%	8%	0%	0%	13%	0%	0%	2%
sum	100%	100%	100%	100%	100%	100%	100%	100%	100%	100%	100%	100%

Table 8.2. Summary of total dissolved solids distributions for select water chemistry samples.

	Geologic Unit											
TDS (mg/L)	Unconsolidated	Uinta-Duchesne River	upper Green River	lower Green River	North Horn	Wasatch-Colton	Mesaverde	Mancos	Dakota-Cedar Mountain	Entrada	Glen Canyon	All Units
<500	33	21	0	0	6	0	0	0	0	2	7	69
500-1000	22	16	5	7	0	1	0	8	0	0	3	62
1000-5000	50	12	98	45	0	41	1	20	4	3	6	280
5000-10,000	1	1	19	63	0	76	18	7	1	1	0	187
10,000-25,000	0	0	25	234	2	140	30	3	1	1	1	437
25,000-50,000	0	2	16	144	1	48	25	2	2	2	0	242
>50,000	0	1	34	37	0	12	9	1	0	3	2	99
total observation	106	53	197	530	9	318	83	41	8	12	19	1376
<500	31%	40%	0%	0%	67%	0%	0%	0%	0%	17%	37%	5%
500-1000	21%	30%	3%	1%	0%	0%	0%	20%	0%	0%	16%	4%
1000-5000	47%	23%	50%	8%	0%	13%	1%	49%	50%	25%	32%	20%
5000-10,000	1%	2%	10%	12%	0%	24%	22%	17%	13%	8%	0%	14%
10,000-25,000	0%	0%	13%	44%	22%	44%	36%	7%	13%	8%	5%	32%
25,000-50,000	0%	4%	8%	27%	11%	15%	30%	5%	25%	17%	0%	18%
>50,000	0%	2%	17%	7%	0%	4%	11%	2%	0%	25%	11%	7%
sum	100%	100%	100%	100%	100%	100%	100%	100%	100%	100%	100%	100%

Table 8.3. Water type distribution for select samples.

Water type	Geologic Unit											
	Unconsolidated	Uinta-Duchesne River	upper Green River	lower Green River	North Horn	Wasatch-Colton	Mesaverde	Mancos	Dakota-Cedar Mountain	Entrada	Glen Canyon	All Units
Na-Cl	0	6	77	386	3	290	61	7	6	5	3	844
Na-HCO_3	20	24	96	61	0	4	21	0	2	0	1	229
Na-SO_4	23	7	10	16	0	16	0	6	0	1	2	81
Ca-Cl	0	0	2	27	0	7	0	0	0	0	1	37
Ca-HCO_3	33	8	2	1	6	0	0	0	0	1	5	56
Ca-SO_4	16	1	0	0	0	0	0	0	0	1	5	23
Mg-Cl	1	0	0	11	0	1	0	0	0	0	0	13
Mg-HCO_3	6	6	0	0	0	0	0	0	0	1	1	14
Mg-SO_4	7	1	0	0	0	0	0	1	0	2	1	12
K-Cl	0	0	0	0	0	0	1	0	0	1	0	2
K-HCO_3	0	0	1	0	0	0	0	0	0	0	0	1
K-SO_4	0	0	0	0	0	0	0	0	0	0	0	0
total observation	106	53	187	502	9	318	82	14	8	11	19	1309
Na-Cl	0%	11%	41%	77%	33%	91%	74%	50%	75%	45%	16%	65%
Na-HCO_3	19%	45%	51%	12%	0%	1%	26%	0%	25%	0%	5%	18%
Na-SO_4	22%	13%	5%	3%	0%	5%	0%	43%	0%	9%	11%	6%
Ca-Cl	0%	0%	1%	5%	0%	2%	0%	0%	0%	0%	5%	3%
Ca-HCO_3	31%	15%	1%	0%	67%	0%	0%	0%	0%	9%	26%	4%
Ca-SO_4	15%	2%	0%	0%	0%	0%	0%	0%	0%	9%	26%	2%
Mg-Cl	1%	0%	0%	2%	0%	0%	0%	0%	0%	0%	0%	1%
Mg-HCO_3	6%	11%	0%	0%	0%	0%	0%	0%	0%	9%	5%	1%
Mg-SO_4	7%	2%	0%	0%	0%	0%	0%	7%	0%	18%	5%	1%
sum	100%	100%	100%	100%	100%	100%	100%	100%	100%	100%	100%	100%

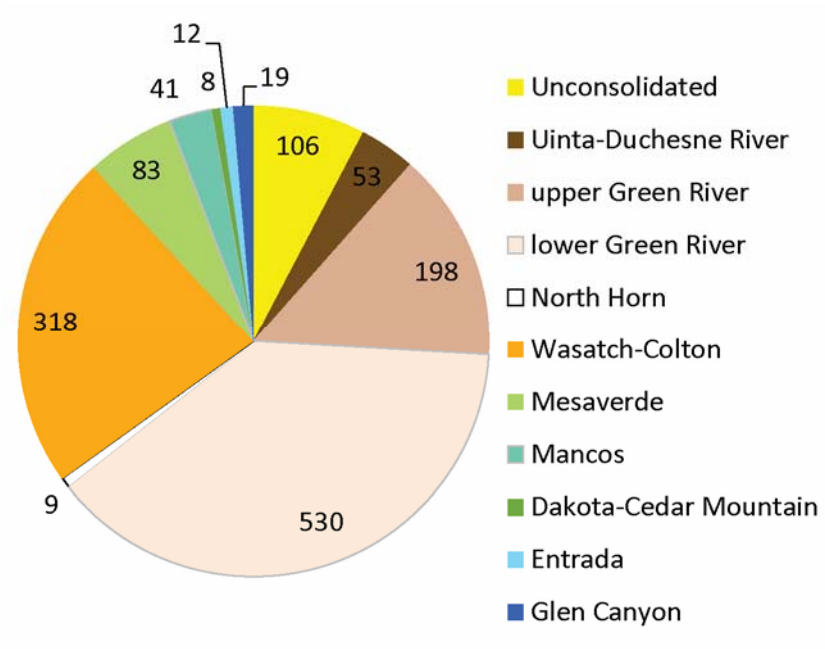

Figure 8.1. Pie graph of the number of samples for each geologic unit.

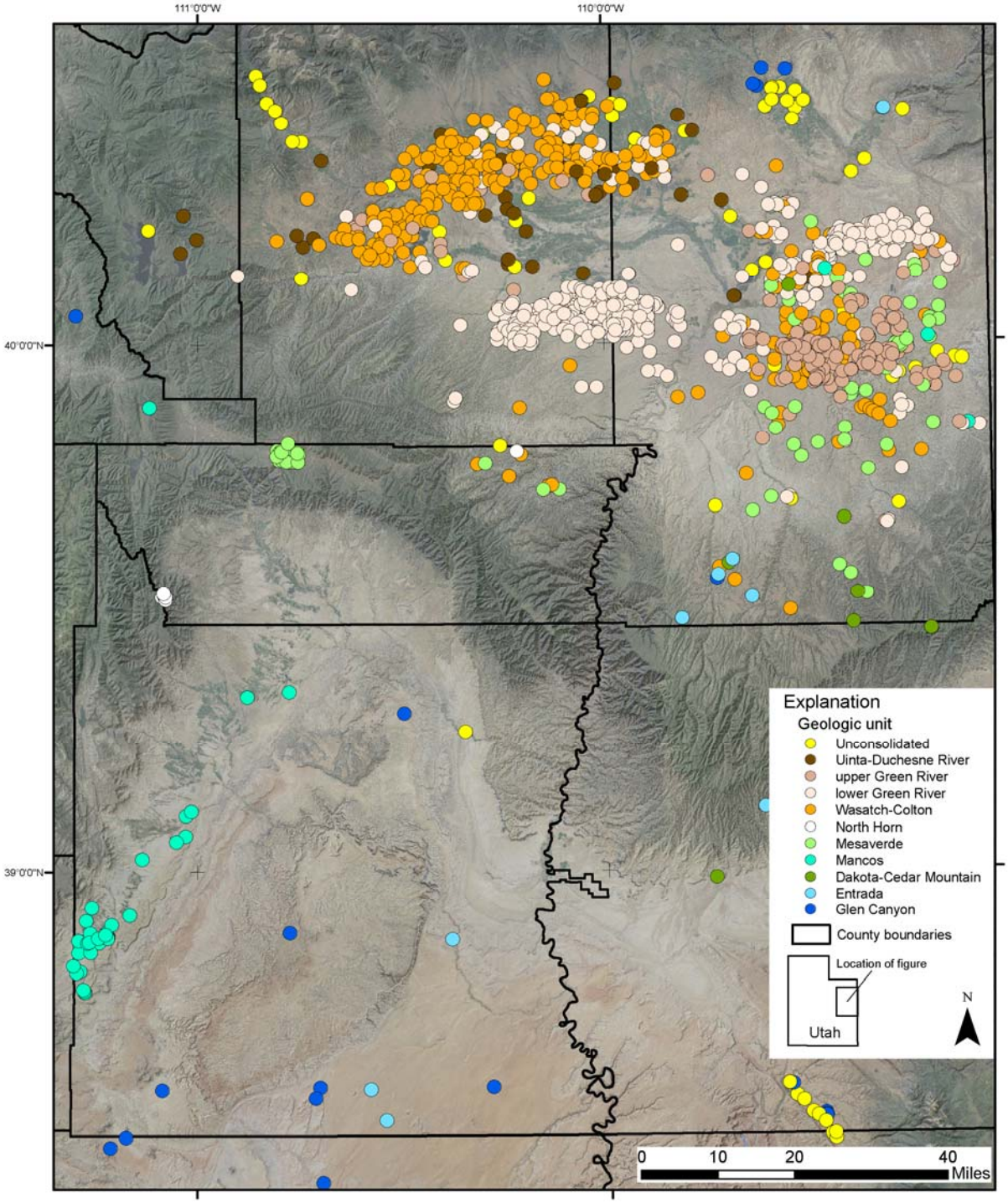

Figure 8.2. Location of select fluid geochemical samples. Samples in this subset of the database were selected to represent geochemistry of simplified geologic units.

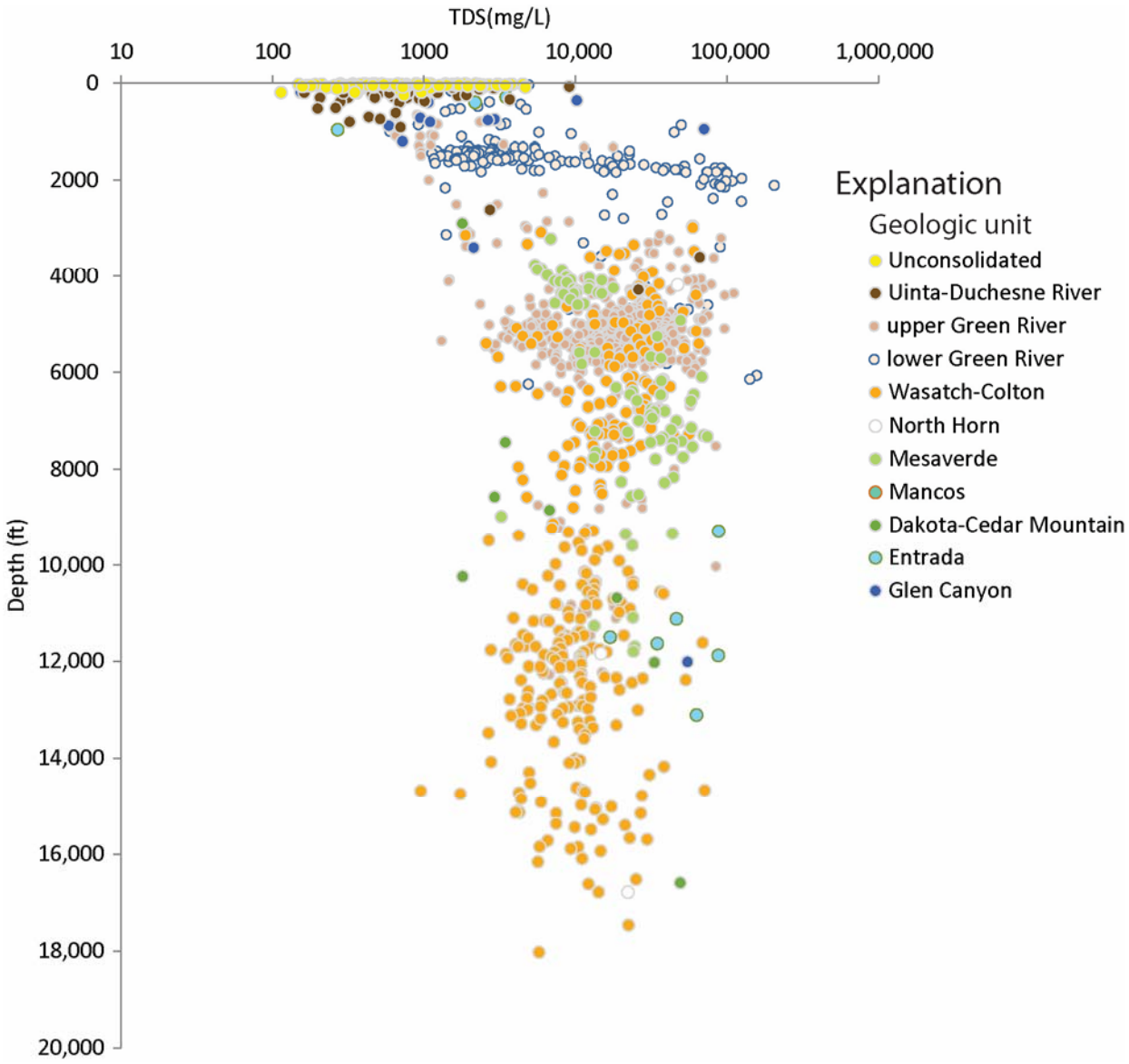

Figure 8.3. Total dissolved solids versus depth for select samples.

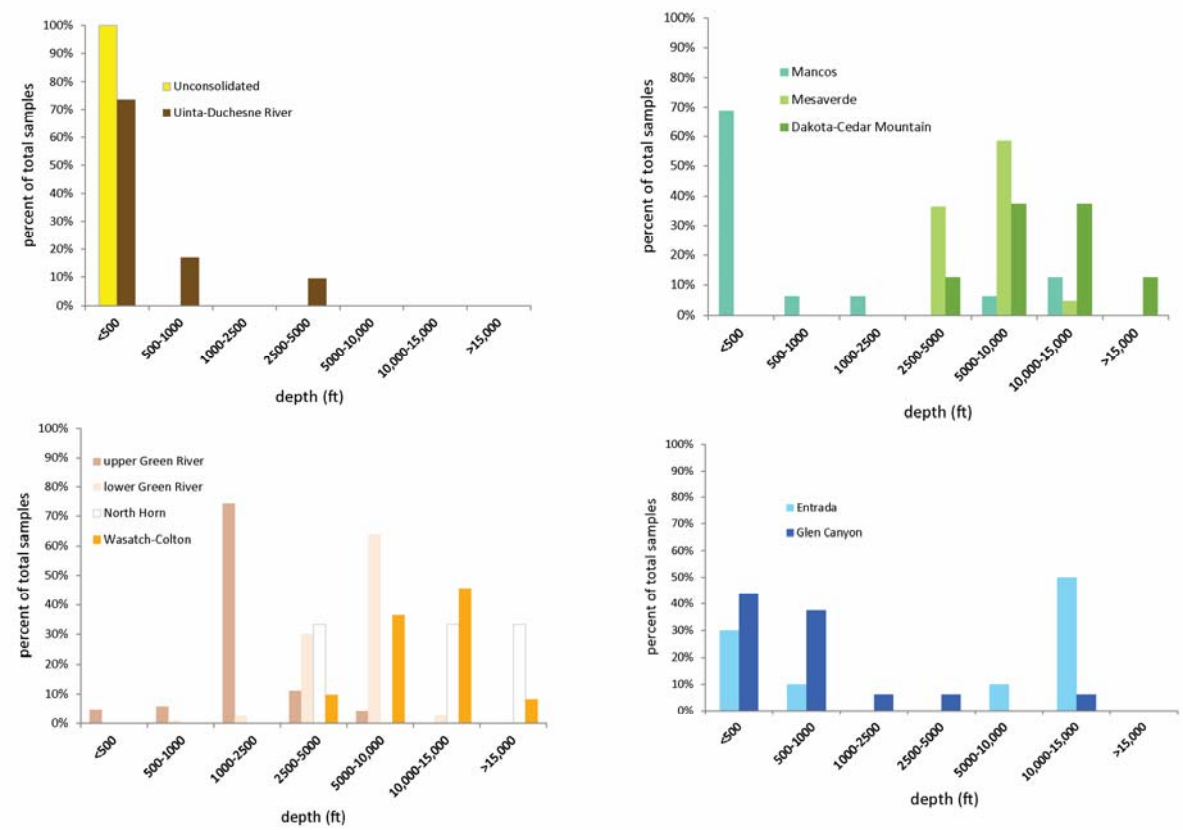

Figure 8.4. Summary of depths of samples by geologic unit. Data correlates with that in table 8.1.

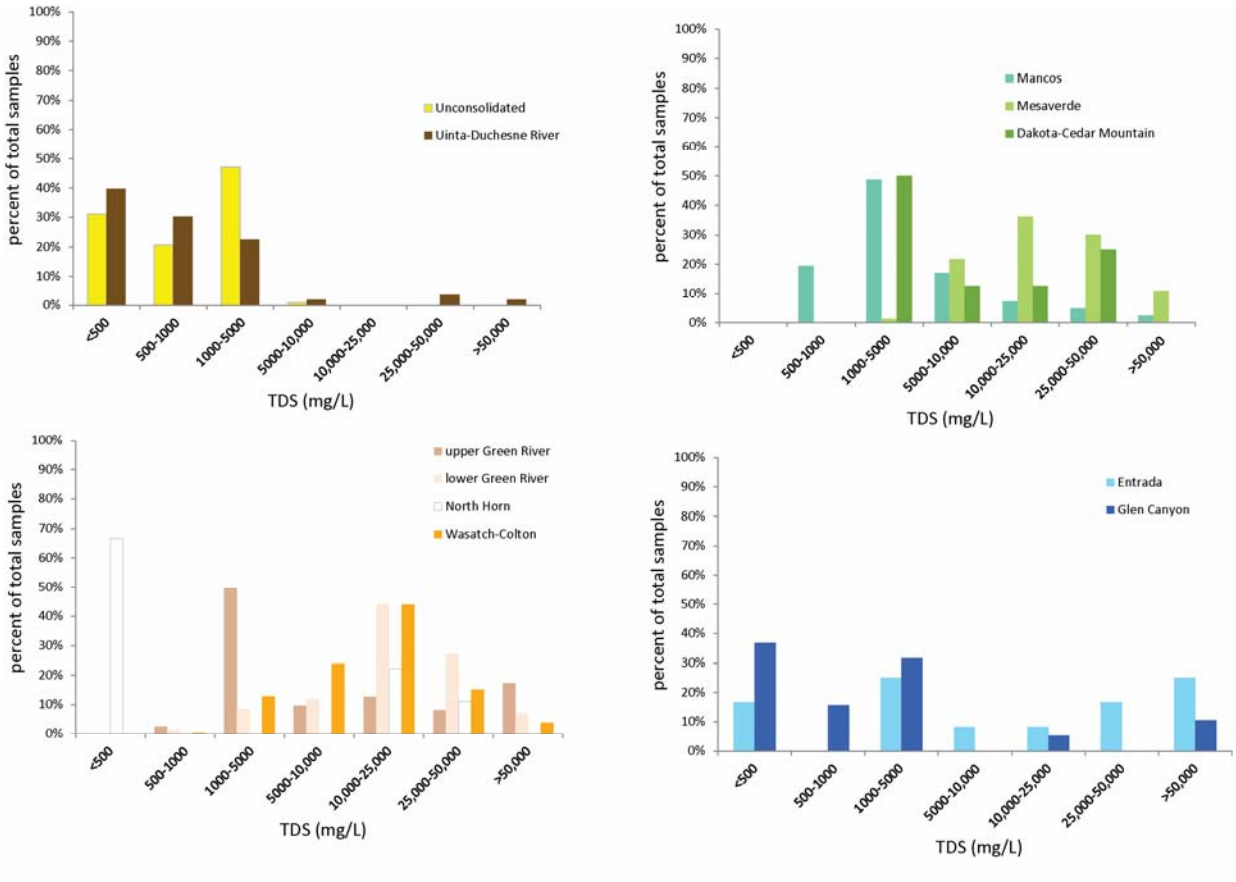

Figure 8.5. Summary of total dissolved solids by geologic unit. Data correlates with that in table 8.2.

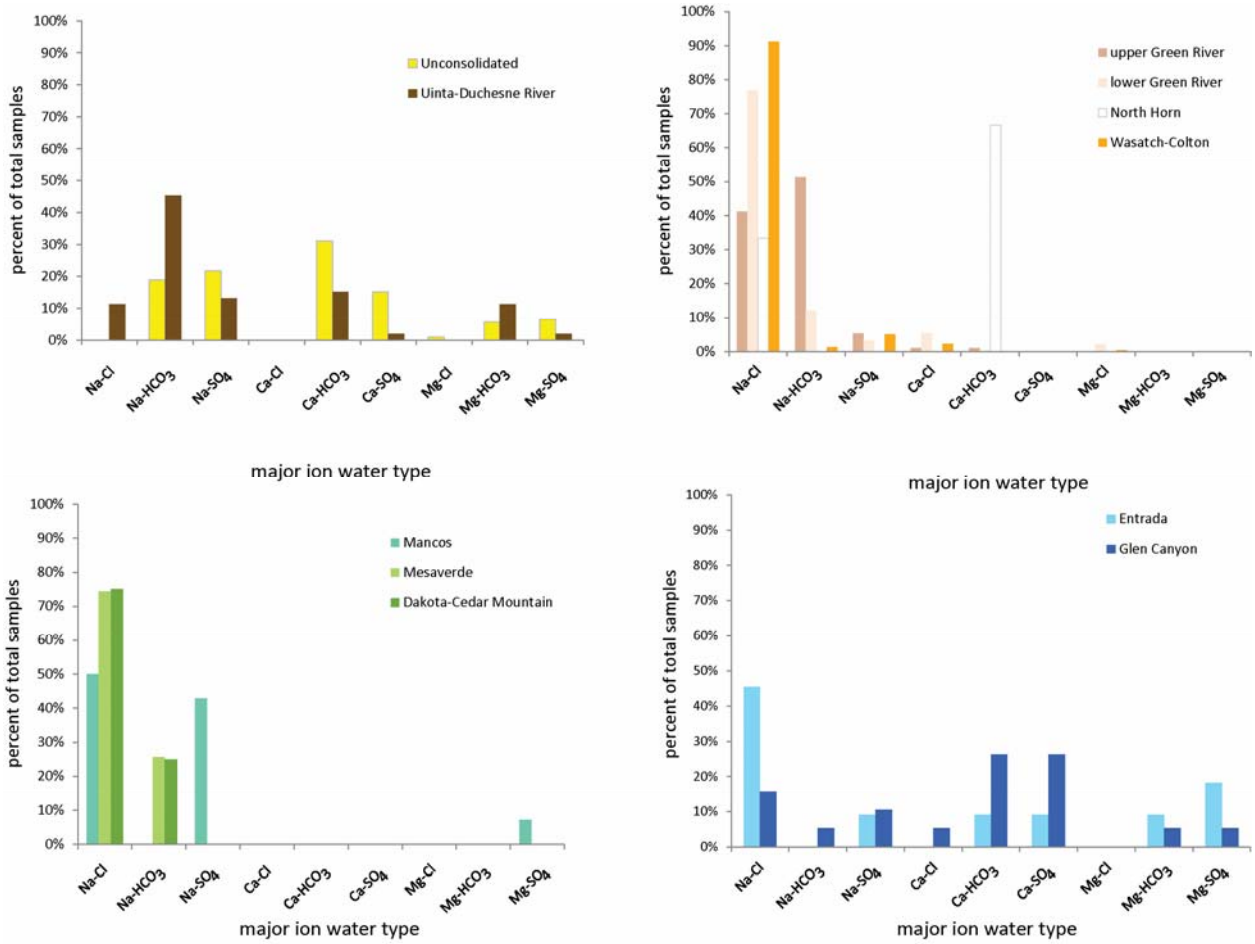

Figure 8.6 Summary of water types by geologic unit. Data correlates with that in table 8.3.

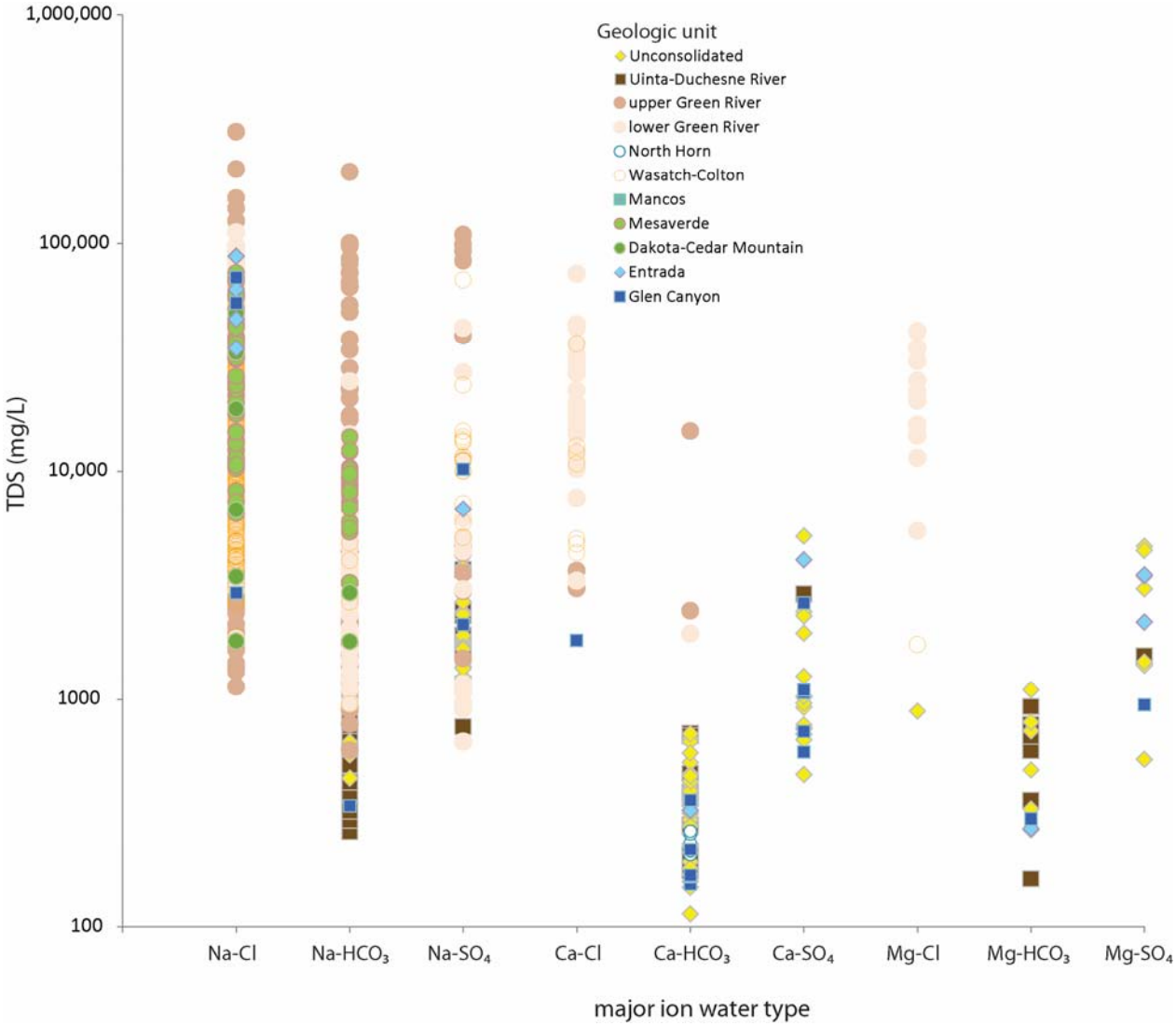

Figure 8.7 Major ion chemistry versus total dissolved solids.

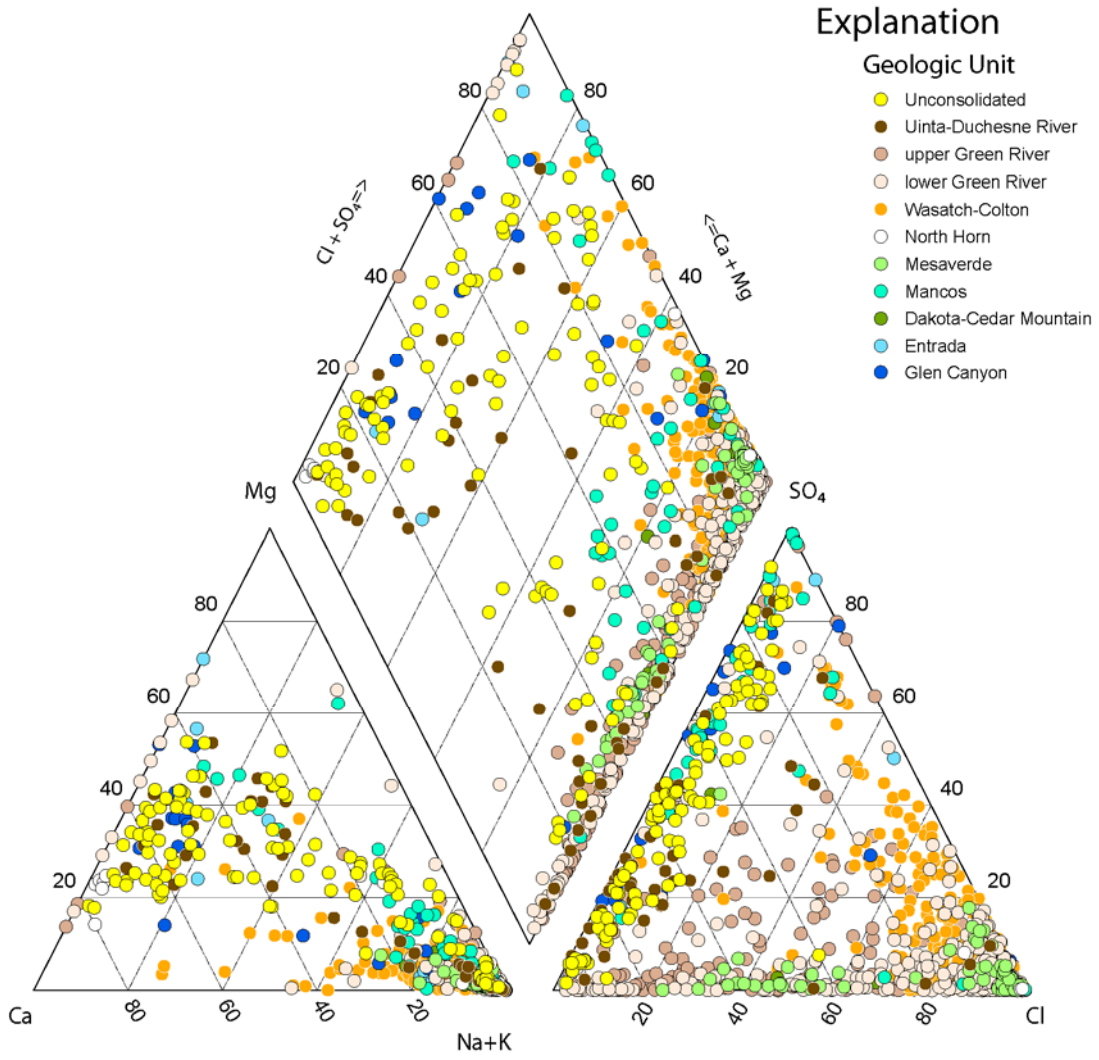

Figure 8.8 Piper diagram of select samples.

CHAPTER IX

GROUNDWATER CHEMISTRY AND WATER QUALITY FOR SHALLOW ALLUVIAL WELLS AND SPRINGS IN THE UINTA BASIN

Janae Wallace

The UB generally lacks sufficient water-quality data to characterize the relatively shallow groundwater. The primary objective of work presented in this chapter is to document water quality in established conventional oil and gas reservoirs, including "tight" sand- and shale-gas reservoirs, (figure 9.1). Production and disposal of produced water especially affects the economics of gas resource development and has potential land-use impacts that may impact vulnerable aquifers of the UB. Characterizing shallow groundwater chemistry will aid in the protection of critical UB alluvial aquifers and springs by establishing baseline water quality. The information collected in this study provides necessary background water-quality information along with historic water-quality data to help create a vulnerability assessment of the UB's shallow aquifers.

PREVIOUS WORK

Hydrogeology

Groundwater in the UB occurs in both unconsolidated valley-fill material and consolidated rocks. In the southeastern UB, the principal productive consolidated aquifers are in the Green River and Wasatch Formations (Holmes, 1980). Price and Miller (1975) provided a reconnaissance of groundwater conditions in the southern UB. Water is generally unconfined in the unconsolidated deposits and confined in the consolidated aquifers.

Recharge to the shallow groundwater system, including imported Duchesne River water, in the southern UB for the 1935–1970 period was estimated at 120,000 acre-feet per year; discharge was estimated at 118,000 acre-feet per year (Price and Miller, 1975). Holmes (1980) indicated the amount of basin-wide recharge was 630,000 acre-feet per year, of which only 20% was derived from the southern half of the basin. Most recharge generally occurs during winter when more widespread and longer-duration snowstorms occur. The fine-grained, low permeability rocks found throughout the recharge area result in slow percolation rates; about 3% of estimated average annual precipitation (~100,000 acre-feet) is recharged (Price and Miller, 1975).

In a later study, groundwater discharge was estimated to be equal to recharge (Holmes and Kimball, 1987) with discharge occurring in the southeastern UB mostly from shallow, alluvial aquifers within valley drainages of the Green and White Rivers and their tributaries. Most discharge occurs from streams, springs, evapotranspiration, and well withdrawal. The hydrologic budgets for the alluvial aquifer and the bedrock aquifers within the Green River Formation vary (Holmes and Kimball, 1987). Recharge for deep groundwater aquifers is primarily from precipitation and stream inflow but can also originate from leaking overlying

formations. Shallow, alluvial aquifer recharge originates from stream infiltration and locally from upward migration of underlying, consolidated aquifer water. Groundwater movement in both unconsolidated and consolidated aquifers typically follows the slope and direction of the major streams (e.g., Strawberry, Duchesne, Green, and White Rivers) (Price and Miller, 1975). Water leaves the basin via the Green River and diversions to the Great Basin region (Holmes, 1985).

The total water volume consumed in the entire UB is estimated by taking the difference between the inputs (surface-water and precipitation inflows) and the outputs (surface-water outflow and diversions to the Great Basin). The water volume consumed in 1985 was about 7.4 million acre-feet (Holmes, 1985). Today, annual consumption is most likely greater due to an increased number of water users. For shallow, alluvial aquifers in the southeastern UB, the estimated volume of recoverable storage water is about 200,000 acre-feet with maximum yields for individual wells of more than 1000 gallons per minute (Holmes and Kimball, 1987).

A 1987 study by Holmes and Kimball of the USGS on groundwater in the southeastern UB examined water quality from the alluvial and bedrock aquifers. They documented variable water quality throughout the southeastern Uinta Basin; their data are from the easternmost part of the study area. Total-dissolved-solids concentrations ranged from 440 to 27,800 mg/L for water in the alluvial aquifers, from 870 to 5810 mg/L in the eastern portion of the Birds Nest aquifer (much higher salinities are found in the western Birds Nest), and from 640 to 6100 mg/L in the Douglas Creek aquifer. They attributed the changes in water quality to several physiochemical processes, including mineral precipitation and dissolution, oxidation and reduction, mixing, ion exchange, and evaporative concentration. Water quality is much poorer in the alluvial aquifers than in the bedrock aquifers. Based on 72 samples from four alluvial aquifers in the southeastern

UB, average TDS was 5432 mg/L. Average TDS concentration (80 water samples) for the eastern Birds Nest aquifer was 2700 mg/L, and average TDS concentration (12 samples) for the Douglas Creek aquifer was 1098 mg/L. Water quality in the deeper part of the basin, especially in the Birds Nest aquifer, has TDS concentrations of more than 100,000 mg/L (Vanden Berg and others, 2013).

Another study in the northwestern UB, within the Altamont-Bluebell field area (figure 1.1), examined the impacts to drinking-water wells from oil and gas wastewater injection into deeper parts of the aquifer (Steiger, 2007). Twenty monitoring wells penetrating alluvial and/or shallow bedrock aquifers of the Duchesne River and Uinta Formations were analyzed for water quality with emphasis on bromide, chloride, and stable isotopes (^{18}O and ^{2}H). The study monitored the wells on a rotating basis from 1993 to 2004 to determine whether saline water disposed in the deeper aquifers (3100 to 10,500 feet below the surface) was influencing the shallow aquifers. Any increase in either bromide or chloride concentrations in the monitoring wells over time could indicate mixing of the two waters, but based on these constituents, no mixing was documented. Stable isotopes from the shallow wells plotted on or near the meteoric water line whereas those from the deep aquifer wells plotted well below the meteoric water line. Based on these chemical results, Steiger (2007) concluded that the deeper groundwater was not reaching the drinking-water aquifers.

Kenney and others (2009) evaluated water quality in the greater Upper Colorado River Basin, including the rivers and tributaries within the Uinta Basin, to determine the impact of land-use practices on water quality using TDS concentrations. Using a Spatially Referenced Regressions on Watershed Attributes (SPARROW) model, they compared relative contributions of dissolved solids from natural sources, agricultural practices, and industrial development (oil

and gas fields). Based only on measured dissolved solids in rivers and streams, the authors concluded the greatest source of TDS is from natural geologic sources (~57%) and agricultural practices (45%) whereas the oil and gas industry contribution was statistically insignificant.

Previous Water-Quality Data

Several water-quality studies were conducted in the southeastern UB where tight-sand gas produce and potential shale-gas reservoirs remain to be evaluated. These studies are mainly of water sampled from oil and gas wells during well installation. In 1970, the USGS drilled six monitoring wells into the shallow, alluvial aquifer and Green River Formation in areas considered for oil-shale development and reported water-quality data from the Douglas Creek and Birds Nest aquifer within the Green River Formation (Holmes, 1980; Wallace, 2012a). The UGS compiled water-quality data for springs and wells sampled during the 1970s (Wally Gwynn, former UGS geologist, written communication, May 2009). A study by Zhang and others (2009) provided water-quality data from 57 wells completed in several different formations. The UGS conducted studies on water-related issues affecting conventional oil and gas recovery as well as potential oil shale development in the UB (Anderson and others, 2012; Wallace, 2012a; Vanden Berg and others, 2013).

Wells and springs dominantly penetrating or issuing from the Green River Formation (and a few in the Wasatch Formation) indicate variable water quality (Wally Gwynn, former UGS geologist, written communication, May 2009). TDS concentrations from 39 springs range from 292 to 23,900 mg/L with an average of 1999 mg/L, and TDS concentrations from 50 wells range from 494 to 9870 mg/L with an average of 2443 mg/L (Wally Gwynn, former UGS

geologist, written communication, June 2009). Zhang and others' (2009) data show 5% of the wells have TDS between 0 and 1000 mg/L, 4% between 1000 and 3000 mg/L, 5% between 3000 and 10,000 mg/L, 68.5% between 10,000 and 50,000 mg/L, and 17.5% greater than 50,000 mg/L. Water samples from the Birds Nest aquifer (from ~200 oil/gas wells, oil-shale wells, and disposal wells) have TDS values that range from 1100 to 205,286 mg/L; 35% of the wells have TDS concentrations less than 3000 mg/L (mainly in the southeast), 28% between 3000 and 10,000 mg/L (south and east) and 37% greater than 10,000 mg/L (north and west) (data provided by several oil and gas industry sources; see Vanden Berg and others, 2013). Anderson and others (2012) re-mapped the BMSW in the UB using 10,000 mg/L TDS as the "boundary" between non-saline (TDS <10,000 mg/L) and saline (TDS>10,000 mg/L) water from data provided by cooperating oil and gas operators (data from ~8000 wells drilled after a report by Howells and others (1987) who mapped the original BMSW).

Wallace (2012a) evaluated water quality from 24 locations in the southeastern UB to assess the alluvial and bedrock aquifers on lands proposed by the BLM as having oil shale development potential. Data from 85 water samples were analyzed from water wells and surface-water sites (figure 9.2) over three different sampling seasons from 2009 to 2011. The actual number of samples obtained each season/year varied depending on the condition of the well/spring. A suite of water-quality constituents were analyzed including general chemistry (including TDS), nutrients (including nitrate, phosphorous, and ammonia), dissolved metals, and volatile organic compounds (VOCs).

Groundwater quality in Wallace (2012a) was variable, and generally good with TDS concentrations primarily below 3000 mg/L; some sites showed elevated nitrate, arsenic, lead, selenium, barium, boron, and gross alpha particle emitter concentrations in the aquifers.

Seasonal changes in water chemistry were minimal for most sampling sites. TDS concentrations for all samples range from 172 to 2832 mg/L. The highest TDS value of 2832 mg/L was from Evacuation Creek during spring 2009; the lowest value (172 mg/L) was from the Green River near Ouray during flood stages in spring 2010. Nitrate concentrations range from <0.1 to 18.8 mg/L for all sampling seasons. Most sites had nitrate concentrations below 0.1 mg/L except alluvial wells downgradient from irrigated fields and a cattle ranch operation in the northwestern part of the study area, and a well penetrating bedrock in the central part of the study area. Twelve different types of VOCs had detectable concentrations, but all were below EPA maximum contaminant levels (MCL). Besides VOCs and boron, only the chemical constituents exceeding EPA standards are discussed below (see Wallace, 2012a).

More recently, sites around Greater Natural Buttes field (figure 1.1) have been and continue to be sampled quarterly as part of a long-term water-resource monitoring project for shallow alluvial and surface water administered by a subsidiary of Anadarko Petroleum Company (InterTech Environmental and Engineering, LLC, 2014). In the most recent monitoring report, TDS concentrations ranged from 820 to 11,800 mg/L for alluvial wells and 331 to 13,500 mg/L for surface water sites (InterTech Environmental and Engineering, LLC), 2014). Detectable VOC concentrations above detection level include: vinyl chloride, acetone, trichlorofluoromethane, trichloroethane, toluene, styrene, pyridine, p-isopropyltoluene, methyl ethylketone, bis (2-ethylhexyl) phthalate, and total petroleum hydrocarbon (TPH) (commonly called gasoline-range organics/diesel-range organics or GRO/DRO).

WATER-QUALITY SAMPLING FOR SPRINGS AND ALLUVIAL WELLS

During summer 2013, water from 12 shallow wells and 10 springs was sampled, representing a widespread distribution without land use bias, to characterize the alluvial aquifers in the UB. During summer 2014, two additional springs were discovered and sampled (figure 9.1). A suite of water-quality constituents was analyzed, including TDS, specific conductance, bicarbonate, hydroxide, carbonate, sulfate, chloride, nitrate, dissolved metals/metalloids (including calcium, magnesium, potassium, sodium, arsenic, aluminum, barium, cadmium, chromium, copper, mercury, manganese, mercury, silver, lead, iron, selenium, boron, and zinc), VOCs, TPH, and stable isotopes (^{18}O and ^{2}H). One well (site 18) was not analyzed for dissolved metals.

WATER-QUALITY RESULTS

Total-dissolved-solids concentrations for all wells and springs sampled range from 214 to 5532 mg/L, and nitrate concentrations range from <0.1 to 5.32 mg/L. Piper and Stiff water chemistry diagrams uniquely show variations in ion concentrations from water wells and springs throughout the study area. Piper diagrams indicate overall water chemistry is variable throughout the area with dominantly sodium-potassium-bicarbonate-, sodium-potassium-sulfate-, and calcium-magnesium-bicarbonate-sulfate-type groundwater (figure 9.3). Stiff diagrams show solute chemistry data for sites sampled in 2012-2014 (all but one site have solute chemistry data) (figure 9.4).

Total-Dissolved-Solids Concentrations

The average TDS concentration from samples in this study is 1229 mg/L, and the median is 747 mg/L (table 9.1). The highest TDS concentration is 5532 mg/L from a spring (site 12) near the White River, and the lowest is 214 mg/L from a water well near the Uinta Mountains recharge area (site 5). Additional TDS data were gathered from 32 public supply sources (water wells and springs). The average TDS for public supply sources is 427 mg/L. Figure 9.5 shows a graduated-symbol TDS concentration map for sites sampled during 2013 and 2014 (this study), the 2009 to 2011 sampled sites, and public supply sources (data from 1978 to 2013). The poorest quality water shown in figure 9.5 is an outlier compared to the rest, in terms of high TDS, and is from a spring (site 12) issuing from the Uinta Formation exposed at the surface near the White River (figure 9.6). The highest quality water is from wells (sites 3, 4, 5, 6, 7, 8) located proximal to the Uinta Mountains recharge area in the north (figure 9.5). Elevated TDS concentrations are possibly due to long residence time in the bedrock aquifers, associated with drilling fluids (reported "lost" circulation driller's mud due to the pervasive vugs within the Birds Nest aquifer), or wastewater disposal from wells drilled in the Green River Formation (though many disposal wells are upgradient from this spring, which warrants additional analysis, discussed below).

Nitrate Concentrations

Nitrate concentrations in groundwater range from less than 0.1 mg/L to 5.32 mg/L (table 9.1). The majority of samples (91%) had nitrate concentrations that were less than 1 mg/L. One

spring (site 19) and one well (site 15) had nitrate concentrations of 4.3 and 5.3 mg/L. Both samples are below the EPA maximum contaminant level (MCL) of 10 mg/L. Average nitrate concentration is 0.59 mg/L and median concentration is 0.08 mg/L.

The highest nitrate concentrations of 5.3 and 4.3 mg/L are in different areas in the basin; site 15 is a shallow monitoring well drilled in the 1970s near Evacuation Creek (figure 9.7) and site 19 is a spring near the Duchesne River downgradient from a gravel pit. No other nearby land use commonly identified as a nitrate source (septic tanks, feed lots, and fertilized cropland) exists in either area.

Arsenic

Arsenic values from sampling sites ranged from less than 1 µg/L to 13 µg/L (table 9.1). One site (2), near a gas development in the Nine Mile Canyon field area (figures 1.1 and 9.1), exceeds the 10 µg/L EPA MCL, and ten sites had arsenic concentrations between 1 and 9 µg/L. Forty-three percent of the sites had concentrations below detection level (< 1 µg/L); the average concentration is 2.5 µg/L and the median is 3.6 µg/L. Overall, arsenic concentrations in the basin aquifers are variable, and the source of arsenic is unknown.

Boron

Boron was analyzed in all but one sample (table 9.1) and ranges from <30 µg/L (site 23, E seep spring) to a high of 28,300 µg/L (site 12, White River spring). The average of all samples, excluding site 23, is 2319 µg/L and the median is 178 µg/L (table 9.1). Boron may be

associated with dissolution of minerals (feldspar) in the Green River Formation (Desborough and others, 1974, 1976) or from drilling fluid loss in the Birds Nest aquifer. Clerico (in press) reports elevated boron concentrations in the Birds Nest aquifer which may be indicative of a perched aquifer underlying areas leased for oil shale development near Evacuation Creek in the southeastern part of the UB. All but one of the boron concentrations were above the detection level of 30 µg/L. Boron does not have an EPA-designated MCL, and is not known to pose a threat to human health. However, the UDWQ has classified the nearby Green River as Class 4 Water and has set a maximum boron concentration of 0.75 mg/L for this class. Eight of the sample sites had boron concentrations that exceed the maximum concentration for Class 4 Waters.

Other Constituents of Concern

Water from seven of 21 sites analyzed for metals concentrations had some constituents with concentrations with detection levels above the reporting level but below the drinking water EPA MCL. The chromium concentrations ranged from <2 to 11.5 µg/L, and may be associated with drilling fluids. Lead levels for 14 sites were above the detection level, ranging from 0.103 µg/L to 4.89 µg/L, but did not exceed the EPA Treatment Technique Action Level of 15 µg/L. Barium was detected at seven sites and concentrations ranged from 104 to 1730 µg/L, but no sites exceeded the EPA MCL of 2000 µg/L.

Volatile Organic Compounds and Total Petroleum Hydrocarbons

Total petroleum hydrocarbons and VOCs were analyzed for all sample sites. No samples had detectable TPH (table 9.1). A total of twelve different VOCs were detected. Chloromethane was the most commonly occurring VOC (14 sites), and toluene and bromomethane were the second most common (5 sites each). Chloromethane concentration ranged from trace amounts to 18 µg/L. Toluene concentrations range from 0.24 to 10.2 µg/L. Vinyl chloride was detected in two wells (6.6 µg/L at site 15 and 3 µg/L at site 18) above the EPA MCL of 2 µg/L. These shallow alluvial monitor wells were drilled by the USGS during the 1970s and are not used for drinking water. Other detectable VOCs include benzene, bromoform, chlorodibromomethane, bromodichloromethane, chlorobenzene, chloroethane, and total xylene (table 9.1).

Chloromethane is on the EPA Contaminant Candidate List 3 but is currently unregulated by the EPA. The Drinking Water Health Advisory, Office of Water, has issued a report on the chemical properties of chloromethane as it is used in the production of other chemical products (U.S. EPA, 2014, accessed December 3, 2014). Toluene is a regulated organic liquid that has been known to cause problems with the nervous system, kidneys, or liver when consumed in concentrations that exceed the MCL over long periods of time. Exposure to vinyl chloride in drinking water can cause long-term problems to the human nervous system and liver cancer (U.S. EPA, 2014, accessed December 3, 2014).

Secondary Constituents

National Secondary Drinking Water Standards set by the EPA were exceeded in 12 samples (table 9.1). The sulfate standard (250 mg/L) was exceeded at seven sites; iron standard (0.3 mg/L) was exceeded at four sites; and chloride standard (250 mg/L) was exceeded for one

site. These constituents are not known to be deleterious to human health but may impart an unpleasant taste, odor, or color to the water.

Oxygen and Deuterium Stable Isotopes

Isotope hydrology uses the isotopes of water molecules to trace water sources and can be used to determine the contributions of old and new water in a groundwater system. Factors such as altitude, latitude, location within a continent (and proximity to a mountain range), and the amount of rainfall affect the enrichment factor of precipitation isotopes (Kendall and Caldwell, 1998). Heavier isotopes of oxygen and deuterium are associated with lower altitudes (on windward mountain sides), decreasing latitude, coastal versus inland areas, and smaller rainfall amounts (not applicable to snowfall) (Kendall and Caldwell, 1998).

Twenty-two sites were sampled for oxygen isotopes and deuterium in 2013. The isotopic ratios in water range from -13.66 to -17.87‰ for oxygen and -134 to -104‰ for deuterium (table 9.2). The stable isotope results indicate that most water in the study area was recharged from different sources: some at moderate elevations and moderate climatic temperatures and others from higher elevations and cooler temperatures. Some locations have anomalous or ambiguous sources.

A plot of the oxygen and deuterium data is shown in figure 9.8. The global meteoric water line (GMWL) is from Clark and Fritz (1997). Most of the groundwater data collected from the area plot on or below the GMWL; groundwater is slightly enriched in ^{18}O relative to deuterium. Enrichment of ^{18}O (less negative isotopic signatures) in groundwater in the western

United States has been attributed to paleoclimate effects (White and Chuma, 1987) such as arid conditions and extensive evaporation prior to recharge.

Samples that are more enriched in ^{18}O (more positive) include the central wells, northern springs, and southern springs (including around Ninemile Creek). The enrichment of ^{18}O in the groundwater shown on figure 9.8 indicates evaporation of surface/soil water or snow sublimation prior to infiltration at these sites. If groundwater is recharged by more ephemeral heavy precipitation, then data for the groundwater may plot on the meteoric water line (which some of the data do). The lighter, or more depleted isotopes include the northernmost wells, the spring in the westernmost part of the study area (site 13), northern wells near Tabiona (site 8), Strawberry Pinnacles (site 9), and sites near the communities of Neola and Ballard (sites 5, 6, and 7) (figure 9.4; table 9.2). The outlier site 10 (another northern well near Myton; figure 9.1) has recharge water likely from another source. The isotopes from the White River spring (site 12) have a unique isotopic signature that likely relates to a different source(s) of recharge water, either connate brine water, hydraulic-fracturing fluid, disposal water, or lost (circulation) drilling fluids, or a mixture of these; the White River spring and its unique water characteristics warrant future investigation (see below).

The isotopic signature for the shallowest well sampled in the northern basin near Myton (site 10) also stands out and likely receives recharge locally from the high water table associated with the nearby Duchesne River. For samples having enriched ^{18}O, spring runoff may be a significant component of recharge in the study area, so the enrichment is most likely a result of sublimation of snow and/or evaporation of water during runoff but prior to recharge. Samples with the more depleted isotopic signatures may have a recharge source from the relatively nearby Uinta Mountains where recharge may take much longer to reach these sites.

WHITE RIVER SPRING COMPLEX

The spring/seep complex issuing from the Uinta Formation, along the White River exhibits anomalous chemistry data and suspect gases warranting further discussion (site 12, figures 9.4 and 9.9). Informal reports from the public (strange odors [rotten egg] and unusual colors [black and pink]) alerted the BLM and UDEQ to further investigate the water quality of this spring/seep complex (Scott Hacking, UDEQ, personal communication, 2013), which is along a popular recreational corridor. The TDS concentration (5532 mg/L) is the highest from the 2012 and 2013 studies (Wallace, 2012a). Anomalously high chemical constituents include arsenic, barium, bicarbonate, boron, chromium, selenium, sodium, sulfate, benzene, and trace xylene (table 9.1); some of these constituents (boron, selenium, sodium, sulfate, and oil/grease) have been reported in streams and streamflow in the UB and environs by other investigators (Lindskov and Kimball, 1984; Gerner and others, 2006; Wingert and others, 2010; Wallace, 2012a). No constituent exceeds EPA MCL for drinking water standards, and the elevated TDS concentration, which is above the Utah Division of Drinking Water's MCL of 2000 mg/L for public-supply sources, does not apply in this case. The source of the relatively high TDS is unknown and needs further investigation, but may be sourced from natural, connate water or long-residence time along a complex groundwater flow path. TDS concentrations from the Uinta Formation for 102 wells in the UB range from 165 mg/L to 222,060 mg/L with an average of 10,900 mg/L and a median of 1615 mg/L (Stephanie Carney, UGS, personal communication, May 2015, unpublished data). Water from the White River has low TDS concentrations

typically near 500 mg/L (Wallace, 2012a); the water in this spring likely is not sourced from the White River. A second field test of water from the spring complex (located about 50 feet from the lab analyzed sample, taken in a nearby stagnant pool of water) had a TDS of 25,452 mg/L and specific conductance of 38,912 µmohs/cm (Ammon McDonald, Utah Division of Oil, Gas, and Mining, personal communication, 2014). The presence of some of the constituents, such as selenium, boron, and zinc may be from natural sources inherent in the bedrock as reported in previous investigations from wells, seeps, and surface water within Green River Formation watersheds (Desborough and others, 1974; Gerner and others, 2006; Wingert and Adams, 2010).

A black powder (noted by recreationists) exists as a substrate in pools in the spring system and contains what is most likely finely ground gilsonite (Taylor Boden and Peter Nielsen, UGS, personal communication, 2012). Gilsonite is a natural, chemically inert, and mechanically very friable hydrocarbon resin. The source of gilsonite in these pools is unknown but may be related to nearby gilsonite veins (Boden and Tripp, 2012). The stretch of the White River at this location trends along the same northwest-southeast direction as mapped gilsonite veins (figure 2.1, plate 1), though no vein has been documented at this location (perhaps due to their smaller size, erosion by the river, or covered by alluvium or the river itself). Gilsonite veins in the area may serve as a conduit for groundwater carrying fluids from the subsurface (Vanden Berg and others, 2013).

During July 2014, staff with UDEQ, BLM, and EPA had the spring water re-analyzed. The analyses yielded similar results to the UGS sampling, with a TDS of 7430 mg/L, 1800 µg/L for barium, 31,500 µg/L for boron, 2970 mg/L sodium, 587 mg/L chloride, 3770 mg/L bicarbonate, and above-detection levels for benzene and TPH (DRO) (Joyel Dhieux, EPA,

written communication, July 2014). No samples were taken to determine the chemical constituents of the bubbling gas.

In order to evaluate the source of the dissolved constituents and gases in the White River spring complex, and whether there may be a link to current or historic oil and gas drilling activity, the following actions are recommend:

- Compare water chemistry of the Birds Nest aquifer, produced water from nearby gas wells, records of mud-water compositions used during drilling of older wells, with the spring complex.

- Collect and analyze produced water and spring complex water samples for oxygen, hydrogen, strontium, boron, radium, and lithium isotopes.

- Collect water and gas samples to analyze for methane, propane, ethane, hydrogen sulfide, and $\delta^{13}C$ of methane, to reveal potential sources of gases associated with the spring.

Integration of mapping and analyses of the geochemical and isotopic tracers listed above may help determine the source(s) and possibly the groundwater transport mechanism (A. Vengosh, Duke University, personal communication, June 2014). For example, previous investigations near the Book Cliffs along the Green River show that integration of the geochemical and isotopic tracers using boron and strontium can help determine sources of dissolved solids (Gerner and others, 2006).

DISCUSSION

Stiff diagrams based on analysis of waters from sample sites show variable water quality throughout the 2012 and 2013 study areas. The variations among sampling sites indicate water is likely from multiple aquifers that are not connected, with the exception of wells and springs in the northernmost area of the basin near the Uinta Mountains recharge area.

Arsenic, boron, chromium, barium, sulfate, iron, and chloride were identified in many of the sampled sites. Some samples had concentrations of arsenic and boron that exceeded limits set by the EPA and UDWQ. Sulfate, iron, and chloride concentrations at some sites exceed the EPA Secondary Drinking Water Quality Standards. As land use changes in the basin and more oil/gas wells are developed, continued sampling of these sites may show any water quality changes.

This baseline study was conducted to establish the current water quality of shallow aquifer(s) and springs in the UB. The overall chemistries of most samples are of good quality. The recommendation to continue to sample wells and springs is a cautionary measure in response to potential and existing energy-resource development. To prevent future degradation and preserve the relatively good quality of water resources in the UB, the locations sampled should be monitored for changes in water chemistry that may herald contamination, especially near the seep/spring along the White River.

SUMMARY

The UB generally lacks sufficient water-quality data from alluvial wells and springs to characterize the area's shallow groundwater. As part of the evaluation of produced water-management issues affecting tight-sand gas reservoir development and potential shale-gas resources in the UB, this component of the study establishes baseline water quality and provides some background data that will help underscore the potential vulnerability of the area's shallow alluvial wells and springs.

During summer 2013, 22 water samples were collected from alluvial water wells and springs in the UB, and augmented the data from two springs sampled by the UDWQ. A suite of water-quality constituents was analyzed, including general chemistry and TDS, nitrate, dissolved metals, VOCs, TPH, and stable isotopes. Overall, samples show variable water quality throughout the study area indicating there are multiple aquifers that are not connected. Dissolved solids were highest from an outcrop spring in the Uinta Formation flowing to the White River and they were lowest from the wells and springs in the northern part of the area proximal to recharge in the Uinta Mountains. Two sites have notable nitrate concentrations (though below the EPA MCL): a shallow monitor well near Evacuation Creek in the southeastern part of the basin and a spring downgradient from a gravel pit near Duchesne, Utah. Some sites have detectable VOCs including benzene, vinyl chloride, bromomethane, chlorobenzene, chloromethane, and toluene.

All of the sites sampled vary in terms of their water resource value. Some are perennial springs, some are water supply sources for the oil/gas industry, some supply water for wildlife, and a few are domestic water supply sources. Most of the water, if treated properly, could be used as drinking water; all but three of the sampling sites have TDS concentrations below the

upper limit (3000 mg/L) set by the Utah Water Quality Board as "Drinking Water Quality." None of these three sites is used as a public supply source, which deems a TDS of less than 2000 mg/L to meet Utah Division of Drinking Water's MCL requirement. To ensure good water quality is preserved, we recommend sampling most of the sites annually or every three years at the least.

Potential water-quality degradation may result from an expected increase in oil and gas activity if sound water-management procedures are not implemented. This project provides supporting data for a complementary study to examine aquifer vulnerability to potential contamination from VOCs (see Chapter X). Together these studies can help to implement integrated management of water production and disposal for shale/tight-sand gas development in the UB. This regional water study will provide Geographic Information Systems- (GIS-) based information to help local planners and potential developers preserve the quality of shallow groundwater and springs by establishing best-management practices through careful land-use planning.

CHAPTER IX FIGURES AND TABLE CAPTIONS

Figure 9.1. Location map of study area showing wells/springs sampled for this study and their site IDs; black dots correspond to sites sampled during 2009-2011 (modified from Wallace, 2012a; Vanden Berg and others, 2013).

Figure 9.2. Sample site locations from a previous baseline water quality study for southeastern Uinta Basin. Well, spring, and surface water sites were sampled seasonally from 2009 to 2011 (from Wallace, 2012a).

Figure 9.3. General solute chemistry for sampling sites in the Uinta Basin. A – Piper plot of samples collected for this study; numbers correspond to site IDs in table 9.1 and figure 9.1. B – Piper plot of all samples collected from a previous study (seasonal samples collected from 2009 to 2011 [Wallace, 2012a]) and this study.

Figure 9.4. Stiff diagrams for solute chemistry in the Uinta Basin. Stiff plots shown in blue are from data collected during 2009-2011 (sites 25 through 46 [Wallace, 2012a]); orange stiff plots (site IDs 1-22) are from data collected during 2013, but include sites 23 and 24 collected by the Utah Division of Water Quality during 2014.

Figure 9.5. Total-dissolved-solids concentrations for samples collected for a previous baseline water quality study (samples collected from 2009 to 2011 [Wallace, 2012a]), for this study, and from public supply wells taken from various years. Site IDs 1-24 are samples collected for this study (see table 9.1), site IDs 25-46 are from samples collected from 2009-2011.

Figure 9.6. White River spring (site 12) located along the White River in the central part of the study area. The spring issues into pools that likely enter the White River and mix with White River overbank flood water during spring runoff.

Figure 9.7. Monitoring well (site 15) drilled by the U.S. Geological Survey during the 1970s for a study to examine water quality in shallow alluvium in the southeastern Uinta Basin. Nitrate concentration for this well is 5.3 mg/L.

Figure 9.8. Plot of deuterium versus oxygen isotope for 22 samples in the Uinta Basin. The global meteoric water line (GMWL) is from Clark and Fritz (1997). See figure 9.1 for site ID locations and table 9.2 for isotope data for each site.

Figure 9.9. White River spring complex along the White River recreational corridor. Pink color may be bacteria/biologic activity; some of the black-colored residue is likely pervasive Uinta Basin gilsonite. A – spring pools, and B – seep in bedrock above spring.

Table 9.1. Water quality data for shallow well and spring sample sites in the Uinta Basin collected during summer 2013 (sites 1-22) and summer 2014 (sites 23 and 24).

Table 9.2. Isotope data for 22 sites in the Uinta Basin collected during 2013.

Table 9.1. Water quality data for shallow well and spring sample sites in the Uinta Basin collected during summer 2013 (sites 1-22) and summer 2014 (sites 23 and 24).

Site ID	Site Name	Lab, Specific Conductance (µmhos)	Solids, residue @180°C, dissolved	Arsenic, dissolved (µg/L)	Barium, dissolved (µg/L)	Bicarbon-ate (mg/L)	Boron, dissolved (µg/L)	Cadmium, dissolved (µg/L)	Chloride (mg/L)	Chromium, dissolved (µg/L)	Iron, dissolved (µg/L)
1	Snyder	2300	1476	1.25	<100	470	1760	<0.1	71.8	5.24	125
2	Prickly	1131	754	13	<100	478	797	<0.1	27.5	3.86	22.6
3	Upalco	532	304	4.51	292	294	70.8	<0.1	8.88	3.27	<20
4	Altamont	788	470	3.03	138	405	132	<0.1	19.5	3.68	22.1
5	Felsch	373	214	1.22	104	179	160	<0.1	3.81	<2	<20
6	Morrill	527	308	<1	<100	229	89.5	<0.1	1.79	<2	<20
7	Cloward	624	366	<1	<100	269	86.7	<0.1	1.61	2.59	29.9
8	Lefler	572	332	<1	110	284	72.4	<0.1	6.87	<2	38.8
9*	Leila	3570	2056	<1	391	1140	4460	<0.1	311	6.64	43.1
10	Bowden	1122	740	<1	<100	388	712	<0.1	24.4	<2	1890
11	Bugsy	715	468	<1	346	238	145	<0.1	25.3	<2	129
12	White River	8370	5532	8.89	1730	3510	28300	<0.2	537	11.5	59
13	I-40	593	392	<1	<100	276	156	<.1	4.69	<2	21.9
14	USGS-1	1616	982	6.18	<100	825	846	<0.1	37.2	<2	52.5
15	USGS-2	4430	3364	<1	<100	469	178	<0.1	31.4	<2	26.5
16	USGS-3	4200	3168	4.98	<100	860	8510	<0.1	87.9	<2	2520
17	PR Spring	690	408	<1	<100	330	61.3	<0.1	**J2.49	<2	25.1
18	USGS-4	1586	1060	-	-	802	-	-	70.9	-	-
19	D.R.	4180	3250	2.33	<100	513	1520	0.135	137	<2	438
20	Preston	640	976	2.484	<100	702	577	0.165	10.2	<2	832
21	Harmon	1036	634	3.597	<100	442	259	<0.1	24	<2	<20
22	Nine mile	1214	854	<1	<100	284	92.9	<0.1	16.2	<2	20.5
23	longshot	719	554	-	-	292	2040	-	3.25	-	-
24	e. Seep Cyn	1174	832	-	-	633	<30	-	7.96	-	-
AVERAGE[1]			1229	2.5			2319				
MEDIAN[1]			747	3.6			178				

Table 9-1. continued.

Site ID	Site Name	Lead, dissolved (µg/L)	Ni-trate as N (mg/L)	Selenium, dissolved (µg/L)	Sodium, dissolved (mg/L)	Sulfate (mg/L)	Zinc, dis-solved (µg/L)	Benzene (µg/L)	Bromomethane (µg/L)	Bromodi-chloro-methane (µg/L)	Bromoform (µg/L)
1	Snyder	0.182	0.142	<1	463	565	<10	u	u	u	u
2	Prickly	<0.1	0.086	<1	90.7	201	<10	u	1.4	u	u
3	Upalco	<0.1	0.205	<1	9.2	19.6	<10	u	0.25	u	u
4	Altamont	0.259	0.053	<1	24.4	65.2	44.9	u	0.36	u	u
5	Felsch	0.265	0.275	<1	52	24.4	<10	u	u	u	u
6	Morrill	0.132	0.061	<1	112	48.5	34.3	u	u	u	u
7	Cloward	<0.1	0.043	<1	135	64.4	<10	u	0.25	u	u
8	Lefler	<0.1	0.385	<1	12.9	55.5	12.3	u	u	u	u
9*	Leila	0.192	0.067	<1	808	35.5	<10	u	6.7	27.9	1.8
10	Bowden	<0.1	0.041	<1	102	253	29.1	u	u	u	u
11	Bugsy	<0.1	0.077	<1	60.9	147	15.5	u	u	u	u
12	White River	<0.2	0.033	8.687	2520	3390	<20	1.2	u	u	u
13	I-40	0.103	0.043	<1	46.6	103	11.6	u	u	u	u
14	USGS-1	0.291	0.019	<1	401	86.6	154	u	u	u	u
15	USGS-2	1.45	5.32	<1	837	1820	473	u	u	u	u
16	USGS-3	0.56	0.001	<1	718	1550	57.4	u	u	u	u
17	PR Spring	0.949	0.213	<1	18.9	94.7	35.2	u	u	u	u
18	USGS-4	-	0.001	-	-	126	-	u	u	u	u
19	D.R.	4.89	4.33	<1	682	1710	822	u	u	u	u
20	Preston	3.498	0.338	<1	144	271	100.55	u	u	u	u
21	Harmon	0.858	0.953	<1	86.4	174	44.896	u	u	u	u
22	Nine mile	0.999	0.195	<1	82.2	381	38.243	u	u	u	u
23	longshot	-	-	-	101	185	-	-	-	-	-
24	e. Seep Cyn	-	-	-	30.8	148	-	-	-	-	-
AVERAGE[1]		0.59									
MEDIAN[1]		0.08									

Table 9-1. continued.

Site ID	Site Name	Chlorobenz-ene (µg/L)	Chlorometh-ane (µg/L)	Chloro-ethane (µg/L)	Chloroform (µg/L)	Chlorodibro-momethane (µg/L)	Vinyl chloride (µg/L)	Total xylene (µg/L)	Toluene (µg/L)	TPH (mg/L)
1	Snyder	0.21	0.9	u	u	u	u	u	0.24	u
2	Prickly	u	18	u	u	u	u	u	u	u
3	Upalco	u	2.1	u	u	u	u	u	u	u
4	Altamont	u	14.3	u	u	u	u	u	u	u
5	Felsch	u	0.98	u	u	u	u	u	u	u
6	Morrill	u	2.8	u	u	u	u	u	u	u
7	Cloward	u	13.4	u	u	u	u	u	u	u
8	Lefler	u	u	u	u	u	u	u	u	u
9*	Leila	u	17.5	u	82	12.1	u	u	u	u
10	Bowden	u	tr	u	u	u	u	u	u	u
11	Bugsy	u	3.9	tr	u	u	u	u	u	u
12	White River	u	u	u	u	u	-	tr	u	u
13	I-40	u	1.6	u	u	u	u	u	u	u
14	USGS-1	u	u	u	u	u	u	u	8.1	u
15	USGS-2	u	*J0.25	u	u	u	6.6	u	10.2	u
16	USGS-3	u	*J0.29	u	u	u	u	u	1.1	u
17	PR Spring	u	*J0.21	u	u	u	u	u	u	u
18	USGS-4	u	u	u	u	u	3	u	3.2	u
19	D.R.	u	4.6	u	u	u	u	u	u	u
20	Preston	u	u	u	u	u	u	u	u	u
21	Harmon	u	u	u	u	u	u	u	u	u
22	Nine mile	u	u	u	u	u	u	u	u	u
23	longshot	-	-	-	-	-	-	-	-	-
24	e. Seep Cyn	-	-	-	-	-	-	-	-	-
AVERAGE[1]										
MEDIAN[1]										

*well owner indicated no water treatment filter existed, VOC data suggest otherwise; **J is above detectable levels; u is undetected, - is no sample collected, 1 available for some data

Table 9.2. Isotope data for 22 sites in the Uinta Basin collected during 2013.

Site ID	Site Name	Conductivity (µhmos/cm)	Temperature (degrees C)	δ18O	+/-	δD	+/-
1	Snyder	2370	20	-14.06	0.4	-111.2	1
2	Prickly	1260	19.9	-15.01	0.4	-117.5	1
3	Upalco	570	10.9	-14.79	0.4	-110.9	1
4	Altamont	3170	10.2	-15.22	0.4	-113.3	1
5	Felsch	2700	13.3	-16.53	0.4	-120	1
6	Morrill	2440	13.6	-17.87	0.4	-133.8	1
7	Cloward	3590	13.8	-17.12	0.4	-126.5	1
8	Lefler	3300	11.6	-16.9	0.4	-126.3	1
9	Leila	3210	13.7	-17.32	0.4	-133.7	1
10	Bowden	1080	14.4	-13.66	0.4	-112.3	1
11	Bugsy	650	16.1	-14.83	0.4	-116.4	1
12	White River	9150	24	-16.34	0.4	-128.6	1
13	I-40	590	12.8	-17.38	0.4	-130.5	1
14	USGS-1	1700	23.5	-14.45	0.4	-109.8	1
15	USGS-2	4610	27	-13.7	0.4	-104.2	1
16	USGS-3	4260	14.3	-14.27	0.4	-110.1	1
17	PR Springs	690	12.7	-15.24	0.4	-111.4	1
18	USGS-4	1450	20.5	-15.14	0.4	-114.7	1
19	D.R.	3700	14.4	-15.07	0.4	-115.7	1
20	Preston	1390	17.3	-14.07	0.4	-107.7	1
21	Harmon	950	12.5	-14.36	0.4	-110.2	1
22	Nine Mile	1160	21	-15.07	0.4	-112.9	1

*highlight in yellow are spring sites

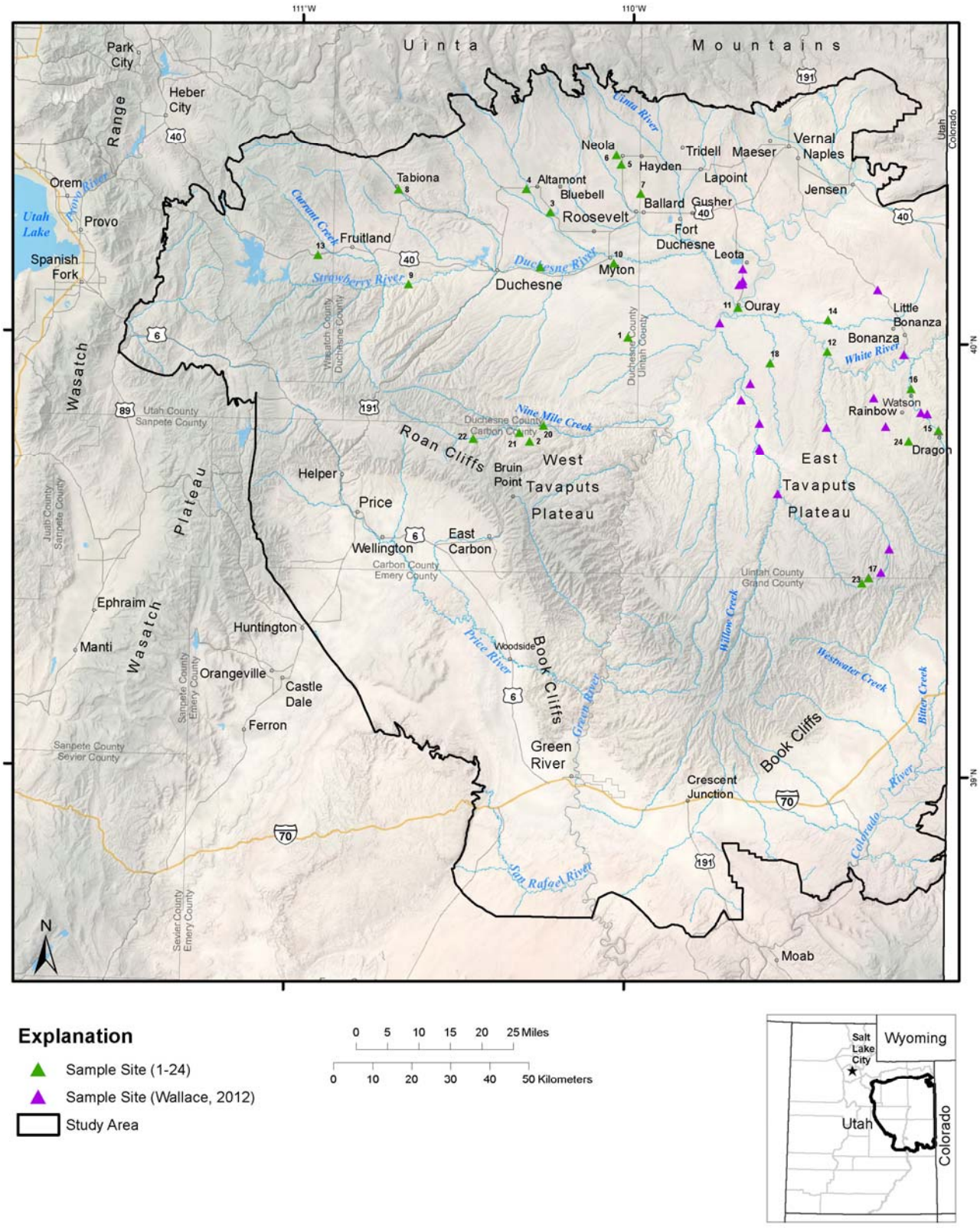

Figure 9.1. Location map of study area showing wells/springs sampled for this study and their site IDs; black dots correspond to sites sampled during 2009-2011 (modified from Wallace, 2012a; Vanden Berg and others, 2013).

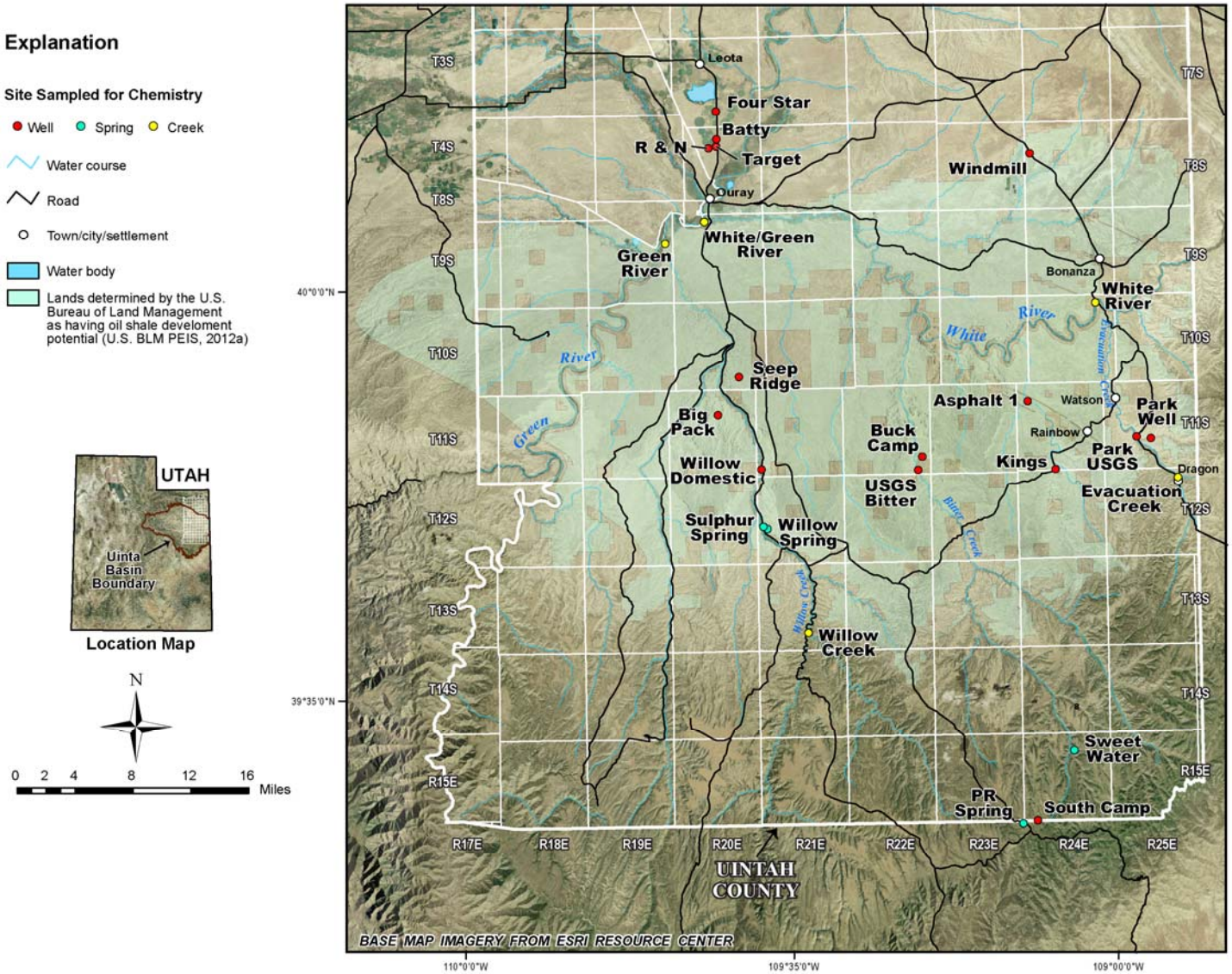

Figure 9.2. Sample site locations from a previous baseline water quality study for southeastern Uinta Basin. Well, spring, and surface water sites were sampled seasonally from 2009 to 2011 (from Wallace, 2012a).

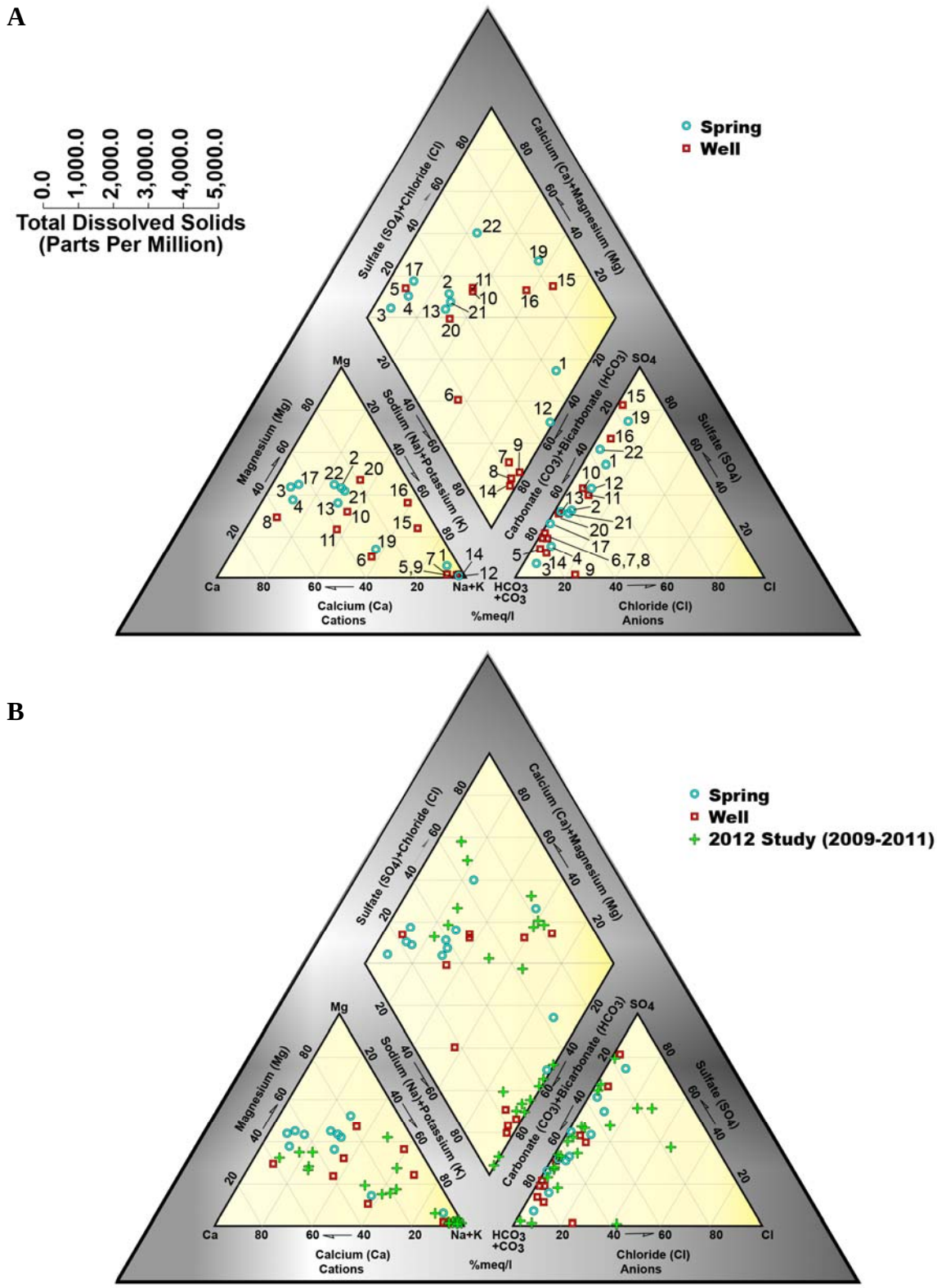

Figure 9.3. General solute chemistry for sampling sites in the Uinta Basin. A – Piper plot of samples collected for this study; numbers correspond to site IDs in table 9.1 and figure 9.1. B – Piper plot of all samples collected from a previous study (seasonal samples collected from 2009 to 2011 [Wallace, 2012a]) and this study.

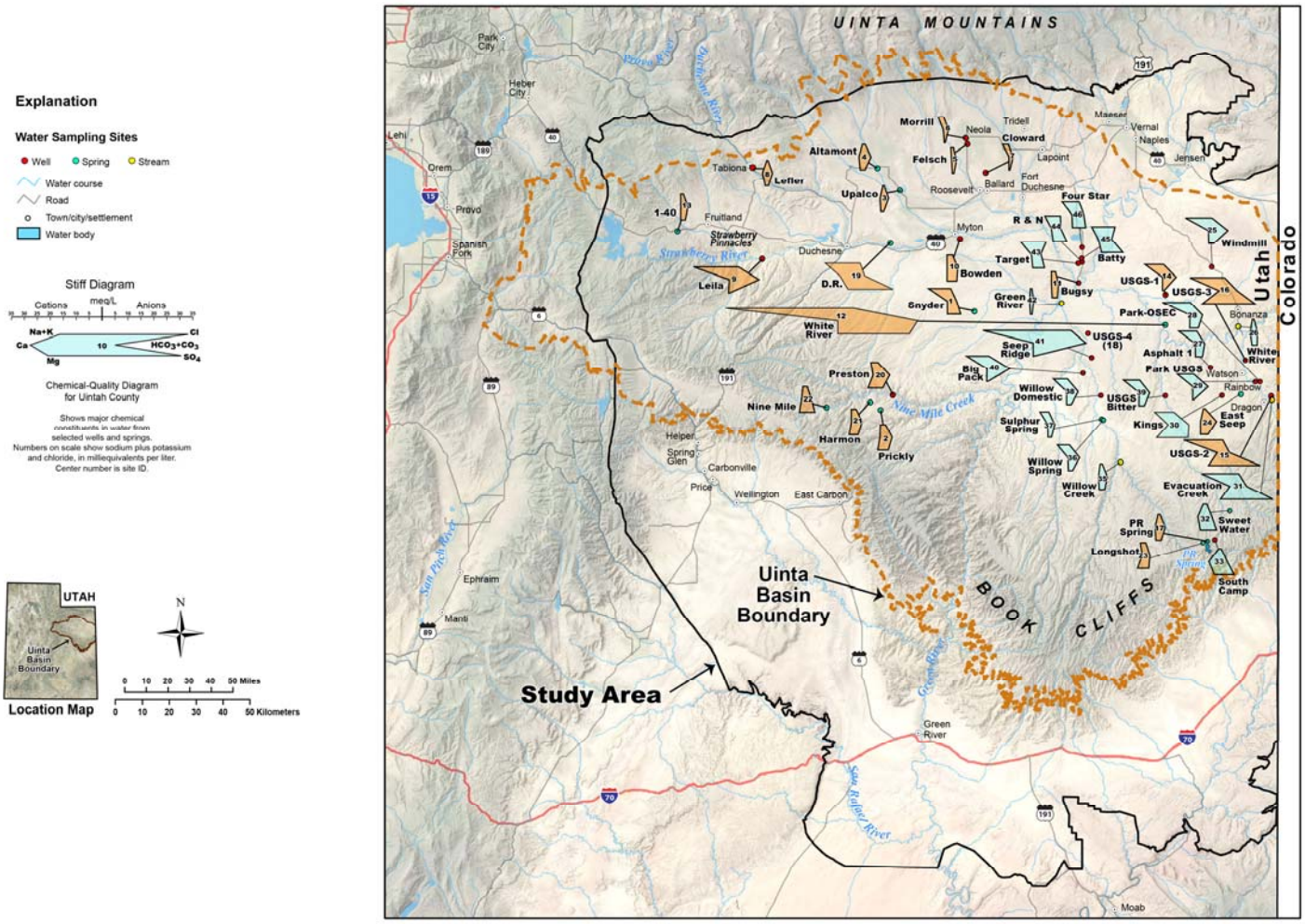

Figure 9.4. Stiff diagrams for solute chemistry in the Uinta Basin. Stiff plots shown in blue are from data collected during 2009-2011 (sites 25 through 46 [Wallace, 2012a]); orange stiff plots (site IDs 1-22) are from data collected during 2013, but include sites 23 and 24 collected by the Utah Division of Water Quality during 2014.

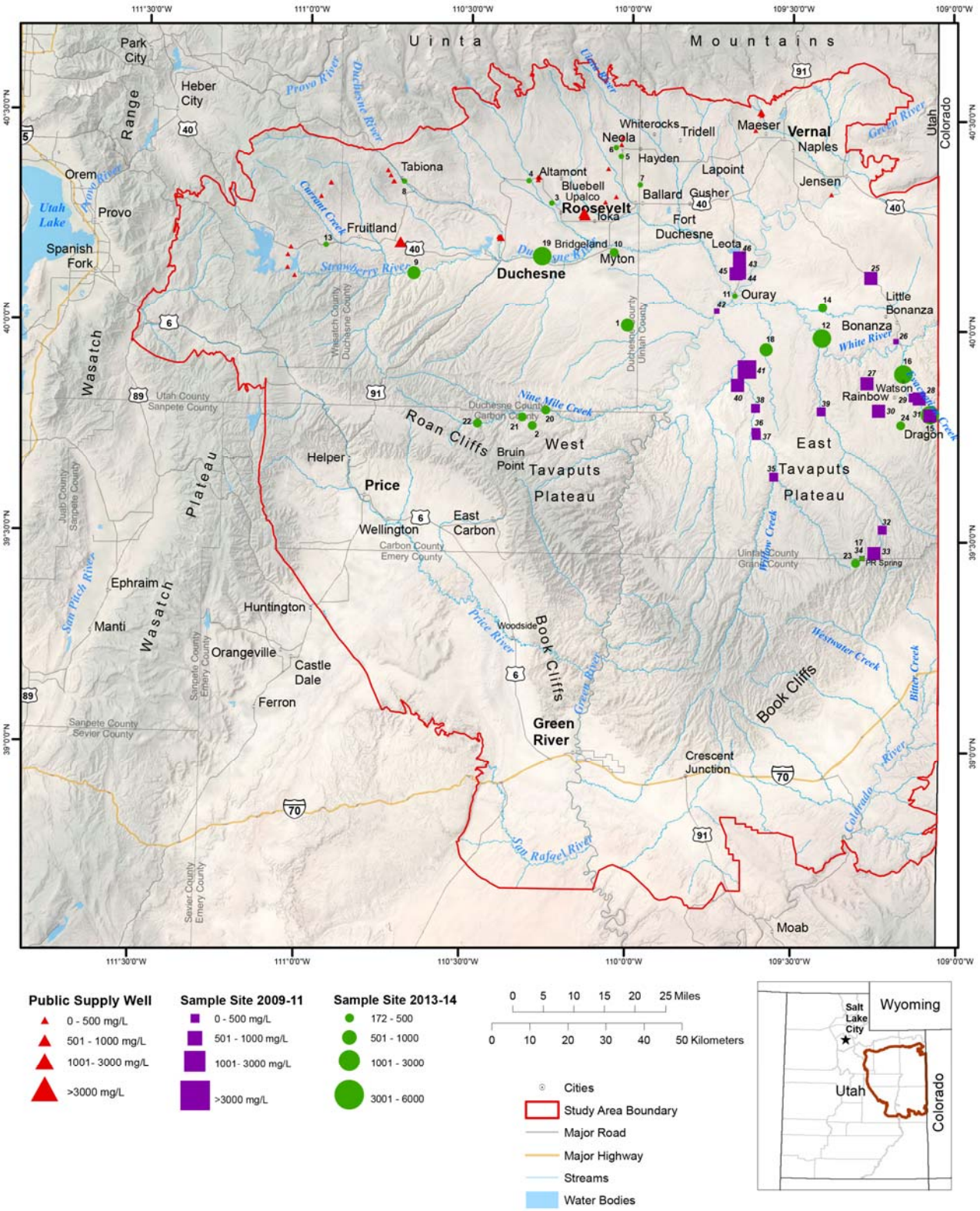

Figure 9.5. Total-dissolved-solids concentrations for samples collected for a previous baseline water quality study (samples collected from 2009 to 2011 [Wallace, 2012a]), for this study, and from public supply wells taken from various years. Site IDs 1-24 are samples collected for this study (see table 9.1), site IDs 25-46 are from samples collected from 2009-2011.

Figure 9.6. White River spring (site 12) located along the White River in the central part of the study area. The spring issues into pools that likely enter the White River and mix with White River overbank flood water during spring runoff.

Figure 9.7. Monitoring well (site 15) drilled by the U.S. Geological Survey during the 1970s for a study to examine water quality in shallow alluvium in the southeastern Uinta Basin. Nitrate concentration for this well is 5.3 mg/L.

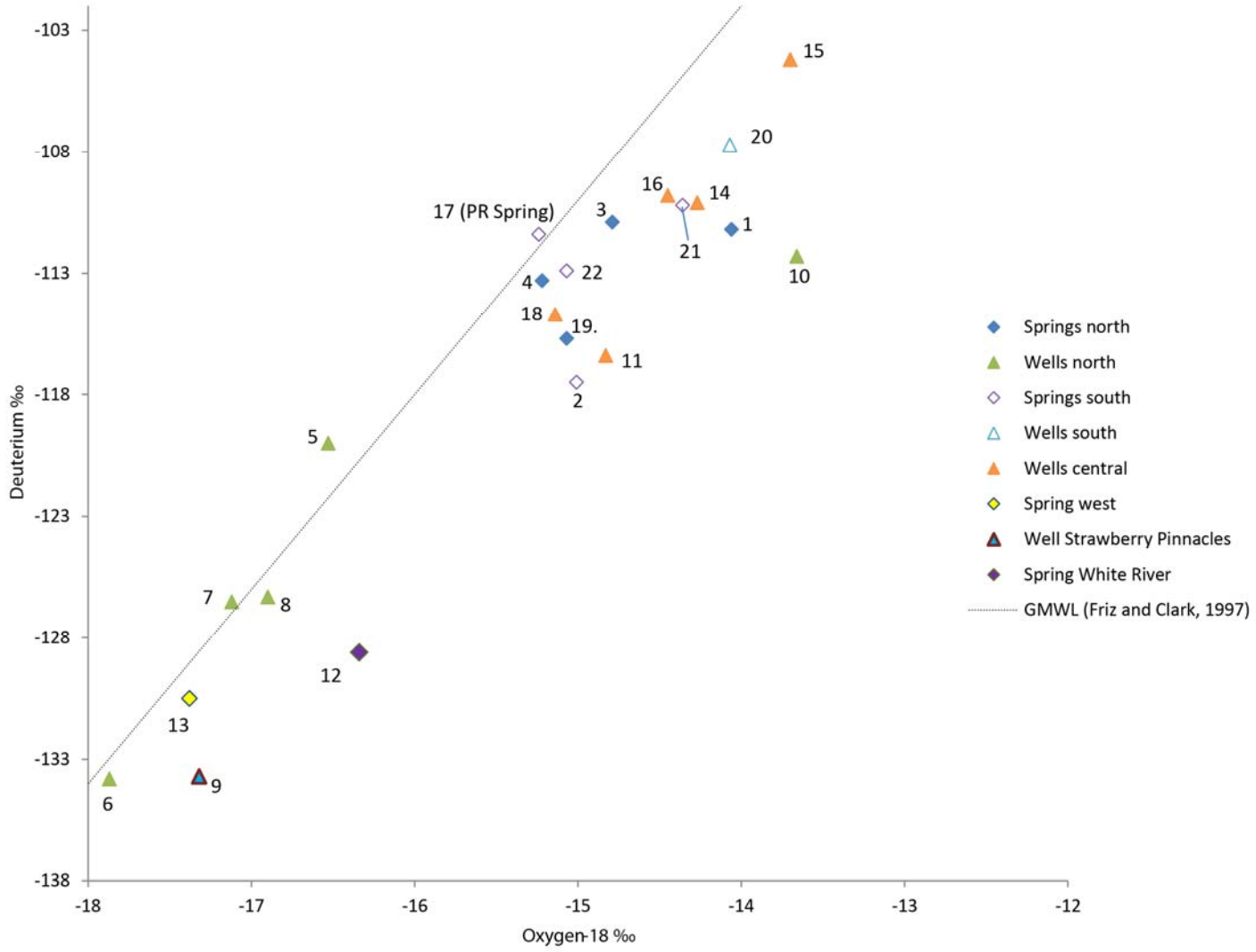

Figure 9.8. Plot of deuterium versus oxygen isotope for 22 samples in the Uinta Basin. The global meteoric water line (GMWL) is from Clark and Fritz (1997). See figure 9.1 for site ID locations and table 9.2 for isotope data for each site.

A

B

Figure 9.9. White River spring complex along the White River recreational corridor. Pink color may be bacteria/biologic activity; some of the black-colored residue is likely pervasive Uinta Basin gilsonite. A – spring pools, and B – seep in bedrock above spring.

CHAPTER X

SENSITIVITY AND VULNERABILITY OF THE AQUIFERS AND SPRINGS IN THE UINTA BASIN, TO POTENTIAL CONTAMINATION ASSOCIATED WITH TIGHT-SAND GAS PRODUCTION AND POTENTIAL SHALE-GAS RESOURCE DEVELOPMENT

Janae Wallace, Nathan Payne, and Richard Emerson

Water resource issues are a primary focus in the UB with continued tight-sand gas reservoir development and exploration for potential shale gas. It is important to address water resources by assessing the sensitivity and vulnerability of the aquifers in the basin. This study provides information on groundwater sensitivity and vulnerability to VOCs in the shallow alluvial aquifers and springs of the UB. Water-quality degradation from naturally occurring VOC sources is not considered in this study. Groundwater and surface water are important sources of water in many rural areas for human consumption and wildlife. Therefore, the potential for VOCs to contaminate water resources represents a threat to public health and the environment. Springs and drains flowing from contaminated aquifers may present a hazard to wildlife that live in or consume the water. Once VOCs are in the environment, they can move between different media of atmosphere, soil, groundwater, and surface water.

Understanding the mechanisms by which VOCs migrate into groundwater allows us to determine which geographic areas are most vulnerable and require more concentrated efforts to protect. The ability to delineate areas of greater and lesser VOC vulnerability will allow for geographically focused mitigation measures and land-use practice restrictions.

The maps presented in this report are intended to provide federal, state, and local government agencies and energy-related development users with information concerning vulnerability of groundwater to VOCs, especially benzene, toluene, ethylbenzene and xylene (collectively BTEX). Geographic variation of sensitivity and vulnerability and hydrologic and soil conditions that cause these variations are described herein. Plates 4 and 5 show the VOC sensitivity and vulnerability, respectively, of the alluvial aquifers and springs in the UB.

APPROACH AND BACKGROUND

We used collected water quality data, existing land-use data, and an attribute ranking system specifically tailored to the western United States to produce sensitivity and vulnerability maps in GIS analysis software. These maps show the sensitivity and vulnerability of the important alluvial aquifer(s) to potential contamination from VOCs associated with oil and gas development based on characteristics of the alluvial aquifer(s) and their geographic relation to tight-sand gas development activities. The maps can show areas with high sensitivity and vulnerability and indicate where extra care should be taken for alluvial aquifer protection.

VOCs were analyzed because of their documented presence within the basin, mostly as atmospheric concentrations (U.S. Environmental Protection Agency, 2012; Edwards and others,

2014). Once these contaminants are released into an environment, their chemical and physical characteristics allow for easy movement between the atmosphere, soil, groundwater, and surface water (Squillace and Moran, 2000; Squillace and others, 2002). VOCs readily dissolve in water or partition into soil vapor and, because of their relatively hydrophilic nature, may not be attenuated by the soil, resulting in long distance transport in groundwater systems (EUGRIS, 2014).

Groundwater chemical sensitivity is determined by assessing natural factors that may lead to the degradation of groundwater if VOCs are introduced into the environment. Some of these natural factors include permeability of geologic surficial units, soil hydraulic conductivity, natural retardation and attenuation of VOCs, and groundwater elevation. The location of active and potential oil/gas wells and their proximity to water bodies and/or water wells is used to determine groundwater vulnerability. Sensitivity to VOCs is determined by assessing natural factors favorable or unfavorable to the degradation of groundwater by VOCs, whereas vulnerability to VOCs is determined by assessing how groundwater sensitivity is modified by the activities of humans. For this study, groundwater sensitivity is assessed using depth to groundwater, permeability of surficial geologic units, and soil properties, including hydraulic conductivity, bulk density, organic content, and field capacity. Groundwater sensitivity also includes the influences of VOC physical properties, such as their capacity to adsorb organic carbon in soil and the half-life of a VOC under typical soil conditions. Specific vulnerability accounts for the presence and type of potential contaminating activities. In the case of the UB, active gas and oil wells are considered. The vulnerability analysis also incorporates well and spring water resources. Groundwater vulnerability includes human-controlled factors such as

proximity to active and producing oil/gas wells, proximity to water bodies, wells, or springs, and types of VOCs commonly associated with natural and synthetic products and by-products.

Groundwater Quality Standards

Maximum contaminant levels (MCLs) for VOCs in drinking water are established in Utah Administrative Code R309-100 through R309-605; organic chemicals are divided into three categories: pesticides/polychlorinated biphenyls (PCBs)/synthetic organic chemicals (SOCs), VOCs, and total trihalomethanes. Federal regulations are based on the EPA's protocols (EPA 816-F-09-0004, May 2009, Title 40, Chapter 1, Part 141, National Primary Drinking Water Regulations) (U.S. Environmental Protection Agency, 2006). MCLs are given in table 10.1 for the common BTEX VOCs. The vulnerability and sensitivity maps generated in this report rely on specific VOC-BTEX compounds; we do not address all VOCs that were analyzed as part of this study.

Volatile Organic Compounds in the Uinta Basin

VOCs are carbon-based chemicals that typically evaporate at the Earth's surface, but can reach groundwater under certain conditions. An estimated 98 to 99% of airborne UB VOCs are from oil and gas operations (Utah State University, 2013), but can be introduced to groundwater from direct industrial or wastewater discharge, leaky underground storage tanks, infiltration from surface spills, and atmospheric deposition of vehicle and industrial emissions.

As part of this study, VOCs were analyzed for 22 sample sites—12 water wells and 10 springs (figures 9.1 and 10.1) (see Chapter IX). Chloromethane is the most commonly occurring VOC (14 sites), and toluene and bromomethane are the second most common (five sites). Vinyl chloride was detected in two wells (sites 15 and 18). Other detected VOCs include benzene, bromoform, chloro dibromomethane, bromo dichloromethane, chlorobenzene, chloroethane, and total xylene. The range of concentrations for detected chloromethane is trace amounts to 18 µg/L. Toluene concentrations range from 0.24 to 10.2 µg/L. Vinyl chloride was above EPA MCL of 2 µg/L for sites 15 and 18 (6.6 and 3 µg/L, respectively), shallow alluvial monitor wells drilled by the USGS during the 1970s. We augmented the VOC data from this study with samples collected annually during 2009 to 2011 for 23 sample sites (figure 10.1; Wallace, 2012a, 2012b). Chlorobenzene, the most commonly occurring VOC, was detected in 18 samples over all sampling intervals, followed by chloroethane (detected in six samples), xylene (five samples), and ethylbenzene (three samples). Other VOCs include benzene, bromoform, bromoethane, toluene, naphthalene, chloro dibromomethane, bromo dichloromethane, and 1, 2, 4-trimethylbenzene (Wallace, 2012a, 2012b, 2013).

PREVIOUS WORK

Previous work of the hydrogeology and water quality within the UB is summarized in Chapter IX. In general, groundwater in the UB occurs in both unconsolidated alluvial material and consolidated rocks. Water quality is variable throughout the basin and even within specific formations (Wallace 2012a, 2012b; Vanden Berg and other, 2013).

The most recent studies evaluated water quality from 24 locations in the southeastern UB as a means to assess the alluvial and bedrock aquifers on lands proposed by the BLM as having oil shale development potential (figure 10.1) (Wallace 2012a, 2012b, 2013). Data from 85 water samples were analyzed from water wells and surface-water sites over three different sampling seasons from 2009 to 2011. Water-quality constituents analyzed included general chemistry (including TDS), nutrients, dissolved metals, and VOCs (listed above). Results indicate groundwater quality was variable, but generally had good TDS concentrations primarily below 3000 mg/L and ranged from 172 to 2832 mg/L. No VOC exceeded EPA maximum contaminant level, but many samples had detectable levels of certain VOCs. The most frequently detected was chlorobenzene (in 17 samples over all sampling intervals) followed by chloromethane and xylene (5 samples).

Data were also collected to augment this study and is discussed in Chapter IX and summarized here. During summer 2013, water was sampled from 12 shallow alluvial wells and 10 springs. Total-dissolved-solids concentrations for all wells and springs sampled range from 214 to 5532 mg/L. Twelve different VOCs were detected (listed above).

METHODS

Methodologies for Groundwater Pollution Assessment

The potential for groundwater pollution can be assessed using index-based methods, process-based methods, overlay methods, or combinations of these. Focazio and others (2002)

provide an overview of these methods, and Bernknopf and others (2001) discuss their underlying theory. Index-based methods, which commonly involve the use of map overlays, assign numerical scores to physical attributes to develop a range of subjective sensitivity/vulnerability categories (Aller and others, 1985). Process-based methods apply physical processes associated with the fate and transport of contaminants in the environment (Rao and others, 1985). Using Drinking Water Source Assessment and Protection (DWSAP) methods, Harter (2001) discussed the uses of index-and-overlay methods by highlighting possible contaminating activities (PCAs) at the land surface.

Rao and others (1985) developed process-based indices for ranking the potential for contamination of groundwater. The method of Rao and others (1985) uses a calculated retardation factor to characterize movement and an attenuation factor to characterize persistence of a chemical constituent(s) in the vadose zone. These factors vary with different soil properties and different characteristics of specific chemical species. Equations for these indices enable calibration of hydrogeologic and other data to more realistically represent actual conditions. However, the results are only a qualitative assessment of a contaminant's potential to pollute groundwater. Quantitative assessment of a contaminant's potential to pollute groundwater, including loss via runoff and leaching, requires complex computer modeling (Rao and others, 2006) that utilizes chemical-suite specific information, soil type, and the amount, frequency, and duration of precipitation events.

Harter (2001) used index-based and overlay methods to evaluate DWSAP vulnerability analyses. The study focused on the type of possible contaminating activities at the land surface to assess vulnerability of groundwater and surface water sourced drinking water in California. This method considers the contaminant type and proximity to the water supply and drinking

water source protection (DWSP) zones of PCAs that could release contaminants. In the case of the UB, PCAs include pre-existing oil/gas wells in addition to unconventional energy resources, particularly tar sands and oil shale deposits.

While efforts to predict the potential for groundwater pollution from VOCs combine index-based and process-based methods (Siegel, 2000; Harter, 2001) (including the one we devised for this study), they remain qualitative rather than quantitative tools because of their inability to incorporate site- and temporal-specific data. The summarized methods above vary in design based on their geographic scale, the subsurface zone of interest, the inclusion of VOC-specific properties (or any other potential contaminant of interest, such as pesticides), and the types of information available to incorporate into the methods. Field-scale evaluations (such as Rao and others, 1985; Meeks and Dean, 1990) require more detailed soils and geological data than evaluations at county- or groundwater-basin scales (such as Shukla and others, 2000; Lowe and Sanderson, 2000, 2003; Schlosser and others, 2002; Lowe and others, 2004; Sinkevich and others, 2005), which, in turn, require more detailed soils and geologic data than regional or statewide evaluations (such as Lowe and others, 2003; Mehnert and others, 2005). The index-based component of the evaluations requires subjective decisions be made regarding the numerical scoring that results in the sensitivity/vulnerability map output.

Combined Methodologies Applied to the Uinta Basin

The project scope is limited to the use and interpretation of existing data to produce VOC sensitivity and vulnerability maps through the application GIS analysis methods. Using GIS, we devised a combined index-based, process-based, and overlay method to determine aquifer

sensitivity and vulnerability in the UB (table 10.2). The interplay between hydrogeology, groundwater recharge, soil conditions, and BTEX behavior in the vadose zone determines whether groundwater in a particular area is likely to become contaminated with a VOC (the type of BTEX is a critical factor since each component has unique physical and chemical properties) (table 10.1).

This is a first attempt to develop VOC sensitivity and vulnerability maps and a lack of some data limits our analysis; better data and tools may become available in the future so that better maps can be produced. For example, recharge is typically a component used in the production of sensitivity/vulnerability maps, but the data we used from the National Soil Survey Center's Soil Survey Geographic (SSURGO) database (National Soil Survey Center, 2006) does not provide recharge amount specific to the UB. We analyzed precipitation and evapotranspiration data in an attempt to determine average annual recharge. By subtracting average annual evapotranspiration from annual precipitation an estimate of annual elevation-based recharge could be determined. The results of this calculation showed zero recharge in low elevation areas where evaporation potential exceeded precipitation. However, recharge can occur in low elevations where streams flow from mountainous areas during spring runoff and prolonged storm events. But since no comprehensive datasets pertain to recharge/discharge zones in the study area, this method of estimating recharge at low elevations was not possible. Therefore, recharge/discharge data were not used in our sensitivity/vulnerability analysis. Soil data for this study were collected at a scale of 1:63,360 or smaller and are too general to accurately depict areas of soil versus areas of bedrock outcrop. Organic carbon in soils is one major factor that determines the potential for VOCs to reach groundwater, but due to the small scale of 1:63,360, the higher sensitivity and vulnerability of these areas are not reflected in our

maps. To produce the maps, we made some subjective decisions regarding the quality and the types of data available based on our knowledge of the hydrogeology of the area. For example, we calculated a weighted average from all soil horizons for organic carbon, field capacity, and bulk density values, and selected 5 feet as the reference depth for applying VOC retardation and attenuation equations. Table 10.2 summarizes the methods we employ, the source(s) of information we use to calculate or derive parameters, and how we determine ranges of values used to rank attributes from our GIS analysis of aquifer sensitivity and vulnerability.

SENSITIVITY ANALYSIS

Groundwater sensitivity to VOCs can be determined by assessing natural factors favorable or unfavorable to the degradation of groundwater by VOCs present and/or leaked onto the land surface. Aquifer permeability, soil hydraulic conductivity, retardation of VOCs, attenuation of VOCs, and estimated depth to groundwater (or permeable layer) are the factors primarily determining groundwater sensitivity to VOCs in the aquifers within the UB. Sensitivity represents the sum of natural influences that facilitate the entry of VOCs into groundwater.

Aquifer Permeability

Permeability was delineated for each geologic unit present in the UB (table 10.3), based on the work of Schlotthaeur and others (1981). For GIS analyses, each unit was assigned a

qualitative permeability rank of (1) low, (2) heterogeneous, or (3) medium to high. The geologic map (plate 1) for the study area was compiled from pre-existing 1:100,000 scale geologic maps (Witkind and Weiss, 2002; Weiss and others, 2003; Gualtieri, 2004; Witkind, 2004; Sprinkel, 2006, 2007, 2009, 2013) and simplified to show surficial exposures that have similar permeability properties.

For our GIS analysis, we characterized terrain directly underlain by hydrostratigraphic units with medium to high permeability as potentially having groundwater and surface water that is more vulnerable to potential contaminants, terrain directly underlain by those units with low permeability as potentially having groundwater and surface water that is less vulnerable to potential contaminants, and terrain directly underlain by geologic units with the heterogeneous permeability rank category intermediate between the medium-to-high and low-permeability. For example, geologic units considered to have medium to high permeability (a rank of 3) included alluvium and unconsolidated deposits. Geologic units considered to be heterogeneous (rank of 2) include the Mesaverde Group and some undivided mapped units (such as the Curtis/Stump, Entrada, and Carmel Formations [figures 1.5 and 2.1, plate 1]). The Mancos Shale is an example of a low permeability layer with a ranking of 1. Localized high, moderate, and/or low permeable units within the study area could not be identified at a map scale of 1:100,000 so were not included in the analysis.

Hydraulic Conductivity of Soils

Hydraulic conductivity is a measure of the rate at which soils can transmit water. Values for soil hydraulic conductivity and depth to groundwater for the UB were obtained from

SSURGO database (National Soil Survey Center [NRCS], 2006). For GIS analysis, areas were divided into two hydraulic conductivity ranges (based on SSURGO data natural divisions): low (<0.57 inch/hour) and high (≤0.57 inch/hour) (table 10.4).

VOC Retardation

Retardation is a measure of the differential between movement of water and the movement of a potential contaminant (e.g., VOCs) in the vadose zone (Rao and others, 1985). Certain VOCs can be adsorbed to organic carbon in soil and thus move through soil more slowly than water. Slower moving BTEX compounds (e.g., toluene and xylene) may be more readily degraded by bacteria in the vadose zone than compounds that move more quickly to the saturated zone (e.g., benzene). The relative rate of movement of a VOC is dependent on many factors and may be calculated using the retardation factor (R_F). The retardation factor is a function of dry bulk density, organic carbon fraction and field capacity of the soil, and the organic carbon sorption distribution coefficient of the specific VOC. A relatively low R_F indicates a contaminant will not be adsorbed to organic carbon and can move more quickly into groundwater, increasing potential for groundwater pollution. Rao and others (1985) presented the following equation:

$$R_F = 1 + (\rho_b F_{oc\ oc})/\theta_{fc} \qquad (10.1)$$

where:

R_F = retardation factor (dimensionless),

ρ_b = bulk density (kg/L),

F_{oc} = fraction, organic carbon,

K_{oc} = organic carbon sorption distribution coefficient (L/kg), and

θ_{fc} = field capacity (volume fraction).

Retardation factors typically range from (1 + 4 Kd) to (1 + 10 Kd) (Freeze and Cherry, 1979) (where Kd is the distribution coefficient) for unconsolidated sediments (ρ_b = 0.06–0.08 lb/in^3[1.7–2.2 kg/L]) with porosity range of 0.2 to 0.4. Dissolved constituents in groundwater with low R_F values (~1), such as nitrate (a relatively mobile cation), move through the subsurface at the same rate as groundwater. Constituents with R_F values that are orders of magnitude larger than 1 are essentially immobile (Freeze and Cherry, 1979). The relative velocity is the reciprocal of the retardation factor and describes the rate at which a contaminant moves relative to solvent-free groundwater.

For this study, data from the SSURGO database were used to help map aquifer sensitivity. The database provided information for bulk density, organic carbon fraction, and field capacity of soil in the UB at a scale of 1:24,000 (table 10.5).

In order to establish a rationale for dividing high and low VOC retardation for GIS analysis, variables in equation 10.1 are set to values that represent conditions likely to be

encountered in the natural environment (table 10.5). Digital soil information unique to particular soil groups from SSURGO data was applied for organic carbon. We used the organic carbon sorption distribution coefficient (table 10.1) for benzene (97), the BTEX compound among the four having the least tendency to adsorb to organic carbon in the soil (Fetter, 1988; Carey and Sundberg, 1990; Weast and others, 1990; Weber, 1994). Bulk density and field capacity were derived from a soil texture triangle hydraulic properties calculator (Saxton, undated). To compute R_F values, bulk density end members of 0.04 and 0.07 pounds per cubic inch (1.2 and 2.0 kg/L) and field capacity end members of 14 and 42%, were applied to represent naturally occurring conditions in the UB, a variable soil organic carbon content, and a water depth of 3 feet. Average organic carbon content in soils in aquifers within the UB ranges from 0.029 to 8.7% (table 10.5); the mass fraction of organic carbon was computed by dividing the organic matter parameter in the SSURGO data by a conversion factor of 1.72 (Siegel, 2000). The organic carbon content end members were used to compute the extreme R_F values; equation 10.1 results in retardation factors ranging from 1.1 to 25, with a median of 5. This means the highest relative velocity from the data is 0.9 and the lowest is 0.04; the former indicates benzene in groundwater moves at a rate about 90% that of groundwater free of benzene, whereas the latter indicates that VOCs in groundwater are essentially immobile. For the GIS analysis, VOC retardation is divided into two ranges: greater than or equal to, and less than 5.

VOC Attenuation

VOC attenuation is the rate at which a potential contaminate can degrade under certain soil conditions (Rao and others, 1985). The rate of attenuation indirectly controls the depth to

which a BTEX compound may reasonably be expected to migrate under specific conditions. The attenuation factor (A_F) is a function of vertical depth or horizontal length of the soil column, net annual groundwater recharge, half-life of the specific VOC considered, and field capacity of the soil. Attenuation factors range between 0 and 1 (Rao and others, 1985); high attenuation factors represent conditions of low attenuation. Rao and others (1985) presented the following equation:

$$A_F = \exp(-0.693 z R_F \theta_{fc} / q t_{1/2}) \qquad (10.2)$$

where:

A_F = attenuation factor (dimensionless),

z = reference depth (m),

R_F = retardation factor (dimensionless),

θ_{fc} = field capacity (volume fraction),

q = net annual groundwater recharge (precipitation minus evapotranspiration) (m), and

$t_{1/2}$ = VOC half-life (years).

Using equation 10.2, we calculated attenuation factors for ranges of values common to soils within the UB, similar to the approach for retardation, to delineate high and low VOC attenuation factors for GIS analysis. To represent naturally occurring conditions in this area that would result in the greatest sensitivity to groundwater contamination, we used the median retardation factor of 5; the half-life for benzene (table 10.1), the BTEX with a half-life the same as other BTEX compounds (and longer than toluene) (Koo, 2012); a field capacity of 14%; and a bulk density value of 0.04 pounds per cubic inch (1.2 kg/L). For the negligible net annual groundwater recharge typical of the most areas across the Uinta Basin, equation 10.2 results in an attenuation factor approaching 0.

Although quantities of VOCs spilled and/or leaked to the ground surface would intuitively seem to have a direct bearing on the amount of VOC impacting groundwater, Rao and others' (1985) equations do not support this. Note that the quantity of VOC does not enter into either equation as a variable; the half-life, however, is essential and remains fairly constant.

Depth to Groundwater (Permeable Layer)

The closer groundwater is to the land surface the more sensitive it is to being degraded by VOCs. Depth to groundwater maps are not available for the study area, so we used the depth to the permeable layer attribute (table 10.4) to estimate depth to groundwater using Soil Hydraulic Conductivity and Depth to Groundwater data from NRCS SSURGO Soils database. We used 5 feet as the depth-to-groundwater attribute to evaluate sensitivity of geographic areas to VOCs. Permeability was determined for each geologic formation based on work from Schlotthauer and

others (1981). A qualitative permeability rank was assigned to formations based on work by Lowe and others (2003).

GIS Analysis Methods

Aquifer sensitivity (intrinsic susceptibility) to VOC compounds is characterized as "low," "moderate," or "high" based on the sum of numerical values (rankings) assigned to soil retardation of benzene, soil attenuation of benzene, permeability, soil hydraulic conductivity, and depth to shallowest groundwater (permeable layer) attributes as shown in table 10.4. Rasters (400 meter-resolution) based on the ranking in table 10.4 were created for each input parameter. Numerical ranking for each attribute category is subjective but reflects the relative level of importance we believe the attribute plays in determining sensitivity of areas to VOCs. A sensitivity attribute of low is assigned when the summed ranking ranges from 3 to 4. A sensitivity attribute of moderate is assigned when the summed ranking ranges from 5 to 6, and a sensitivity attribute of high is assigned when the summed ranking ranges from 7 to 9.

VULNERABILITY ANALYSIS

As discussed above, sensitivity to oil and gas development is determined by assessing natural factors favorable or unfavorable to the degradation of groundwater by anthropogenic chemicals, whereas groundwater vulnerability is determined by assessing how groundwater sensitivity is modified by the activities of humans. Vulnerability includes human-controlled

factors such as proximity to a water well, boundaries of DWSPs, proximity to active oil/gas well(s), and types of chemicals produced. Our vulnerability analysis includes input of three parameters: (1) groundwater sensitivity, (2) proximity to streams, water bodies, water wells, and public supply wells and (3) oil/gas well density (table 10.6). All of the input parameters, except sensitivity, are derived from a combined index- and overlay-based method (table 10.2). Absolute numerical ranking for each attribute category is arbitrary and subjective, but reflects the relative level of importance the attribute plays in determining vulnerability to the area's aquifers.

Groundwater Sensitivity

We mapped aquifer sensitivity based on hydrostratigraphy (using primary and secondary permeability of geologic units), soil properties (including hydraulic conductivity, bulk density, organic content, and field capacity), BTEX (specifically benzene) chemical properties (such as the capacity of molecules to adsorb to organic carbon in soil), and depth to groundwater (permeable layer).

We consider groundwater sensitivity (intrinsic susceptibility) to be the principal factor that determines the vulnerability of aquifers in the UB to degradation from VOCs (table 10.6). For example, we believe sensitivity is the most important attribute with respect to groundwater vulnerability (e.g., based on the inherent properties of the surficial/geologic material) and weighted this attribute heavier than the other parameters, which we rank equally (table 10.6). Consequently, low, moderate, and high sensitivity input rankings were assigned numerical values for the vulnerability analysis that are more heavily weighted than the other parameters, which we rank equally.

Proximity to Wells, Rivers, and Streams

Streams and water bodies used to create a proximity-to-water-bodies GIS layer were sourced from the National Hydrology Dataset. We selected major streams and water bodies larger than three acres for the analysis. Water well and spring locations were compiled from data collected from this study, Wallace's 2012 study, and public supply wells (Mark Jensen, Utah Division of Drinking Water, written communication, December 2014) (figure 10.1). DWSP zones were also provided by the Utah Division of Drinking Water. A low ranking is for water bodies and wells located greater than 3 miles, a moderate ranking is for 1 to 3 miles, and a high ranking is for those located less than 1 mile away. We use a buffer of 1-mile proximity to be protective of groundwater quality (see table 10.6).

Active/Producing Well Density

A list of active oil and gas wells was obtained from the DOGM database (Utah Automated Geographic Reference Center portal [gis.utah.gov]). The final oil/gas well density GIS layer was calculated with the Kernel Density tool in ArcGIS 10.2.2 at a resolution of 400 meters (610 ft) and a search radius of 1.6 miles (1 km). Polygons with greater than five producing wells per square kilometer (0.4 mi^2) were selected as having a greater influence since active wells are more likely to contribute potential VOCs in the UB (figure 10.2; table 10.6).

GIS Analysis Methods

VOC vulnerability is "low," "moderate," and "high" based on all three input parameters discussed above (table 10.6). Rasters (400-meter resolution) based on these rankings (table 10.6) were created for each input parameter. Low vulnerability is assigned when the summed ranking ranges from -2 to 1, moderate vulnerability is assigned when the summed ranking ranges from 2 to 5, and high vulnerability is assigned when summed ranking ranges from 6 to 10. Once again, numerical ranking for each attribute category is subjective, but reflects the relative level of importance the attribute plays in determining vulnerability of areas potentially contributing VOCs. As stated above, we believe aquifer sensitivity is the most important attribute with respect to groundwater vulnerability to VOCs, and therefore, weighted it more heavily than other parameters.

RESULTS OF MAPPING

Groundwater Sensitivity

Plate 4 shows the aerial extent of aquifer sensitivity. Most of the study area is moderately sensitive to VOC contamination. The breakdown in sensitivity is: 43% low sensitivity, 48% moderate, and 10% high.

Much of the UB having low sensitivity (43%) to VOC contamination is due to protective clay layers or unmapped permeable layers. VOCs in these areas are unlikely to degrade

groundwater quality but could, however, affect surface water. Areas with high hydraulic conductivities (≥0.57 inches/hour), high VOC retardation factors, and low VOC attenuation factors coincide with high sensitivity (10%). Most high sensitive areas are near streams and lakes where shallow alluvium covers the land surface and shallow groundwater likely exists.

Groundwater Vulnerability

Plate 5 shows groundwater vulnerability to VOCs of aquifers for the UB. Areas of high vulnerability are near water bodies, water wells, and oil/gas wells. Less than 2% of the surface area of the aquifers within the UB has high vulnerability. Of particular concern are areas where groundwater is shallow or where oil/gas wells are near open water bodies. Areas of moderate vulnerability coincide, in general, with areas of moderate or high sensitivity. About 37% of the aquifer surface area has moderate vulnerability. Low-vulnerability areas generally coincide with areas farther away from public supply wells and with low density of active oil/gas wells. About 62% of the aquifer surface area within the UB has low vulnerability. Most DWSP zones are located within moderately vulnerable areas. We recommend these areas be monitored for VOCs on a regular basis to ensure groundwater protection from potential pollution associated with any nearby development.

DISCUSSION

In areas of the UB where groundwater is unconfined or in aquifers categorized as having high permeability, degradation of the aquifers by VOCs could occur whenever chemicals infiltrate through the vadose zone to the aquifer. In confined or lower permeability aquifer settings, VOCs would need to find pathways through confining layers to cause water-quality degradation. Thus, the ability of soils at the surface to retard or attenuate the downward movement of VOCs, and the hydrogeologic setting where VOCs may be present, have a fundamental effect on the likelihood that they can travel downward to the aquifer. Withdrawal of water from the aquifers via water wells could cause changes in vertical head gradient that may increase the potential for water-quality degradation. Wells themselves, if not properly constructed, or poorly developed in fractured/faulted areas near springs, could provide pathways for water with VOCs to reach the aquifers.

Areas of moderate and high vulnerability are primarily where greatest density of oil/gas development occurs within main or tributary drainages where groundwater sensitivity to VOCs is high. Of particular concern are streams that flow across the basin. Streams may be important sources of recharge to some, if not all of the aquifers. Efforts to preserve water quality at these locations would help to preserve groundwater quality in the UB.

SUMMARY

This part of the study examined the aquifer sensitivity and vulnerability of areas currently producing oil and gas in the UB which generally lacks sufficient shallow, groundwater quality data to determine the effects that current and future oil and gas development, particularly tight-

sand gas reservoirs and potential shale-gas resources, may have on the area's aquifers. We used existing data and made assumptions for areas lacking data, to produce sensitivity and vulnerability maps by applying an attribute-ranking system specifically tailored to the arid conditions of the western United States using GIS analysis methods. This study established a snapshot of recent water quality and examined the vulnerability of the area's shallow alluvial wells and springs.

Thousands of wells within the UB tap groundwater, but at depths tens of hundreds of feet below the surface where water is classified as too salty for human consumption. Most of the wells exist as part of the vast energy extraction industry of the UB, namely oil and natural gas that could contain VOCs, among other chemical constituents of concern. VOCs, once released into the environment, can readily move among the atmosphere, soil, groundwater, and surface water. Potential VOC contamination from chemical spills, defective oil and gas wells, or other industrial use threatens drinking water sources, recreation areas, and wildlife habitats.

The areas with the highest potential for water-quality degradation associated with VOCs in the UB occur where near-surface permeable layers are near water bodies, water wells/springs, and high-density oil/gas development, some within DWSP zones. VOC groundwater monitoring may be necessary in areas of high sensitivity or high vulnerability areas in and near DWSP zones. Water sampling and testing in areas of the basins characterized by low and moderate sensitivity and vulnerability may also be warranted, but at a lower frequency than for areas with higher sensitivity and vulnerability. The maps and accompanying report are based on analyses of 1:100,000 or smaller scale data, and are not applicable for site-specific evaluations. This study is based on GIS analysis of available land-use data and some data collected from groundwater wells and springs, and therefore has many limitations for vulnerability assessments.

CHAPTER X FIGURE AND TABLE CAPTIONS

Figure 10.1. Location of sites sampled for water quality for this study, a previous water quality study (Wallace, 2012a, 2012b), public water supply wells, and drinking water source protection (DWSP) zones. DWSP transient zones refer to public supply sources that are used on a seasonal or intermittent basis.

Figure 10.2. Density of active oil/gas wells obtained from Utah Division of Oil, Gas, and Mining.

Table 10.1. Chemical and physical properties of BTEX compounds and the U.S. EPA maximum contaminant levels for select VOCs (BTEX) in drinking water (table modified from Koo [2012]; Weast and others [1990] using some data from Lawrence [2006]; EUGRIS [2014]).

Table 10.2. Summary of methods used, data sources used to calculate and derive parameters, and determination of ranges of values used to rank attributes from our GIS analysis of aquifer sensitivity and vulnerability in the Uinta Basin.

Table 10.3. Permeability ranking of geologic units in the Uinta Basin (modified from Schlotthauer and others [1981]). The units from the compiled 1:100,000 scale geologic map have been grouped and simplified from 328 units to 32 units. Permeability is ranked based on

Schlotthauer's permeability ranking (as feet per day), transmissivity data for each unit (in feet squared per day, if available), and well or spring yield (in gallons per minute, if available). A low ranking for permeability ranges from 0.5 to 5 feet/day, and moderate ranking ranges from 51 to 50 feet/day, and a high ranking ranges from 51 to 500 feet/ day.

Table 10.4. VOC sensitivity and the attribute rankings used to assign sensitivity for the Uinta Basin.

Table 10.5. Hydrologic soil groups, field capacity, bulk density, and fraction of organic carbon content generalized for Utah soils. Soil description and organic content from National Soil Survey Center (2006). Field capacity based on sediment grain size calculated from a soil texture triangle hydraulic properties calculator (Saxton, undated).

Table 10.6. VOC vulnerability and the attribute rankings used to assign vulnerability for Uinta Basin.

Table 10.1. Chemical and physical properties of BTEX compounds and the U.S. EPA maximum contaminant levels for select VOCs (BTEX) in drinking water (table modified from Koo [2012]; Weast and others [1990] using some data from Lawrence [2006]; EUGRIS [2014]).

Parameters	Benzene	Toluene	Ethylbenzene	Xylene
U.S. EPA MCL (mg/L)	0.005	1	0.7	10
Soil organic carbon-water partitioning coefficient (K_{OC})	97	242	622	570**
half life (days) not in () is uncontaminated***	238 (58 field contaminated matrix)	135-238 (5 in field with contaminated matrix)	238	238
Half life (years) converted	0.65	0.37-0.65	0.65	0.65

*Table is modified from Koo (2012) and Weast and others (1990), who used data from Carey and Sundberg (1990) and Fetter (1988).
**Average values.
***From Lawrence (2006).

Table 10.2. Summary of methods used, data sources used to calculate and derive parameters, and determination of ranges of values used to rank attributes from our GIS analysis of aquifer sensitivity and vulnerability in the Uinta Basin.

Sensitivity Input Parameters	Method	Derived or Calculated	Source
BTEX Retardation Factor (RF)	Process	Calculated	Rao and others (1985)
BTEX Attenuation Factor (AF)	Process	Derived	Rao and others (1985)
Permeability (See Table 10.3)	Index and Overlay	Derived	SSURGO* and Geologic Maps
Soil Hydraulic Conductivity	Index	Derived	SSURGO*
Depth to Groundwater	Index and Overlay		SSURGO* and Geologic Maps
Sensitivity Output	**Method**	**Derived or Calculated**	**Source**
Sensitivity Map	GIS Analysis (Combined Process, Index, and Overlay)	Both	This study
Vulnerability Input Parameters	**Method**	**Derived or Calculated**	**Source**
Sensitivity	GIS Analysis (Combined Process, Index, and Overlay)	Both	This study
Active/Producing Well Density	Index and Overlay	Derived	DOGM** See figure 10.2
Located Within Oil Shale/Tar Sand Areas	Index and Overlay	Derived	See figure 10.1
Proximity to Public Supply Well	Index and Overlay	Derived	See figure 10.1
Proximity to River/Stream	Index and Overlay	Derived	See figure 10.1
Vulnerability Output	**Method**	**Derived or Calculated**	**Source**
Vulnerability Map	GIS Analysis (Combined Process, Index, and Overlay)	Both	This study

* SSURGO: National Soil Survey Center's Soil Survey Geographic Database
** Utah Division of Oil, Gas, and Mining

Table 10.3. Permeability ranking of geologic units in the Uinta Basin (modified from Schlotthauer and others [1981]). The units from the compiled 1:100,000 scale geologic map have been grouped and simplified from 328 units to 32 units. Permeability is ranked based on Schlotthauer's permeability ranking (as feet per day), transmissivity data for each unit (in feet squared per day, if available), and well or spring yield (in gallons per minute, if available). A low ranking for permeability ranges from 0.5 to 5 feet/day, and moderate ranking ranges from 51 to 50 feet/day, and a high ranking ranges from 51 to 500 feet/ day.

Geologic Unit Description	Permeability Ranking
Water	3
Human disturbance	3
Mass wasting	2
Eolian deposits	3
Spring tufa deposits	2
Alluvium	3
Talus	3
Colluvium	3
Pediment mantle deposits	3
Young and Old alluvium - undifferentiated	3
Older pediment mantle	3
Volcanic rocks - undifferentiated	2
Uinta and Duchesne Formations - undivided	2
Green River Formation	1
Colton/Wasatch Formation	1
Flagstaff, North Horn, and Currant Creek Formations - undivided	2
Tertiary - undifferentiated	2
Mesaverde Groupe - undivided	2
Mancos Shale - undivided	1
Mancos Shale and Dakota Sandstone - undivided	2
Morrison, Summerville, Dakota, Burro Canyon, and Cedar Mountain Formations - undivided	2
Cretaceous rocks - undifferentiated	2
Summerville, Curtis/Stump, and Preuss Formations - undivided	1
Entrada Sandstone Formation	2
Curtis/Stump, Entrada and Carmel Formations - undivided	2
Twin Creek Limestone Formation	2
Carmel Formation	2
Navajo/Nugget Sandstone Formation	2
Glen Canyon Group - undifferentiated	2
Jurassic rocks - undifferentiated	2
Triassic - undifferentiated	2
Permian and Pennsylvanian undifferentiated	2
Pennsylvanian and Mississippian rocks - undifferentiated	2
Proterozoic and Archean rocks - undifferentiated	2

Table 10.4. VOC sensitivity and the attribute rankings used to assign sensitivity for the Uinta Basin.

Aquifer Sensitivity Input Parameters	Attribute	Ranking
BTEX Retardation Factor (RF)	High if RF>5	0
	Low if RF<5	1
BTEX Attenuation Factor (AF)	Low if AF is 0	0
	High if AF>0	1
Permeability (see table 2)	Low	1
	Heterogeneous	2
	Medium to High	3
Soil Hydraulic Conductivity	Less than 0.57 inch/hour low transmissivity)	1
	Greater than or equal to 0.57 inch/hour high transmissivity)	2
Depth to Groundwater	Greater than 5 feet to permeable layer	1
	Less than 5 feet permeable layer	2
Aquifer Sensitivity Output	**Attribute**	**Ranking**
Sensitivity	Low	3 to 4
	Moderate	5 to 6
	High	7 to 9

Table 10.5. Hydrologic soil groups, field capacity, bulk density, and fraction of organic carbon content generalized for Utah soils. Soil description and organic content from National Soil Survey Center (2006). Field capacity based on sediment grain size calculated from a soil texture triangle hydraulic properties calculator (Saxton, undated).

Soil Group	Soil Description	Grain size (mm) (Field Capacity %)	Bulk Density Range (kg/L) (average)	Organic Carbon Content, Fraction (F_{oc})*
A	Sand, loamy sand, or sandy loam; low runoff potential and high infiltration rates even when thoroughly wetted; consists of deep, well to excessively drained sands or gravels with high rate of water	0.1 – 1.0 (14-21)	1.5 – 2.0 (1.75)	Variable and ranges from 0.029 to 8.7 %
B	Silt loam or loam; moderate infiltration rate when thoroughly wetted; consists of moderately deep to deep, moderately well to well-drained soils with moderately fine to moderately coarse textures.	0.015 - 0.15 (25-28)	1.3 - 1.61 (1.4)	Variable and ranges from 0.029 to 8.7 %
C	Sandy clay loam; low infiltration rates when thoroughly wetted; consists of soils with layer that impedes downward movement of water; soils with moderately fine to fine structure.	0.01 - 0.15 (26)	1.3 - 1.9 (1.6)	Variable and ranges from 0.029 to 8.7 %
D	Clay loam, silty clay loam, sandy clay, silty clay, and/or clay; highest runoff potential of all soil groups; low infiltration rates when thoroughly wetted; consists of clay soils with a high swelling potential, soils with a permanent high water table, soils with a hardpan or clay layer at or near the surface, and shallow soils over nearly impervious material.	0.0001 - 0.1 (32-42)	1.2-1.3 (1.25)	Variable and ranges from 0.029 to 8.7 %
G	Gravel	2.0 and greater (less than 12)	2.0 (2)	0.029 %**

* F_{oc} is calculated from SSURGO organic matter data divided by 1.72 and is unique for soil polygons.

**No value for F_{oc} exists in the SSURGO database for gravel; we assigned the lowest value in the SSURGO database.

Table 10.6. VOC vulnerability and the attribute rankings used to assign vulnerability for Uinta Basin.

Aquifer Vulnerability Input Parameters	Attribute	Ranking
Sensitivity	Low	-2
	Moderate	0
	High	2
Active/Producing Well Density*	<1 well per sq. km.	0
	1-5 wells per sq. km.	1
	>5 wells per sq. km.	2
Located Within Oil Shale/Tar Sand Area	Y	0
	N	2
Proximity to Well/Spring*	>3 miles	0
	1-3 miles	1
	<1 mile	2
Proximity to Water Body*	>3 miles	0
	1-3 miles	1
	<1 mile	2
Aquifer Vulnerability Output	Attribute	Ranking
Vulnerability	Low	-2 to 1
	Moderate	2 to 5
	High	6 to 10

*The attributes and ranking are subjective as part of the index-based method we employed (see table 10.2). We selected a range of values for each parameter that more realistically modeled land-use patterns based on the output of values generated from GIS analysis. The ranges represent a natural break in the distribution of GIS generated values that we modified and lumped together to minimize the number of classifications that were generated by GIS analysis. For example, we use a range category for proximity to water bodies as <1, 1-3, and >3 miles with "1" mile as a buffer zone surrounding a water body to be protective of water quality.

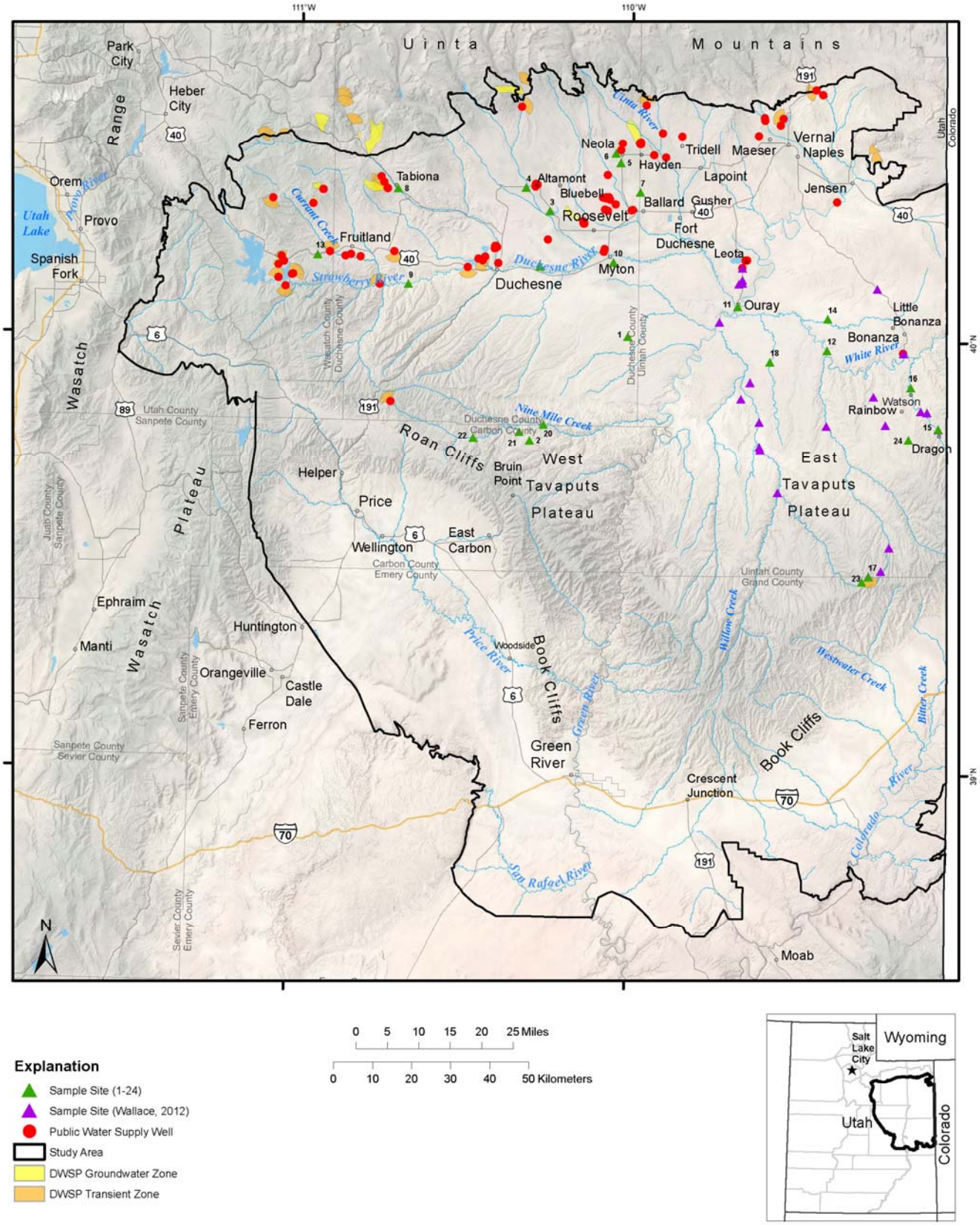

Figure 10.1. Location of sites sampled for water quality for this study, a previous water quality study (Wallace, 2012a, 2012b), public water supply wells, and drinking water source protection (DWSP) zones. DWSP transient zones refer to public supply sources that are used on a seasonal or intermittent basis.

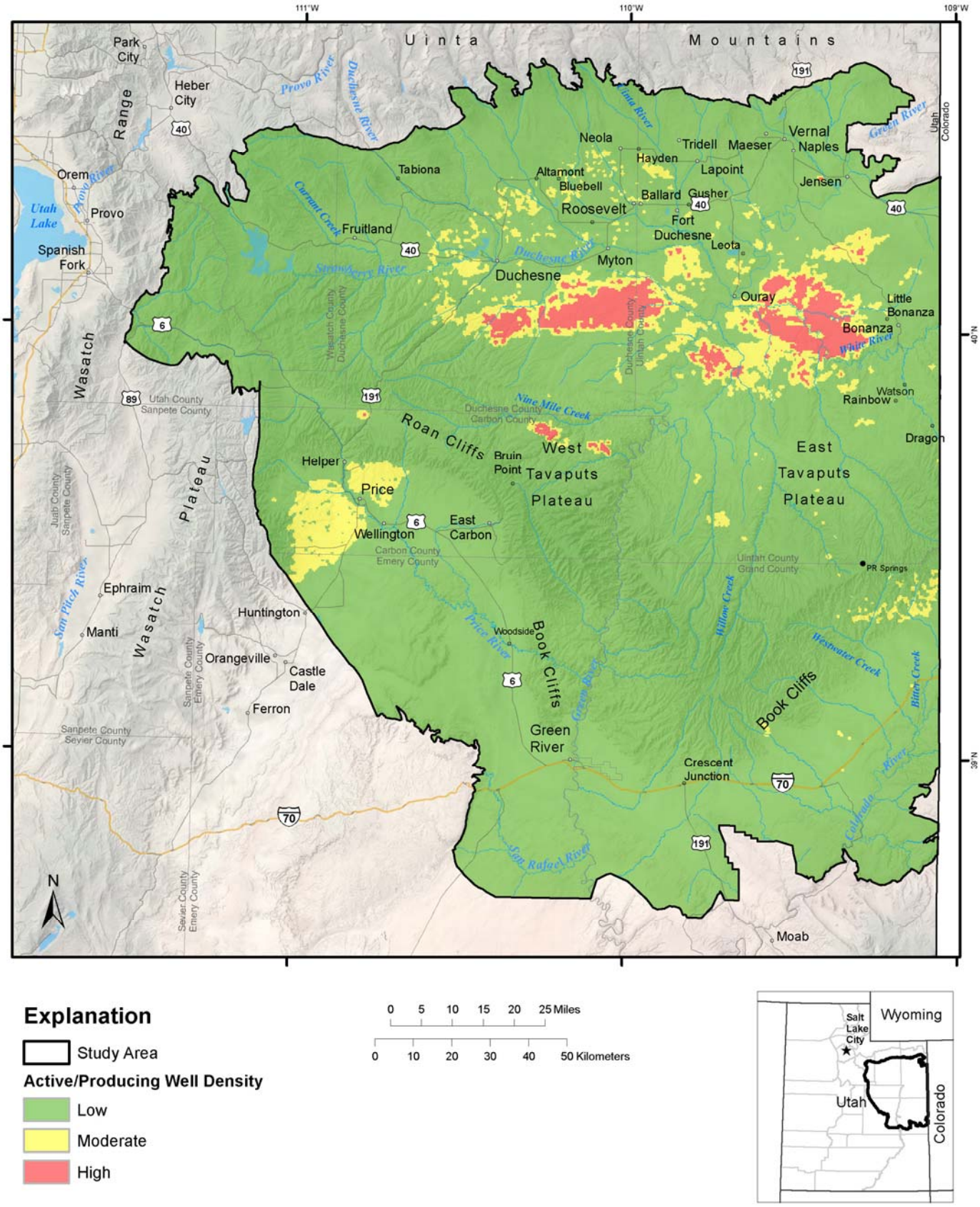

Figure 10.2. Density of active oil/gas wells obtained from Utah Division of Oil, Gas, and Mining.

CHAPTER XI

HANDLING AND MANAGEMENT OF WATER PRODUCED FROM OIL AND GAS RESERVOIRS IN THE UINTA BASIN

David E. Tabet

According to Clark and Veil (2009), produced water is the largest by-product and waste stream associated with gas and oil production in the United States. Water handling and management practices for waste water resulting from gas and oil production in the UB are subject to regulation from various federal and state agencies including the UDWQ within the Utah Department of Environmental Quality (UDEQ), DOGM, the EPA, as well as by local county regulatory bodies.

Regulation of water-use associated with the petroleum industry has evolved over time, and presently is designed mainly to protect underground and surface fresh-water supplies and surface habitat, including fauna, flora, and the atmosphere. Water management issues related to gas and oil development in Utah primarily involve water used for drilling and completion of wells, water for flushing of certain reservoirs to enhance oil recovery, water to suppress dust emissions from dirt roads, as well as the disposal of water produced as a byproduct of gas and oil production. Some synoptic studies of produced water management have been carried out in the past, but when local case studies are provided, they mostly tend to focus waters associated with

CBM or on the larger producing basins such as the Denver and Piceance of Colorado, the Marcellus of Pennsylvania, the Anadarko and Arkoma of Oklahoma, the Fort Worth and Permian of Texas, the Williston of North Dakota, and Big Horn, Green River, Powder River, and Wind River of Wyoming, rather than on the waters associated with conventional oil and gas production in the UB of Utah (IOGCC and ALL Consulting, 2006; Benko and Drewes, 2008; Guerra and others, 2011; Dahm and Chapman, 2014). The best previous synopsis of produced water production and disposal in Utah was for the Argonne National Laboratory (Clark and Veil, 2009), which gave a snapshot for 2007. This chapter first defines the water quality standards established in Utah. It next provides an extensive updated discussion that attempts to describe and quantify the water streams involved in water management practices associated with gas- and oil-well drilling and completion, EOR waterflooding, and water disposal via deep underground injection wells since quantities used annually are reported and available for evaluation for the UB. The amount of water used for suppression of dust on dirt access roads is not reported on a regular basis to a regulatory agency and therefore was not included in this chapter.

The chapter also reviews petroleum water management practices by specific companies, as well as trends as far back as records are easily available, but concentrates mainly on practices and quantities of water usage in the 10 years prior to 2014. For example, water used in hydraulic fracture stimulation of gas and oil wells was not required to be reported to FracFocus (2015) by the Utah DOGM until November 1, 2012, before which such reporting was simply voluntary, and so earlier records for such usage are scant and incomplete.

UTAH WATER QUALITY STANDARDS

Utah Groundwater Classification Scheme

The UDWQ the (Utah Department of Environmental Quality, 2015a) has established a groundwater classification scheme in Utah with four major classes, and three subclasses under the highest class, I - A, I - B, and I - C. Each of the groundwater classes and subclasses has different management prescriptions to protect groundwater quality.

Groundwater Class	Class Name	TDS Range
Class1 – A	Pristine	0 – 499 mg/L, and no contaminant concentrations exceeding the groundwater quality standard
Class 1 – B	Irreplaceable	0 – 1999 mg/L; any contaminants present must not exceed the groundwater quality standard or 1.1 times background concentration
Class 1 – C	Ecologically Important	0 – 1999 mg/L
Class II	Drinking Water	500 – 2999 mg/L
Class III	Limited use	3000 – 9999 mg/L
Class IV	Saline	$\geq$ 10,000 mg/L

Class I Groundwater

- CLASS IA groundwater is referred to as "pristine" and is classified as such by exhibiting both of the following characteristics:

- TDS of less than 500 mg/L, and

- no contaminant concentrations that exceed the groundwater quality standard.

- For facilities located above CLASS IA groundwater, that discharge or will probably discharge to the groundwater, and that are under the regulatory authority of the Ground Water Quality Protection Program (GWQPP), groundwater quality protection levels will be established as follows.

  - TDS may not exceed the greater of 1.25 times the background or background plus two standard deviations.

  - When a contaminant is not present in a detectable amount as a background concentration, the concentration of the pollutant may not exceed the greater of 0.1 times the groundwater quality standard, or the limit of detection.

  - When a contaminant is present in a detectable amount as a background concentration, the concentration of the pollutant may not exceed the greater of 1.25 times the background concentration, 0.25 times the groundwater quality standard, or background plus two standard deviations; however, in no case will the concentration of a pollutant be allowed to exceed the groundwater quality standard.

- CLASS IB groundwater is referred to as “irreplaceable” when it is a source of water for an existing community public drinking water system for which no reliable supply of comparable quality and quantity is available because of economic or institutional constraints.

- For facilities located above CLASS IB groundwater, that discharge or will probably discharge to the groundwater, and that are under the regulatory authority of the GWQPP groundwater quality protection levels will be established as follows.

    - TDS may not exceed the lesser of 1.1 times the background value or 2000 mg/L.

    - When a contaminant is not present in a detectable amount as a background concentration, the concentration of the pollutant may not exceed the greater of 0.1 times the groundwater quality standard, or the limit of detection.

    - When a contaminant is present in a detectable amount as a background concentration, the concentration of the pollutant may not exceed the greater of 1.1 times the background concentration or 0.1 times the groundwater quality standard; however, in no case will the concentration of a pollutant be allowed to exceed the groundwater quality standard.

- CLASS IC groundwater is referred to as “ecologically important” when it is a source of groundwater discharge important to the continued existence of an existing wildlife habitat.

- Class IC groundwater will be protected as a source of water for potentially affected wildlife habitat. Limits on increases of TDS, and organic and inorganic chemical compounds will be determined in order to meet applicable surface water standards.

Class II Groundwater

CLASS II groundwater is also referred to as “drinking water quality” and is classified as such by exhibiting both of the following characteristics:

- TDS greater than 500 mg/L and less than 3000 mg/L, and

- no contaminant concentrations that exceed ground water quality standards.

For facilities located above CLASS II groundwater, that discharge or will probably discharge to the groundwater, and that are under the regulatory authority of the GWQPP, groundwater quality protection levels will be established as follows.

- TDS may not exceed the greater of 1.25 times the background value or background plus two standard deviations.

- When a contaminant is not present in a detectable amount as a background concentration, the concentration of the pollutant may not exceed the greater of 0.25 times the groundwater quality standard, or the limit of detection.

- When a contaminant is present in a detectable amount as a background concentration, the concentration of the pollutant may not exceed the greater of 1.25 times the background concentration, 0.25 times the groundwater quality standard, or background plus two standard deviations; however, in no case will the concentration of a pollutant be allowed to exceed the groundwater quality standard.

Class III Groundwater

CLASS III ground water is also referred to as "limited use" and is classified as such by exhibiting one or both of the following characteristics:

- TDS greater than 3000 mg/L and less than 10,000 mg/L, or

- one or more contaminants that exceed the groundwater quality standards.

For facilities located above CLASS III groundwater, that discharge or will probably discharge to the groundwater, and that are under the regulatory authority of the GWQPP, groundwater quality protection levels will be established as follows.

- TDS may not exceed the greater of 1.25 times the background value or background plus two standard deviations.

- When a contaminant is not present in a detectable amount as a background concentration, the concentration of the pollutant may not exceed the greater of 0.5 times the groundwater quality standard, or the limit of detection.

- When a contaminant is present in a detectable amount as a background concentration, the concentration of the pollutant may not exceed the greater of 1.5 times the background concentration, 0.5 times the groundwater quality standard, or background plus two standard deviations; however, in no case will the concentration of a pollutant be allowed to exceed the groundwater quality standard.

Class IV Groundwater

CLASS IV groundwater is also referred to as "saline" and is classified as such by containing greater than 10,000 mg/L of TDS. Most water produced as a byproduct of oil and gas production in Utah is CLASS IV, or saline in quality, although some of Utah's produced water falls in the 3000 to 9999 mg/L TDS category, or CLASS III.

No protection levels for CLASS IV groundwater have been established to date by the Executive Secretary of the GWQPP to protect human health and the environment.

Utah Total Maximum Daily Loads

Section 303(d) of the U.S. Clean Water Act requires states to develop Total Maximum Daily Loads (TMDLs) to establish allowable loadings of pollutants, or other quantifiable factors, for water bodies in the state based on the relationships between pollutant sources and in-stream water quality conditions (U.S. Environmental Protection Agency, 2015). These load limits are designed for waters that do not meet water quality standards even after technology-based controls are used.

Several watershed areas in the UB have been listed by the UDEQ (2015b) as impaired waters for TDS. The bedrock formations in the basin can contain soluble saline minerals, particularly the Green River and Wasatch Formations plus the Mancos Shale (figure 2.1, plate 1), with dissolved salts contributing TDS to water flowing over or through them. In addition to natural salt loading from runoff, seepage of water from irrigation canals, de-icing salts along roads, and deep percolation of irrigation waters contributes to salt loading in tributaries of the Duchesne River (plates 4 and 5). Other man-made disturbances of salt-bearing strata, such as oil and gas development, can lead to increased runoff and potential salt loading.

Fortunately for Utah, a report by the U.S. Geological Survey (Vaill and Butler, 1999) on dissolved-solids trends in the Colorado River Basin waterways from 1970 through 1996 noted that there has been a historic downward trend in TDS concentrations in the Duchesne River watershed. Therefore, it appears that the land owners and surface management agencies in Utah have put in place practices that are effectively reducing dissolved solid loads entering the Duchesne River and probably other Uinta Basin watersheds. The improvements in TDS concentration are mainly the result of better irrigated agricultural practices, but also from close

monitoring and regulation of land disturbing activities like petroleum development. A new study looking at trends since 1996 would be helpful.

WATER FACILITIES

History of Utah Water Facility Development and Use

Regulation of petroleum development operations by the State of Utah formally began in 1955 with the creation of the Oil and Gas Conservation Commission, which was charged to prevent the waste of oil and gas, encourage conservation, and protect the correlative rights of oil and gas owners. The regulations prior to 1970 mainly involved sound well drilling, construction, spacing, and abandonment to protect the petroleum resource and the surrounding environment during development. In 1968, the Utah Legislature reorganized the Division of Oil and Gas Conservation as part of the Department of Natural Resources, and in 1975 renamed it the Division of Oil, Gas, and Mining. Following the creation of the EPA in December 1970, as new federal laws were passed through the 1970s and 1980s to help mitigate the potential impacts of petroleum development activities on the local and regional air, fauna, flora, cultural, socio-economic and water resources, the DOGM periodically updated its regulations to match those required in new federal laws. For example, in 1982 DOGM received primacy from the EPA in the regulation of Class II water injection wells (see DOGM history at: http://linux1.ogm.utah.gov/WebStuff/wwwroot/division/aboutus.html).

Strategies and technologies utilized by the petroleum industry to address produced water management generally fall into one of three categories: (1) minimization of produced water; (2) recycling or reuse of produced water; and (3) some form of disposal (National Petroleum Council, 2011). Also, in general as field development has increased in area and number of wells over time, operators in Utah have moved from small isolated systems, either commercially run or company owned, to more integrated and comprehensive, generally company-owned, water-handling and treatment facilities as economies of scale and centralization could be realized as field size grew or field consolidation occurred through mergers or acquisitions. One major example of this type of development was the consolidation of more than 15 smaller individual EOR, waterflood units into the single giant Greater Monument Butte waterflood unit in 2010 by Newfield Exploration Company.

Also, as demand for fresh water has grown with increased petroleum development, certain companies, and no doubt more in the future, have looked for ways to increase water reuse and reduce their demand for limited fresh water supplies. Notably Anadarko/Kerr-McGee has developed water handling systems to reuse water for drilling and fracture stimulation of wells and cut its fresh water usage for these development steps close to 100%. In addition, EOG Resources plans to use waste water from the Bonanza coal-fired power plant (about 40 mile southeast of Vernal) of Deseret Generation and Transmission for 88% of the water needed to drill and complete the 2808 new gas wells it proposes at the Chapita Wells unit of Greater Natural Buttes field (figure1.1). Most of the larger UB petroleum operators have, or are in the process of installing, centralized water collection and treatment plants to reduce or eliminate water storage at individual well sites and the need to have trucks transport the produced water from well sites to disposal or reuse sites, resulting in less dust and diesel emissions from reduced

trucking and less traffic and human activity in their fields which might disturb flora and fauna living in the area. One regulatory and operational trend in the past five years has been an effort to reduce or minimize the use of surface ponds for storage and evaporation of produced water. Both companies and regulators see pond facilities as costly and difficult to maintain over time, possessing a large disturbance footprint, and having a higher potential for leakage and emissions in a sensitive environment.

Service industries understand that water management for petroleum companies in the U.S. is a growing industry and are looking for new and more cost-effective ways to serve this greater than $6-billion dollar industry (Bluefield Research, 2014). Several of the larger UB operators have developed and posted company water policies on their websites and are actively looking for ways to reduce water use and waste water production, and find ways to reuse existing water supplies, and anticipate or adapt to an ever-changing regulatory landscape. The State of Utah encourages voluntary efforts to conserve and reuse water in Utah (Utah Division of Water Resources, 2005), and although initial emphasis was placed on municipal water systems, the State will no doubt encourage and foster petroleum company efforts in this regard.

Produced Water Volume in the Uinta Basin

The amount of water produced in association with petroleum production in the four-county (Uintah, Duchesne, Carbon, and northern Grand) area comprising the UB has increased about 35% from 2008 to 2014, with the volume rising about 86 to 116 MMB over that time frame. The increase in produced water reflects a similar increase in petroleum development over

that period as the number of active wells increased nearly 41% from 9070 in 2008 to 12,780 in 2014 (table 11.1).

All of the counties, except for Grand County, have seen the number of wells increase over the years tabulated above, and the greatest increases in new active wells and produced water volumes has taken place in Duchesne and Uintah Counties. Since the wells in Duchesne County are mainly developed for oil production and those in Uintah County are mainly focused on gas production, the number of bbls of produced water per county in table 11.1 were divided by the number of active wells to arrive at a tabulation of BW per well for each county by year as shown in table 11.2 below.

Table 11.2 show different trends over time for each of the counties involved, but cumulatively the amount of produced water per well from the four-county area has decreased for most years over the seven-year study period. Most of the cumulative decline in bbls per well can be attributed to the major decline in produced water per well coming from the CBM fields of Carbon County, and the fact that more recent wells in that county have been conventional gas wells that typically are lower volume water producers. The amount of water produced per well has generally decreased over the time frame studied for the predominantly Wasatch and Mesaverde formations gas wells of Uintah County. Interestingly, in the predominantly Green River Formation oil producing wells of Duchesne County the amount of water produced per well has been generally increasing over the 2008 to 2014 time frame, so it is evident that oil and gas wells in the UB operate differently in terms of their produced water behavior. Grand County's UB gas wells generally produce from older Dakota-Cedar Mountain-Morrison Formation reservoirs and are the lowest volume water producers per well in the basin. Thus, the data above illustrates that the amount of water produced per well across the UB is affected by the formation

being produced as well as the type of product predominantly being produced, either oil or gas. Other factors, such as depth of the producing formation, well completion technology (vertical versus horizontal), and well spacing variations from field to field may also affect the amount of water produced per well, and some of this local detail is provided in discussions of the individual operators activities below.

Water Disposal Wells

The DOGM's website information on wells classified as water disposal wells indicates that the number of disposal wells in the UB has grown from a single well in 1961 to 92 in 2014 (figures 11.1 and 11.2). Over this period it appears that 106 disposal wells were completed and 14 were subsequently plugged and abandoned or converted to gas wells. Whereas 91 wells are classified as water disposal wells in the DOGM well file records, examination of the Disposal Well Volumes part of the DOGM website, found disposal volumes for 92 wells for 2014 since one well is both a gas producer and a disposal well but is classified as a gas well. The first major growth spurt was in 1975, when 10 disposal wells were completed as part of the development of the Altamont and Bluebell fields (figure 1.1). Disposal well additions averaged about one well every five years from 1977 to 1988, then increased to an average of one new disposal well per year from 1989 to 1995. From 1996 through 2008 the average annual increase in disposal well completions rose to about three new wells per year, when coalbed gas development in Carbon County and tight-sand gas development in Uintah County were undergoing steady development. The UB disposal well completion rate increased from 2009 through 2014 at an average rate of about six new disposal wells per year, although the rate has slowed somewhat in the past couple

years. As of the end of 2014, the 92 active produced-water disposal wells listed in the DOGM's Disposal Well Volumes files for the UB study area were distributed among the four counties as such: 21 in Carbon County, 38 in Duchesne County, 2 in Grand County, and 31 in Uintah County (table 11.3).

The volume of water disposed via injection annually in the UB has increased with the added number of disposal wells, from 43.07 MMB in 2008 to 67.55 MMB in 2014 (table 11.4). Within the four-county UB area all the counties, except Carbon County, have seen their annual and average per well water disposal volumes increase over time. In the period from 2008 through 2014, the water disposal volume has increased 174% in Duchesne County, 251% in Uintah County, and from nothing to over 330,000 BW in Grand County. Meanwhile, Carbon County has seen the annual amount of water disposed in wells decrease from 16.06 MMB in 2008 down to 12.05 MMB in 2014. The average amount of water disposed per well has been similar in Carbon, Duchesne, and Uintah Counties, averaging about 0.8 MMB per well annually, while ranging on average between 0.4 and 1.4 MMB per well annually. However, in Grand County the average water disposed per well annually has been less than 0.2 MMB, ranging between 0.13 and 0.19 MMB per well per year.

Half of the produced-water disposal wells (46) are associated with gas fields, both CBM and tight-gas sand developments, whereas the remaining 46 produced-water disposal wells are associated with oil field developments in the UB (figure 11.2), mainly in those fields not employing waterflood, EOR techniques such as Altamont and Bluebell oil fields. Natural Buttes gas field has the greatest number of water disposal wells (22) of any field in the UB, but at least five different companies operate individual disposal wells in their portion of the field. Several fields (Buck Canyon, Duchesne, Nine Mile Canyon, and Wonsits Valley) have had disposal

wells in the past or have wells that were inactive in 2014. New fields adding water disposal wells in 2014 in the UB included the Three Rivers and Windy Ridge oil fields. Whereas most of the UB disposal wells are operated by producing companies for their own disposal needs, at least six disposal wells were operated in 2014 by commercial ventures that would accept water from any operator willing to pay for water disposal. Altamont, Bluebell, and Greater Cisco fields each had two commercial disposal wells operating within the field area. In 2014, the 92 water disposal wells were distributed among 22 producing UB fields and one wildcat area as follows:

Field Name (commodity – producing formation)	**Disposal Wells**
Altamont (oil – Green River Fm.)	15
Antelope Creek (oil – Green River Fm.)	1
Bluebell (oil – Green River Fm.)	9
Brundage Canyon (oil – Green River Fm.)	10
Castlegate (CBM – Mesaverde Fm.)	1
Cedar Rim (oil – Green River Fm.)	1
Clear Creek (gas – Ferron Ss. Mbr. of the Mancos Sh.)	1
Devils Playground (gas – Mesaverde Gp. and Wasatch Fm.)	1
Drunkards Wash (CBM – Ferron Ss. Mbr. of the Mancos Sh.)	9
Gordon Creek (gas – Ferron Ss. Mbr. of the Mancos Sh.)	1
Greater Cisco (gas – Morrison, Cedar Mountain, and Dakota Fms.)	2
Helper (CBM – Ferron Ss. Mbr. of the Mancos Sh.)	6
Moffat Canal (oil – Wasatch and Green River Fms.)	1
Natural Buttes (gas – Mesaverde Gp., Wasatch and Green River Fms.)	22
North Myton Bench (oil – Green River Fm.)	2
Pariette Bench (oil – Green River Fm.)	1
Peters Point (gas – Mesaverde Gp. and Wasatch Fm.)	2
Randlett (oil – Green River Fm.)	1
Red Wash (oil – Green River and Uinta Fms.)	2
Stone Cabin (gas – Mesaverde Gp. and Wasatch Fm.)	1
Three Rivers (oil – Green River Fm.)	1
Windy Ridge (oil – Green River Fm.)	1
wildcat gas (gas – Ferron Ss. Mbr. of the Mancos Sh.)	1

Waterflood Injection Projects

Since 2010, the UB has had 16 active EOR, waterflood injection projects in operation (figure 11.3). All of these projects inject water, produced or fresh, via wells into Green River Formation reservoirs to flush residual oil left behind after primary production toward other producing wells in the same field. The 16 active EOR, waterflood injection projects in the UB involve 1586 permitted water injection wells. Collectively all these EOR, water-injection wells pumped 44.29 MMBW underground in 2014. Water produced with the oil from all the same fields where EOR, water injection occurred totaled 24.91 MMB in 2014, and assuming all the produced water was re-injected for EOR, then the UB operators needed to use over 19 MMB of fresh water to achieve the full water volumes used in the EOR efforts in 2014.

Most of these waterflood projects are small, and only six involve more than ten water-injection wells (table 11.5). The Antelope Creek project of Petroglyph Operating Company, the Gypsum Hills, Red Wash, and Wonsits Valley projects of QEP Energy Company, and the Walker Hollow project of Citation Oil and Gas Corporation each operated between 11 and 109 water injection wells at their sites in 2014. By far the largest EOR, waterflood injection project in the UB in 2014 was Newfield Production Company's Greater Monument Butte Unit (GMBU) project that involves 1347 water injection wells and injected 35.75 MMBW by itself. Newfield created this giant waterflood injection project in 2010 by combining at least 19 smaller projects, including Ashley, Beluga, Blackjack, Canvasback, Castle Draw, East Pariette, Fenceline, Hawkeye, Humpback, Jonah, Lone Tree, Monument Butte, Monument Butte East, Monument Butte NE, Pariette, Pleasant Valley, Sand Wash, S. Monument Butte, South Wells Draw, Sundance, West Point, and West Willow Creek, into one unified project. Merging many smaller waterflood projects into one larger one can offer an operator economies of scale in terms of water handling, processing, procurement, transportation, and overall project management leading

to improved project operating costs. Newfield has plans to drill over 5700 new oil wells at the GMBU, of which perhaps half will eventually be converted to injection wells, so the amount of water injected for EOR will likely more than double as the GMBU progresses toward full-field development. It remains to be seen if further waterflood project consolidation occurs in other areas of the UB as oil development expands there as well.

According records posted on the internet by the DOGM (see web address: http://oilgas.ogm.utah.gov/Data_Center/LiveData_Search/injection.htm), the amount of water injected annually by all 16 of the UB EOR, waterflood injection projects has increased from 25.45 MMB in 2008 to over 44.29 MMB in 2014 (table 11.6). Over the same time period the water produced annually with the oil from the fields where these EOR projects occur has risen from 12.9 MMB in 2008 to over 24.9 MMB in 2014. The annual deficit of produced water to injected water for the combined UB EOR, waterflood projects has increased from about 12.5 MMB in 2008 to over 19.3 MMB in 2014, although the deficit temporarily dipped below the 2008 level between 2009 and 2011. Whereas the overall volume of water injected for EOR has increased over time, the increase has not been uniform across all the EOR projects. In fact, as shown in table 11.6, only the GMBU waterflood project has had significant increases in the volume of water injected annually, with the volume of water injected for EOR in 2014 more than tripling the 10.71 MMB injected in 2008. Meanwhile, the remaining 15 projects have had relatively flat to declining volumes of water injected during the same period. It is also of note that the GMBU waterflood project has steadily increased its portion of the total volume of water injected for EOR from 42% in 2008 to over 80% in 2014, at 35.75 of the 44.29 MMBW injected that year. In 2008, the GMBU project involved water injection volumes only 33% above those at the Red Wash project, but by 2014 the Red Wash water injection project had shrunk and the

GMBU project had grown such that the water injected at GMBU was 1084% greater than at the Red Wash project.

Water Evaporation Ponds

Within Uintah County, where most of Utah's tight gas production comes, produced water evaporation ponds associated with disposal facilities must have a conditional use permit (CUP) according to Uintah County (2015) rules, and all such facilities are subject to the annual reviews. All facilities must comply with State of Utah DOGM General Rules, and the CUP application must include a copy of the DOGM application and approval. A Uintah County Operations Certificate must be issued prior to an applicant receiving any production water.

All evaporation ponds and water treatment plants must be located a minimum of 2 miles from any state or federal highway, city, town, or residential use (as determined by the Uintah County tax rolls) and from the property line of a parcel containing a primary residential use. Any site located within 5 miles of a residence shall have a real time meteorological station on the site for data collection and analysis of at least wind speed and direction. Copies of the meteorological data shall be filed quarterly with Uintah County. The site must be a minimum of 40 acres in size.

The number of produced water disposal ponds are limited to the amount approved on the CUP certificate. Sites cannot be enlarged, or modified, without approval from the Uintah County Planning Commission. Copies of DOGM's quarterly inspection reports must be filed with the County Planning and Zoning office. Any leaks must be reported to Uintah County within 24 hours of an occurrence.

Sites must be fenced with a minimum 6-foot, chain-link fence to sustain safety, and prevent access by livestock, wildlife, and unauthorized personnel. Signs providing emergency contact information must be provided at the receiving areas and adjacent to ponds. An operator must be on site at all times for monitoring of the site during receiving operations unless specific approval is given by Uintah County for the site to be unmanned. Spray evaporation systems must be operated such that all spray-borne suspended or dissolved solids remain within the perimeter of the lined pond area (figure 11.4A). Odors must be controlled to prevent nuisance complaints. A wind sensor is required on all open ponds to automatically shut down spray devices if wind speed causes any spray to leave the lined pond area. If there is reasonable indication that spray has left the lined pond area, an analysis of soils outside the pond area shall be required at the expense of the CUP holder.

A mandatory bond or other assurance must be furnished to Uintah County on all CUP permitted property prior to the receipt of water. The bond or assurance shall be in the amount of 125% of a contractor's estimate to remove buildings and tanks, reclaim roads and driving surfaces, remove fencing and re-vegetate the site to a standard agreed to by the property owner and Uintah County. The contractor's estimate and bond amount shall be re-calculated every five years. The County's bond is in addition to Utah DOGM General Rules (R649-9-9), which requires bonding to treat or remove waste from the site and secure the site to prevent future contamination. A copy of the bond with DOGM shall be provided and kept on file with Uintah County.

DOGM rules R649-9-3 and R649-9-4 cover specific requirements applicable to petroleum field waste disposal and evaporation facilities, respectively. Siting a petroleum waste disposal facility must conform to the following requirements:

(1) be located on level, stable ground, and an acceptable distance from any established of intermittent drainage;

(2) at least 1 mile from residences or occupied buildings not associated with the facility; and

(3) not within aquifer recharge areas, protection zones for public drinking water sources, flood plains, drainage bottoms, areas on or near faults; not within 500 feet of a wetland, water-course or lakebed; and not over permeable soil where ground water is less than 50 feet below the surface, or areas above a subsurface mine.

A DOGM petroleum waste disposal facility permittee must provide a waste-stream management plan that details the estimated quantity and quality of the liquid and solid waste materials accepted at the facility and a description of the physical and chemical processes used in the treatment of the waste streams, as well as the method and schedule of disposal of all solid and liquid waste streams produced at the facility, including how odors will be managed and kept from creating an environmental or nuisance problem. The disposal facility plan must include a contingency plan designed to minimize any hazards to fresh water, public health and safety, or the environment in the event of an unplanned fire, explosion, or an accidental release of oil field wastes to the air, soil, surface or groundwater.

If a DOGM petroleum waste disposal facility permittee plans to include evaporation ponds, in addition to meeting the siting requirements above, the evaporation ponds shall be designed for 10 acre-feet or less of water, and the pond capacity should be adequate to contain all

produced water delivered, even in times of minimum evaporation rates. The applicant must provide an estimate of the maximum daily quantity and representative quality of the produced water to be disposed at the evaporation site, including concentrations of chlorides, sulfates, pH, TDS, and any other significant constituents required by DOGM. The evaporation ponds need to be constructed with a double liner system including a leak detection system between the primary (minimum 60-mil high-density polyethylene [HDPE] or equivalent) and secondary (minimum 40-mil HDPE or equivalent) liner systems. The pond liner material shall be impervious and resistant to weather, tears and punctures, sunlight, hydrocarbons, aqueous acids, alkalis, salt, fungi, or other substances that may be contained in the produced water. Water unloading systems associated with the ponds may also require a leak detection system. The ponds are to be constructed with 2-foot free-board at all times and the grade of the pond levee is to be no steeper than 3:1 on the inside of the levee and no steeper than 2:1 on the outside of the levee (figure 11.4B). Any hydrocarbon accumulation on a pond, other than de minimis quantities, is considered an operating violation and must be corrected immediately.

The above summary provide the basic highlights of the Utah rules governing petroleum waste disposal facilities and evaporation ponds. For the exact particulars of the DOGM rules regarding waste disposal facilities and evaporation ponds the reader is referred to the DOGM rules webpage found at: http://oilgas.ogm.utah.gov/Rules/Rules.htm.

DOGM collects quarterly information from operators of evaporation ponds, both commercial and private, on the amount of water delivered to each pond, as wells as information on whether leaks were detected or not. Commercial ponds are those that take water for disposal for a fee, and private ponds are those operated by a company for their own needs. The UGS was

kindly provided by the DOGM with water delivery volume data for 2010 through 2013 and the annual results are summarized in table 11.7.

Table 11.7 shows the amount of water delivered annually to all evaporation ponds in the UB is varied from 12.2 to 17.3 MMB per year with a four-year annual average of 13.76 MMB. The percentage of water delivered to commercial evaporation ponds varied over the four years between 60 to 73%, and averaged 67.3% of the total delivered to all ponds. The amount of produced water deliver to evaporation ponds varied from year to year and a long term trend is difficult to discern with only four years of data. The least amount of water delivered to evaporation ponds was in 2011, and the greatest amount was in 2012.

A list of commercial disposal facilities, which often have evaporation ponds, is provided on the DOGM web site. The 20 commercial facilities in the UB are listed in table 11.8; the locations are shown on figure 11.5.

Water Used for Hydraulic Fracturing

The amount of water used in hydraulic fracturing of wells in Utah is the hardest water stream to pin down because reporting of such water use was not mandatory in Utah until November 2011, when the DOGM began requiring companies to report the amount of water and additives used in hydraulic fracturing well completions to the FracFocus' chemical disclosure registry website (see: http://fracfocus.org/). Thus, reported water volumes used in hydraulic fracturing before 2012 are incomplete because not all companies participated in the voluntary reporting effort, and FracFocus only began collecting data itself in 2011. As of mid-2015, the FracFocus website did not have its records available in a digital tabular format, only in PDF

image format, which makes compilation of the hundreds of UB fracture stimulation records cumbersome, tedious, and subject to more clerical data entry errors. DOGM kindly provided the UGS with a batch download in digital format of all the wells fracture stimulation in Uintah County during 2013 for use in our study. Data for other years and counties for this study were tallied one at time from the PDF records available on the FracFocus website. Some wells received more than one fracture stimulation in a year and care was taken to tally such wells only once with a cumulative amount of water used in all treatments. Occasionally duplicate records were encountered and the duplicates were removed from our final well tally and volume of water used. As of mid-2015, FracFocus had only posted records for the first half of 2014, so the information posted in the tables and chart below for 2014 only reflect one half of a year.

For the two full years (2012 and 2013) reported in table 11.9, the number of wells fracture stimulated in the UB averaged 1010, and the two years with only partial reporting each were about half that amount. Uintah County, where most of the natural gas development is occurring, has generally had the greatest proportion of fracture stimulated wells, except for the first half of 2014 when Duchesne County took the lead. Only a small number of fracture stimulations of wells has occurred in Carbon or Grand Counties in the four years tabulated.

Table 11.10 provides a tally of the number of BW used in fracture stimulations of wells by county for the four years with data available for the UB, and shows that the two years with full reporting averaged about 10 MMB per year. Some of the wells tallied have had more than one fracture stimulation at a given time (multiple intervals), and some have been fracture stimulated more than once (multiple times in the same interval or subsequent stimulations of new intervals). If the second half of 2014 equals the first half of the year as reported to FracFocus, then the full year for 2014 may also entail over 10 MMBW use for fracture stimulations in the

UB. The annual water usage in fracture stimulations by county is also depicted graphically in figure 11.6.

Since the data reporting water used in fracture stimulations of oil and gas wells is not complete for all the years studied, one way to look for changes in usage from year to year is to convert the data to water used per well treated by dividing the total water used in a year by the number of wells fracture stimulated during that year. Table 11.11 shows that the BW per well used in fracture stimulations varies for each county and over time. Carbon County has the most variable water usage per well over time, ranging from none in 2014 to over 19,000 bbls per well for the two wells in 2013. The amount of water used per well for fracture stimulation for Duchesne County has been the most consistent over time averaging about 8665 bbls per well for the four years for which we have data. With only one full year and one partial year of data, and only five wells stimulated, Grand County does not have any discernable trend or consistency in terms of water usage per well. The water usage per well for fracture stimulation completions in Uintah County appears to be rising gradually over time, increasing from the average of 7778 bbls used per well in 2011 to the average of 12,760 bbls used in 2014. Many factors can contribute to changes in the amount of water used for fracture stimulating a well such as well depth, number or intervals stimulated, the thickness of the interval(s) stimulated, whether the well is vertical or horizontal, and the susceptibility of the reservoir rocks to fracturing. Also, in some instances it has been found that larger fracture stimulation treatments may be more effective than smaller treatments, which may cause water usage to increase over time.

Table 11.12 show that during 2013, water used in fracture stimulations in Uintah County varied based on the purpose of the well completed. The wells for this county for 2013 were divided into two classes, either gas (Greater Natural Buttes) or oil wells. Each category

cumulatively used about the same amount of water for fracture stimulations during 2013, but since there were more gas wells than oil wells, the amount used per well was about 28% more for oil wells than gas wells. Interestingly the amount of water used for fracture stimulations during 2013 in Duchesne County, where oil completions predominate, averaged 8807 bbls per well compared to an average of 12,089 bbls per well in Uintah County for the same year. Thus, even wells drilled for the same purpose can vary from county to county for the average amount of water used per well in fracture stimulations.

UINTA BASIN PETROLEUM-RELATED WATER HANDLING PRACTICES

Introduction

Water management/handling practices in the UB, Utah, cover a range of possibilities. Small operators are generally dependent on outside vendors to haul and dispose of produced water at commercial disposal wells or pits. Large operators commonly design and construct complex centralized water collection, handling, and disposal facilities that allow for minimizing trucking needs, capture and reuse of flow-back formation fracturing fluids, centralized facilities for treatment of produced water, and a series of injection wells or evaporation ponds for water disposal. Water treatments may include settling tanks which skim oil off the top and settle sediments at the base, oil-water separators, hydrocyclones, floatation cells, chemical flocculation of clays, and filtration systems (walnut shell, sock, or ceramic) before final disposal. To help

understand the range of operational practices used or possible we review the practices employed by various gas and oil operators from the UB in the following section. Other practices are employed in other states in the U.S. and no doubt some new practices that find success elsewhere may be tried in Utah in the future to see the same successes can be replicated here.

Current Practices of Selected Companies

Anadarko Petroleum/Kerr-McKee (Natural Buttes Gas Field)

Drilling and completion practices: Anadarko Petroleum received approval for full-field development from the BLM in 2012 (U.S. Bureau of Land Management, 2012b). For well drilling, Anadarko uses only closed-loop drilling procedures to ensure that no fluids are lost from the drill site and that other emissions are best contained (Kenny Gathings, Anadarko Petroleum, personal communication, November 2013). Air drilling is not used since dust from a site could not be completely contained. Drilling of a typical well might use between 3000 to 6000 gallons of water for a 9000- to 10,000-foot-deep well. As of mid-2014, Anadarko had 2796 gas wells (2679 producing, 92 shut-in, and 25 temporarily abandoned), 9 water disposal wells, and 1 water supply well in Uintah County. Anadarko has recently employed from one to four rigs to maintain its development schedule of 200 to 400 wells per year. At the end of 2014, Anadarko had reduced the number of drill rigs operating to one. As of mid-2014, the company also had 626 approved Applications for Permit to Drill (APDs) new wells, and had three locations where approved drilling operations had commenced, but had been temporarily suspended. For full field development, Anadarko anticipates drilling over 4700 new wells (Kenny Gathings, Drilling

Manager, Anadarko Petroleum, personal communication, November 2013). Assuming an average of 150 new wells per year, Anadarko will be adding these new wells for over 31 years, until about 2045, to finish drilling 4700 new gas wells at Natural Buttes field.

For gas well completions, Anadarko typically fracture stimulates the tight-sand reservoirs to increase gas-flow connectivity between the reservoir and the wellbore. Anadarko estimates that a single fracturing job would entail about 60,000 gallons (1430 bbls) of water (Kenny Warren, Anadarko Petroleum, personal communication, November 2013). This estimate reflects a single stage of fracture stimulation since reports by Anadarko to the Frac-Focus website (see http://fracfocus.org/) showed water volumes for an individual well ranging from 200,000 to 700,000 gallons per well, no doubt because some wells had multiple perforation segments (stages) that were individually fracture stimulated. Thus, to drill and complete a new gas well at Natural Buttes field could require from 203,000 to 706,000 gallons (4833-16,810 BW; 0.62-2.17 acre-feet). If we assume 150 new wells are drilled and fracture stimulated per year, then associated annual water usage for fracture stimulations could range from 30.45 to 105.9 million gallons (724,950-2,521,500 bbls; 93-325.5 acre-feet).

Water for fracture stimulation is contained on a well site in portable tanks of 500 to 1000 gallons. To reduce fresh-water consumption for fracture stimulations, Anadarko uses its Anadarko Completion Technology System (ACTS) to catch flow-back water from a series one to six of wells on a single pad in lined and netted pits. The pits allow the solid drill cuttings to settle out in the bottom and then the settled water is treated (generally with bleach) to kill bacteria and settle out iron. The treated flow-back water is transferred via aluminum pipe or truck to the next site for use in fracturing other wells. Piping by temporary surface lines is the predominant transfer method between a group of closely spaced wells to reduce truck traffic and

related emissions (figure 11.7); trucking is mainly employed where the pumping distance via pipe is prohibitively expensive. With a slight loss of fluid in each well, Anadarko (2015) needed to make up less than 10% of its water required for fracture stimulation from fresh-water sources and over 90% of its water used in fracture stimulations was recycled water, thereby reducing fresh-water usage and trucking costs. If annual water usage for fracture stimulations is estimated at 30.45 to 105.9 million gallons (see above paragraph), then if reuse is estimated at 90%, Anadarko's ACTS program will use 27.4 to 95.3 million gallons (0.65-2.27 million bbls) of flowback water annually and significantly reduce the use of freshwater needed for field development.

Rather than flaring gas during the flow-back phase of the well completion, Anadarko connects the well up to the gas sales pipeline as soon as possible. This practice avoids product loss due to flaring and its associated air emissions.

Produced water management practices: Anadarko has no use for the water produced from a well other than collecting the initial flow-back water portion from the fracture stimulation phase of well completion, which is reused at new wells for other fracture stimulations. Therefore, water produced with gas is considered a waste stream and Anadarko has determined that within its operating area the best and most cost effective way to handle to waste water is disposal in deep saline aquifers via Class II disposal wells. To handle the disposal of produced water from 2700+ existing wells and 4700+ future wells, Anadarko has designed and built an integrated field-wide water handling, treatment and disposal system for its produced water waste stream. In 2013, Anadarko had nine disposal wells, and eight water treatment facilities designed to handle 60,000 bbls of produced water per day, but at that time was handling in the range of 30 to 40,000

BPD (John Kynaston and Mike Merrill, Anadarko Petreoleum, personal communications, November 2013). According to the Record of Decision (ROD) document for the Greater Natural Buttes Final Environmental Impact Statement (EIS) (U.S. Bureau of Land Management, 2012c), full gas field development will entail an average annual produced water volume of 1385 acre-feet of water (10,745,338 bbls; 451,304,208 gallons), of which, Anadarko estimated 75% would be disposed of by underground injection, and 25% would be disposed by evaporation. Three of the water treatment facility sites have pits for evaporation and overflow capacity in case a disposal/treatment plant went offline. All of the water treatment and disposal well facilities are interconnected by a system of pipelines which can be controlled to move water to any water treatment site or disposal well should any one need to be taken off line for maintenance or repair. The UGS toured two of the eight water treatment facilities, Blue Feather and Pipeline, to get an understanding of the water treatment technologies employed in preparing the produced water for final disposal in an underground saline aquifer.

Anadarko's produced water disposal system network represents, particularly the Blue Feather site, the newest and best water treatment technology whereby even the truck unloading part of the facility offers a pretreatment separation of the water, other liquids and solids by pumping the off-loaded water through a centrifugal spiral that separates different densities of materials to the various water processing or product tanks on site. Liquid hydrocarbons go to the products tank, and clean water to the bulk disposal tank, and dirty water to the settling or Induced Gas-Flotation Tank (IGT) tanks. Water is trucked mainly from newly completed wells before they are fully connected to the water gathering system, or selected wells that periodically need to be disconnected from the water gathering system. A water treatment plants' first set of gun barrel tanks are simple gravity settling tanks where solids sink, and are collected from the

bottom, condensate hydrocarbon liquids are skimmed from the tops and the left over dirty water is sent to the intermediate IGT tanks for further cleaning. In the IGT tanks, gas is pumped into water at the bottom of the tank as small bubbles and the dirty water is introduced from the top of the tank at an angle in such a way as to create a downward spiraling of the fluid. This downward spiral reacts with the gas to float oil droplets off the top of the tank in a frothing action that further cleans the water from the initial gravity settling tanks before the water is sent to the final bulk storage tanks, where the water can be pumped to one of nine injection wells for ultimate disposal. When the water is pumped from the "bulk" water storage tanks to the disposal well it is sent through a system of 5-micron sock filters to further clean the water and help protect the disposal well and pipeline gathering system from corrosion and abrasion. The piping in the system is all stainless steel to handle the inherent high-salinity and corrosive nature of the produced water (John Kynaston and Mike Merrill, Anadarko Petroleum, personal communication, November 2013). Water can be sent from a water treatment site to any of the nine injection wells operated by Anadarko, and it meters the water sent from each treatment plant so that deliveries to each disposal well maintain a constant injection rate, or adjustments can be made to the injection rate to accommodate flows from one or several water treatment facilities. The maximum injection rate for each injection well is capped by the results of mechanical integrity tests performed on each injection well before it is put into service, and routinely performed every five years to test that the well is still in good working condition.

At the second water treatment site visited, Anadarko had a similar progressive system of treatment tanks installed with initial gravity settling tanks, and then "bulk" water holding and liquid-hydrocarbon condensate storage tanks. An intermediate IGT tank was tested at this site, but either because the water offloading system did not offer water pretreatment, or the delivered

water was somehow different, or some other reason, the IGT tanks did not work properly at this site but simply made a mixed suspension of oil in the water rather than actively separating the oil as expected. This second site also included a new solid "sludge" treatment set of tanks where the solids were heated and treated before landfilling to recover residual condensate product from the solids before ultimate disposal offsite. Anadarko had learned that the landfill operator was treating the solids before disposal and recovering the oil and decided to recover the product for themselves before landfilling the produced solids. This second water treatment site also included legacy evaporation/settling ponds that Anadarko had used previously for water handling and disposal. When water was pumped to the ponds it can be sent through a network of sock, walnut shell, and MyCelX coated filters to ensure that 99% of the oil is removed before the water enters the ponds. Anadarko is moving away from the use of open evaporation pits as a primary disposal method since they no longer find them an economic or environmentally acceptable water handling technique.

Expansion of the number of evaporation ponds and the use of water cannons on ponds has been discontinued. These practices were discontinued because the cannons floated on the ponds to spray water into the air to enhance evaporation frequently plugged and needed servicing, it was difficult to keep waterfowl off the ponds, filtering the water going into the ponds was costly, and open ponds (rather than closed tanks) allowed for more airborne hydrocarbon emissions than Anadarko preferred. Therefore, the evaporation ponds are mainly used for backup storage when the existing storage tanks and disposal wells are unable to handle all the produced water on a daily basis.

EOG Resources (Natural Buttes Gas Field)

Field development activities: EOG Resources operates the Chapita Wells unit of Natural Buttes gas field. For development work in the past few years, where practical, EOG has been drilling up to five directional wells per drill site to reduce overall footprint for roads, well pads, and collection lines in this unit. The number of producing gas wells EOG operated at the Chapita Wells unit was 1250 as of November 2014. In 2014, EOG also operated 10 active water disposal wells at the Chapita Wells unit of Natural Buttes gas field, 51 shut-in gas wells, and 68 plugged and abandoned wells, for a success ratio of over 99% of the wells drilled. EOG also had permits to drill another 275 gas wells. According to production records from the DOGM through June 2014, EOG's gas wells each averaged 70 MCFG and 13 BW per day during the first half of the year.

According to plans filed with the BLM, EOG hopes to drill up to 2808 new gas wells on its land holdings, and drilling and completion of each well could use up to 16,850 BW for a cumulative water requirement of 47,314,800 BW over the life of the project. EOG's plans to minimize fresh water usage in the drilling and completion of new wells by only using 12% from fresh water sources, and obtaining the remaining 88% from recycled water from the Bonanza power plant of Deseret Generation and Transmission. Assuming the drilling development period spans 15 years, then EOG could use 378,518 bbls of fresh water and 2,775,802 bbls of recycled power plant water annually.

Produced water management practices: In the past EOG has used commercial produced water disposal facilities, and it presently has regulatory approval to use commercial disposal facilities run by R N Industries in the Uinta Basin if necessary. In 2012, all of EOG's gas wells had

individual water holding tanks and the produced water was trucked to disposal wells or holding ponds that EOG operated at the Chapita Wells unit. In addition to disposal of produced water in its own disposal wells, EOG had disposed produced water at the Brennan Bottom commercial site located in section 19, T. 6 S., R. 21 E., SLBL&M, Uintah County. In 2013, when EOG only completed and hydraulically fractured one well due to low gas prices, its plan for an integrated liquids-gathering system (LGS) at the Chapita Wells unit was approved by the BLM (U.S. Bureau of Land Management, 2013a). Because mineral ownership differences preclude EOG from commingling the products from the Mesaverde and Wasatch reservoirs, EOG's new, centralized, LGS will only address the products from the Mesaverde reservoirs, whereas the fluids from the wells tapping the Wasatch reservoirs will still be stored in tanks at each well site until they are trucked to a disposal or marketing site. According to the April 2013 BLM ROD for the LGS (U.S. Bureau of Land Management, 2013a), EOG's proposed project would consist of an integrated system of buried pipelines connecting and coordinating the transport of hydrocarbon, and fresh and produced water, among Mesaverde gas wells, up to 14 centralized gas-processing plants, existing freshwater supply ponds, existing produced water disposal ponds, water disposal wells, and gas and oil sales points. The LGS system is planned to be connected to only about half of the wells in the field at full development. As of early 2015 at the Chapita Wells unit, EOG's three centralized LGS facilities simply separate produced water from salable hydrocarbons, and send the produced water to any of three produced water underground disposal facilities, or in an emergency to pond at the Red Wash site (section 2, T. 9 S., R. 22 E., SLBL&M, Uintah County), at the White River site, or ponds at its Coyote Wash disposal well facility (section 16, T. 9 S., R. 23 E., SLBL&M, Uintah County). The three existing and 11 proposed LGS and centralized gas processing facilities will reduce truck traffic and associated

emissions at the Chapita Wells unit, and through centralization create economies of operating scale in water handling that may allow EOG to experiment with further treatment and possible reuse of some produced water there.

According to EOG's website, the company is committed to actively managing and conserving water resources where it operates. For example, EOG continues to test water reuse technologies, take steps to minimize overall water usage in the drilling and completion of wells, properly dispose of produced water, evaluate alternative sources of water, and responsibly manage the water used, produced, and disposed of at its operations. In March 2014, EOG installed water treatment and reuse facilities at its Eagle Ford play development operations in west Texas. Perhaps in the future when natural gas prices rise, EOG will also test water reuse technologies in the Natural Buttes field area in combination with its recently completed centralized water handling system.

XTO Energy (Natural Buttes Gas Field)

Field development activities: XTO Energy purchased its holdings in the UB from Dominion Energy in July 2007, but development of these leases began as early as the 1950s. Through August 2014, XTO operated 571 gas and 5 oil wells in Uintah County, with the majority (500) in Natural Buttes gas field, and the remaining 76 producing wells scattered among Alger Pass (9), Fence Canyon (2), Hill Creek (51), Love (8), and Rock House (1) gas fields, and the Uteland Butte (1) and West Willow Creek (4) oil fields. In addition to these producing oil and gas wells, XTO had 42 shut-in gas wells and 1 shut-in oil well, 2 temporarily abandoned gas wells, 44 plugged and abandoned gas wells and 4 plugged and abandoned oil wells, and 4 water-disposal

wells in Natural Buttes gas field. According to DOGM records through August 2014, each of XTO's 576 Uintah County wells averaged about 0.6 BO, 71.8 MCFG, and 3.6 BW per day through the first eight months of 2014. In August 2014, XTO had permits to drill 83 new gas wells, 55 at Natural Buttes, 21 at Hill Creek, and 7 at Love fields.

Produced water management practices: According to the BLM's environmental assessment (U.S. Bureau of Land Management, 2013b) for XTO's planned infill development at the River Bend unit of Natural Buttes gas field, produced water and condensate are separated and stored in steel tanks at each well pad. Potential spills from the tanks are protected by containment dikes of compacted earth or steel to hold 110% of the largest tank on site. Currently, the water from each tank is pumped periodically as needed and transported to existing water-injection disposal wells in the River Bend unit area, or to permitted evaporative disposal sites. XTO disposes of the majority of the produced water (93%) via injection wells, with the remainder via evaporation (U.S. Bureau of Land Management, 2013b).

GASCO Energy (West Tavaputs Plateau Gas Development)

Field development activities: As of June 2012, GASCO's Uinta Basin natural gas development project EIS had been approved by the BLM, allowing for the drilling of nearly 1300 new wells from 575 well pads. GASCO Energy operated 137 wells, including 2 shut-in oil well and 7 shut-in gas wells, in the UB in 2014, distributed between seven different fields mainly in the area between Monument Butte and Natural Buttes fields along the Uintah-Duchesne County line (figure 1.1). The majority of GASCO's wells are in the Pariette Bench (56 wells), Uteland Butte

(28 wells), and 8 Mile Flat North (26 wells) fields, with a lesser number of wells in the 8 Mile Flat (11), Gate Canyon (5), Middle Bench (2), and Natural Buttes (1) fields. The 129 producing wells are mainly for gas (113), with only 16 producing oil wells. During 2014, GASCO had started drilling, but not completed, 12 new gas wells, and had approved APD's another 30 gas wells, 6 oil wells, and 1 water disposal well. Within its lease holdings, GASCO had drilled and abandoned 9 wells, indicating a drilling success rate of nearly 94% of the wells drilled.

In 2014, GASCO's operating wells produced 49,289 BO, 4.495 BCFG, and 466,968 BW through August of that year. In August 2014, GASCO's 136 actively producing wells individually averaged 1.7 BO, 155.9 MCFG, and 16.2 BW per day.

Produced water management practices: As part of the BLM ROD on the GASCO final EIS (U.S. Bureau of Land Management, 2012c), GASCO had agreed to:

(1) institute an aquifer/groundwater monitoring plan to routinely check for evidence of any contamination from oil and gas development activities over the life of the project;

(2) investigate the use of recycled water for drilling and completion operations;

(3) use a closed loop drilling system in areas with porous soils over fractured bedrock when drilling through a DWSP zone or Sole Source Aquifer, or in areas with shallow groundwater; and

(4) limit the new water evaporation facility to 12 pits totaling 78 acres (proposed locations in either section 21, T. 9 S., R. 18 E., SLBL&M, Uintah County, or section 13, T. 4 S., R. 3W., UBL&M, Duchesne County), and five years after the ROD re-evaluating the need for evaporation ponds and possibly then moving to alternate means such as disposal wells.

In July 2013, the BLM approved the permit to drill GASCO's first salt (produced) water disposal well, which is to be drilled on an existing well pad in section 20, T. 9 S., R. 19 E., SLBL&M, Uintah County, in Pariette Bench field, Uintah County (figure 11.2). A class II injection well permit had been received from the EPA for the well, which would dispose produced saline water into sands of the Douglas Creek Member in the lower part of the Green River Formation (figures 2.28 and 7.7). The proposed disposal sandstone units would have to have their water tested to see that they contains at least 10,000 ppm TDS or more. The water disposal facilities associated with the well were planned to include two 500-bbl tanks to hold produced water delivered to the site, and containment berms around the tanks to conform to EPA's spill prevention, control, and countermeasure regulations. However, the application for the permit to drill was rescinded as of January 8, 2015, due to lack of activity at the site. Complicating GASCO's decision to use disposal wells instead of evaporation ponds, is the fact that produced water from the Mesaverde Group and Wasatch Formation often has in excess of 50,000 ppm TDS and contains major scaling constituents of calcium and iron carbonate (U.S. Bureau of Land Management, 2012c). In wells producing from these two reservoirs where their waters are mixed, GASCO has been forced to insert a capillary string next to the production string of tubing to allow scale inhibitors to be continuously pumped to the bottom of the wells to

provide scale protection throughout the wellbores. According to the BLM (U.S. Bureau of Land Management, 2012c), GASCO has been unable to dispose of its produced waters at other operator's disposal wells due to the other owner's concerns that scale would plug the accepting formations. Before drilling its own disposal well, GASCO has been using either its own Desert Spring evaporation facility (located in section 36, T. 9 S., R. 18 E., SLBL&M, Uintah County), or using other state-approved UB commercial disposal facilities, primarily the one operated by Integrated Water Management, LLC (section 30, T. 2 S., R. 4 W., UBL&M, Duchesne County), or various commercial sites operated by LaPoint Recycle and Storage (section 12, T. 5 S., R. 19 E., SLBL&M, Uintah County; temporarily closed as of December 2014), R N Industries (sections 4 and 9, T. 2 S., R. 2 W, UBL&M, Duchesne County), and Western Water Solutions (sections 9 and 10, T. 4 S., R. 1 W., UBL&M, Duchesne County) to dispose of its produced water.

Enervest Operating, LLC (West Tavaputs Plateau Gas Development)

Field development activities: Bill Barrett Corporation (BBC) purchased leases in 2002 on the West Tavaputs Plateau of the southwestern UB, which had been originally drilled as far back as the 1960s, and discovered new potential in the area around 2005. An EIS for BBC's full field development of 596 new wells on 85 new and 57 prior drill pads was approved by the BLM in July 2010 (U.S. Bureau of Land Management, 2010). Enervest Operating, LLC assumed ownership of the project from BBC in early 2013 and as of August 2014, operated 327 gas wells, including 9 shut-in gas wells, 6 that still had no reported production, and 4 disposal wells on the West Tavaputs Plateau (figure 11.2). These wells are found in northeastern Carbon County and

are predominantly distributed between three different fields: Nine Mile Canyon (197 wells), Peters Point (112 wells), and Stone Cabin (9 wells) fields (figure 11.2). Only nine wells were listed in 2014 with undesignated as a field name. The 308 wells with reported production are all classified as gas wells. In 2014, Enervest had started drilling, but not yet completed, 33 new gas wells, and had approved APDs another 164 more gas wells. Within Enervest's lease holdings, past and present operators have drilled and abandoned 37 wells, indicating a success rate of about 90% of the wells drilled to date.

In August 2014, Enervest's operated wells generated 4144 BO (condensate), 1.831 BCFG, and 48,690 BW for the month. Individually, each of Enervest's 308 actively producing wells averaged 0.4 BO, 191.7 MCFG, and 5.1 BW per day for the month of August 2014.

Future development will consist of multiple wells per drill pad, up to eight, drilled and completed from a single well pad, in order to minimize the surface disturbance of individual well pads and access roads. This development scheme will also reduce truck traffic in the area for well servicing.

Produced water management practices: Before October 2008, when the first deep-injection water disposal well was completed, water production from the current Enervest leases was stored at individual well sites in storage tanks and trucked to commercial disposal operations, such as the RNI disposal site near Roosevelt, Utah, as mentioned in a 2002 annual waste management plan filed with DOGM. Subsequently, more deep-injection water disposal wells have been completed in the West Tavaputs Plateau area, one in September 2010, and one each in March and October 2013. Although one of these wells initially attempted disposal in the Castlegate Sandstone of the Mesaverde Group (figure 2.13), all now dispose of water in the Wasatch

Formation, one of the hydrocarbon producing formations. To avoid impairing hydrocarbon production from the Wasatch, the deep-injection water disposal wells are located at least 0.5 miles outside the structurally controlled producing areas. These disposal areas are structurally downdip from the gas at the top of the anticlinal traps and in the water legs of the reservoirs.

Under the stipulations for full field development provided in the BLM's EIS and ROD (U.S. Bureau of Land Management, 2010), the field operator is committed to: (1) protect groundwater in the 100-year floodplain of the valley bottoms or other sensitive sites within the development area by using closed-loop drilling techniques for more completed management of drilling and completion fluids; (2) reduce the amount of road and pad disturbance by drilling up to eight wells from a single pad, thereby eliminating 356 pads and 85 miles of access roads that would have been required for one well per pad; (3) where in-ground pits are used, they will be lined by an impermeable layer to prevent leakage of drilling fluids and the company will have an approved Spill Prevention, Control, and Countermeasure Plan; (4) produced water and condensate will be stored in 400-bbl tanks on the well pads and generally connected via pipelines to centralized storage and disposal facilities to avoid most truck traffic and potential leakage at loading and unloading truck transfer points; (5) any shallow fresh water (<10,000 TDS) zones encountered during drilling will be isolated and protected by suitable casing and cement from lower producing horizons, and the company will sample groundwater at three monitoring well sites four times a year to test for any potential leakage from producing wells; and (6) disposal of produced water will only occur at properly tested, permitted, and inspected company-owned or commercial Class II injection sites.

Newfield Exploration (Monument Butte Oil Field)

Field development activities: As of November 2014, Newfield Exploration operated approximately 3395 oil and gas wells in Monument Butte field area (figure 1.1) and had plans to add an addition 5750 new wells. Development could entail drilling and completion of up to 360 new wells per year until the resource base is fully developed. Under this maximum drilling rate scenario, construction, drilling, and completion of the 5750 new wells would encompass approximately 16 years. The annual rate and total number of wells actually drilled will depend largely on outside factors such as production success, engineering technology, reservoir characteristics, drilling economics, commodity prices, rig availability, and lease stipulations. The anticipated life of an individual well is 20 to 30 years, and the anticipated time it would take for field abandonment and final reclamation is five years. Therefore, the anticipated life of the Monument Butte project could be up to 46 years.

Produced water management practices: Newfield recycles its produced water through water treatment plants and then reuses the produced water for EOR waterflood. Produced water is either trucked directly to the water treatment facilities or initially processed through new centralized Gas-Oil-Separation (GOS) plants before being piped to the water treatment facilities. Starting in November 2012, Newfield opened its first GOS plant, designed to process up to 30,000 BPD of produced water and oil mixture (emulsion) from more than 200 wells. At the GOS plant, the produced oil is separated and prepared for sale, while the water is sent to the Sand Wash plant for final cleansing and recycling. This GOS facility, along with an associated gathering system, allows Newfield to collect water and oil from over 200 wells at a single delivery point, and eliminate the need for up to 300 truckloads of produced water per day to the

Sand Wash water treatment plant. The GOS facility reduces VOCs and nitrogen oxides (NOx) emissions as well as reducing truck traffic in the field.

The Sand Wash water treatment facility was built in 2010 and commissioned in April 2011. The Sand Wash plant includes two processes for treating produced water that is trucked in or water delivered via pipeline from a nearby GOS facility including: (1) conventional gravity separation technology to handle up to 10,000 BW per day, and (2) technology designed and run by Environmentally Clean Systems (ECS), a joint venture of Dickinson, Texas-based MPR Services and Salt Lake City, Utah-based Jet Oil Solutions according to the Houston Chronicle (May 28, 2012), which uses an electrocoagulation process to treat up to 20,000 bbls per day of water. Prior to entering the ECS system, Newfield may first run the water through a series of gun-bbl tanks to perform conventional separation of solids and hydrocarbons from the water. The ECS process involves additional cleaning of the water by passing it through tanks containing electrified plates to form ions in the water that attach themselves via electrocoagulation to contaminants, such as Ca, Fe, Ba, Mn, and S, clustering these contaminants into larger bundles of particles that are screened out of the water. Prior to development of its Sand Wash facility, injection facilities did not have the ability to treat pit water, flow-back water from hydraulic fracturing activities, or production water high in iron sulfide. With the completion of its Sand Wash facility in 2011, Newfield now treats produced water, removing oil and gas byproducts and removing solids, so it can be re-injected into the oil-producing formation to EOR and also to conserve valuable fresh water resources. Assuming each waterflood well requires 100 BW per day, the Sand Wash water treatment facility provides for water treatment and supply for about 200 waterflood wells per day.

In 2014, Newfield completed another water treatment facility named Beluga (figure 11.8), which employs a different water cleaning systems designed and operated by Veolia Water Solutions and Technologies (2014). The Veolia system combines a multi-flow chemical (alkali) softening and flocculation process with filtration through silicon-carbide ceramic filters (figure 11.9) to prepare the water for recycling in the waterflood EOR process. This system includes softening, oil and grease removal, as well as removal of suspended solids and scale formers in a compact, modular design. The flocculated dense solids are removed in a settling zone using lamella plates. Excess solids are intermittently purged from the process for dewatering and subsequent landfill disposal. The solids from the ceramic ultrafiltration unit are continuously recycled back to the crystallization tank of the multi-flow unit, providing seed for further crystal growth. The treated alkaline water is neutralized with acid to prepare it for reuse in the EOR, waterflood recovery operations, reducing fresh water demand. Finally for waterflooding operations, a de-aeration gas stripper removes dissolved oxygen from the treated water, preventing corrosion in the injection piping network in the oil field. (See table 11.13 for Veolia's reported feed water and output processed water quality results.) Some benefits of Veolia's trade-marked "removal of oil and suspended solids" (ROSS) system are:

- effective removal of scale formers (hardness, silica, iron, barium, strontium);
- effective removal of particulates (oil, solids, bacteria, algae, clay);
- high system-recovery rates (>98%), minimizing liquid waste generated;

- excellent thermal resistance (up to 210°F); and

- modular, shop-fabricated, pre-piped, pre-wired treatment system.

Preliminary operational results of the new Beluga water-treatment plant, which can process up to 18,000 BPD, are reported to have been very positive for Newfield. Assuming each waterflood well requires 100 BW per day, the Beluga water-treatment facility provides water for another 180 waterflood wells per day.

Following treatment at a water-recycling plant, initial water storage would be at on-site tanks before transfer by pipeline to one of the central water injection facilities: Ashley, Monument Butte, Jonah, or Beluga for waterflood injection into approved Class II wells to enhance Newfield's EOR secondary oil recovery project. Water pumped from a treatment plant is passed through sock filters before going to a re-injection site.

When the BLM finally approves a plan of operations for full field development, perhaps in 2015, Newfield plans to construct eight or more centralized GOS plants and six or more water treatment plants to allow recycling of produced water for reuse in EOR, waterflood operations to cover the water needs for about 2200 approved, Class II, waterflood injection wells, and reduce truck traffic needed to move production fluids within the greater Monument Butte field area. Construction of four to six water pump stations will also be needed to move the water around the field from production well to processing and treatment plants, and back to an injection well. Produced water that cannot be cleaned to meet waterflood quality standards will be disposed at Newfield's Pariette Bench Unit No.4 disposal well (; section 7, T. 9 S., R. 19 E., SLBL&M,

Uintah County, API No. 43-047-15681), its sole water disposal well, or at other State of Utah-approved surface disposal facilities (U.S. Bureau of Land Management, 2013c).

Opportunities for Water Reuse in Utah

The greatest opportunities for water reuse of produced water is within the petroleum industry itself, and these opportunities are already being used to some extent as explained in the discussions above of the individual Utah petroleum operator's practices. Produced water is reused by Utah gas producers for drilling and well completions, and by Utah oil producers for EOR waterflooding operations. However, as has been found in studies elsewhere, more could be done to encourage the sharing of water and treatment options among petroleum companies (Colorado Energy Office, 2014). The Colorado study found the following industry concerns about produced water reuse that would also be present with Utah's industry:

(1) the desire for produced water reuse technologies to be economically practical for energy companies to employ;

(2) the desire for regulatory flexibility in terms of options for produced water reuse and disposal, particularly in light of the variability in water quality, supply, and demand over the life of a well or field, and from reservoir to reservoir;

(3) the desire for regulatory predictability to enable energy companies to make long-term plans and investments in produced water sharing and reuse;

(4) the desire to find ways to facilitate the pooling of produced water supply and demand among smaller operators to allow them to achieve the economies of scale needed to enable produced water reuse; and

(5) the desire to find economical and environmentally acceptable water storage and transport means to allow operators producing excess water to efficiently meet the needs of operators requiring water.

To address these industry concerns and promote further produced water reuse will require the future collaboration of industry, state and federal regulators, and the general public.

In addition to the reuse of produced water within the energy industry in the UB, there are other wastewater streams that could be reused in petroleum development activities there to reduce the use of fresh water supplies. XTO Energy has proposed making use of some industrial wastewater from the nearby Bonanza electric generation plant for future well drilling and completion operations at its Chapita Wells unit of Natural Buttes field, and other industrial wastewater streams might be available for reuse by Utah's petroleum industry.

Another potential source of wastewater for reuse by the petroleum industry in the UB would be seven publicly operated wastewater treatment facilities located in Duchesne and Uintah Counties, which cumulatively processed 30.3 MMBW (1273.4 million gallons) per year in 2004 according to the Utah Division of Water Resources (2005). The list of these facilities and their average annual flow is provided in table 11.14.

The reuse of municipal waste water by the petroleum industry would likely be considered a Type II reuse, where human exposure is unlikely. Such water is not required to be cleaned to the same level as water used where human exposure is likely. While the TDS content of Type II water is low, Type II water would probably need minor additional petroleum industry treatment to eliminate bacteria that might lead to hydrogen sulfide generation in the reservoir environment. For the municipal waste water to be reused by the petroleum industry the following factors would be considered by the State of Utah before approval: (1) the point of discharge must be changed, (2) a change application must be approved if the new water use is inconsistent with the underlying right, and (3) the petroleum industry's reuse of municipal waste water may be viewed as a consumptive one, which could diminish the amount of water that can be used since it will not be returned to the source (Utah Division of Water Resources, 2005; Western Energy Alliance, 2014). Factor 3 could limit the amount of municipal waste water available for petroleum industry reuse.

Best Water Handling Practice Recommendations

Based on the discussions above, it appears that the best water handling practices in the UB vary depending on the size of the field or unit being developed, whether the product is gas or oil, the completion techniques and well spacing employed in field development, and the reservoir rocks being developed and their varying associated water characteristics. According to the EPA (CDM Smith, 2012) the best approach to produced water treatment and management must balance factors such as produced water quality, simplicity of operations, treatment objectives, and cost. Thus, no single set of best management practices can be advocated or applied across

the entire UB. The State of Utah's goals in managing the use and disposal of water associated with gas and oil development in the UB can be summarized in the following guidelines:

(1) protect the Class I, II, and III water (pristine, drinking water and limited use classes with less than 10,000 TDS) from contamination as a result of activities associated with gas and oil development;

(2) encourage companies to minimize the use of Class I through III waters in oil and gas development;

(3) encourage companies to reuse water employed or produced in petroleum development activities; and

(4) encourage petroleum company reuse of suitable available waste-water streams, such as power plant or other industrial waste water and municipal water treatment plant effluent, in petroleum development activities.

The State of Utah adequately protects Class I, II, and III waters through a variety of regulatory efforts administered by the DOGM, Utah Division of Water Resources, Utah Division of Water Rights, and UDWQ, as well as companion federal regulatory programs in the BLM and EPA. These regulations control such petroleum development activities as well siting and spacing, well and production facilities construction approval and oversight, production facilities inspection and monitoring, safe handling of petroleum products and waste streams, and proper

well abandonment and field reclamation oversight (Ground Water Protection Council, 2009). Such regulations are periodically reviewed and updated to allow for adaptive management as a result of the development of newer or improved best management practices and to respond to the implementation of new technologies, such as the use of hydraulic fracturing.

Regulatory agencies are encouraging petroleum development companies to reuse drilling wastes such as produced water (Environmental Protection Agency, 2008). However, many of the best management practices are practical only when the developments in an area reach a critical size where implementing centralized water collection, handling, treatment, and reuse or disposal achieves the economies of scale to become cost effective. At the large greater Monument Butte oil field area, Newfield Exploration has implemented centralized water gathering and treatment facilities that allow most of the produced water to be reused in EOR, waterflooding operations, reducing fresh water use by up to 10 MMBW in 2014. At Natural Buttes gas field, Anadarko Petroleum has developed the ACTS program to recover water used in hydraulic fracturing and reduce fresh water use by 90%, resulting in a 2014 savings of up to a couple MMB of fresh water used for hydraulic fracturing. Also, EOG's plans to minimize fresh water usage in the drilling and completion of new wells at the Chapita Wells unit of Natural Buttes field by only using 12% of its water needs from fresh water sources, and obtaining the remaining 88% from recycled water from the Bonanza power plant of Deseret Generation and Transmission. Assuming the EOG's future drilling development period spans 15 years, then EOG might use 378,518 bbls of fresh water and 2,775,802 bbls of recycled power plant water annually for field development drilling, again reducing fresh water usage by a few MMB per year. As the larger and more developed areas of the UB test and find economic ways to handle and reuse produced water for drilling, completion, or EOR practices, these methods will likely be

adopted by smaller operators as their fields grow, or perhaps smaller operators may join together to unitize operations into larger operating areas, and allow economies of scale to permit centralized water treatment and handling to be implemented elsewhere in the basin. At the same time, competition among petroleum service companies that see a growing market in offering cost-effective centralized water treatment, handling, or disposal services will likely lead to reduced costs associated with produced-water management and make these services more widely available to small and large petroleum companies in the UB and elsewhere in the U.S.

SUMMARY

The management of produced water associated with petroleum development in the Uinta Basin of Utah can be summarized in the following eleven points.

(1) Produced water management in the UB has evolved over time from very little government oversight prior to 1955, to basic efforts at the conservation of resources in the period from 1955 to late 1970, and finally to increasingly detailed and complex regulation since the creation of the EPA in December 1970.

(2) Produced water volumes from petroleum development in the four-county UB study area have increased over the last seven years (2008-2014) from 86 to 116 MMB per year.

(3) Current water management practices used by petroleum companies in the UB, in decreasing order of usage, include disposal in deep injection wells, reuse in EOR waterflood, delivery to evaporation ponds for disposal via evaporation, and reuse in hydraulic fracturing.

(4) Disposal of produced water in deep injection wells has increased from 43 to nearly 68 MMB per year from 2008 through 2014; the corresponding number of deep disposal wells has increased over that same period from 56 to 92.

(5) The amount of produced water delivered to commercial and private evaporation ponds has varied from 11.9 to 17.3 MMB over the four-year period for which records were available from 2010 through 2013, and averaged about 13.7 MMB per year.

(6) The amount of water used in EOR waterflood projects has increased from over 25 to over 44 MMBW per year from 2008 through 2014. With the unitization of 19 smaller waterflood projects into one large Greater Monument Butte unit by Newfield in 2010, the reuse of produced water for EOR was implemented in a large way allowing Newfield to reuse up to 10 MMB of produced water in 2014 for its waterflood needs. One approach that should be investigated in detail is to transport the excess produced water from the gas fields in the eastern part of the basin for use in waterflooding in the oil fields of the central part of the basin.

(7) Anadarko fully implemented the ACTS technology at its greater Natural Buttes gas operations in 2010, and as of 2014 was claiming it recycled nearly 100% of the water it recovers after the hydraulic fracturing process and reuses it in new well-completions, which conserves fresh water and reduces truck traffic. On average this reuse is estimated involve about 1.5 MMB of flow-back produced water.

(8) As of late 2014, EOG's plans to minimize fresh water usage in the drilling and completion of 2808 new wells by only using 12% from fresh water sources, and obtaining the remaining 88% from recycled water from the Bonanza power plant of Deseret Generation and Transmission. Assuming the drilling development period spans 15 years, then EOG could eliminate 2,775,802 bbls of fresh water use annually by substituting recycled power plant water.

(9) The estimated disposition of the 116 MMB of produced water from the four-county study area for 2014 is as follows:

- 68 MMB (58.6%) to disposal wells,
- 24 MMB (20.7%) used for EOR,
- 13.7 MMB (11.8%) sent to evaporation ponds,
- 1.5 MMB (1.3%) reused in hydraulic fracturing, and

- 8.8 MMB (7.6%) lost to evaporation.

(10) Regulatory agencies in Utah are encouraging petroleum development companies to reuse drilling wastes such as produced water to reduce fresh water consumption; however, many of the best management practices are practical only when the developments in an area reach a critical size where implementing centralized water collection, handling, treatment, and reuse or disposal achieves the economies of scale to become cost effective.

(11) Produced water management in Utah is a large and dynamic management challenge that requires a flexible, adaptive regulatory scheme to meet ever changing conditions and technologies in fields of variable size and with differing product and waste streams.

CHAPTER XI FIGURE AND TABLE CAPTIONS

Figure 11.1. Graph of cumulative number of produced-water disposal wells in the Uinta Basin, from 1968 through 2014 (source: Division of Oil, Gas, and Mining website).

Figure 11.2. Location of water disposal wells by field in the Uinta Basin. Number of disposal wells shown in parentheses beneath field names.

Figure 11.3. Location of enhanced-oil recovery, waterflooding projects and wells in the Uinta Basin.

Figure 11.4. Water evaporation ponds in the Uinta Basin. A – Spray evaporation system at Brennan Bottom disposal facility evaporation pond, Uintah County. B – Liner system and levee at the Sand Pass Ranch evaporation pond, Duchesne County. Photos courtesy of Brad Hill, Utah Division of Oil, Gas, and Mining.

Figure 11.5. Location of water evaporation ponds (blue squares) in the Uinta Basin. From Utah State University, 2013.

Figure 11.6. Graph showing the annual amount of water used in fracture stimulations by county for the Uinta Basin from 2011 through 2014 (note: 2011 and 2014 are only partial year tallies).

Figure 11.7. Example of Anadarko's Completion Technology System (ACTS) at Natural Buttes field showing closely spaced drilling pads containing multiple wells and temporary surface pipeline to transport and reuse hydraulic fracturing flow-back fluids. Illustration courtesy of Anadarko Petreolum.

Figure 11.8. Exterior view of water and oil storage tanks at Newfield's Beluga water treatment facility. Photo from article in the Salt Lake Tribune, August 19, 2012, by Dawn House.

Figure 11.9. Schematic diagram of the Newfield Beluga plant's Veolia water-treatment process with water moving from left to right; note M = mixer. Multiflo and CeraMem are registered trade names of Veolia Water Solutions and Technologies (source: veoliawaterstna.com/news-resources/information-files/ross-flowback-produced-water.htm webpage accessed October 2014).

Table 11.1. Uinta Basin active wells and annual produced water volumes by county, 2008–2014 (in million barrels).

Table 11.2. Uinta Basin annual produced water volumes per well by county, 2008–2014.

Table 11.3. Uinta Basin disposal-well numbers with active disposal volumes by county, 2008–2014.

Table 11.4. Uinta Basin disposal well injection volumes, 2008–2014 (in million barrels).

Table 11.5. 2014 Uinta Basin enhanced-oil recovery water injection and produced water volumes (in millions of barrels).

Table 11.6. Uinta Basin enhanced-oil recovery water injection volumes, 2008–2014 (in millions of barrels).

Table 11.7. Produced water delivered to Uinta Basin evaporation ponds, 2010–2013 (barrels).

Table 11.8. Utah Division of Oil, Gas, and Mining approved commercial disposal facilities as of June 9, 2015.

Table 11.9. Annual number of wells with fracture stimulations in the Uinta Basin by county for the years 2011–2014 (note: 2011 is a partial year and 2014 is for the first half only).

Table 11.10. Annual number of barrels of water used in fracture stimulations in the Uinta Basin by county for the years 2011–2014 (note: 2011 is a partial year and 2014 is for the first half only).

Table 11.11. Annual number of barrels of water used per well in fracture stimulations in the Uinta Basin by county for the years 2011–2014 (note: 2011 is a partial year and 2014 is for the first half only).

Table 11.12. Annual number of wells fracture stimulated, barrels of water used in stimulations, and the number of barrels used per well in Uintah County for the year 2013.

Table 11.13. Veolia's reported processing performance data for waterflood applications.

Table 11.14. Publicly operated waste water treatment plants in Duchesne and Uintah Counties, Utah and their average annual flow in barrels per year (note: 1 barrel equals 42 gallons).

Table 11.1. Uinta Basin active wells and annual produced water volumes by county, 2008–2014 (in million barrels).

	2008		2009		2010		2011		2012		2013		2014	
County	# of Wells	Bbls	# of Wells	Bbls	# of Wells	Bbls	# of Wells	Bbls	# of Wells	Bbls	# of Wells	Bbls	# of Wells	Bbls
Uintah	5612	47.91	5837	46.46	6182	51.51	6564	52.84	7055	48.61	7519	53.56	7797	61.33
Duchesne	1981	20.93	2062	21.39	2340	24.21	2611	29.74	2841	34.91	3093	39.14	3340	43.44
Carbon[1]	899	17.31	942	19.21	967	17.47	1050	16.94	1090	14.07	1084	12.37	1099	11.21
Grand[2]	578	0.05	578	0.03	567	0.03	565	0.04	572	0.03	556	0.08	544	0.24
TOTAL	9070	86.20	9419	87.09	10,056	93.22	10,790	99.56	11,558	97.62	12,252	105.14	12,780	116.23

[1]includes some CBM wells

[2]includes some Paradox Basin wells

Table 11.2. Uinta Basin annual produced water volumes per well by county, 2008–2014.

	2008	2009	2010	2011	2012	2013	2014
County	Bbls/well	Bbls/well	Bbls/well	Bbls/well	Bbls/well	Bbls/well	Bbls/well
Uintah	8537	7960	8332	8050	6890	7124	7866
Duchesne	10,565	10,373	10,346	11,390	12,288	12,653	13,007
Carbon[1]	19,255	20,393	18,066	16,133	12,908	11,411	10,202
Grand[2]	87	52	53	71	52	135	447
TOTAL	38,444	38,778	36,798	35,644	32,139	31,322	31,522

[1]includes CBM wells

[2]includes some Paradox Basin wells

Table 11.3. Uinta Basin disposal-well numbers with active disposal volumes by county, 2008–2014.

	2008	2009	2010	2011	2012	2013	2014
County	# of Wells	# of Wells	# of Wells	# of Wells	# of Wells	# of Wells	# of Wells
Uintah	15	26	29	29	16	30	31
Duchesne*	23	23	24	28	27	28	38
Carbon*	18	19	20	19	19	20	21
Grand	0	0	1	1	1	1	2
TOTAL	56	68	74	77	63	79	92

* includes CBM disposal wells

Table 11.4. Uinta Basin disposal well injection volumes, 2008–2014 (in million barrels).

	2008	2009	2010	2011	2012	2013	2014
County	**Bbls**	**Bbls**	**Bbls**	**Bbls**	**Bbls**	**Bbls**	**Bbls**
Uintah	10.67	12.46	20.27	23.53	22.21	23.68	26.81
Duchesne*	16.34	16.64	16.73	20.78	24.47	28.06	28.36
Carbon*	16.06	20.75	18.47	16.81	14.68	12.97	12.05
Grand	0.00	0.00	0.00	0.13	0.19	0.17	0.33
TOTAL	43.07	49.85	55.47	61.26	61.54	64.88	67.55

* includes CBM disposal wells

Table 11.5. 2014 Uinta Basin enhanced-oil recovery water injection and produced water volumes (in millions of barrels).

Project Name (oil field)	Project Number	County	# of Wells	Injected Water 2014	Produced Water 2014	Short/ Excess 2014
Antelope Creek	390	Duchesne	109	1.596	1.412	-0.184
Brundage Canyon	700	Duchesne	9	0.258	1.838	1.580
Uteland Butte	338	Duchesne	2	0.004	0.100	0.096
Greater Monument Butte Unit	398	Duchesne-Uintah	1347	35.747	10.704	-25.043
Calf Canyon (Left Hand Canyon)	360	Grand	2	0.009	0.000	-0.009
Brennan Bottom	490	Uintah	2	0.030	0.223	0.193
Coyote Basin	350	Uintah	2	0.000	0.010	0.010
Duck Creek (Pariette Bench)	370	Uintah	5	0.027	0.440	0.412
Glen Bench Enh. Rec. (White River)	480	Uintah	5	0.369	0.085	-0.285
Gypsum Hills	300	Uintah	11	0.206	0.142	-0.064
Horseshoe Bend	530	Uintah	1	0.000	0.078	0.078
Leland Bench	600	Uintah	1	0.090	1.533	1.443
Red Wash	140	Uintah	52	3.019	4.533	1.514
Walker Hollow & Pearl Broadhurst	190 & 590	Uintah	16	1.669	1.719	0.050
Wonsits Valley	230	Uintah	22	1.261	2.089	0.828
TOTAL			1586	44.286	24.907	-19.379

Source: Division of Oil, Gas, and Mining website

Notes:

(1) Shortages are made up with fresh water supplies.

(2) Excesses are disposed in deep wells or evaporation ponds.

(3) 1 barrel = 42 gallons

Table 11.6. Uinta Basin enhanced-oil recovery water injection volumes, 2008–2014 (in millions of barrels).

Enhanced-Oil Project Name	County	2008	2009	2010	2011	2012	2013	2014
Antelope Creek	Duchesne	1.88	1.71	1.48	1.20	1.25	1.40	1.60
Brundage Canyon	Duchesne	0.00	0.02	0.17	0.36	0.74	0.37	0.26
Uteland Butte	Duchesne	0.04	0.03	0.01	0.03	0.03	0.01	0.00
Greater Monument Butte	Duchesne-Uintah	10.71	11.08	15.12	16.55	22.26	29.96	35.75
Calf Canyon	Grand	0.00	0.00	0.00	0.00	0.00	0.00	0.01
Brennan Bottom	Uintah	0.09	0.08	0.06	0.07	0.04	0.04	0.03
Coyote Basin	Uintah	0.00	0.00	0.00	0.00	0.00	0.00	0.00
Duck Creek	Uintah	0.00	0.28	0.13	0.05	0.06	0.05	0.03
Glen Bench (Enhanced Recovery)	Uintah	0.44	0.42	0.42	0.47	0.43	0.38	0.37
Gypsum Hills	Uintah	0.35	0.25	0.38	0.25	0.36	0.24	0.21
Horseshoe Bend	Uintah	0.00	0.00	0.01	0.00	0.02	0.11	0.00
Leland Bench	Uintah	0.01	0.03	0.03	0.07	0.11	0.11	0.09
Pearl Broadhurst	Uintah	0.16	0.13	0.13	0.14	0.11	0.11	0.15
Red Wash	Uintah	8.05	4.87	4.33	3.94	3.39	3.00	3.02
Walker Hollow	Uintah	1.30	1.21	1.25	1.24	1.29	1.31	1.52
Wonsits Valley	Uintah	2.41	2.72	2.07	1.96	1.37	1.32	1.26
TOTAL		25.45	22.82	25.59	26.33	31.46	38.40	44.29

Note: volumes in millions of barrels of water

Table 11.7. Produced water delivered to Uinta Basin evaporation ponds, 2010–2013 (barrels).

Type	2010	2011	2012	2013
Commercial	9,076,507	7,196,591	12,495,939	8,569,282
Private	4,569,698	4,704,461	4,759,001	3,678,693
TOTAL	13,646,205	11,901,052	17,254,940	12,247,975

Table 11.8. Utah Division of Oil, Gas, and Mining approved commercial disposal facilities as of June 9, 2015.

Type/Operator	Sec.	Township	Range	County	Facility/Area
*/Brennan Bottom Disposal	19	06 South	21 East	Uintah	12 Mile Wash
- /Brennan Bottom Disposal	09	09 South	22 East	Uintah	Glen Bench
*/Dalbo, Inc.	35	5 South	20 East	Uintah	Ace Disposal
	& 2	6 South	20 East		
*/Dalbo, Inc.	5	9 South	22 East	Uintah	Glen Bench
- /Danish Flats Env. Services	8	20 South	24 East	Grand	Danish Flats
- /Eastern Water Solutions	12	6 South	19 East	Uintah	EWS E. Gusher
*/Integrated Water Management, LLC	30	2 South	4 West	Duchesne	IWM/N. Blue Bench
*/Iowa Tanklines, Inc.	30	4 South	2 West	Duchesne	Pleasant Valley
*/LaPoint Recycle & Storage	12	5 South	19 East	Uintah	LaPoint
- /Monarch Natural Gas, LLC	36	9 South	18 East	Uintah	Desert Spring
- /Monarch Natural Gas, LLC	29	9 South	18 East	Uintah	Eight Mile Flat
- /New Water Financial, LLC	10	19 South	25 East	Grand	Harley Dome 1
- /OWL SWD Operating, LLC	8	20 South	24 East	Grand	Danish Flats
*/R N Industries, Inc	4, 9	2 South	2 West	Duchesne	Bluebell
*/R N Industries, Inc	26, 35	8 South	21 East	Uintah	Wonsit
- /R N Industries, Inc	2	9 South	22 East	Uintah	Chapita
- /R N Industries, Inc	5	9 South	22 East	Uintah	Glen Bench
- /R N Industries, Inc	36	10 South	20 East	Uintah	Seep Ridge
- /R N Industries, Inc	25, 26, & 35, 36	4 South	3 West	Duchesne	Pleasant Valley
*/Western Water Solutions (temporarily closed as of June 9, 2015)	9, 10	4 South	1 West	Duchesne	Sand Pass Ranch

- Facility is approved to accept only produced water and associated RCRA exempt fluids.
* Facility is approved to accept produced water and associated RCRA exempt fluids and waste material resulting from crude oil spill clean-up operations.

Table 11.9. Annual number of wells with fracture stimulations in the Uinta Basin by county for the years 2011–2014 (note: 2011 is a partial year and 2014 is for the first half only).

County	2011 (part)	2012	2013	2014 (1/2)
Carbon	25	34	2	0
Duchesne	138	326	490	299
Grand	0	0	4	1
Uintah	330	576	588	228
TOTAL	493	936	1084	528

Table 11.10. Annual number of barrels of water used in fracture stimulations in the Uinta Basin by county for the years 2011–2014 (note: 2011 is a partial year and 2014 is for the first half only).

County	2011 (part)	2012	2013	2014(1/2)
Carbon	150,949	198,006	38,533	0
Duchesne	1,136,421	3,058,977	4,315,481	2,461,673
Grand	0	0	21,121	1422
Uintah	2,566,602	6,243,948	6,234,542	2,909,366
TOTAL	3,853,972	9,500,932	10,609,677	5,372,461

Table 11.11. Annual number of barrels of water used per well in fracture stimulations in the Uinta Basin by county for the years 2011–2014 (note: 2011 is a partial year and 2014 is for the first half only).

County	2011 (part)	2012	2013	2014 (1/2)
Carbon	6038	5824	19,267	none
Duchesne	8235	9383	8807	8233
Grand	none	none	5280	1422
Uintah	7778	10,840	10,603	12,760

Table 11.12. Annual number of wells fracture stimulated, barrels of water used in stimulations, and the number of barrels used per well in Uintah County for the year 2013.

Field Name	Wells Fractured	Barrels Used	Barrels Per Well
Greater Natural Buttes	329	3,103,534	9433
various Green River oil fields	259	3,131,008	12,089
TOTAL	588	6,234,542	10,603

Table 11.13. Veolia's reported processing performance data for waterflood applications.

Contaminant	Feed Water	MULTIFLO Effluent	CeraMem Effluent	Deaerator Effluent
Hardness, ppm as $CaCO_3$	1000 - 5000	< 20	< 20	< 0.5
Total iron, ppm	2 - 30	< 1.0	< 0.5	< 0.5
Free oil, ppm (>20 µm)	10 - 300	< 10	< 0.2	< 0.2
Suspended solids, ppm	10 - 300	< 10	< 0.2	< 0.2
Bacteria, cells / ml	100 - 9999	100 - 9999	non-detect	non-detect
Oxygen, ppm	2 - 8	2 - 8	2 - 8	< 0.05

Table 11.14. Publicly operated waste water treatment plants in Duchesne and Uintah Counties, Utah and their average annual flow in barrels per year (note: 1 barrel equals 42 gallons).

County	Facility	Average Annual Flow/Year
Duchesne	Altamont	519,800
Duchesne	Duchesne	1,823,200
Duchesne	Myton	5,128,300
Duchesne	Neola	605,150
Duchesne	Roosevelt*	4,430,000
Duchesne	Tabiona	85,300
Uintah	Ashley Valley	17,727,850
TOTAL		30,319,600

*Note: this facility already uses all of its flow in a land application water reuse project.

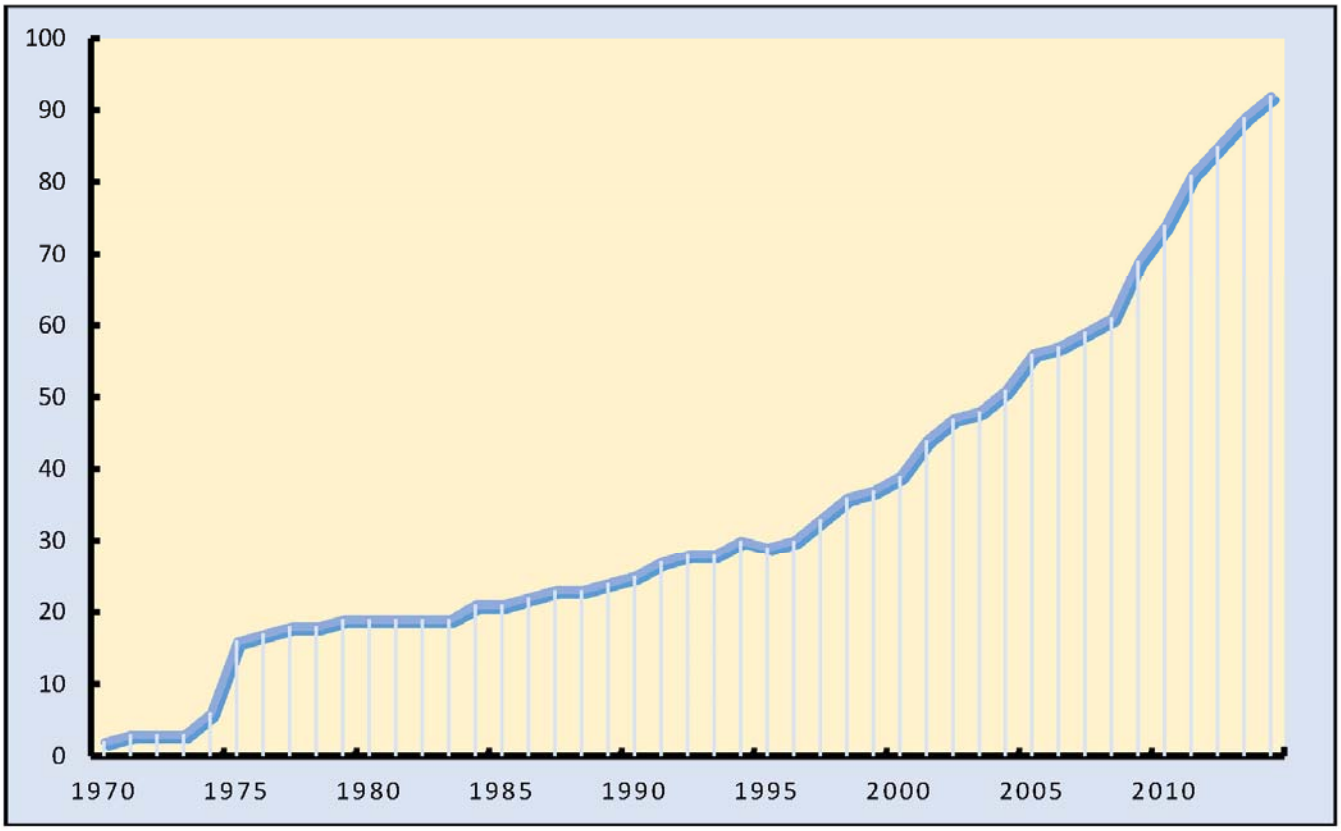

Figure 11.1. Graph of cumulative number of produced-water disposal wells in the Uinta Basin, from 1968 through 2014 (source: Division of Oil, Gas, and Mining website).

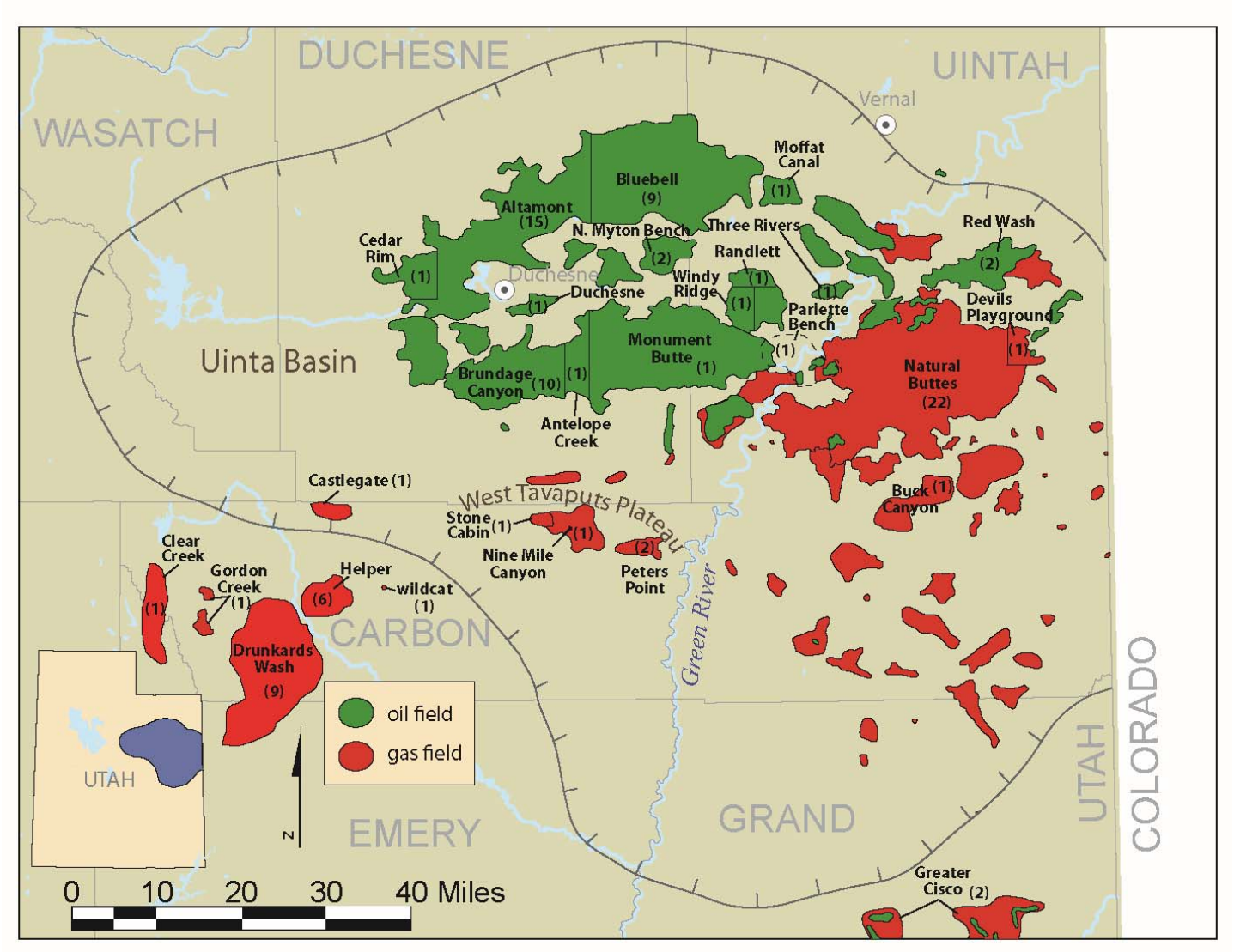

Figure 11.2. Location of water disposal wells by field in the Uinta Basin. Number of disposal wells shown in parentheses beneath field names.

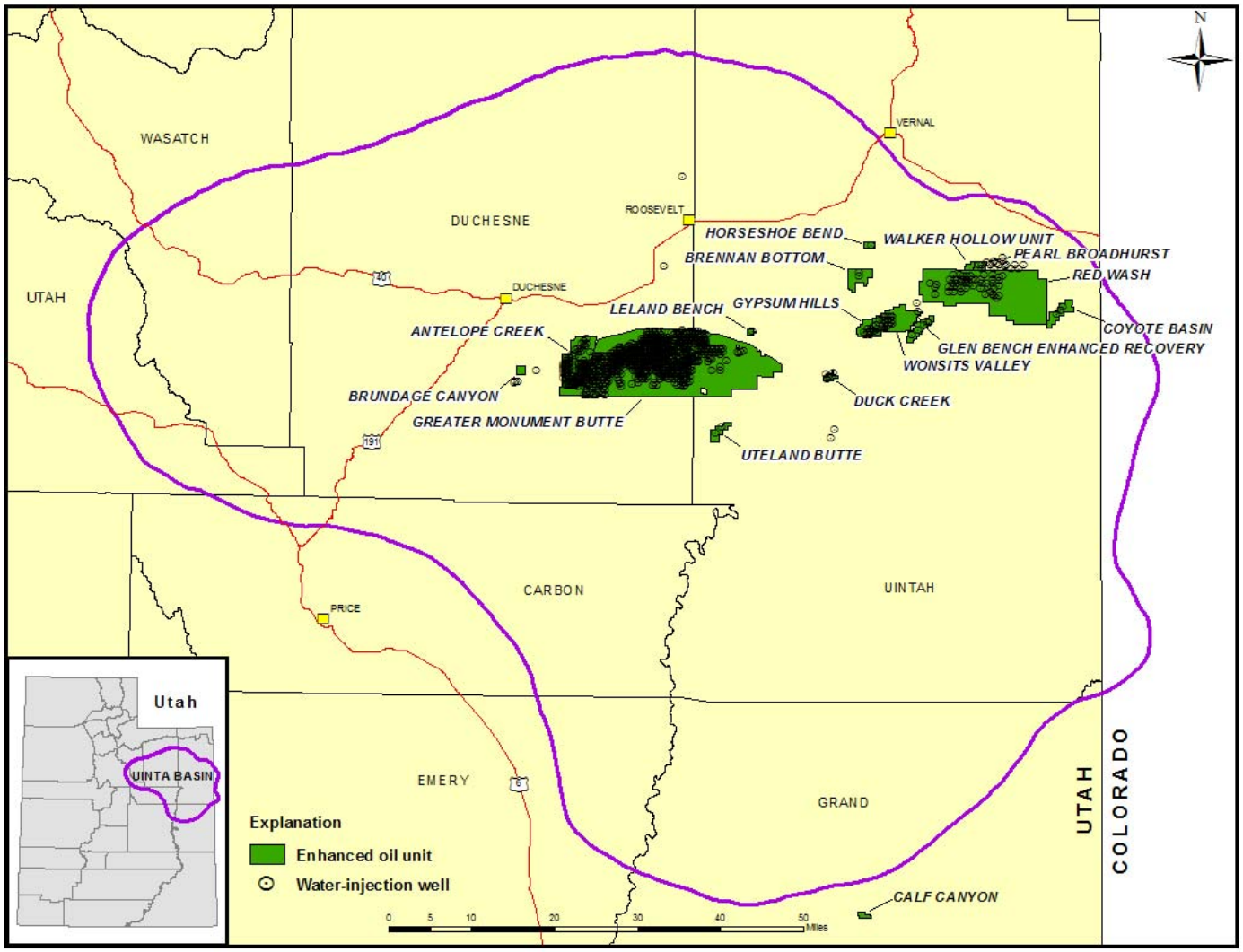

Figure 11.3. Location of enhanced-oil recovery, waterflooding projects and wells in the Uinta Basin.

A

B

Figure 11.4. Water evaporation ponds in the Uinta Basin. A – Spray evaporation system at Brennan Bottom disposal facility evaporation pond, Uintah County. B – Liner system and levee at the Sand Pass Ranch evaporation pond, Duchesne County. Photos courtesy of Brad Hill, Utah Division of Oil, Gas, and Mining.

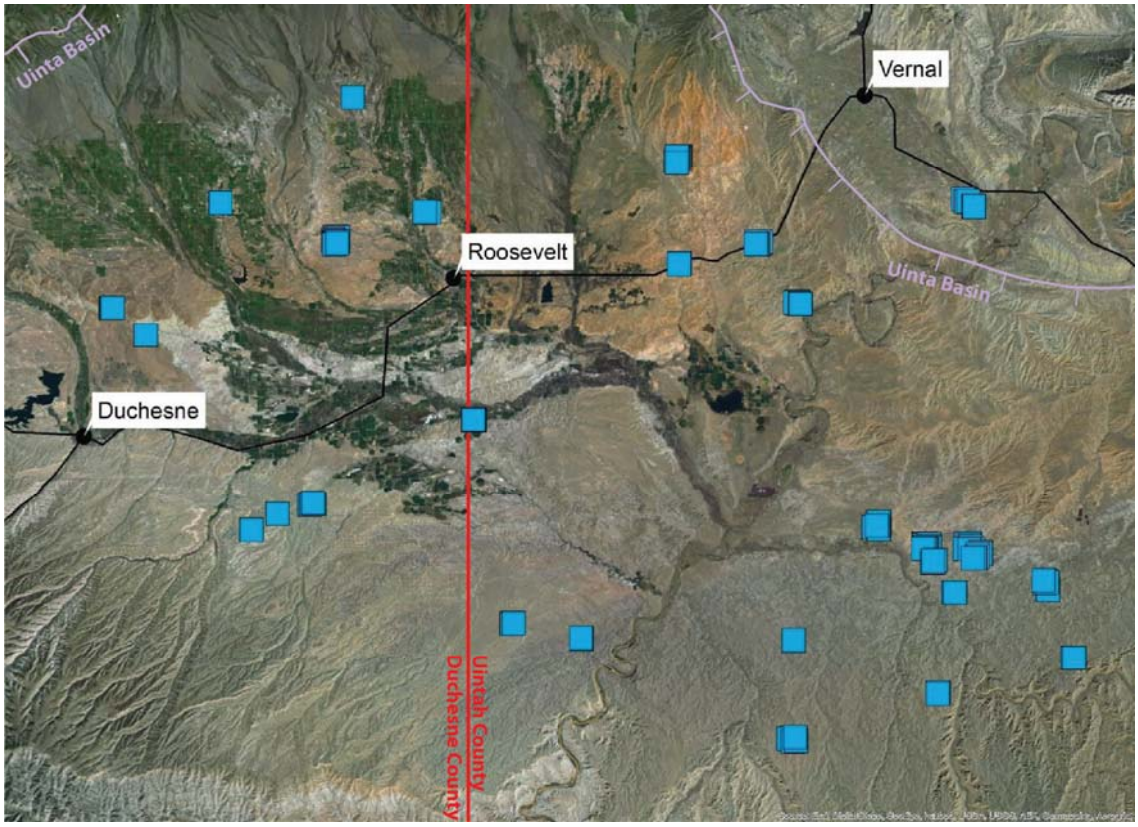

Figure 11.5. Location of water evaporation ponds (blue squares) in the Uinta Basin. From Utah State University, 2013.

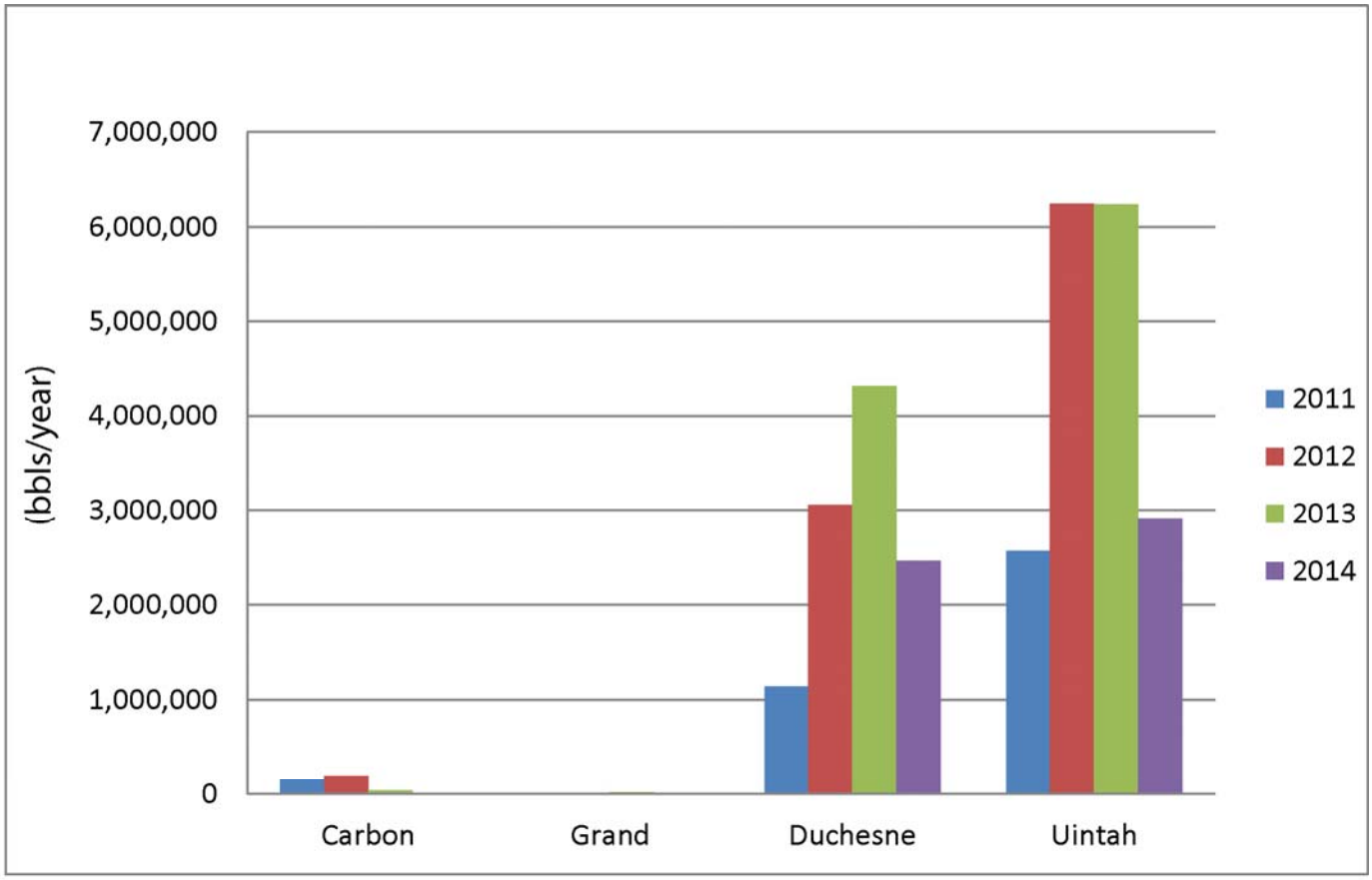

Figure 11.6. Graph showing the annual amount of water used in fracture stimulations by county for the Uinta Basin from 2011 through 2014 (note: 2011 and 2014 are only partial year tallies).

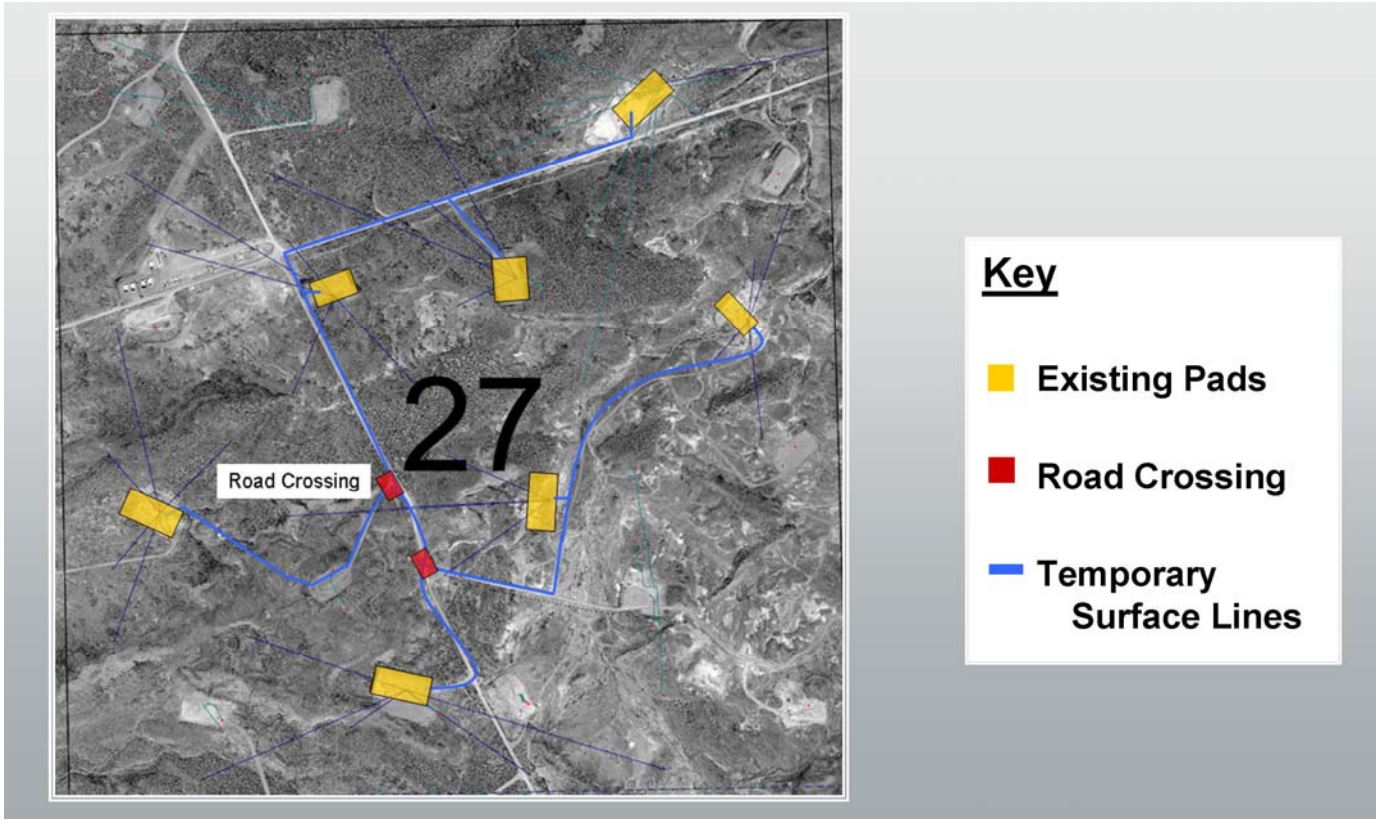

Figure 11.7. Example of Anadarko's Completion Technology System (ACTS) at Natural Buttes field showing closely spaced drilling pads containing multiple wells and temporary surface pipeline to transport and reuse hydraulic fracturing flow-back fluids. Illustration courtesy of Anadarko Petreolum.

Figure 11.8. Exterior view of water and oil storage tanks at Newfield's Beluga water treatment facility. Photo from article in the Salt Lake Tribune, August 19, 2012, by Dawn House.

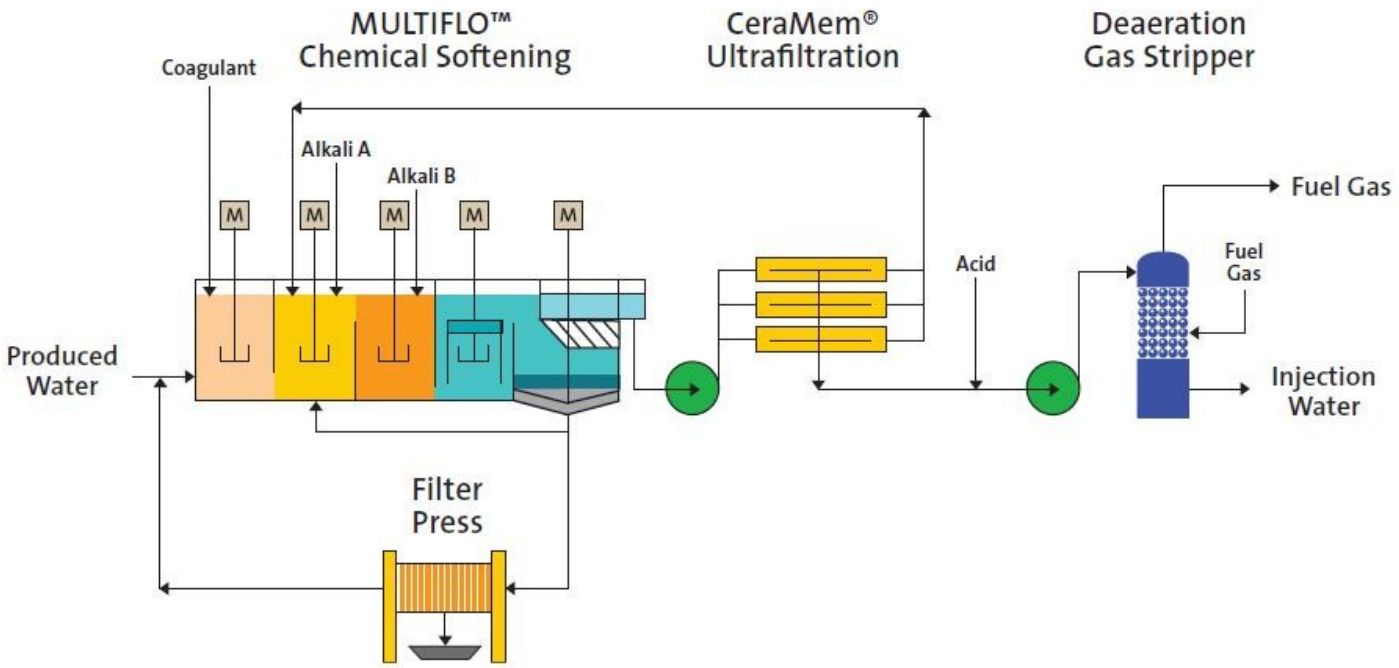

Figure 11.9. Schematic diagram of the Newfield Beluga plant's Veolia water-treatment process with water moving from left to right; note M = mixer. Multiflo and CeraMem are registered trade names of Veolia Water Solutions and Technologies (source: veoliawaterstna.com/news-resources/ information-files/ross-flowback-produced-water.htm webpage accessed October 2014).

CHAPTER XII

GEOTHERMAL ASSESSMENT AND MODELING OF THE UINTA BASIN

Christian L. Hardwick, Hobie W. Willis, and Mark L. Gwynn

The thermal regime of a sedimentary basin controls the maturity of hydrocarbon systems within the basin and the overall geothermal energy potential (Luheshi, 1983; Willett and Chapman, 1987; Deming and Chapman, 1988, 1989; Prensky, 1992; Hermanrud and others, 1990; Förster, 2001; Kutasov and Eppelbaum, 2005; Zschocke, 2005; Goutorbe and others, 2007). This limited, yet robust, study focuses on the geothermal energy potential of fluids co-produced from hydrocarbon reservoirs in the UB by examining temperature data and other thermal properties from oil and gas wells (figure 12.1). Over 15,700 wells have been drilled across large tracts of the UB (U.S. Bureau of Land Management, 2012a). Bottom-hole temperatures extracted from oil and gas well logs constitute a majority of the subsurface temperature data throughout the world and this is certainly true of the UB. These data are typically readily available, relatively inexpensive, and abundant in many study locations (Förster and Merriam, 1995; Henrikson, 2000; Henrikson and Chapman, 2002; Morgan and Scott, 2014). Aside from sporadic temperatures recorded in relatively shallow water supply wells, BHTs often constitute the only available subsurface temperature data. Heat flow and geothermal energy potential can be calculated from BHTs, associated thermal conductivities, and the consequent thermal gradient inherent in each well (Chapman and others, 1984).

However, there is a major problem with BHT data because the temperature of the surrounding rock is temporarily altered during the drilling process. Although some frictional heat is generated by the drill bit, the predominant effect is cooling that comes from the circulation of relatively cold drilling fluids (Guyod, 1946; Bullard, 1947; Lachenbruch and Brewer, 1959; Dowdle and Cobb, 1975; Fertl and Wichmann, 1977; Harrison and others, 1983; Luheshi, 1983; Keho, 1987; Willett and Chapman, 1987; Cao and others, 1988; Deming, 1989; Deming and others, 1990; Prensky, 1992; Förster and Merriam, 1995; Blackwell and others, 1999; Förster, 2001; Andaverde and others, 2005; Zschocke, 2005; Goutorbe and others, 2007; Edwards, 2013; Morgan and Scott, 2014). This is a major reason BHTs should be considered low precision, low reliability data that need to be carefully evaluated (Willett and Chapman, 1987). Additionally, noise is a typical component of BHT datasets for a wide range of reasons (Kehle and others, 1970; Luheshi, 1983; Speece and others, 1985; Cao and others, 1988; Deming and Chapman, 1988; Deming, 1989; Deming and others, 1990; Förster and Merriam, 1995; Henrikson, 2000; Beardsmore and Cull, 2001; Henrikson and Chapman, 2002). In a deep well, the upper part of the wellbore will frequently be heated while the lower section is cooled as drilling mud is circulated throughout the well bore (Guyod, 1946; Bullard, 1947; Glenn and others, 1980; Speece and others, 1985; Deming and others, 1990; Edwards, 2013). While the disturbed temperatures throughout the wellbore will eventually re-equilibrate, the time required is typically 10 to 20 times the duration of the drilling, which may mean many months for deep wells (Bullard, 1947; Steeples and Stavnes, 1982; Luheshi, 1983; Beardsmore and Cull, 2001). The magnitude of the perturbation is smallest at the bottom of the well near where temperatures are recorded (depending on the position of the thermometer on the tool string and other factors), but considerable time is still required to regain equilibrium temperatures (Deming and others,

1990; Blackwell and others, 1999; Henrikson, 2000; Henrikson and Chapman, 2002; Morgan and Scott, 2014). Unfortunately, geophysical logging in oil and gas wells is almost always initiated shortly (usually within 24 hours) after drilling and mud circulation has ceased, so the thermal disturbance is still great (Willett and Chapman, 1987; Prensky, 1992; Beardsmore and Cull, 2001; Förster, 2001; Morgan and Scott, 2011; Edwards, 2013). Since oil and gas wells will typically be plugged and abandoned or in some other phase of development or production long before the wellbore has time to recover to pre-drilling temperatures, numerous methods have been developed to correct for the drilling induced temperature disturbance.

BHT DATA

BHT Correction Methods

Hermanrud and others (1990) tested 22 methods developed between 1946 and 1988 against drill-stem test (DST) control data. Drill-stem tests typically draw fluids from some distance beyond the thermally disturbed volume of rock surrounding the wellbore and are therefore commonly considered as a close approximation to the virgin rock temperature (VRT) (Harrison and others, 1983; Ben Dhia, 1988; Hermanrud and others, 1990; Förster and Merriam, 1995; Beardsmore and Cull, 2001; Shalev and others, 2008). However, DST reports sometimes record estimated temperatures, and other factors such as slow fluid flow and expanding gasses may decrease fluid temperatures and underestimate the VRT (Beardsmore and Cull, 2001). Ben Dhia (1988) notes other potential sources for error including the possibility that friction and

compression could result in the overestimation of the VRT. Still, despite the potential inaccuracies, DSTs generally constitute the best available temperature data at depth. Unfortunately, DST data quantity is usually dwarfed by BHT data quantity and availability.

Goutorbe and others (2007), Crowell and Gosnold (2011), Crowell and others (2012), and Edwards (2013) compared various correction techniques. These comparison studies showed that most methods reliably estimate formation temperatures within about ±10°C (±18°F). Some methods are much more accurate but complex, requiring data that are rarely available. Many common methods use depth-dependent equations. These equations are typically derived from specific locations where sufficient quantities of DST or other reliable temperature data are used to develop an empirical correction, scaled by depth, which can be applied to an uncorrected BHT. Examples of these methods include Kehle and others (1970; see Gregory and others, 1980), Harrison and others (1983), Willett and Chapman (1987), Ben Dhia (1988), Blackwell and Richards (2004), Förster and Merriam (1995), Morgan and Scott (2011, 2014), and Crowell and others (2012). Because these methods were all derived for specific basins, they are not necessarily applicable to other sedimentary basins (Crowell and Gosnold, 2011; Crowell and others, 2012; Edwards, 2013; Morgan and Scott, 2014; Welhan and Gwynn, 2014).

Although a number of minor variations exist (mainly in certain assumptions that typically need to be made), Horner-type BHT corrections are commonly used in the petroleum industry and in geothermal investigations (Luheshi, 1983; Chapman and others, 1984; Hermanrud and others, 1990; Prensky, 1992; Kutasov and Eppelbaum, 2005). The basis of these corrections is rooted in the work of Bullard (1947) and Lachenbruch and Brewer (1959), but the "Horner" name comes from the mathematically similar technique developed by Horner (1951) for examining pressure build-up in wells. Unlike the empirical methods that require only a single

BHT measurement, Horner-type corrections are time-sequential, requiring BHT data from two or (preferably) more logging runs at the same depth. The premise of the technique is based on the formula from Chapman and others (1984):

$$T_B(t) = T_{B\infty} + \mathrm{A}\log\left(\frac{T_c + T_e}{T_e}\right) \tag{12.1}$$

where:

$T_B(t)$ = the time-dependent BHT (in °C),

$T_{B,\infty}$ = temperature at infinite time (in °C),

A = constant derived by linear regression for a given BHT set,

t_c = the circulation time (in hours), and

t_e = the elapsed time since circulation stopped (in hours).

By plotting log $(t_c + t_e / t_e)$ against $T_B(t)$ for two or more logging runs, the rate of temperature rebound can be extrapolated to infinite time, thereby providing an estimate of the undisturbed VRT.

Values for t_c are almost never recorded. So, in practice, most investigators use an estimated duration and apply it to all corrections (Deming, 1989). Undocumented values for t_e are another problem that frequently precludes using this method. Wells containing multiple time-temperature pairs needed for Horner-type corrections are uncommon in many locations. For example, Chapman and others (1984), Keho (1987), and Willett and Chapman (1987) found that only about 5% of the UB wells were suitable for Horner-type corrections. Ben Dhia (1988), Shalev and others (2008), and Morgan and Scott (2014), describe similar situations for their investigations. Although not quantified, the proportion of wells suitable for Horner-type corrections in the UB is still small despite a large increase in the number of wells drilled since the 1980s. This is due to logging tool developments that often now allow all desired logs to be run concurrently.

Dowdle and Cobb (1975), Luheshi (1983), Hermanrud and others (1990), and Welhan and Gwynn (2014) suggest that Horner-type corrections tend to underestimate the VRT to some degree. However, we feel that for most geothermal studies, it is preferable to report more conservative (lower) VRT estimates.

Henrikson (2000) and Henrikson and Chapman (2002) used Horner-type corrections where possible, and then compiled those data to develop empirical correction equations that can be applied to wells where only a single time since circulation-temperature datum exists (i.e., BHTs from single logging runs at a given depth). Edwards (2013) compared the results of Horner-type corrections (assumed to represent the VRT) with the single-BHT equations of Henrikson (2000) and Henrikson and Chapman (2002). He found that the single-BHT corrections usually overcorrected by about 1°C (1.8°F) with a standard deviation of 11°C (19.8°F).

Horner and Horner-derived single point correction methods of Henrikson (2000) and Henrikson and Chapman (2002) have been used with reasonable success throughout Utah and surrounding states by Allis and others (2011, 2012), Edwards (2013), Gwynn and others (2013, 2014) and Welhan and others (2014). Within the inherent limitations of all BHT correction methods (see Deming, 1989 and Deming and others, 1990), we feel the Henrikson (2000) and Henrikson and Chapman (2002) methods provide reasonable estimated BHTs for the UB.

BHT Data Compilation

Of several thousand wells currently producing fluids, a sample of 776 were selected for this study (figure 12.1). Other thermal studies tend to combine thermal data from the UB with data from the entire Colorado Plateau for a large-scale thermal regime such as in Henrikson (2000). In this study, wells were chosen to represent as much of the entire area of the UB as possible in order to understand the thermal properties and regime on a basin-wide scale rather than a regional, lithospheric scale. However, the number of wells and spatial density of the data studied does not provide enough information for the research of shallow depth, intra-basin scale thermal characteristics.

Two sets of BHT data for the UB were combined in this study. The first has data processed from 136 wells where sufficient, credible data were available to correct for the drilling-induced temperature perturbations using both Horner-type and single-point BHT correction methods of Henrikson (2000) and Henrikson and Chapman (2002) compiled for the National Geothermal Data System (NGDS) by the UGS. Many of these data were used by Chapman and others (1984), Keho (1987), and Willett and Chapman (1987) in previous heat-

flow studies. These wells are primarily distributed among the Altamont-Bluebell-Cedar Rim oil fields in Duchesne County and Natural Buttes gas field in Uintah County (figure 1.1) (Chapman and others, 1984; Keho, 1987). Many of these wells had multiple data points at a given depth, allowing Horner-type corrections to be made, and are presumed to represent the highest-quality corrected BHTs in the study area. The correction factor assumes that the Horner-type correction provides a reliable estimate of the VRT in a given well (Fertl and Wichmann, 1977; Edwards, 2013).

Bottom-hole temperatures for the remaining 640 wells were extracted from geophysical logs via the online DOGM database. A depth-dependent correction factor specific to the UB was derived and applied to the uncorrected BHTs of this dataset. This correction factor was determined using Horner-corrected BHTs from the 136 previously corrected wells. The difference between each uncorrected BHT and the Horner-corrected temperature was calculated and the average of these values was found to be 2.0°Celsius/kilometer (°C/km) (0.11°F/100 ft). This correction, a linear function of depth, was applied to the remaining 640 wells.

These corrections, though less rigorous than the other methods, generally result in corrected gradients very similar to those of the first dataset. Therefore, we feel confident that the corrected BHTs in this dataset are reasonable, especially when viewed with the inherent limitations and uncertainties of BHT data. Together, the two datasets generate a BHT database for 776 wells within the UB (figure 12.2) that is left-skewed, normally distributed around a mean BHT of about 96°C (205°F).

Heat Flow

In this study, corrected BHTs are combined with additional thermal data and used as inputs of the Simple Gradient and Thermal Resistance Methods (figure 12.3) for calculating one-dimensional (1D) heat-flow values following Chapman and others (1984), Keho (1987), and Henrikson (2000). The thickness of lithofacies encountered in each well in this study were taken from existing UGS data. Thermal conductivity values directly measured by the divided-bar method are taken from Keho (1987) and Henrikson (2000) when available. Otherwise, lithofacies were assigned a typical thermal conductivity value sourced from common industry data compiled by Beardsmore and Cull (2001). Mean annual surface ground temperature (SGT) values for each well were extrapolated from Edwards (2013). First, a thermal gradient is calculated using the Simple Gradient Method given by:

$$T_B = T_0 + \left(\frac{\partial T}{\partial Z}\right) B \tag{12.2}$$

where:

T_B = the temperature at depth B (in ^{o}C),

T_0 = the mean annual surface ground temperature (in ^{o}C),

$(\partial T/\partial Z)$ = the thermal gradient (in ^{o}C/meters [m]), and

B = the depth the BHT was recorded (in meters).

An initial estimate of heat flow based on the Simple Gradient Method and Fourier's Law is then computed using the calculated gradient and a thickness weighted (arithmetic) mean of thermal conductivities, k, for all stratigraphic layers within the gradient interval. Fourier's law of heat conduction in 1D is:

$$q_0 = k \frac{\partial T}{\partial Z} \tag{12.3}$$

where:

q_0 = surface heat flow (in watts per meter squared [W/m^2]),

k = thermal conductivity (in watts per meter kelvin [W/mK]), and

$(\partial T/\partial Z)$ = the thermal gradient (in $^oC/m$).

With this estimate, a starting value of surface heat flow is determined and then used in the Thermal Resistance Method. The thermal resistance is the relation between a lithological unit of thickness Δz and the associated thermal conductivity k. This method allows for lateral differences in subsurface temperature, thermal conductivity, and heat flow which does not restrict oil and gas fields to a homogenized, single gradient, or conductivity value. The governing equation for the Thermal Resistance Method is:

$$T_B = T_0 + q_0 \sum_{z=0}^{B} \left(\frac{\Delta z}{k} \right) \tag{12.4}$$

where:

T_B = the temperature at depth where z = B (in ^oC),

T_0 = the mean annual SGT at each well location (in ^oC),

q_0 = surface heat flow (in W/m^2),

Δz = the vertical interval (in m), and

k = thermal conductivity (in W/mK).

Thermal resistance is summed for all layers between the surface and depth B (Keho, 1987) to compute the temperature value at B (also known as bootstrapping). In this study, temperature is calculated with the Thermal Resistance Method in an iterative, forward-modeling approach by adjusting the heat-flow parameter which is guided by the residual of the observed and calculated BHTs until the data are within a tolerance of 1%. The Thermal Resistance Method gives a better approximation for the final surface heat-flow value compared to the Simple Gradient Method because it incorporates all subsurface layers in the computation.

Heat Flow Results

The Thermal Resistance Method was applied to the 776 wells in this study (figure 12.4). The mean surface heat flow for all wells studied is 67 milliwatts per square meter (mW/m^2) with a standard deviation of 12 mW/m^2. The mean thermal gradient for the data is 31°C/km (1.7°F/100 ft) with a standard deviation of 6°C/km (0.33°F/100 ft). However, these data reveal the presence of several anomalous wells with heat-flow values exceeding 100 mW/m^2. While some spatial variation is expected, a single well with a heat-flow value on the order of 50 mW/m^2 greater than several neighboring wells is unlikely. Many of these wells were eliminated from the final calculations due to potentially erroneous BHT data based on comparing the heat flow of an anomalous well to that of several neighboring wells. A heat flow value of 65 ±10 mW/m^2 and a mean geothermal gradient of 27 ±5°C/km (1.48 ±0.27°F/100 ft) were calculated after filtering the anomalous wells (figures 12.5 and 12.6).

The mean surface heat flow falls within a reasonable range when compared with previous studies, although the overall accuracy would be improved with additional high-quality BHT data. A heat-flow study detailed by Chapman and others (1984) and Keho (1987) of 97 wells located primarily in the northwest portion of the UB resulted in a mean heat flow of 57 ±11 mW/m^2 from a range of 40 to 65 mW/m^2. A study of the entire Colorado Plateau by Henrikson (2000) reports a mean heat-flow value of 62 ±2 mW/m^2 which includes around 100 heat-flow values for the UB. Keho (1987) and Henrikson (2000) used fewer, but more accurate, BHTs in their work, which may partly explain the differences. Another factor may be our use of more wells spread over a greater expanse of the UB, a major goal of this study.

THERMAL MODELS

Background Data and Methods

Building upon the observed and computed thermal data from above, we created a conductive thermal model of the UB using COMSOL Multiphysics 4.4, a finite element method modeling program. This initial thermal model is intended to bracket the regional background heat flow so that more detailed models exploring spatial heterogeneities can be developed. The methods used by Hardwick and others (2014) to generate a similar model of the Black Rock Desert of western Utah were used in this study. Model framework (figure 12.7) consists of surface topography from a 5-meter digital elevation model, a basement interface as determined by well data, and isopach maps from previous UGS UB work. In this study, a simple layer-cake model is implemented consisting of only two material layers (basement rock and basin fill material). In areas where basin-fill thickness is zero, we set the bedrock contact at 10 meters depth so that the layers are continuous without any overlap. Model layers are then smoothed within COMSOL in order to simplify the meshing and speed up computing time. We use the mean annual SGT from Edwards (2013) as the upper boundary condition and a spatially uniform basal heat flux as the lower boundary condition. Both boundary conditions are invariant with respect to time.

The range of thermal conductivities chosen for the model are determined by the measured properties of core and chip samples recovered from UB wells (Keho, 1987; Henrikson, 2000) and typical values for the lithology recorded in the well logs. Thermal conductivities for the basin fill layer (k_1) range from 2.0 to 3.0 W/mK (9 total) and for the basement rock layer (k_2)

range from 3.5 to 4.5 W/mK (9 total). Increments of 0.125 W/mK were modeled for each layer. The lower boundary condition, basal heat flow (q_b), is uniform and a range of values from 60 to 80 mW/m^2 are used (5 total). The upper and lower limits of the range for all parameters is intentionally extended slightly beyond known values as a check of the model behavior and to help define global and local minimums. A parametric sweep scheme using COMSOL results in 81 models per q_b value (405 models in total).

Model Results and Discussion

Temperature and heat-flow residuals (figure 12.8) indicate where the thermal models correlate with the observed data. The residuals are computed from 776 observed subsurface temperature points and the respective surface heat-flow values compared to the modeled temperatures at the same locations reported as the mean, standard deviation, and maximum difference. Temperature residuals show that the models are more sensitive to changes in the basin fill thermal conductivity than to changes in basement rock. This is expected because the UB is a deep basin (exceeding 4.5 kilometers [14,760 ft]) and the primary effects on temperature are the insulating properties of the basin fill material. The 70 mW/m^2 basal heat-flow value results in the best-fit models according to temperature residuals and shows a global minimum for the k_1 parameter. This overall best-fit model uses $k_1 = 2.375$ and $k_2 = 4.0$, with residuals of 9.8, 9.0, and 61.9ºC (50, 48, and 143°F) for mean, standard deviation, and maximum.

Heat-flow residuals vary only slightly for changes in k_1 and k_2 values. As with the temperature residuals, the basal flux of 70 mW/m^2 contains the best-fit model as well as the lowest model residuals for all combinations of k_1 and k_2 compared to other basal-flux values.

The best-fit basal flux model for heat-flow residuals has the same k_1 and k_2 values as the best temperature residual model. The heat-flow residuals are 8.0, 7.0, and 46.0 mW/m^2 for the mean, standard deviation, and maximum difference.

Temperature slices at depth shown in figure 12.9 of the UB thermal model are produced at approximate depths of 2, 3, 4, and 5 kilometers (6560, 9840, 13,120, and 16,400 ft) below the average surface elevation of the basin. For an area of 16,000 square kilometers (6180 mi^2) we find that temperatures are generally greater than 75°C (167 ^{o}F) at a depth of 2 kilometers (6560 ft) and in some areas exceed 100°C (212°F). In this assessment, the calculated minimum temperature required for direct use applications (greenhouses, etc.) is 50°C (122°F) which is met at 2 kilometers (6560 ft) depth in the entire basin model. Modeled temperatures reach 150°C (302°F) at a depth of 5 kilometers (16,400 ft) below the basin which exceeds the minimum temperature of 140°C (284°F) required for binary geothermal power production.

The modeled surface heat flow in the UB ranges from 50 to over 80 mW/m^2 (figure 12.10). Values are generally highest in the mountains and lowest in the valleys. Due to the refraction of heat flow along the basin/basement interface we expect bedrock values to exceed the uniform basal flux of 70 mW/m^2. This is observed in the model along the margins of the UB where basin-fill thickness is thin and bedrock is at or near the surface. Average heat flow for the UB based using the thermal resistance method is 67 mW/m^2 which agrees reasonably with the best-fit thermal model and suggests that the thermal regime of the basin may be primarily conductive.

When comparing the three-dimensional (3D) model to the 1D calculations there are some key differences to point out. Since the primary intention of the initial 3D model is to constrain the background regional heat flow, disparities are expected when examined against the 1D

values. These differences typically can be due to the result of heat transport in modes other than that of conduction (i.e., advection, convection). We find that differences are most prominent at the northern end of the UB where the thermal model over predicts the 1D values by up to 30 mW/m^2 or more. One proposed explanation for this difference is that regional groundwater flow is flushing the heat (cooling the host rock) via recharge pathways originating in the Uinta Mountains and moving southward into the basin. This hypothesis of groundwater flow is also suggested by a number of saline water studies of the UB (Howells and others, 1987; Freethey, 1992; Glover, 1996; Zhang and others, 2009; Anderson and others, 2012) in order to explain the great depth to the base of the saline water in the northern part of the basin. We find that this deep trend is coincident with low heat-flow values (figure 12.11) and most likely a cause and effect relation. An east-west trend of under predicted heat flow is observed through the central part of the basin where model results are lower than 1D values by 15 mW/m^2 on average. This trend aligns with the Duchesne fault zone as well as a shallow trend of the moderately saline fluid base. The shallow base is thought to be related to the upward mobility of fluids enabled by the fault-and-fracture system (among other factors) according to Anderson and others (2012). Heat transport within these upward moving fluids could explain the elevated heat flow in the central part of the basin, coincident with the Duchesne fault zone. In order to facilitate a more in-depth study of the UB, revised versions of the 3D thermal models should incorporate fluid flow to better address the effects of the groundwater flow hypotheses.

GEOTHERMAL RESOURCE POTENTIAL

This study shows that co-produced fluids from oil and gas wells within the UB may represent a significant, yet unused, geothermal resource. The mean thermal gradient of 27°C/km (1.48°F/100 ft) for the basin implies that any well deeper than 2 kilometers (6500 ft) could have a fluid temperature of about 65°C (149°F) when using a mean annual SGT of 11°C. This temperature is well above the minimum threshold required for heated fluids to be used in direct-use applications such as aquaculture, greenhouses and space heating (Boyd, 2008). Since the average depth of wells in this study is 3 kilometers (9840 ft), higher temperatures can be expected from the majority of producing wells.

Fluid production volumes from UB wells have been averaged using available data, which, in many cases, represents the entire production period for a given well. With documented flow and temperature values we can calculate the heat content and thermal output of each well. The heat-energy content can be calculated by:

$$Q = mc\Delta T \tag{12.5}$$

where:

m = the mass of the fluid (in kilograms [kg]),

c = 4200 J/kgK (the specific heat of water in joules per kilogram kelvin), and

ΔT = the change in temperature from produced depth to surface (in °C).

Applying this equation to our UB dataset results in an average thermal output of 88 kilowatts (kW), but a maximum output of up to 10 megawatts (MW) was calculated for wells with exceptionally high volumes of produced fluids (figure 12.12). Of the wells studied, 587 of the 776 fall in a range of 25 to 100 kW of thermal output. The most significant parameter affecting thermal output is the volume of produced fluid, which varies significantly in the UB (figures 4.21, 4.46, 4.69, 6.23, and 7.19). Slighter higher fluid output volume would drastically increase thermal power output.

Binary geothermal power systems are commonly used to generate electricity from intermediate-temperature reservoirs. Resource fluid temperatures between 120 and 150°C (248-302°F) are suitable for binary-cycle power plants (Blackett and others, 2004). In a binary system, geothermal water passes through a heat exchanger to heat a secondary working fluid. This working fluid flashes to steam at a lower temperature and pressure than water and is used to drive the generator turbine. The cooled geothermal fluid is then injected back into the geothermal reservoir. Temperatures above 120°C (248°F) are found in 127 wells in our dataset. However, useable heat content is limited by the temperature difference between the surface and the production depth. In addition, the efficiency of existing geothermal power plants demonstrates that a resource temperature at or above 140°C (284°F) is preferred (Blackett and others, 2004). Such temperatures are observed in 36 wells in this study, so geothermal power generation may be viable from wells with sufficient fluid production and adequate temperature (figure 12.13).

Alternatively, produced fluids could be used for direct-use geothermal applications such as greenhouse heating. The Newcastle area near Cedar City in southwestern Utah, currently sustains nine greenhouses covering an area of 3135 square meters (33,750 ft^2) growing crops in a

hydroponic system (Boyd, 2008). However, the resource may be able to sustain greenhouses covering an area up to 25 acres (approx. 100,000 m^2) according to findings from Blackett and others (2004). Greenhouse heating requirements are highly variable depending on several factors including, but not limited to greenhouse size/volume, structural materials, heat delivery methods, crop requirements, and weather (Boyd, 2008). We can, in general, compute peak energy requirements by using the following equation:

$$Q_g = AU\Delta T \tag{12.6}$$

where:

Q_g = the total energy requirement (in J),

A = the area of the green house construction material (in m^2),

U = the heat loss factor of the greenhouse material (unitless), and

ΔT = the change in temperature from mean annual SGT and the desired internal temperature (in ^oC).

A common type of greenhouse is the fiberglass-plastic style, where the walls are made of fiberglass and a domed roof is made of a double layer of plastic film enclosing an air space. Such a greenhouse covering an area of 468 square meters (5037 ft^2) would require 51 kW

(174,676 Btu/hr) of power to maintain an internal temperature of 21°C (70°F) with a mean external temperature of 10°C (50°F). Additional design parameters from Boyd (2008) and Lund (2011) reveal that a single well must produce 10 to 22 gallons per minute (3-5 m^3/hr) of >50°C (122°F) fluids to sustain the greenhouse described above. It should be noted this is a general calculation and specific greenhouse requirements vary according to materials, location, and desired crop to be grown. Minimum temperatures are found in 740 wells in our dataset, and 29 of these also meet the flow requirements of our example greenhouse. These wells could support 86 greenhouses (figure 12.13). Regardless of volumetric production, the high number of existing wells producing fluids above 50°C (122°F) make direct-use geothermal applications (i.e., greenhouses) in the UB an attractive option.

SUMMARY

This geothermal assessment of the UB presents encouraging results related to geothermal potential in a number of ways. With a well-distributed sampling of thermal data in the basin, we are able to identify key thermal characteristics that are important to geothermal prospecting and the possibility of future development. Average background heat flow of 67 mW/m^2 and an average geothermal gradient of 27ºC/km (1.48°F/100 ft) result in adequate temperatures (>50ºC [122ºF]) at depths greater than 2 kilometers (6562 ft) for direct use applications such as greenhouses. This is important because of the large number of wells that are deeper than 2 kilometers and the pre-existing well infrastructure (significant cost savings for development) in the basin. Preliminary thermal models of the UB give some support to existing interpretations

that the thermal regime is primarily conductive with the exception of groundwater flushing from the Uinta Mountains. A conductive regime implies that the thermal aspects, intra-basin systems and responses are more predictable and likely are uniformly spread across the basin, resulting in a larger geothermal prospect. Future models incorporating basin-scale fluid flow will provide better estimates of the resource potential within the basin. From this small subset of UB well data, we find 740 wells meeting the temperature requirement of 50ºC (122ºF) for direct-use applications and 36 wells meeting the temperature requirement of 140ºC (284ºF) for binary geothermal power production. The average thermal output per well is 88 kW and maximum output is as high as 10 MW. For each well, produced oil or gas volumes decrease and co-produced fluids increase and the door opens to even more geothermal resource that could be used locally.

CHAPTER XII FIGURE CAPTIONS

Figure 12.1. Map of Uinta Basin showing geographic distribution of wells studied.

Figure 12.2. Histogram showing the distribution of bottom-hole temperatures (BHT).

Figure 12.3. Simple Gradient (A) and Thermal Resistance Methods (B) plots (modified from Chapman and others, 1984).

Figure 12.4. Histogram showing the distribution of calculated heat-flow values.

Figure 12.5. Thermal gradients of oil and gas wells. These wells, categorized by corrected BHTs, show the general trend of thermal gradients in the Uinta Basin. Gradients are slightly higher than the average of 27°C/km (1.48°F/100 ft) along the center of the basin with cooler than average gradients to the north and south. Gradients may be cooler along the northern margins due to groundwater recharge from the south flank of the Uinta Mountains.

Figure 12.6. Temperatures at depth. The average thermal gradient of 27°C/km (1.48°F/100 ft) is bracketed over a range of surface temperatures. Well depth distribution in upper-right corner.

Figure 12.7. Thermal model framework including upper and lower boundary conditions.

Figure 12.8. Residuals of model results to observed data for each model parameter set represented as mean, standard deviation, and maximum. Top panel shows temperature residuals and bottom panel shows surface heat-flow residuals.

Figure 12.9. Maps of the temperature field at planes of constant elevation below the average elevation of the Uinta Basin.

Figure 12.10. Surface heat flow from Uinta Basin thermal model and corrected well data (symbols colored according to heat-flow values). Black lines are contours of heat flow in 10 mW/m^2 intervals.

Figure 12.11. Map of depth in kilometers to the base of the moderately saline water (data from Anderson and others, 2012) in the Uinta Basin. Well locations and calculated heat-flow values (symbols colored according to heat-flow values) are shown. Magenta lines are faults. A noticeable spatial correlation between the depths to the base of the moderately saline water and heat flow can be observed. Heat-flow values are lower in the northern area where the base to the saline water is deep and heat-flow values are higher in the central part of the basin where the base to the saline water is shallow.

Figure 12.12. Histogram showing the distribution of calculated thermal output.

Figure 12.13. Map of wells co-producing water at a sufficient volume to support at least one 5037-square-foot (468 m^2) greenhouse (square symbol, indicated when more than three can be supported) and wells meeting required temperature threshold (> 140°C) for binary power generation (triangles). The potential is greatest for wells in Ashley Valley field near Vernal (see figure 1.1), in the northwest quadrant of the map, due to high volumetric output of co-produced fluid.

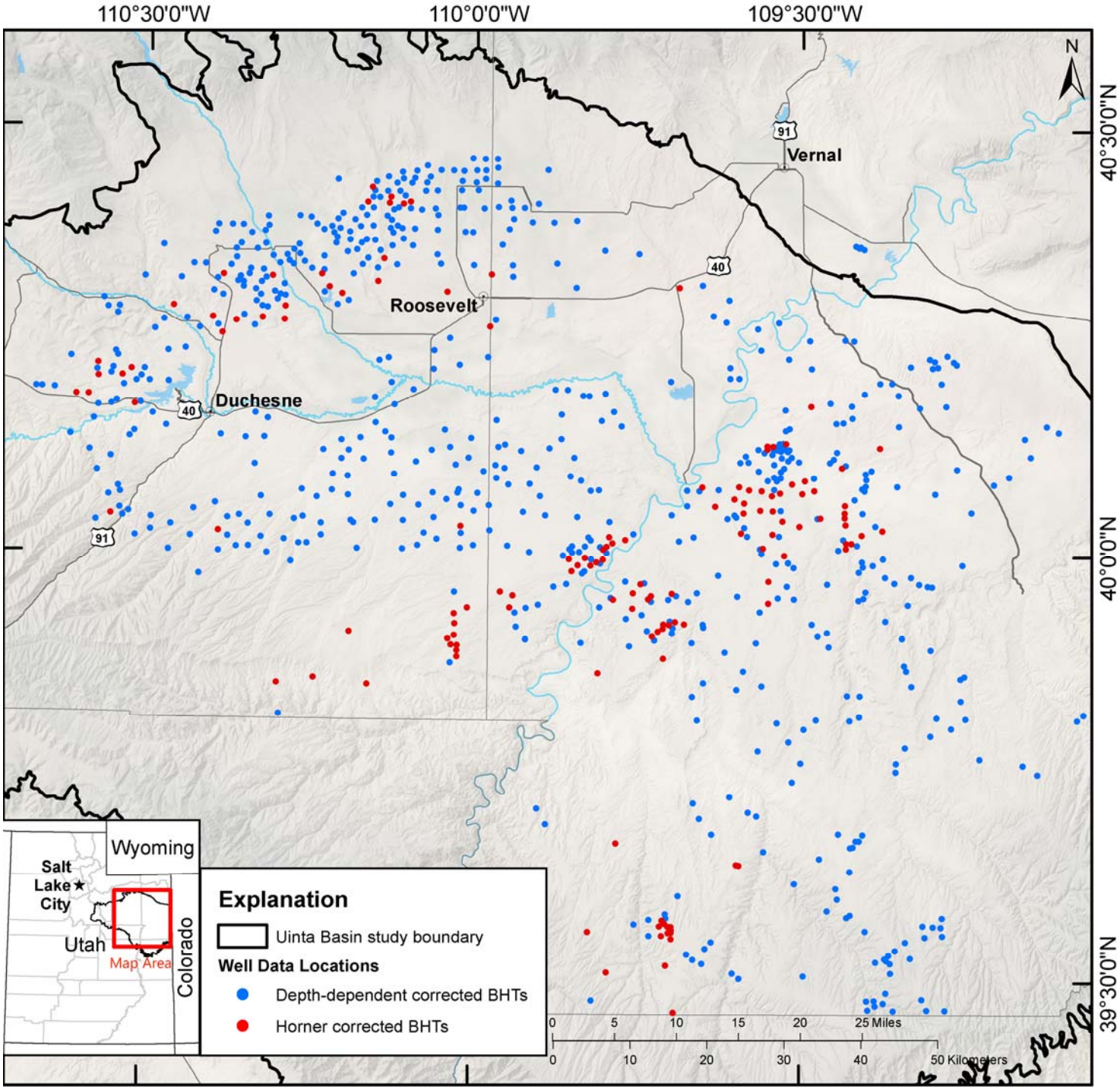

Figure 12.1. Map of Uinta Basin showing geographic distribution of wells studied.

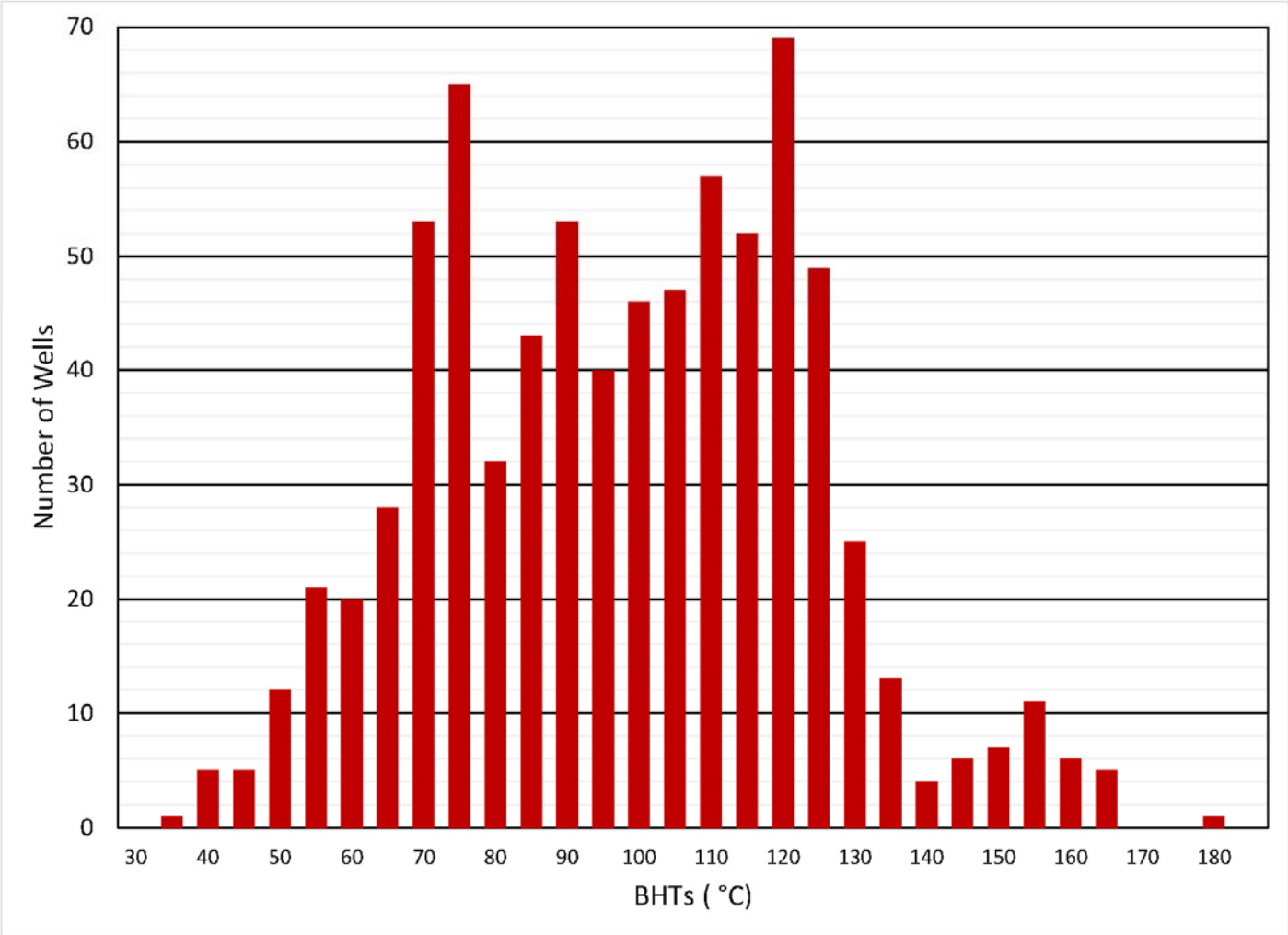

Figure 12.2. Histogram showing the distribution of bottom-hole temperatures (BHT).

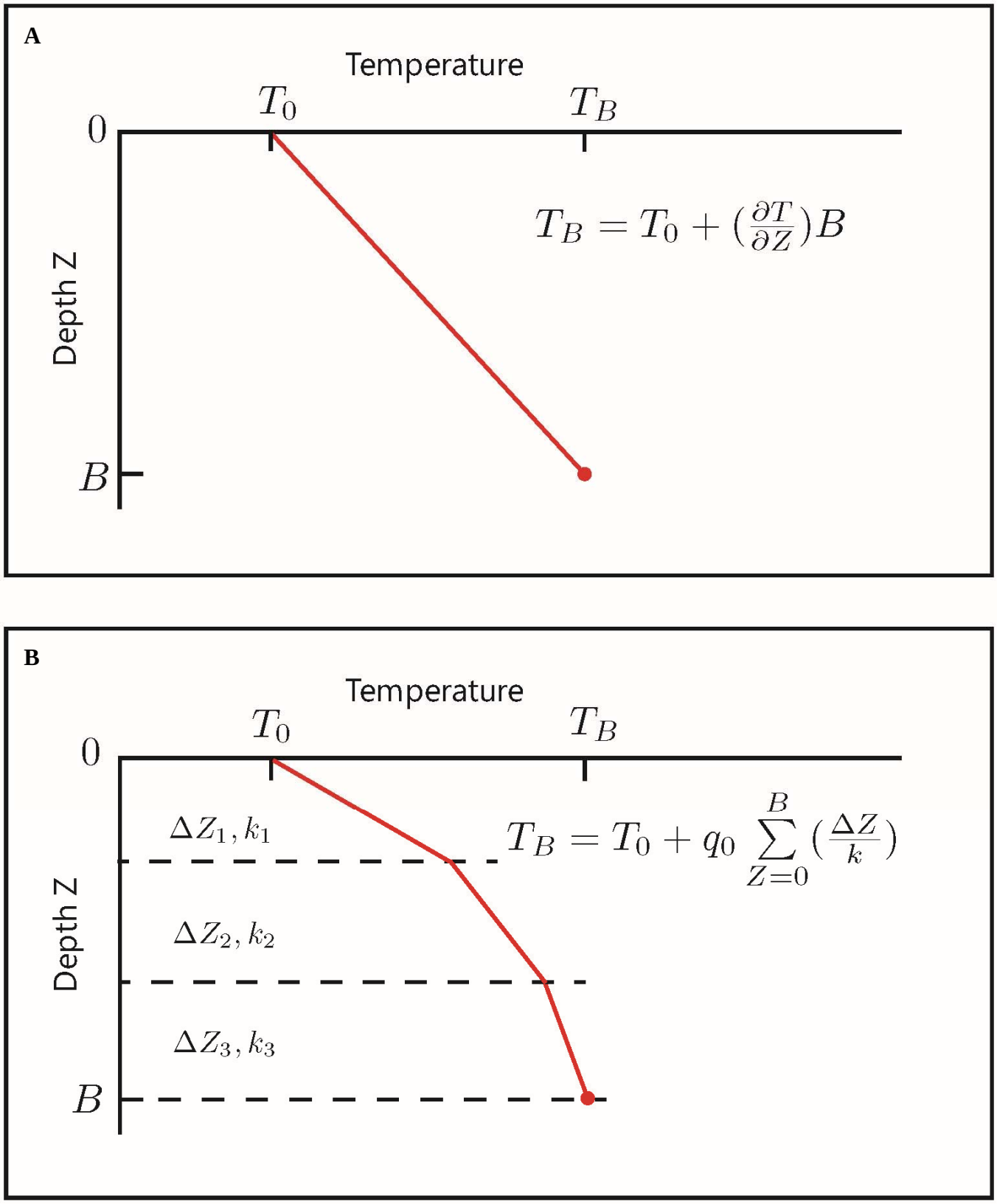

Figure 12.3. Simple Gradient (A) and Thermal Resistance Methods (B) plots (modified from Chapman and others, 1984).

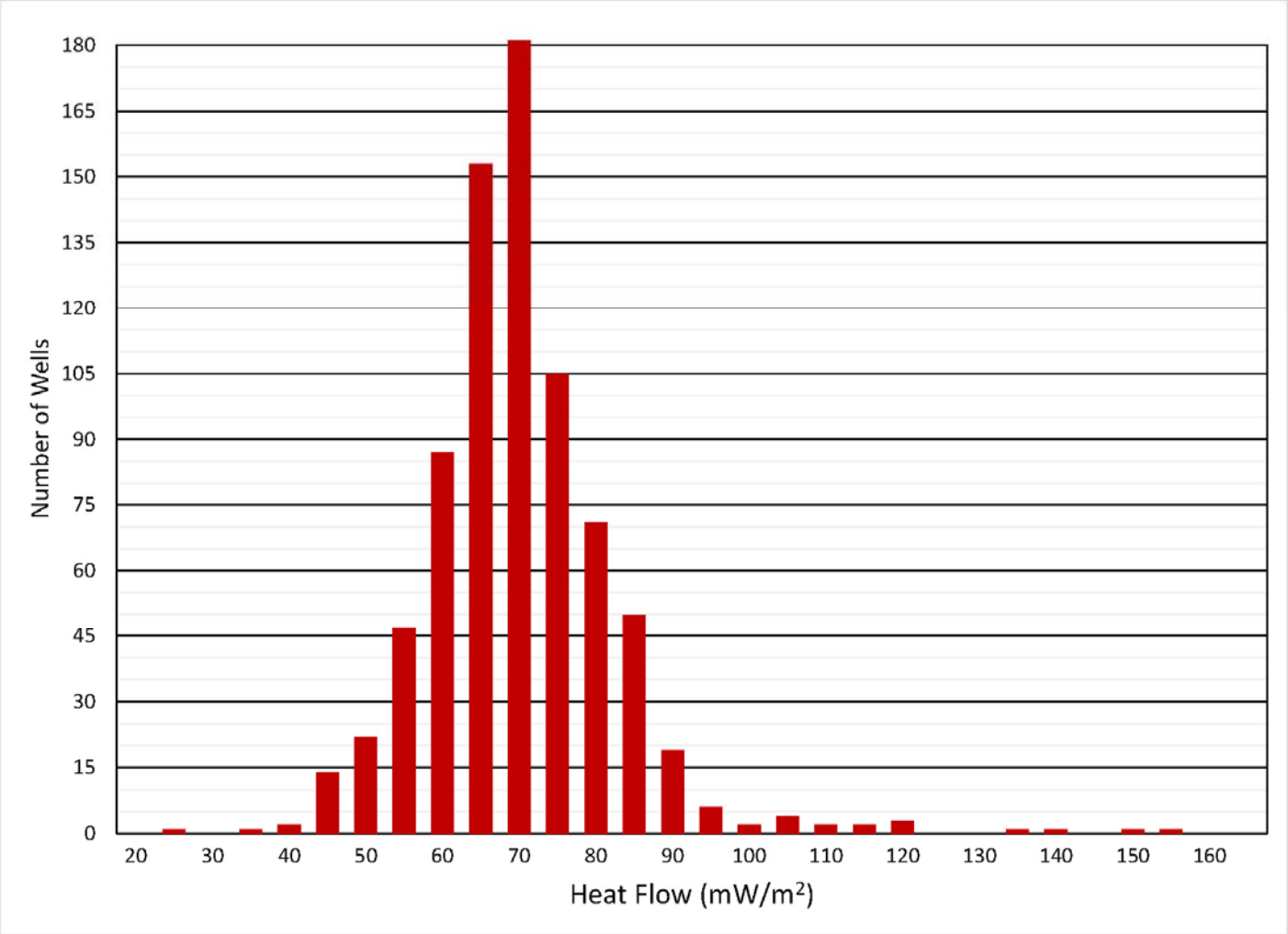

Figure 12.4. Histogram showing the distribution of calculated heat-flow values.

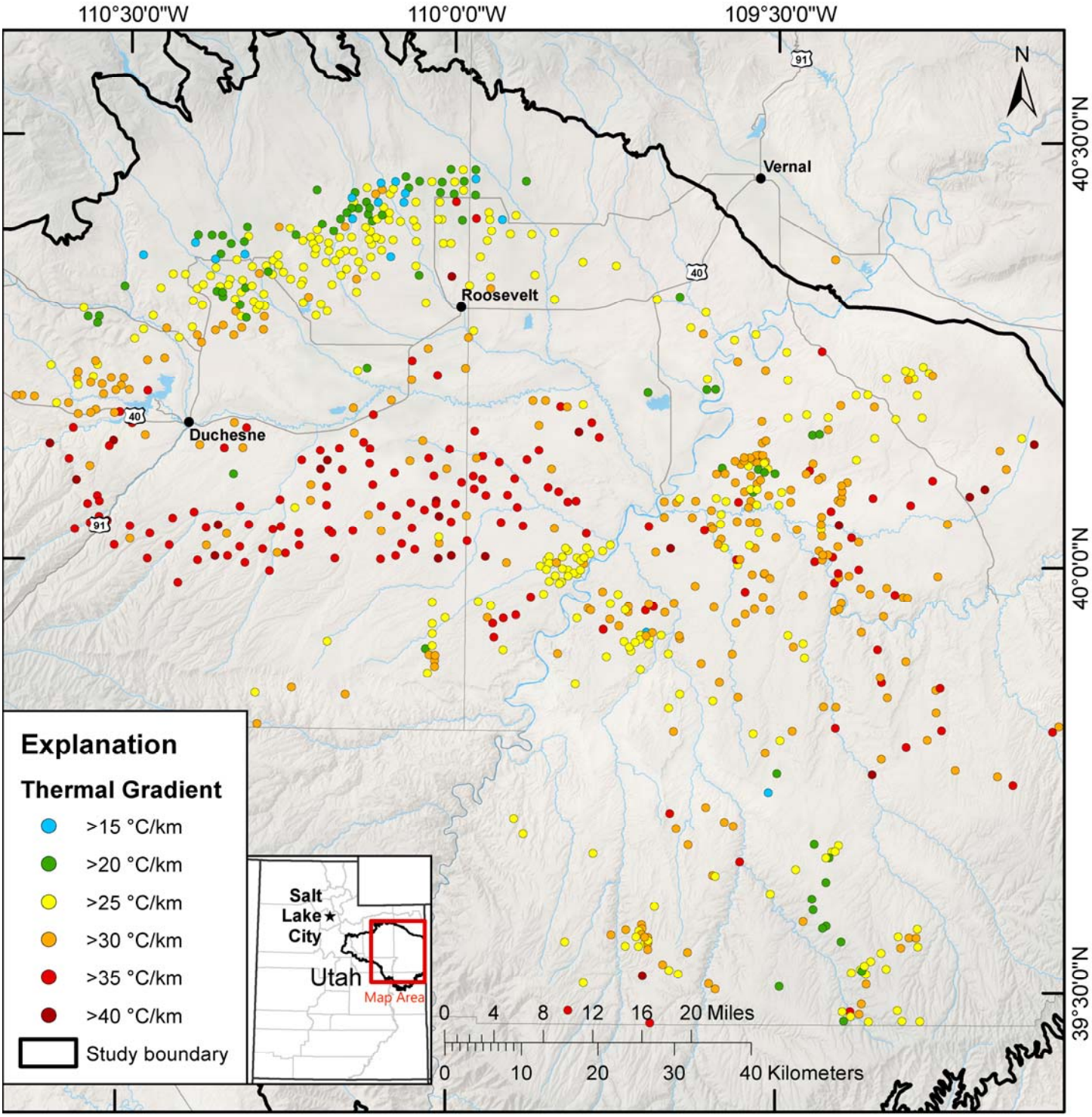

Figure 12.5. Thermal gradients of oil and gas wells. These wells, categorized by corrected BHTs, show the general trend of thermal gradients in the Uinta Basin. Gradients are slightly higher than the average of 27°C/km (1.48°F/100 ft) along the center of the basin with cooler than average gradients to the north and south. Gradients may be cooler along the northern margins due to groundwater recharge from the south flank of the Uinta Mountains.

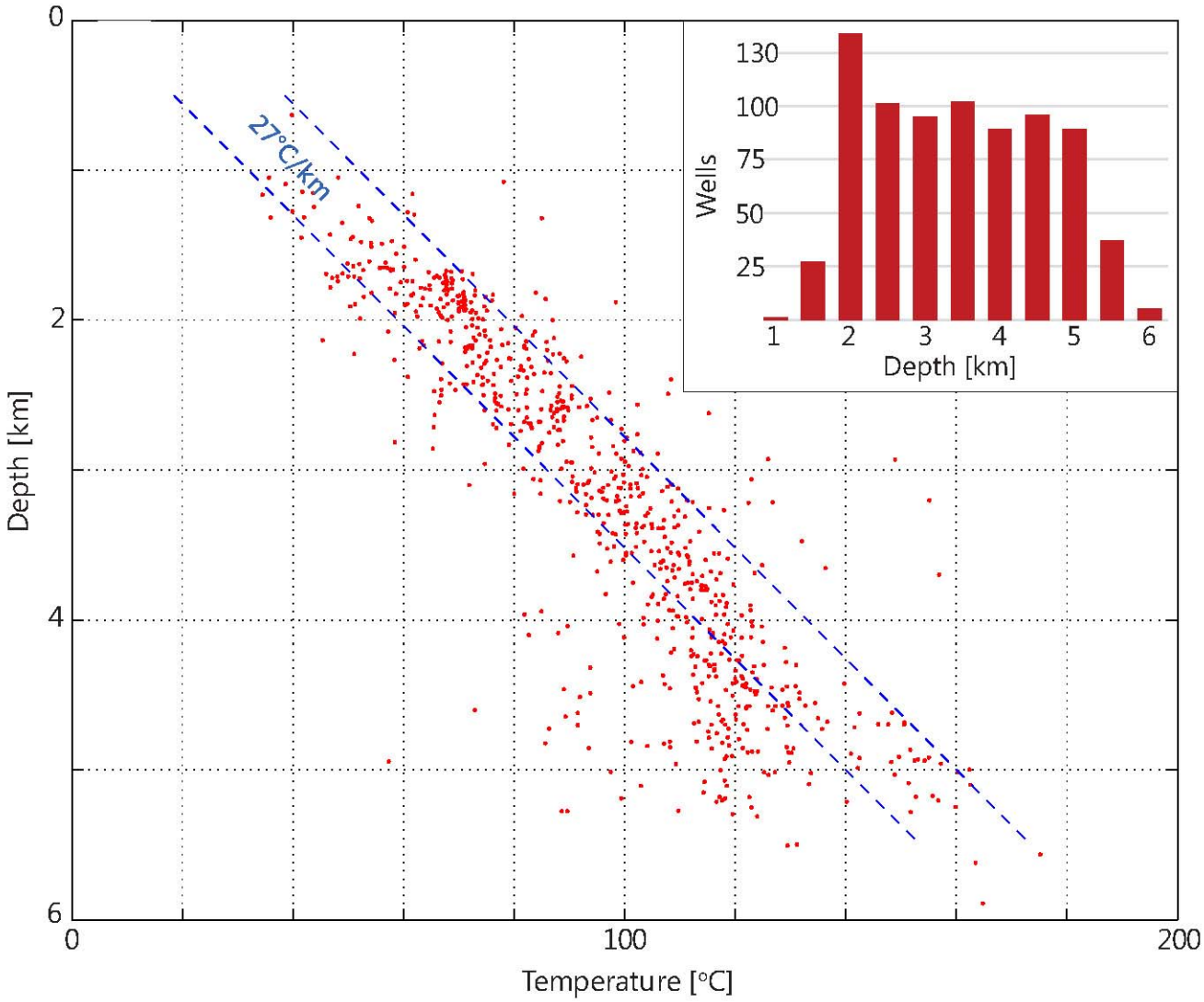

Figure 12.6. Temperatures at depth. The average thermal gradient of 27°C/km (1.48°F/100 ft) is bracketed over a range of surface temperatures. Well depth distribution in upper-right corner.

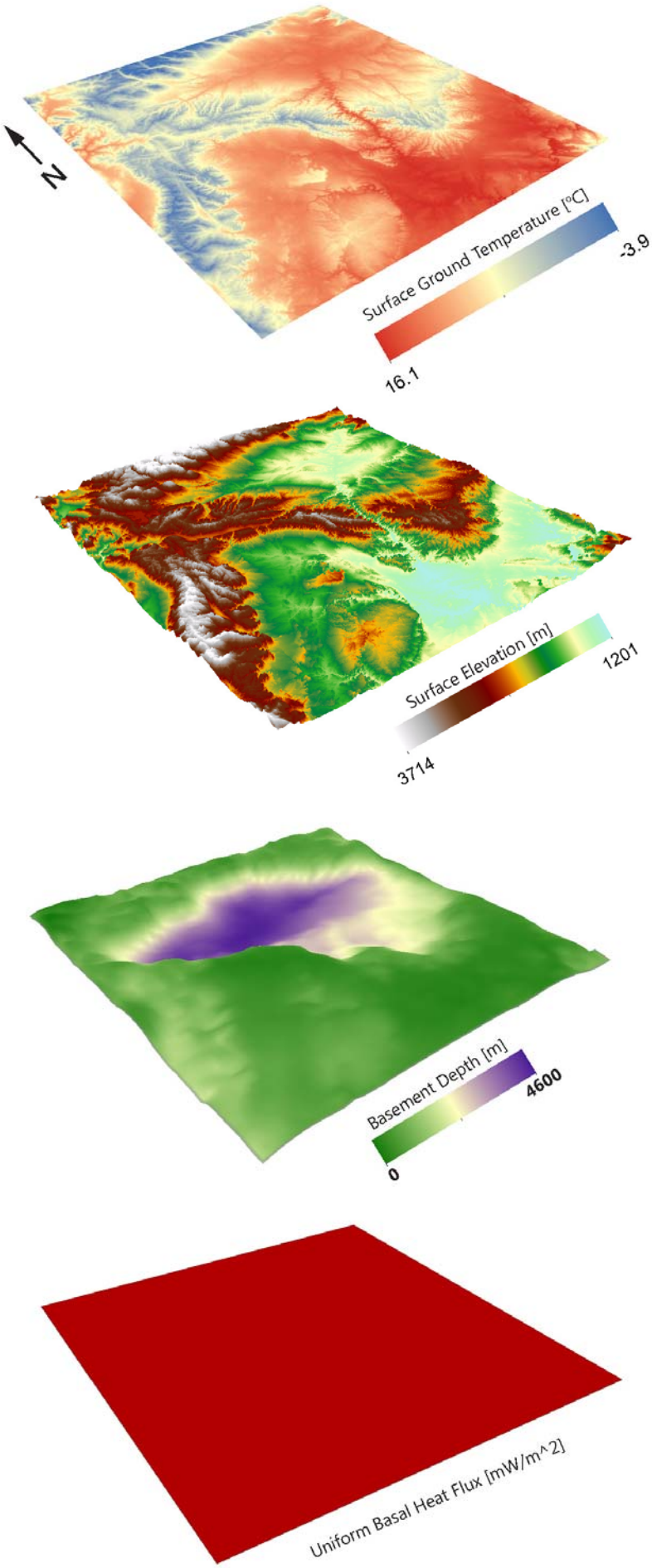

Figure 12.7. Thermal model framework including upper and lower boundary conditions.

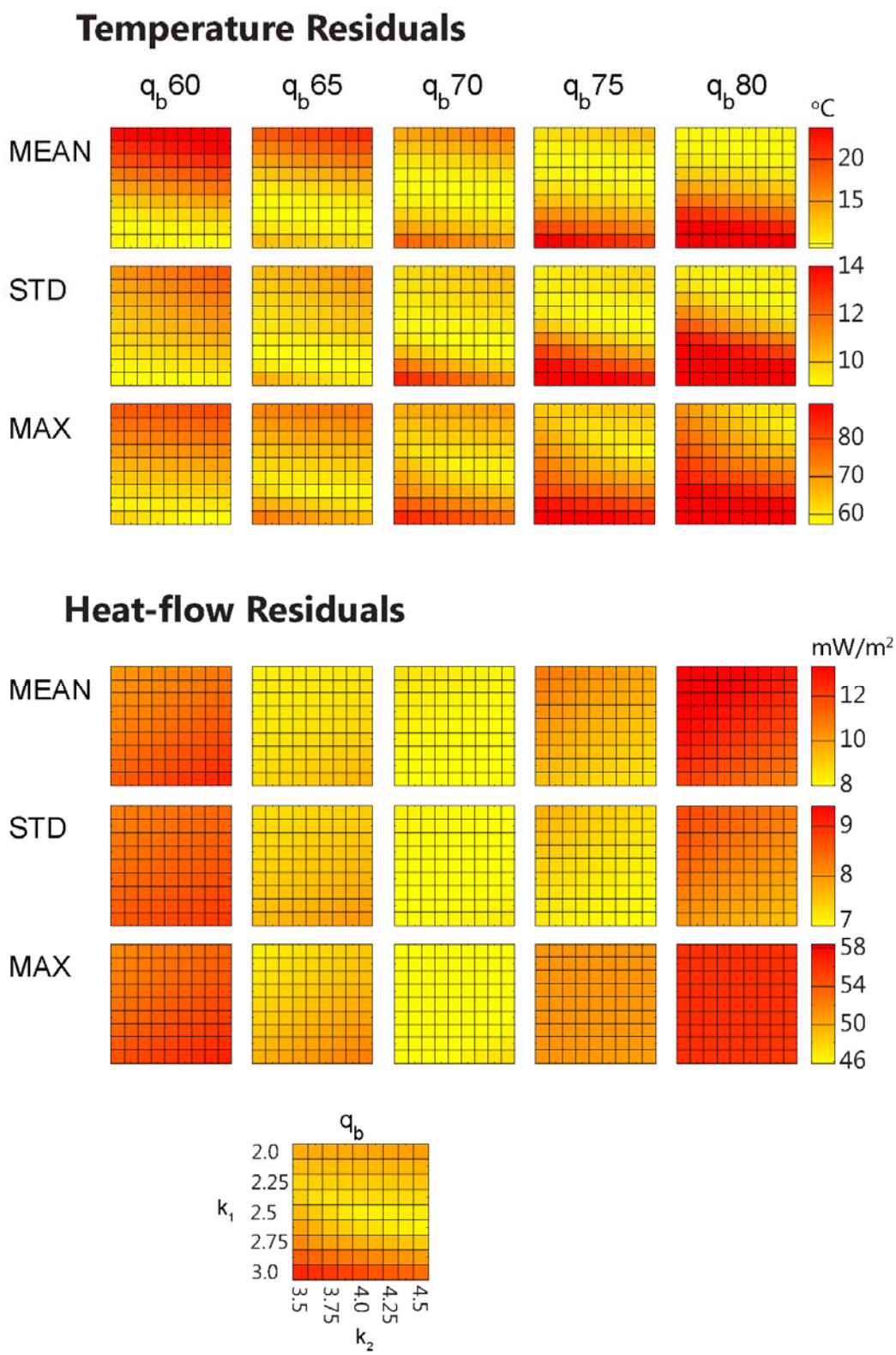

Figure 12.8. Residuals of model results to observed data for each model parameter set represented as mean, standard deviation, and maximum. Top panel shows temperature residuals and bottom panel shows surface heat-flow residuals.

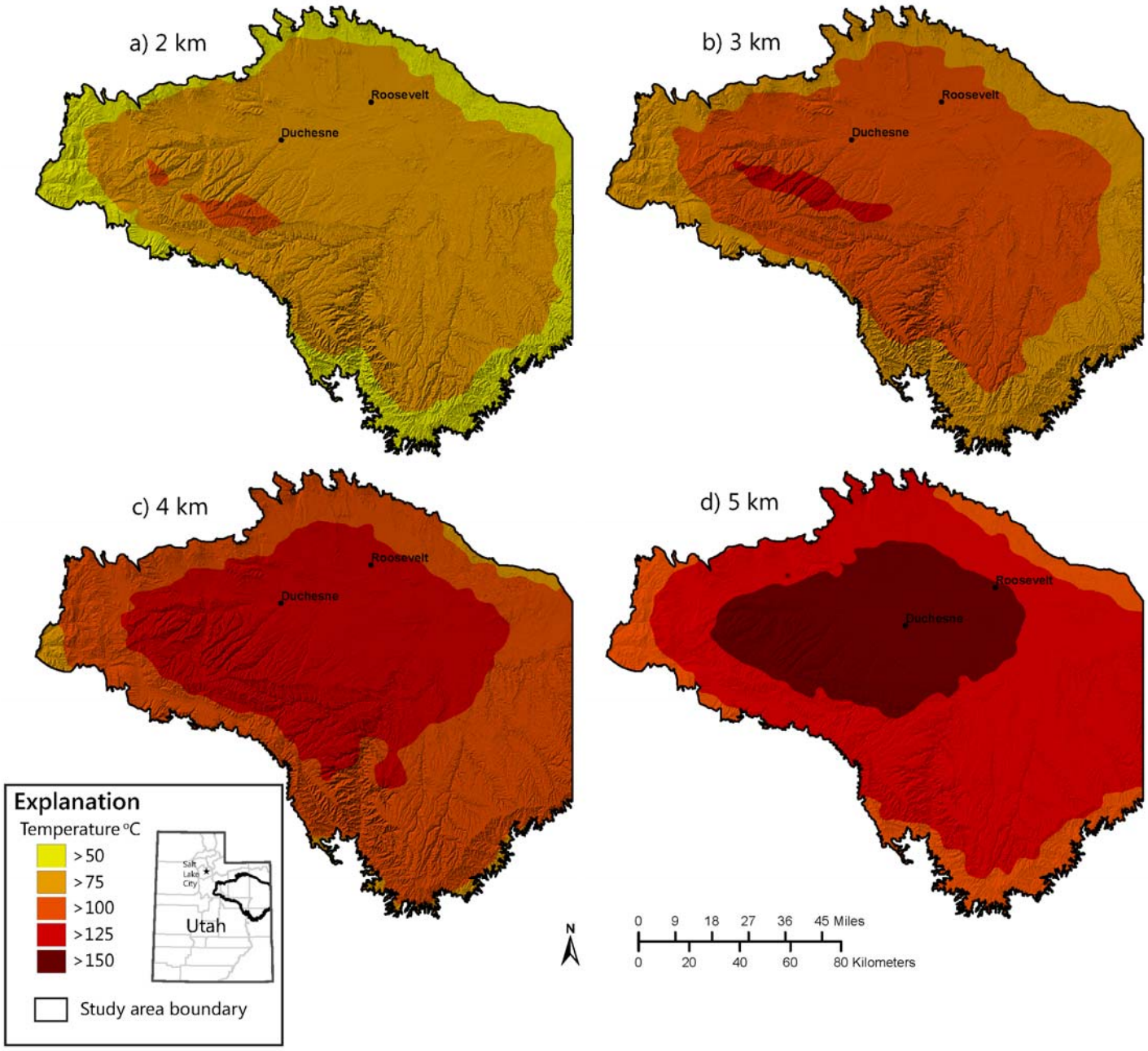

Figure 12.9. Maps of the temperature field at planes of constant elevation below the average elevation of the Uinta Basin.

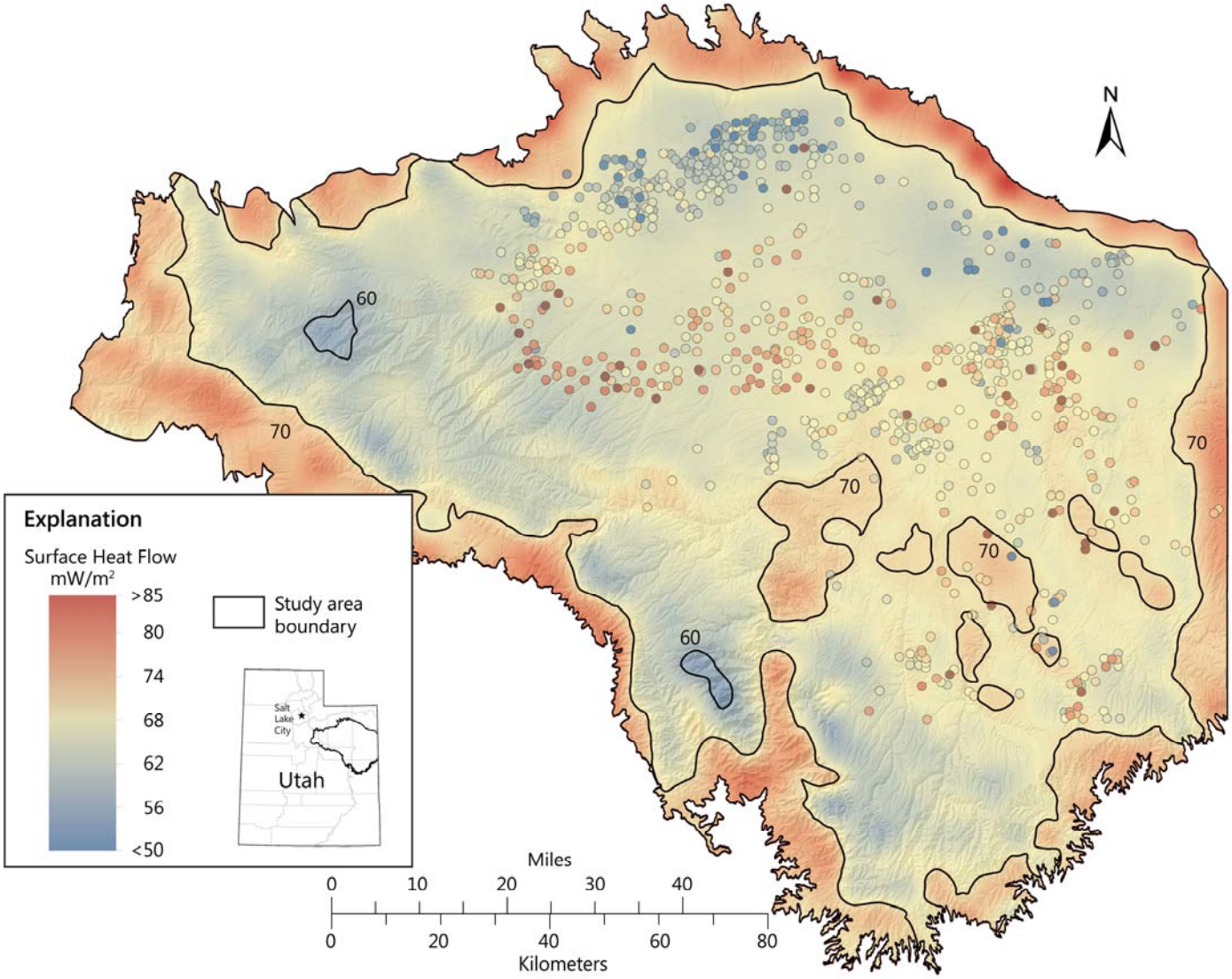

Figure 12.10. Surface heat flow from Uinta Basin thermal model and corrected well data (symbols colored according to heat-flow values). Black lines are contours of heat flow in 10 mW/m^2 intervals.

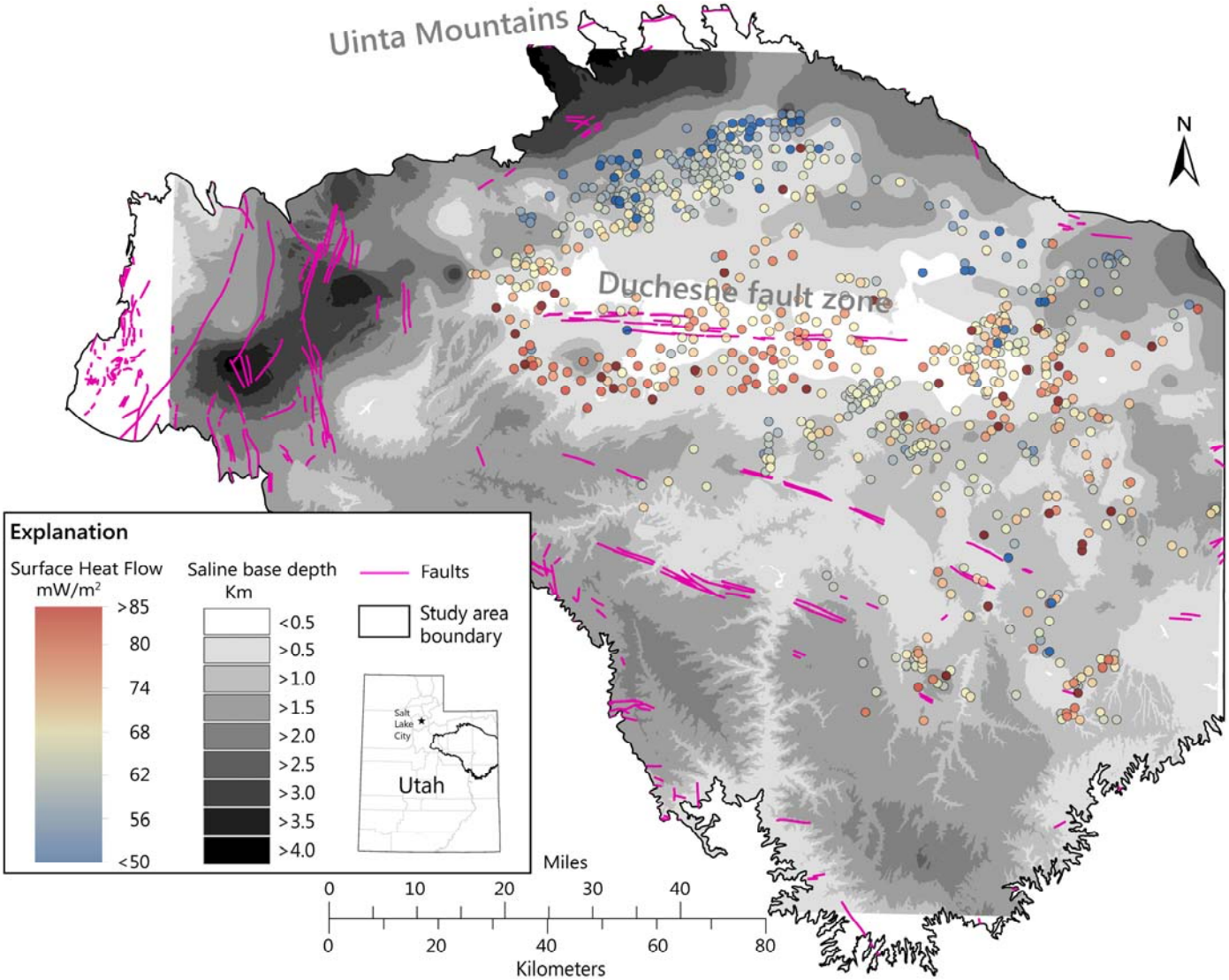

Figure 12.11. Map of depth in kilometers to the base of the moderately saline water (data from Anderson and others, 2012) in the Uinta Basin. Well locations and calculated heat-flow values (symbols colored according to heat-flow values) are shown. Magenta lines are faults. A noticeable spatial correlation between the depths to the base of the moderately saline water and heat flow can be observed. Heat-flow values are lower in the northern area where the base to the saline water is deep and heat-flow values are higher in the central part of the basin where the base to the saline water is shallow.

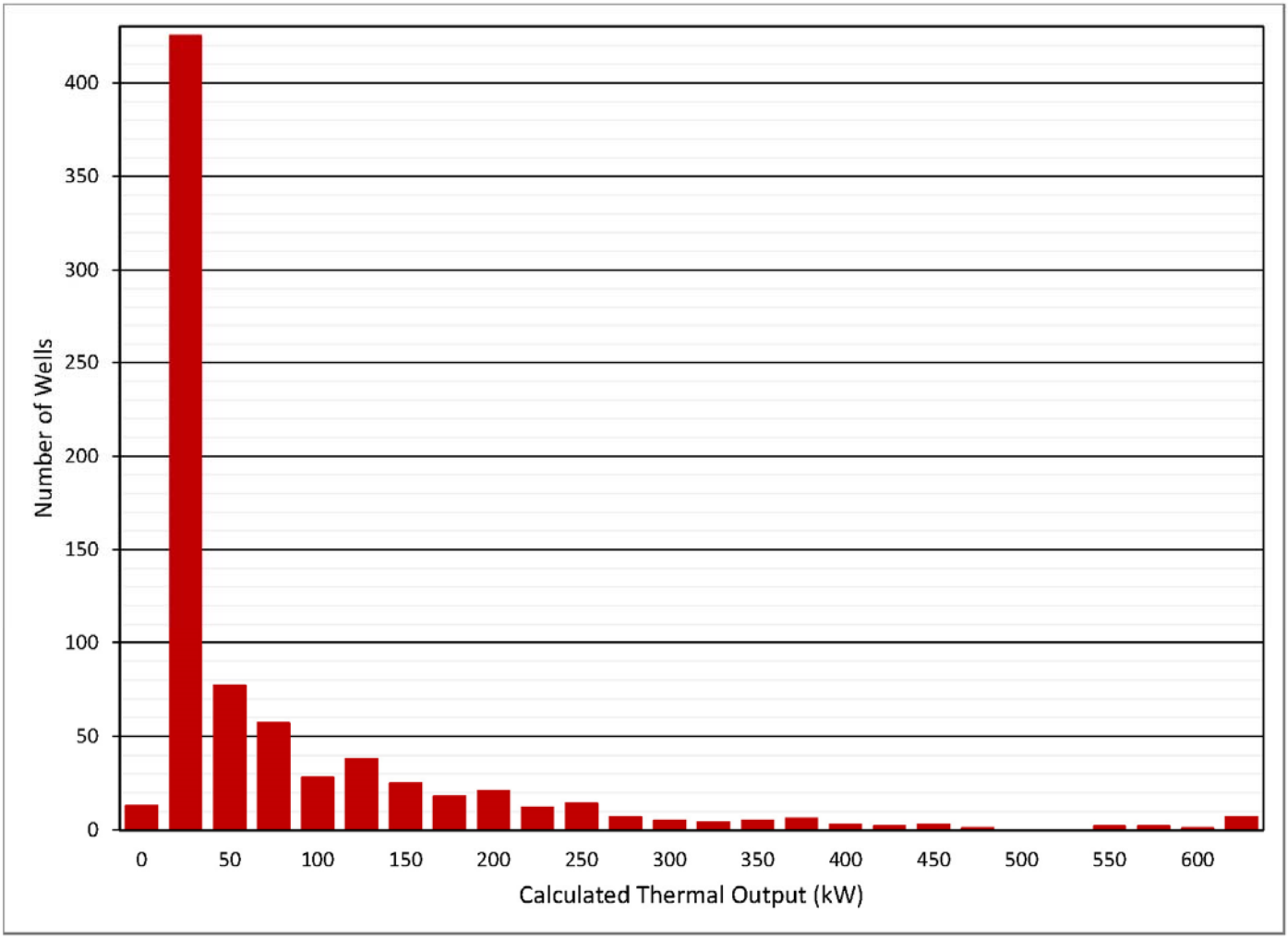

Figure 12.12. Histogram showing the distribution of calculated thermal output.

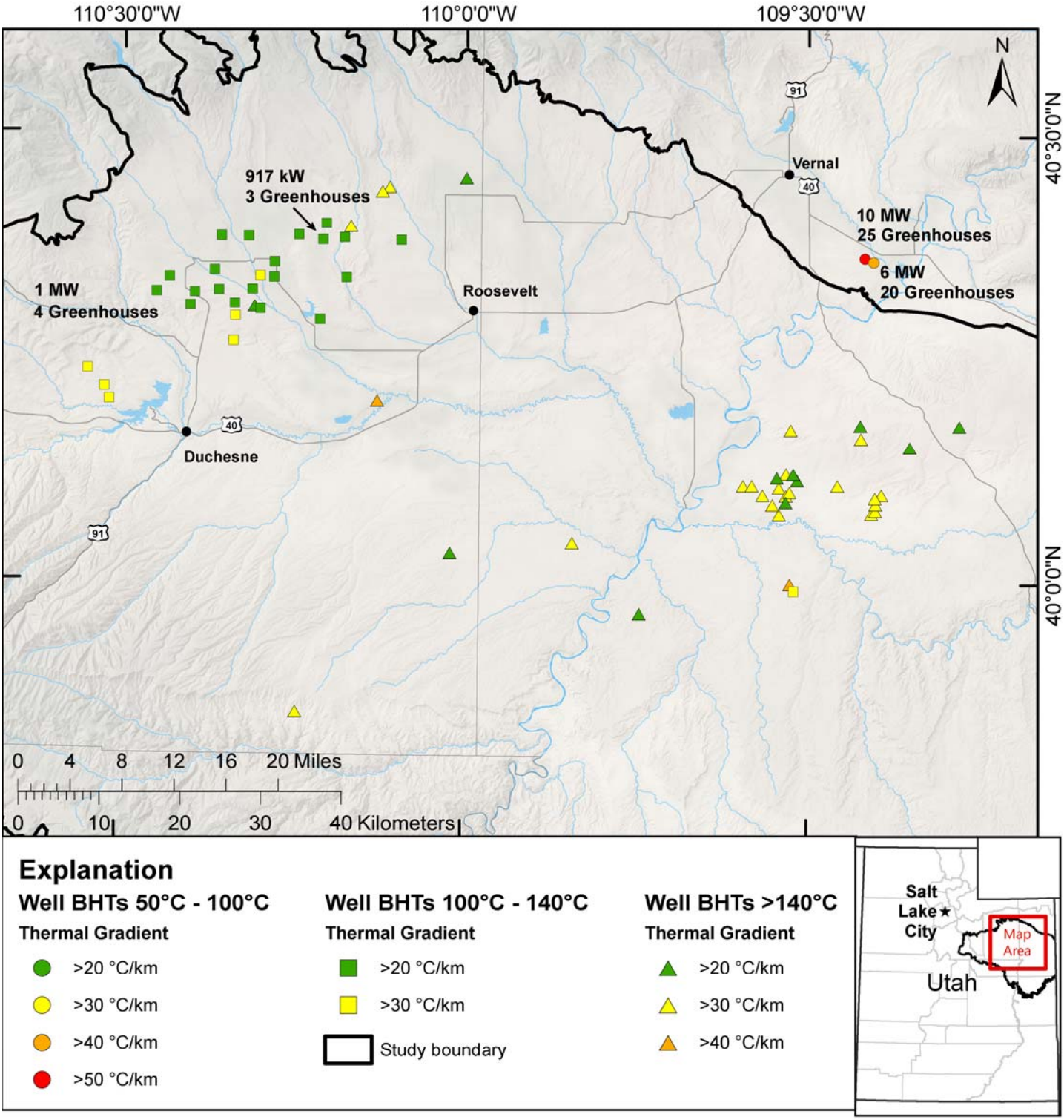

Figure 12.13. Map of wells co-producing water at a sufficient volume to support at least one 5037-square-foot (468 m^2) greenhouse (square symbol, indicated when more than three can be supported) and wells meeting required temperature threshold (> 140°C) for binary power generation (triangles). The potential is greatest for wells in Ashley Valley field near Vernal (see figure 1.1), in the northwest quadrant of the map, due to high volumetric output of co-produced fluid.

CHAPTER XIII

CONCLUSIONS AND RECOMMENDATIONS

Taylor Boden, Stephanie M. Carney, Thomas C. Chidsey, Jr., Richard Emerson, Christian Hardwick, Stefan Kirby, Craig D. Morgan, Peter Nielsen, Nathan Payne, Robert Ressetar, Rebekah W. Stimpson, David E. Tabet, Michael D. Vanden Berg, Janae Wallace, and Hobie W. Willis

The production and disposal of water from tight-sand gas reservoirs and potential shale-gas resources in the UB of eastern Utah, and elsewhere affects the economics of gas resource development and has recently become a topic of much public debate because produced water is the largest-volume waste stream associated with these unconventional gas plays. Managing produced water can be a significant cost fraction of the value of the gas extracted, thus there is an economic incentive to minimize this waste stream, and/or generate revenue from treating and reusing produced water in hydrocarbon production or other applications.

The major tight-gas sand reservoirs in the UB are the Tertiary Wasatch Formation and several formations in the Upper Cretaceous Mesaverde Group. Oil and gas fields in the basin produced nearly 33 MMBO and 363 BCFG in 2014 from the Green River (Eocene) and Wasatch Formations, and Mesaverde Group. Nearly 105 MMBW was also produced with these hydrocarbons. Balancing the water-use needs associated with Green River waterflood projects in the central part of the UB (Monument Butte field trend) and produced-water disposal requirements associated with shale/tight-sand gas development in the eastern part of the basin

creates significant material handling challenges to both industry and regulators. These challenges are complicated by an operating environment where many individual producers of varying sizes exist within a field, each with differing water needs and production, and a production timescale of decades for the basin as wells play out and new ones are completed.

Our study consisted of four major components: (1) compilation and analysis of past and new information on the thickness, structure, depth, lithology, water quality, and temperature of all aquifer/reservoir units in the UB from the Tertiary down through the Jurassic Glen Canyon Group; (2) statistical analysis of water production quantity and quality for each discrete tight-sand gas-producing interval; (3) development of alluvial aquifer sensitivity/vulnerability models to potential contamination from fluids associated with tight-sand gas development; and (4) an evaluation of the existing infrastructure for produced water management/reuse and recommendations for best management practices and the energy generation potential of geothermal-produced waters. The major conclusions and recommendations of these components are described in the following sections.

UINTA BASIN RESERVOIRS/AQUIFERS: TRIASSIC-JURASSIC GLEN CANYON GROUP THROUGH TERTIARY GREEN RIVER FORMATION

Triassic-Jurassic Nugget and Jurassic Navajo and Entrada Sandstones

- The Upper Triassic-Lower Jurassic Nugget and Lower Jurassic Navajo Sandstone is an excellent potential aquifer for produced water disposal where less than 10,000 feet in depth;

porosity decreases at greater depths. However, there are relatively few Navajo penetrations in the UB and the economics for drilling new disposal wells at the required depths are difficult to justify. Old wells that encountered Navajo/Nugget could be re-entered and completed as water disposal wells.

- The Jurassic Entrada Sandstone is projected to have less than 20 feet of porous sandstone throughout much of the basin. The amount of sandstone with 6% usable porosity in begins to decrease rapidly below 5000 feet drill depth. There are few penetrations of the Entrada in the deeper portion of the basin but areas of high porosity and permeability could exist which could either be hydrocarbon bearing or store produced water depending on the depth and proximity to oil and gas production.

Cretaceous Cedar Mountain and Dakota Formations

- The Cretaceous Cedar Mountain and Dakota Formations are predominantly fluvial channel deposits. There is an overall northeast-southwest thickness trend in study area. Thickness ranges from less than 25 feet in southeast part of the UB, to over 250 feet in the northeast part of the basin.

- A porous sand trend is parallel, but slightly southeast of net sandstone thickness trend. Thickness of porous sand with at least 6% porosity is generally less than half of the total sandstone thickness. However, porosity and permeability within the channel sandstones can be highly variable and difficult to predict.

- Channel deposits provide additional stratigraphic traps for hydrocarbons throughout the UB. Production can be spotty and volumes highly variable due to the heterogeneity of the lenticular channel deposits. These sandstones have very limited potential for produced water disposal.

Upper Cretaceous Mancos Shale

- The Mancos Shale is one of the thickest confining units in the Colorado Plateaus aquifer, separating the Dakota-Glen Canyon and Mesaverde aquifers.

- The sandstone content of the Mancos Shale, based on gamma-ray logs, show (not surprisingly) that sandstone constitutes less than 1% of the formation except where the Tununk and Blue Gate Shale Members interfinger with the Ferron and Emery Sandstone Members.

- The only produced-water disposal into the Mancos is local injection of water from CBM operations in the Ferron Sandstone Member on the southwestern margin of the Uinta Basin.

- With very low permeability, in the range of 0.05 to 160 nD, the Mancos is likely a poor candidate for produced-water disposal in most of the Uinta Basin. It continues to be a secondary drilling target for shale gas.

Upper Cretaceous Mesaverde Group

- The sandy formations in the upper part of the Mesaverde Group could make favorable produced water injection units, particularly around the margins of the UB where their water saturation is lower. The Tuscher and Farrer Formations are good candidates for disposal wells on the eastern side of the basin. Both formations, especially the Tuscher, have thick-blocky sandstones with good porosity. The Farrer has significant candidate sandstone channels for water disposal that are generally finer-grained, thinner, and less massive than the Tuscher channels. We calculated that three sandstone channels in the upper Tuscher, or approximately 40 feet of sandstone, would store up to 4.2 MMBW in a 1000-foot radius around a well.

- Further subdivision of the Mesaverde Group into units or facies would provide a more accurate representation of high and low porosity zones within each formation, but this level of detail was beyond the scope of this project. Additional studies of the Mesaverde should be conducted to correlate TDS and NaCl waters from laboratory analyses to formation water resistivity from well logs.

Upper Paleocene to Lower Eocene Wasatch/Colton Formation

- The Colton/Wasatch Formation contains sandstones that are candidates for water disposal. However, the thickness and continuity of any sandstone channel will be localized and will require long perforated zones and targeted perforations for disposal. Generally higher NGR

and PHIA in Colton/Wasatch suggest favorable conditions for water disposal. The Wasatch is an oil reservoir in the central parts of the basin and would lend itself to water flooding using produced water.

- There are two options recommended for disposing of produced water from the Mesaverde Group and the Colton/Wasatch Formation. One treatment option would desalinate produced water to decrease the volume of disposal, particularly where the water can be used in hydraulic fracturing operations, possibly for irrigation water, or for other surface uses. The second option is injecting produced water into sandstone beds of the Mesaverde or Colton/Wasatch either for waterflooding to enhance hydrocarbon production or as waste disposal.

Eocene Green Formation

- The GRF is a complex lacustrine sedimentary deposit that is up to 7000 feet thick and contains a wide range of lithologies. Main reservoir rocks are typically isolated lenticular sands with varying amounts of connectivity. As a result, water chemistry varies significantly both laterally and vertically.

- Water quality in the complex lower GRF varies widely from 650 to 112,000 mg/L of TDS. Recharge is mostly from the Wasatch Range to the west, the Douglas Creek arch and Uncompahgre uplift to the east-southeast, and the Uinta Mountains to the north.

Groundwater in the lower GRF seems to travel toward the Green River in the central portion of the basin coinciding with an area of higher TDS water.

- Water quality in the upper GRF also varies widely from 600 mg/L to over 200,000 mg/L TDS. Groundwater in the upper GRF is highly influenced by the location of saline mineral deposition, which occurs in three distinct phases and locations.

- The unique Birds Nest aquifer (phase 2 saline zone) in the upper GRF in the eastern part of the UB and the area located around the phase 3 saline interval in the western part of the basin, as well as select areas in the lower GRF, serve as excellent produced water disposal zones since reservoir water already exceeds 10,000 TDS (mg/L).

SUMMARY OF THE COMPILED FLUID GEOCHEMISTRY DATABASE FOR THE UINTA BASIN

- Highest TDS tends to correlate with sodium chloride or sodium bicarbonate water types that are typical of the upper and lower Green River, Wasatch-Colton, and Mesaverde units. These samples are predominately produced water and the high TDS and may be the result of oil and gas generation processes, long residence time, and or increased water rock interaction within these units. Lower TDS values and bicarbonate water types area typical of the Unconsolidated, Uinta-Duchesne River, Glen Canyon units. These chemistries likely result

from a relatively active meteoric groundwater system within these units where they are near surface.

- The samples in this database represent a unique regional scale snapshot of fluid geochemistry across an active petroleum province including both the shallow meteoric groundwater system and the deeper basin fluid system. Further study and geochemical analysis of these data could yield insight into large scale fluid evolution in both active petroleum provinces and similar geographic setting elsewhere.

GROUNDWATER CHEMISTRY AND WATER QUALITY FOR SHALLOW ALLUVIAL WELLS AND SPRINGS IN THE UINTA BASIN

- The UB generally lacks sufficient water-quality data to characterize the area's relatively shallow groundwater. To establish a baseline of water quality for springs and alluvial wells, water samples representing a widespread distribution of sites were collected throughout the the basin. Shallow groundwater-quality information will help apply environmentally sound, water-management solutions for the continued development of tight-sand gas reservoirs and potential shale-gas resources in the UB.

- Water samples were collected from 12 water alluvial wells and 10 springs in the UB, and augmented the data from two springs sampled by the UDWQ. A suite of water-quality

constituents was analyzed, including: general chemistry and TDS, nitrate, dissolved metals (including lead, iron, and zinc), VOCs, TPH, and stable isotopes (^{18}O and ^{2}H).

- Overall, samples show variable water quality throughout the study area indicating there are multiple aquifers that are not connected. TDS concentrations for all samples range from 214 to 5532 mg/L and nitrate concentrations range from <0.1 to 5.32 mg/L for all samples. Dissolved-solids concentrations were highest from a spring along the White River and lowest from a shallow well located in the northern part of the UB near recharge from the Uinta Mountains to the north.

- Most sites have nitrate concentrations below 0.1 mg/L (the detection limit) with the exceptions of one alluvial well near Evacuation Creek in the southeastern part of the basin and one spring north of Duchesne, downgradient from an active gravel pit. Some samples had detectable VOCs, but all were below the EPA's maximum contaminant levels, except for some sites having elevated chloromethane. No samples had detectable TPH. Oxygen and deuterium isotopes in sampled water indicate multiple recharge locations, except for northern wells that may receive recharge from a common area from the nearby high-elevation Uinta Mountains.

- If sound water management practices are not implemented, water-quality degradation may result from an increase in mining activity/energy resource development. This regional baseline water study provides information to help local planners and potential developers preserve the quality of groundwater and surface water by establishing best management

practices through careful land-use planning. To ensure good water quality is preserved, we recommend sampling most of the sites annually or every three years at the least.

SENSITIVITY AND VULNERABILITY OF THE AQUIFERS AND SPRINGS IN THE UINTA BASIN, TO POTENTIAL CONTAMINATION ASSOCIATED WITH TIGHT-SAND GAS PRODUCTION AND POTENTIAL SHALE-GAS RESOURCE DEVELOPMENT

- The UB is better known for productive oil and gas wells than for water resources. The principal goal of this part of the study was to investigate sensitivity and vulnerability of groundwater resources in the UB to contamination from industrial and natural chemicals (e.g., VOCs) commonly associated with energy resource extraction, especially tight-sand gas reservoirs and potential shale-gas resources in the eastern part of the basin. The project scope was limited to the use and interpretation of existing data to produce VOC sensitivity and vulnerability maps through the application of GIS analysis methods.

- Analysis of water samples collected from water wells and springs in the UB show overall good water quality, but some sites have VOC concentrations above detection levels including benzene, vinyl chloride, bromomethane, chlorobenzene, chloromethane, and toluene. We recognized the potential for these contaminants to reach groundwater in the basin and used benzene as the representative VOC in our sensitivity/vulnerability analyses and assessment.

- Using GIS analyses, we combined index-based, process-based, and overlay methods to determine aquifer sensitivity and vulnerability in the UB. The resultant attribute and ranking assessment shows that the areas most sensitive to groundwater contamination by VOCs occur where near-surface permeable layers are near streams and lakes, especially in areas having relatively high hydraulic conductivities, high VOC retardation factors, and low VOC attenuation factors. High vulnerability areas are located near water bodies, water wells/springs, and in close proximity to high-density oil/gas wells, some within DWSP zones.

- Potential groundwater and surface water-quality degradation may result from continued production and drilling activity if sound water-management practices are not enforced. Our regional water study will provide GIS-based information to help local planners and potential developers preserve the quality of shallow groundwater and springs by establishing best-management practices through careful land-use planning. The maps produced are intended to be used to advise water users on proper disposal of wastewater associated with non-conventional oil/gas development in the Uinta Basin and ultimately to provide local, state, and federal government agencies and industry operators with a base of information concerning sensitivity and vulnerability of groundwater to VOCs in the UB.

- We recommend VOC groundwater monitoring may be necessary in areas of high sensitivity or high vulnerability areas in and near DWSP zones. Water sampling and testing in areas of

the basins characterized by low and moderate sensitivity and vulnerability may also be warranted, but at a lower frequency than for areas with higher sensitivity and vulnerability.

HANDLING AND MANAGEMENT OF WATER PRODUCED FROM OIL AND GAS RESERVOIRS IN THE UINTA BASIN

- Produced water volumes from petroleum development in the four-county UB study area have increased over the last seven years (2008-2014) from 86 to 116 MMB per year. Current water management practices used by petroleum companies in the UB for the disposition of the 116 MMB of produced water in 2014 is estimated as follows: 68 MMB (58.6%) to disposal wells, 24 MMB (20.7%) used for EOR, 13.7 MMB (11.8%) sent to evaporation ponds, 1.5 MMB (1.3%) reused in hydraulic fracturing, and 8.8 MMB (7.6%) lost to evaporation.

- Disposal of produced water in deep injection wells has increased from 43 to nearly 68 MMB per year from 2008 through 2014; the corresponding number of deep disposal wells has increased over that same period from 56 to 92. The amount of water used in EOR waterflood projects has increased from over 25 to over 44 MMBW per year from 2008 through 2014. Newfield Exploration reused up to 10 MMB of produced water in 2014 for its waterflood needs at Monument Butte oil field; one approach that should be investigated in detail is to transport the excess produced water from the gas fields in the eastern part of the basin for use in waterflooding in the oil fields of the central part of the basin. The amount of produced

water delivered to commercial and private evaporation ponds has varied from 11.9 to 17.3 MMB, and averaged about 13.7 MMB per year.

- Anadarko's ACTS technology at Natural Buttes gas field recycled nearly 100% of the water recovered after the hydraulic fracturing process and reused it in new well-completions, which conserves fresh water and reduces truck traffic. On average this reuse is estimated involve about 1.5 MMB of flow-back produced water. EOG's plans to minimize fresh water usage in the drilling and completion of new wells by only using 12% from fresh water sources, and obtaining the remaining 88% from recycled water from the Bonanza power plant of Deseret Generation and Transmission. Assuming the drilling development period spans 15 years, then EOG could eliminate 2,775,802 bbls of fresh water use annually by substituting recycled power plant water.

- Regulatory agencies in Utah are encouraging petroleum development companies to reuse drilling wastes such as produced water to reduce fresh water consumption; however, many of the best management practices are practical only when the developments in an area reach a critical size where implementing centralized water collection, handling, treatment, and reuse or disposal achieves the economies of scale to become cost effective. Produced water management in Utah is a large and dynamic management challenge that requires a flexible, adaptive regulatory scheme to meet ever changing conditions and technologies in fields of variable size and with differing product and waste streams.

GEOTHERMAL ASSESSMENT AND MODELING OF THE UINTA BASIN

- Co-produced waters from sedimentary basins may represent a significant geothermal resource. This regional assessment of the geothermal potential for co-produced waters from oil and gas fields in the UB used BHT and co-produced water data from 776 oil and gas wells along with available lithological information.

- For 136 of the wells, a BHT correction is applied using Horner and single-BHT correction methods to account for drilling-induced temperature field disturbances. A conservative depth-dependent correction of +2.0°C/km (+0.11°F/100 ft) was derived from 50 UB wells with reliable Horner corrections and is applied to BHTs with insufficient data for other correction methods. Corrected temperatures and typical thermal conductivities are used to calculate thermal gradients and surface heat-flow values for each well.

- Calculations reveal an average geothermal gradient of about 27°C/km (1.48°F/100 ft), implying wells producing from depths greater than 2 kilometers (6562 ft) in the basin will likely have temperatures greater than 65°C (149°F). The average heat-flow value from wells with corrected BHTs is 67 mW/m^2. These results are generally typical for gradient and heat-flow values in the Colorado Plateau.

- Thermal outputs are calculated using well production rates and fluid temperatures. The average thermal output is 88 kW per well with a maximum output as high as 10 MW—

energy which is currently lost to waste water. The highest output wells are mostly a result of high volumetric production rates and are located in Ashley Valley field.

- Preliminary thermal models of the UB give some support to existing interpretations that the thermal regime is primarily conductive with the exception of groundwater flushing from the Uinta Mountains. These models reveal an area of approximately 16,000 square kilometers (6180 mi^2) with temperatures above 75°C (167°F) at 2 kilometers (6560 ft) depth, and an area of 5500 square kilometers (2120 mi^2) with temperatures above 150°C (302°F) at 5 kilometers (16,400 ft) depth. In order to facilitate a more in-depth study of the UB, future versions of the 3D thermal models should incorporate basin-scale fluid flow to better address the effects of the groundwater flow hypotheses and will provide more accurate estimates of the resource potential within the basin.

- Co-produced water temperatures in 740 wells are above 50°C (122°F) and may be suitable for direct-use applications such as greenhouses, space heating, and aquaculture. Binary geothermal power plants generally require a minimum temperature of 140°C (284°F) to achieve acceptable efficiency and 36 wells (~5%) across the basin meet or exceed such temperatures. The thermal regime and existing infrastructure make the UB a candidate for extensive direct-use geothermal applications and possibly binary geothermal power generation.

ACKNOWLEDGMENTS

Funding for this project was provided by the Research Partnership to Secure Energy for America (RPSEA) through the "Small Producer Program," authorized by the U.S. Energy Policy Act of 2005. RPSEA (www.rpsea.org) is a nonprofit corporation whose mission is to provide a stewardship role in ensuring the focused research, development and deployment of safe and environmentally responsible technology that can effectively deliver hydrocarbons from domestic resources to the citizens of the United States. RPSEA, operating as a consortium of premier U.S. energy research universities, industry, and independent research organizations, manages the program under a contract with the U.S. Department of Energy's National Energy Technology Laboratory (DOE NETL).

The research for the *Basin-Scale Produced-Water Management Tools and Options – GIS-Based Models and Statistical Analysis of Shale Gas/Tight Sand Reservoirs and Their Produced-Water Streams* project was performed under the direction of the UGS, Thomas C. Chidsey, Jr., Principal Investigator. Partial funding was also provided by the UGS. Industry partners and contributors (consortium) for this project included the following: Anadarko Petroleum Corp.; EOG Resources, Inc.; Wind River Resources, Inc.; and QEP Resources, Inc. Collaborating regulatory agencies included the Utah Department of Natural Resources (Division of Oil, Gas, and Mining; Division of Water Rights; Utah Division of Water Resources), the Utah Department of Environmental Quality, U.S. Bureau of Land Management, and again, U.S. Environmental Protection Agency. We especially thank Kenny Gathings, Kenny Warren, John Kynaston, and Mike Merrill of Anadarko Petroleum for providing access to operator's waste-water facilities in Natural Buttes field and providing valuable best pracices information for the project. J.D.

Horrocks, Newfield Exploration provided access to operator's waste-water facilities in Monument Butte field. We also thank Tricia Pfeiffer, Cindy Beeler, and Carol Russell of the EPA's Region 8 office (Denver) for their support.

Vicky Clarke, Cheryl Gustin, Kim Nay, Nathan Payne, Jay Hill, and Nikki Simon of the UGS, prepared the figures, tables, and maps. Cheryl Gustin prepared the manuscript and appendices for submission. The Utah Division of Oil, Gas, and Mining provided information and photographs of produced water facilities and infrastructure in the Uinta Basin. Scott Hacking (UDEQ) helped with field reconnaissance and provided information on potential well sites.

This report was carefully reviewed by following: Scott Hacking (UDEQ); Mike Lowe, Brittany Dame, Mike Hylland, Kimm Harty, and Richard Allis (UGS); and ?? RPSEA, Sugar Land, Texas, and ??, NETL. Their careful reviews and constructive criticism greatly improved the manuscript.

REFERENCES

Allen, J., Si-Young, L., and Potter, S., 2011, Three dimensional geologic model of the eolian Jurassic Navajo Sandstone in central Utah for the evaluation of CO_2 sequestration: Utah Geological Association Guidebook 42, p. 223-260 (Ch-4).

Aller, L., Bennett, T., Lehr, J.H., and Petty, R.J., 1985, DRASTIC—a standardized system for evaluating groundwater pollution potential using hydrogeological settings: Ada,

Oklahoma, U.S. Environmental Protection Agency, Office of Research and Development, Robert S. Kerr Environmental Research Laboratory, 163 p. (Ch-10).

Allis, R., Blackett, R., Gwynn, M., Hardwick, C., Moore, J.N., Morgan, C., Schelling, D., and Sprinkel, D., 2012, Stratigraphic reservoirs in the Great Basin—the bridge to enhanced geothermal systems in the U.S.: Transactions, Geothermal Resources Council, v. 36, p. 351–357 (Ch-12).

Allis, R., Moore, J., Blackett, B., Gwynn, M., Kirby, S., and Sprinkel, D., 2011, The potential for basin-centered geothermal resources in the Great Basin: Transactions, Geothermal Resources Council, v. 35, p. 683–688 (Ch-12).

Anadarko Petroleum Corporation, 2015, Utah fact sheet: Online, http://www.anadarko.com/content/documents/apc/news/Fact_Sheets/Utah_Fact_Sheet.pdf, accessed on April 1, 2015 (Ch-11).

Andaverde, J., Verma, S.P., and Santoyo, E., 2005, Uncertainty estimates of static formation temperatures in boreholes and evaluation of regression models: Geophysics Journal International, v. 160, p. 1112–1122 (Ch-12).

Anders, D.E., Palacas, J.G., and Johnson, R.C., 1992, Thermal maturity of rocks and

hydrocarbon deposits, Uinta Basin, Utah, *in* Fouch, T.D., Nuccio, V.F., and Chidsey, T.C., Jr., editors, Hydrocarbon and mineral resources of the Uinta Basin, Utah and Colorado: Utah Geological Association Publication 20, p. 53-76 (Ch-7).

Anderson, D.S., and Harris, N.B., 2006, Integrated sequence stratigraphic and geochemical resource characterization of the lower Mancos Shale, Uinta Basin, Utah: Utah Geological Survey Open-File Report 483, compact disk (Ch-5).

Anderson, P.B., 1983, Geologic map of the Pine Canyon quadrangle, Carbon County, Utah: Utah Geological and Mineral Survey Map 72, scale 1:24,000 (Ch-2).

Anderson, P.B., 2005, Mesaverde gas of southeastern Uinta Basin: Utah Geological Survey, Open-File Report 460, 42 p. (Ch-6).

Anderson, P.B., Vanden Berg, M.D., Carney, S., Morgan, C., and Heuscher, S., 2012, Moderately saline groundwater in the Uinta Basin, Utah: Utah Geological Survey Special Study 144, 35 p. (Ch-4, Ch-7, Ch-8, Ch-9, Ch-12).

Anderson, P.B., Willis, G.C., Chidsey, T.C., Jr., and Sprinkel, D.A, 2010, Geology of Glen Canyon National Recreation Area, Utah-Arizona, *in* Sprinkel, D.A., Chidsey, T.C., Jr., and Anderson, P.B., editors, Geology of Utah's parks and monuments (3rd edition): Utah Geological Association Publication 28, p. 309-347 (Ch-3).

Archie, G.E., 1942, The electrical resistivity log as an aid in determining some reservoir characteristics: Journal of Petroleum Technology, v. 5, p. 54-62 (Ch-6).

Armstrong, R.L., 1968, Sevier orogenic belt in Nevada and Utah: Geological Society of America Bulletin, v. 79, p. 429-458 (Ch-2).

Aschoff, J.L., 2010, Preliminary regional sequence stratigraphic framework and characterization of potential fluvial reservoirs of the upper Mesaverde Group, Uinta Basin, Utah: Utah Geological Survey Open-File Report 569, 43 p. (Ch-6).

Asquith, G., and Krygowski, D., 2004, Basic well log analysis: American Association of Petroleum Geologists Methods in Exploration Series No. 16, 244 p. (Ch-6).

Bader, J.W., 2009, Structural and tectonic evolution of the Douglas Creek arch, the Douglas Creek fault zone, and environs, northwestern Colorado and northeastern Utah—implications for petroleum accumulation in the Piceance and Uinta Basins: Rocky Mountain Geology, p. 121-145 (Ch-6).

Banton, O., and Villeneuve, J., 1989, Evaluation of groundwater vulnerability to VOCs—a comparison between the VOC DRASTIC index and the PRAM leaching quantities: Journal of Contaminant Hydrology, v. 4, p. 285–296 (Ch-10).

Beardsmore, G.R., and Cull, J.P., 2001, Crustal heat flow—a guide to measurement and modeling: Cambridge, Cambridge University Press, 334 p. (Ch-12).

Ben Dhia, H., 1988, Tunisian geothermal data from oil wells: Geophysics, v. 53, no. 11, p. 1479–1487 (Ch-12).

Benko, K.L., and Drewes, J.E., 2008, Produced water in the western United States—geographical distribution, occurrence, and composition: Environmental Engineering Science, v. 25, no. 2, p. 239-246 (Ch-11).

Bereskin, S.R., Taff, D.E., and Ballou, R.L., 1993, Enhanced fracture permeability and unconventional production potential along the Duchesne fault zone, Uinta Basin, Utah [abs.]: American Association of Petroleum Geologists Bulletin, v. 77, p. 1442 (Ch-3).

Bernknopf, R.L., Dinitz, L.B., and Loague, K., 2001, An interdisciplinary assessment of regional-scale nonpoint source groundwater vulnerability—theory and application: U.S. Geological Survey Professional Paper 1645, 21 p. (Ch-10).

Birgenheier, L.P., McCauley, A., Horton, B., and Ressetar, R., in preparation, Chapter 2—geologic setting, *in* Ressetar, R., and Birgenheier, L.P., editors, Cretaceous Mancos Shale, Uinta Basin, Utah—resource potential and best practices for an emerging shale gas play: Utah Geological Survey contract report (Ch-5).

Blackett, R.E., Sowards, G.M., and Trimmer, E., 2004, Utah's high temperature geothermal resource potential—analysis of selected sites: Utah Geological Survey Open-File Report, 124 p. (Ch-12).

Blackwell, D.D., Beardsmore, G.R., Nishimori, R.K., and McMullen, R.J., Jr., 1999, High resolution temperature logs in a petroleum setting—examples and applications, *in*, Förster, A., and Merriam, D.F., editors, Geothermics in basin analysis: New York, Plenum Press, p. 1-34 (Ch-12).

Blackwell, D.D., and Richards, M., 2004, Calibration of the AAPG geothermal survey of North America BHT data base [abs.]: American Association of Petroleum Geologists Extended Abstract 87616 (Ch-12).

Blakey, R.C., and Ranney, W., 2008, Ancient landscapes of the Colorado Plateau: Grand Canyon Association, 156 p. (Ch-2, Ch-4, Ch-6, Ch-7).

Bluefield Research, 2014, Water for U.S. hydraulic fracturing—competitive strategies, solutions, and outlook, 2014-2020: Online, http://bluefieldresearch.com/water-for-fracking-2014/, accessed July 1, 2015 (Ch-11).

Boden, T., and Tripp, B.T., 2012, Gilsonite veins of the Uinta Basin: Utah Geological Survey Special Study 141, 50 p. (Ch-2, Ch-3, Ch-9).

Borer, J., 2003, Day 3: High-resolution stratigraphy of the Green River Formation at Raven Ridge and Red Wash field, NE Uinta Basin–Facies and stratigraphic patterns in a high-gradient, high-energy lacustrine system, *in* Keighley, D., Borer, J., Morgan, C., McClure, K., and Griffen, R., editors, Facies asymmetry in alluvial-lacustrine basins—a transect across the Uinta Basin, eastern Utah and western Colorado: Guidebook, Field Trip #4, American Association of Petroleum Geologists Annual Convention, Salt Lake City, May 2003, p. 46-55 (Ch-7).

Borer, J., and McPherson, M., 1998, High-resolution stratigraphy of the Green River Formation, Raven Ridge, northeast Uinta Basin: Guidebook, Field Trip # 17, American Association of Petroleum Geologists Annual Convention, Salt Lake City, May 1998, 117 p. (Ch-7).

Boyd, T., 2008, Geothermal greenhouse information package: Oregon Institute of Technology, 287 p. (Ch-12).

Bradley, W.H., 1931, Origin and microfossils of the oil shale of the Green River Formation of Colorado and Utah: U.S. Geological Survey Professional Paper 168, 58 p. (Ch-7).

Bredehoeft, J.D., Wesley, J.B., and Fouch, T.D., 1994, Simulations of the origin of fluid pressure, fracture generation, and the movement of fluids in the Uinta Basin, Utah: American Association of Petroleum Geologists Bulletin, v. 78, p. 1729-1747 (Ch-6).

Brownfield, M.E., Johnson, R.C., Dyni, J.R., 2010, Sodium carbonate resources of the Eocene Green River Formation, Uinta Basin, Utah and Colorado, *in* U.S. Geological Survey Oil Shale Assessment Team, 2010, Oil shale resources of the Uinta Basin, Utah and Colorado: U.S. Geological Survey Digital Data Series DDS–69–BB, 7 chapters, pages variable (Ch-7).

Bryant, B., 1992, Geologic map of the east half of the Salt Lake City 1°x2° quadrangle (Duchesne and Kings Peak 30' x 60' quadrangles), Duchesne, Summit, and Wasatch Counties, Utah, and Uinta County, Wyoming: U.S. Geological Survey Miscellaneous Investigation Series Map I-1997, scale 1:100,000 (plate 1).

Bryant, B., 2010, Geologic map of the east half of the Salt Lake City 1° x 2° quadrangle (Duchesne and Kings Peak 30′ x 60′ quadrangles), Duchesne, Summit, and Wasatch Counties, Utah, and Uinta County Wyoming: Utah Geological Survey Miscellaneous Publication 10-1 DM, 2 plates, scale 1:125,000 (Ch-3).

Bryant, B., and Nichols, D.J., 1990, Geologic map of the Salt Lake City 30' x 60' quadrangle, north-central Utah and Uinta County, Wyoming: U.S. Geological Survey Map I-1944, scale 1:100,000 (plate 1).

Bullard, E.C., 1947, The time necessary for a borehole to attain temperature equilibrium: Monthly Notices, Royal Astronomical Society, Geophysical Supplement, v. 5, no. 5, p. 127-130 (Ch-12).

Burchfiel, B.C., Lipman, P.W., and Zoback, M.L., editors, 1992, The Cordilleran orogen—conterminous U.S.: Geological Society of America, Decade of North American Geology, 734 p. (Ch-3).

Burton, D., Greenhalgh, B.W., Britt, B.B., Kowallis, B.J., Elliott, W.S., Jr., and Barrick, R., 2006, New radiometric ages from the Cedar Mountain Formation, Utah and the Cloverly Formation, Wyoming—implications for contained dinosaur faunas [abs.]: Geological Society of America Abstracts with Programs, v. 38, no. 7, p. 52 (Ch-2).

Cao, S., Lerche, I., and Hermanrud, C., 1988, Formation temperature estimation by inversion of borehole measurements: Geophysics, v. 53, p. 979–988 (Ch-12).

Campbell, J.A., 1975, Structural geology and petroleum potential of the south flank of the Uinta Mountain uplift, northeastern Utah: Utah Geology, v. 2, no. 2, p. 129-132 (Ch-3).

Caputo, M.V., and Pryor, W.A., 1991, Middle Jurassic tide- and wave-influenced coastal facies and paleogeography, upper San Rafael Group, east-central Utah, *in* Chidsey, T.C., Jr., editor, Geology of east-central Utah: Utah Geological Association Publication 19, p. 9-27 (Ch-2).

Carey, F.A., and Sundberg, R.J., 1990, Advanced organic chemistry, part A—structures and mechanisms: New York, Plenum Press, 1199 p. (Ch-10).

Cashion, W.B., 1967, Geology and fuel resources of the Green River Formation, southeastern Uinta Basin, Utah and Colorado: U.S. Geological Survey Professional Paper 548, 48 p. (Ch-7).

Castle, J.W., 1990, Sedimentation in Eocene Lake Uinta (GRF), northeastern Uinta Basin, Utah, *in* Katz, B.J., editor, Lacustrine basin exploration case studies and modern analogues: American Association of Petroleum Geologists Memoir 50, p. 243-263 (Ch-7).

CDM Smith, 2012, Guidelines for water reuse – 2012: U.S. Environmental Protection Agency, Report EPA/600/R-12/618, 9 chapters, 7 appendices, individually paginated (Ch-11).

Chan, M.A., and Pfaff, B.J., 1991, Fluvial sedimentology of the Upper Cretaceous Castlegate Sandstone, Book Cliffs, Utah, *in* Chidsey, T.C., Jr., editor, Geology of east-central Utah: Utah Geological Association Publication 19, p. 95-110 (Ch-6).

Chapman, D.S., Keho, T.H., Bauer, M.S., and Picard, D.M., 1984, Heat flow in the Uinta Basin determined from bottom hole temperature (BHT) data: Geophysics, v. 49, no. 4, p. 453–466 (Ch-12).

Chidsey, T.C., Jr., and Laine, M.D., 1992, The fractured Green River and Wasatch Formations of the Uinta Basin, Utah—targets for horizontal drilling, *in* Fouch, T.D., Nuccio, V.F., and

Chidsey, T.C., Jr., editors, Hydrocarbon and mineral resources of the Uinta Basin, Utah and Colorado: Utah Geological Association Publication 20, p. 123-134 (Ch-3, Ch-6).

Chidsey, T.C., Jr., Vanden Berg, M.D., and Eby, D.E., 2015, Petrography and characterization of microbial carbonates and associated facies from modern Great Salt Lake and Uinta Basin's Eocene Green River Formation in Utah, USA, *in* Bosence, D.W.J., Gibbon, K.A., Le Heron, D.P., Morgan, W.A., Pritchard, T., and Vining, B.A., editors, Microbial carbonates in space and time—implications for global exploration and production: The Geological Society, London, Special Publication 418, http://dx.dio.org/10.1144/SP418.6 (Ch-2).

Cifelli, R.L., Kirkland, J.I., Weil, A., Deinos, A.R., and Kowallis, B.J., 1997, High-precision $^{40}Ar/^{39}Ar$ geochronology and the advent of North America's Late Cretaceous terrestrial fauna: Proceedings of the National Academy of Science of the United States of America, v. 94, p. 11163-1167 (Ch-2).

Cifelli, R.L., Nydam, R.L., Gardner, J.D., Weil, A., Eaton, J.G., Kirkland, J.I., and Madsen, S.K., 1999, Medial Cretaceous vertebrates from the Cedar Mountain Formation, Emery County, the Mussentuchit local fauna, *in* Gillette, D., editor, Vertebrate paleontology in Utah: Utah Geological Survey Miscellaneous Publication 99-1, p. 219-242 (Ch-2).

Clark, C.E., and Veil, J.A., 2009, Produced water volumes and management practices in the United States: Argonne National Laboratory, Environmental Sciences Division, Report 09/1, Contract DE-AC02-06CH11357, 59 p. (Ch-11).

Clark, I., and Fritz, P., 1997, Environmental isotopes in hydrogeology: Boca Raton, CRC Press, Inc., 328 p. (Ch-9).

Clem, K., 1985, Oil and gas production summary of the Uinta Basin, *in* Picard, M.D., editor, Geology and energy resources, Uinta Basin of Utah, Utah Geological Association Publication 12, p. 159-167 (Ch-3).

Clerico, R., 2015, Hydrology baseline study in the southeastern Uinta Basin—a summary of Enefit American Oil's program to inform project planning and permitting, *in* Vanden Berg, M.D., Ressetar, R., and Birgenheier, L., editors, Geology of Utah's Uinta Basin and Uinta Mountains: Utah Geological Association Publication 44, in preparation (Ch-9).

Colburn, J.A., Bereskin, S.R., McGinley, D.C., and Schiller, D.M., 1985, Lower Green River Formation in the Pleasant Valley producing area, Duchesne and Uintah Counties, Utah: *in* Picard, M.D., editor, Geology and energy resources, Uinta Basin of Utah: Utah Geological Association Publication 12, p. 177-186 (Ch-7).

Cole, R.D., White, H., and Kirschbaum, M., 2008, Stops 1-4 through 1-10, Thompson Canyon-Sego Canyon, *in* Longman, M.W., and Morgan, C.D., editors, Hydrocarbon systems and

production in the Uinta Basin, Utah: Rocky Mountain Association of Geologists and Utah Geological Association Publication 37, p. 417-437 (Ch-2, Ch-6).

Cole, R.D., Young, R.G., and Willis, G.C., 1997, The Prairie Canyon Member, a new unit of the Upper Cretaceous Mancos Shale, west-central Colorado and east-central Utah: Utah Geological Survey Miscellaneous Publication 97-4, 23 p. (Ch-5).

Colorado Energy Office, 2014, Produced water beneficial use dialogue—opportunities and challenges for re-use of produced water on Colorado's western slope: Report prepared by CDR Associates for the Colorado Energy Office and Colorado Mesa University, 16 p., 2 appendices (Ch-11).

Constenius, K.M., Clark, D.L., King, J.K., and Ehler, J.B., 2011, Interim geologic map of the Provo 30' x 60' quadrangle, Salt Lake, Utah, and Wasatch Counties, Utah: Utah Geological Survey Open-File Report 586, scale 1:100,000 (Ch-2, plate 1).

Crowell, A.M., and Gosnold, W., 2011, Correcting bottom-hole temperatures—a look at the Permian Basin (Texas), Anadarko and Arkoma Basins (Oklahoma), and Williston Basin (North Dakota): Transactions, Geothermal Resources Council, v. 35, p. 735–738 (Ch-12).

Crowell, A.M., Ochsner, A.T., and Gosnold, W., 2012, Correcting bottom-hole temperatures in the Denver Basin—Colorado and Nebraska: Transactions, Geothermal Resources Council, v. 36, p. 201–206 (Ch-12).

Currie, B.S., McPherson, M.L., Dark, J.P., and Pierson, J.S., 2007, Reservoir characterization of the Cretaceous Cedar Mountain and Dakota Formations, southern Uinta Basin (year 2): Utah Geological Survey Open-File Report 516, 67 p. (Ch-4).

Currie, B.S., 1998, Upper Jurassic – Lower Cretaceous Morrison and Cedar Mountain Formations, NE Utah – NW Colorado—relationships between nonmarine deposition and early Cordilleran foreland–basin development: Journal of Sedimentary Geology, v. 68, p. 632-652 (Ch-2).

Currie, B.S., McPherson, M.L., Hokanson, W., Pierson, J.S., Horman, M.B., Pyden, T., Schellenbach, W., Purcell, R., and Nicklaus, D., 2011, Reservoir characterization of the Lower Cretaceous Cedar Mountain and Dakota Formations, northern Uinta Basin, Utah: Utah Geological Survey Open-File Report 597, 34 p. (Ch-4).

Currie, B.S., and Reeder, M.D., 2002, Sequence stratigraphy of the Jurassic Curtis, Summerville, and Stump Formations, Utah-Colorado [abs.]: Geological Society of America Abstracts with Programs, v. 34, no. 6, p. 278 (Ch-2).

Currie, B.S., Schwartz, R.K., and Wilcox, W.T., 2005, Sequence stratigraphy of a regional-scale tidal embayment, Upper Jurassic Curtis and Summerville Formations, central Utah [abs.]: Geological Society of America Abstracts with Programs, v. 37, no. 7, p. 141 (Ch-2).

Curtice, R., in preparation, Chapter 18—best completion practices—review of the Mancos shale-gas wells in Utah, *in* Ressetar, R., and Birgenheier, L.P., editors, Cretaceous Mancos Shale, Uinta Basin, Utah—resource potential and best practices for an emerging shale gas play: Utah Geological Survey contract report (Ch-5).

Dahm, K., and Chapman, M., 2014, Produced water treatment primer—case studies of treatment applications: U.S. Bureau of Reclamation Science and Technology Research Report for Project 1617, 58 p. (Ch-11).

Dane, C.H., 1954, Stratigraphic and facies relationships of the upper part of the Green River Formation in Duchesne, Uintah, and Wasatch Counties, Utah: American Association of Petroleum Geologists Bulletin, v. 38, p. 405-425 (Ch-7).

Davis, S.J., Dickinson, W.R., Gehrels, G.E., Spencer, J.E., Lawton, T.F., and Carroll, A.R., 2010, The Paleogene California River—evidence of Mojave-Uinta paleodrainage from U-Pb ages of detrital zircons: Geology, v. 38, p. 931-934 (Ch-6).

Davis, S.W., Davis, M.E., Lucchitta, I., Hanks, T.C., Finkel, R.C., and Caffee, M., 2001, Erosional history of the Colorado River through Glen and Grand Canyons, *in* Young, R.A., and Spamer, E.E., editors, Colorado River origin and evolution—proceedings of a symposium held at Grand Canyon National Park in June, 2000: Grand Canyon Association, p. 135-139 (Ch-3).

DeCelles, P.G., and Coogan, J.C., 2006, Regional structure and kinematic history of the Sevier fold-and-thrust belt, central Utah: Geologic Society of America Bulletin, v. 118, no. 7/8, p. 841-864 (Ch-2).

Deming, D., 1989, Application of bottom-hole temperature corrections in geothermal studies: Geothermics, v. 18, no. 5/6, p. 775–786 (Ch-12).

Deming, D., and Chapman, D.S., 1988, Inversion of bottom-hole temperature data—the Pineview field, Utah-Wyoming thrust belt: Geophysics, v. 53, no. 5, p. 707–720 (Ch-12).

Deming, D., and Chapman, D.S., 1989, Thermal histories and hydrocarbon generation—examples from Utah-Wyoming thrust belt: American Association of Petroleum Geologists Bulletin, v. 73, no. 12, p. 1455–1471 (Ch-12).

Deming, D., Nunn, J.A., Jones, S., and Chapman, D.S., 1990, Some problems in thermal history studies, *in* Nuccio, V.F., and Barker, C.E., editors, Applications of thermal maturity studies to energy exploration: Rocky Mountain Section, Society for Sedimentary Geology, p. 61-80 (Ch-12).

Desborough, G.A., Pitman, J.K., and Huffan, A.C., Jr., 1974, Concentration and mineralogical residence of elements in rich oil shales of the Green River Formation, Piceance Creek Basin, Colorado, and the Uinta Basin, Utah—a preliminary report: U.S. Geological Survey Open-File Report 74-77, 14 p. (Ch-9).

Desborough, G. A., Pitman, J.K., and Huffman, A.C., Jr., 1976, Concentration and mineralogical residence of elements in rich oil shales of the Green River Formation, Piceance Creek Basin, Colorado, and the Uinta Basin, Utah—a preliminary report: Chemical Geology, v. 17 p. 13-26 (Ch-9).

Dickinson, W.R., Fiorello, A.R., Hall, D.L., Monreal, R., Potochnik, A.R., and Swift, P.N., 1989, Cretaceous strata of southern Arizona, *in* Jenney, J.P., and Reynolds, S.J., editors, Geologic evolution of Arizona: Tucson, Arizona Geological Society Digest 17, p. 447-461 (Ch-3).

Dickinson, W.R., Klute, M.A., Hayes, M.J., Janecke, S.U., Lundin, E.R., McKittrick, M.A., and Olivares, M.D., 1988, Paleographic and paleotectonic setting of Laramide sedimentary basins in the central Rocky Mountain region: Geological Society of America Bulletin, v. 100, p. 1023-1039 (Ch-6).

Dickinson, W.R., Lawton, T.F., and Inman, K.F., 1986, Sandstone detrital modes, central Utah foreland region—stratigraphic record of Cretaceous-Paleogene tectonic evolution: Journal of Sedimentary Petrology, v. 56, p. 276-293 (Ch-6).

Dickinson, W.R., Lawton, T.F., Pecha, M., Davis, S.J., Gehrels, G.E., and Young, R.A., 2012, Provenance of the Paleogene Colton Formation (Uinta Basin) and Cretaceous-Paleogene

provenance evolution in the Utah foreland—evidence from U-Pb ages of detrital zircons, paleocurrent trends, and sandstone petrofacies: Geosphere, v. 8, p. 854-880 (Ch-6).

Difley, R., and Ekdale, A.A., 2002, Faunal implications of an environmental change before the Cretaceous-Tertiary (K-T) transition in central Utah: Cretaceous Research, v. 23, p. 315-331 (Ch-2).

Doelling, H.H., 2001, Geologic map of the Moab and the eastern part of the of the San Rafael Desert 30' x 60' quadrangles, Grand and Emery Counties, Utah, and Mesa County, Colorado: Utah Geological Survey Map 180, scale 1:100,000 (plate 1).

Doelling, H.H., 2002, Interim geologic map of the San Rafael Desert 30' x 60' quadrangle, Emery and Grand Counties, Utah: Utah Geological Survey Open-file Report 404, scale 1:100,000 (Ch-2).

Doelling, H.H., 2004, Interim geologic map of the eastern half of the Salina 30' x 60' quadrangle, Emery, Sevier, and Wayne Counties, Utah: Utah Geological Survey Open-file Report 438, scale 1:62,500 (Ch-2).

Doelling, H.H., Blackett, R.E., Hamblin, A.H., Powell, J.D., and Pollock, G.L., 2010, Geology of Grand Staircase-Escalante National Monument, *in* Sprinkel, D.A., Chidsey, T.C., Jr., and Anderson, P.B., editors, Geology of Utah's parks and monuments (3rd edition): Utah Geological Association Publication 28, p. 193-235 (Ch-2).

Doelling, H.H., and Davis, F.D., 1989, The geology of Kane County, Utah—geology, mineral resources, geologic hazards: Utah Geological and Mineral Survey Bulletin 124, 192 p., 10 plates, map scale 1:100,000 (Ch-2).

Doelling, H.H., and Kuehne, P.A., 2012, Geologic map of the Short Canyon quadrangle, Emery County, Utah: Utah Geological Survey Map 255DM, scale 1:24,000, 13 p. (Ch-2).

Doelling, H.H., Kuehne, P.A., and Kirkland, J.I., 2009, Geologic map of the Willow Springs quadrangle, Sevier and Emery Counties, Utah: Utah Geological Survey Map 237, scale 1:24,000, 14 p. (Ch-2).

Doelling, H.H., Kuehne, P.A, Willis, G.C., and Ehler, J.B., 2015, Geologic map of the San Rafael Desert 30‘ x 60‘ quadrangle, Emery and Grand Counties, Utah, Utah Geological Survey Map 267, scale 1:100,000.

Dowdle, W.L., and Cobb, W.M., 1975, Static formation temperature from well logs—an empirical method: Journal of Petroleum Technology, v. 27, no. 11, p. 129–135 (Ch-12).

Dubiel, R.F., Kirschbaum, M.A., Roberts, L.N.R., Mercier, T.J., and Heinrich, A., 2000, Geology and coal resources of the Blackhawk Formation in the southern Wasatch Plateau, central Utah, *in* Kirschbaum, M.A., Roberts, L.N.R., and Biewick, L.R.H.,

editors, Geologic assessment of coal in the Colorado Plateau—Arizona, Colorado, New Mexico, and Utah: U.S. Geological Survey Professional Paper 1625-B, 61 p. (Ch-6).

Dubiel, R.F., 2000, Summary of geology and coal resources of the Blackhawk Formation in the southern Wasatch Plateau, central Utah, *in* Kirschbaum, M.A., Roberts, L.N.R., and Biewick, L.R.H., editors, Geologic assessment of coal in the Colorado Plateau, Arizona, Colorado, New Mexico, and Utah: U.S. Geological Survey Professional Paper 1625-B, 29 p. (Ch-6).

Dyer, J., and Donoho, D., 2008, Gas-filled Jurassic Entrada erg-sandstones at Flat Rock field, Uintah County, Utah, *in* Longman, M.W., and Morgan, C.D., editors, Hydrocarbon systems and production in the Uinta Basin, Utah: Rocky Mountain Association of Geologists and Utah Geological Association Publication 37, p. 155-178 (Ch-4).

Dyni, J. R., 1976, Trioctahedral smectite in the Green River Formation, Duchesne County, Utah: U.S. Geological Survey Professional Paper 967, 14 p. (Ch-7).

Dyni, J.R., 1996, Sodium carbonate resources of the Green River Formation: U.S. Geological Survey Open-File Report 96-729 (Ch-7).

Dyni, J.R., Milton, C., and Cashion, W.B., Jr., 1985, The saline facies of the upper part of the Green River Formation near Duchesne, Utah, *in* Picard, M.D., editor, Geology and energy resources, Uinta Basin, Utah: Utah Geological Association Publication 12, p. 51-

60 (Ch-7).

Edwards, M.C., 2013, Geothermal resource assessment of the Basin and Range Province in western Utah: Salt Lake City, University of Utah, M.S. thesis, 133 p. (Ch-12).

Edwards, P.M., Brown, S.S., Roberts, J.M., Ahmadov, R., Banta, R.M., deGouw, J.A., Dube, W.P., Field, R.A., Flynn, J.H., Gilman, J.B., Graus, M., Helmig, D., Koss, A., Langford, A.O., Lefer, B.L., Lerner, B.M., Li, R., Li, S.M., McKeen, S.A., Murphy, S.M., Parrish, D.D., Senff, C.J., Soltis, J., Stutz, J., Sweeney, C., Thompson, C.R., Trainer, M.K., Tsai, C., Veres, P.R., Washenfelder, R.A., Warneke, C., Wild, R.J., Young, C.J., Yuan, B., and Zamora, R., 2014, High winter ozone pollution from carbonyl photolysis in an oil and gas basin: Nature, v. 514, p. 351–354 (Ch-10).

Energy Information Administration, 2015, Oil and gas production ranking by states – 2013: Online, http://www.eia.gov/state/rankings/#/series/47 (Ch-1).

Estes-Jackson, J.E., Shefte, S.W., and Siguaw, S.G., 2008, Hydrocarbon systems and production in the Uinta Basin, Utah, *in* Longman, M.W., and Morgan, C.D., editors: Rocky Mountain Association of Geologists and Utah Geological Association Publication 37, p. 267-281 (Ch-6).

EUGRIS, 2014, EUGRIS—portal for soil and water management in Europe, Online: http://www.eugris.info/FurtherDescription.asp?e=6&Ca=2&Cy=0&T=Benzene,%20toluene,%20ethylbenzene,%20and%20xylene, accessed April 10, 2014 (Ch-10).

Fertl, W.H., and Wichmann, P.A., 1977, How to determine static BHT from well log data: World Oil, v. 184, p. 105–106 (Ch-12).

Fetter, C.W., 1988, Applied hydrogeology, 2nd edition: Columbus, Merrill Publishing Company, 488 p. (Ch-10).

Fisher, D.J., 1936, The Book Cliffs coal field in Emery and Grand Counties, Utah: U.S. Geological Survey Bulletin 852, 104 p. (Ch-6).

Focazio, M.J., Reilly, T.E., Rupert, M.G., and Helsel, D.R., 2002, Assessing groundwater vulnerability to contamination—providing scientifically defensible information for decision makers: U.S. Geological Survey Circular 1224, 33 p. (Ch-10)

Förster, A., 2001, Analysis of borehole temperature data in the northeast German Basin—continuous logs versus bottom-hole temperatures: Petroleum Geoscience, v. 7, p. 241–254 (Ch-12).

Förster, A., and Merriam, D.F., 1995, A bottom-hole temperature analysis in the American Midcontinent (Kansas)—implications to the applicability of BHTs in geothermal studies,

in World Geothermal Congress, Firenze, Italy, May 18–31, 1995, Proceedings: International Geothermal Association, v. 2, p. 777-782 (Ch-12).

Fouch, T.D., 1975, Lithofacies and related hydrocarbon accumulations in Tertiary strata of the western and central Uinta Basin, Utah, *in* Bolyard, D.W., editor, Symposium on deep drilling frontiers in the central Rocky Mountains: Rocky Mountain Association of Geologists Guidebook, p. 163-173 (Ch-1, Ch-2, Ch-7).

Fouch, T.D., 1976, Revision of the lower part of the Tertiary System in the central and western Uinta Basin, Utah: U.S. Geological Survey Bulletin 1405-C, 7 p. (Ch-2).

Fouch, T.D., Lawton. T.F., Nichols, D.J., Cashion, W.A., and Cobban, W.A., 1983, Patterns and timing of synorogenic sedimentation in Upper Cretaceous rocks of central and northeast Utah, *in* Reynolds, M.W., and Dolly, E.D., editors, Mesozoic paleogeography of the west-central United States: Rocky Mountain Section, Society of Economic Paleontologists and Mineralogists, Rocky Mountain Paleogeography Symposium 2, p. 305-336 (Ch-2).

Fouch, T.D., Nuccio, V.F., Osmond, J.C., MacMillan, L., Cashion, W.B., and Wandrey, C.J., 1992, Oil and gas in uppermost Cretaceous and Tertiary rock, Uinta Basin, Utah, *in* Fouch, T.D., Nuccio, V.F., and Chidsey, T.C., Jr., editors, Hydrocarbon and mineral resources of the Uinta Basin, Utah and Colorado: Utah Geological Association Publication 20, p. 9-47 (Ch-1, Ch-2, Ch-3).

Fouch, T.D., Nuccio, V.F., Anders, D.E., Rice, D.D., Pitman, J.K., and Mast, R.F., 1994, Green River (!) petroleum system, Uinta Basin, Utah, USA, *in* Magoon, L.B., and Dow, W.G., editors, The petroleum system—from source to trap: American Association of Petroleum Geologists Memoir 60, p. 399–421 (Ch-7).

Fouch, T.D., Nuccio, V.F., Osmond, J.C., MacMillan, L., Cashion, W.B., and Wandrey, C.J., 1992a, Oil and gas in uppermost Cretaceous and Tertiary rock, Uinta Basin, Utah, *in* Fouch, T.D., Nuccio, V.F., and Chidsey, T.C., Jr., editors, Hydrocarbon and mineral resources of the Uinta Basin, Utah and Colorado: Utah Geological Association Publication 20, p. 9-47 (Ch-7).

Fouch, T.D., Wandrey, C.J., Pitman, J.K., Nuccio, V.F., Schmoker, J.W., Rice, D.D., Johnson, R.C., and Dolton, G.L., 1992b, Natural gas accumulations in low-permeability Tertiary and Cretaceous (Campanian and Maastrichtian) rock, Uinta Basin, Utah: U.S. Department of Energy, Report No. DE-A121-83MC20422, 81 p. (Ch-3, Ch-7).

FracFocus, 2015, A digital chemical disclosure registry: Online, http://fracfocus.org/, accessed various times (Ch-11).

Franczk, K.J., Pitman, J.K., and Nichols, D.J., 1990a, Sedimentology, mineralogy, palynology, and depositional history of Upper Cretaceous and lower Tertiary rocks along the Book

and Roan Cliffs east of the Green River: U.S. Geological Survey Bulletin 1787-N, 27 p. (Ch-2, Ch-6).

Franczyk, K.J., Fouch, T.D., Johnson, R.C., Molenaar, C.M., and Cobban, W.A., 1990b, Cretaceous and Tertiary paleogeographic reconstructions for the Uinta-Piceance Basin study area, Colorado and Utah: U.S. Geological Survey Bulletin 1787-Q, 48 p. (Ch-6).

Freethey, G.W., 1992, Maps summarizing geohydrologic information in an area of salt-water disposal, eastern Altamont-Bluebell petroleum field, Uinta Basin, Utah: U.S. Geological Survey Water Resource Investigation Report WRIR 92-4043, 2 plates (Ch-12).

Freethey, G.W., and Cordy, G.E., 1991, Geohydrology of Mesozoic rocks in the upper Colorado River basin in Arizona, Colorado, New Mexico, Utah, and Wyoming, excluding the San Juan Basin: U. S. Geological Survey Professional Paper 1411-C, 130 p. (Ch-4).

Freethey, G.W., and Stolp, B.J., 2010, Simulation of ground-water flow and solute transport in the Glen Canyon aquifer, East-Central Utah: U. S. Geological Survey Scientific Investigations Report 2009-5037, 28 p. (Ch-4)

Freeze, A.R., and Cherry, J.A., 1979, Groundwater: Englewood Cliffs, New Jersey, Prentice Hall Inc., 604 p. (Ch-10).

Fryberger, S.G., 1990, Ancient eolian deposits of the Navajo and Weber Sandstones, northeast Utah and Colorado, *in* Fryberger, S.G., Krystinik, L.F., and Schenk, C.J., editors, Modern and ancient eolian deposits—petroleum exploration and production: Society for Sedimentary Geology (SEPM), Rocky Mountain Section Publication, Chapter 19, 12 p. (Ch-2).

Gardner, M.H., Cross, T.A., and Levorsen, M., 2004, Stacking patterns, sediment volume partitioning, and facies differentiation in shallow-marine and coastal-plain strata of the Cretaceous Ferron Sandstone, Utah, *in* Chidsey, T.C., Jr., Adams, R.D., and Morris, T.H., editors, Regional to wellbore analog for fluvial-deltaic reservoir modeling—the Ferron Sandstone of Utah: American Association of Petroleum Geologists Studies in Geology 50, p. 95–124 (Ch-5).

Gerner, S.J., Spangler, L.E., Kimball, B.A., Wilberg, D.E., and Naftz, D.L., 2006, Hydrology and water quality in the Green River and surrounding agricultural areas near Green River in Emery and Grand Counties, Utah, 2004-05: U.S. Geological Survey Scientific Investigations Report 2006-5186, 42 p. (Ch-9).

Glenn, W.E., Chapman, D.S., Foley, D., Capuano, R.M., Cole D., Sibbett, B., and Ward, S.H., 1980, Geothermal exploration program Hill Air Force Base, Davis and Weber Counties, Utah: U.S. Department of Energy Report, Contract DE-AC07-78ET28392, 77 p. (Ch-12).

Glover, K.R., 1996, Ground-water flow in the Duchesne River–Uinta aquifer in the Uinta Basin, Utah and Colorado: U.S. Geological Survey Water Resource Investigation Report 92-4161, p. 24 (Ch-12).

Goutorbe, B., Lucazeau, F., and Bonneville, A., 2007, Comparison of several BHT correction methods—a case study on an Australian data set: *Geophysics Journal International, v.* 170, no. 2, p. 913–922 (Ch-12).

Graf, W.L., Hereford R., Laity, J., and Young, R.A., 1987, Colorado Plateau, *in* Graf, W.L., editor, Geomorphic systems of North America: Geological Society of America Centennial Special Volume 2, p. 259–302 (Ch-3).

Gregory, A.R., Dodge, M.M., Posey, J.S., and Morton, R.A., 1980, Volume and accessibility of entrained (solution) methane in deep geopressured reservoirs—Tertiary formations of the Texas Gulf Coast: U.S. Department of Energy Final Report DOE/ET/11397-1, 361 p. (Ch-12).

Gregson, J.D., Chure, D.J., and Sprinkel, D.A., 2010, Geology and paleontology of Dinosaur National Monument, *in* Sprinkel, D.A., Chidsey, T.C., Jr., and Anderson, P.B., editors, Geology of Utah's parks and monuments (3rd edition): Utah Geological Association Publication 28, p. 161-192 (Ch-2).

Groeger, A. and Bruhn, R.L. 2001, Structure and geomorphology of the Duchesne graben, Uinta Basin, Utah and its enhancement of a hydrocarbon reservoir: American Association of Petroleum Geologists Bulletin, v. 85, p. 1661-1678 (Ch-3).

Ground Water Protection Council, 2009, State oil and natural gas regulations designed to protect water resources: U.S. Department of Energy, National Energy Technology Laboratory Report, Contract DE-FC26-04NT15455, 63 p. (Ch-11).

Gualtieri, J.L., 1988, Geologic map of the Westwater 30' x 60' quadrangle, Grand and Uintah Counties, Utah, and Garfield and Mesa Counties, Colorado: U.S. Geological Survey Map I-1765, scale 1:100,000 (Ch-2, Ch-6, Ch-10, plate 1).

Guerra, K., Dahm, K., and Dundorf, S., 2011, Oil and gas produced water management and beneficial use in the western United States: U.S. Bureau of Reclamation Science and Technology Program Report No. 157, 113 p. (Ch-11).

Guyod, H., 1946, Temperature well logging [a seven-part series]: Oil Weekly, v. 123, no. 8–11, (October 21, 28; November 4, 11), v. 124, no. 1–3 (December 2, 9, 16) (Ch-12).

Gwynn, J.W., 1992, The oil well saline-water resources of the Uinta Basin, Utah—their character and distribution, *in* Fouch, T.D., Nuccio, V.F., and Chidsey, T.C., Jr., editors, Hydrocarbon and mineral resources of the Uinta Basin, Utah and Colorado: Utah Geological Association Publication 20, p. 289–308 (Ch-7).

Gwynn, J.W., 1995, Resistivities and chemical analyses of selected oil and gas field, water well, and spring waters, Utah: Utah Geological Survey Circular 87, 142 p. (Ch-7).

Gwynn, M., Allis, R., Blackett, R., and Hardwick, C., 2013, New geothermal resource delineated beneath Black Rock Desert, Utah, *in* 38th Workshop on Geothermal Reservoir Engineering, Stanford, California, February 11–13, 2013, Proceedings: Stanford University, SGP-TR-198, 9 p. (Ch-12).

Gwynn, M., Allis, R., Sprinkel, D., Blackett, R., and Hardwick, C., 2014, Geothermal potential in the basins of northeastern Nevada: Transactions, Geothermal Resources Council, v. 38, p. 1029–1039 (Ch-12).

Hamblin, W.K., 2004, Beyond the visible landscape – aerial panoramas of Utah' geology: Provo, Utah, Brigham Young University, 300 p. (Ch-1).

Hampson, G.J., 2010, Sediment dispersal and quantitative stratigraphic architecture across an ancient shelf: Sedimentology, v. 57, p. 96–141 (Ch-5).

Hanks, T.C., Lucchitta, I., Davis, S.W., Davis, M.E., Finkel, R.C., Lefton, S.A., Garvin, C.D., 2001, The Colorado River and the age of Glen Canyon, *in* Young, R.A., and Spamer, E.E., editors, Colorado River origin and evolution—proceedings of a symposium held at

Grand Canyon National Park in June, 2000: Grand Canyon Association, p. 129–133 (Ch-3).

Hansen, W.R., 1986, Neogene tectonics and geomorphology of the eastern Uinta Mountains in Utah, Colorado, and Wyoming: U.S. Geological Survey Professional Paper 1356, 78 p. (Ch-3).

Hansen, W.R., Rowley, P.D., and Carra, P.E., 1983, Geologic map of Dinosaur National Monument and vicinity: U.S. Geological Survey Miscellaneous Investigation Series Map I-1407, scale 1:50,000 (Ch-2).

Hardwick, C.L., Kirby, S., and Gwynn, M., 2014, Geothermal prospecting in Utah—a new thermal model of the Black Rock Desert: Transaction, Geothermal Resources Council, v. 38, p. 1041-1045 (Ch-12).

Harrison, W.E., Luza, K.V., Prater, M.L., and Cheung, P.K., 1983, Geothermal resource assessment in Oklahoma: Oklahoma Geological Survey Special Publication 83–1, 42 p. (Ch-12).

Harter, T., 2001, Chapter 11—assessing vulnerability of groundwater, *in* Harter, T., and Rollins, L., editors, Watersheds, groundwater, and drinking water—a practical guide: Oakland, University of California Agriculture and Natural Resources, p.183–203 (Ch-10).

Henrikson, A., 2000, Heat flow determination from oil and gas wells in the Colorado Plateau and Basin and Range of Utah: Salt Lake City, University of Utah, M.S. thesis, 69 p. (Ch-12).

Henrikson, A., and Chapman, D.S., 2002, Terrestrial heat flow in Utah: Salt Lake City, University of Utah, unpublished report, 47 p. (Ch-12).

Herbst, S.R., and Morris, T.H., 2011, Unexpected reservoir quality sandstone within the mudstone-rich portion of the Middle Jurassic Entrada Sandstone, San Rafael Swell, Utah [abs.]: Geological Society of America, Abstracts with Programs, v. 43, p. 610 (Ch-2).

Hermanrud, C., Cao, S., and Lerche, I., 1990, Estimates of virgin rock temperature derived from BHT measurements—bias and error: Geophysics, v. 55, no. 7, p. 924–931 (Ch-12).

Hettinger, R.D., and Kirschbaum, M.A., 2002, Stratigraphy of the Upper Cretaceous Mancos Shale (upper part) and Mesaverde Group in the southern part of the Uinta and Piceance Basins, Utah and Colorado: U.S. Geological Survey Investigative Report I-2764, 21 p. (Ch-2, Ch-6).

Hettinger, R.D., and Kirschbaum, M.A., 2003, Stratigraphy of the Upper Cretaceous Mancos Shale (upper part) and Mesaverde Group in the southern part of the Uinta and Piceance Basins, Utah and Colorado, *in* USGS Uinta-Piceance Assessment Team, compilers, Petroleum systems and geologic assessment of oil and gas in the Uinta-Piceance

Province, Utah and Colorado: U.S. Geological Survey Digital Data Series DDS–69–B, chapter 12, compact disk (Ch-5).

Hicks, T.C., Morris, T.H., and Fairbanks, M.D., 2010, Facies analysis of the transitions between subtidal, intertidal, and supratidal zones of the Entrada Sandstone, south central Utah—a provisional sequence stratigraphic analysis, *in* Carney, S.M., Tabet, D.E., and Johnson, C.L., editors, Geology of south-central Utah: Utah Geological Association Publication 39, p. 317-337 (Ch-2, Ch-4).

Hilchie, D.W., 1978, Applied open hole log interpretation: Golden, Colorado, D.W. Hilchie Inc., 161 p. (Ch-6).

Hill, B.G., and Bereskin, S.R., editors, 1993, Oil and gas fields of Utah: Utah Geological Association Publication 22, non-paginated (Ch-1).

Hintze, L.F., 1975, Geological highway map of Utah: Provo, Brigham Young University Geology Studies Special Publication 3, scale 1:1,000,000 (Ch-2, Ch-3).

Hintze, L.F., 1980, Geologic map of Utah: Utah Geological Survey Map M-A-1, 2 sheets, scale 1:500,000 (Ch-3).

Hintze, L.F., and Kowallis, B.J., 2009, Geologic history of Utah: Brigham Young University Geology Studies Special Publication 9, 225 p. (Ch-1, Ch-2, Ch-3, Ch-4, Ch-5, Ch-7).

Hintze, L.F., Willis, G.C., Laes, D.Y.M., Sprinkel, D.A., and Brown, K.D., 2000, Digital geologic map of Utah: Utah Geological Survey Map 179DM, scale 1:500,000 (Ch-3, Ch-7).

Holmes, W.F., 1980, Results of test drilling for ground water in the southeastern Uinta Basin, Utah and Colorado: U.S. Geological Survey Water-Resources Investigations 80-951, 89 p., 6 plates (Ch-9, Ch-10).

Holmes, W.F., 1985, Water budget and ground-water occurrence in the Uinta Basin of Utah, *in* Picard, M.D., editor, Geology and energy resources, Uinta Basin of Utah: Utah Geological Association Publication 12, p. 271–275 (Ch-9, Ch-10).

Holmes, W.F., and Kimball, B.A., 1987, Ground water in the southeastern Uinta Basin, Utah and Colorado: U.S. Geological Survey Water Supply Paper 2248, 47 p., 1 plate, scale 1:250,000, (Ch-9).

Horner, D.R., 1951, Pressure build-up in wells, *in* 3rd World Petroleum Congress, The Hague, the Netherlands, May 28–June 6, 1951, Proceedings: World Petroleum Congress, p. 25–43 (Ch-12).

Horton, B.K., 2012, Variability of the Mancos Shale—developing preliminary depositional and sequence stratigraphic models of a developing shale gas play: Salt Lake City, University of Utah, M.S. thesis, 386 p. (Ch-5).

House, D., 2012, Giant operation in Utah gives rise to oil boom, though challenges loom: Salt Lake Tribune, with photo gallery by Kim Raff: Online, http://www.sltrib.com/sltrib/money/54641000-79/oil-newfield-utah-basin.html.csp, accessed July 1, 2015 (Ch-11).

Howell, J., and Flint, A., 2005, Tectonic setting, stratigraphy and sedimentology of the Book Cliffs, *in* Coe, A.L., editor, The sedimentary record of sea-level change: New York, The Open University and Cambridge University Press, p. 156 (Ch-6).

Howells, L., Longson, M.S., and Hunt, G.L., 1987, Base of moderately saline ground water in the Uinta Basin, Utah, with an introductory section describing the methods used in determining its position: Utah Department of Natural Resources Technical Publication 92, 59 p., 2 plates, scale 1:250,000. Also available as: U.S. Geological Survey Open-File Report 87-394 (Ch-7, Ch-9, Ch-12).

Hunt, C.B., 1956, Cenozoic geology of the Colorado Plateau: U.S. Geological Survey Professional Paper 279, 99 p. (Ch-1, (Ch-3).

InterTech Environmental & Engineering, LLC, 2014, Greater Natural Buttes project area baseline water quality monitoring: unpublished technical report prepared for Anadarko and Kerr McGee, 61 p. (Ch-9).

IOGCC and ALL Consulting, 2006, A guide to practical management of produced water from onshore oil and gas operations in the United States: U.S. Department of Energy National Petroleum Technology Office Report, Contract DE-PS26-04NT15460-02, 179 p., 1 appendix (Ch-11).

Jennings, G.R., 2014, Facies analyses and paleogeography of Utah's Entrada Sandstone—traps, tectonic implications and outcrop analog: Provo, Utah, Brigham Young University, M.S. thesis, 66 p. (Ch-4).

Johnson, R.C., 1985, Early Cenozoic history of the Uinta and Piceance Creek Basins, Utah and Colorado, with special reference to the development of Eocene Lake Uinta, *in* Flores, R.M., and Kaplan, S.S., editors, Cenozoic paleogeography of the west-central United States: Denver, Colorado, Society of Sedimentary Geology, Rocky Mountain Section, p. 247-276 (Ch-6).

Johnson, R.C., 2002, Northwest to southeast cross section of Cretaceous and lower Tertiary rocks across the eastern part of the Uinta Basin, Utah: U.S. Geological Survey Digital Data Series DDS-69-B, plate 1 (Ch-6).

Johnson, R.C., 2003, Northwest to southeast cross section of Cretaceous and lower Tertiary rocks across the eastern part of the Uinta Basin, Utah, *in* USGS Uinta-Piceance Assessment Team, compilers, Petroleum systems and geologic assessment of oil and gas in the Uinta-Piceance Province, Utah and Colorado: U.S. Geological Survey Digital Data Series DDS–69–B, chapter 11, compact disk (Ch-5).

Johnson, R.C., and Roberts, S.B., 2003, The Mesaverde total petroleum system, Uinta-Piceance Province, Utah and Colorado, *in* Petroleum systems and geologic assessment of oil and gas in the Uinta-Piceance Province, Utah and Colorado: U.S. Geological Survey Digital Data Series DDS–69–B, chapter 7, 68 p. (Ch-6).

Jones, E., and Plink-Björklund, P., 2013, The effects of early Eocene climate change on the composition of fluvial sandstones, Uinta Basin, Utah: American Association of Petroleum Geologists, Search and Discovery article #50880 (Ch-6).

Jones, E., and Plink-Björklund, P., 2015, Revisiting the depositional environment and provenance of the Wasatch Formation in the Uinta Basin, Utah—implications for the early Eocene paleogeography of western North America: American Association of Petroleum Geologists, Search and Discovery Article #90216 (Ch-6).

Keele, D., and Evans, J., 2008, Analysis of reservoir properties of faulted and fractured eolian thrust-belt reservoirs: Utah Geological Survey Open-File Report 529, 55 p. (Ch-4).

Kehew, A.E., 2000, Applied chemical hydrogeology: Upper Saddle River, New Jersey, Prentice Hall, 368 p. (Ch-8).

Kehle, R.O., Schoeppel, R.J., and DeFord, R.K., 1970, The AAPG geothermal survey of North America, *in* U.N. Symposium on the Development and Utilization of Geothermal Resources, Pisa, Italy, 1970: Geothermics Special Issue 2, p. 358–367 (Ch-12).

Keho, T.H., 1987, Heat flow in the Uinta Basin determined from bottom hole temperature (BHT) data: Salt Lake City, University of Utah, M.S. thesis, 99 p. (Ch-12).

Keighin, C.W., and Fouch, T.D., 1981, Depositional environments and diagenesis of some nonmarine Upper Cretaceous reservoir rocks, Uinta Basin, Utah: Society of Sedimentary Geology Special Publication No. 31, p. 109-125 (Ch-6).

Keighley, D., 2015, Phosphatic carbonate shale of the "Bird's Nest saline zone," upper Green River Formation, Uinta Basin, Utah, *in* Smith, M.E., and Carrol, A.R., editors, Stratigraphy and paleolimnology of the Green River Formation, western USA: Syntheses in Limnology 1, p. 251-276 (Ch-6).

Keighley, D., Flint, S., Howell, J., Anderson, D., Collins, S., Moscariello, A., and Stone, G., 2002, Surface and subsurface correlation of the Green River Formation in central Nine Mile Canyon, SW Uinta Basin, Carbon and Duchesne Counties, east-central Utah: Utah Geological Survey Miscellaneous Publication 02-1 (Ch-7).

Keighley, D.G., and Flint, S.S, 2008, Fluvial sandbody geometry and connectivity in the middle Green River Formation, Nine Mile Canyon, southwestern Uinta Basin, *in* Longman, M.W., and Morgan, C.D, editors, Hydrocarbon systems and production in the Uinta Basin, Utah: Rocky Mountain Association of Geologists and Utah Geological Association Publication 37, p. 101-119 (Ch-7).

Kelly, J.M., and Castle, J.W., 1992, Red Wash field-U.S.A., Uinta Basin, Utah, *in* Foster, N.H., and Beaumont, E.A., editors, Stratigraphic traps III: American Association of Petroleum Geologists, Treatise of Petroleum Geology, Atlas of Oil and Gas Fields, p. 231-256 (Ch-7).

Kendall, C., and Caldwell, E.A., 1998 Chapter 2—fundamentals of isotope geochemistry, *in* Kendall C., and McDonnell, J.J., editors, Isotope tracers in catchment hydrology: Amsterdam, Elsevier Science, B.V., p. 519–576 (Ch-9).

Kenney, T.A., Gerner, S.J., Buto, S.G., and Spangler, L.E., 2009, Spatially referenced statistical assessment of dissolved-solids load sources and transport in streams of the Upper Colorado River Basin: U.S. Geological Survey Scientific Investigations Report 2009-5007, 50 p. (Ch-9).

Kirkland, J.I., Lucas, S.G., and Estep, J.W., 1998, Cretaceous dinosaurs of the Colorado Plateau, *in* Lucas, S.W., Kirkland, J.I., and Estep, J.W., editors, Lower to middle Cretaceous non-

marine Cretaceous faunas: New Mexico Museum of Natural History and Science Bulletin 14, p. 67-89 (Ch-2).

Kirkland, J.I., and Madsen, S.K., 2007, The Lower Cretaceous Cedar Mountain Formation, eastern Utah—the view up an always interesting learning curve, *in* Lund, W.R., and Simon, D.B., editors, Field guide to excursions in southern Utah: Utah Geological Association Publication 35, 108 p. (Ch-2).

Kirschbaum, M.A., and Schenk, C.J., 2011, Sedimentary and reservoir heterogeneity of a valley-fill deposit—a field guide to the Dakota Sandstone of the San Rafael Swell, Utah: U.S. Geological Survey Scientific Investigations Report 2010-5222, 36 p., 1 plate (Ch-2).

Kocurek, G., and Dott, R.H., Jr., 1983, Jurassic paleogeography and paleoclimate of the central and southern Rocky Mountains region, *in* Reynolds, M.W., and Dolly, E.D., editors, Symposium on Mesozoic paleogeography of West-central U.S.: Rocky Mountain section of Society of Economic Paleontologists and Mineralogists, Denver, Colorado, p. 101-116 (Ch-2, Ch-4).

Koo, D.H., 2012, Assessment and calculation of BTEX permeation through HDPE water pipe final report: Unpublished report in IUPUI School of Engineering and Technology: Online, http://plasticpipe.org/pdf/permeation-report.pdf, accessed April 15, 2014 (Ch-10).

Kutasov, I.M., and Eppelbaum, L.V., 2005, An improved Horner method for determination of formation temperature, *in* World Geothermal Congress 2005, Antalya, Turkey, April 24–29, 2005, Proceedings: International Geothermal Association, 8 p. (Ch-12).

Lachenbruch, A.H., and Brewer, M.C., 1959, Dissipation of the temperature effect of drilling a well in Arctic Alaska: U.S. Geological Survey Bulletin 1083-C, p. 73–109 (Ch-12).

Larson, T.E., and Skold, R.V., 1958, Laboratory Studies Relating Mineral Quality of Water to Corrosion of Steel and Cast Iron: Illinois State Water Survey, Report ISWS C-71, p. 43-46 (Ch-8).

Lawrence, S.J., 2006, Description, properties, and degradation of selected volatile organic compounds detected in ground water—a review of selected literature: Online, http://pubs.usgs.gov/of/2006/1338/pdf/ofr2006-1338.pdf, accessed April 15, 2014 (Ch-10).

Lawton, T.F., 1983, Tectonic and sedimentologic evolution of the Utah foreland basin: Tucson, University of Arizona, Ph.D. dissertation, 217 p. (Ch-6)

Lawton, T.F., 1985, Style and timing of frontal structures, thrust belt, central Utah: American Association of Petroleum Geologists Bulletin, v. 69, p. 1145-1159 (Ch-3).

Lawton, T.F., 1986, Fluvial systems of the Upper Cretaceous Mesaverde Group and North Horn Formation, central Utah—a record of transition from thin-skinned to thick-skinned deformation in the foreland region, *in* Peterson, J.A., editor, Paleotectonics and sedimentation in the Rocky Mountain region, United States: American association of Petroleum Geologists Memoir 41, p. 423-442 (Ch-2, Ch-3).

Lawton, T.F., Talling, P.J., Hobbs, R.S., Trexler, J.H., Jr., Weiss, M.P., and Burbank, D.W., 1993, Structure and stratigraphy of the Upper Cretaceous and Paleocene strata (North Horn Formation), eastern San Pitch Mountains, Utah—sedimentation at the front of the Sevier orogenic belt: U.S. Geological Survey Bulletin 1787-II, p. 1-33 (Ch-2).

Lemmon, R.E., and others, 1998, Advanced fracture modeling in the Uinta Basin (Utah) for optimized primary and secondary recovery—final report: U.S. Department of Energy, DOE/PC/91008-21, 39 p. (Ch-3).

Lillis, P.G., Warden, A., and King, J.D., 2003, Petroleum systems of the Uinta and Piceance Basins—geochemical characteristics of oil types, *in* Petroleum systems and geologic assessment of oil and gas in the Uinta-Piceance province, Utah and Colorado: U.S. Geological Survey Digital Data Series DDS-69-B, chapter 3, 28 p. (Ch-3, Ch-6).

Lockley, M.G., Lucas, S.G., Hunt, A.P., and Gaston, R., 2004, Ichnofaunas from the Triassic-Jurassic boundary sequences of the Gateway area, western Colorado—implications for

faunal composition and correlations with other areas: Ichnos, v. 11, no. 1, p. 89-102 (Ch-2).

Lowe, M., and Sanderson, I., 2000, Assessing aquifer sensitivity and vulnerability to pesticides—examples from two Utah valleys [abs.]: Geological Society of America Abstracts with Programs, v. 32, no. 7, p. A-345 (Ch-10).

Lowe, M., and Sanderson, I., 2003, Groundwater sensitivity and vulnerability to pesticides, the southern Sevier Desert and Pahvant Valley, Millard County, Utah: Utah Geological Survey Miscellaneous Publication 03-1, 28 p., scale 1:380,160 (Ch-10).

Lowe, M., Wallace, J., Burk, N., Butler, M., Johnson, A., and Riding, R., 2004, Groundwater sensitivity and vulnerability to pesticides, Morgan Valley, Morgan County, Utah: Utah Geological Survey Miscellaneous Publication 04-4, 23 p., scale 1:87,000, compact disk (Ch-10).

Lowe, M., Wallace, J., Hurlow, H.A., Sanderson, I.D., and Butler, M., 2003, Groundwater sensitivity and vulnerability to pesticides in Utah: Utah Geological Survey Miscellaneous Publication MP-03-3, 40 p., 2 plates, scale 1:750,000, compact disk.

Lucas, P.T., and Drexler, J.M., 1975, Altamont-Bluebell - a major naturally fractured and overpressured stratigraphic trap, Uinta Basin, Utah, *in* Bolyard, D.W., editor, Symposium

on deep drilling frontiers in the central Rocky Mountains: Rocky Mountain Association of Geologists Guidebook, p. 265-273 (Ch-3, Ch-7).

Lucas, S.G., Tanner, L.H., and Heckert, A.B., 2005, Tetrapod biostratigraphy and biochronology across the Triassic-Jurassic boundary in northeastern Arizona, *in* Heckert, A.B., and Lucas, S.G., editors, Vertebrate paleontology in Arizona: New Mexico Museum of Natural History and Science Bulletin 29, p. 83-92 (Ch-2).

Lucchitta, I., 1979, Late Cenozoic uplift of the southwestern Colorado Plateau and adjacent Colorado River region: Tectonophysics, v. 61, p. 63-95 (Ch-1, Ch-3).

Lucchitta, I., 1989, History of the Grand Canyon and of the Colorado River in Arizona, *in* Jenney, J.P., and Reynolds, S.J., editors, Geologic evolution of Arizona: Arizona Geological Society Digest 17, p. 701-715 (Ch-3).

Luheshi, M.N., 1983, Estimation of formation temperature from borehole measurements: Geophysical Journal, Royal Astronomical Society, v. 74, p. 747– 776 (Ch-12).

Lund, J.W., 2011, Development of Direct-Use Projects, *in* 36th Workshop on Geothermal Reservoir Engineering, Stanford, California, January 31–February 2, 2011, Proceedings: Stanford University, SGP-TR-191, 11 p. (Ch-12).

Lynds, R., and Hajek E., 2006, Conceptual model for predicting mudstone dimensions in sandy

braided-river reservoirs: American Association of Petroleum Geologists Bulletin, v. 90, no. 8, p. 1273-1288 (Ch-2).

Maberry, J.O., 1971, Sedimentary features of the Blackhawk Formation (Cretaceous) in the Sunnyside district, Carbon County, Utah: U.S. Geological Survey Professional Paper 688, 58 p. (Ch-6).

Marchetti, D.W., and Cerling, T.E., 2001, Bedrock incision rates for the Fremont River tributary of the Colorado River, 2001, *in* Young, R.A., and Spamer, E.E., editors, Colorado River origin and evolution—Proceedings of a symposium held at Grand Canyon National Park in June, 2000: Grand Canyon Association, p. 125-127 (Ch-3).

Marino, J.E., 1992, Erg margin and marginal marine facies analysis of the Entrada Sandstone, San Rafael Swell, Utah—implications to hydrocarbon entrapment: Provo, Utah, Brigham Young University, M.S. thesis, 140 p. (Ch-4).

Marino, J.E., and Morris, T.H., 1996, Erg margin and marginal marine facies analysis of the Entrada Sandstone—implications to depositional models and hydrocarbon entrapment, *in* Morales, M., editor, The continental Jurassic: Museum of Northern Arizona, Bulletin 60, p. 483-496 (Ch-2, Ch-4).

Masters, G.M., and Ela, W.P., 2007, Introduction to environmental engineering and science: Prentice Hall (third edition), 720 p. (Ch-6).

McCauley, A.D., 2013, Sequence stratigraphy, depositional history, and hydrocarbon potential of the Mancos Shale, Uinta Basin, Utah: Salt Lake City, University of Utah, M.S. thesis, 173 p. (Ch-2).

McPherson, M.L., Currie, B.S., and Pierson, J.S., 2006, Reservoir characterization of the Cretaceous Cedar Mountain and Dakota Formations, southern Uinta Basin (year 1): Utah Geological Survey Open-File Report 492, 20 p. (Ch-4).

Meeks, Y.J., and Dean, J.D., 1990, Evaluating groundwater vulnerability to pesticides: Journal of Water Resources Planning and Management, v. 116, no. 5, p. 693–707 (Ch-10).

Mehnert, E., Keefer, D.A., Dey, W.S., Wehrmann, H.A., Wilson, S.D., and Ray, C., 2005, Aquifer sensitivity to pesticide leaching—testing a soils and hydrogeologic index method: Ground Water Monitoring & Remediation, v. 25, no. 4, p. 60–67 (Ch-10).

Milner, A.R.C., and Kirkland, J.I., 2006, Preliminary review of the Early Jurassic (Hettangian) freshwater Lake Dixie fish fauna in the Whitmore Point Member, Moenave Formation in southwest Utah, *in* Harris, J.D., Lucas, S.G., Spielmann, J.A., Lockley, M.G., Milner, A.R.C., and Kirkland, J.I., editors, Tracking dinosaur origins—the Triassic/Jurassic terrestrial transition: New Mexico Museum of Natural History and Science Bulletin 37, p. 510-521 (Ch-2).

Milton, C., Axelrod, J.M., and Grimaldi, F.S., 1954a, New minerals reedmergnerite ($Na_2O•B_3O_3•6SiO_2$) and eitelite ($Na_2O•MgO•CO_2$) associated with leucosphenite, shortite, searesite, and crocidolite in the Green River Formation, Utah [abs.]: Geological Society of America Bulletin, v. 65, p. 1286-1287 (Ch-7).

Milton, C., Axelrod, J.M., and Sherwiid, A.M., 1954b, New occurrence of leucosphenite, in oil shale from Utah [abs.]: American Mineralogist, v. 39, p. 337 (Ch-7).

Molennar, C.M., and Cobban, W.A., 1991, Middle Cretaceous stratigraphy on the south and east sides of the Uinta Basin, northeastern Utah and northwestern Colorado: U.S. Geological Survey Bulletin 1787, p. P1-P34 (Ch-2, Ch-3, Ch-5).

Molina-Garza, R.S., Geissman, J.W., and Lucas, S.G., 2003, Paleomagnetism and paleomagnetostratigraphy of the lower Glen Canyon and upper Chinle groups, Triassic-Jurassic of northern Arizona and northeastern Utah: Journal of Geophysical Research, v. 108, no. B4, p. 1-24 (Ch-2).

Morgan, C.D., 2003a, Geologic guide and road logs of the Willow Creek, Indian, Soldier Creek, Nine Mile, Gate, and Desolation Canyons, Uinta Basin, Utah: Utah Geological Survey Open-File Report 407, 79 p. (Ch-2, Ch-6).

Morgan, C.D., 2003b, The Bluebell oil field, Uinta Basin, Duchesne and Uintah Counties, Utah—characterization and oil well demonstration: Utah Geological Survey Special Study 106, 95 p. (Ch-7).

Morgan, C.D., Chidsey, T.C., Jr., McClure, K.P., Bereskin, S.R., and Deo, M.D., 2003, Reservoir characterization of the lower Green River Formation, southwest Uinta Basin, Utah: Utah Geological Survey Open-File Report 411, CD-ROM, 216 p. 28 plates (Ch-2)

Morgan, C.D., McClure, K.P., Bereskin, S.R., and McPherson, M., 2002, A preliminary discussion of fault styles in the southwest Uinta Basin, Utah [abs.]: American Association of Petroleum Geologists Rocky Mountain Section Meeting Program with Abstracts, p. (Ch-6).

Morgan, P., and Scott, B., 2011, Bottom-hole temperatures data from the Piceance Basin, Colorado—indications for prospective sedimentary basin EGS resources: Transactions, Geothermal Resources Council, v. 35, p. 477–485 (Ch-12).

Morgan, P., and Scott, P., 2014, New geothermal-gradient maps for Colorado's sedimentary basins: Transactions, Geothermal Resources Council, v. 38, p. 155–162 (Ch-12).

Morris, T.H., and Hicks, T.C., 2011, Facies analysis and reservoir characterization of the mudstone-rich portion of the Entrada Sandstone, south-central Utah—emphasis on the

Bitter Seep Wash Sandstone at South Salt Wash and Bitter Seep Wash: Utah Geological Survey unpublished report, 110 p. (Ch-4).

Morris, T.H., Richmond, D.R., and Marino, J.E., 1991, The Paleocene/Eocene Colton Formation—a fluvial-dominated lacustrine deltaic system, Roan Cliffs, Utah, *in* Chidsey, T.C., Jr., editor, Geology of east-central Utah: Utah Geological Association Publication 19, p. 129-140 (Ch-6).

Morris, T.H., McBride, J.H., and Monn, W.D., 2005, A multidisciplinary approach to reservoir characterization of the Entrada erg-margin gas play, Utah: Utah Geological Survey Open-File Report 459, 52 p. (Ch-4).

Myubg-uk, Y., and Cross, A.T., 1997, Palynostratigraphy of Upper Cretaceous-Lower Tertiary strata, Price Canyon, Utah: Review of Paleobotany and Palynology, v. 97, p. 53-66 (Ch-2).

Narr, W.N., and Currie, J.B., 1982, Origin of fracture porosity - example from Altamont field, Utah: American Association of Petroleum Geologists Bulletin, v. 66, no. 9, p. 1231-1247 (Ch-3, Ch-7).

National Petroleum Council, 2011, Management of produced water from oil and gas wells: National Petroleum Council Operations and Environment Task Group Paper 2-17, 32 p. (Ch-11).

National Soil Survey Center, 2006, Soil Survey Geographic (SSURGO) data base: Online, http://soildatamart.nrcs.usda.gov/Survey.aspx?State=UT, accessed February 17, 2006 (Ch-10).

Nelson, P.H., and Hoffman, E.L., 2009, Gas, water, and oil production from the Wasatch Formation, Greater Natural Buttes field, Uinta Basin, Utah: U.S. Geological Survey Open-File Report 2009-1049, 19 p. (Ch-6).

Newman, K.F., and Chan, M.A., 1991, Depositional facies and sequences in the Upper Cretaceous Panther Tongue Member of the Star Point Formation, Wasatch Plateau, Utah, *in* Chidsey, T.C., Jr., editor, Geology of east-central Utah: Utah Geological Association Publication 19, p. 65-76 (Ch-2).

Nixon, R.P., 1973, Oil source beds in the Cretaceous Mowry Shale of northwestern interior United States: American Association of Petroleum Geologists Bulletin, v. 57, no. 1, p. 136-157 (Ch-2).

Nuccio, V.F., and Condon, S.M., 1996, Burial and thermal history of the Paradox Basin, Utah and Colorado, and petroleum potential of the Middle Pennsylvanian Paradox Formation, *in* Huffman, A.C., Jr., Lund, W.R., and Godwin, L.H., editors, Geology of the Paradox Basin: Utah Geological Association Publication 25, p. 57-76 (Ch-3).

Nuccio, V.F., and Roberts, L.N.R., 2003, Chapter 4 – Thermal maturity and oil and gas generation history of petroleum systems in the Uinta – Piceance province, Utah and Colorado, *in* Petroleum systems and geologic assessment of oil and gas in the Uinta – Piceance province, Utah and Colorado: U.S. Geological Survey Digital Data Series, DDS-69-B, 39 p. (Ch-3).

Osborn, S.G., Vengosh, A., Warner, N.R., and Jackson, R.B., 2011, Methane contamination of drinking water accompanying gas-well drilling and hydraulic fracturing: Proceedings of the National Academy of Sciences, v. 108, p. 8172–8176.

Osmond, J.C., 1964, Tectonic history of the Uinta Basin, Utah, *in* Sabatka, E.F., editor, Guidebook to the geology and mineral resources of the Uinta Basin—Utah's hydrocarbon storehouse: Intermountain Association of Petroleum Geologists, Thirteenth Annual Field Conference, p. 47-58 (Ch-6).

Osmond, J.C., 1985, Reservoir sandstone patterns, Green River Formation, Duck Creek oil field, Uintah County, Utah, *in* Picard, M.D., editor, Geology and energy resources, Uinta Basin of Utah: Utah Geological Association Publication 12, p. 187-192 (Ch-7).

Osmond, J.C. 1986, Petroleum geology of the Uinta Mountains – White River uplift, Colorado and Utah, *in* Stone, D.S., editor, New interpretations of northwest Colorado geology: Rocky Mountain Association of Geologists Guidebook, p. 213-221 (Ch-3).

Pederson, J., Karlstrom, K., Sharp, W., and McIntosh, W., 2002, Differential incision of the Grand Canyon related to Quaternary faulting—constraints from U-series and Ar/Ar dating: Geology, v. 30, p. 739-742 (Ch-3).

Peterson, F., 1988, Pennsylvanian to Jurassic eolian transportation systems in the western United States: Sedimentary Geology, v. 56, p. 207-260 (Ch-2).

Peterson, J.A., 1994, Regional geology of the eastern Great Basin and paleotectonic history of the Railroad Valley area, eastern Nevada, *in* Schalla, R.A., and Johnson, E.H., editors, Oil fields of the Great Basin: Nevada Petroleum Society Special Publication, p. 15-40. (Ch-4).

Picard, M.D., 1975, Facies, petrography and petroleum potential of Nugget Sandstone (Jurassic), southwestern Wyoming and northeastern Utah, *in* Bolyard, D.W., editor, Symposium on deep drilling frontiers of the central Rocky Mountains: Rocky Mountain Association of Petroleum Geologists Guidebook, p. 109-127 (Ch-2).

Pipiringos, G.N., and O'Sullivan, R.B., 1978, Principal unconformities in Triassic and Jurassic rocks, Western Interior United States—a preliminary survey: U.S. Geological Survey Professional Paper 1035-A, 29 p. (Ch-2, Ch-4).

Pitman, J.K., Fouch, T.D., and Goldhaber, M.B., 1982, Depositional setting and diagenetic evolution of some Tertiary unconventional reservoir rocks, Uinta Basin, Utah: American Association of Petroleum Geologists Bulletin, v. 66, no. 10, p. 1581-1596 (Ch-7).

Potochnik, A.R., and Faulds, J.E., 1998, A tale of two rivers—Tertiary structural inversion and drainage reversal across the southern boundary of the Colorado Plateau, *in* Duebendorfer, E.M., editor, Geologic excursions in northern and central Arizona: Field Trip Guidebook for Geological Society of America Rocky Mountain Section Meeting (Ch-3).

Potter, C.J., Tang, R., and Hainsworth, T.J., 1991, Late Paleozoic structure of the southern part of the Uinta Basin, Utah, from seismic reflection data: U.S. Geological Survey Bulletin 1787-V, 18 p. (Ch-6).

Prensky, S., 1992, Temperature measurements in boreholes—an overview of engineering and scientific applications: The Log Analyst, v. 33, no. 3, p. 313–333 (Ch-12).

Price, D., and Miller, L.L., 1975, Hydrologic reconnaissance of the southern Uinta Basin, Utah and Colorado: Utah Department of Natural Resources Technical Publication 49, 66 p., 3 plates (Ch-7, Ch-9, Ch-10).

Rao, P.S.C., Hornsby, A.G., and Jessup, R.E., 1985, Indices for ranking the potential for VOC contamination of groundwater: Soil and Crop Science Society of Florida Proceedings, v. 44, p. 1–8 (Ch-10).

Rao, P.S.C., Mansell, R.S., Baldwin, L.B., and Laurent, M.F., 2006, VOCs and their behavior in soil and water: Online, http://pmep.cce.cornell.edu/facts-slides-self/facts/gen-pubre-soil-water.html, accessed February 8, 2006 (Ch-10).

Ray, R.G., Kent, B.H., Dane, C.H., 1956, Stratigraphy and photograph-geology of the southwestern part of Uinta Basin, Duchesne and Uintah Counties, Utah: U.S. Geological Survey Oil and Gas Inventory Map OM 171, 2 plates, scale 1:63,360 (Ch-3).

Remy, R.R, 1992, Stratigraphic of the Eocene part of the Green River Formation in the south-central part of the Uinta Basin, Utah: U.S. Geological Survey Bulletin 1787, 79 p. (Ch-7).

Ressetar, R., Birgenheier, L.P., and McCauley, A., in preparation, Chapter 4—regional correlations and thickness trends, *in* Ressetar, R., and Birgenheier, L.P., editors, Cretaceous Mancos Shale, Uinta Basin, Utah—resource potential and best practices for an emerging shale gas play: Utah Geological Survey contract report (Ch-5).

Rice, D.D, Fouch, T.D, and Johnson, R.C., 1992, Influence of source rock type, thermal maturity, and migration on composition and distribution of natural gases, Uinta Basin, Utah, *in* Fouch, T.D., Nuccio, V.F., and Chidsey, T.C., Jr., editors, Hydrocarbon and mineral resources of the Uinta Basin, Utah and Colorado: Utah Geological Association Publication 20, p. 95-109 (Ch-3).

Rider, M., and Kennedy, M., 2011, The geological interpretation of well logs (third edition): Scotland, Rider-French Consulting Ltd., 432 p. (Ch-6).

Riggs, N.R., and Blakey, R.C., 1993, Early and Middle Jurassic paleogeography and volcanology of Arizona and adjacent areas: Society of Economic Paleontology and Mineralogy, Pacific Section, Mesozoic Paleogeography, Book 71, p. 347-375 (Ch-4).

Roberts, L.N.R., 2003, Structure contour map of the top of the Dakota Sandstone, Uinta-Piceance Province, Utah and Colorado, *in* USGS Uinta-Piceance Assessment Team, Petroleum systems and geologic assessment of oil and gas in the Uinta-Piceance Province, Utah and Colorado: U.S. Geological Survey Digital Data Series 69-B, Chapter 16, 11 p. (Ch-4).

Rose Petroleum, 2015, Mancos operations update—Uinta Basin, Utah: online at http://www.rosepetroleum.com/press/pressreleases/view/502, accessed July 2015 (Ch-5).

Rowley, P.D., Hansen, W.R., Tweto, O., and Carrara, P.E., 1985, Geologic map of the Vernal 1° x 2° quadrangle, Colorado, Utah, and Wyoming: U.S. Geological Survey Miscellaneous Investigation Series Map I-1526, 1 plate, scale 1:250,000 (Ch-3).

Ruble, T.E., 1996, Geochemical investigation of the mechanisms of hydrocarbon generation and accumulation in the Uinta Basin, Utah: Norman, University of Oklahoma, Ph.D. dissertation, 268 p. (Ch-7).

Ryder, R.T., Fouch, T.D., and Elison, J.H., 1976, Early Tertiary sedimentation in the western Uinta Basin, Utah: Geological Society of America Bulletin, v. 87, no. 4, p. 496-512 (Ch-2, Ch-7).

Saxton, K.E., undated, Soil texture triangle hydraulic properties calculator: Online, http://wilkes-fs1.wilkes.edu/~boram/grphtext.htm, accessed February 24, 2006 (Ch-10).

Schamel, S., 2015, Shale oil resource play potential of the Green River Formation, Uinta Basin, Utah: Utah Geological Survey Open-File Report 639, 65 p. (Ch-7).

Schlosser, S.A., McCray, J.E., Murray, K.E., and Austin, B., 2002, A subregional-scale method to assess aquifer vulnerability to pesticides: Groundwater, v. 40, no. 4, p. 361–367 (Ch-10).

Schlotthauer, W.E., Nance, B.W., and Olds, J.D., 1981, Identification and characteristics of aquifers in Utah: Salt Lake City, Utah Division of Water Rights, 240 p., 4 plates, scale 1:1,000,000 (Ch-10).

Schlumberger, 2009, Log interpretation charts: Sugarland, Texas, Schlumberger, 310 p. (Ch-6).

Schmoker, J.W., Nuccio, V.F., and Pitman, J.K., 1992, Porosity trends in predominately nonmarine sandstones of the Upper Cretaceous Mesaverde Group, Uinta and Piceance

Basins, Utah and Colorado, *in* Fouch, T.D., Nuccio, V.F., and Chidsey, T.C., Jr., editors, Hydrocarbon and mineral resources of the Uinta Basin, Utah and Colorado: Utah Geological Association Publication 20, p. 111-122 (Ch-6).

Schuh, M.L., 1993, Red Wash, *in* Hill, B.G., and Bereskin, S.R., editors, Oil and gas fields of Utah: Utah Geological Association Publication 22, non-paginated (Ch-3).

Sendziak, K.L., 2012, Stratigraphic architectural and avulsion deposits of a low net sand content fluvial succession—lower Wasatch Formation, Uinta Basin: Golden, Colorado School of Mines, M.S. thesis, 53 p. (Ch-6).

Shalev, E., Levitte, D., Gabay, R., and Zemach, E., 2008, Assessment of geothermal resources in Israel: Geological Survey of Israel Report GSI /29/ 2008, 26 p. (Ch-12).

Shier, D.A., 2004, Well log normalization—methods and guidelines: Petrophysics, v. 45, p. 268-280 (Ch-6).

Shukla, S., Mostaghimi, S., Shanholt, V.O., and Ross, B.R., 2000, A county-level assessment of groundwater contamination by pesticides: Groundwater Monitoring & Remediation, v. 20, no. 1, p. 104–119 (Ch-10).

Siegel, D.I., 2000, Pesticides in groundwater—vulnerability, transport and fate: Ostrander, Ohio, Environmental Education Enterprises, Inc., short course, 259 p. (Ch-10).

Sinkevich, M.G., Jr., Walter, M.T., Lembo, A.J., Jr., Richards, B.K., Peranginangin, N., Aburime, S.A., and Steenhuis, T.S., 2005, A GIS-based groundwater contamination risk assessment tool for pesticides: Groundwater Monitoring & Remediation, v. 25, no. 4, p. 82–91 (Ch-10).

Smith, J.L., 2004, Investigation of fracture mechanisms in the Duchesne fault zone, Uinta Basin, northeastern Utah—the role of fluid overpressures and other processes: Socorro, New Mexico Institute of Mining and Technology, M.S. thesis, 157 p. (Ch-3)

Smith, L.S., 1976, Paleoenvironments of the upper Entrada Sandstone and the Curtis Formation on the west flank of the San Rafael Swell, Emery County, Utah: Brigham Young University Geology Studies, v. 23, pt. 1, p. 113-171 (Ch-2, Ch-4).

Smith, A.G., Hurley, A.M., and Briden, J.C., 1981, Phanerozoic paleocontinental world maps: Cambridge University Press, Cambridge Earth Science Series, 102 p. (Ch-2)

Speece, M.A., Bowen, T.D., Folcik, J.L., and Pollack, H.N., 1985, Analysis of temperatures in sedimentary basins—the Michigan Basin: Geophysics, v. 50, p. 1218–1334 (Ch-12).

Spieker, E.M., 1946, Let Mesozoic and early Cenozoic history of central Utah: U.S. Geological Survey Professional Paper 205-D, p. 117-161 (Ch-2, Ch-6).

Sprinkel, D.A., 2006, Interim geologic map of the Dutch John 30' x 60' quadrangle, Daggett and Uintah Counties, Utah, Moffat County, Colorado, and Sweetwater County, Wyoming: Utah Geological Survey Open-File Report 491, scale 1:100,000 (Ch-2, Ch-3, Ch-10, plate 1).

Sprinkel, D.A., 2007, Interim geologic map of the Vernal 30' x 60' quadrangle, Uintah and Duchesne Counties, Utah, and Moffat and Rio Blanco Counties, Colorado: Utah Geological Survey Open-File Report 506, scale 1:100,000 (Ch-3, Ch-6, Ch-7, Ch-10, plate 7).

Sprinkel, D.A., 2009, Interim geologic map of the Seep Ridge 30' x 60' Quadrangle, Uintah, Duchesne, and Carbon Counties, Utah, and Garfield and Rio Blanco Counties, Colorado: Utah Geological Survey Open-File Report 549, scale 1:100,000 (Ch-2, Ch-3, Ch-7, Ch-10, plate 1).

Sprinkel, D.A., 2010, Geology of Flaming Gorge National Recreation Area, Utah-Wyoming, *in* Sprinkel, D.A., Chidsey, T.C., Jr., and Anderson, P.B., editors, 2010, Geology of Utah's parks and monuments (third edition): Utah Geological Association and Bryce Canyon Natural History Association, p. 285-308 (Ch-3).

Sprinkel, D.A., 2013, Interim geologic map of the easternmost part of the Duchesne 30' x 60' quadrangle, Duchesne and Wasatch Counties, Utah—Year 1 of 6: Utah Geological Survey Open-File Report 625, scale 1:100,000 (Ch-10, plate 1).

Sprinkel, D.A., 2014, Interim geologic map of the easternmost part of the Duchesne 30' x 60' quadrangle, Duchesne and Wasatch Counties, Utah—Year 2: Utah Geological Survey Open-File Report 634, 19 p., scale 1:100,000 (Ch-3).

Sprinkel, D.A., Castaño, J.R., and Roth, G.W., 1997, Emerging plays in central Utah based on a regional geochemical, structural, and stratigraphic evaluation [abs.]: American Association of Petroleum Geologists Bulletin Annual Convention, Official Program with Abstracts, v. 6, p. A110 (Ch-3).

Sprinkel, D.A., Kowallis, B.J., and Jensen, P.H., 2011a, Correlation and age of the Nugget Sandstone and Glen Canyon Group, Utah, *in* Sprinkel, D.A., Yonkee, W.A., and Chidsey, T.C., Jr., editors, The Sevier thrust belt—northern and central Utah and adjacent areas: Utah Geological Association Publication 40, p. 131-149 (Ch-2).

Sprinkel, D.A., Doelling, H.H., Kowallis, B.J., Waanders, Gerald, and, Kuehne, P.A., 2011b, Early results of a study of Middle Jurassic Strata in the Sevier fold and thrust belt, *in* Sprinkel, D.A., Yonkee, W.A., and Chidsey, T.C., Jr., editors, The Sevier thrust belt—northern and central Utah and adjacent areas: Utah Geological Association Publication 40, p. 151-172 (Ch-2).

Sprinkel, D.A., Madsen, S.K., Kirkland, J.I., Waanders, G., and Hunt, G.J., 2012, Cedar Mountain and Dakota Formations around Dinosaur National Monument—evidence of the

first incursion of the Cretaceous Western Interior Seaway into Utah: Utah Geological Survey Special Study 143, 20 p. (Ch-2)

Sprinkel, D.A., Doelling, H.H., Waanders, Gerald, and Kowallis, B.J., in preparation, Stratigraphy, correlation, and paleogeography of Middle Jurassic (Bajocian to Callovian) formations in Utah: Utah Geological Survey Bulletin (Ch-2).

Squillace, P.J., and Moran, M.J., 2000, Estimating the likelihood of MTBE occurrence in drinking water supplied by ground-water sources in the Northeast and Mid-Atlantic Regions of the United States: U.S. Geological Survey Open-File Report 00-343, 10 p. (Ch-10).

Squillace, P.J., Scott, J.C., Moran, M.J., Nolan, B.T., and Kolpin, D.W., 2002, VOCs, pesticides, nitrate, and their mixtures in groundwater used for drinking water in the United States: Environmental Science Technology, v. 36, p. 1923–1930 (Ch-10).

Stancel, S.G., Cuzella, J.J., Macmillan, L., and Ragas, A., 2008, Controls on gas production along the southern flank of greater Natural Buttes field—a case study of the Love area, Uinta Basin, Utah, *in* Longman, M.W., and Morgan, C.D., editors, Hydrocarbon systems and production in the Uinta Basin, Utah: Utah Geological Association Publication 37, p 237-266 (Ch-6).

Stanton, R.G., 1976, The paleoenvironment of the Summerville Formation on the west side of the San Rafael Swell, Emery County, Utah: Brigham Young University Geology Studies, v. 23, pt. 1, p. 37-73 (Ch-2).

Stearns, D.W., and Friedman, M., 1972, Reservoirs in fractured rocks, in King, R.E., editor, Stratigraphic oil and gas fields—classification, exploration methods, and case histories: American Association of Petroleum Geologist Memoir 16, p. 82-106 (Ch-3).

Steeples, D.W., and Stavnes, S.A., 1982, Assessment of geothermal resources of Kansas: U.S. Department of Energy Final Report DOE/ET/27204-T1, v. 1, sec. 1, 59 p. (Ch-12).

Steiger, J.I., 2007, Effects of saline-wastewater injection on water quality in the Altamont-Bluebell oil and gas field, Duchesne County, Utah, 1990-2005: U.S. Geological Survey Scientific Investigations Report 2007-5192, 29 p. (Ch-9).

Stoddard, T., and McLennan, J., in preparation, Chapter 12—log evaluation, *in* Ressetar, R., and Birgenheier, L.P., editors, Cretaceous Mancos Shale, Uinta Basin, Utah—resource potential and best practices for an emerging shale gas play: Utah Geological Survey contract report (Ch-5).

Stone, D.S., 1977, Tectonic history of the Uncompahgre uplift, *in* Veal, H.K., editor, Exploration frontiers of the central and southern Rockies: Rocky Mountain Association of Geologists Guidebook, p. 23-30 (Ch-3).

Stone, D.S., 1986, Rangely field summary 2 - seismic profile, structural cross section, and geochemical comparisons, *in* Stone, D.S., editor, New interpretations of northwest Colorado geology: Rocky Mountain Association of Geologists Guidebook, p. 226-228 (Ch-3).

Stone, D.S., 1993, Tectonic evolution of the Uinta Mountains—palinspastic restoration of a structural cross section along longitude 109º15', Utah: Utah Geological Survey Miscellaneous Publication 93-8, 19 p., 3 plates (Ch-2, Ch-3).

Sweeny, J.J., Burnham, A.K., and Braun, R.L., 1987, A model of hydrocarbon generation from type I kerogen—application to Uinta Basin, Utah: American Association of Petroleum Geologist Bulletin, v. 71, no. 8, p. 967-985 (Ch-3).

Tänavsuu-Milkeviciene, K., and Sarg, F.J., 2012, Evolution of an organic-rich lake basin—stratigraphy, climate and tectonics: Piceance Creek basin, Eocene Green River Formation: Sedimentology, v. 59, no. 6, p. 1735–1768 (Ch-7).

Tiab, D., and Donaldson, E.C., 2011, Petrophysics—theory and practice of measuring reservoir rock and fluid transport properties: Gulf Professional Publishing (third edition), 976 p. (Ch-6).

Toms, L.C., 2014, Spatial and temporal variations in lacustrine depositional controls from the middle to upper Green River Formation, central and western Uinta Basin, Utah: Salt Lake City, University of Utah, M.S. thesis, 255 p. (Ch-7).

Tripp, B.T., 2004, Gilsonite—an unusual Utah resource: Utah Geological Survey, Survey Notes, v. 36, no. 3, p. 1-3 (Ch-3).

Uintah County, 2015, Uintah County, Utah, Rules Chapter 17.140 – produced water disposal facilities and evaporation ponds: Online, http://www.co.uintah.ut.us/planning/minutes/2009/agendas/11-04-09/Evaporative.pdf, accessed April 1, 2015 (Ch-11).

U.S. Bureau of Land Management, 2010, Greater Natural Buttes Final Environmental Impact Statement FES 12-8: U.S. Department of Interior, Bureau of Land Management, 9 chapters, individually paginated, 17 appendices (Ch-11).

U.S. Bureau of Land Management, 2012a, Greater Uinta Basin oil and gas cumulative impacts technical support document: U.S. Bureau of Land Management technical report, 27 p. (Ch-9, Ch-12).

U.S. Bureau of Land Management, 2012b, Greater Natural Buttes Final Environmental Impact Statement FES 12-8: U.S. Department of Interior, Bureau of Land Management, 9 chapters, individually paginated, 17 appendices, online,

http://www.blm.gov/ut/st/en/fo/vernal/planning/nepa_.html, accessed May 1, 2013 (Ch-11).

U.S. Bureau of Land Management, 2012c, Final Environmental Impact Statement – Gasco Uinta Basin Natural Gas Project: U.S. Department of Interior, Bureau of Land Management, 5 chapters, individually paginated, 19 appendices, and project maps, online, http://www.blm.gov/style/medialib/blm/ut/vernal_fo/planning/gasco_eis/gasco_folder_7.Par.81638.File.dat/GASCO%20EIS%20Entire%20Document.pdf, accessed May 5, 2014 (Ch-11).

U.S. Bureau of Land Management, 2013a, Finding of No Significant Impact (FONSI) for EOG Resources, Inc. Chapita Wells Unit Liquids Gathering System Phase 1 Project Environmental Assessment BLM-UT-G010-2012-113: U.S. Department of Interior, Bureau of Land Management, 106 p., online, http://www.blm.gov/style/medialib/blm/ut/vernal_fo/planning/environmental_documents/eog_gathering.Par.6185.File.dat/EOG%20Liquids%20Gathering%20FINAL%20EA_FONSI_DR.pdf, accessed May 15, 2014 (Ch-11).

U.S. Bureau of Land Management, 2013b, XTO Energy's River Bend Unit Infill Development Environmental Assessment and Biological Assessment EA Number UT-080-07-772: U.S. Department of Interior, Bureau of Land Management, 7 chapters, individually paginated, 15 appendices, online, http://www.blm.gov/style/medialib/blm/ut/vernal_fo/planning/gasco_eis/gasco_folder_7.

Par.81638.File.dat/GASCO%20EIS%20Entire%20Document.pdf, accessed May 22, 2014 (Ch-11).

U.S. Bureau of Land Management, 2013c, Newfield Exploration Corporation Monument Butte Oil and Gas Development Project in Uintah and Duchesne Counties, Utah, Draft Environmental Impact Statement UT-G010-2009-0217: U.S. Department of Interior, Bureau of Land Management, 7 chapters, individually paginated, 9 appendices, online, http://www.blm.gov/ut/st/en/fo/vernal/planning/nepa_.html, accessed June 2, 2014 (Ch-11).

U.S. Environmental Protection Agency, 2004, Evaluation of impacts to underground sources of drinking water by hydraulic fracturing of coalbed methane reservoirs: Environmental Protection Agency, Attachment 4, 10 p. (Ch-6).

U.S. Environmental Protection Agency, 2006, Current drinking water standards: Online, http://www.epa.gov/safewater/mcl.html, accessed February 6, 2006 (Ch-10).

U.S. Environmental Prptection Agency, 2008, An assessment of the environmental implications of oil and gas production—a regional case study, EPA Region 8: U.S. Environmental Protection Agency Sector Strategies Working Draft Report, 4 chapters, 5 appendices, individually paginated (Ch-11).

U.S. Environmental Protection Agency, 2012, Overview of final amendments to air regulations for the oil and natural gas industry: Fact sheet, Online, http://www.epa.gov/airquality/oilandgas/pdfs/20120417fs.pdf, accessed February 4, 2015 (Ch-10).

U.S. Environmental Protection Agency, 2014, Chloromethane health advisory: http://yosemite.epa.gov/water/owrccatalog.nsf/7322259e90d060c885256f0a0055db68/ac4215744f22d0d285256b0600723232!opendocument, accessed December 3, 2014 (Ch-9).

U.S. Environmental Protection Agency, 2015, U.S. Environmental Protection Agency water – total maximum daily loads (303d): Online, http://www.blm.gov/ut/st/en/fo/vernal/planning/nepa_.htmlhttp://water.epa.gov/lawsregs/lawsguidance/cwa/tmdl/index.cfm, accessed April 1, 2015 (Ch-11).

U.S. Geological Survey, 2009, Ground water atlas of the United States, chapter C, Colorado Plateaus aquifers: Online at http://pubs.usgs.gov/ha/ha730/pub/ch_c/C-text.ascii, accessed August 2015 (Ch-5).

U.S. Geological Survey Oil Shale Assessment Team, 2010a, Oil shale and nahcolite resources of the Piceance Basin, Colorado: U.S. Geological Survey Digital Data Series DDS–69–Y, 7 chapters, pages variable (Ch-7).

U.S. Geological Survey Oil Shale Assessment Team, 2010b, Oil shale resources of the Uinta Basin, Utah and Colorado: U.S. Geological Survey Digital Data Series DDS–69–BB, 7 chapters, pages variable (Ch-7).

U.S. Geological Survey, 2014, National Water Information System database: Online, <http://waterdata.usgs.gov/nwis>, accessed May 14th, 2014 (Ch-8).

Utah Department of Environmental Quality, 2015a, Division of Water Quality, Ground Water Protection Program: Online, http://www.deq.utah.gov/ProgramsServices/programs/water/groundwater/classes.htm, accessed April 1, 2015 (Ch-11).

Utah Department of Environmental Quality, 2015b, Division of Water Quality, Water Management Program: Online, http://www.deq.utah.gov/ProgramsServices/programs/water/watersheds/approvedtmdls.htm, accessed April 1, 2015 (Ch-11).

Utah Division of Oil Gas and Mining, 2014, DOGM Live Data website: Online, <http://oilgas.ogm.utah.gov/Data_Center/LiveData_Search/well_data_lookup.cfm>, accessed March 15th, 2014 (Ch-8).

Utah Division of Oil, Gas, and Mining, 2015a, Oil and gas summary production report by county, December 2014: Online,

fs.ogm.utah.gov/pub/Oil&Gas/Publications/Reports/Prod/County/Cty_Dec_2014.pdf, accessed May 2015 (Ch-1).

Utah Division of Oil, Gas, and Mining, 2015b, Application for permits to drill (APD) – by county: Online, http://oilgas.ogm.utah.gov/Statistics/APD_county.cfm, accessed May 2015 (Ch-1).

Utah Division of Oil, Gas, and Mining, 2015c, Oil and gas summary production report by field, December 2014: Online, fs.ogm.utah.gov/pub/Oil&Gas/Publications/Reports/Prod/Field/Fld_Dec_2014.pdf, accessed May 2015 (Ch-1, Ch-6).

Utah Division of Oil, Gas, and Mining, 2015d, Oil and gas summary production report by well, December 2014: Online, fs.ogm.utah.gov/pub/Oil&Gas/Publications/Reports/Prod/Well/Fld_Dec_2014.pdf, accessed May 2015.

Utah Division of Oil, Gas, and Mining, 2015e, Data research center: Online, http://oilgas.ogm.utah.gov/Data_Center/DataCenter.cfm, accessed July 2015 (Ch-7).

Utah Division of Water Resources, 2005, Water reuse in Utah: Utah Division of Water Resources Report as part of the Utah State Water Plan, online, http://www.water.utah.gov/WaterReuse/WaterReuse.pdf, accessed July 1, 2014 (Ch-11).

Utah State Univerity, 2013, Uintah Basin winter ozone and air quality study—final report, Lyman, S. and Shorthill, H., editors: Utah State University Commercialization and Regional Development, Document Number CRD13-320.32, 281 p. (Ch-10, Ch-11).

Vaill, J.E., and Butler, D.L., 1999, Streamflow and dissolved-solids trends through 1996, in the Upper Colorado River Basin upstream from Lake Powell – Colorado, Utah, and Wyoming: U.S. Geological Survey Water Resources Investigations Report 99-4097, 47 p. (Ch-11).

Vanden Berg, M.D., 2008, Basin-wide evaluation of the uppermost Green River Formation's oil-shale resource, Uinta Basin, Utah and Colorado: Utah Geological Survey Special Study 129, compact disk (Ch-7).

Vanden Berg, M.D., 2011, Exploring Utah's other great lake: Utah Geological Survey, Survey Notes, v. 43, no. 2, p. 1-2 (Ch-1).

Vanden Berg, M.D., in preparation, An examination of the saline phases of Eocene Lake Uinta, Uinta Basin, Utah (Ch-7).

Vanden Berg, M.D., and Birgenheier, L., 2014, Hypersaline facies and the termination of Lake Uinta, upper Green River Formation, Uinta Basin, Utah [abs.]: American Association of Petroleum Geologists, Rocky Mountain Section Annual Meeting, July 20-22, 2014:

Online: http://www.searchanddiscovery.com/abstracts/html/2014/90193rms/abstracts/1952854.html, accessed March 2015 (Ch-7).

Vanden Berg, M.D., Lehle, D.R., Carney, S.M., and Morgan, C.D., 2013, Geological characterization of the Birds Nest aquifer, Uinta Basin, Utah—assessment of the aquifer's potential as a saline water disposal zone: Utah Geological Survey Special Study 147, 53 p. (Ch-7, Ch-9, Ch-10).

Vanden Berg, M.D., Wood, R.E., Carney, S.M., and Morgan, C.D., 2014, Geological characterization of the Uteland Butte Member of the Eocene Green River Formation—an emerging unconventional carbonate tight oil play in the Uinta Basin, Utah [abs.]: American Association of Petroleum Geologists, Rocky Mountain Section, July 2014 (Ch-7).

Veolia Water Technologies, North America, 2014, ROSS™ Technology – Frac flowback and produced water treatment: Online, http://www.veoliawaterstna.com/news-resources/information-files/ross-flowback-produced-water.htm, accessed 2015 (Ch-11).

Verbeek, E.R., and Grout, M.A., 1993, Geometry abd structural evolution of gilsonite dikes in the eastern Uinta Basin, Utah, in Evolution of sedimentary basins—Uinta and Piceance Basin: U.S. Geological Survey Bulletin 1787-HH, 42 p. (Ch-3).

Wallace, J., 2012a, Baseline water quality and quantity for selected sites in the southeastern Uinta Basin, Utah: Utah Geological Survey Open-File Report 595, 70 p. (Ch-7, Ch-9, Ch-10).

Wallace, J., 2012b, Seasonal analysis of water chemistry to establish baseline water quality for selected sites in the southeastern Uinta Basin, Utah, *in* Hylland, M.D., and Harty, K., editors, Selected topics in engineering and environmental geology in Utah: Utah Geological Association Publication 41, p. 155–173 (Ch-10).

Wallace, J., 2013, Establishing baseline water quality conditions in the southeastern Uinta Basin: Utah Geological Survey, Survey Notes, v. 45, p. 5–6 (Ch-10).

Wanty, R.B., Pitman, J.K., and Fouch, T.D., 1991, Groundwater chemistry and diagenetic reactions in Tertiary sandstone of the Green River and Wasatch Formations, Uinta Basin, Utah, *in* Evolution of sedimentary basins, Uinta and Piceance Basins: U.S. Geological Survey Bulletin, no. 1787, 21 p. (Ch-7).

Weast, R.C., Lide, D.R., Astle, M.J., and Berger, W.H., 1990, CRC handbook of chemistry and physics: Boca Raton, CRC Press, Inc., variously paginated (Ch-10).

Weber, J.B., 1994, Properties and behavior of pesticides in soil, *in* Honeycutt, R.C., and Shabacker, D.J., editors, Mechanisms of movement into groundwater: Boca Raton, CRC Press, Inc., p. 15–41 (Ch-10).

Weiss, M.P., Witkind I.J., and Cashion W.B., 1990, Geologic map of the Price 30' x 60' quadrangle, Carbon, Duchesne, Uintah, Utah, and Wasatch Counties, Utah: U.S. Geological Survey Miscellaneous Investigations Series Map I-1981, scale 1:100,000 (Ch-2, Ch-3, Ch-6, Ch-7, Ch-10, plate 1).

Welhan, J., and Gwynn, M., 2014, High heat flow in the Idaho thrust belt—a hot sedimentary geothermal prospect: Transactions, Geothermal Resources Council, v. 38, p. 1055–1066 (Ch-12).

Welhan, J.A., Gwynn, M.L., Payne, S., McCurry, M.O., Plummer, M., and Wood, T., 2014, The Blackfoot volcanic field, southeast Idaho—a hidden high-temperature geothermal resource in the Idaho thrust belt, *in* 39th Workshop on Geothermal Reservoir Engineering, Stanford, California, February 24–26, 2014, Proceedings: Stanford University, SGP-TR-202, 13 p. (Ch-12)

Wernicke, B., 2011, The California River and its role in carving Grand Canyon: Geological Society of America Bulletin, v. 123, p. 1288-1316 (Ch-6).

Western Energy Alliance, 2014, Oil and natural gas exploration and production water sources and demand study – Colorado, Montana, New Mexico, North Dakota, Utah, and Wyoming: Western Energy Alliance report 1302226 prepared by Golder and Associates, 56 p. (Ch-11).

White, D.E., and Chuma, N.J., 1987, Carbon and isotopic mass balance models of Oasis Valley-Forty Nine Mile Canyon ground water basin, southern Nevada: Water Resources Research, v. 23, no. 4, p. 571–582 (Ch-9).

White, H., Cole, R., Stancel, S., Lee, C., and MacMillan, L., 2008, "Window" outcrop analogues for Greater Natural Buttes field, Uinta Basin Utah, *in* Longman, M.W., and Morgan, C.D., editors, Hydrocarbon systems and production in the Uinta Basin, Utah: Rocky Mountain Association of Geologists and Utah Geological Association Publication 37, p. 209-236 (Ch-2, Ch-6).

Willett, S.D., and Chapman, D.S., 1987, Analysis of temperatures and thermal processes in the Uinta Basin, *in* Beaumont, C., and Tankard, A.J., editors, Sedimentary basins and basin-forming mechanisms: Canadian Society of Petroleum Geologists Memoir No. 12, p. 227–261 (Ch-12).

Wilcox, W.T., 2007, Sequence stratigraphy of the Curtis, Summerville, and Stump Formations, Utah and northwest Colorado: Oxford, Miami University (Ohio), M.S. thesis, 108 p. (Ch-2)

Willis, G.C., and Biek, R.F., 2001, Quaternary incision rates of the Colorado River and major

tributaries in the Colorado Plateau, Utah, *in* Young, R.A., and Spamer, E.E., editors, Colorado River origin and evolution—proceedings of a symposium held at Grand Canyon National Park in June, 2000: Grand Canyon Association, p. 119-123 (Ch-3).

Wingert, S., and Adams, C., 2010, TMDLs for total dissolved solids, selenium, and boron in the Pariette Draw Watershed: Online, http://www.waterquality.utah.gov/TMDL/Pariette%20Draw%20TMDL%20Final.pdf, accessed March 18, 2015 (Ch-9).

Witkind, I.J., 1979, Reconnaissance geologic map of the Wellington quadrangle, Carbon County, Utah: U.S. Geological Survey Miscellaneous Investigations Series Map I-1178, scale 1:24,000 (Ch-2).

Witkind, I.J., 1980, Reconnaissance geologic map of the Mounds quadrangle, Carbon and Emery Counties, Utah: U.S. Geological Survey Miscellaneous Investigations Series Map I-1202, scale 1:24,000 (Ch-2).

Witkind, I.J., 1988, Geologic map of the Huntington 30’ x 60’ quadrangle, Carbon, Emery, Grand, and Uintah Counties, Utah: U.S. Geological Survey Miscellaneous Investigations Series Map I-1764, scale 1:100,000 (Ch-2, Ch-6, Ch-10, plate 1).

Witkind, I.J., and Weiss, M.P., 1991, Geologic map of the Nephi 30' x 60' quadrangle, Carbon, Emery, Juab, Sanpete, Utah, and Wasatch Counties, Utah: U.S. Geological Survey Map I-1937, scale 1:100,000 (Ch-10, plate 1).

Witkind, I.J., Weiss, M.P., and Brown, T.L., 1987, Geologic map of the Manti 30' x 60' quadrangle, Carbon, Emery, Juab, Sanpete, and Sevier Counties, Utah: U.S. Geological Survey Map I-1631, scale 1:100,000 (plate 1).

Wood, L.J., and Dutton, S.P., 1999, Sequence stratigraphy and reservoir architecture of tide-influenced shoreline systems in the Late Cretaceous Sego Sandstone: Texas Bureau of Economic Geology, Clastic Reservoirs Group Field Trip Guidebook, 132 p. (Ch-2).

Wood, R.E., and Chidsey, T.C., Jr., 2015, Oil and gas fields map of Utah: Utah Geological Survey Circular 119, scale 1:700,000 (Ch-6).

Wyllie, M.R., Gregory, A.R., and Gardner, G.H.F., 1958, An experimental investigation of the factors affecting elastic wave velocities in porous media: Geophysics, v. 23, p. 459-493 (Ch-6).

Yingling, V.L., 1987, Timing and initiation of the Sevier Orogeny—Morrison and Cedar Mountain Formations and Dakota Sandstone, east-central Utah: Laramie, University of Wyoming, M.S. thesis, 169 p. (Ch-2).

Young, R.G., 1973, Depositional environments of basal Cretaceous rocks of the Colorado Plateau, *in* Fassett, J.E., editor, Cretaceous and Tertiary rocks of the southern Colorado Plateau: Four Corners Geological Society Memoir, p. 10-27 (Ch-4).

Young, R.A., and Spamer, E.E., editors, 2001, Colorado River, origin and evolution: Grand Canyon Natural History Association, symposium volume, 280 p. (Ch-3).

Zhang, Y., Gable, C.W., Zyvoloski, G.A., and Walter, L.M., 2009, Hydrogeochemistry and gas compositions of the Uinta Basin—a regional-scale overview: American Association of Petroleum Geologists Bulletin, v. 93, no. 8, p. 1087–1118 (Ch-7 Ch-9, Ch-10, Ch-12).

Zschocke, A., 2005, Correction of non-equilibrated temperature logs and implications for geothermal investigations: Journal of Geophysics and Engineering, v. 2, p. 364–371 (Ch-12).

LIST OF ACRONYMS AND ABBREVIATIONS

ACTS – Anadarko Completion Technology System
A_F – attenuation factor
APDs – Applications for Permit to Drill
API – American Petroleum Institute
BBC – Bill Barrett Corporation
bbls – barrels
BCF – billion cubic feet
BCFG – billion cubic feet of gas
BHT – bottom-hole temperature
BLM – Bureau of Land Management
BMSW – base of moderately saline water
BO – barrels of oil
BOPD – barrels of oil per day
BPD – barrels per day
BTEX – benzene, toluene, ethylbenzene, and xylene
BVW – bulk volume of water
BW – barrels of water
Ca/Na ratio – calcium/sodium ratio
CBM – coal-bed methane
Ch-1, Ch-2,… – Chapter 1, Chapter 2,…
CMKD – Cretaceous Cedar Mountain and Dakota Formations
CO_2 – carbon dioxide
CUP – conditional use permit
DEM – digital elevation model
DFZ – Duchesne fault and fracture zone
DOGM – Utah Division of Oil, Gas, and Mining
DST – drill-stem test
DT – sonic log, Delta T
DWSAP – Drinking Water Source Assessment and Protection
DWSP – drinking water source protection
ECS – Environmentally Clean Systems
EIS – Environmental Impact Statement
EOR – enhanced oil recovery
EPA – U.S. Environmental Protection Agency
Fm. – Formation
GAPI – gamma ray measurements in American Petroleum Institute units
GCG/N – Glen Canyon Group/Nugget Sandstone
GIS – Geographic Information System
GMBU – Greater Monument Butte Unit
Gp. – Group
GWQPP – Ground Water Quality Protection Program
GMWL – global meteoric water line
GOR – gas-oil ratio
GOS – Gas-Oil-Separation

GR – gamma-ray log
GRF – Green River Formation
GRO/DRO – gasoline-range organics/diesel-range organics
HDPE – high-density polyethylene
IDW – Inverse Distance Weighting
IFP – initial flowing potential
IGT – Induced Gas-Flotation Tank
I-70 – Interstate 70
K-T boundary – Cretaceous-Tertiary boundary
kW – kilowatts
LGS – liquids-gathering system
LSN – large-saline-nodule [facies]
Ma – million years ago
MB – thousand barrels
MBO – thousand barrels of oil
Mbr. – Member
MBW – thousand barrels of water
MCL – maximum contaminant levels
mD – millidarcies
MCF – thousand cubic feet
MCFG – thousand cubic feet of gas
MCFGPD – thousand cubic feet of gas per day
mg/L – milligrams/liter
MMB – million barrels
MMBO – million barrels of oil
MMBW – million barrels of water
MMCF – million cubic feet
MMCFG – million cubic feet of gas
MW – megawatts
mW/m^2 – milliwatts per square meter
nD – nanodarcies
NGR – net-to-gross sand ratios
NOx – nitrogen oxides
NRCS – National Soil Survey Center
NWIS – National Water Information System
OWR – oil-water ratio
PCA – possible contaminating activities
PHIA – average porosity
PhiE – effective porosity
ppm – parts per million
RES – resistivity log
RESD – deep resistivity
R_F – retardation factor
RMCCS – Rocky Mountain Carbon Capture and Storage
Rmf – resistivity of mud filtrate
Rmfft – resistivity of mud filtrate at formation temperature

ROD – Record of Decision
ROSS – removal of oil and suspended solids
RPSEA – Research Partnership to Secure Energy for America
Rw – water resistivity
Rwe – equivalent formation water resistivity
SGT – surface ground temperature
Sh. – Shale
SLBL&M – Salt Lake Base Line & Meridian
SP – spontaneous potential log
SPHI – sonic porosity readings or curve values
SPHIS – sonic porosity – sandstone
SPHIS_GAS – sonic porosity curve adjusted for gas
SPARROW – Spatially Referenced Regressions on Watershed Attributes
SRS – San Rafael Swell
Ss. – Sandstone
SSC – small-saline-crystal [facies]
SSP – static spontaneous potential
SSURGO – National Soil Survey Center's Soil Survey Geographic
TCFG – trillion cubic feet of gas
TDS – total dissolved solids
TMDL – total maximum daily loads
TPH – total petroleum hydrocarbon
TWT – two-way time
UB – Uinta Basin
UBMBF – Uinta Basin-Mountain boundary fault
UBL&M – Uinta Base Line & Meridian
UDEQ – Utah Department of Environmental Quality
UDWQ – Utah Division of Water Quality
UGS – Utah Geological Survey
USGS – U.S. Geological Survey
UU – University of Utah
VOC – volatile organic compounds
VRT – virgin rock temperature
Vsh – V-shale
W/m^2 – watts per meter squared
W/mK – watts per meter Kelvin

APPENDIX A: TECHNOLOGY TRANSFER

Project Presentations

Basin Scale Produced Water Management Tools and Options – GIS Based Models and Statistical Analysis of Shale Gas/Tight Sand Reservoirs and their Produced Water Streams, Uinta Basin, Utah (posted on UGS project website), presented by Thomas C. Chidsey, Jr. at the quarterly meeting of the Uinta Basin Oil and Gas Collaborative Group, January 17, 2013, Vernal, Utah.

Basin Scale Produced Water Management Tools and Options – GIS Based Models and Statistical Analysis of Shale Gas/Tight Sand Reservoirs and their Produced Water Streams, Uinta Basin, Utah: Progress Report (posted on UGS project website), presented by Thomas C. Chidsey, Jr. at the quarterly meeting of the Uinta Basin Oil and Gas Collaborative Group, July 11, 2013, Vernal, Utah.

Water Quality from Alluvial Wells and Springs in the Uinta Basin, Eastern Utah (posted on UGS project website), presented by Janae Wallace at the Geological Society of America Annual Meeting, October 27-30, 2013, Denver, Colorado.

Basin-Scale Analysis, Management Tools, and Options for Produced Water from Tight-Gas Sand Reservoirs, Uinta Basin, Utah (posted on UGS project website), presented by David E. Tabet at the American Association of Petroleum Geologists (AAPG) Annual Convention, April 6-9, 2014, Houston, Texas. Note: this presentation was awarded the AAPG Division of Environmental Geosciences *Excellence of Presentation Award, Best Poster*.

Produced Water Modeling of Upper Cretaceous Mesaverde Group Tight-Sandstone Reservoirs in the Uinta Basin, Utah (posted on UGS project website), presented by Peter Nielsen at the AAPG Rocky Mountain Section Meeting, July 20-23, 2014, Denver, Colorado.

Basin-Scale Analysis, Management Tools, and Options for Produced Water from Tight-Gas Sand Reservoirs, Uinta Basin, Utah (posted on UGS project website), presented by David E. Tabet at the AAPG Rocky Mountain Section Meeting, July 20-23, 2014, Denver, Colorado.

Geothermal Assessment and Modeling of the Uinta Basin, Utah (posted on UGS project website), presented by Christian Hardwick at the AAPG Rocky Mountain Section Meeting, July 20-23, 2014, Denver, Colorado.

Development of Produced Water Management Tools for the Uinta Basin, Utah (posted on UGS project website), presented by David E. Tabet at the RPSEA On-Shore Production Conference, September 10, 2014, Salt Lake City, Utah.

Geology of the Uinta Basin and Oil and Gas Resource Potential, presented by Thomas C. Chdsey, Jr. at the Utah Petroleum Association Quarterly Community Outreach meeting, October 21, 2014, Roosevelt, Utah.

Oil and Gas in the Uinta Basin, Utah – What to do with the Produced Water? (posted on UGS project website), presented by Thomas C. Chidsey, Jr. at the Environmental Protection Agency, Region 8 Oil & Gas Muster, November 10, 2014, Denver, Colorado.

Development of Produced Water Management Tools for the Uinta Basin, Utah: A Project Overview and Progress Report, presented by Thomas C. Chidsey, Jr. at the quarterly meeting of the Uinta Basin Oil and Gas Collaborative Group, January 8, 2015, Vernal, Utah.

Oil and Gas in the Uinta Basin, Utah – What to do with the Produced Water?, presented by Thomas C. Chidsey, Jr. at the American Petroleum Institute, Uinta Basin Chapter monthly meeting, May 13, 2015, Roosevelt, Utah.

Basin-Scale Modeling of Jurassic and Late Cretaceous Reservoirs in the Uinta Basin, Utah, for Produced-Water Management and CO_2 Storage, presented by Craig D. Morgan at the AAPG Annual Convention, June 2, 2015, Denver, Colorado.

Oil and Gas in the Uinta Basin, Utah – What to do with the Produced Water? (posted on UGS project website), presented by Thomas C. Chidsey, Jr. at the AAPG Annual Convention, June 2, 2015, Denver, Colorado.

Basin-Scale Produced Water Management Tools and Options—GIS Based Models and Statistical Analysis of Shale Gas/Tight Sand Reservoirs and Their Produced Water Streams, Uinta Basin, Utah (posted on UGS project website), presented by Thomas C. Chidsey, Jr., at the RPSEA Onshore Technology Workshop, August 11, 2015, Denver, Colorado.

Project Publications

Abstracts

Wallace, J., 2013, Water quality from alluvial wells and springs in the Uinta Basin, eastern Utah [abs.]: Geological Society of America Abstracts with Programs, v. 45, p. 784.

Tabet, D.E., and Chidsey, T.C., Jr., 2014, Basin-scale analysis, management tools, and options for produced water from tight-gas sand reservoirs, Uinta Basin, Utah [abs.]: American Association of Petroleum Geologists Annual Convention Abstracts Volume, (1837451).

Tabet, D.E., Chidsey, T.C., Jr., Morgan, C.D., Ressetar, R., Nielsen, P.J., Wood, R.E., Boden, T., Carney, S.M., Vanden Berg, M.D., Kirby, S., Willis, H., Hardwick, C., and Emerson, R., 2014, Basin-scale analysis and options for produced water from tight-gas sand reservoirs, Uinta Basin, Utah [abs.]: American Association of Petroleum Geologists, Rocky Mountain Section Official Meeting Program, p. 43, (1960262).

Nielsen, P.J., Wood, R.E., and Chidsey, T.C., Jr., 2014, Produced water modeling of Upper Cretaceous Mesaverde Group tight-sandstone reservoirs in the Uinta Basin, Utah [abs.]: American Association of Petroleum Geologists, Rocky Mountain Section Official Meeting Program, p. 37, (1960221).

Hardwick, C., Willis, H., and Gwynn, M., 2014, Geothermal assessment and modeling of the Uinta Basin, Utah [abs.]: American Association of Petroleum Geologists, Rocky Mountain Section Official Meeting Program, p. 28-29, (1965777).

Chidsey, T.C., Jr., Tabet, D.E., Morgan, C.D., Ressetar, R., Nielsen, P., Wood, R.E., Boden, T., Carney, S.M., Vanden Berg, M.D., Kirby, S., Willis, H., Hardwick, C., Emerson, R., and Wallace, J., 2015, Oil and gas in the Uinta Basin, Utah – what to do with the produced water? [abs.]: American Association of Petroleum Geologists Annual Convention Abstracts Volume, (2088117).

Morgan, C.D., Kirby, S., Nielsen, P., Quick, J.C., Tabet, D.E., and Willis, H., [abs.]: Basin-scale modeling of Jurassic and Late Cretaceous reservoirs in the Uinta Basin, Utah, for produced water management and CO_2 storage [abs.]: American Association of Petroleum Geologists Annual Convention Abstracts Volume, (2091557).

Technical Papers

Hardwick, C.L., Willis, H.W., and Gwynn, M.L., 2015, Geothermal assessment and modeling of the Uinta Basin, Utah, *in* Vanden Berg, M., Ressetar, R., and Birgenheier, L., editors, Geology of Utah's Uinta Basin and Uinta Mountains: Utah Geological Association Publication 44, in press.

Wallace, J., 2015, Groundwater chemistry for shallow alluvial wells and springs in the Uinta Basin, Utah, *in* Vanden Berg, M., Ressetar, R., and Birgenheier, L., editors, Geology of Utah's Uinta Basin and Uinta Mountains: Utah Geological Association Publication 44, in press.

Wallace, J., Payne, N., and Emerson, R., 2015, Sensitivity and vulnerability of the aquifers and springs in the Uinta Basin, Utah, to potential contamination associated with energy resource development, *in* Vanden Berg, M., Ressetar, R., and Birgenheier, L., editors, Geology of Utah's Uinta Basin and Uinta Mountains: Utah Geological Association Publication 44, in press.

Non-Technical Article

Chidsey, T.C., Jr., and Tabet, D.E., 2013, New Utah Geological Survey study to determine what best to do with water produced from gas fields in the Uinta Basin: Utah Geological Survey, Survey Notes, v. 45, no. 1, p. 10-11.

Field Review

A project field review was conducted May 21-22, 2014. The UGS project team took attendees to outcrops of the Jurassic Navajo Sandstone through the Tertiary Green River Formation that have been a major focus of the study in eastern and central Utah. Both potential produced water storage formations and tight gas reservoirs were observed and described. We also visited a unique spring water-sample site and the examined the infrastructure of Natural Buttes field area. Attendees included members of our project consortium composed of Uinta

Basin field operator and collaborating regulatory agencies (Utah Division of Oil, Gas, and Mining, and the U.S. Environmental Protection Agency, for example).

Project Displays at the American Association of Petroleum Geologists (AAPG) Annual and Other Meetings

Project materials, objectives, plans, activities, and results were displayed at the UGS exhibit booth during the meetings and conventions listed below:

Annual Governor's Energy Development Summit, January 9-10, 2013, Salt Lake City, Utah

AAPG Annual Convention, May 19-22, 2013, Pittsburgh, Pennsylvania.

AAPG Rocky Mountain Section Meeting, September 22-24, 2013, Salt Lake City, Utah.

AAPG Annual Convention, April 6-9, 2014, Houston, Texas.

AAPG Rocky Mountain Section Meeting, July 20-23, 2014, Denver, Colorado.

AAPG Annual Convention, May 31-June 3, 2015, Denver, Colorado.

Utah Geological Survey Web Site

The UGS maintains a website on the Internet, http://geology.utah.gov. The UGS site includes a page under the heading *Oil, Coal, & Energy* which describes the studies past and present. Each UGS RPSEA/DOE cooperative study also has its own separate page on the UGS website. The Uinta Basin produced water project page is found under Uinta Basin water studies at http://geology.utah.gov/resources/energy/oil-gas/produced-water/, and contains (1) a project location map, (2) a description of the project, and (3) poster and oral presentations.

Technical Advisory Board (Industry Consortium) and Collaborating Regulatory Agencies

Anadarko Petroleum Corp., Denver, Colorado
EOG Resources, Inc., Denver, Colorado
Wind River Resources, Inc., Salt Lake City, Utah
QEP Resources, Inc., Vernal, Utah
U.S. Environmental Protection Agency, Region 8, Denver, Colorado
Utah Department of Natural Resources (Division of Oil, Gas, and Mining, Division of Water Rights, Utah Division of Water Resources), Salt Lake City, Utah
Utah Department of Environmental Quality, Salt Lake City, Utah
U.S. Bureau of Land Management, Vernal, Utah